



Kent Academic Repository

Bird, Emma Elizabeth (2022) *Functional adaptation of internal bone structure in the wrist of extant hominids and fossil hominins*. Doctor of Philosophy (PhD) thesis, University of Kent, University of Kent.

Downloaded from

<https://kar.kent.ac.uk/96957/> The University of Kent's Academic Repository KAR

The version of record is available from

<https://doi.org/10.22024/UniKent/01.02.96957>

This document version

UNSPECIFIED

DOI for this version

Licence for this version

CC BY-NC (Attribution-NonCommercial)

Additional information

Versions of research works

Versions of Record

If this version is the version of record, it is the same as the published version available on the publisher's web site. Cite as the published version.

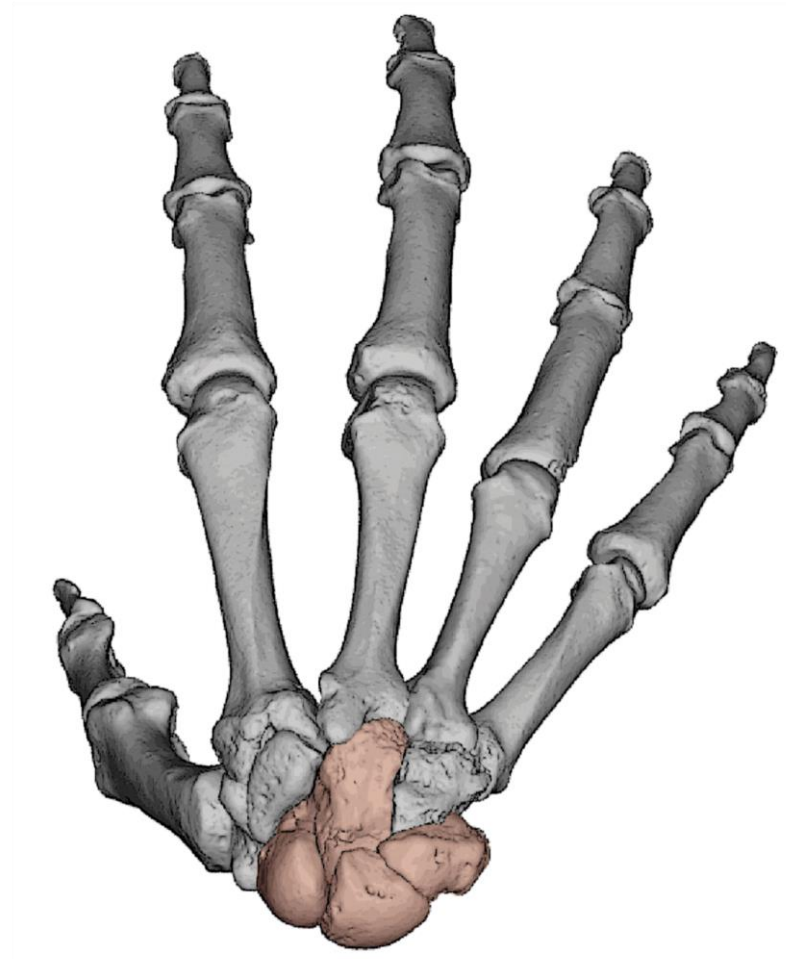
Author Accepted Manuscripts

If this document is identified as the Author Accepted Manuscript it is the version after peer review but before type setting, copy editing or publisher branding. Cite as Surname, Initial. (Year) 'Title of article'. To be published in *Title of Journal*, Volume and issue numbers [peer-reviewed accepted version]. Available at: DOI or URL (Accessed: date).

Enquiries

If you have questions about this document contact ResearchSupport@kent.ac.uk. Please include the URL of the record in KAR. If you believe that your, or a third party's rights have been compromised through this document please see our [Take Down policy](https://www.kent.ac.uk/guides/kar-the-kent-academic-repository#policies) (available from <https://www.kent.ac.uk/guides/kar-the-kent-academic-repository#policies>).

Functional adaptation of internal bone structure in the wrist of extant hominids and fossil hominins



Emma Elizabeth Bird

School of Anthropology and Conservation

University of Kent

Submitted in partial fulfilment of the requirements for the degree of
Doctor of Philosophy in Anthropology at the University of Kent, May
2022

The hand is not to be looked on as one organ but as many;
for it is, as it were, an instrument for further instruments

Aristotle, On the Parts of Animals

Abstract

The shape of wrist bones (carpals) in living hominids are thought to be adapted to the primary function of the hand, which in *Homo sapiens* is for manipulation, and in non-human hominids, locomotion. However, the hominid hand is inherently versatile in its use, and parsimony would suggest that the hominid last common ancestor was capable of manipulating and using simple tools. Therefore, key questions in palaeoanthropology ask when, why, and how tool use moved from facultative, as it is in other hominids, to obligate, as it is in *H. sapiens*. Inferring this transition within the fossil record is challenging as habitual behaviours are not always reflected in the external morphology of the skeleton. As the internal microstructure of bone is known to adapt to load dynamically, bone functional adaptation analyses provide an avenue to investigate how a joint has actually been loaded over an individual's lifetime. The central question asked by this thesis was: **'How and why does the internal structure of wrist bones differ among extant and extinct hominids?'**. To achieve this aim, I investigated 1) whether functionally meaningful differences exist in the microarchitecture of extant hominid carpals; 2) how to detect signals of functional adaptation within the complex biomechanical environment of the wrist; 3) what can be inferred about hand use from the proximal capitate bone of fossil hominins?

This thesis undertook three research projects, which all use 'whole-bone' methodologies for investigating functional signals of hand use. Using micro-computed tomography, I quantified and compared trabecular and cortical bone microarchitecture in 264 individual carpal bones across four extant hominids (*Pongo*, *Gorilla*, *Pan*, and *H. sapiens*) and four extinct hominins (*Australopithecus sediba*, *Homo naledi*, *Homo floresiensis* and Neanderthals).

In the first project, I used inter- and intraspecific analyses to compare the trabecular and cortical microstructure of the proximal and distal capitate in extant hominids. Unique combinations of microarchitecture across the two segments of the bone differentiated the extant taxa. Notably, non-human hominids exhibited a distinctive pattern of extremely thick cortical bone in the distal capitate. This result suggested that highly localised functional adaptation responses were occurring across the capitate, and studying biomechanically distinct subregions of the carpus may be required to detect signals of functional adaptation.

I then conducted intraspecific analyses on the scaphoid, lunate and triquetrum's trabecular and cortical bone microstructure across extant hominids. Results identified that microarchitectural differences across the three bones could be linked to the known or assumed biomechanics of the proximal row. Relative differences in the three bones

differentiated locomotor mode between the genera: *Gorilla* and *Pan* expressed the same relative patterns of architecture, with *Pongo* and *H. sapiens* showing unique patterns. This project demonstrated that establishing relative patterns across a biomechanically distinct subregion of the wrist can differentiate hand use among extant hominids.

Using a novel canonical holistic morphometric analysis, my final research project indicated that extant hominids have statistically distinct distributions of relative bone volume in the proximal capitate. Neanderthals and fossil *H. sapiens* exhibited the same pattern of relative bone distribution in the proximal capitate as modern *H. sapiens* suggesting a functional commitment to tool use leaves a distinct distribution of bone in the proximal capitate. Despite being the geologically oldest fossil, *A. sediba* was the only other species to exhibit a human-like distribution of bone, with evidence of a highly strained capitulate and capitoscapoid joint. Although *H. naledi* has human-like carpal morphology, it showed no evidence for human-like force transfer and loading at the midcarpal joint suggesting its hand use was not similar to a typical modern *H. sapiens*. The distribution of bone in *H. floresiensis* suggested that Oldowan-type tools were made and used with high ulnar-side loading of the hand and relatively lower loading of the thumb.

This thesis demonstrated that a hand used primarily for manipulation has distinctive and statistically differentiated microarchitecture in the carpal bones. Unique microarchitectural features within the hominin species support a model of adaptive radiations of hand and tool behaviours among hominins. The similarity in microarchitecture at the midcarpal joint of *H. sapiens* and Neanderthals suggests it may be a strong signal of human-like commitment to tool use but is unlikely to capture variation in tool behaviour. Further analyses are needed to better understand how manipulation and arboreality are reflected in bone architecture. In particular, this thesis discussed how both climbing and transverse grips might be biomechanically compatible behaviours, as both emphasise high loading at the ulnar side of the hand and wrist and deemphasise the use of the thumb. Thus the use of transverse-type grips may have provided fossil hominins with an opportunity to improve the functional efficiency of tool behaviours without highly compromising climbing ability. Future analyses are likely to be most informative when numerous bones across biomechanically meaningful subregions of the wrist are analysed together. Analyses at the ulnar side of the wrist may be informative for identifying signals of climbing and grip preference differences in *H. sapiens* and Neanderthals.

Acknowledgements

Firstly I would like to acknowledge my supervisors, Matt Skinner and Tracy Kivell. Your support, encouragement and flexibility made it possible for me to complete a PhD, which historically has been difficult for people with disabilities. You have built and fostered a collaborative, constructive and, importantly, friendly working environment at the University of Kent, the importance of which cannot be understated. I'm truly grateful for the opportunity you have given me to contribute to the field of palaeoanthropology. I am also thankful to the School of Anthropology and Conservation for their award of the 50th Anniversary Scholarship, which supported me over the completion of this thesis. A very big thank you to my two examiners, Brandon Wheeler and Matt Tocheri, for their deep engagement and thoughtful commentary on my thesis. Thank you also to the administrative staff at the school for their support, which has always been prompt and helpful. Everybody who has constituted part of the Skinner/Kivell lab groups since 2018, you have been an invaluable part of my experience; thank you for your expert opinions and friendship. In particular, I would like to thank Chris Dunmore for tireless technical training and support, similarly Ameline Bardo, Kim Deckers and Zewdi Tsegai for their helpful discussions, and Mykolas Imbrasas for the million jobs big and small he did to keep the technical aspects of our work accessible. I would also like to acknowledge the non-human hominids used in this research. They had lives and priorities of their own, yet many were shot and killed in the pursuit of science. I respect and thank these primates and acknowledge how much I owe them.

External to the university, this thesis would not have been possible without significant help from my family. Firstly, to my mum and dad, Marie and David Bird, thank you - this is also your achievement. My husband, Chavez Hyndman, who, by this point in time, deserves an honorary degree in palaeoanthropology. Thank you for helping me write my R script, discussing statistics with me, feeding me, and for the endless kindness and empathy you have had for me during this process. A big thank you also to my best friend, Jack Hancock, who kindly produced several illustrations for this thesis.

And finally, my cats Solomon and Mimi, and my dog Figgy Pudding, for reminding me what was really important while writing this thesis during a global pandemic: enjoying the sunshine, napping, regular meals, and daily walkies.

Contents

ABSTRACT	I
ACKNOWLEDGEMENTS	III
LIST OF FIGURES	VI
LIST OF TABLES.....	VIII
ABBREVIATIONS.....	IX
1. INTRODUCTION	1
1.1. STATEMENT OF THE PROBLEM	1
1.2. THESIS AIMS	3
1.3. CHAPTER SUMMARIES.....	4
1.4. HOMINID LOCOMOTION, POSTURE AND BEHAVIOUR	6
1.5. ANATOMY AND BIOMECHANICS OF THE WRIST	14
1.6. BONE FUNCTIONAL ADAPTATION.....	37
1.7. ALLOMETRY	43
1.8. MORPHOLOGY AND FUNCTIONAL ANATOMY IN FOSSIL HOMININS	45
2. MATERIALS AND METHODS	61
2.1. MATERIALS.....	61
2.2. METHODS	69
3. CORTICAL AND TRABECULAR BONE STRUCTURE IN THE HOMINOID CAPITATE	93
3.1. ABSTRACT	93
3.2. INTRODUCTION	94
3.3. HYPOTHESES.....	102
3.4. MATERIALS AND METHODS	104
3.5. RESULTS.....	108
3.6. DISCUSSION	122
3.7. CONCLUSION	128
3.8. SUPPLEMENTARY TABLES	129
3.9. SUPPLEMENTARY FIGURES.....	134
4. PATTERNS OF INTERNAL BONE STRUCTURE AND FUNCTIONAL ADAPTATION IN THE HOMINOID SCAPHOID, LUNATE, AND TRIQUETRUM	138
4.1. ABSTRACT	138
4.2. INTRODUCTION	139
4.3. MATERIALS AND METHODS	147

4.4.	RESULTS.....	150
4.5.	DISCUSSION.....	157
4.6.	CONCLUSION	166
4.7.	SUPPLEMENTARY TABLES	166
5.	INTERNAL STRUCTURE OF THE CAPITATE AND ITS IMPLICATIONS FOR HAND USE IN FOSSIL HOMININS.....	174
5.1.	ABSTRACT	174
5.2.	INTRODUCTION	174
5.3.	MATERIALS.....	180
5.4.	METHODS	181
5.5.	RESULTS.....	185
5.6.	DISCUSSION.....	193
5.7.	CONCLUSION	201
5.8.	SUPPLEMENTARY FIGURES.....	203
5.9.	SUPPLEMENTARY TABLES	214
6.	DISCUSSION AND CONCLUSIONS	218
6.1.	DO DIFFERENCES EXIST BETWEEN EXTANT SPECIES?.....	218
6.2.	LIMITATIONS AND IMPLICATIONS FOR FUTURE FUNCTIONAL ADAPTATION ANALYSES OF SHORT BONES	222
6.3.	WHAT DOES THE INTERNAL STRUCTURE OF THE CAPITATE SUGGEST ABOUT HAND USE AMONG EXTINCT PLIO- PLEISTOCENE HOMININS?	225
6.4.	CONCLUSION	230
6.5.	FUTURE DIRECTIONS	232
7.	REFERENCES.....	235
8.	APPENDICES.....	263
8.1.	APPENDIX A SAMPLE PREPARATION.....	263
8.2.	APPENDIX B: PUBLISHED WORK	286
8.3.	FURTHER ACKNOWLEDGEMENTS	310

List of Figures

Main Figures

FIGURE 1.1 AXES OF ROTATION OF THE HAND AND WRIST.	16
FIGURE 1.2 MOVEMENT OF THE CAPITATE AROUND THE AXES OF ROTATION SHOWN ON A <i>P. TROGLODYTES</i> CAPITATE. .	17
FIGURE 1.3 COMPARATIVE ANATOMY OF THE RIGHT CAPITATE ACROSS HOMINIDS.....	19
FIGURE 1.4 COMPARATIVE ANATOMY OF THE RIGHT SCAPHOID ACROSS HOMINIDS.....	20
FIGURE 1.5 COMPARATIVE ANATOMY OF THE RIGHT LUNATE IN HOMINIDS.	21
FIGURE 1.6 COMPARATIVE ANATOMY OF THE RIGHT TRIQUETRUM IN HOMINIDS.....	23
FIGURE 1.7 MOVEMENT THROUGH THE DART-THROWER’S MOTION (DTM).....	31
FIGURE 1.8 MORPHOLOGY OF THE CAPITATE IN EXTANT AND EXTINCT HOMINIDS.....	46
FIGURE 2.1 SURFACE MODELS OF THE 14 FOSSIL SPECIMENS.	65
FIGURE 2.2 SEGMENTATION OF CAPITATE BY MIA.....	67
FIGURE 2.3 THREE EXAMPLES OF FUNCTIONS USED IN AVIZO TO CLEAN FOSSIL SEGMENTATIONS.	68
FIGURE 2.4 ILLUSTRATION OF WHOLE-BONE METHODOLOGIES VERSUS VOI METHODS.....	69
FIGURE 2.5 WORKFLOW OF MEDTOOL FOR WHOLE-BONE DATA COLLECTION FOR THE BINARY AND TISSUE SEGMENTATION OF A μ CT SCAN.	71
FIGURE 2.6 EXAMPLES OF VISUALISATIONS OF MEDTOOL DATA.	74
FIGURE 2.7 VISUALISATION OPTIONS FOR BV/TV IN A <i>H. SAPIENS</i> SCAPHOID.....	74
FIGURE 2.8 A <i>H. SAPIENS</i> LUNATE SHOWING THICK AND POROUS TISSUE MORPHOLOGY AT THE CAPITATE ARTICULAR SURFACE.	78
FIGURE 2.9 A <i>PONGO</i> LUNATE ILLUSTRATING THE EFFECTS OF DIFFERENT KERNEL SIZES ON TISSUE SEGMENTATION.	79
FIGURE 2.10 EXAMPLES OF PROBLEMATIC TISSUE SEGMENTATION ON SIX <i>PONGO</i> LUNATES.	80
FIGURE 2.11 FIVE SLICES FROM DIFFERENT PLANES THROUGH A <i>G. GORILLA</i> SPECIMEN.	81
FIGURE 2.12 BOXPLOT OF TRABECULAR BV/TV, DA, Ct.TH AND TOTAL BV/TV RESULTS.	84
FIGURE 2.13 PROCESS OF CELL SELECTION TO ANALYSE THE PROXIMAL AND DISTAL CAPITATE SEPARATELY.	89
FIGURE 2.14 CHMA VISUALISATION OPTIONS.	90
FIGURE 2.15 EXAMPLES OF THE PC LOADINGS MODELS.	91
FIGURE 3.1 CT-DERIVED SURFACE MODELS OF A LEFT CAPITATE FROM EACH GENUS SHOWING VARIATION IN EXTERNAL MORPHOLOGY.....	101
FIGURE 3.2 IMAGES SHOWING THE MORPHOLOGICAL FILTERS APPLIED IN MEDTOOL 4.3 FOR THE WHOLE-BONE ANALYSIS.	107
FIGURE 3.3 THREE CROSS-SECTIONS FROM THE FOUR STUDY GENERA SHOWING INTERNAL BONE PATTERNING.	110
FIGURE 3.4 SPLIT VIOLIN PLOTS SHOWING THE DISTRIBUTION OF TRABECULAR RESULTS IN THE PROXIMAL AND DISTAL VOI OF EACH GENUS.....	113
FIGURE 3.5 BOXPLOTS OF THE FIVE TRABECULAR RATIOS FOR EACH GENUS AS WELL AS RESULTS FOR THE INTRASPECIFIC WILCOXON SIGNED-RANK TEST AND INTERSPECIFIC PAIRWISE RANK-SUM TESTS.....	114

FIGURE 3.6 SPLIT VIOLIN PLOTS SHOWING THE DISTRIBUTION OF TOTAL BV/TV (A) AND Ct.Th (B) RESULTS IN THE PROXIMAL AND DISTAL VOI OF EACH GENUS.	115
FIGURE 3.7 CROSS-SECTIONS FROM REPRESENTATIVE INDIVIDUALS OF EACH GENUS SHOWING RELATIVE TRABECULAE AND CORTEX THICKNESS ACROSS THE CAPITATE.....	118
FIGURE 4.1 EXTERNAL MORPHOLOGY OF THE SCAPHOID, LUNATE AND TRIQUETRUM OF THE PROXIMAL CARPAL ROW FROM ONE REPRESENTATIVE INDIVIDUAL OF EACH TAXON.	145
FIGURE 4.2 PROCESS OF μ -CT SEGMENTATION AND DATA COLLECTION USING MIA-CLUSTERING AND MEDTOOL.	149
FIGURE 4.3 CROSS-SECTIONS OF EACH CARPAL SPECIMEN REPRESENTED IN FIGURE 4.1 SHOWING DIFFERENCES IN THE INTERNAL ARCHITECTURE.....	152
FIGURE 4.4 BOX-AND-WHISKER PLOTS SHOWING THE DISTRIBUTION OF BV/TV (A) AND DA (B) RESULTS BY BONE AND TAXON.....	155
FIGURE 4.5 LINE GRAPHS PLOTTING BV/TV (A) AND DA (B) RESULTS ACROSS EACH BONE BY INDIVIDUAL AND TAXON.	156
FIGURE 5.1 ANATOMY OF THE CAPITATE AND FUNCTION IN THE WRIST.	177
FIGURE 5.2 MIA SEGMENTATION AND MEDTOOL ANALYSIS USED IN THIS STUDY.	182
FIGURE 5.3 OVERVIEW OF THE CANONICAL HOLISTIC MORPHOMETRIC ANALYSIS (CHMA) WORKFLOW.	184
FIGURE 5.4 THE AVERAGE RELATIVE BONE DISTRIBUTION IN THE CAPITATE HEAD OF EACH EXTANT TAXON.	186
FIGURE 5.5 RESULTS OF THE PCA ANALYSIS.	189
FIGURE 5.6 RELATIVE BONE VOLUME (RBV) DISTRIBUTION MAPS OF THE FOSSIL SPECIMENS.....	192

Supplementary Figures

SUPPLEMENTARY FIGURE 3.1 EXAMPLE OF EXCLUDED <i>PAN TROGLODYTES</i> SPECIMEN.....	134
SUPPLEMENTARY FIGURE 3.2 PLOTS OF THE SEVEN RMA REGRESSIONS TESTING FOR ALLOMETRY.	137
SUPPLEMENTARY FIGURE 5.1 MAPS ILLUSTRATING THE STANDARD DEVIATIONS IN THE TAXON-SPECIFIC DISTRIBUTION OF RELATIVE BONE VOLUME.	203
SUPPLEMENTARY FIGURE 5.2 MAPS ILLUSTRATING THE RELATIVE BONE VOLUME DISTRIBUTION OF EVERY INDIVIDUAL IN THE SAMPLE.	213

Appendices

APPENDIX A FIGURE 8.1 ILLUSTRATIONS OF THE STEP BY STEP PROCESS OF TISSUE SEGMENTING THE FOSSIL SPECIMENS.	283
APPENDIX A FIGURE 8.2 BOX AND WHISKER PLOTS OF ABSOLUTE SURFACE DISTANCE MOVEMENTS DURING THE REGISTRATION OF MEAN CAPITATE SHAPE FOR CHMA ANALYSIS.....	284
APPENDIX A FIGURE 8.3 VISUAL REPRESENTATION OF INDIVIDUALS REGISTERED IN THE MEAN CAPITATE SHAPE.	285

List of Tables

Main Tables

TABLE 1.1 SUMMARY OF 11 WRIST LIGAMENTS IDENTIFIED IN THE KINETIC THEORY PROPOSED BY GARCIA-ELIAS (2017)	34
TABLE 1.2 SUMMARY OF GROSS CAPITATE MORPHOLOGY AMONG THE HOMININS	47
TABLE 2.1 SUMMARY OF THESIS SAMPLE	61
TABLE 2.2 SPECIMENS USED IN THE REPEATABILITY STUDY	75
TABLE 2.3 RESULTS OF REPEATABILITY STUDY	75
TABLE 2.4 DESCRIPTIVE STATISTICS OF REPEATABILITY STUDY	76
TABLE 2.5 <i>GORILLA</i> AND <i>PONGO</i> SPECIMENS INCLUDED IN SEGMENTATION TEST AND THEIR INDIVIDUAL MEDTOOL RESULTS	82
TABLE 2.6 RESULTS OF INTRASPECIFIC MANN-WHITNEY U TESTS	84
TABLE 3.1 SUMMARY OF THE HYPOTHESES, PREDICTIONS AND STATISTICAL TESTS USED IN THIS STUDY	102
TABLE 3.2 SUMMARY OF THE STUDY SAMPLE	104
TABLE 3.3 RMA REGRESSION RESULTS OF THE INTER- AND INTERSPECIFIC ALLOMETRY	120
TABLE 4.1 SUMMARY OF STUDY SAMPLE	148
TABLE 4.2 DESCRIPTIVE STATISTICS FOR BV/TV AND DA ACROSS THE STUDY TAXA	150
TABLE 4.3 MEAN RANK OF EACH BONE BY TAXA WITH FRIEDMAN'S TEST P-VALUE AND KENDALL'S EFFECT SIZE (W)	152
TABLE 4.4 INTRASPECIFIC DIFFERENCES BETWEEN CARPAL BONES USING WILCOXON RANK-SUM TESTS WITH BONFERRONI CORRECTION FOR BV/TV (BOTTOM LEFT OF TABLE) AND DA (TOP RIGHT OF TABLE)	153

Supplementary Tables

SUPPLEMENTARY TABLE 3.1 SEE APPENDIX A TABLE 1. FULL LIST OF EXTANT AND EXTINCT SPECIMENS USED IN THIS THESIS	129
SUPPLEMENTARY TABLE 3.2 DESCRIPTIVE STATISTICS FOR THIS STUDY	129
SUPPLEMENTARY TABLE 3.3 RESULTS OF THE KRUSKAL-WALLIS AND POST-HOC PAIRWISE COMPARISON TESTS OF THE MEAN PARAMETERS IN THE PROXIMAL AND DISTAL SEGMENTS	131
SUPPLEMENTARY TABLE 3.4 RESULTS OF THE NINE RATIOS AND THE ASSOCIATED INTER- AND INTRASPECIFIC WILCOXON TESTS	132
SUPPLEMENTARY TABLE 3.5 DESCRIPTIVE STATISTICS FOR THE NINE RATIOS CALCULATED IN THIS STUDY	133
SUPPLEMENTARY TABLE 4.1 SPECIMEN INFORMATION AND INDIVIDUAL PARAMETER RESULTS	166
SUPPLEMENTARY TABLE 4.2 RESULTS OF THE WILCOXON INTRASPECIFIC PAIRWISE COMPARISONS	173
SUPPLEMENTARY TABLE 5.1 SPECIMEN INFORMATION AND INDIVIDUAL PARAMETER VALUES	214
SUPPLEMENTARY TABLE 5.2 SUMMARY OF THE QUALITATIVE DESCRIPTIONS OF THE TYPICAL RBV FOR KEY REGIONS IN THE PROXIMAL CAPITATE	216
SUPPLEMENTARY TABLE 5.3 PERMUTATIONAL MULTIVARIATE PAIRWISE COMPARISONS OF EXTANT HOMINOIDS	217

Appendices

APPENDIX A TABLE 8.1 FULL LIST OF EXTINCT AND EXTANT SPECIMENS USED IN THIS THESIS	263
--	-----

Abbreviations

μ CT	Micro-Computed Tomography (Micro-CT)
A.	<i>Australopithecus</i>
BFA	Bone functional adaptation
BV/TV	Bone volume to total volume
CMc	Carpometacarpal
Ct.Th	Cortical thickness
DA	Degree of anisotropy
ka	Thousands of years ago
LB1	Liang Bua 1, <i>Homo floresiensis</i> holotype
LB6	Liang Bua 6, <i>Homo floresiensis</i>
LCA	Last common ancestor
Ma	Millions of years ago
Mc	Metacarpal
Mc1	First metacarpal
Mc2	Second metacarpal
Mc3	Third metacarpal
Mc4	Fourth metacarpal
Mc5	Fifth metacarpal
MH2	Malapa Hominin 2, <i>Australopithecus sediba</i> paratype.
MIA	Medical imaging analysis
PC	Principle component
PCA	Principle component analysis
RBV	Relative bone volume to total volume
Tb.N	Trabecular number
Tb.Sp	Trabecular spacing
Tb.Th	Trabecular thickness
Total BV/TV	Bone volume to total volume of the cortical and trabecular bone combined
VOI	Volume of interest

1. Introduction

1.1. Statement of the problem

A dexterous, grasping hand is a shared feature of all primates (Lewis 1989; Cartmill 1992; Bloch and Boyer 2002; Fragaszy and Crast 2016); however, the only living species that requires extensive manufacture and use of tools to survive is *Homo sapiens* (Marzke 1997; Shea 2017). While once considered a defining characteristic of the genus *Homo* (Leakey, Tobias and Napier 1964), tool use is now known to be exploited by several primate species (Malaivijitnond et al. 2007; Ottoni and Izar 2008; Falótico et al. 2019); indeed, all hominids¹ are capable of making and using tools to varying degrees (Washburn 1960; Leakey, Tobias and Napier 1965; Toth et al. 1993; Breuer, Ndongou-Hockemba and Fishlock 2005; Meulman and van Schaik 2013; Sanz, Call and Boesch 2013). Therefore, key questions in palaeoanthropology ask when, why and how did tool use move from facultative, as in other non-human primates, to obligate, as in *H. sapiens*?

Due to their diverse locomotor strategies, carpal morphology among the hominids is more variable than in other primate clades (Kivell, Barros and Smaers 2013; Kivell 2016a). The degree of behavioural and concomitant morphological variability among hominids offers an opportunity to correlate the form of the carpus to hand function within a phylogenetically-constrained group of primates. The hand of *H. sapiens* is morphologically adapted² to the biomechanical requirements of precise, forceful and fine manual manipulation (Napier 1956; Lewis 1989; Marzke 1997). Similarly, non-human hominids exhibit carpal morphology adapted to the primary function of their hand, locomotion (Sarmiento 1988; Lewis 1989; Richmond, Begun and Strait 2001; Alba, Moyà-Solà and Köhler 2003; Begun 2004; Tocheri 2007; Orr 2010, 2017, 2018; Preuschoft 2019). For palaeoanthropologists, establishing the form-function relationship of the carpus in extant hominids provides a framework to infer behaviour among fossil hominins³ and elucidate the evolution of morphological traits.

Drawing these behavioural inferences from skeletal morphology has distinct challenges as, while the skeleton provides information on the capacity for movement, it is not *ipso facto* evidence of behaviour. For example, most researchers agree that *Australopithecus* species

¹ Hominid refers to extinct and extant 'great apes'. Great apes include *Pongo*, *Pan*, *Gorilla*, *Homo sapiens*, and all of their fossil ancestors. Hominid is sometimes used in this thesis when the inclusion of family Hylobatidae is relevant.

² See section 1.6 for a discussion on the definition of adaptation as used in this thesis.

³ A hominin is any species more closely related to *H. sapiens* than it is to *Pan*, e.g., Neanderthals, *Australopithecus*.

were committed bipeds when terrestrial (Aiello and Dean 1990; Ward 2002; Raichlen et al. 2010; Barak et al. 2013; Ward 2013a, b; Williams et al. 2021). However, the degree of arboreality is more contentious as, to varying degrees, *Australopithecus* expresses skeletal morphology considered advantageous for arboreality, such as long and curved fingers and toes (Marzke 1983; Ward 2002; Green and Gordon 2008; Kivell et al. 2011; Rein et al. 2017). From external morphology alone, it can be challenging to differentiate between morphology that is retained from an ancestor but is no longer functionally relevant to that which is still relevant to the behavioural niche of the species (Ward 2002; Tocheri 2007). In part due to this, palaeoanthropologists have reached conflicting conclusions when inferring the functional significance of skeletal morphology in fossils. In the case of *Australopithecus*, some argue the arboreal traits represent current adaptations to a behavioural niche dependent on arboreal substrates (Jungers 1982; Stern and Susman 1983; Rose 1984; Kivell et al. 2011), while others argue they are primitive retentions from a more arboreal ancestor, retained via neutral or stabilising evolution (Latimer 1991; Richmond and Jungers 2008; Ward 2013a).

It has been hypothesised that through evolutionary time, reduced reliance on arboreal substrates removed functional constraints on the hands for locomotion, allowing hand morphology to instead specialise for manipulation at the expense of efficient climbing and other arboreal locomotor modes (Washburn 1960; Alba, Moyà-Solà and Köhler 2003). This morphological evolution went together with increasingly human-like behaviours and ecological niches; tool use opened up access to high-quality food resources such as bone marrow, which is argued to have led to encephalisation and enhanced cognition, alongside increasingly complex tool manufacture (Leakey, Tobias and Napier 1964; Aiello and Dean 1990; McHenry and Coffing 2000). Under this model, 'ape-like' carpal morphology among hominins became more 'human-like' over time. Although a human-like capitate first appears in *Homo antecessor* (800ka) (Lorenzo, Arsuaga and Carretero 1999; Lorenzo et al. 2015), it is not until the appearance of Neanderthals^{4,5}, that we have evidence for the full-suite of derived features at the hand and wrist considered evidence of a functional commitment to tool manufacture and use (Tocheri et al. 2008). The earliest archaeological evidence, however, suggests that late Pliocene hominins were capable of stone tool manufacture (Harmand et al., 2015) and use (McPherron et al. 2010). The current paucity of carpal material throughout the Plio-Pleistocene leaves a ~3 million year gap between the

⁴ The term Neanderthal is used in place of the species name, as the taxonomic affinity is debated.

⁵ Neanderthals are known as early as 400ka, although wrist bones are only known from ~130-50ka (Kivell et al. 2018c).

archaeological evidence for hominin tool behaviour and the morphological evidence for commitment to it.

Bone is a living, “plastic” material that has been demonstrated to alter its architectural properties to reflect the strain it has experienced over the lifetime of the individual, reflecting the force vectors inflicted via movement (Pontzer et al. 2006b; Ruff, Holt and Trinkaus 2006; Barak, Lieberman and Hublin 2011). Thus, behaviourally sensitive aspects of skeletal morphology provide an avenue to address the gap between the archaeological and skeletal evidence for tool behaviours. Bone functional adaptation (BFA) research aims to detect these behavioural signals, supplementing and extending the inferences from external morphological analyses. Furthermore, when fossils are analysed within a comparative context, BFA provides an avenue to differentiate functional and non-functional morphology. For this thesis, BFA analysis provides an opportunity to explore the biomechanical loading history of an individual, potentially elucidating hand use from carpal bones of fossil species.

1.2. Thesis aims

This thesis explores how and why internal wrist bone microstructure differs among extant and extinct hominids. This thesis first asks the question: **Does the microarchitecture of trabecular and cortical bone differ between extant species, and how do we best detect these differences within the distinct biomechanical environment of the wrist?** This question is explored in the first research project in relation to the capitate and again in the second research project in relation to the three bones of the proximal row (scaphoid, lunate, triquetrum). The BFA methodologies used in this thesis have predominantly been developed on long bones (e.g., Tsegai et al. 2013; Gross et al. 2014; Bachmann et al. 2022), and it should not be presumed *a priori* that the assumptions underlying these methodologies are applicable to the study of short bones, such as those of the carpus. In order to establish a robust framework for the interpretation of fossil carpus, some of the key assumptions of the methodologies need to be systematically tested on an extant sample.

Within this comparative framework, this thesis then addresses the question: **What does the internal structure of the capitate in *Australopithecus sediba*, *Homo naledi*, *Homo floresiensis*, Neanderthals and fossil *H. sapiens* suggest about hand use among Plio-Pleistocene hominins?** The carpals of *H. sapiens* and non-human hominids are adapted to the primary function of their hand (Tocheri 2007). The morphological differences reflect variable adaptations to the biomechanically distinct force vectors imposed by that primary function, which in *H. sapiens* is manipulative and, in non-human hominids, locomotor

(Tocheri, 2007, Richmond, 2006, Lewis, 1989, Sarmiento, 1988). While it is reasonable to assume *a priori* that all fossil hominins were capable of manipulating tools, it is not clear whether they were facultative tool users like non-human hominids, and continued to use their hands primarily for locomotion, committed tool users with a hand used primarily for manipulation, or somewhere in-between.

Although separated spatiotemporally, *A. sediba* (South Africa, 1.977Ma (Pickering et al. 2011)), *H. naledi* (South Africa, ~250Ka (Dirks et al. 2017)) and *H. floresiensis* (Indonesia, ~100-60ka (Sutikna et al. 2016)) provide a unique opportunity to investigate this question. *H. floresiensis* is the only one of these three species to be, thus far, found associated with stone tools (Morwood et al. 2004; Morwood et al. 2005; Moore and Brumm 2009; Sutikna et al. 2018), although exhibiting none of the derived carpal features considered evidence for a functional commitment to obligate tool behaviour (Tocheri 2007; Orr et al. 2013). Conversely, both *A. sediba* and *H. naledi* express several of these derived features (Kivell et al. 2015; Kivell et al. 2018a), although both have been hypothesised to utilise arboreal substrates habitually, and their capacity for tool use is largely unknown (Berger et al. 2010; Berger et al. 2015). This thesis will compare the microarchitecture of these fossils to known committed tool users (modern and fossil *H. sapiens* as well as Neanderthals) alongside extant non-human hominids (*Pongo*, *Pan*, *Gorilla*). Within this context, an analysis of the BFA in these fossils will allow, for the first time, an insight into the loading history of their wrists.

1.3. Chapter summaries

This thesis is organised into six chapters. The remainder of this **introductory chapter (Chapter 1)** outlines the hominid locomotion, posture and behaviour that may influence bone functional adaptation in the carpus. Detailed descriptions of the anatomy and biomechanics of the wrist follow, focusing specifically on the four carpals included in this thesis. I then discuss bone functional adaptation and why this approach can be useful for investigating and reconstructing past behaviour from skeletal material. Finally, I review the morphology and functional anatomy of fossil hominins as it pertains to the four main extinct species included for analysis, *A. sediba*, *H. naledi*, *H. floresiensis* and Neanderthals.

Chapter 2 gives a detailed summary of the materials and methods used in each research project. In addition, the approaches' limitations are also discussed, and some basic proof of concept analyses are detailed.

Chapter 3 outlines the manuscript published in the *Journal of Anatomy* (Bird, Kivell and Skinner 2021). This research project centres on establishing whether differences exist in the

capitate bone of extant hominids and how best to detect these differences within the complex biomechanical environment of the wrist. It explores: 1) interspecific differences in the structure of the trabecular and cortical bone of the proximal and distal capitate; 2) intra- and interspecific differences in the proximal and distal capitate; 3) allometry. The final published manuscript is included in Appendix B: Published Work.

Chapter 4 outlines the manuscript published in the *American Journal of Biological Anthropology* (Bird, Kivell and Skinner 2022). This project focuses on establishing whether intraspecific patterns of bone architecture across the proximal row carpus can be correlated to what we know about the loading regimes at the radiocarpal and midcarpal joints. The final published manuscript is included in Appendix B: Published Work.

Chapter 5 outlines the manuscript 'Internal structure of the capitate and its implications for hand use in fossil hominins' prior to input from the additional co-authors. The manuscript will be submitted for publication in due course. This project is the first to apply the novel canonical holistic morphometric analysis (cHMA) method (outside testing and validating projects), which combines statistical shape modelling and wholistic trabecular bone analysis. In order to investigate signals of functional adaptation within extant and extinct hominins, I quantify and statistically compare the distribution of relative bone volume within the proximal capitate with the ultimate goal to infer loading and hand use in *A. sediba*, *H. naledi*, *H. floresiensis* and Neanderthals.

Chapter 6 is the Discussions and Conclusions chapter, which summarises the three research projects and directly answers the **key questions of this thesis**:

- Are there structural differences in the carpal microarchitecture of extant species, and how do we best detect these differences within the distinct biomechanical environment of the wrist?
- What does the internal structure of the capitate suggest about force transfer and hand use in Plio-Pleistocene hominins?

1.4. Hominid locomotion, posture and behaviour

Extant hominids include *H. sapiens* and all *Pan*, *Gorilla* and *Pongo* species. As the closest living relatives to *H. sapiens*, their ecology, behaviour, life history, and anatomy provide an important comparative context in which to analyse fossil hominin species. *Homo sapiens* is conspicuous among extant hominids as the only habitual bipeds. Many aspects of *H. sapiens*' skeletal morphology decrease its efficiency for exploiting arboreal substrates relative to the extant non-human hominids, and the evolution of many of these features in the hand and wrist have been tracked through evolutionary time (Sarmiento 1988; Lewis 1989). However, fossils such as *A. sediba*, *H. naledi*, and *H. floresiensis* exhibit, in variable proportions, a combination of features throughout the skeleton advantageous for both arboreality and manipulation, complicating the inference of behavioural repertoires from skeletal remains (Jungers et al. 2009b; Kivell et al. 2011; Orr et al. 2013; Kivell 2015; Kivell et al. 2015).

Defining prehension and tool behaviour

All primates are capable of prehension, including tool use, object manipulation, locomotion, foraging, feeding and grooming (Boesch and Boesch 1993; Bardo et al. 2016; Fragaszy and Crast 2016; Bardo et al. 2017). Tool behaviour, tool use and tool manufacture are used throughout this thesis, and the definitions are as follows: tool behaviour is a general term encapsulating both tool use and manufacture (Marzke 1997); tool use is the application of an unattached object from the external environment to alter the condition of another object in some way to benefit the user (Alba, Moyà-Solà and Köhler 2003); tool manufacture is making modifications to an object in order to improve its functionality for a specific task (Alba, Moyà-Solà and Köhler 2003). Below I define power and precision grips as they relate to hominids, and a comprehensive review of the use of these grips across all primates can be found in Fragaszy and Crast (2016). Primate prehensile grips were first defined by Napier (1956) and then expanded by Marzke et al. (1992) and Marzke (1997). Grips are generally categorised as belonging to either power or precision grip types and then one of several sub-categories within each type. Grip choice is influenced by the properties of the object, such as size and weight, as well as the objective of the task (Napier 1956). In addition, grips are differentiated by the role of the fingers, thumb and palm. In **power grips**, the fingers flex around an object and hold it against the palm, and the thumb may or may not be used as a stabilising buttress (Napier 1956; Marzke, Wullstein and Viegas 1992). In **precision grips**, objects are held away from the palm and held in place by the thumb and another finger(s) (Napier and Tuttle 1993; Marzke 1997).

Below I begin by summarising the dominant locomotor postures of non-human hominids in arboreal and terrestrial contexts. I will then briefly summarise the known tool behaviours among non-human hominids. Finally, I will summarise the locomotor postures for *H. sapiens* in arboreal and terrestrial contexts and elaborate on what differentiates their tool behaviour.

1.4.a. *Pongo*

1.4.a.1. Arboreal behaviour

Pongo locomotion is characterised by its incredible complexity (Thorpe and Crompton 2006). Utilising all four prehensile limbs across a variety of supports in a predominantly arboreal environment, *Pongo* uses suspension, as well as torso pronograde and orthograde clambering, climbing vertically in ascent and descent, swing and sway (Thorpe and Crompton 2005, 2006, 2009; Manduell, Morrogh-Bernard and Thorpe 2011). Broadly, *P. abelii* (Sumatran) and *P. pygmaeus* (Bornean) positional repertoires are the same but differ in their frequency (Thorpe and Crompton 2009). Interestingly, age and sex have been shown to have little to no influence on substrate choice and locomotor mode (Thorpe and Crompton 2005; Manduell, Morrogh-Bernard and Thorpe 2011; Davies et al. 2017). The only study explicitly exploring ontogeny and locomotion showed that mothers aid juveniles to cross gaps in the canopy up to the age of weaning (6-7 years), by which point the juveniles utilise adult patterns of movement (Chappell et al. 2015).

1.4.a.2. Terrestrial behaviour

Pongo spends more time arboreally than any other hominid. *P. abelii* is almost exclusively arboreal, whereas *P. pygmaeus* has been observed to engage more frequently in terrestrial locomotion (Thorpe and Crompton 2009; Ancrenaz et al. 2014; Thorpe, McClymont and Crompton 2014). While the preferred stratum of *Pongo* is arboreal, their habitat type is perhaps more versatile than previously thought (particularly in light of intense logging in South East Asia) (Manduell, Morrogh-Bernard and Thorpe 2011; Davies et al. 2017). Recent research has emphasised that terrestriality, and differences between species, are likely strongly influenced by canopy coverage, as the degree of coverage either allows or restricts forward movement and may necessitate a greater degree of terrestrial locomotion (Thorpe and Crompton 2005; Manduell, Morrogh-Bernard and Thorpe 2011).

Palaeoanthropological literature frequently mentions fist walking during terrestrial locomotion (Tuttle 1967, 1969; Sarmiento 1988; Richmond, Begun and Strait 2001). However, most references come from a small number of observations of captive animals (Tuttle 1967; Susman 1974), where a greater proportion of their time is spent terrestrially

relative to wild animals. Other postures such as bipedalism, palmigrady and 'modified fist walking' are also noted in these studies (Sarmiento 1988). Terrestrial postures in *Pongo* appear similar to their arboreal postures; their locomotor repertoire is versatile, and they appear to adapt their behaviours to suit their environment. The flexed-fingered postures described for *Pongo* is likely a necessary posture for an animal with relatively long fingers to adopt while on the ground (Sarmiento 1988). It has not yet been demonstrated that these postures are routinely adopted in the wild.

1.4.b. *Gorilla*

1.4.b.1. Arboreal behaviour

Gorilla is divided into two species, *G. gorilla* (western gorillas) and *G. beringei* (eastern / mountain gorillas), each with two subspecies (*G. g. gorilla* and *G. g. diehli*; *G. b. beringei* and *G. b. graueri*) (Wilson and Reeder 2005). The large body mass of *Gorilla* limits its capacity to utilise arboreal substrates (Remis 1999). As adults, *G. beringei* exhibits the lowest level of arboreality of any of the non-human hominids, spending only 3-7% of the time in trees (Doran 1996; Remis 1998; Ruff et al. 2013), while *G. gorilla* is more arboreal, with an estimate that it spends ~20% of its time in trees (Remis 1998). In both species, females are generally more arboreal than males, although other factors such as seasonality, group size, tree size, and tree availability also affect the degree of arboreality (Remis 1995; Doran 1996; Remis 1999). Arboreal (and terrestrial) behaviours in *Gorilla* consist primarily of passive behaviours such as lying, resting, and feeding (Hunt 1992; Doran 1996). Locomotion constitutes only a small proportion of total arboreal behaviour, with studies suggesting that only ~10% of arboreal time is spent in active movement (Hunt 1992; Doran 1996). *Gorilla beringei* uses an arboreal setting almost exclusively for eating and rarely climbs above 7m, while *G. gorilla* also spends time resting and nesting up to 40m high (Remis 1995, 1998, 1999). Neither species engage in long-distance arboreal locomotion, preferring to descend and move terrestrially between feeding and resting spots (Tuttle and Watts 1985; Doran 1996; Remis 1998). Research also suggests a difference in the type of arboreal behaviours between the two species. *G. gorilla* spends about 2/3 of arboreal behaviours climbing, followed by quadrupedalism (Doran 1996; Remis 1998). On the other hand, *G. beringei* uses quadrupedal postures in equal or greater proportions than climbing (Doran 1996). Suspensory behaviours constitute less than 8% of all arboreal behaviours in both species (Doran 1996; Remis 1998).

1.4.b.2. Terrestrial behaviour

Terrestrial locomotor positional behaviour is broadly similar among the two *Gorilla* species. Both are primarily terrestrial knuckle-walkers and use this substrate and posture to move

between feeding and nesting sites (Tuttle and Watts 1985; Doran 1996; Remis 1999). Recent research has reiterated the predominance of knuckle-walking during terrestrial locomotion in *G. beringei*, with 85% of observed locomotion using this posture (Thompson et al. 2018).

1.4.b.3. Ontogeny

Changes in locomotion during ontogeny have been studied in one group of *G. b. beringei* in the Parc National des Volcans, Rwanda (Doran 1997). During the juvenile period, there is an increase in terrestrial quadrupedalism and a decrease in arboreality until terrestrial knuckle-walking constitutes the majority of locomotor activity (Doran 1997). Juvenile *Gorilla* reach adult levels of knuckle-walking around the age of four, although their arboreality remains higher than adult levels up until five (Doran 1997). Terrestrially, sub-adults tend to predominantly use knuckle-walking, similar to adults (Doran 1997; Thompson et al. 2018); however, when arboreal sub-adults utilise climbing, suspensory and bipedal postures in greater proportions (Doran 1992, 1997).

1.4.c. *Pan paniscus* and *Pan troglodytes*

1.4.c.1. Arboreal behaviour

Reports on the degree of arboreality in *Pan* have a large degree of variation and underscore the variability of ape behaviour. Studies of *Pan troglodytes* report values from 30-80% of time spent in trees, and the variation is hypothesised to be due to differences in availability of fruit, presence of predators, group size and sex, among other factors (van Lawick-Goodall 1968; Susman, Badrian and Badrian 1980; Doran and Hunt 1994; Doran 1996; Remis 1998; Ramos III 2014). Generally, the most frequent arboreal locomotor behaviour is similar to that recorded for *G. gorilla*: climbing and vertical scrambling is the most frequent locomotor mode (60%⁶), followed by quadrupedalism (20%), then suspensory (6%), and finally bipedalism (2.5%) (Hunt 1992; Doran 1993a; Doran and Hunt 1994; Doran 1996).

Based on comparisons between Lomako Forest *P. paniscus* and Tai Forest *P. troglodytes* it has been hypothesised that *P. paniscus* is relatively more arboreal than *P. troglodytes* (Hunt 1991a; Doran 1993a). Increased arboreality in *P. paniscus* has been correlated with a greater use of suspensory postures and less climbing (Susman, Badrian and Badrian 1980; Hunt 1992; Doran 1993a; Doran and Hunt 1994). However, Doran (1993a) noted that low habituation levels among *P. paniscus* may have increased bouts of arboreality in order to hide from observers. More recent studies on fully habituated *P. paniscus* at Lui Kotale

⁶ The percentages here are rounded, sex-pooled *P. troglodytes* means as reported by Remis (1998). A more nuanced breakdown by sub-species and sex can be found in Doran and Hunt (1994).

(Democratic Republic of Congo) support Doran's (1993a) habituation theory, as this group used arboreal substrates as frequently, if not less so than Mahale, Gombe, or Tai Forest *P. troglodytes* (Doran 1996; Ramos III 2014). Excluding sitting and lying postures (53% of total time), arboreal postures such as cling, climb, scramble, and brachiate constituted less than 1% of the positional behaviours used by Lui Kotale *P. paniscus* (Ramos III 2014).

1.4.c.2. Terrestrial behaviour

Both *Pan* species use knuckle-walking most frequently when terrestrial (Doran 1993a). Evidence suggests *P. troglodytes* exclusively uses terrestrial knuckle-walking for long-distance movement between sites, while *P. paniscus* are considered to predominantly use terrestrial knuckle-walking for long-distance travel (van Lawick-Goodall 1968; Hunt 1992; Doran 1993a; Doran and Hunt 1994; Ramos III 2014); however, as discussed above, the habituation levels of the Lomako Forest *P. paniscus* may have overestimated long-distance arboreal travelling (Doran 1993a). When travelling between resting and nesting sites the Lui Kotale *P. paniscus* used terrestrial knuckle-walking 98% of the time (Ramos III 2014).

1.4.c.3. Ontogeny

Changes in locomotion during ontogeny have been studied in one group of *P. troglodytes* from the Tai National Forest, Ivory Coast (Doran 1997). In this study, juvenile *Pan* engaged in greater proportions of arboreal locomotion until two years of age and reached adult proportions of terrestrial knuckle-walking around six years (Doran 1997). During their first five years, *Pan* engaged in more climbing, suspension and bipedalism than adults (Doran 1997). This pattern of locomotor development is similar to what has been observed in *Gorilla*, although movement through this pattern occurs more slowly in *Pan* (Doran 1992; Inouye 1994; Doran 1997).

1.4.d. Tool behaviour in non-human hominids

Tool behaviour among non-human hominids is of interest to palaeoanthropologists as it provides clues to infer the behaviour of hominid fossil ancestors, as well as how a non-human hominid hand may meet the biomechanical demands of different manipulative tasks. Manipulative behaviours (tool-based and non tool-based) exert fitness benefits to the individual and as such, all non-human hominids are likely under some selective pressures to maintain manual dexterity (Marzke, Wullstein and Viegas 1994; Alba, Moyà-Solà and Köhler 2003). Nevertheless, the non-human hominid hand is predominantly shaped by and adapted to its locomotor function (Tocheri 2007; Preuschoft 2019). This is likely because the biomechanical stresses induced by arboreality and other forelimb-dominated locomotion

are stronger than the manipulative ones (Alba, Moyà-Solà and Köhler 2003; Preuschoft 2019). Furthermore, natural selection pressures for efficient arboreality are also likely to be extremely high, as failure (i.e. falling) is likely to lead to severe consequences such as injury or death. As such, tool behaviour among non-human hominids remains largely facultative, expressing only small degrees of modification to the natural shape of the object, and affording limited fitness benefits (as per definition in Shea 2017). For a hominid hand to begin to adapt to the lower biomechanical forces of tool behaviours, particularly at the expense of locomotor ones, the fitness benefits of that tool behaviour must have significantly increased relative to what they currently are for extant non-human hominids.

As above, palaeoanthropological literature frequently refers to tool behaviours as facultative, habitual, or obligate (Shea 2017). All non-human hominids are classified as facultative tool users, while *H. sapiens* are obligate tool users. Marzke (1997) discusses and defines these concepts in detail, although a more recent definition has been given by Shea (2017) in reference to hominin commitment to tool use since the Plio-Pleistocene. In summary:

- (1) **Facultative tool users** produce tools using basic core reduction methods such as freehand or anvil percussion, with the end result not looking much different from their original geometry. The materials used for the tools originate from local areas (Shea 2017). Oldowan tools and tools produced by chimpanzees could be considered evidence of facultative tool users (Shea 2017).
- (2) **Habitual tool users** create defined objects that no longer reflect their original geometry and are instead shaped to improve their functionality for their intended task (Shea 2017). They were likely created to be portable and carried by the user, but their use is periodic and with variable fitness advantages (Shea 2017). Shea (2017) proposes that habitual tool use is associated with Early-Middle Pleistocene assemblages.
- (3) **Obligate tool users** cannot survive without the consistent application of their tools to their environment. Obligate tool users make the most complex tools, which probably require language capacity in order to instruct how to make and use them efficiently (Shea 2017). The toolkits of *H. sapiens* and Neanderthals are evidence of obligate-tool users.

1.4.e. *Homo sapiens*

1.4.e.1. Arboreal behaviour

Today, most modern *H. sapiens* rarely use arboreal substrates for daily life and subsistence. Nevertheless, unaided tree climbing amongst modern hunter-gatherers is well documented across global populations and provides access to high-quality food resources such as honey, animal prey, fruit, nuts and seeds (Kraft, Venkataraman and Dominy 2014). During the late 19th century, tools to assist vertical climbing were developed, and ever since, *H. sapiens* have regularly climbed rock faces and mountains purely for adventure, exercise and leisure (Bright 2014). Thus, the evolution of efficient striding bipedalism in the lower limb and manipulation in the upper limb has not completely excluded *H. sapiens* from utilising arboreal substrates.

1.4.e.2. Terrestrial behaviour

As *H. sapiens* is an efficient terrestrial biped (Bramble and Lieberman 2004; Pontzer, Raichlen and Sockol 2009; Gruss and Schmitt 2015), the hand is used predominately to interact with and manipulate the environment rather than traverse it. During locomotion, the hands are used alongside the forelimb as propellers and stabilisers (Sarmiento 1988; Gruss and Schmitt 2015). When *H. sapiens* places its hands terrestrially to aid in locomotion, it is capable of palmigrady, digitigrady, fist-walking and knuckle-walking postures (Sarmiento 1988).

1.4.e.3. Tool use

As the capacity to perform power and precision grips is not novel to *H. sapiens* (Napier 1962a), numerous studies have investigated what distinguishes their hand postures from other primates. While *H. sapiens'* hand is extraordinarily dexterous, capable of finely adjusting its grip to suit the unique geometry of the object (Marzke 2013; Key, Merritt and Kivell 2018), there are three aspects which are hypothesised to differentiate *H. sapiens* from all other animals, which are listed below (Napier 1962a; Marzke 1983; Marzke, Wullstein and Viegas 1992; Marzke 1997).

(1) **Precision handling:** While precision handling is not specifically a grip type, it is a distinct behaviour correlated to the unique ability of the *H. sapiens* hand for rapid and precise tool manufacture. Precision handling is the capacity to use just the fingertips of one hand to adjust the grip on an object (Marzke 1997). Non-human hominids generally drop an object, hold it in the mouth or use the palm to readjust the grip, increasing the time and effort required to achieve a manipulative task (Marzke 1997; Bardo et al. 2016; Bardo et al. 2017) (but see Crast and Fragaszy (2009) for the use of in-hand movement in *P. troglodytes*).

(2) **Forceful precision gripping:** Precision gripping can be simply defined as holding an object between the pad of the thumb and one or more fingers and has been observed in several non-human primates, including *P. troglodytes* and *Papio* (Marzke, Wullstein and Viegas 1992; Marzke 1997; Bardo et al. 2017). *Homo sapiens* is distinguished in its use of precision grips by the relatively large amount of force it can exert on the held object (Marzke 1997). Forceful precision grips can better withstand displacement from high reaction forces (Marzke 1997). There are several sub-categories of precision gripping, which variably use a different number, or parts, of fingers to secure the object. A recent comprehensive study by Key et al. (2018) reemphasised the large number of precision grips used by *H. sapiens*. Their conclusions ultimately supported the original conclusions of Marzke (1997) that the 2/3 jaw chuck, buttressed pad-to-side and cradle grip constitute the majority of precision grips used by *H. sapiens* (Key, Merritt and Kivell 2018).

(3) **Power squeeze grip:** The power squeeze grip places objects obliquely across the palm, held in place by flexed fingers and buttressed by an adducted thumb (Napier 1956; Marzke, Wullstein and Viegas 1992). Non-human hominids also use power grips, although the thumb cannot exert the same force, stability, or control as it does in *H. sapiens* (Napier 1956; Bardo et al. 2017). What precision and power squeeze grips have in common is the degree of force that can be generated and withstood by the joints of the hands while manipulating and using tools in these postures.

1.4.f. Functional conclusions

Non-human hominid's inter- and intraspecific locomotor variation is important as quadrupedal, manipulative and suspensory movements are propelled by different kinetic forces. We, therefore, may expect to see different microarchitecture and signals of functional adaptation in the carpus of taxa using these divergent locomotor modes. During climbing and, particularly, suspensory behaviour, there is substantial tensile loading throughout the upper limb as gravity pulls the body downwards (Swartz, Bertram and Biewener 1989). Although muscle contractions impose compressive loads, the strength of tensile forces more strongly opposes those stressors, limiting their biomechanical impact on axial bone strain (Sarmiento 1988; Swartz, Bertram and Biewener 1989; Carlson and Patel 2006). This contrasts torso-orthograde quadrupedal locomotion (e.g., knuckle-walking), whereby body mass is supported above the hand. In this position, forces originate from gravity and muscle contractions and are therefore predominantly compressive (Sarmiento 1988; Swartz, Bertram and Biewener 1989). Finally, during manipulation, forces arise from muscle contractions and the resultant reaction forces of manipulation and are thus also

compressive (Sarmiento 1988; Swartz, Bertram and Biewener 1989). However, as no muscles attach directly to the carpals, tensile forces arising from the stabilising role of ligaments constitute a significant proportion of force resisted and transferred by the carpal bones (Caler and Carter 1989; Swartz, Bertram and Biewener 1989; Pattin, Caler and Carter 1996; Kijima and Viegas 2009). Section 1.5 below discusses the functional anatomy and biomechanics of the hominid wrist joint and how the shared and derived morphology is hypothesised to facilitate and support the habitual behaviours described in this section.

1.4.f.1. Limitations

It is important to acknowledge the limitations to our knowledge of non-human hominid locomotion. The bulk of our resources are drawn from a limited number of populations and studies. For example, in *Gorilla*, we draw from a single population each of *G. g. gorilla* (Remis 1998) and *G. b. beringei* (Doran 1997; Thompson et al. 2018). Many of these studies have demonstrated the profound impact ecology, sub-species, sex, rainfall, habituation, and more, have on the behaviours expressed by these species. Notably, *Pongo* locomotion has been studied far less than the African apes. Many studies that quantify behaviour in *Pongo* focus reasonably on conservation questions (e.g., Ancrenaz et al. 2014; Davies et al. 2017) and do not quantify locomotion in the fine-grained detail we often require as palaeoanthropologists. Conservation research, in particular, has emphasised how changing habitats influence primate behaviour and locomotion (e.g., Manduell, Morrogh-Bernard and Thorpe 2011; Ancrenaz et al. 2014; Chappell et al. 2015; Davies et al. 2017). While studies on captive non-human hominids fill an important gap, it is often impossible for captive animals to express behaviours in the same proportions as their wild counterparts. Studying live, wild, non-human hominids is costly, financially and potentially physically; it is also constrained ethically and politically. Thus, we do not yet completely understand the full nuance of locomotion among these extraordinarily complex and behaviourally versatile primates. This point must be considered when interpreting results.

1.5. Anatomy and biomechanics of the wrist

The wrist is biomechanically complex, consisting of at least 28 joints and eight or nine carpals, including articulations with five metacarpals (Mc), distal radius, and distal ulna (Kivell 2016a; Ayhan and Ayhan 2020). Although no muscles attach directly to the carpus, there are numerous ligaments that cross and attach to the wrist, playing a key role in facilitating or restricting movement of the bones (Buijze et al. 2011; Ayhan and Ayhan 2020). Traditionally, the bones of the wrist are divided into two sections; the proximal row, which includes (from ulnar to radial) the pisiform, triquetrum, lunate, os centrale (if unfused from the scaphoid),

and scaphoid, and the distal row, which includes the hamate, capitate, trapezoid and trapezium (Kivell 2016a). While biomechanical data indicates that the scaphoid may act as an anchoring link between the two rows and that the triquetrum variably participates in both the proximal and distal row in *Pongo* (Wolfe, Neu and Crisco 2000; Crisco et al. 2005; Orr and Atkinson 2016; Orr 2017), for conciseness and clarity, the scaphoid and triquetrum will be considered part of the proximal row in this thesis, unless otherwise stated.

Every articulation between the bones within the wrist and hand constitute a joint, although motion is often simplified into three major joint complexes; the **radiocarpal**, which is between the radius, ulna and proximal row; the **midcarpal**, which is between the proximal row and distal row; and the **carpometacarpal (CMC)**, which is between the distal carpal row and the metacarpals (Kivell et al. 2016). In the radiocarpal joint of hominids, the ulna is mostly or completely removed from articulating with the proximal row, although in most other animals, the radiocarpal joint is called the antebrachial joint as it includes a bony articulation between the ulna and the carpus (Lewis 1989; Kivell 2016a).

Section 1.5 outlines the functional anatomy relevant to this thesis. I will first define and illustrate the axes of movement in the carpus, then I will describe the anatomy of each carpal, and finally describe the functional anatomy and movement of the wrist within each extant taxon. Detailed consideration of the comparative anatomy of each carpal bone is important as the orientation, and relative size of the intercarpal joint surfaces can indicate adaptive differences between extant species in regards to forces across the hand and wrist (Marzke, Wullstein and Viegas 1992; Tocheri et al. 2003; Tocheri et al. 2005; Tocheri 2007). This is because deformation from joint reaction forces is most efficiently resisted when the articular surface is perpendicular to the origin of force and/or has a large surface area over which force can be dispersed (Sarmiento 1988; Hamrick 1996; Currey 2002; Tocheri 2007). It, therefore, provides critical context to interpreting patterns of adaptation. Each part of the following section is written such that it can be read in isolation. As such, a discussion of some anatomical features will be included in more than one section.

1.5.a. Axes of movement

Research on the wrist generally refers to mobility or stability across joints or anatomical planes. 'Stability' is the capacity for a joint to resist displacement within a plane of motion, whereas 'mobility' is the joint's range of movement within a plane of motion (Hamrick 1996). Traditional methods for studying kinematics have been lacking in precision when applied to the carpals, and there is a lack of precise data for the biomechanical movements and

anatomical significance of carpal morphology (Orr et al. 2010; Ayhan and Ayhan 2020). However, recent computational advances have facilitated more nuanced quantitative measurements of individual carpal bones. Research on wrist bone kinematics generally discusses joint movement in relation to three axes of motion (six degrees of freedom): radial-ulnar deviation, flexion-extension, and pronation-supination. The axes and motion within the carpal bones are explicitly defined below and illustrated in Figure 1.1 and Figure 1.2.

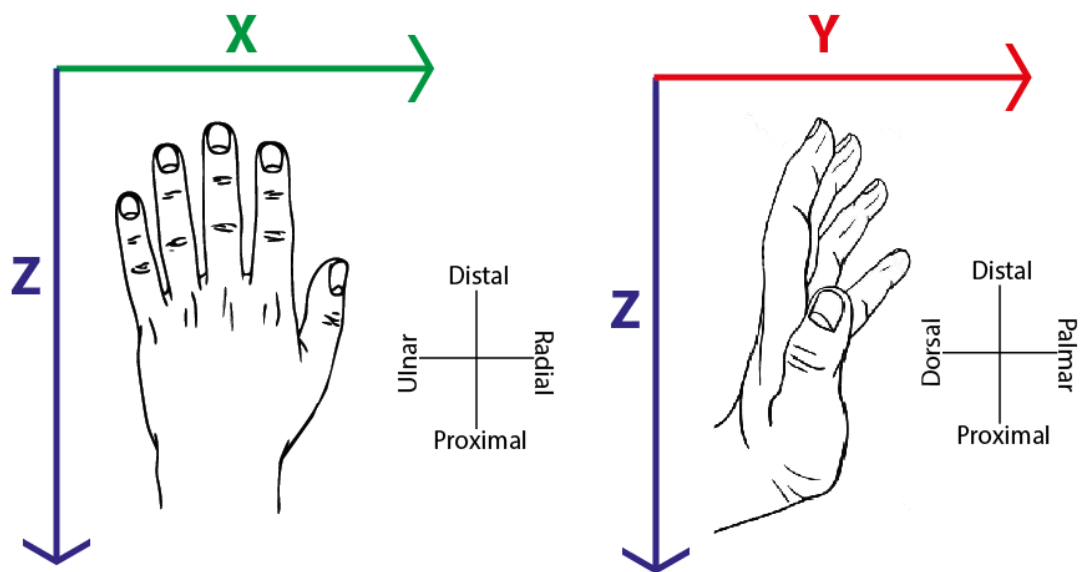


Figure 1.1 Axes of rotation of the hand and wrist. The X-, Y- and Z-axes are illustrated using a *H. sapiens* left hand in two different perspectives.

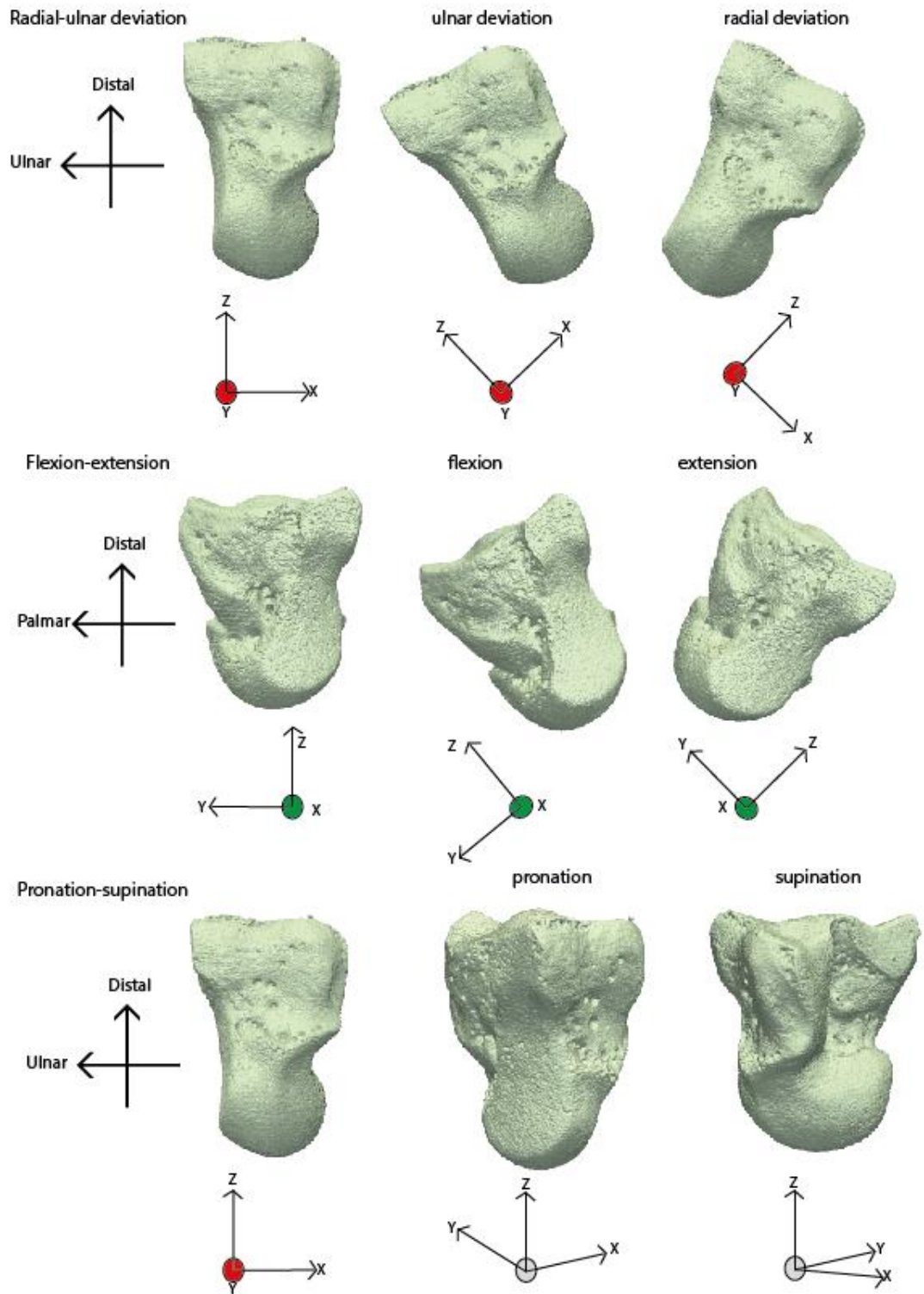


Figure 1.2 Movement of the capitate around the axes of rotation shown on a *P. troglodytes* capitate.

Top row: radial-ulnar deviation. The Y-axis is stable. Middle row: Flexion-extension. The X-axis is stable. Bottom row: pronation-supination. The Z-axis is stable.

Figure 1.1 shows the axes in relation to the entire hand, while Figure 1.2 illustrates the six degrees of freedom around these axes. The Z-axis is the coronal plane; it runs proximo-distally and follows the long axis of the radius and metacarpals. The X-axis is the transverse plane; it runs medio-laterally through the radius, which is radio-ulnarly through the wrist and hand. The Y-axis is the sagittal plane; it runs antero-posteriorly in the radius, which is palmar-dorsally in the wrist and hand. In pronation-supination, the Z-axis remains stable as the bones spin around the axis. This movement rotates the dorsal surface towards the palmar surface (volar surface) and vice versa. Supination is the motion that rotates the bone towards or into anatomical position, turning the palmar surface to face anteriorly. Pronation is the opposite of this movement. For radio-ulnar deviation, the Y-axis remains stable. The carpals slide around this axis to point more radially (laterally) for radial deviation (wrist abduction, i.e., movement away from the midline of the body) or more ulnarly (medially) for ulnar deviation (wrist adduction, i.e., movement towards the midline of the body). In flexion-extension, the X-axis remains stable. The carpals slide about this axis towards the palmar or dorsal surface. When a bone is described as flexing, it moves towards the palm; when it is extending, it moves towards the dorsum.

1.5.b. Carpal anatomy

1.5.b.1. Anatomy of the capitate

The capitate sits in the middle of the distal row forming part of the midcarpal joint proximally and carpometacarpal joints distally (Figure 1.3) (Lewis 1989). It articulates distally with the Mc3 and sometimes Mc4, ulnarly with the hamate, disto-radially with the trapezoid and Mc2, proximo-ulnarly with the lunate and hamate, and proximally with the scaphoid or os centrale in *Pongo* (Lewis 1989). It is bound to the hamate and trapezoid by short and tight ligaments, and thus the bones of the distal row have little to no capacity for intercarpal movement and instead move in unison during flexion and extension (Garcia-Elias et al. 1994; Richmond, Begun and Strait 2001; Moojen et al. 2003). In *H. sapiens*, the dorso-disto-radial surface is bevelled to accommodate a styloid process on the Mc3 (Marzke 1983). The proximal aspect of the capitate, also known as the head, has no ligamentous attachments and so there is greater range of motion (ROM) at the midcarpal joint than in the distal row or carpometacarpal joints (Moojen et al. 2003; Crisco et al. 2005; Kijima and Viegas 2009; Regal, Maschke and Li 2020). *Gorilla* and *Pan* have the lowest ROM in extension at the midcarpal joint as a result of a radially expanded capitate head, creating an embrasure into which the os centrale aspect of the scaphoid is rapidly engaged during extension (Tuttle 1967; Jenkins and Fleagle 1975; Richmond, Begun and Strait 2001; Orr 2010). The dorsal ridge running

radio-ulnarly across the head provides further stability during extension (Richmond, Begun and Strait 2001; but see Kivell & Schmitt (2009) for a counterview). *Homo sapiens* also express the fused scaphoid-centrale morphology, as well as the radially expanded head (Lewis 1989). However, an expansion of the palmo-radial region results in a less ‘waisted’ capitate in *H. sapiens*, providing more surface area for the scaphoid to extend and a concomitant greater ROM in extension relative to the African apes (Lewis 1989; Orr 2017). *Pongo* has the highest ROM of all the extant hominids (Orr 2018). As the os centrale is not fused in *Pongo*, it sits between the scaphoid and capitate, excluding the scaphoid from participating in the midcarpal joint and allowing a higher extension ROM (Begun 2004; Orr 2018).

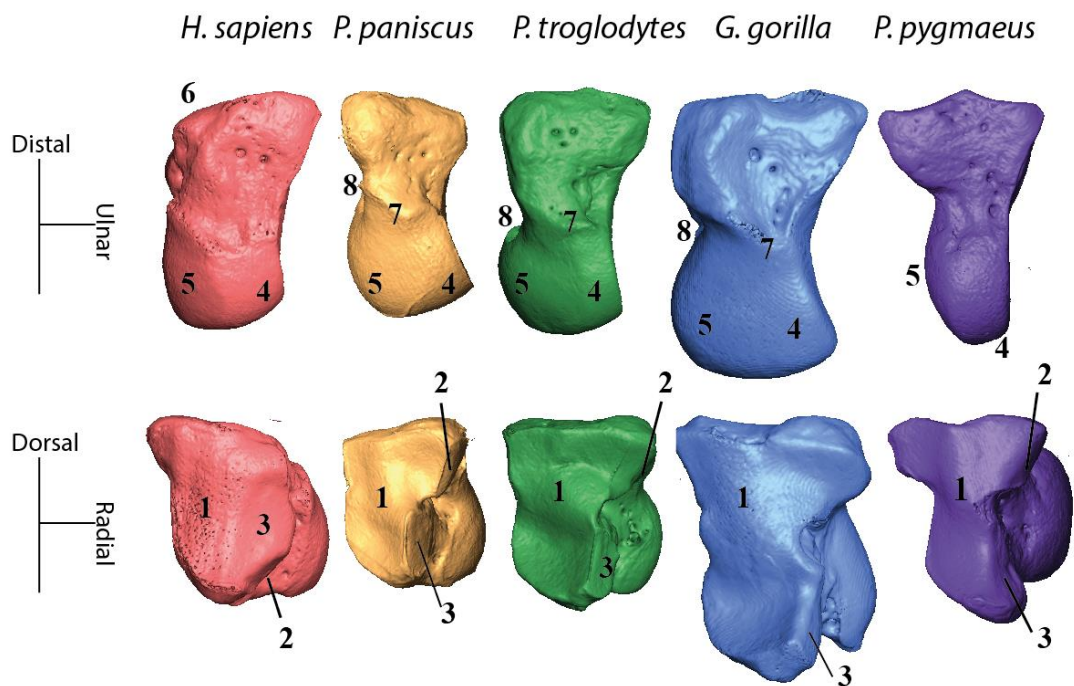


Figure 1.3 Comparative anatomy of the right capitate across hominids. The top row is in a dorsal perspective, and the bottom row is in a distal perspective. 1 = Mc3 articulation; 2 = trapezoid articulation; 3 = Mc2 articulation; 4 = lunate articulation; 5 = scaphoid articulation or os centrale articulation in *Pongo*; 6 = Bevelled surface for Mc3 styloid process. Bones are scaled to relative size.

1.5.b.2. Anatomy of the scaphoid

The scaphoid is the radial-most bone of the proximal row carpus (Figure 1.4). In most primates, as in most non-primate mammals, the scaphoid is a separate bone from the os centrale (Lewis 1989; Kivell 2016a). In *H. sapiens*, African apes and some strepsirrhines, the scaphoid bone incorporates the os centrale (Kivell and Begun 2007). Given the sporadic presence of this morphology across primates, scaphoid morphology has received greater

attention than most other carpals (Richmond, Begun and Strait 2001; Kivell and Begun 2007). The scaphoid possesses a distinct and highly vascularised dorsal-radial ridge, which separates the proximal and ulnar articular surfaces from the disto-dorsal ones (Buijze et al. 2011; Ayhan and Ayhan 2020). Proximally, the scaphoid articulates with the scaphoid fossa of the distal radius and proximo-ulnarly with the lunate (Lewis 1989; Buijze et al. 2011). The dorsal body of the scaphoid extends radially, and the trapezium and trapezoid articulate distally (Buijze et al. 2011). In *H. sapiens*, this articulation extends further palmarly onto the tubercle (Lewis 1989; Kivell 2016a). In *H. sapiens*, *Gorilla*, and *Pan*, the ulnar portion articulates with the capitate (Richmond, Begun and Strait 2001; Tocheri 2007). Together with the lunate, the ulnar scaphoid forms a confluent concave articular surface for the proximal capitate (Lewis 1989; Richmond, Begun and Strait 2001; Tocheri 2007). As the os centrale is a separate bone in *Pongo*, the ulnar portion of the scaphoid articulates only with the os centrale and usually does not articulate with the capitate (Richmond, Begun and Strait 2001). The palmar surface of the scaphoid is non-articular and highly concave (Buijze et al. 2011). It extends radio-palmarly, terminating with a distinct tubercle, which is the attachment site for several ligaments (Buijze et al. 2011; Ayhan and Ayhan 2020).

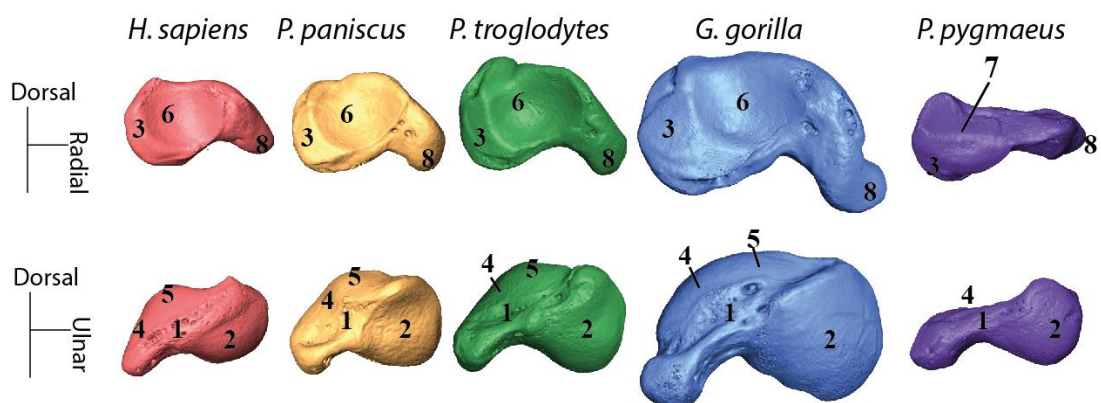


Figure 1.4 Comparative anatomy of the right scaphoid across hominids.

The top row is in a distal perspective and the bottom row is in a proximal perspective. 1 = dorsal-radial ridge; 2 = radial articulation; 3 = lunate articulation; 4 = trapezium articulation; 5 = trapezoid articulation; 6 = capitate articulation; 7 = os centrale articulation. Bones are scaled to relative size.

1.5.b.3. Anatomy of the lunate

The lunate sits within the middle of the proximal row, articulating radially with the scaphoid and ulnarly with the triquetrum (Figure 1.5) (Kivell 2016a). The proximal surface is convex and articulates with the radius' lunate fossa radially and the triangular fibrocartilage complex (TFCC) ulnarly (Koebke 1993; Kivell 2016a). The dorsal surface is narrower, flatter and more

vascularised than the palmar surface (Ayhan and Ayhan 2020). The distal articular surface is highly concave and is the primary articulation for the head of the capitate (Kivell 2016a; Ayhan and Ayhan 2020).

The presence or absence of a lunatohamate joint is an intriguing morphological variant within the hominids but one that has yet to generate a large amount of research. Hominids have two types of lunate morphologies, one in which the lunate and hamate do not have an articulation (Type 1), and one which possesses an additional disto-ulnar facet to articulate with the hamate (Type 2) (Marzke, Wullstein and Viegas 1994). In all hominids, the majority of individuals possess the hamate articulation, with 65% of *H. sapiens*, 90% of *P. troglodytes*, 62% of *G. gorilla*, and 87% of *Pongo* sp. expressing Type 2 lunates (Marzke, Wullstein and Viegas 1994). This is the opposite condition in *Papio anubus*, as the majority of individuals lack the lunatohamate joint (Marzke, Wullstein and Viegas 1994). The Type 2 morphology appears to interrupt radio-ulnar deviation at the midcarpal joint, and while this may provide a mechanical advantage for knuckle-walking in African apes, it is associated with a greater incidence of joint degeneration in *H. sapiens* compared to Type 1 lunates (Marzke, Wullstein and Viegas 1994; Bain et al. 2015). Type 1 lunates also appear to allow greater movement at the radiocarpal joint during flexion and extension than Type 2 (Bain et al. 2015).

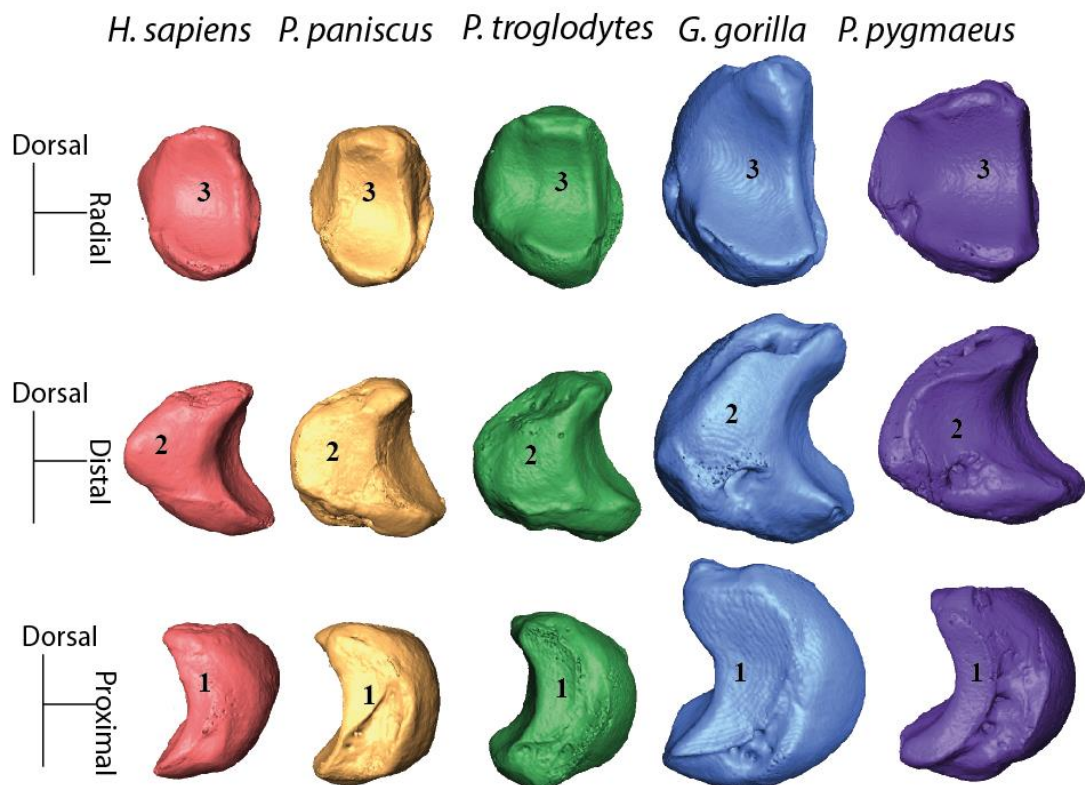


Figure 1.5 Comparative anatomy of the right lunate in hominids.

The top row is in a proximal perspective, the middle row is from an ulnar perspective, and the bottom row is in a radial perspective. 1 = scaphoid articulation; 2 = triquetrum articulation; 3 = capitate articulation. Bones are scaled to relative size.

1.5.b.4. Anatomy of the triquetrum

The triquetrum is perhaps the least described and compared bone of the carpus (but see Cartmill and Milton 1977; Kivell 2011), although there are intriguing morphological similarities (and differences) across the hominids that hint at the importance of supination and wrist adduction in the evolutionary history of the hominids. The proximal retraction of the ulnar styloid process is a distinct synapomorphy amongst the hominoids. While the styloid process and intervening soft tissue structures are fully elaborated in *Gorilla* and *Homo*, such that there is no hard tissue articulation with the triquetrum, in *Pan*, it is common for there to be a small articulation on the proximal surface via an aperture in the meniscus (Lewis 1989) (Figure 1.6). Lewis (1989) notes he observed ulnotriquetral articulation in up to 8% of *H. sapiens* and that when present, the joint resembles *P. troglodytes*. The proximal triquetrum has an articular surface for the TFCC, indicating a capacity for force transfer with the soft tissue complex (Sarmiento 1988; Lewis 1989). The proximo-radial aspect of the triquetrum articulates with the palmar radiocarpal ligament and the ulnar aspect with the lunate; distally, it articulates with the hamate and palmarly with the pisiform. The concave pisiform facet covers almost the entire palmar surface (Lewis 1989).

In *Pongo*, the triquetrum is notably different to other hominids (Figure 1.6). *In situ*, it is displaced distally by the large, ulnarly expanded lunate such that it does not form part of the proximal articular row. Indeed, it has been observed that the proximal surface does not possess an articular facet for the triangular fibrocartilaginous complex (Lewis 1989). The bone is rod-shaped rather than pyramid-shaped, and the concave articular facet for the pisiform is relatively small and highly distally placed (Sarmiento 1988; Lewis 1989; Vanhoof et al. 2021). The elongation of the bone and its distal displacement results in the pisiform sometimes articulating with the hamate hook (Sarmiento 1988; Lewis 1989). Like the other hominids, it articulates with the lunate radially, proximo-radially with the palmar radiocarpal ligament, distally with the hamate, and palmarly with the pisiform.

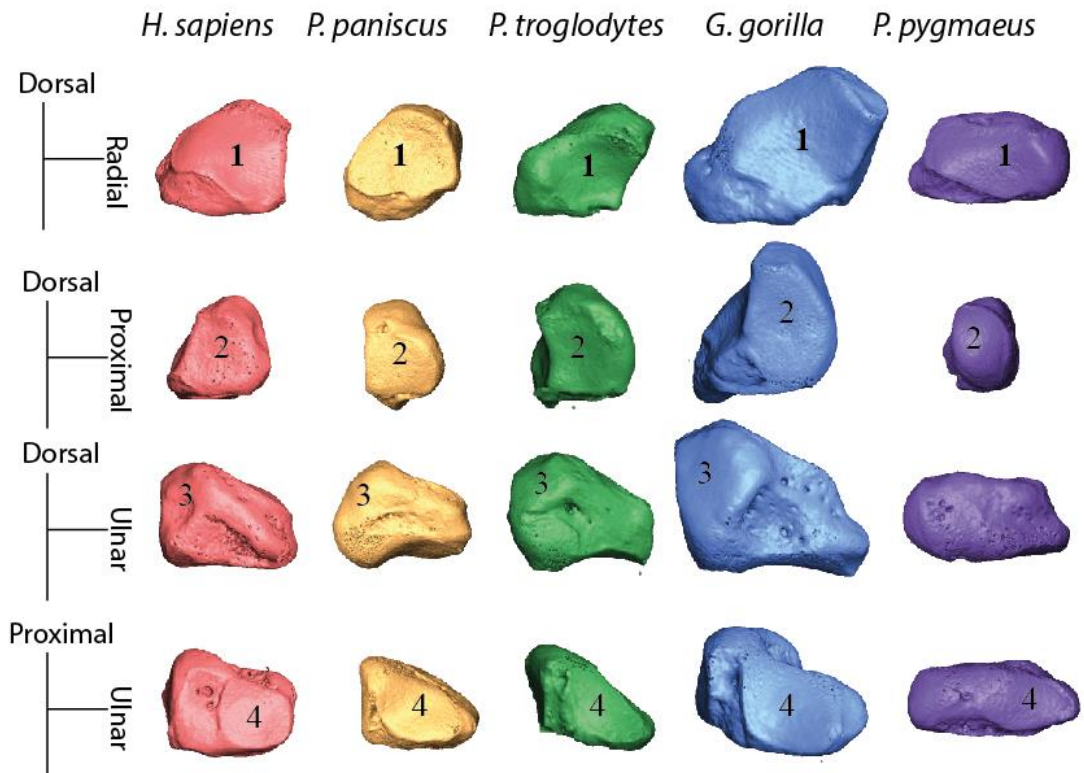


Figure 1.6 Comparative anatomy of the right triquetrum in hominids.

The first row is in a distal perspective, the second row is in an ulnar perspective, the third row is in a dorsal perspective, and the fourth row is in a palmar perspective. 1 = hamate articulation; 2 = lunate articulation; 3 = TFCC articulation; 4 = pisiform articulation. Bones are scaled to relative size.

1.5.c. Wrist functional morphology of the hominids

As a clade, hominids share several derived features relative to other primates, but some of the most notable synapomorphies in the hand are found within soft tissue structures (Lewis 1989): firstly, the novel TFCC between the ulna and proximal row; secondly, a fully synovial joint between the distal ulna and radius; and finally, the loose and flexible ligamentous structures between the proximal row bones (Lewis 1989; Kivell 2016a; Orr 2017). The TFCC is fully developed in both *Homo* and *Gorilla* as the meniscus, and triangular disc components are separate entities, while in *Pan* and *Pongo*, they may be merged (Lewis 1989). In all taxa, the ulnar styloid process is reduced and is either fully (*Pongo*, *Gorilla* and *Homo*) or mostly (*Pan*) prevented from articulating with the proximal row by the TFCC (Lewis 1989). Alongside the synovial radio-ulnar joint, this morphological configuration allows high degrees of pronation and supination (Lewis 1989; Jouffroy and Medina 2002; Kivell 2016a; Orr and Atkinson 2016). Bones within the proximal row of hominids are only loosely tethered to one another via lax ligaments, which allow a high degree of intercarpal motion (Lewis 1989;

Garcia-Elias et al. 1994). This is in stark contrast to the distal row, which has strong intercarpal ligaments and generally moves as a single unit, tracking the motion of the Mc3 (Lewis 1989; Garcia-Elias et al. 1994; Kivell 2016a; Ayhan and Ayhan 2020). Orr (2017) quantified this functionality and found it to be a biomechanically differentiating feature of Hominoidea compared to Cercopithecidae, which showed more intrinsic stiffness within the proximal row.

While soft tissue structures reflect a shared common ancestry of hominids, analyses of the hard tissue have underscored a functional and adaptive dichotomy between non-human hominids and *H. sapiens*. During quadrupedal locomotion, substrate reaction forces are incurred by the Mc2-5 either directly (e.g. power grasping during climbing) or indirectly (e.g., via the phalanges during knuckle-walking) and are transferred proximally through the hand of non-human hominids (Sarmiento 1988; Wunderlich and Jungers 2009; Matarazzo 2013). The external morphology of the wrist reflects these biomechanical forces, as intercarpal joint surfaces are generally orthogonal to the long axis of the metacarpals, dispersing stress oriented towards the forearm and increasing stability radio-ulnarly to resist displacement and shear (Tocheri 2007). In comparison, *H. sapiens* displays joint surfaces oriented obliquely to the radio-ulnar axis. In other words, rather than being oriented toward the fingers as they are in non-human hominids, the joint surfaces are oriented toward the thumb (Marzke 1983; Lewis 1989; Tocheri et al. 2005; Tocheri 2007; Tocheri et al. 2008; Marzke et al. 2010). This oblique orientation efficiently disperses and resists deformation, shear and displacement from compressive forces arising from the thumb and strong thenar musculature and subsequently transfers it radio-ulnarly across the wrist (Tocheri 2007). Below I will discuss the morphology and functional anatomy of each extant hominid taxon in more detail.

1.5.c.1. *Pongo* functional morphology

Pongo carpals exhibit morphologies that distinguish them from African apes and *H. sapiens*. Most notably, *Pongo* retains the scaphoid and os centrale as separate bones (Lewis 1989). Scaphoid-centrale fusion occurs in greater than 95% of *Pan*, *Gorilla* and *H. sapiens* and begins early during growth (Kivell and Begun 2007). Less than 7% of *Pongo* wrists show the fused morphology, and this fusion usually only occurs in individuals of advanced age (Lewis 1989; Kivell and Begun 2007). Morphologically, a free centrale excludes the scaphoid from articulating with the capitate. Functionally, this excludes the scaphoid from forming part of the midcarpal joint, but it also allows greater freedom of movement between the capitate and scaphoid, creating a higher range of motion in extension in *Pongo* compared to the other hominids (Orr 2018). Importantly, in the rare occasion that centrale fusion does occur in

Pongo, it does not reorient the capitocentrale joint to match the radial orientation seen in African apes and *H. sapiens*. Instead, the centrale portion maintains its dorsal position on the capitate head, indicating a clear functional differentiation between the fused and unfused centrale of the hominids (Richmond, Begun and Strait 2001; Richmond 2006).

1.5.c.1.1. The proximal row

Relative to the African apes, the *Pongo* scaphoid is smaller and has smoother articular surfaces that allows a greater range of motion at the radiocarpal joint before maximum joint congruence is reached (Begun 2004). The lunate dominates the proximal carpal row and in contrast to African apes and *H. sapiens*, contributes relatively more surface area and more range of motion to the radiocarpal joint (Corruccini 1978; Orr 2017). Although articulation with the distal dorsal ridge in *Pan* and *Gorilla* has traditionally been associated with knuckle-walking postures and limitations to the radiocarpal mobility, kinematic analyses indicate that the scaphoid ridge in *Pongo* also contacts the radius in maximum extension and thus, it may be the subtle repositioning of the scaphoid by the enlarged lunate that provides more intrinsic excursion of the scaphoid before articulating at maximum congruence at the radius (Sarmiento 1988; Orr 2017). The distal radius articulates with a more radially-oriented scaphoid and more ulnarly-oriented lunate, which contrast the co-planar orientation in African apes and *H. sapiens* (Sarmiento 1988; Richmond, Begun and Strait 2001; Begun 2004). This radiocarpal joint configuration, alongside the distally migrated triquetrum, results in the most acute (highly concave) radiocarpal joint contour among the hominids (Sarmiento 1988). The enlarged size of the lunate and transverse triquetral articulation is interpreted as increasing the capacity for wrist adduction while also aligning the ulnar carpals to the ulnar metacarpals, which are frequently loaded during locomotion. More recent computational analyses of ulnar-side carpal biomechanics supported the hypothesis that the large lunate allows greater radio-ulnar deviation in *Pongo* (Orr and Atkinson 2016).

1.5.c.1.2. The distal row

The radio-ulnarly narrow capitate head is in stark contrast to that of African apes and *H. sapiens*, and it is this feature, along with the similarly-narrow hamate of *Pongo*, produces a ball-and-socket midcarpal joint (Richmond, Begun and Strait 2001). As the *Pongo* capitate lacks the convex-concave articular surface for the scaphoid, the solely convex facet does not narrow distally (i.e. capitate 'waisting') as dramatically as seen in *Gorilla* or *Pan* (Lewis 1989). The *Pongo* capitate lacks the extension limiting morphology seen in African apes, and as such, the proximal row has a far greater range of motion at the midcarpal joint, particularly greater excursion across the dorsal surface of the capitate (Richmond 2006; Orr 2017). Indeed,

kinematic analyses support the notion that it is mobility at the midcarpal joint specifically that allows hyperextended hand postures such as palmigrady in *Pongo* (Orr 2017). The midcarpal joint does not show the generalised proximo-distal joint orientation as seen in African apes and *H. sapiens*; instead, the configuration allows greater degrees of radial and ulnar deviation as the centrale-capitate articulations are oriented radially and the hamate-triquetral articulations oriented ulnarly (Kivell 2016a). At the carpometacarpal joints, the topology in *Pongo* is smoother and less “jagged”, with continual, flatter, concave surfaces to receive relatively convex surfaces of the distal metacarpals (Richmond, Begun and Strait 2001; Begun 2004; Kivell 2016a).

Fist walking is often noted for *Pongo* because it is unusual among primates. During fist walking, the phalanges are flexed, the wrist is predominantly ulnarly deviated, and weight is born on the dorsum of the phalanges (Tuttle 1967; Sarmiento 1988). However, fist walking remains rare among *Pongo*, and it is therefore unlikely to be functionally important to trabecular bone analysis. Together, the *Pongo* wrist morphology is advantageous for allowing freedom of movement at all three major wrist complexes, which is consistently interpreted as being an adaptation to arboreal and suspensory locomotion (Sarmiento 1988; Richmond 2006). Terrestrial postures are likely a compromise position to compensate for the long metacarpals and phalanges.

1.5.c.2. *Gorilla* and *Pan* functional morphology

The carpal morphology of *Pan* and *Gorilla* has generated substantial research interest because of their distinctive knuckle-walking locomotion. During knuckle-walking, both *Pan* and *Gorilla* flex their distal phalanges, hyperextend the metacarpophalangeal joint and bear weight on the dorsal surface of the middle phalanges (Richmond, Begun and Strait 2001; Orr 2005). Knuckle-walking has been shown to have beneficial energetic costs as the rigid metacarpals, wrist, and forearm align to elongate the effective length of the limb, allowing more kinetic energy to be actualised via pendula dynamics (Orr 2017). Knuckle-walking, therefore can be reasonably interpreted as an efficient trade-off solution to maintaining arboreally beneficial morphology, such as long fingers, while minimising terrestrial energetic costs. The kinematics of knuckle-walking in *Pan* and *Gorilla* are not identical (Wunderlich and Jungers 2009; Matarazzo 2013), although I will begin by reviewing some similar biomechanical features of their wrist before discussing their differences.

1.5.c.2.1. The os centrale

African apes and *H. sapiens* have eight rather than nine carpals as there is no cavitation in the mesenchyme between the os centrale and scaphoid. This feature has a long research

history, although the biomechanical purpose of the incorporation is still not well understood (Orr 2005; Kivell and Begun 2007; Kivell 2016a). Morphologically, an incorporated os centrale brings the scaphoid into the midcarpal joint complex, as it is the centrale portion that articulates with the capitate and trapezoid (Richmond, Begun and Strait 2001). During dynamic knuckle-walking hand posture, compression is incurred by the phalanges, and sheer stresses are incurred by the distal wrist as peak pressure moves from the ulnar side of the wrist towards the radial side during locomotion (Wunderlich and Jungers 2009; Matarazzo 2013). Recent computational modelling has demonstrated that centrale-scaphoid morphology decreases the ROM between the scaphoid, capitate and at the midcarpal joint, creating a more stable radial wrist relative to the unfused morphology (Orr 2018; Püschel et al. 2020).

1.5.c.2.2. Radiocarpal, midcarpal and carpometacarpal extension

Pan and *Gorilla* display low degrees of radiocarpal and midcarpal extension (dorsiflexion) compared to habitually palmigrade or brachiating anthropoids (Orr 2017). Derived carpal morphology (such as the above-discussed fused centrale-scaphoid) is hypothesised to reduce mobility at these joints to stabilise the wrist for quadrupedal locomotion (Tuttle 1969; Jenkins and Fleagle 1975; Richmond 2006; Orr 2017). Extension at the radiocarpal joint is hypothesised to be limited via the scaphoid dorsal concavity and beak, which engages a projected dorsal ridge on the distal radius (Richmond, Begun and Strait 2001; but see Orr 2017 for analysis indicating that when adjusted for size, *Pan* and *Gorilla* do not have greater radial distal projection than Asian apes). The capitate head has a radial expansion that produces a 'waist', forming an embrasure with the trapezoid into which the centrale portion of the scaphoid is wedged during extension (Wolfe et al. 2006; Kivell 2016a; Orr 2018). Together, the hamate and capitate are described as creating a midcarpal articular surface which is radio-ulnarly broad (Richmond, Begun and Strait 2001).

Stability during knuckle-walking is hypothesised to be achieved via the 'screw-clamp mechanism', a series of interdependent movements at the carpus describing the functional complex limiting extension at the midcarpal joint in African apes. During the initial phases of extension, the scaphoid quickly engages with the dorsum of the capitate, and the centrale portion of the scaphoid becomes wedged underneath the laterally expanded capitate head (Lewis 1989; Orr 2005). The triquetrum moves about a hamate facet, which is tightly helical, impacting and stabilising the lunate against the scaphoid (Lewis 1989; Orr 2010). The topology of the distal row joint surfaces for the metacarpals is also complex and irregular in

Pan and *Gorilla*, and has been interpreted as increasing resistance to dislocation or subluxation during knuckle-walking (Richmond, Begun and Strait 2001; Begun 2004).

The phylogenetic status of knuckle-walking has been a strongly debated topic within palaeoanthropology (Napier 1962a; Tuttle 1967; Jenkins and Fleagle 1975; Dainton and Macho 1999; Richmond, Begun and Strait 2001; Kivell and Schmitt 2009). For example, a systematic analysis of osteological features purported to be functional adaptations to knuckle-walking has been shown to be generally absent or weakly developed in *Gorilla* compared to *Pan*, which is contrary to predictions given that *Gorilla* knuckle-walks at a higher frequency with a greater body mass (Kivell and Schmitt 2009). It is not the explicit purpose of this thesis to contribute to this ongoing debate; suffice to say, the homology of knuckle-walking in *Pan* and *Gorilla*, and whether it is a reasonable contender for the locomotor mode of the last common ancestor of the African apes and *H. sapiens* remains unsolved. As with most contentious debates in palaeoanthropology, it would benefit from more fossil discoveries. What is important to this thesis, are key differences in the kinematics between the two genera.

1.5.c.2.3. Differences between *Gorilla* and *Pan*

Pan and *Gorilla* utilise knuckle-walking as the preferred mode of locomotion, although *Pan* knuckle-walk arboreally in greater proportions than *Gorilla* (Doran 1996). Arboreal substrates are more irregular than terrestrial ones, and Kivell and Schmitt (2009) argue that qw several wrist features of *Pan* are shared with arboreal non-knuckle-walking Catarrhini, they may be advantageous to navigating variable arboreal substrates. While both *Pan* and *Gorilla* hold their wrists in slight extension during knuckle-walking (Finestone et al. 2018; Thompson et al. 2018; Thompson 2020), *Pan* variably uses palm-in and palm-back postures, while *Gorilla* consistently adopts palm-back (Tuttle 1967, 1969; Inouye 1994; Wunderlich and Jungers 2009; Matarazzo 2013). A greater use of palm-in postures is potentially associated with greater ulnar-side force transfer as ulnar deviation is higher during palm-in versus palm-back postures (Patel and Carlson 2007). *Pan troglodytes* has been observed to utilise high degrees of ulnar deviation relative to cercopithecoids (Thompson 2020), while *Gorilla* has been observed to use high degrees of ulnar deviation during climbing (Neufuss et al. 2017). Finally, as *Pan* has greater diversity in ray length and engages more variable hand and forelimb postures, it does not bear weight as evenly across the manus, almost always removing the 5th Mc from weight bearing (Inouye 1994; Wunderlich and Jungers 2009; Matarazzo 2013). In contrast, *Gorilla* tends to produce even pressure across the hand and includes the fifth digit in weight-bearing (Matarazzo 2013).

1.5.c.3. *Homo sapiens* functional anatomy

While the function of the *H. sapiens* hand is distinct among primates, many of the hand and wrist hard and soft tissue structures are plesiomorphic for mammals in general (Wood Jones 1942; Napier 1960; Lewis 1989; Marzke 2009; Lemelin and Schmitt 2016). Nevertheless, numerous derivations of the hand suggest a joint complex adapted to efficient and powerful tool behaviour, resisting compressive forces arising from a hypertrophied thumb (Lewis 1989). Many of the morphological correlates considered key indicators of a human-like adaptation to tool manufacture are found in the derived morphology of the radial carpus.

1.5.c.3.1. Joint reorganisation in the radial-side carpus

It has been suggested that the trapezoid may be the key to the reorganisation of the *H. sapiens* radial wrist, as its derived 'boot-shaped' morphology has significant consequences for the surrounding carpals (Tocheri 2007). The palmar expansion causes supination of the trapezium, aligning the distal row radio-ulnarly (Tocheri 2007). This supination of the trapezium displaces it radio-palmarly on the scaphoid, resulting in the characteristic position on the scaphoid tubercle (Tocheri 2007). Just as the relatively flatter, more mobile trapezium-Mc1 articulation allows freedom of movement without loss of surface area for force dispersal (Rose 1992; Tocheri et al. 2005; Tocheri 2007; Bardo et al. 2020), the palmar expansion of the trapezoid allows movement and subtle repositioning between the capitate-scaphoid-trapezoid joints, to ensure a consistent perpendicular joint orientation relative to the thumb, whether the thumb is in adduction, abduction, flexion or extension (Tocheri 2007).

Alongside the trapezoid, the capitate has several derived articular surfaces that are advantageous for transferring force arising from the thumb radio-ulnarly across the wrist. The trapezoid articular surface is enlarged and displaced palmarly, reorienting it more orthogonal to the radio-ulnar axis, improving the dispersal of load and resistance to sheer originating from the thumb (Tocheri 2007). Indeed, Lewis (1989) suggested that this palmar trapezoid articular surface may be the key diagnostic feature for the capacity of human-like power squeeze grips. The articular relationship with the Mc2 is also critical to forceful precision grips. While in non-human hominids, the Mc2 articulates with the capitate on its disto-radial surface, in *H. sapiens*, this surface has reoriented to face predominantly distally (Lewis 1989; Marzke, Wullstein and Viegas 1992; Marzke 1997; Tocheri 2007; Marzke 2013). The distal orientation stabilises the Mc2 from sliding distally when compressed radio-ulnarly as well as allows it to pronate towards the thumb for greater precision and force during grip (Marzke 1997; Tocheri 2007).

Despite the hand not being recruited for locomotion, the amount of force generated via tool use and subsequently resisted by joints is not insignificant. As the forces arise from the musculature, they are predominantly compressive (Napier 1956). The hand can experience up to 120kg of compressive force at the trapezium-MC1 joint during power grips (Cooney and Chao 1977), and even delicate tasks such as pipetting have been shown to produce force at the carpometacarpal joints of up to 18kg (Wu et al. 2014). However, no muscles attach directly to the wrist. Instead, the carpus is compressed at the bone-to-bone articular surfaces indirectly by muscular compression and directly by the tensional strain imposed by the stabilising forces of the ligaments.

While these reorientations at the radial carpus are undoubtedly critical to the distinctive biomechanics of the *H. sapiens* wrist, relatively less research has been conducted on the functional morphology of the ulnar-side carpus. This is perhaps because, due to the contraction of the ulnar styloid process, this side of the wrist receives relatively little of the load from the forearm (Viegas et al. 1987; Hara et al. 1992; Viegas et al. 1993; Gíslason et al. 2009). Nevertheless, the shared soft tissue features of the apes at the ulnar wrist, such as the TFCC, and the recently published importance of the fifth finger of the non-dominant hand during tool manufacture (Key, Dunmore and Marzke 2019) makes this region a fruitful region for future biomechanical research.

1.5.c.3.2. The dart-thrower's motion

In *H. sapiens*, the proximal capitate has been demonstrated to be the functional crux of wrist movement (Edirisinghe et al. 2014). *Homo sapiens* use the dart-thrower's motion (DTM) for almost all activities in daily life, from pouring water, and answering a mobile phone, to throwing and hammering (Wolfe et al. 2006; Kaufman-Cohen et al. 2018). The DTM describes a plane of motion which moves from extension with radial deviation to flexion with ulnar deviation (Figure 1.7) (Crisco et al. 2005). During the DTM the scaphoid and lunate are virtually motionless as the capitate head moves across their concave reciprocal facets, the rotation axis remaining perpendicular to the orientation of the capitate head (Crisco et al. 2005; Edirisinghe et al. 2014; Garcia-Elias, Alomar Serrallach and Monill Serra 2014). The capitulunate joint is considered the hinge of the DTM, as the centre of rotation is at that region of the midcarpal joint (Edirisinghe et al. 2014). Several morphological features of the *H. sapiens* hand have been identified as markers of the DTM functional anatomy. These features predominantly relate to the carpal articular surfaces of the proximal row, which are oriented oblique to the radio-ulnar plane, and thus guide movement along the oblique axis of the DTM (Moritomo et al. 2007). Examples can be found in the oblong-shaped

scapholunate distal articular surface and the obliquely oriented dorsal ridge on the scaphoid, which helps constrain and guide the scaphotrapeziotrapezoid joint motion along the DTM path (Moritomo et al. 2007). The *H. sapiens* wrist appears to be highly adapted to the path of the DTM, as even when the wrist is allowed to fall passively against gravity, it moves along the DTM; that is to say, wrist extension is always accompanied by radial deviation and wrist flexion is always accompanied by ulnar deviation (Moritomo et al. 2007). Figure 1.7B illustrates how even in delicate tasks with relatively little movement or force, such as sewing, the position of the wrist is held along the DTM axis.

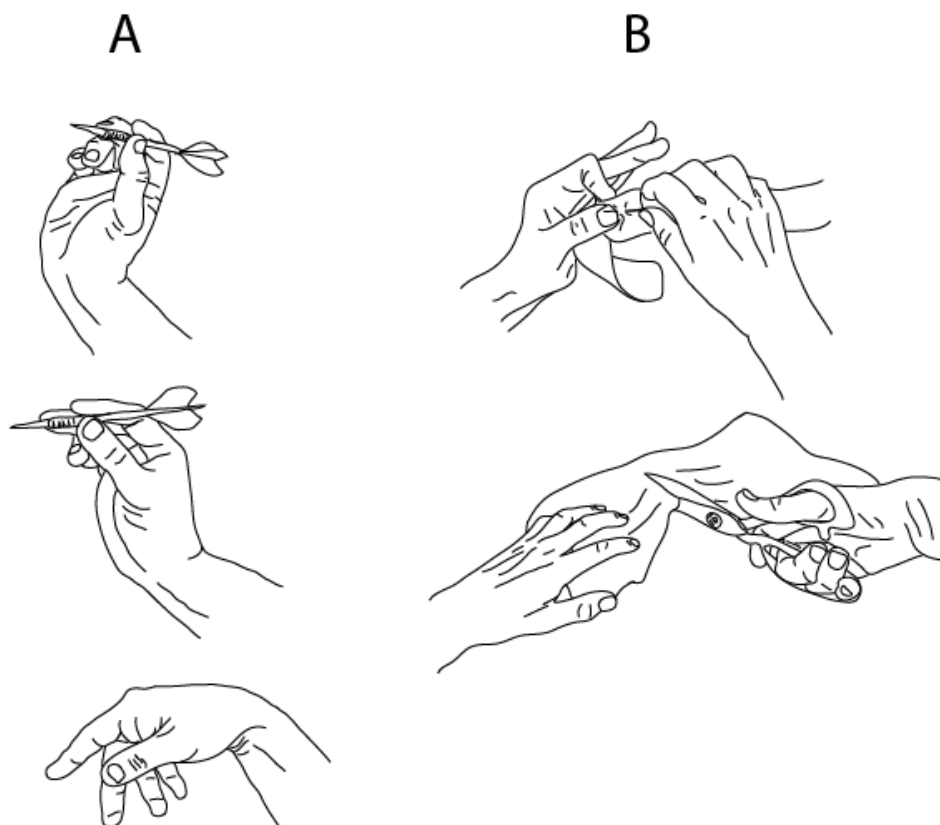


Figure 1.7 Movement through the dart-thrower's motion (DTM)

A) The top figure is the starting position of the DTM with the wrist in extension and radial deviation. The bottom figure is the end position of the DTM, the wrist is in flexion with ulnar deviation. B) The wrist is held across the DTM axis while sewing. In the top figure the left hand is in the starting position of the DTM as it grips a piece of cloth. In the bottom figure, the right hand is cutting with a pair of scissors and is held in the end position of the DTM.

A high ROM in extension is an essential component of the DTM. During the initial phases of motion, the DTM maintains extension and minimises inertia, allowing the muscles to contract quickly. This increases the torque and velocity of the tool, resulting in increased force upon impact (Young 2003; Wolfe et al. 2006; Williams, Gordon and Richmond 2010,

2014). The high extension also reduces the chance of injury as the wrist experiences the reaction forces of high-magnitude strikes (Williams-Hatala et al. 2021). It has yet to be reported whether non-human hominids use the DTM, or an oblique axis of motion, at their midcarpal joints. As such, it is currently unclear whether the underlying anatomical structures facilitating the DTM are an adaptation or exaptation among *H. sapiens* for tool behaviour.

Today, living *H. sapiens* rarely use stone tools, although the DTM continues to be used during activities of daily living. It has been demonstrated in activities such as lifting and pouring a jug of water, brushing your own hair, and lifting a mobile phone to answer a call, as well as less common activities such as vocational behaviours such as hammering or using a screwdriver (Rohde, Crisco and Wolfe 2010; Kaufman-Cohen et al. 2018; Kaufman-Cohen et al. 2019). Stephens et al. (2018) demonstrated that pre- and post-Neolithic *H. sapiens* generally exhibited similar patterns of trabecular bone across their hand and wrist, although pre-Neolithic populations showed evidence for heavier loading of the joints and more varied use of the hand. It is unclear, however, what activities of living *H. sapiens* would lead to functional adaptation at the wrist, particularly if loading is habitually low.

1.5.d. Functional anatomy of the wrist ligaments

Alongside the bone-to-bone articulations described above, the individual carpals interact with one another via soft tissue ligament structures that induce tension and provide stability. As tension within the carpal ligaments is induced by movement and behaviour (Garcia-Elias, de la Bellacasa and Schouten 2017), they are a potential cause of functional adaptation in wrist bones. Morphologically, ligaments are classified as either extrinsic (attachments from a long bone [radius, ulna, metacarpal] to one or more carpals) or intrinsic (attaching between two or more carpals – also called intercarpal ligaments) (Taleisnik 1976; Kijima and Viegas 2009). However, the identification of ligament attachment sites and their specific function is inconsistent and disputed among researchers (Buijze et al. 2011; Ayhan and Ayhan 2020). Critical to this thesis, few studies provide detailed descriptions of non-human hominid ligaments in the carpus (but see Lewis 1989). Furthermore, there is interspecific variation in ligament attachments and even an absence of certain ligaments in some individuals (Kijima and Viegas 2009; Buijze et al. 2011; Garcia-Elias, de la Bellacasa and Schouten 2017; Casado et al. 2021).

Within this context, describing the individual function of each ligament is fraught with inconsistencies and contradictions. By looking at the isodynamic (interdependent)

relationships between the different carpal ligaments, Garcia-Elias (2017) proposed a kinetic theory of unified ligament functionality. In brief, two important systems of ligaments were identified, which both surround the wrist and hand in a helical spiral, with the capitate as the central pillar (Garcia-Elias, de la Bellacasa and Schouten 2017). Firstly, there are six ligaments that work together to prevent displacement of the carpals when the hand is under axial compression, called the anti-pronators. Secondly, there are five ligaments that prevent carpal displacement when the hand is under axial tension, known as the anti-supinators. These 11 ligaments are summarised in Table 1.1 below. This theory is a constructive way to approach ligament functional anatomy within a multispecies framework as it focuses on the interdependent nature of wrist anatomy, emphasising the overall functionality of the hand under different forces. Across hominids, the hand experiences axial compression during quadrupedalism or tool behaviours and axial traction during arboreal arm-swinging/hanging or climbing. Although this theory has only been tested on *H. sapiens* wrists, the gross similarity of the carpus and ligaments between the apes suggests the kinetic theories of the anti-pronators and anti-supinators may also apply to non-human hominids.

Table 1.1 Summary of 11 wrist ligaments identified in the kinetic theory proposed by Garcia-Elias (2017)

Name	System	Comments	Attachments	Function	Controversies
Long radiolunate	Anti-pronator		Radius, lunate	Prevent ulnar or distal translocation of lunate (Kijima and Viegas 2009; Garcia-Elias, de la Bellacasa and Schouten 2017)	
Proximal and distal lunotriquetral	Anti-pronator		Lunate, triquetrum	Check triquetrum extension (Garcia-Elias, de la Bellacasa and Schouten 2017)	Sometimes considered part of the radio-triquetral ligament (Kijima and Viegas 2009)
Distal scaphotriquetral	Anti-pronator		Scaphoid, triquetrum	Prevent flexion and pronation of scaphoid (Garcia-Elias, de la Bellacasa and Schouten 2017)	May be part of Radio-scapho-capitate ligament (Buijze et al. 2011)
Distal scapholunate interosseous	Anti-pronator	1 stiff ligament with 3 portions. Proximal portion is membranous and weakest portion. Dorsal portion is the strongest (Buijze et al. 2011)	Scaphoid and lunate	Primary stabiliser between the two bones 2; Prevent flexion and pronation of scaphoid (Garcia-Elias, de la Bellacasa and Schouten 2017)	
Radio-scaphocapitate (RSC)	Anti-pronator		Radius, scaphoid, capitate	Secondary stabilisers to the scapholunate interosseous (Short et al. 2002); checks distal row pronation (Garcia-Elias, de la Bellacasa and Schouten 2017)	Some controversies surrounding exact constitution and attachment sites (Buijze et al. 2011)

Scapho-capitate	Anti-pronator	Insertion area on scaphoid much larger than that on the capitate, covers a large area on the palmar and ulnar scaphoid (Buijze et al. 2011)	Scaphoid, capitate	Important stabiliser of midcarpal joint (Buijze et al. 2011); checks distal row pronation (Garcia-Elias, de la Bellacasa and Schouten 2017)	Includes a connection to the radius (Buijze et al. 2011)
Dorsal radiotriquetral	Anti-supinator	Part of radiocarpal ligament (Garcia-Elias, de la Bellacasa and Schouten 2017)	Radius, triquetrum	Midcarpal stability (Garcia-Elias, de la Bellacasa and Schouten 2017)	
Palmar triquetrohamocapitate	Anti-supinator	Part of arcuate ligament (Garcia-Elias, de la Bellacasa and Schouten 2017)	Triquetrum, hamate, capitate	Midcarpal stability (Garcia-Elias, de la Bellacasa and Schouten 2017)	
Ulnocarpal	Anti-supinator			Stability on the medial side of the wrist (Garcia-Elias, de la Bellacasa and Schouten 2017)	
Palmar scapholunate interosseous	Anti-supinator	1 stiff ligament with 3 portions. Proximal portion is membranous and weakest portion. Dorsal portion is the strongest (Buijze et al. 2011)	Scaphoid, lunate	Stability at the medial wrist (Garcia-Elias, de la Bellacasa and Schouten 2017)	

Dorsolateral scaphotrapezotrapezoidal	Anti-supinator		Scaphoid, trapezium, trapezoid.	Secondary stabilisers to the scapholunate interosseous 1 stabilise the carpal-Mc1 joints	Possibly more than one ligament (Buijze et al. 2011)
---------------------------------------	----------------	--	---------------------------------	--	--

Finally, different ligaments across the wrist have different patterns of proprioceptive function, with the ligaments attached to the triquetrum having the highest density of mechanoreceptors (Hagert, Forsgren and Ljung 2005; Garcia-Elias, de la Bellacasa and Schouten 2017). Proprioceptive ligaments feed signals to the central nervous system about the wrist's position, movement and functionality (Garcia-Elias, de la Bellacasa and Schouten 2017). When ligaments are approaching their failure limit, the mechanoreceptors alerts the CNS, initiating safety factors to prevent injury (Garcia-Elias, de la Bellacasa and Schouten 2017; Ayhan and Ayhan 2020). Given the density of mechanoreceptors in the triquetrum, it must play a key role in the overall stability of the wrist, at least in *H. sapiens* (Short et al. 2002; Garcia-Elias, de la Bellacasa and Schouten 2017).

1.6. Bone functional adaptation

Bone is commonly categorised as cortical (compact, external) or trabecular (cancellous, surrounded by a cortical shell) (Currey 2002). Although they are almost chemically identical, the material property of cortical and trabecular bone is distinct and relates to their different biological and biomechanical roles. In the simplest sense, cortical bone resists fracture and deformation during loading, whereas trabecular bone provides support to cortical bone and channels load away from the cortex (Currey 2002; Pearson and Lieberman 2004; Barak, Weiner and Shahar 2008; Cotter et al. 2009).

The elasticity of bone is referred to by Young's modulus (or elastic- / e-modulus), which measures the degree to which a bone can undergo deformation due to strain and return to its original shape without breaking (Pearson and Lieberman 2004). The higher Young's modulus of a material or structure, the greater amount of force it is able to withstand before permanent deformation. Compared to cortical bone, trabecular bone is more porous, less compacted and has a lower Young's modulus (Guo 2001; Currey 2002). It is therefore considered more elastic and less stiff than cortical bone. However, while the trabecular bone is generally reported to be lower, the ranges of Young's modulus reported for trabecular bone have varied and sometimes overlapped with cortical measurements (Rho, Ashman and Turner 1993; Turner et al. 1999; Currey 2002). With its lower Young's modulus and higher surface-to-volume ratio, trabecular bone is capable of a 25% cell turn-over rate per year (Huiskes et al. 2000; Currey 2002). This compares to the stiff, compact cortical bone that sees only 2-5% cell turnover annually (Currey 2002; Hadjidakis and Androulakis 2006; Li et al. 2017). The study of morphological changes to bone due to mechanical stress has a long history of research and continued refinement (Wolff 1892; Ruff, Holt and Trinkaus 2006; Kivell 2016b). Today, the process whereby bone changes its architectural and material

properties over time in response to biomechanical loading is commonly referred to in anthropological literature as 'bone functional adaptation' (BFA).

BFA uses the word 'adaptation' to describe how bone alters its structural properties in response to biomechanical loading (Cowin 2001; Ruff, Holt and Trinkaus 2006). This form of 'adaptation' occurs at the individual level and cannot be inherited by offspring. Adaptation is also a core concept in evolutionary biology, although the definition in this context predicates genetic heritability. In evolutionary biology, an adaptation is a morphology that confers a fitness benefit to a species relative to another without that particular morphology (Coddington 1988; Baum and Larson 1991). Adaptations first arise as random mutations within a population, but as a result of their fitness benefits, they are maintained in subsequent populations by natural selection (Coddington 1988; Baum and Larson 1991). For palaeoanthropologists, detecting adaptations by this definition can be difficult due to the patchy fossil record and uncertainty of phylogenetic relationships (Ross et al. 2002; Ward 2002; Tocheri 2007); however, this discussion is beyond the scope of my thesis (see Tocheri 2007 for a detailed discussion). For the purpose of this thesis, when 'functional adaptation' or 'modelling' is discussed, this references a non-heritable change in morphology as a result of biomechanical strain; when adaptation is discussed, this references a species-level morphotype that confers fitness benefits relative to species without these same morpho-types.

To date, there has been contention within the literature as to whether BFA is a process of 'modelling' or 'remodelling'. Some literature describes bone remodelling as responsible for absorption of old tissue and deposition of new tissue and bone modelling as responsible for growth and biomechanical adaptation (Pearson and Lieberman 2004; Raggatt and Partridge 2010). However, other literature defines bone modelling as a process that occurs only during childhood and is primarily responsible for growth and the genetic architecture of bone, whereas remodelling occurs during the lifetime of an individual and is responsible for homeostasis, repair and functional adaptation (Martin, Burr and Sharkey 1998; Currey 2002). Recently, Barak (2019) argued for all future work on BFA to be referred to as modelling due to the fact that, by its original definition, the process of bone remodelling always couples the process of bone removal and replacement such that only pre-existing structures are replaced. This is in contrast to modelling that can deposit or absorb bone as an independent process and never replaces bone in the exact same location as the original structure (Barak 2019). In line with this commentary, this thesis will use the term **modelling** to refer to the process of functional absorption or bone deposition as a result of mechanical loading.

The response of bone to mechanical stressors, both in modelling and remodelling, is a normal biological process occurring throughout an individual's entire lifetime. It is responsible for growth, repair, homeostasis, and functional adaptation (Pearson and Lieberman 2004; Raggatt and Partridge 2010). Ruff et al. (2006) emphasize that the process of functional adaptation is due to strain rather than stress. **Stress** is the biomechanical load placed on the bone, while **strain** is the physical deformation of bone, and BFA can only occur in response to strain. Therefore, it is not the load causing the modelling, but the tissue's non-optimal response to that imposed load. Both cortical and trabecular bone are capable of modelling, however the greater rate of cell turn-over in trabecular bone means this tissue has a much higher potential rate of modelling and dynamic response compared to cortical bone (Hadjidakis and Androulakis 2006).

Of course, bone fulfils a biological function beyond its mechanical role. The shape, material properties, and modelling behaviour are determined by a combination of genetic, biochemical and mechanical factors; untangling these factors to detect biomechanical signals is a significant challenge for this research. The role of genes in determining bone structure has received considerable research attention (Lovejoy et al. 2003; Yeni et al. 2011; Paternoster et al. 2013). Genetics certainly play a role in bone structure, especially the major species-specific, evolutionary features (Smith et al. 1973; Paternoster et al. 2013). However, it is generally accepted that genetics and the environment interface to produce internal and external bone morphology (Huiskes et al. 2000; Ruff, Holt and Trinkaus 2006; Kivell 2016b). Volkman et al. (2003) studied the effect of genes on the morphology of cortical bone in mice and concluded that only 8.2-21.7% of variation could be explained by genetics, with the remainder determined by non-genetic factors such as hormones, age, weight, nutrition and functional adaptation. Within the clinical literature, research has focused on the determinates of fracture risk. While certain genes have been identified as a predictor of risk factors such as low bone mass, genetic factors alone cannot adequately explain differences in fracture risk (Huiskes et al. 2000; McGuigan et al. 2002). Interestingly, it appears that as humans age, environmental factors account for increasingly greater proportions of bone volume (Smith et al. 1973; Pollitzer and Anderson 1989).

Besides the role of genetics, another big question in the application of BFA research is whether the ability to respond to load is age-dependent (Ruff, Holt and Trinkaus 2006; Pettersson et al. 2010). Bertram and Swartz (1991) argued that previous *in vivo* studies had not used satisfactory methods to prove BFA could occur in healthy adult tissue. They argued that BFA is an important factor for trabecular bone's form, but it is only sensitive to

mechanical loading during the sub-adult growth period. However, in the 30 years since the Bertram and Swartz (1991) study, BFA has been shown experimentally to occur in adult tissue (Robling et al. 2002; Barak, Lieberman and Hublin 2011; Birkhold et al. 2014; Best et al. 2017; Sundaramurthy et al. 2019). While adult bone has a reduced sensitivity to loading and a slower capacity to model compared to sub-adults, adult bone still has the capacity to model its structure in response to mechanical load (Martin, Burr and Sharkey 1998; Currey 2002; Ruff, Holt and Trinkaus 2006).

Another consideration linked to age and genetics is the biochemical environment within which bone tissue exists. The endocrine system has a powerful influence on bone modelling in the maintenance of homeostasis. Bone is an important mineral reserve for the body, particularly calcium, and absorption or deposition of bone is regulated by several hormones aimed at maintaining serum calcium homeostasis (Hadjidakis and Androulakis 2006). For example, Turner et al. (2001) argues that the bone loss observed during spaceflight is more consistently explained by changes in calcium balance rather than a reduction in mechanical load. Menopause (Lindsay et al. 1997; Eriksen et al. 2002), pregnancy (Naylor et al. 2000), lactation (Kent et al. 1993; Kalkwarf and Specker 1995) and hormone therapy (Turner et al. 2004; Eriksen 2010) have all been shown to affect bone turnover rates.

Finally, the frequency and magnitude of loading are important factors when considering which behaviours within the repertoire of a species may be reflected in cortical and trabecular architecture. Up to this point, I have referred to bone altering its structure to habitually incurred forces, although it is unlikely that many habitual positional behaviours will elicit an adaptive response. Sitting or lying down are behaviours that constitute a large proportion of an animal's daily positional repertoire (Hunt 1991a; Ramos III 2014), and yet they are unlikely to be loading the bones in a way that would stimulate sufficient strain to produce a modelling response. This then begs the question as to which frequencies and magnitudes of strain are capable of eliciting functional adaptation. Several studies comparing the outcomes of high and low impact exercise on bone mineral density accord with the model that it is *strain* rather than *stress* which elicits BFA (Heinonen et al. 1993; Taaffe et al. 1995; Kerr et al. 1996; Morel et al. 2001; Tsuzuku et al. 2001; Stengel et al. 2005). Kerr et al. (1996) tested this hypothesis directly by unilaterally loading one arm of each participant. They concluded that exercise regimes designed for strength rather than endurance produced the greatest increase in bone mineral density. That is to say, the intensity of the load rather than the duration or frequency was a greater driver for BFA. However, these peak loads are likely habitual, as novel high-intensity loads can lead to bone fracture (Doblaré, Garcia and

Gómez 2004; Tanck et al. 2009). In contrast to the concept that peak loads predominantly determine the functional adaptation of bone, Rubin et al. (2002) found evidence that low impact, high-frequency loads (such as standing in *H. sapiens*) could result in functional adaptation in the trabecular, although not the cortical, bone.

Given the powerful deductive opportunity afforded by mechanically sensitive tissue, many researchers have investigated the link between BFA and locomotor behaviour. Several *in vivo* experiments have measured trabecular properties such as bone volume to total volume (BV/TV), mean thickness of individual trabeculae (Tb.Th), the mean number of trabeculae (Tb.N), and the degree of alignment across the individual trabeculae, more commonly referred to as the degree of anisotropy (DA). Variable combinations of these parameters have been measured before and after exercise, regimes to assess whether bone changed in predictable ways to the novel biomechanical environment (Pontzer et al. 2006a; Barak, Lieberman and Hublin 2011; Izard et al. 2016; Sundaramurthy et al. 2019). For example, Barak et al. (2011) measured changes in tarsal joint trabecular parameters in sheep exercised at an incline. Changes in trabecular orientation between the experimental and control groups correlate closely to the peak loading orientation. More commonly, studies have investigated the link between locomotor mode and trabecular architecture to assess whether there is a relationship between bony correlates of strength and the expected joint loading position.

Given the postural diversity among primates, many studies have analysed the trabecular and cortical architecture across numerous elements of the skeleton, although the success in correlating locomotor mode with expected joint loading and bone strength has had mixed results. For example, although the proximal femur is hypothesised to be under strong and predictable loads, numerous studies have failed to find strong, diagnostic differences in trabecular architecture across primates of diverse locomotor behaviours (Fajardo et al. 2007; Ryan and Walker 2010; Ryan and Shaw 2012; Shaw and Ryan 2012). However, other work has found functionally meaningful differences in elements such as the proximal humerus (Fajardo and Müller 2001; Kivell et al. 2018b), metacarpals (Tsegai et al. 2013; Matarazzo 2015; Skinner et al. 2015; Stephens et al. 2018; Dunmore et al. 2020a), metatarsals (Komza and Skinner 2019), talus (DeSilva and Devlin 2012; Su and Carlson 2017; Tsegai et al. 2017) and tibia (Barak et al. 2013). Differences in osteological elements, comparative taxa, and quantitative methodology likely all impact the ability to detect functionally meaningful differences in architecture.

Thus, although the correlation between locomotion and functional adaptation is complex, the continued exploration of bone architecture and habitual mechanical load represents a significant opportunity for reconstructing the locomotor behaviour of fossil taxa. It is reasonable to conclude that we cannot and should not dichotomise the role of genes, biochemistry, environment and biomechanics; bone morphology represents a complex interaction between these competing factors, and any interpretations must proceed with caution and consideration of these extraneous variables (Ruff, Holt and Trinkaus 2006).

1.6.a. Bone functional adaptation in short bones

BFA research provides a method for drawing behavioural inferences from the microarchitecture as a reflection of habitual behaviour, providing an appealing methodology for overcoming limitations to traditional external functional analyses. As the internal structure of bone is known to model in response to habitual loading during life (Pontzer et al. 2006a; Barak, Lieberman and Hublin 2011; Doube et al. 2011), its structural and mechanical properties may provide an informative avenue for understanding the biomechanics and kinematics of the hominid wrist. To date, two studies have analysed BFA in carpals across multiple primate taxa (Schilling et al. 2014; Ragni 2020). Both studies used a single volume of interest (VOI) to quantify trabecular architecture, although functionally meaningful interspecific differences were limited (Schilling et al. 2014; Ragni 2020). Whole-bone methodologies, which use hundreds of VOIs across an entire subregion of bone, have been more functionally informative for studies on hand bones (Tsegai et al. 2013; Dunmore 2019). To date, this methodological approach has not been applied to the carpals of non-human hominids. Therefore, a whole-bone approach to quantifying and analysing the microarchitecture of hominid carpus represents a significant opportunity. More detail on the difference between these two approaches is given in section 2.2.a.

Whole-bone methodologies, however, have primarily been developed on long bones such as the Mc3 and femur (Pahr and Zysset 2009b, a; Tsegai et al. 2013; Gross et al. 2014; Steiner, Synek and Pahr 2021; Bachmann et al. 2022). Carpals are defined as 'short' bones as they are small, irregularly shaped, and generally as long as they are wide (Currey 2002). In *H. sapiens*, short bones consist of a thin cortical shell, with trabecular tissue filling the entire internal space (Currey 2002; Schilling et al. 2014). This is in contrast to long bones, which have an epiphysis, metaphysis and diaphysis with trabecular bone volume varying in each component. Curry (2002) focuses on long bone functional adaptation but notes that short bones are likely to bear a significant portion of the load imposed upon the anatomical region as they resist compressive forces and transfer load through the bone from one joint

articulation to another. While the ends of long bones have thin cortical shells filled with trabecular tissue, such as in short bones, the cortical bone of the diaphysis is much thicker, and trabecular bone in the epiphysis transfers load towards the mechanically stronger diaphyseal cortex (Martin, Burr and Sharkey 1998; Currey 2002). However, this model of diaphysis-oriented load transfer is not applicable to short bones as they lack this morphology.

The geometry, biomechanical function and biological environment of short bones, such as those that comprise the carpus, differentiate them in comparison to long or flat bones. Therefore, there are important considerations for the application of BFA research to short bones. Crucially, it is not clear whether the small bones of the wrist in non-human hominids, which bear a significant load from quadrupedal locomotion, will conform to the described *H. sapiens* pattern of thin cortical bone surrounding trabeculae.

1.7. Allometry

Allometry is the investigation of scale: what are the mechanical and functional consequences of size differences across different animals (Jungers 1984). Interspecific research incorporating species of variable body mass should consider the effect of this variation in order to differentiate between differences that confer the same mechanical output at variable body sizes to those reflecting biomechanical and behavioural adaptations (Ruff, Holt and Trinkaus 2006). As animals increase in body size, the loads imposed upon their joints by mass and gravitational forces also increase (Doubé et al. 2011). As bones get longer, they tend to become more robust (Doubé et al. 2011), although as bone modelling aims to maximize stiffness and minimise weight (Currey 2003), the comparatively less dense trabecular bone is an efficient way to increase whole bone strength without adding too much mass, by altering any of several properties such as volume, thickness or number (Doubé et al. 2011).

Although research on the effects of body mass on trabeculae has yet to find consistent results, there are some general trends. In many studies, BV/TV and DA show no significant correlation with body mass, while trabecular thickness, spacing and number do show relationships (Cotter et al. 2009; Doubé et al. 2011; Barak, Lieberman and Hublin 2013; Ryan and Shaw 2013). While trabeculae in smaller mammals are thinner on an absolute scale relative to size, they are thicker, more widely spaced and more numerous than in larger mammals (Cotter et al. 2009; Doubé et al. 2011; Barak, Lieberman and Hublin 2013). Small mammals have absolutely less space for trabecular bone, and while their body mass is less,

many of the demands of homeostasis and bone cell physiology are the same as in large mammals (Cowin 2001; Barak, Lieberman and Hublin 2013). Thus, as BV/TV is relatively constant across species of various sizes, several biomechanical and homeostatic hypotheses have been posited to explain the differences in trabecular architecture.

Trabecular thickness may have a functional minimum and maximum, restricting the amount that trabeculae can alter in this aspect (Barak, Lieberman and Hublin 2013). Trabeculae are unlikely to be thinner than the lacunae created by osteoclasts as they need to be wide enough to withstand the 30-50 μ m channels without being sliced in half, and as osteoclasts do not change size between species, thickness cannot scale allometrically (Cowin 2001; Doube et al. 2011; Barak, Lieberman and Hublin 2013). On the other side of the spectrum, maximum thickness is likely capped by the limitations of osteocyte metabolism (Doube et al. 2011; Christen, Ito and van Rietbergen 2015). Thickness may also be limited in small mammals as space must be reserved in the trabecular cavity to ensure there is room for bone marrow (Barak, Lieberman and Hublin 2013). Small animals also must preserve the integrity of their trabecular bone at low body weight as it is likely there is a minimum threshold of strain that trabecular bone needs to experience before it starts to be reabsorbed (Huiskes et al. 2000). These competing demands placed on bone provide a reasonable explanation as to why mammals cannot simply thicken or thin their trabeculae to deal with stress, and instead use variable trabecular geometry to provide mechanical solutions.

When analysing closely related species, there is potential for trabecular patterns to reflect similarities due to their close phylogenetic relationship rather than shared loading patterns. The effect of genes on trait variance has been analysed inter- and intraspecifically, and results suggest bone volume does have a degree of interspecific trends across the skeleton (Havill et al. 2010; Chirchir et al. 2015; Tsegai et al. 2018). However, studies that have examined phylogenetic effects on trabecular parameters have generally found that they do not strongly influence form (Barak, Lieberman and Hublin 2013; Ryan and Shaw 2013; Tsegai et al. 2013). Interestingly, different trabecular parameters may be more or less phenotypically plastic and different elements of the skeleton are not likely to exhibit consistent degrees of phylogenetic constraint. For example, the importance of the skeletal element to the peak mechanical loading regime may reduce the phylogenetic constraints on that element's trabecular structure (Ryan and Shaw 2013). Therefore, while the low phylogenetic influence over trabecular bone means closely related species can reasonably be included in analyses, the evolutionary relationships between species should not be excluded from consideration during interpretations.

While this thesis will not necessarily focus on fine-grained intraspecific trabecular differences, there is evidence indicating that underlying differences within populations affects bone structure. Clinical research provides some insight, with most research focusing on the significant differences in bone mineral density between people of different ethnicities and the consequent higher fracture risk in certain populations (Pollitzer and Anderson 1989; Micklesfield, Norris and Pettifor 2011; Popp et al. 2017). Most palaeoanthropological trabecular research focuses on broad differences between taxonomic groups, and there is much less data contributing to our nuanced understanding of within-group differences (Saers et al. 2016). This may be because multiple, differentiated populations with demographic data and high preservation is not easy to come across in osteological collections; nevertheless, this area of research is understudied in palaeoanthropology and affords a major opportunity for future research. The small number of studies that have looked within later *Homo*, have focused on the effects of divergent subsistence strategies on population-wide trabecular patterns (Nikita et al. 2011; Chirchir et al. 2015; Ryan and Shaw 2015; Stephens et al. 2018; Saers, Ryan and Stock 2019b). This is an important consideration when including fossil hominins in trabecular bone research as the low bone volume observed in modern *H. sapiens* appears to have a very recent origin, coinciding with the advent of agriculture and subsequent reduction in long distance food foraging (Chirchir et al. 2017). Fossil hominins, therefore, are unlikely to have trabecular bone volumes within the agricultural or post-industrial *H. sapiens* range of variation (Chirchir et al. 2015; Ryan and Shaw 2015; Saers et al. 2016).

1.8. Morphology and functional anatomy in fossil hominins

Below I review some of key literature on our current understanding of the morphology and archaeology of the fossil hominins included in this thesis, laying the backdrop to the interpretation of their habitual hand use. This thesis will analyse only the capitate bone of the fossil species. A large sample of capitate material across extant and fossil species was available for analysis providing a unique opportunity to test the application of whole-bone functional adaptation analysis to a carpal bone to infer hand use and behaviour. Further, given the importance of the capitate to the midcarpal, carpometacarpal and range of motion and its correlation to hand posture differences across primates (Orr 2017), it is an ideal bone to use in BFA analyses. A summary of key morphological correlates of manipulation in the *H. sapiens* capitate is summarised below in Table 1.2, and the character trait of the fossils are noted.

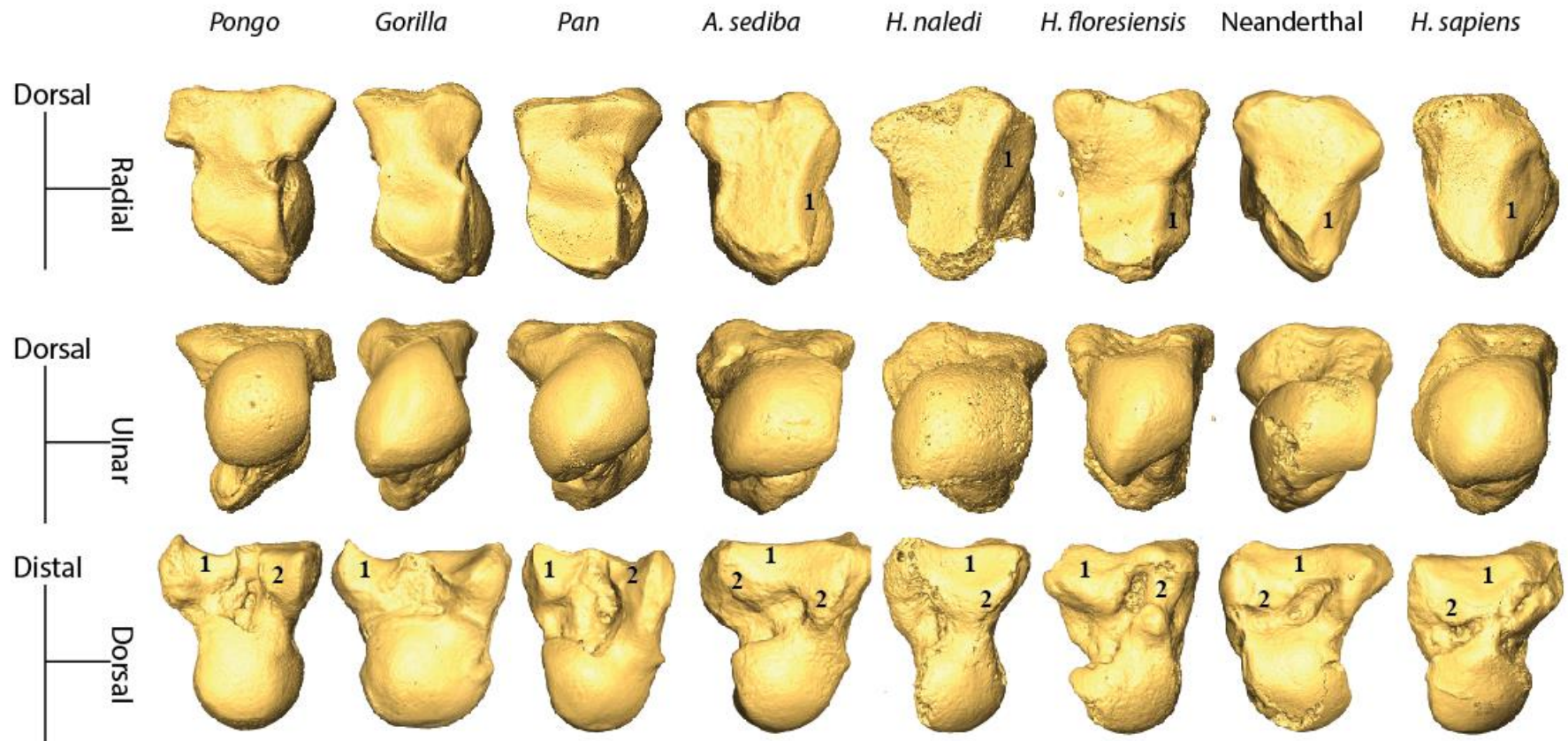


Figure 1.8 Morphology of the capitate in extant and extinct hominids

The top row is in a distal perspective; the middle row is in a proximal perspective; the bottom row is in a radial perspective. 1 = Mc2 articulation; 2 = trapezoid articulation. More details of these features are given in Table 1.2. *A. sediba* is the left from MH2; *H. naledi* is Hand 1, *H. floresiensis* is LB1, Neanderthal is SD-1034.

Table 1.2 Summary of gross capitate morphology among the hominins.

Feature on the capitate ¹	Mc2 orientation ¹	Position of trapezoid articular surface ¹	Shape of head ¹	Presence of a surface for an Mc3 styloid process?
Non-human hominid	Radial	Dorsal	Varies by taxon ²	No
<i>H. sapiens</i>	Distal	Palmar	Radially expanded	Yes
Neanderthal	Disto-radial	Palmar	Radially expanded	Yes
<i>A. sediba</i>	Disto-radial	Dorsal and palmar	Small degree of radial expansion	No
<i>H. naledi</i>	Distal	Dorsal	Radially expanded	No
<i>H. floresiensis</i>	Radial	Dorsal	Not radially expanded	No

¹Kivell et al., 2015, Kivell et al., 2011, Lewis, 1989, Marzke et al., 1992. ²The shape of the capitate head differs between the non-human hominid. *Pongo* does not have a laterally expanded head, while *Pan* and *Gorilla* do. *Homo* is differentiated from *Pan* and *Gorilla* as the lateral expansion extends distally.

1.8.a. *Australopithecus sediba*

Dated to the late Pliocene at 1.977Ma, two individuals with relatively well-preserved skeletal elements represent the species *A. sediba* (Dirks et al. 2010; Pickering et al. 2011). The holotype, Malapa Hominin 1 (MH1), is a juvenile and is thought to be male based on muscle attachment robusticity (Berger et al. 2010). The paratype, Malapa Hominin 2 (MH2), is an adult, and as the mandible and postcrania are smaller and more gracile than the MH1, it is thought to be female (Berger et al. 2010). Although there are notable derived features in the pelvis, cranium, and hand, the persistence of primitive cranial morphology and an overall *Australopithecus*-like body plan places the affinity of the Malapa skeletons with *Australopithecus* rather than *Homo* (Berger et al. 2010).

1.8.a.1. Cranium

The cranial volume of MH1 is 420 cm³ making it smaller than *A. afarensis* and *A. africanus*, at the bottom of the range of variation among australopiths (Berger et al. 2010; Carlson et al. 2011). Although small in size, the skull mirrors several cranial morphologies evident in *H. erectus*, but missing from *H. habilis* and *H. rudolfensis* (Berger et al. 2010). The post-canine teeth are reduced in size, a feature typically attributed to *Homo*, although the cusp pattern more closely resembles *Australopithecus* (Berger et al. 2010). This unique combination of craniodental features not seen in any other Pliocene australopith has led some authors to suggest *A. sediba* may be ancestral to the genus *Homo* (Berger et al. 2010; Pickering et al.

2011; Berger 2012). However, this hypothesis has not gone unchallenged, particularly as the Malapa Hominins are dated 800ka after the first appearance of the earliest members of *Homo* (Du and Alemseged 2019).

1.8.a.2. Lower limb

The lower limb and pelvis present a combination of primitive and derived morphology not found in any other *Australopithecus* species (DeSilva et al. 2018). For example, the axial skeleton indicates *A. sediba* was an obligate biped, although the foot, and especially the calcaneus, shows some surprisingly primitive morphological features that are more similar to *Pan* than to earlier *A. afarensis* (Berger et al. 2010; Kibii et al. 2011; Zipfel et al. 2011; DeSilva et al. 2018). Specifically, *A. sediba* appears to have a mid-tarsal break, a feature associated with arboreality in African apes (but absent in *A. africanus* and *A. afarensis*), which allows a high degree of flexion at the foot (DeSilva 2010; Zipfel et al. 2011; DeSilva et al. 2013). In light of this unique combination of features, *A. sediba* has been hypothesised to indicate a unique kinematic solution to combining climbing with extended knee bipedalism (Zipfel et al. 2011; DeSilva et al. 2013).

1.8.a.3. Upper limb

While other regions of the *A. sediba* anatomy exhibit a combination of primitive and derived morphology, the long upper limb of *A. sediba* exhibits mostly primitive morphology relative to *Homo*, and fits well within the *Australopithecus* morphotype (Churchill et al. 2013). The upper limb is long relative to stature, partly due to the relatively long forearm, a feature strongly correlated with forelimb-dominated suspensory behaviour (Churchill et al. 2013; Rein, Harvati and Harrison 2015). In sum, the shoulder and elbow joint configurations, as well as the location and robusticity of muscle insertions, all indicate an adaptation to climbing and suspension (Berger et al. 2010; Churchill et al. 2013; Rein et al. 2017).

1.8.a.4. Hand and wrist

The MH2 hand is mostly complete (missing only seven of the 27 hand and wrist bones), displaying some features consistent with *Australopithecus* and others consistent with *Homo*. Numerous features of the metacarpals suggest muscles associated with precise gripping and cupping were well developed in *A. sediba* (Kivell et al. 2011). The distal pollical phalanx has a broad apical tuft and gabled attachment for the *flexor pollicis longus*, the Mc heads are asymmetrical, and the base of the Mc5 is robust and has a strong attachment site for the *flexor carpi ulnaris* muscle (Kivell et al. 2011; Kivell et al. 2018a). The thumb is also long relative to the fingers; thus, it appears the hand was capable of pad-to-pad precision grips, with thumb and fifth finger adduction (Kivell et al. 2011). Nevertheless, some key muscles

correlated to large and heavy object manipulation appear underdeveloped based on the enthesal morphology (Kivell et al. 2011). There are also morphological features considered to be adaptations to climbing. The proximal and intermediate phalanges are moderately curved and display robust flexor sheath ridges, both features correlated with powerful flexion during arboreal grasping and climbing (Kivell et al. 2011).

The MH2 left and right capitates have several derived features; however, it is still morphologically distinct from modern *H. sapiens*. The shape is overall 'boxy', particularly because the mid-section waisting is reduced (as it is in *H. sapiens*) in combination with a notably large and square distal palmar projection (on which numerous ligaments attach). The Mc2 articulation is oriented more distally than African apes but not as extremely distally oriented as in *H. sapiens* (Kivell et al. 2011). Similarly, the trapezoid articulation expresses both the primitive and derived conditions as it has a dorsal and palmar articular surface (Kivell et al. 2011). In line with the overall less-derived carpometacarpal configuration, the capitate does not have a bevelled distodorsal surface for an Mc3 styloid process.

The functional interpretation of these features is not straightforward, as their combination is not seen in any extant species. While the *flexor carpi ulnaris* muscle is recruited during Oldowan tool manufacture, it is also strongly recruited in climbing (Marzke et al. 1998b; Berger et al. 2010). Although the phalanges are moderately curved, they are gracile and of similar length to modern *H. sapiens*, making them less competent at resisting the strong bending forces of flexion during arboreal locomotion relative to *Pan* (Kivell et al. 2011). The Mc1 exhibits several features correlated with tool-making in *H. sapiens*, including broad apical tufts and robust muscle attachments for the flexors and abductors (Kivell et al. 2011). The carpometacarpal articulations (notably the Mc1-trapezium) are similar to *Australopithecus* (Kivell et al. 2011), suggesting the palm was not well adapted to withstand large and repetitive strike forces. A recent study analysing trabecular and cortical bone in the metacarpals of *A. sediba* within a broad comparative hominid sample provides some additional context for interpreting the external morphology (Dunmore et al. 2020b). This study found that *A. sediba* likely combined arboreal locomotion with habitual manipulation as it displayed a *Pongo*-like pattern of bone distribution in the fingers but human-like patterning in the thumb (Dunmore et al. 2020b).

1.8.a.5. Stone tools

At this point, no stone tools have been found in association with *A. sediba*, although this species existed after the earliest stone tools in both East (3.3Ma, Harmand et al. 2015) and South Africa (2.2Ma, Granger et al. 2015; Kuman et al. 2021). South African stone tools

contemporaneous with the dates of *A. sediba* are Oldowan-type and are currently only associated with *Paranthropus* and early *Homo* (Kuman and Clarke 2000; Chazan et al. 2008; Kuman et al. 2021; Shaar et al. 2021).

1.8.a.6. Conclusions

The external morphology of the hand, combined with the BFA study, suggests *A. sediba* was habitually utilising both power-grasping with flexed fingers for arboreal locomotion, as well as using their thumbs to grasp and manipulate objects commensurate with tool manufacture and use. The combination of these features suggests a hand not as well suited for arboreality as *P. troglodytes*, but neither as an obligate tool user. The developed muscles along the ulnar and radial aspects of the hand would suggest it could withstand a degree of force encountered during tool manufacture; however, the gracility of the metacarpals and lack of certain key intrinsic muscles may indicate there was a cap on the weight of objects they could grasp.

1.8.b. *Homo naledi*

The morphology of the 15+ individuals recovered from the Rising Star Cave in South Africa has consistently been described as a mosaic of primitive and derived morphology relative to *H. sapiens*. Prior to the discovery of *H. naledi*, the fossils of the African Middle Pleistocene were large-brained species of *Homo* (Dusseldorp, Lombard and Wurz 2013; Berger et al. 2017; Dusseldorp and Lombard 2021). Based on this evidence, traditional hypotheses postulated that across evolutionary time, there had been a continually increasing brain size, which correlated to an increased reliance on tool use, reduced dentition, and decreasing use of arboreal substrates (Napier 1962b; Wood and Collard 1999; Berger et al. 2017; Holloway et al. 2018). Therefore, the late Middle Pleistocene date of 250ka, places *H. naledi* as contemporaneous with *H. sapiens* in southern Africa (Berger et al. 2017; Dusseldorp and Lombard 2021).

1.8.b.1. Cranium

The small size of the *H. naledi* cranium is particularly salient in one morphological analysis, which concluded that based on cranial morphology alone, the *H. naledi* material should date to 2Ma (Thackeray 2015). At 465–610 cm³ (Hawks et al. 2017; Laird et al. 2017) the *H. naledi* cranial capacity is comparable to *Paranthropus* and *Australopithecus* (Berger et al. 2017; Holloway et al. 2018). Derived aspects of endocranial morphology are shared with numerous *Homo* species, including *H. habilis*, *H. floresiensis* and *H. sapiens*, is linked to language processing, speech production, social behaviours and planning (Stout et al. 2008; Holloway

et al. 2018). Some authors have drawn the conclusion that the development of these neurological features indicates a greater capacity for tool manufacture, as the ability for planning, communication, and group cohesion underlie the same brain structures (Stout et al. 2008; Holloway et al. 2018).

1.8.b.2. Lower limb

The lower limb of *H. naledi* has numerous human-like features. The configuration of the ankle joint, limited movement at the mid-foot, proportions of the metatarsals, and an adducted hallux all indicate *H. naledi* was adapted to striding bipedalism (Berger et al. 2015; Harcourt-Smith et al. 2015). These derived features are combined with a degree of curvature in the proximal pedal phalanges similar to non-human hominids and australopiths, indicative of greater capacity to flex and possibly grasp with the toes (Harcourt-Smith et al. 2015). While the morphology of the upper and lower leg is described as 'intermediate' between *Homo* and australopiths, the presence of a femoral linear aspera, a valgus knee, and a long tibia support the conclusions from the analysis of the foot; that *H. naledi* was well adapted to striding, long-distance bipedalism (Berger et al. 2015; Marchi et al. 2017).

1.8.b.3. Upper limb

The upper limb is notably more primitive than the lower limb, implying that the evolution of the limbs has a degree of independence rather than evolving as a single morphological package (Sylvester 2006; Berger et al. 2015; Feuerriegel et al. 2017). In brief, a wider, more ape-like thorax, stronger, more *Pan*-like clavicle, cranially elevated scapula position, cranially oriented glenoid fossa and low humeral torsion have been interpreted as reflecting the continued importance of overhead reaching, hanging and climbing in *H. naledi* (Berger et al. 2015; Feuerriegel et al. 2017; Feuerriegel et al. 2019). Indeed, a recent 3D geometric morphometric analysis concluded that the *H. naledi* humerus appears better adapted to arboreal locomotion than any *Australopithecus* species (Feuerriegel et al. 2019). Although the lower limb appears well adapted to long-distance bipedalism, the trunk and upper limb morphology suggest a reduced capacity for running or overarm throwing, as the trunk does not possess the capacity to stabilise against the torque produced by these behaviours (Feuerriegel et al. 2017).

1.8.b.4. Hand and wrist

The combination of primitive and derived morphology is also found in an almost complete right hand, missing only the pisiform, known as Hand 1. The thumb's metacarpal and phalangeal proportions, broad apical tufts, and robust muscle attachments resemble *H. sapiens* and Neanderthals (Kivell et al. 2015). Conversely, the intermediate and proximal

phalanges are highly curved, with the degree of curvature in proximal phalanges similar to *Australopithecus* and intermediate phalanges similar to *Pongo* (Kivell et al. 2015). Despite this unusual combination, the morphology of the fingers and palm is suggestive of a strong thumb, fully capable of adduction and opposition with the other fingers, an adaptive feature of powerful, human-like precision grips.

Kivell et al. (2015) undertook a 3D morphometric analysis of the trapezium, trapezoid, capitate, hamate, and scaphoid. Measuring angles, relative areas and curvature, the carpal morphology and joint configuration of Hand 1 falls within the range of variation displayed by *H. sapiens* and Neanderthals. Notably, the trapezoid of *H. naledi* is boot-shaped. The boot-shaped trapezoid, with the palmarly expanded non-articular surface, has been hypothesised to be key to the synapomorphic rearrangement of the radial carpus in *H. sapiens* and Neanderthals (Tocheri 2007; Kivell et al. 2015). In conjunction with the derived shape, the articulation on the capitate is palmarly placed, as it is in *H. sapiens* and Neanderthals (Kivell et al. 2015). The capitate, however, lacks the disto-dorsal-radial bevelling for the Mc3 styloid process and in this way, deviates from the derived condition (Kivell et al. 2015). In part due to the derived trapezoid shape, the radial joint articulations are oblique to the radio-ulnar axis of the hand, indicating an adaptation to resist and transfer the compressive forces associated with precision and oblique power grips (Tocheri 2007; Kivell et al. 2015).

In combination, the features of the *H. naledi* hand and wrist suggest that a hominin species could adapt its morphology for intensified stone tool behaviour without compromising all adaptations for arboreality. Phalangeal curvature has a strong functional benefit to flexed-finger grasping postures such as climbing and arm-hanging as it aligns the bones with the direction of stress, greatly reducing the strain experienced by the fingers (Sarmiento 1988; Richmond 2007; Nguyen et al. 2014). In *Pan* and *Gorilla*, phalangeal curvature first increases during infancy when degrees of arboreality are high, and subsequently decreases with age (Paciulli 1995; Richmond 2007). This pattern has been interpreted as a functional adaptation to differing levels of climbing and arm-hanging throughout life (Stern, Jungers and Susman 1995; Richmond 2007; Kivell 2015). However, a post-mortem analysis of a domesticated *P. troglodytes*, who was raised essentially as a human in New York City, showed manual and pedal phalangeal curvature within the range of wild *P. troglodytes*, challenging the hypothesis that curvature is directly correlated to the use of arboreal substrates throughout life (Wallace, Burgess and Patel 2020). While this study reemphasises the difficulty in differentiating the effects of genetics and environment on skeletal morphology, a sample size of just one limits the application of its conclusions. Generally, the phalangeal length and

degree of curvature *H. naledi* has been interpreted as a clear signal of significant proportions of grasping or climbing during locomotion (Kivell et al. 2015).

1.8.b.5. Stone tools

To date, no stone tools have been found in direct association with *H. naledi*. At 250ka, *H. naledi* sits within the technologically diverse Middle Stone Age, which saw the relatively advanced tools, including hand axes, cleavers, and prepared core technologies, exist alongside the more primitive and less cognitively demanding technology of the Oldowan (Shea 2017; Dusseldorp and Lombard 2021). Most archaeological material in South Africa comes from surface finds, making dating difficult, although technology from South African sites, including prepared core, blade production and bifacial cutting tools, all overlap with the dates of *H. naledi* (Dusseldorp, Lombard and Wurz 2013; Berger et al. 2017; Dusseldorp and Lombard 2021).

1.8.b.6. Conclusions

When it comes to the behavioural repertoire of *H. naledi*, few authors disagree that 1) arboreal substrates were an important niche and 2) they were efficient bipeds (Harcourt-Smith et al. 2015; Kivell et al. 2015; Berger et al. 2017; Marchi et al. 2017; Feuerriegel et al. 2019; Dusseldorp and Lombard 2021). What type of tools *H. naledi* was capable of manufacturing and using is more difficult to diagnose from morphology alone. Dusseldorp and Lombard (2021) argue that *H. naledi* and *H. sapiens* must have had significantly differentiated niches in order to co-exist within the same South African grassland biome; therefore it is unlikely *H. naledi* made and utilised hafted tools and points. They support this hypothesis by arguing that the shoulder and upper-limb anatomy of *H. naledi* precludes them as hunters and overhead throwers, something for which points and hafted tools are routinely utilised (as per analyses in Feuerriegel et al. 2017; Feuerriegel et al. 2019). Instead, they argue that *H. naledi* was a habitual, rather than an obligate, tool user, most likely utilising simple Oldowan or large cutting tools with few reduction sequences, heavily reliant on climbing and consuming plant foods (Dusseldorp and Lombard 2021). Indeed, the lack of a bevelled surface for the Mc3 styloid process on the capitate would suggest a reduced ability to resist injury from repeated heavy blows at the mid-palm (Marzke and Marzke 1987). On the other hand, Berger et al. (2017) argue that as the only currently known hominin species from this period in South Africa, we cannot currently discount *H. naledi* as the creator of the more sophisticated prepared core technology.

1.8.c. *Homo floresiensis*

In 2004, fossils attributed to *H. floresiensis* were recovered from Liang Bua, a large, open cave on the Indonesian island of Flores (Brown et al. 2004). The holotype, LB1, is represented by a relatively complete skeleton (Brown et al. 2004; Aiello 2010). Although LB1 was first dated to 18ka (Morwood et al. 2004), revised stratigraphy indicates an age of 100-60ka for all *H. floresiensis* skeletal material (Sutikna et al. 2016). Based on cranial analyses, researchers have proposed that *H. floresiensis* may have arisen from *H. erectus* (Brown et al. 2004; Falk et al. 2005; Gordon, Nevell and Wood 2008) or an as-yet-unknown earlier hominin species (Argue et al. 2006; Tocheri et al. 2007; Aiello 2010; Orr et al. 2013). Stone tools are known as early as 1Ma at the Wolo Sege site, but those dated to ~700ka from the Mata Menge cave on Flores are the earliest associated with fossil material and are identified as a species ancestral to *H. floresiensis* (Brumm et al. 2010; Brumm et al. 2016; Van den Bergh et al. 2016). While it is not certain whether *H. floresiensis* and *H. sapiens* overlapped or interacted in Wallacea, a recent meta-analysis of the stratigraphy and faunal remains on Flores over the past 200,000 years suggests that *H. floresiensis* was extinct by 50ka, with modern *H. sapiens* arriving at the same time or shortly thereafter (Sutikna et al. 2018).

1.8.c.1. Cranium

At 400-426cm³, the cranial capacity of *H. floresiensis* is notably small, similar to *A. afarensis*, and *A. sediba*, but smaller than any temporarily contemporaneous hominin (Brown et al. 2004; Falk et al. 2005; Kubo, Kono and Kaifu 2013). Despite the small brain size, the reduced post-canine teeth, reduced prognathism, facial shape and endocranium organisation indicate an affinity with *Homo* rather than *Australopithecus* (Brown et al. 2004). Indeed, relative to estimated stature, *H. floresiensis* brain size fits well within an allometric *Australopithecus-H. habilis* trend (Kubo, Kono and Kaifu 2013), although the overall shape of the cranium most closely resembles African *H. erectus* (Brown et al. 2004; Falk et al. 2005; Gordon, Nevell and Wood 2008). An analysis of the LB1 endocranium revealed it exhibits a unique organisation, more derived in some aspects than *Australopithecus* and *H. erectus*, while also not resembling *H. sapiens* (Falk et al. 2005). The LB1 endocranium exhibits enlarged prefrontal and temporal regions, areas that are linked to higher cognitive powers, including strategic planning and memory recall (Falk et al. 2005; Aiello 2010).

1.8.c.2. Lower limb

The overall morphology and configuration of the *H. floresiensis* lower limb is indicative of obligate bipedalism, although less derived features of the foot and pelvis suggest unique walking kinematics (Brown et al. 2004; Morwood et al. 2005; Jungers et al. 2009b). In some

respects, the pelvis of *H. floresiensis* is similar to *A. afarensis*; for example, the acetabulum is small and the iliac blades are flared (Brown et al. 2004; Jungers et al. 2009b). However, the overall shape of the acetabulum is derived toward the *H. sapiens* condition, distinguishing it from *Australopithecus* (Jungers et al. 2009b; Aiello 2010). The long bones are described as short but robust, with thick cortices (Brown et al. 2004; Morwood et al. 2005). The foot is remarkably long relative to the length of the lower limb, and although it exhibits a fully adducted hallux and a metatarsal robusticity sequence that matches *H. sapiens*, the first metatarsal is relatively much shorter than the second metatarsal (Jungers et al. 2009a). The pedal phalanges are also relatively longer than modern *H. sapiens* and slightly to moderately curved (Jungers et al. 2009a). The long toes and lack of longitudinal arch indicate that the bipedal kinetics and kinematics of *H. floresiensis* would not match modern *H. sapiens* suggesting this species was not well adapted to running, either long distances or at high speeds (Jungers et al. 2009a).

1.8.c.3. Upper limb

Similar to the long bones of the lower limb, the shafts of the humerus and ulna are robust relative to the length (Morwood et al. 2005). The length of the humerus relative to the ulna falls within the range of variation among modern *H. sapiens*; however, relative to the lower limb, the upper limb is long and falls within the estimated range of *A. afarensis* (Morwood et al. 2005). The humerus displays a low level of torsion, contrasting the high torsion seen in *Pan*, *Gorilla*, *A. afarensis*, *H. sapiens* and Neanderthals (Morwood et al. 2005; Larson et al. 2007). The low humeral torsion is in combination with a more derived scapula but a primitive clavicle (Larson et al. 2009). Larson et al. (2007) argue that the shoulder configuration in LB1 would not have precluded knapping, as the elbow would still operate efficiently in the sagittal plane. Like *H. naledi* (Feuerriegel et al. 2017), the shoulder configuration is likely to preclude overhand throwing, as abducted elbow and posterior overhead movement would be limited (Larson et al. 2007).

1.8.c.4. Hand and wrist

The hand bones attributed to *H. floresiensis* have not received a great deal of attention, perhaps because of their fragmentary nature. Of the available descriptions (i.e., Larson et al. 2009) there are some notable features. Firstly, where bases are preserved, allowing measurement, the shafts of the metacarpals and phalanges exhibit slight curvature. LB6 has better-preserved phalanges than LB1, and the degree of curvature seen in the proximal components is in the extreme ranges of *H. sapiens*, more similar to *Gorilla* (Larson et al. 2009). Secondly, the descriptions suggest the fingers are robust, exhibiting extremely radio-

ulnarly expanded apical tufts, falling within the fourth interquartile range of *H. sapiens* variation (Mittra et al. 2007; Larson et al. 2009). The apical tuberosities are described as rugose, and muscle attachments for the flexor sheaths, *flexor pollicis longus*, and interosseous soft tissues are well developed (Larson et al. 2009).

The recovered wrist bones from LB1 and LB6 do not show the derived morphology of *H. sapiens*; instead, they resemble the basal configuration of all hominids (Tocheri et al. 2007; Orr et al. 2013). The capitate lacks derived features such as the bevelled disto-dorsal-radial corner and a distally oriented Mc2 facet (Tocheri et al. 2007; Orr et al. 2013). The radial mid-section of the capitate is highly excavated, creating a 'waisted' morphology, mimicking the morphology seen in *Pan* (Larson et al. 2009; Orr et al. 2013). The trapezoid does not exhibit the characteristic palmar expansion of an *H. sapiens* trapezoid and has a *Pan*-like wedge shape (Tocheri et al. 2007). The scaphoid is also similar to a non-human hominid, whereby the trapezium articular surface is not extended onto the tubercle, as in *H. sapiens* and Neanderthals (Tocheri et al. 2007). The hamulus of the hamate is notably robust and long relative to its length (Orr et al. 2013). Numerous muscles that are important to wrist flexion attach onto the hamulus, and thus the robusticity may indicate a capacity for powerful flexion (Orr et al. 2013). Some of these muscles, specifically the *flexor digiti minimi brevis* and *opponens digiti minimi*, are critical to performing a cupping action whereby the fifth finger is adducted towards the midline of the hand (Orr et al. 2013). This grip is used during the production of Oldowan tools, increasing the degree of control over the held object (Marzke, Wullstein and Viegas 1992).

In combination, the wrist features of *H. floresiensis* indicate that the kinetics and kinematics of tool use would be substantially different from *H. sapiens*. The wrist anatomy lacks all features considered adaptive in later *Homo* for efficient, committed, high-impact tool use (Tocheri et al. 2008). Nevertheless, some hand features suggest *H. floresiensis* may have been able to perform some aspects of precision handling. Firstly, it has been hypothesised that expanded apical tufts may improve precision gripping of tools (Mittra et al. 2007). Large apical tufts would increase the size of the fingertip, or pulp, allowing greater handling and improved grip (Marzke 1997; Mittra et al. 2007). However, further evidence is required to strongly support this hypothesis, as expanded apical tufts are also correlated to warm climates (Mittra et al. 2007). Secondly, both LB1 and LB6 have distinctive 'J-hook' morphologies on the radial of the capitate. The J-hook is caused by a distal projection of the scaphoid articular surface and, in both capitates, also expands radially, causing a knob-like protrusion such that it can be seen when the bone is viewed proximally (Larson et al. 2009).

A J-hook is also seen in *A. afarensis* and both *Pan* species but is only variably present in *Gorilla* (Orr et al. 2013). Although this character has never received formal biomechanical analysis, it may improve compressive midcarpal load transfer, particularly in flexion, where it would securely engage the scaphoid (Orr et al. 2013).

1.8.c.5. Stone tools

What is particularly intriguing about *H. floresiensis* is its capacity for tool production. Tools are found as early as 1Ma in the Wolo Sege site on Flores, right through to the Holocene (Moore and Brumm 2009; Brumm et al. 2010). The Pleistocene tools on Flores are comparable to early Pleistocene Oldowan tools and are largely indistinguishable from those made by modern *H. sapiens* occupying Flores directly after *H. floresiensis*, up until 3ka (Moore and Brumm 2009; Brumm et al. 2016; Sutikna et al. 2018). Material culture directly attributed to *H. floresiensis* is known from 190-50ka (Brumm et al. 2006; Sutikna et al. 2016). Moore and Brumm (2009) analysed the tools found on Flores relative to the 1.2-1.9Ma Olduvai Gorge assemblage, which typify the Oldowan technocomplex. Oldowan tools found in association with *H. floresiensis* and modern *H. sapiens* on Flores include bifacial tools, choppers, polyhedrons, burins and awls (Moore and Brumm 2009). Moore and Brumm (2009) emphasise that the same techniques were used on Flores as in the African Oldowan, including a predominance of freehand hard hammer percussion.

While the Holocene tools are differentiated from the Pleistocene ones by increased exposure to fire and edge glossing, the most conspicuous difference is the stark change in raw material preference (Moore and Brumm 2009). The tools associated with *H. floresiensis* are predominantly made of silicified tuff, a volcanic material readily found in the immediate vicinity of the Liang Bua cave (Moore and Brumm 2009; Sutikna et al. 2018). However, at ~50ka, chert, transported from elsewhere on the island, becomes the predominant material used, despite the fact that silicified tuff continues to be abundant (Moore and Brumm 2009). This evidence is used to support hypotheses that: 1) as small-brained hominins made these tools-types during the African early Pleistocene, their production is not outside the cognitive capacities of *H. floresiensis*; 2) at ~50ka, *H. floresiensis* was replaced by *H. sapiens*; and 3) the replacement of old technologies with new ones is not a consistent feature of global hominin evolution.

1.8.c.6. Conclusions

This model supports the hypothesis that *H. floresiensis* evolved from a more primitive hominin that maintained symplesiomorphic carpal morphology (Tocheri 2007; Tocheri et al. 2007; Orr et al. 2013). Whether this primitive hominin was *H. erectus* is unresolved, as

insufficient carpal material exists from this species. The *H. floresiensis* carpal morphology also supports the hypothesis that derived carpal configurations were not necessary to produce the earliest tool types. Finally, it also supports the hypothesis that the derived suite of carpal features characterising later *Homo* may have arisen during the Middle Palaeolithic alongside the Acheulian technocomplex (Tocheri 2007).

1.8.d. Neanderthals

Although it has been hypothesised that the subtle morphological differences between *H. sapiens* and Neanderthals indicate divergent ecology (e.g., Niewoehner, Weaver and Trinkaus 1997), the archaeological evidence and the high degree of variation within *H. sapiens* suggests drawing such a dichotomy may not be so straightforward. In the hand, hypertrophied intrinsic and extrinsic muscle insertions and broader apical tufts differentiate the Neanderthals from typical modern *H. sapiens* (Musgrave 1973; Niewoehner 2006; Trinkaus 2016). The large and flaring entheses seen on the Neanderthal pollex and fifth digit have been suggested to indicate higher grip strength than most *H. sapiens* and, therefore, a mechanical advantage for power grips over precision grips (Trinkaus and Villemeur 1991; Niewoehner, Weaver and Trinkaus 1997; Niewoehner 2001). Subtle differences in the carpometacarpal articular configurations have been used to support the hypothesis of different grip preferences in Neanderthals. The Neanderthal capitate-Mc2 facet is more radially oriented relative to the extreme distal orientation in *H. sapiens* (Riley and Trinkaus 1989; Trinkaus et al. 1991; Niewoehner, Weaver and Trinkaus 1997). Further, the Mc2 facet is larger in *H. sapiens* relative to Neanderthals, which instead have larger Mc3 facets (Niewoehner, Weaver and Trinkaus 1997). Additionally, in Neanderthals, the Mc3 styloid process is less proximally projected, resulting in a smaller degree of bevelling on the corresponding capitate surface (Riley and Trinkaus 1989; Trinkaus et al. 1991).

Niewoehner et al. (1997) argue that these differences are a result of an adaptation to differing force vectors experienced by the hand. The Mc2 joint in the Neanderthal hand is argued to be better adapted to axial rather than oblique force transfer. Therefore, their carpus would be better able to resist the forces experienced via transverse power squeeze grips, which places the tool radio-ulnarly across the palm (Niewoehner, Weaver and Trinkaus 1997). Supporting this conclusion, a recent analysis by Bardo et al. (2020) showed that the trapeziometacarpal joint configuration in Neanderthals is best suited to adducted thumb postures associated with power grips compared to the joint configuration in *H. sapiens*, which is advantageous for abducted thumb precision grips.

However, a high degree of interspecific variation among both *H. sapiens* and Neanderthals is noted within joint configuration patterns (Trinkaus 1983; Bardo et al. 2020). This variation is consistent with the large range of variation in numerous aspects of hard and soft tissue anatomy known to exist within the *H. sapiens* hand and wrist, including the axis of the DTM, carpal shape, and range of motion (Marzke, Wullstein and Viegas 1994; Wolfe, Neu and Crisco 2000; Moojen et al. 2003; Moritomo et al. 2004; Crisco et al. 2005; Rainbow et al. 2008; Buijze et al. 2011; Bain et al. 2015; Best et al. 2019; Stirling et al. 2021). Recently, Karakostis et al. (2018) analysed entheses robusticity across the hands of a historical population with highly detailed vocational records to determine whether there was a correlation between patterns of muscle robusticity and profession. It was concluded that there is a correlation between muscle attachment robusticity and occupation, as those who routinely performed power grips (bricklayers, carpenters) were statistically differentiated from those who routinely performed precision grips (tailors, painters). In this analysis, Neanderthals consistently fell among those who performed delicate precision tasks and never among those who routinely performed heavy manual workers' power grips. The authors suggest that this is functional adaptation to precision grasping in Neanderthals. Finally, the archaeological evidence does not strongly support a behavioural dichotomy between *H. sapiens* (preferring precision grips) and Neanderthals (preferring power grips). Within similar landscapes, *H. sapiens* and Neanderthals produced and used similar tool-kits (Churchill 2001; Villa and Roebroeks 2014), which included tools requiring both precision (e.g., hafted tools and sewing needles) and power (e.g., spears) grips (Hardy et al. 2013; Sykes 2015; Borel, Dobosi and Moncel 2017; Hardy et al. 2020; Blinkhorn et al. 2021).

It is important to remember that *H. sapiens* and Neanderthals are more similar to one another in their hand morphology than they are to any other extant ape (Kivell, Barros and Smaers 2013; Skinner et al. 2015; Galletta et al. 2019). Archaeological evidence suggests that *a priori* assumptions of Neanderthals being less technological or culturally advanced than *H. sapiens* are no longer valid (Rodríguez-Vidal et al. 2014; Leder et al. 2021). However, statistically significant differences in mean angles of wrist articulations have been identified (e.g., Niewoehner, Weaver and Trinkaus 1997), and as a result of these differences, Neanderthals potentially face a biomechanical disadvantage when using certain grips compared to *H. sapiens*. For example, the less developed Mc3 styloid process would make the palm more prone to injury from repeated hammering, and reduced mobility of the Mc2 might restrict the ability to forcefully oppose the thumb in some postures. It should be noted though, that in these studies, the range of variation overlap in *H. sapiens* and Neanderthals

(Niewoehner, Weaver and Trinkaus 1997; Niewoehner 2001; Bardo et al. 2020). The *H. sapiens* hand could be interpreted as the 'fine-tuning' to an increased commitment to obliquely oriented force transfer and greater reliance on precision grips; however, this does not preclude Neanderthals from habitually utilising precision grips (Trinkaus 2016). More work is needed across the entire hand to better understand whether the subtle morphological differences between *H. sapiens* and Neanderthals are functional. These differences may represent phylogenetic lag or are 'overbuilt' for their function rather than a commitment to distinctly different grips and behavioural adaptations to *H. sapiens*.

2. Materials and Methods

2.1. Materials

2.1.a. Sample

This thesis analysed 264 individual carpal bones from four carpal elements (capitate, scaphoid, lunate and triquetrum) across four extant (*Pongo*, *Gorilla*, *Pan*, *H. sapiens*) and four extinct (*A. sediba*, *H. naledi*, *H. floresiensis*, and Neanderthals) hominid taxa (Table 2.1). Although the internal structure of the capitate, lunate and scaphoid across a comparative primate sample has been analysed previously (Schilling et al. 2014), the development of whole-bone methodologies provides a new avenue for the investigation of functional adaptation in the carpus of hominids. A summary of the sample is given below in Table 2.1; Appendix A Table 8.1 gives more detail on the sample, including specimen provenance, side, and additional references.

Table 2.1 Summary of thesis sample.

Taxon	N	Sex		
		Female	Male	Unknown
<i>P. abelii</i>	3	1	2	0
<i>P. pygmaeus</i>	15	8	5	2
<i>G. beringei</i>	1	0	0	1
<i>G. gorilla</i>	18	7	10	1
<i>P. troglodytes</i>	9	2	6	1
<i>P. paniscus</i>	8	4	4	0
modern <i>H. sapiens</i>	32	6	14	12
fossil <i>H. sapiens</i> <ul style="list-style-type: none"> - Arene Candide 2 - Barma Grande 2 - Ohalo 2 - Qafzeh 9 	4	0	4	0
<i>A. sediba</i> <ul style="list-style-type: none"> - Malapa Hominin 2 <ul style="list-style-type: none"> ○ UW88_156 ○ UW88_105 	2 (from the same individual)	1	0	0
Neanderthals	5	1	3	1

- Kebara 2 - Amud 1 - Feldhofer 1 LVRB-NN21 - El Sidrón SD-1034 - Tabun C1				
<i>H. floresiensis</i> - Liang Bua 1 LB-VII-59-2003 - Liang Bua 6 LB-XI-51-2004	2	2	0	0
<i>H. naledi</i> - UW101_1730_Hand_1	1	0	0	1

2.1.a.1. *Homo sapiens*

In order to capture the known variation in bone volume among *H. sapiens*, this thesis utilises a spatio-temporally diverse sample of modern *H. sapiens*. The sample can be categorized into pre-industrialised and post-industrialised groups. While these categories provide a useful delineation to approximate mobility and intensity levels of manual behaviours, it should be noted that they are undoubtedly an oversimplification. This is particularly true for the pre-industrialised group, for which we have little primary data to understand the social and behavioural context of the societies in which they were collected. Appendix A Table 8.1 gives detailed information on provenance, curatorial organisation, sex, side and which research project each individual was included in; below, I will provide a brief overview. The pre-industrial group includes four indigenous Inuit from Greenland, two Mori-ori people from the Chatham Islands, two Aboriginal Australians, eight Nubian Egyptians, one Medieval Briton, and one Tierra del Fuegian. The post-industrialized group includes two from Syracuse, Italy, seven from Inden, Germany, and four recovered crewmen from the Mary Rose Tudor warship wreck.

Consideration was given to producing a sample with a balanced sex ratio; however, as many of these individuals came from cemeteries or historical collections with poor provenance records, sex could not always be determined, and 12 individuals had unknown sex. In total, six females and 14 males were confidently identified in this sample. The two Mori-ori individuals from the Duckworth Collection may be female, as a publication by W. Duckworth (1900) outlines that two skeletons recovered from the Chatham islands are female. However, since the hand bones can no longer be associated with a pelvis or skull for independent analysis, I have classified them as unknown sex. Another factor contributing to the sex imbalance is the inclusion of the Mary Rose collection. All of these specimens are classified

as male as it was not customary for women to be aboard a warship, and no analysed material indicative of female sex has been observed (Stirland 2005).

Consideration was also given to producing a sample with a balanced ratio of lefts and rights; however, sample constraints reduced the number of left hands available for analysis. Across the whole sample, there were 15 right, and 15 left capitates, and from the proximal row carpus (scaphoid, lunate, triquetrum), six left hands and 11 rights. The role of the hands during tool manufacture and use is bilaterally differentiated; however, it has been demonstrated that the biomechanics are not (Key and Dunmore 2015; Karakostis et al. 2018; Kaufman-Cohen et al. 2018). Thus it could be expected that signals of loading may be higher in the right hand sample, but relative patterns across the three bones may be similar between the two sides.

Capitates from archaeological collections were also included in this thesis. Firstly, there are four late Pleistocene *H. sapiens*⁷, Qafzeh 9, Ohalo II, Barma Grande 2, and Arene Candide 2. Regarding preservation, Qafzeh 9 has significant cortical and trabecular erosion at the proximodorsal region, at the lunate articular surface. Ohalo 2 and Arene Candide 2 have mild cortical erosion on the distal articular surface. Barma Grande 2 has no damage.

2.1.a.2. Non-human hominid

This thesis includes four non-human hominid genera. Appendix A Table 8.1 gives detailed information on the curatorial organisation, sex, side and which research project each individual was included in; below, I will provide a summary. The total sample of *Pan* includes 11 *P. troglodytes* and eight *P. paniscus*. The total sample of *Gorilla* has 18 *G. gorilla*, and one *G. beringei*. The total sample of 18 *Pongo* includes four *P. abelii*, and 15 *P. pygmaeus*. Three *P. pygmaeus* are captive zoo animals. All other non-human hominids in this sample were wild shot. The inclusion of zoo animals is a potential limitation as captive animals may not have the capacity to perform behaviours at the same proportions as their wild counterparts. However, as detailed in section 1.4.f.1, small sample sizes are a particular limitation of this research, and thus the decision was made to include zoo animals to produce the largest sample size possible.

⁷ Only three of these specimens were included in analysis as Qafzeh 9 was excluded due to preservation, but I include it here as it was prepared for analysis and is included in Appendix A Figure 8.1, detailing the segmentation processes.

2.1.a.3. Extinct hominin genera

The sample includes capitates from four genera of extinct hominins, *A. sediba*, *H. floresiensis*, *H. naledi* and Neanderthals⁸. See Appendix A Table 8.1 for more information on provenance, sex and age. Three Neanderthal capitates derive from Israel: Tabun C1, Amud 1, and Kebara 2. Two Neanderthals derive from Europe: El Sidrón SD-1034 and Feldhofer 1 LVRB-NN21. Regarding preservation (Figure 2.1), the distodorsal surface of Amud 1 is missing; it also has small amounts of surface erosion on the proximal head. LVRB-NN21 has significant cortical erosion on the proximal head at the dorso-lunate articular surface. Moderate cortical erosion is also seen at the disto-palmar, disto-dorsal and proximo-palmar regions. SD-1034 has moderate cortical erosion on the proximodorsal surface, and a crack is also seen at the scaphoid articular surface. Kebara 2 and Tabun C1 have no damage.

⁸ Only three of these specimens were included in analysis as the two Spanish Neanderthals were excluded from analysis due to preservation, but I include them here as they were prepared for analysis and are included in Appendix A Figure 8.1, detailing the segmentation processes.

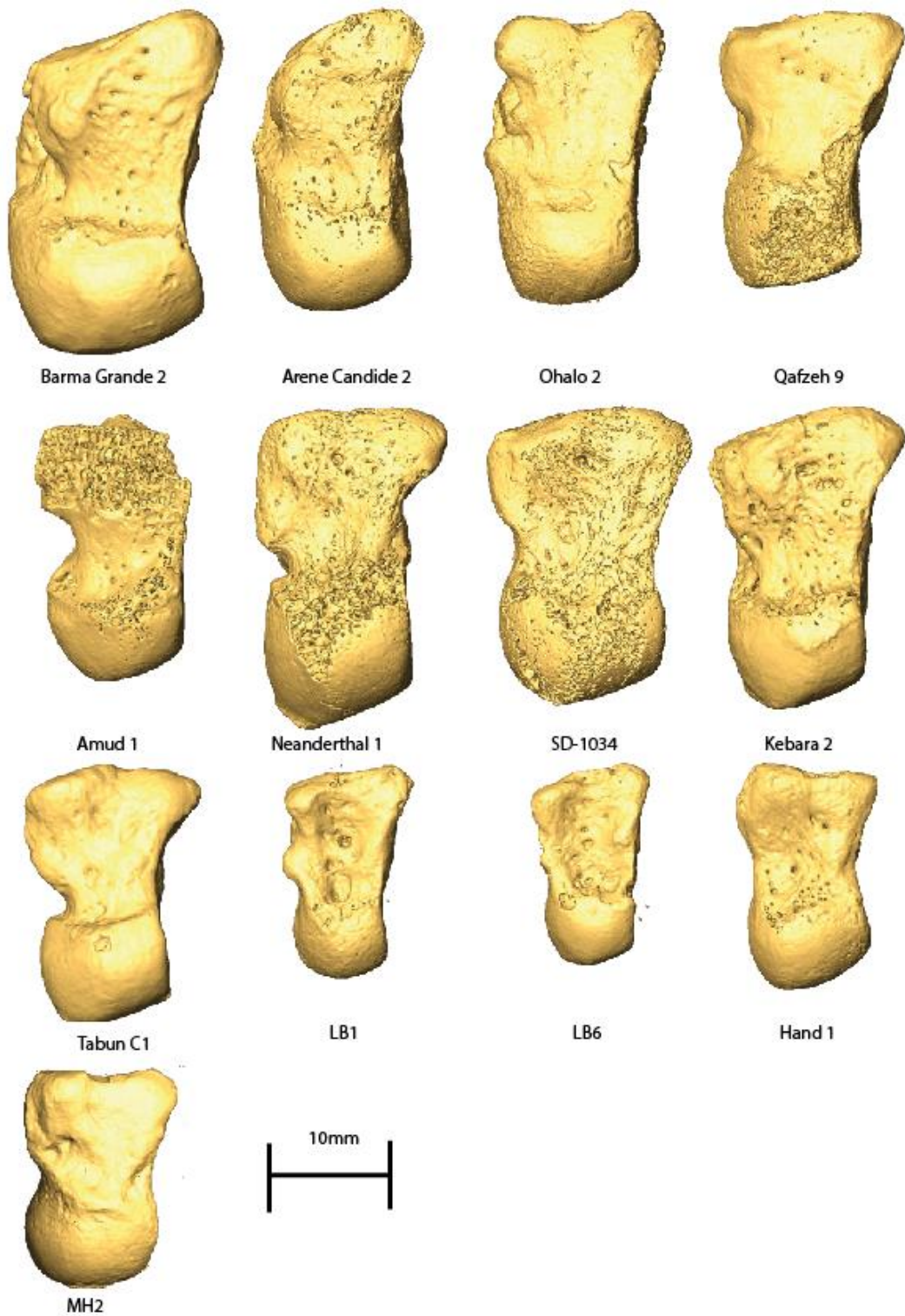


Figure 2.1 Surface models of the 14 fossil specimens. The dorsal surface is shown, and the radial side is to the left. Left capitates have been flipped. Images are to scale.

The *H. floresiensis* material consists of two capitates from LB1 and LB6, both interpreted as female, originating from the Liang Bua caves on the Indonesian island of Flores, dated to 100-

60ka (Sutikna et al. 2016). LB1 has a portion missing at the disto-palmar surface and cortical erosion on the proximo-palmar head. LB6 has no damage. The *H. naledi* material includes a single capitate from the South African dinaledi hominin, Hand 1, dated at 235-335ka (Dirks et al. 2017). This capitate has two regions of moderate cortical erosion at the proximo-palmar head and disto-palmar surface. Finally, the left and right capitate from the 1.9ma *A. sediba* specimen MH2 from Malapa, South Africa (Dirks et al. 2010; Pickering et al. 2011). Both specimens have no damage.

2.1.a.4. Computed tomography

Specimens were scanned using micro-computed tomography (μ -CT). Conventional x-rays produce 2D images that average the attenuation of materials within the specimen. This results in a loss of dimension and a loss of detail between different material elements of the scan (Buzug 2011). Computed tomography (CT) improves the traditional x-ray by taking images from different angles, allowing a 3D reconstruction and more accurate and nuanced delineation between different material densities within an object (Buzug 2011). However, the resolution of medical-grade CT has proven incapable of accurately quantifying and differentiating between individual trabeculae as voxel size is typically the same or greater than the thickness of one trabecula strut (Fajardo and Müller 2001 and references therein). The development of μ -CT reduced the voxel size of a scan to below 100 μ m (Buzug 2011). Two decades of research have established that trabecular architecture can be accurately quantified with a resolution of less than 60 μ m, making μ -CT an ideal method for data collection (Müller et al. 1996; Müller et al. 1998; Isaksson et al. 2011; Christen et al. 2016).

All extant specimens were scanned with either a BIR ACTIS 225/300 high-resolution microCT scanner or a Diondo D3 high-resolution microCT scanner at the Department of Human Evolution, Max Planck Institute for Evolutionary Anthropology, Germany, or a Nikon 225/XTH scanner at the Cambridge Biotomography Centre, University of Cambridge, United Kingdom. Specimens were scanned with an acceleration voltage of 100-160 kV and 100-140 μ A using a 0.2-0.5mm copper or brass filter. Images were reconstructed as 16-bit volumetric TIFF stacks. For modern *H. sapiens*, the scan resolution was between 0.20 and 0.44 microns. For extant non-human hominids, it was between 0.025 and 0.048 microns. For fossil specimens, the scan resolution was between 0.021 and 0.035 microns. Differences in the ranges are due to different scan setups and scanning conditions. After scanning, images were reoriented into approximately the same orientation using Avizo 6.0 or 9.0 (Visualization Sciences Group, SAS).

The reoriented images are then segmented into binary images representing only bone and background voxels (Figure 2B). The medical image analysis (MIA) clustering method (Dunmore, Wollny and Skinner 2018) was used to segment the μ -CT scans and to remove extraneous non-bone material such as soft tissue, curatorial material such as glue, or soil matrix. MIA was used because it has been shown to produce accurate material segmentation while reducing subjective input parameters via a semi-automated, machine learning-based approach to material delineation (Dunmore, Wollny and Skinner 2018).

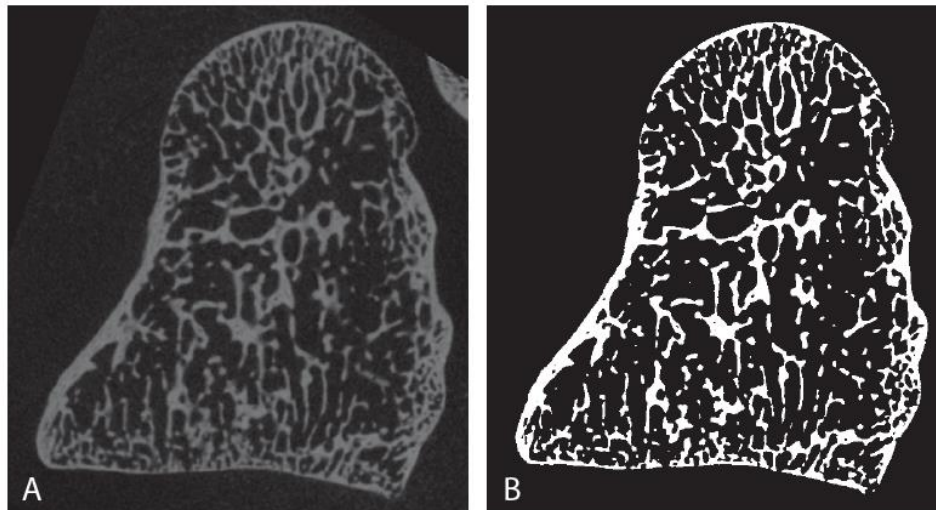


Figure 2.2 Segmentation of capitata by MIA.
A) original micro-CT scan. B) Result of MIA segmentation.

Figure 2.2 shows the original μ CT scanned image and the result of MIA segmentation. MIA requires the user to define the number of materials to be identified and grid size to iteratively perform k-means algorithms and fuzzy c-means clustering. The image is divided into the user-defined grid, and the MIA program first applies the k-mean algorithm to sort the greyscale densities into groups based on the number defined by the user (Dunmore, Wollny and Skinner 2018). Fuzzy c-means clustering then identifies which voxels belong to the same class based on their greyscale value. A class is defined such that each member should be as similar to one another as possible and as dissimilar as possible to non-members (Pham and Prince 1999; Dunmore, Wollny and Skinner 2018). As class membership is based on the probability that a particular voxel belongs to that class, i.e., it is 90% likely this voxel is grey, and 10% likely this voxel is white (Dunmore 2019), this probability threshold can be manipulated by the user such that class membership is highly restrictive (high probability threshold) or more inclusive (lower probability threshold). MIA will output a binary, trinary, quaternion, etc., depending on the number of classes specified. The labelsfield feature of Avizo 6.3

(Visualization Sciences Group, Berlin, Germany) is used to isolate the bone material and save the image stacks as a binary .raw file for data collection.

As segmentation is based on differentiating materials by their greyscale values, scans that have low differentiation between material densities or highly heterogeneous materials may be challenging to segment. This challenge is frequently encountered in fossil specimens due to fossilisation and taphonomic processes. The steps taken to segment each fossil are illustrated in Appendix A Figure 8.1. Each fossil was segmented with an individualised protocol to produce the best segmentation with minimal manual cleaning, although in a few specimens (*H. naledi* capitate, SD-1034 capitate, LB1 and LB6 capitate), manual cleaning was applied. Alongside MIA, the in-built functionality of Avizo 6.3 was used to segment difficult fossils. This includes the 'Remove Islands' (Figure 2.3A) and 'Smooth Labels' (Figure 2.3B) functions, which identify voxels connected to larger regions by fewer than a user-defined number of voxels, for example, 15. This results in small accretions on the edges of trabeculae or 'islands' being removed. In some circumstances, a median filter kernel (Figure 2.3C) was also applied. By applying a kernel across the scan, small irregularities within the trabeculae, such as cracks or small amounts of accretion, are removed. All fossil segmentations were performed by myself and approved by M. Skinner, T. Kivell and C. Dunmore.

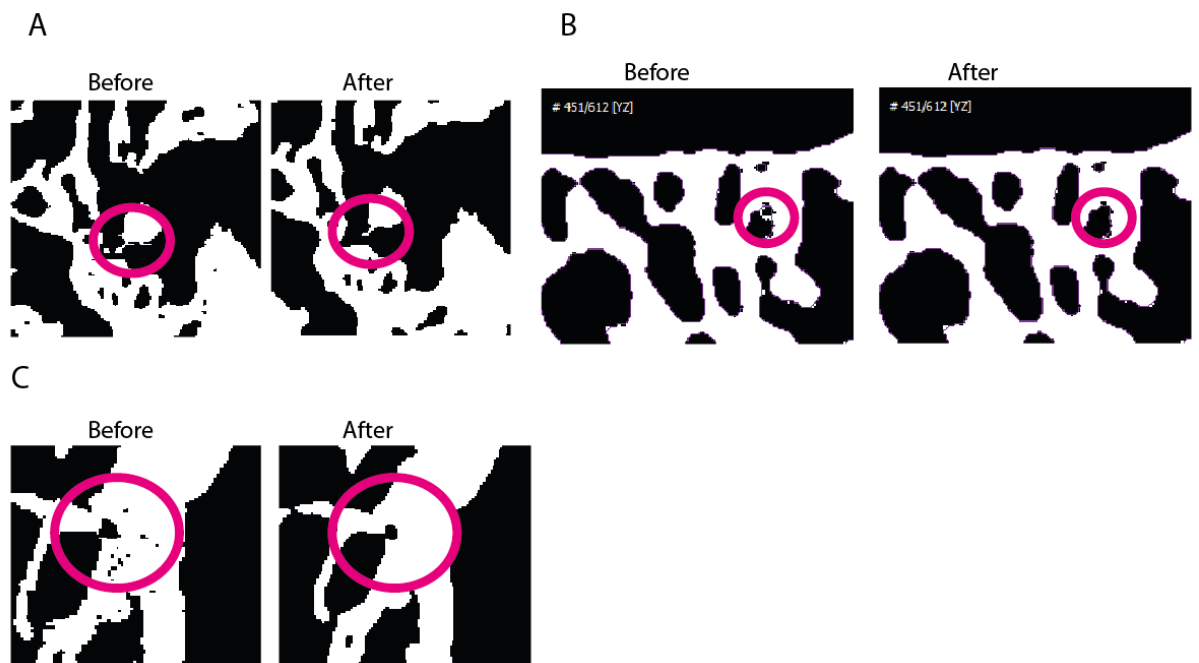


Figure 2.3 Three examples of functions used in Avizo to clean fossil segmentations. A) Remove Islands function. B) Smooth labels function. C) Median filter.

2.2. Methods

2.2.a. Data collection

This thesis explores the application of whole-bone methodologies to detect functional adaptation signals in the carpus of hominids. Whole-bone trabecular bone analysis is an expansion of previous methods that analysed a single volume-of-interest, or VOI, from within the trabecular network (Figure 2.4A). In contrast, whole-bone methodologies can quantify trabecular (and/or cortical) architecture within an entire bone by iteratively applying numerous VOIs (sometimes hundreds depending on the region's size). Figure 2.4 illustrates the differences between single VOI and whole-bone methodologies. For a single VOI (A), a spherical 3D volume is identified, and the architecture within this sphere can be analysed (represented by the rainbow scalar). In a whole-bone methodology (B), the entire trabecular space is quantified (represented by the rainbow scalar).

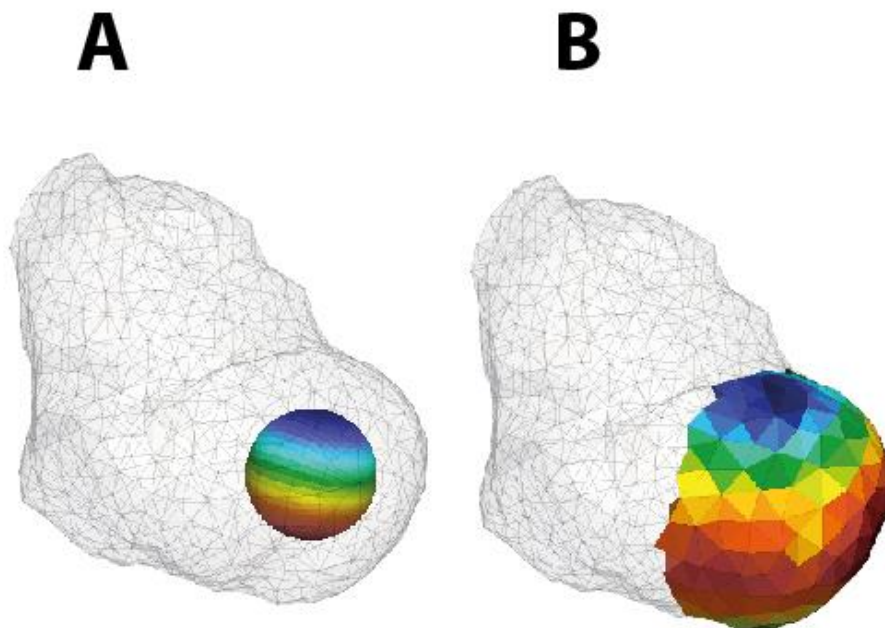


Figure 2.4 Illustration of whole-bone methodologies versus VOI methods.

A) illustrates the extractive VOI method. A 3D portion of bone (rainbow sphere) is extracted from the region of interest (proximal capitate). B) illustrates the whole-bone method. The entire region of interest (proximal capitate) can be quantified and analysed.

All trabecular and cortical parameters were collected using medtool 4.3(<http://www.dr-pahr.at/medtool/>), a software package allowing whole-bone analysis. An in-house script run through medtool applies a series of morphological filters to define and analyse the cortical, trabecular, internal and background regions of a micro-CT scan in three dimensions. Medtool

outputs a number of volumetric image stacks, each of which has had different filters applied. These image stacks will be identified in ***bold and italics***. Detailed descriptions of this workflow are outlined in Gross et al. (2014) and Pahr and Zysset (2009a, b) and a summary will be given below.

After MIA segmentation, a binary image stack is produced in which bone voxels can be classified as 1 (white) and non-bone voxels classified as 0 (black). To identify the outer contour of the bone, arbitrary mathematical rays are cast from the edges of the scan and move inwards. When the ray reaches a bone voxel, movement stops. In order to define and delineate the trabecular and cortical regions, small holes (pores) in the cortical bone are identified and artificially filled as bone, resulting in the ***close*** image stack (Figure 2.5C). By first identifying and filling pores, the rays are able to continue moving inwards until inter-trabecular space is identified. If pores are not first filled, the cortical bone would be artificially thinned (Pahr and Zysset 2009b). To produce this result, medtool must be able to identify the difference between a black voxel representing a pore in the cortex and a black voxel representing space between trabeculae. Medtool makes this differentiation using a kernel. A kernel is a mathematical matrix imposed upon all of the voxels in the original binary segmentation to produce a new image filtered by that mathematical matrix. The kernel's physical size is defined as the radius of a sphere in voxels and requires the trabecular thickness and voxel size of the scan. The kernel size (k_c) is defined in the below formulae (as per Gross et al. 2014) whereby $Tb.Th$ refers to the trabecular thickness, and Vox refers to the size of voxels (resolution) in the scan. By using the individual $Tb.Th$ and voxel size, the kernel is smaller than the trabeculae struts and will only close holes smaller than one trabeculae, ensuring that it does not artificially fill space between trabeculae.

Formulae for the ***close*** and ***OuterMask***:

$$k_c = \text{floor}\left(\frac{Tb.Th}{2*Vox}\right)$$

Formula for the ***InnerMask***:

$$k_1 = \text{floor}\left(\frac{Tb.Th}{Vox}\right)$$

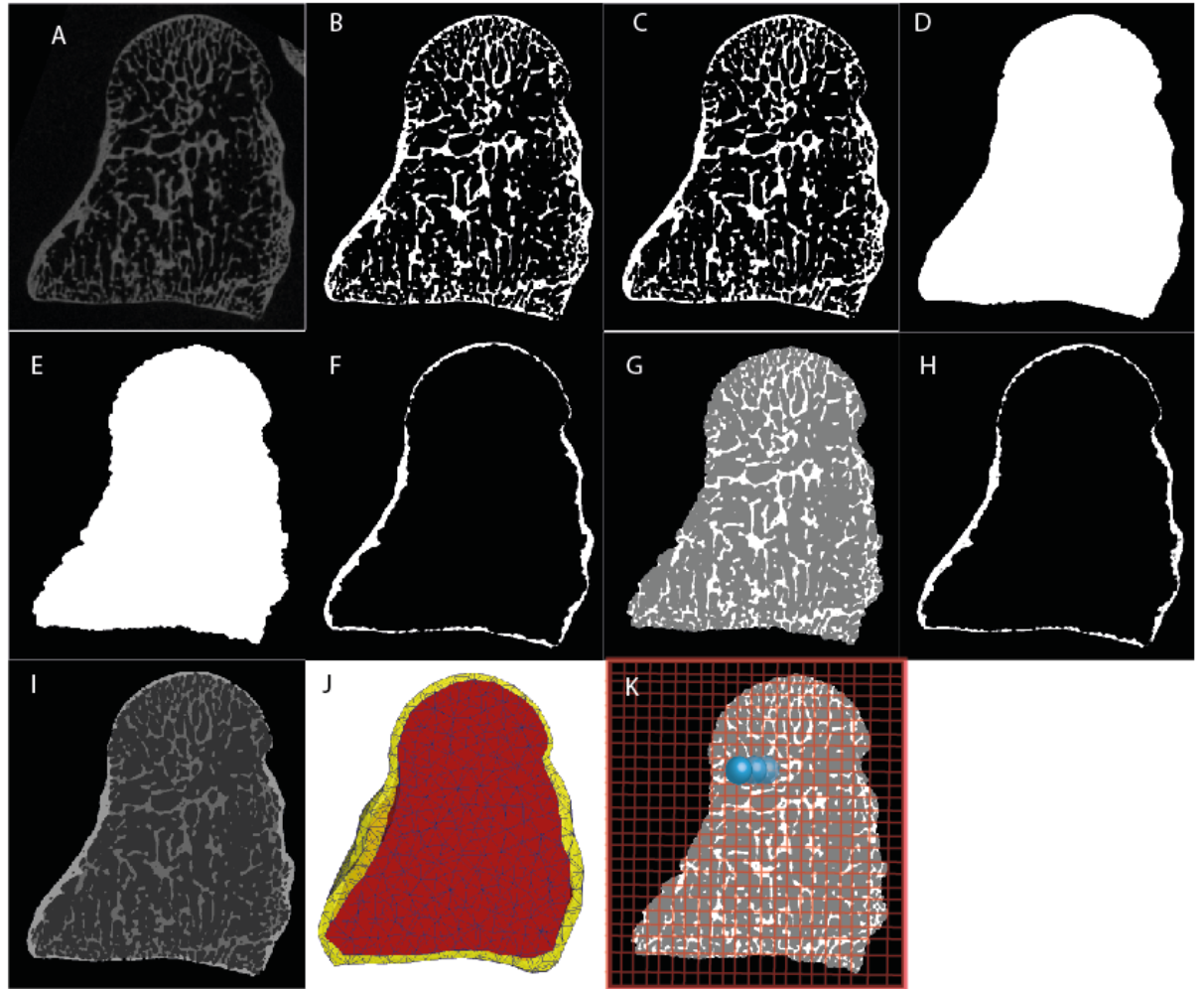


Figure 2.5 Workflow of medtool for whole-bone data collection for the binary and tissue segmentation of a μ ct scan.

Steps A-B are part of the MIA binary segmentation, while C-I are part of the tissue segmentation. A) original micro-CT scan. B) Result of the MIA binary segmentation process. C) Close filter applied to close small pores in the cortical bone. D) **OuterMask**. E) **InnerMask**. F) **ThicknessMask**. G) **MaskSegIn**. H) **MaskSegOut**. I) **MaskSeg**. J) Tetrahedral mesh filling **MaskSegOut** and **MaskSegIn** regions. K) Representation of the 3D grid placed over the **MaskSegIn**, with a sampling sphere (blue) moving from node to node to collect data.

Secondly, medtool creates an **OuterMask** (Figure 2.5D). The **OuterMask** is defined using the **close** image stack. Rays detect the outer contour of the whole bone, and as such, the image stack defines the overall geometry of the bone. Next, the **OuterMask** kernel (k_o) is defined using the same formula as the **close** mask kernel (k_c). Next, an **InnerMask** is defined (Figure 2.5E). The **InnerMask** is similar to the **OuterMask** in that it defines the 3D geometric limitations of the trabecular bone region within the whole bone. Finally, a **ThicknessMask** is created (Figure 2.5F). Simply, this is a mask of the cortical bone thickness only (with the closed pores) and is created by subtracting the **InnerMask** from the **OuterMask**.

Medtool interpolates these image stacks into three final stacks, which are passed for analysis. **MaskSegIn** (Figure 2.5G) has had the **ThicknessMask** removed, leaving only the trabecular bone and internal marrow; **MaskSegOut** (Figure 2.5H) has had the **InnerMask** removed, leaving only the cortical bone (including pores); and **MaskSeg** (Figure 2.5I) which maintains all elements of cortical bone and pores, trabeculae and internal marrow. These final 3D image stacks have a unique scalar applied to the external background of the scan, the cortical bone, the trabecular bone and the internal 'air' or marrow voxels. It is important to note that cortical pores are maintained in these final interpolated image stacks and therefore, for data collection. Medtool identifies the boundary on an artificially non-porous image stack (the **close**) and then superimposes this boundary onto the original image stack. Pores within cortical bone play an important part in overall bone strength and elasticity and are therefore integral to accurately interpreting bone volume (Cooper et al. 2016).

The CGAL 4.9 mesher is then applied to the **InnerMask** and **ThicknessMask** to create a finite element model of the cortical and trabecular area (Figure 2.5J). The mesh contains no architectural information, but it is this mesh onto which we can interpolate the material property data. The mesh is optimised through a series of iterative processes to ensure a smooth boundary, with no overlap or holes between the tetrahedra. Tetrahedra are preferred to a hexahedron as the geometry results in a smooth boundary and less loss of trabecular architectural information (Müller and Rüeegsegger 1995; Ulrich et al. 1998; Alberich-Bayarri et al. 2007). In order to collect material property data, a 3D grid with 2.5mm cells is placed as a bounding box over the **MaskSegIn** or **MaskSegOut** image stacks (Figure 2.5K). Next, a 5mm sampling sphere moves between the grid nodes across the entire bounding box, iteratively measuring trabecular parameters.

2.2.a.1. Trabecular parameters

The strength of bone is principally determined by bone volume and degree of anisotropy (DA), which explains up to 98% of Young's modulus (stiffness) of the bone (Cotter et al. 2009; Maquer et al. 2015; Hart et al. 2017). In this study, bone volume is calculated as the ratio of bone voxels to non-bone voxels (BV/TV) within each sampling sphere, which is then averaged for the entire bone or region. The measurement of Total BV/TV includes the cortical bone and is described in section 2.2.c below. BV/TV is determined by a combination of trabecular thickness (Tb.Th), trabecular separation (Tb.Sp), trabecular number (Tb.N) and if measuring 'Total BV/TV' cortical thickness (Ct.Th) as well. Their calculation is also dependent on one another. For example, the computation of Ct.Th, Tb.Sp and Tb.Th are all calculated using the Hildebrand and Rüeegsegger thickness computation algorithm (1997). Spheres are grown

within cortical or trabecular bone, and thickness is measured as the largest sphere that fits within that bone region. To calculate Tb.Sp, medtool inverts the scalar values of the **MaskSegIn** so that the internal air voxels are now represented by the bone scalar (1). Spheres are grown within the internal voxels and calculated in the same way. In this way, Tb.Th and Tb.Sp are the inverse of one another. Tb.N is calculated using Tb.Th and Tb.Sp and is made via the formula $1/(Tb.Th+Tb.Sp)$. Further, Tb.Th, Tb.Sp and Tb.N have been demonstrated to be sensitive to allometric and genetic factors (see section 2.2.g). On the other hand, BV/TV and DA have often been demonstrated to be largely independent of body mass (Cotter et al. 2009; Doube et al. 2011; Barak, Lieberman and Hublin 2013; Christen, Ito and van Rietbergen 2015). Further, studies that have regressed the two measures against one another have found them to be uncorrelated (Tsegai et al. 2013; Georgiou et al. 2018; Kivell et al. 2018b; Tsegai et al. 2018; Komza and Skinner 2019).

DA is calculated using the Mean Intercept Length (MIL) method (Whitehouse 1974). A value constrained between 0 (complete isotropy) and 1 (complete anisotropy) is produced via the formula $1 - (\text{min. eigenvalue}/\text{max. eigenvalue})$. DA can provide strength in two ways; highly aligned trabeculae (high DA) provide strength along the axis of alignment, while highly diffuse trabeculae (low DA) provide strength across multiple different origins of force. In sum, BV/TV and DA explain up to 98% of stiffness (Maquer et al. 2015) and thus provide considerable information about the biomechanical structure of bone. While Ct.Th, Tb.Th, Tb.Sp, and Tb.N are included in Bird et al. (2021); based on the above discussion, they were not included in subsequent studies.

2.2.b. Data visualisation

Medtool 4.3 outputs quantitative data as well as options for the visualisation of that data. Firstly, by aligning the finite element mesh with the sampling sphere nodes, BV/TV and DA results can be interpolated onto the mesh to produce a graphical representation of these parameters (Figure 2.6A and B, respectively) (Pahr and Zysset 2009b; Tsegai et al. 2013; Gross et al. 2014). These interpolated meshes are visualised in Paraview (3.98.0; Sandia Corporation, Kitware, Inc). Maps of cortical or trabecular thickness can be visualised (Figure 2.6C) using the 3D Volume Viewer plugin (<http://rsb.info.nih.gov/ij/plugins/volume-viewer.html>) for ImageJ (1.50b) (<https://imagej.nih.gov/ij/>) although as of 2022, this plugin is no longer supported.

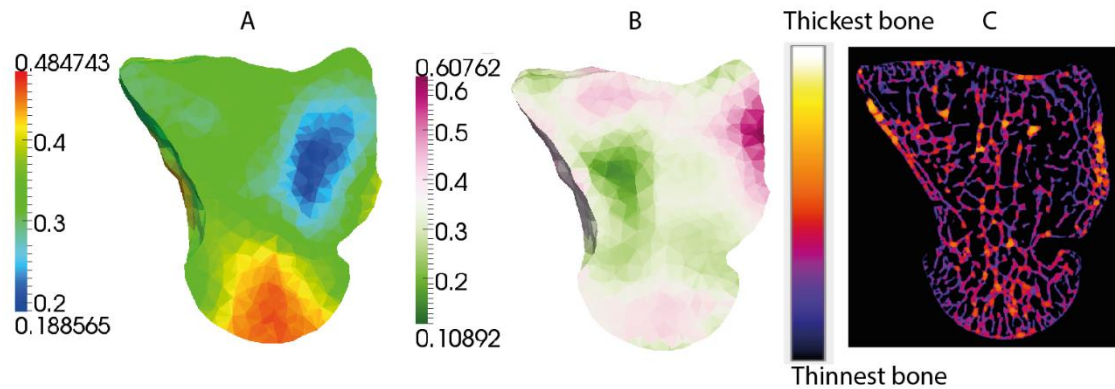


Figure 2.6 Examples of visualisations of medtool data.
 A) Map of BV/TV (%) distribution; B) Map of DA (0-1); C) Maps of cortical or trabecular thickness.

2.2.b.1. BV/TV visualisation relative and absolute values

By default, BV/TV is visualised on an absolute scale (Figure 2.6A). Therefore, the values represented by the scale bar are different for every specimen. Absolute data is useful for understanding mean BV/TV differences between individuals and species; however, it is known to differ systemically between species and have a large range of variation between hominids (Tsegai et al. 2013; Tsegai et al. 2018). Outliers also influence absolute scales in the data. Relative scales mitigate these issues. By dividing each node value by the mean, values are normalised so that mean BV/TV is represented by one (1) on the scale bar. This provides critical and easy-to-interpret visual information on where bone volume has increased or decreased relative to the mean. Figure 2.7 compares the same BV/TV data from a *H. sapiens* scaphoid represented on a relative (A) and absolute (B) scale.

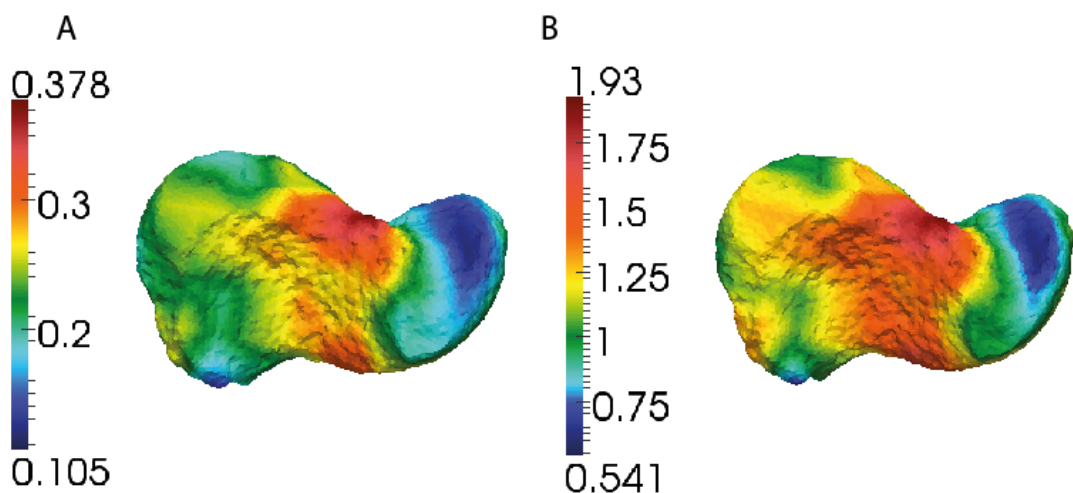


Figure 2.7 Visualisation options for BV/TV in a *H. sapiens* scaphoid. Scaphoids are visualised using an absolute (A) and relative (B) scale. In B, the value of 1 represents the mean BV/TV for that individual.

2.2.c. Customising the medtool workflow

Up to this point, I have described the standard workflow for collecting data using medtool 4.3. However, during data analysis, there were a number of instances where I customised the standard workflow. These will be detailed in the next section.

2.2.c.1. Partitioning bones

In Chapter 3, trabecular and cortical parameters were calculated separately for the proximal and distal regions. The capitate was partitioned within medtool 4.3 via an in-house plugin script. This script instructs medtool to split the tetrahedral mesh at a user-defined point in the bone. The 2.5mm 3D grid is then applied to the partitioned mesh zone separately; data collection runs again as normal on this section only of the **MaskSeg**, **MaskSegIn** or **MaskSegOut**.

2.2.c.1.1. Partitioning bones repeatability study

A repeatability study was run on the capitate to test whether variability in slice choice may affect parameter results. One right capitate was chosen for each of the *Pongo*, *Gorilla*, *Pan* and *Homo* groups. The capitate was partitioned at the most distal aspect of the lunate articulation on the capitate head, as seen in the dorsal view (this cut is defined in detail in Bird et al. (2021). This was identified as Cut 0 (Table 2.2). Additional partitions were made three slices more distal (Cut 1), three slices more proximal (Cut 2), 10 slices more distal (Cut 3) and 10 slices more proximal (Cut 4) from Cut 0. Data was collected for BV/TV and DA in the proximal and distal regions of each variation in the partition.

Table 2.2 Specimens used in the repeatability study

Specimen	Slice number in the Z-axis (Cut 0)
<i>H. sapiens</i> NHMW_K24-2	345
<i>P. paniscus</i> MRAC_29045	350
<i>G. gorilla</i> ZMB_Mam_83530	321
<i>P. pygmaeus</i> ZSM_1907_0633b	391

Table 2.3 Results of repeatability study

Taxa	Cut	Distal BV/TV (%)	Distal DA (0-1)	Proximal BV/TV (%)	Proximal DA (0-1)
<i>Homo</i>	0	0.199	0.195	0.214	0.266
	1	0.200	0.195	0.214	0.270
	2	0.200	0.196	0.214	0.270
	3	0.200	0.194	0.216	0.265

	4	0.200	0.197	0.214	0.271
<i>Pan</i>	0	0.329	0.258	0.345	0.240
	1	0.329	0.258	0.346	0.240
	2	0.330	0.258	0.345	0.240
	3	0.329	0.259	0.345	0.239
	4	0.330	0.258	0.346	0.240
<i>Gorilla</i>	0	0.280	0.231	0.310	0.152
	1	0.280	0.232	0.310	0.152
	2	0.280	0.231	0.310	0.153
	3	0.279	0.234	0.309	0.151
	4	0.281	0.229	0.310	0.154
<i>Pongo</i>	0	0.416	0.270	0.508	0.274
	1	0.416	0.270	0.507	0.274
	2	0.416	0.270	0.508	0.273
	3	0.416	0.269	0.505	0.274
	4	0.416	0.270	0.510	0.273

Table 2.4 Descriptive statistics of repeatability study

Taxa	Region	Standard deviation	Min-Max	Difference between minimum and maximum
<i>Homo</i>	Distal BV/TV	<0.001	0.199-0.200	0.001
	Distal DA	<0.001	0.196-0.197	0.002
	Proximal BV/TV	<0.001	0.214-0.216	0.002
	Proximal DA	0.002	0.265-0.271	0.006
<i>Pan</i>	Distal BV/TV	<0.001	0.329-0.330	<0.001
	Distal DA	<0.001	0.258-0.259	0.001
	Proximal BV/TV	<0.001	0.345-0.346	<0.001
	Proximal DA	<0.001	0.239-0.240	0.001
<i>Gorilla</i>	Distal BV/TV	<0.001	0.279-0.281	0.001
	Distal DA	0.001	0.229-0.234	0.004
	Proximal BV/TV	<0.001	0.309-0.310	<0.001
	Proximal DA	0.001	0.151-0.154	0.003
<i>Pongo</i>	Distal BV/TV	<0.001	0.416-0.416	<0.001
	Distal DA	<0.001	0.269-0.270	0.001
	Proximal BV/TV	0.001	0.505-0.510	0.005
	Proximal DA	<0.001	0.273-0.274	0.001

Results indicate that there was little variation in BV/TV or DA results across the slices (Table 2.3). Across all taxa and parameters, the standard deviation between the five results was consistently <0.01. Similarly, across all taxa and parameters, the difference between the maximum and minimum was <0.01 (Table 2.4). As this variation was consistently low, further sampling and statistical testing were not pursued. It was concluded that potential variation

between researchers on slice selection is not likely to substantially alter the results of the study.

2.2.c.2. Bounding boxes

Pahr and Zysset (2009b) note medtool encounters issues when segmenting 'c-shaped' contours within bone, in other words, shapes with a >45 degree concavity. This is because the rim of the concavity blocks some of the rays from reaching the inner contour. Bounding boxes were developed by Georgiou et al. (2018) to improve poor cortical-trabecular separation at c-shaped contours found in the intercondyloid fossa of the distal femur. This same method was applied to c-shape issues found at the highly concave capitate waist of non-human hominids. Using Avizo 6.3, the user can identify the 3D coordinates of a bounding box that encapsulates the concavity. Medtool 4.3 uses these coordinates to re-run the ray casting process, with the origin of the ray from within the bounding box rather than at the edges of the scan. The process is iterated 15 times and the final result is checked by the user (Georgiou et al. 2018).

2.2.c.3. Total BV/TV

Conventionally, medtool 4.3 measures bone volume from the **MaskSegIn**. This means our result is a ratio of trabecular bone to internal air voxels. It is possible to make this measurement on the original MIA output file, in other words, to measure BV/TV with trabecular and cortical bone combined. This provides a ratio of trabecular and cortical bone voxels to internal air voxels (referred to in this thesis as Total BV/TV). There are benefits and limitations to this approach which are discussed in detail in Chapter 3; however, methodologically, c-shape and tissue segmentation issues (Discussed below in section 2.2.c.4.1) are resolved, as medtool does not need to identify the cortical-trabecular boundary prior to analysis.

2.2.c.4. Closing kernel size

One underlying assumption of the medtool 4.3 methodology is that pores within the cortex region will be less than the thickness of one trabecular strut. This assumption is used to define the **close** and **OuterMask** kernel. It has been shown experimentally to produce consistent and reliable segmentation of trabecular and cortical regions in the femoral head (Pahr and Zysset 2009b; Georgiou et al. 2019), metacarpals (Tsegai et al. 2013; Dunmore et al. 2019), first metatarsal (Komza and Skinner 2019) and humeral head (Kivell et al. 2018b) across a range of hominoids. However, unusual morphology at the cortical-trabecular boundary of carpal bones appeared to undermine this assumption of the methodology.

2.2.c.4.1. Segmentation issues: A study

A study was undertaken in order to better understand how to accurately and consistently segment the unusual tissue morphology shown in some carpals. Medtool 4.3 uses a local calculation of trabecular thickness to differentiate cortical pores and inter-trabecular space. If holes are smaller than half the mean thickness of trabeculae, they will be classified as cortical pores, and the bone surrounding this pore will be classified as cortical bone. Cortical bone will continue to be classified until a space larger than mean trabecular thickness is identified. Highly porous cortices can undermine our ability to identify a smooth and accurate cortical-trabecular boundary.

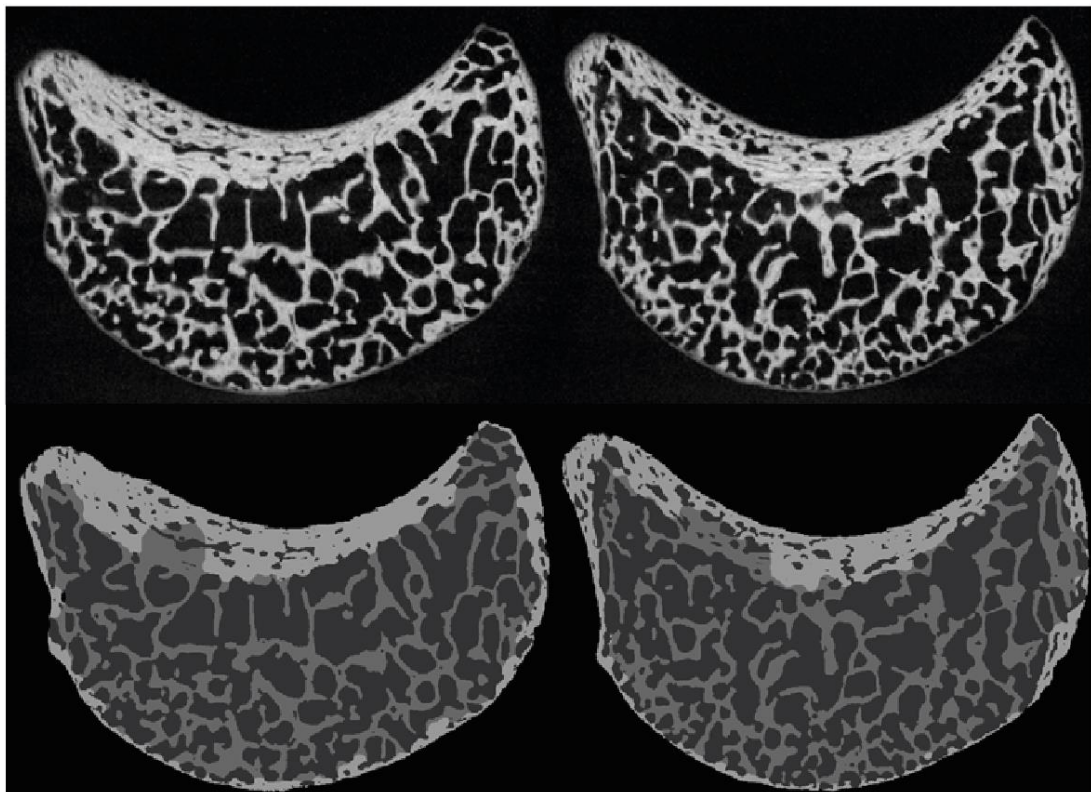


Figure 2.8 A *H. sapiens* lunate showing thick and porous tissue morphology at the capitate articular surface.

Top row: two slices from the original micro-CT scan. Bottom row: the same two slices from the top row after tissue segmentation with a kernel size of 4.

As seen in Figure 2.8, bone at the distal lunate (capitate articular surface) is both extremely thick and porous; many specimens across all analysed genera exhibited this morphology. While a histological analysis would be able to differentiate between the two tissues, medtool 4.3 is unable to differentiate between extremely porous cortex and thick trabeculae. Figure 2.8 shows two different slices from a *H. sapiens* lunate (DCW_AM_3_0_2) that have been segmented with four kernel sizes. In some areas, the thick block of distal bone is identified

entirely as cortical bone, while in other regions, where the pores are slightly larger, the thick block is identified as trabecular bone.

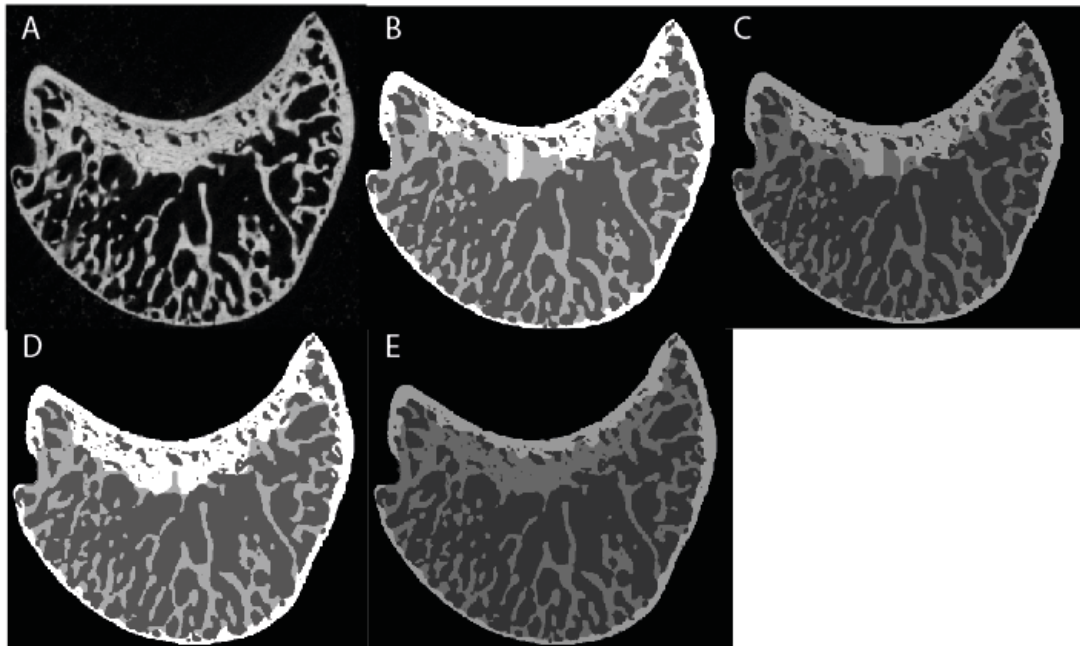


Figure 2.9 A *Pongo* lunate illustrating the effects of different kernel sizes on tissue segmentation.

A) the original micro-CT scan; B) Segmentation with a kernel size of 3; C) Segmentation with a kernel size of 4; D) Segmentation with a kernel size of 5; E) Segmentation with a kernel size of 5 combined with a close kernel of 2.

One of the strengths of medtool 4.3 is that it removes some subjectivity in deciding where to draw the border between cortical and trabecular bone. However, the extremely porous bone at the trabecular-cortical boundary undermines some of the assumptions. Fixing these segmentations requires additional user input on how to alter the medtool script to improve segmentation. In order to reduce user assumptions about what should or should not be included in the cortex or trabecular segment, segmentation parameters which provide the smoothest boundary between tissues should be chosen. In the above example (Figure 2.9), the kernel size is iteratively enlarged in each segmentation of a *Pongo* lunate. Each time the kernel size increases, more of this thick distal region is identified as cortical bone. However, when the kernel size is large enough to identify the entire block as cortical bone, trabeculae within the palmar beak (Figure 2.9D) is misidentified as cortical bone. Figure 2.9E uses a combination of kernel sizes during the masking process and is the only result with a consistent and smooth internal boundary. Figure 2.10 models the trabecular structure of a specimen with tissue segmentation issues. Features of irregular segmentations are seen, such as holes at the edges of the lunate beaks, irregular peaks and pitted trabecular regions.

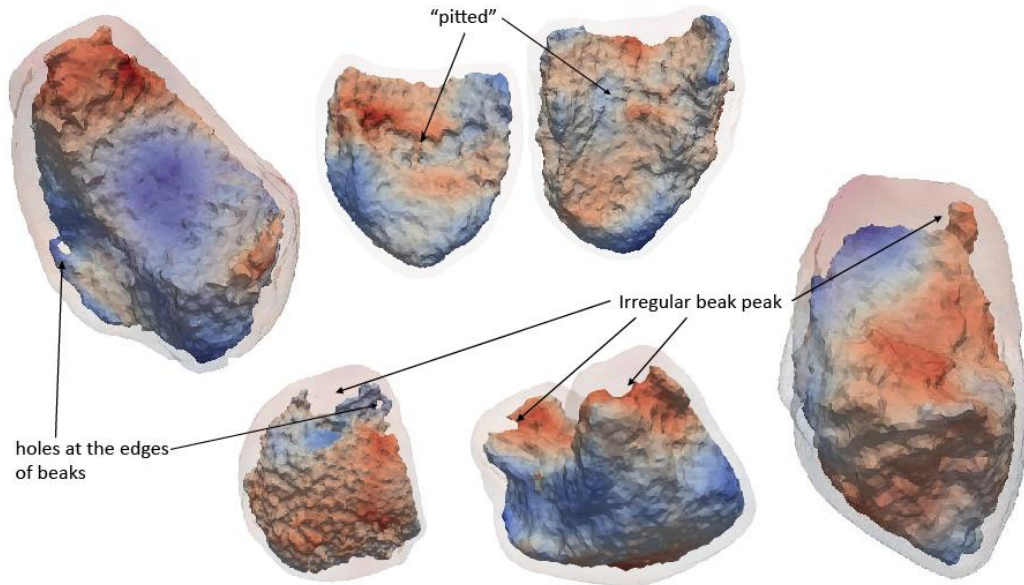


Figure 2.10 Examples of problematic tissue segmentation on six *Pongo* lunates. Examples of holes at the edges of beaks, irregular beak peaks and pitted bodies are pointed out.

Figure 2.9 illustrates how changing the kernel size alters the tissue segmentation. As is standard protocol, segmentations shown in Figure 2.9B-D use the same kernel for the **close** and **InnerMask** operation, while the segmentation shown in Figure 2.9E used a kernel of 5 for the **InnerMask** and a kernel of 2 for the **close** mask. Using the smaller kernel size to close pores allows a smooth boundary to be defined both at the radial articular surface, where the cortex is thin, and the capitate articular surface, where the thick porous block of bone is found. The segmentation seen in Figure 2.9E was used in the analysis for this *Pongo* specimen. This method is successful at creating a smooth cortical-trabecular boundary in most specimens. However, in a number of specimens, it continued to be difficult to create a smooth internal boundary; an example from *Gorilla* is given in Figure 2.11. These specimens appear to all have an exaggerated version of the thick and porous trabecular-cortical boundary morphology described above.

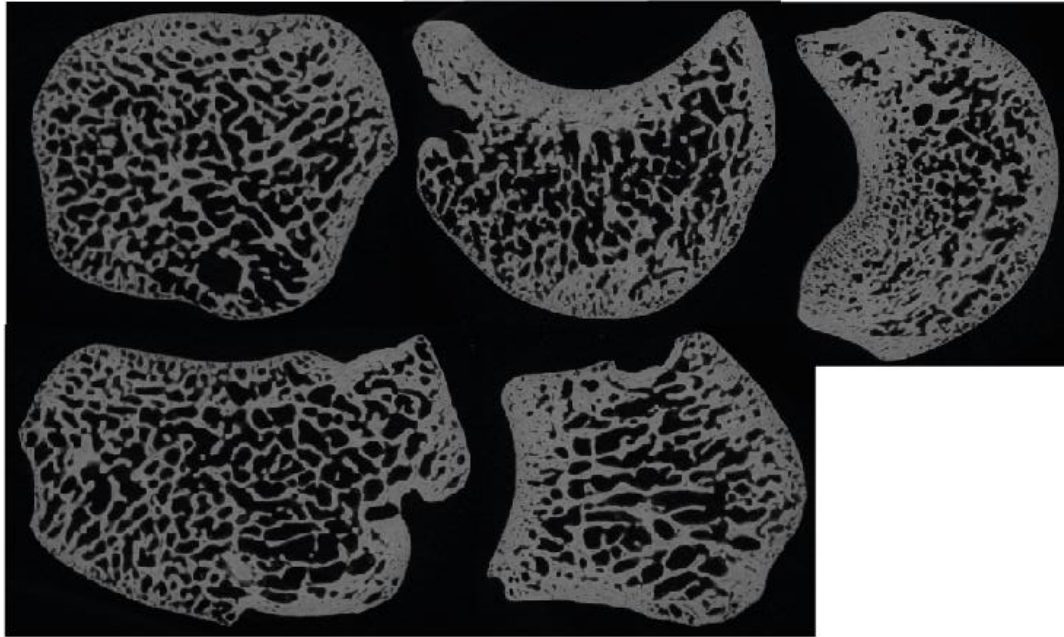


Figure 2.11 Five slices from different planes through a *G. gorilla* specimen. This specimen illustrates the extremely porous and thick bone at the trabecular-cortical boundary posing methodological problems to tissue segmentation.

A question in the research design then arose: should these specimens be excluded from analysis if a smooth delineation between cortical and trabecular bone cannot be established? An experiment was run to test whether specimens that were classified as having segmentation issues have significantly different structural parameters to those classified as not having segmentation issues. For this test, lunates from *Pongo* ($n=13$) and *Gorilla* ($n=16$) were segmented as part of Chapter 4. During the segmentation process, mesh issues were classified as present if a smooth trabecular-cortical boundary could not be produced with either standard protocols or an altered closing kernel, as described above. At the end of the segmentation process, five *Gorilla* and three *Pongo* specimens were identified as having mesh issues (Table 2.5). All specimens were then segmented and processed through medtool via the regular protocol. In medtool, trabecular BV/TV, DA, Ct.Th and Total BV/TV were measured. Total BV/TV measures the bone volume of the trabeculae and cortical combined and, as such, does not rely on the differentiation and segmentation of the two tissues. Using R (v4.1.0), a within-species Mann-Whitney U test was run to assess whether values from specimens with and without mesh issues were significantly different from one another.

Table 2.5 *Gorilla* and *Pongo* specimens included in segmentation test and their individual medtool results.

Under Mesh Issues, N indicates specimen has no mesh issues and Y indicates specimens did have mesh issues. Under sex, F indicates female, M indicates male and UK unknown sex.

Scan ID	Mesh Issues	Taxon	Sex	Side	Trabecular BV/TV	DA	Total BV/TV	Ct.Th	Tb.N	Tb.Sp	Tb.Th
10000737	N	<i>Gorilla</i>	F	Left	0.310	0.281	0.460	0.511	0.924	0.781	0.301
10000989	N	<i>Gorilla</i>	M	Right	0.385	0.277	0.533	0.675	0.697	0.997	0.438
X0010000	N	<i>Gorilla</i>	F	Left	0.362	0.231	0.540	0.651	0.951	0.717	0.334
X0010019	Y	<i>Gorilla</i>	M	Left	0.476	0.255	0.614	0.808	0.804	0.815	0.429
X0010023	N	<i>Gorilla</i>	M	Right	0.418	0.267	0.627	0.621	0.924	0.730	0.352
X0010030	N	<i>Gorilla</i>	F	Right	0.417	0.237	0.579	0.573	0.932	0.708	0.365
X0010043	N	<i>Gorilla</i>	M	Right	0.356	0.266	0.522	0.516	0.820	0.889	0.331
X0010064	N	<i>Gorilla</i>	M	Right	0.333	0.269	0.463	0.338	0.981	0.728	0.291
X0010068	N	<i>Gorilla</i>	F	Left	0.335	0.309	0.500	0.332	1.310	0.543	0.220
X0010174	Y	<i>Gorilla</i>	M	Left	0.465	0.257	0.612	0.582	0.979	0.645	0.377
X0010191	N	<i>Gorilla</i>	F	Left	0.401	0.253	0.509	0.432	1.079	0.618	0.309
X0010204	N	<i>Gorilla</i>	M	Right	0.330	0.271	0.448	0.297	1.295	0.549	0.223
X0010208	N	<i>Gorilla</i>	F	Right	0.393	0.251	0.514	0.388	1.117	0.600	0.295
X0010219	Y	<i>Gorilla</i>	F	Left	0.451	0.286	0.605	0.582	0.972	0.667	0.362
X0010260	Y	<i>Gorilla</i>	M	Left	0.346	0.292	0.477	0.613	0.865	0.812	0.344
X0010279	Y	<i>Gorilla</i>	M	Right	0.482	0.236	0.699	0.705	0.811	0.768	0.465
10001259	N	<i>Pongo</i>	F	Left	0.415	0.228	0.621	0.525	1.052	0.627	0.324
10001261	N	<i>Pongo</i>	F	Left	0.320	0.315	0.468	0.400	1.164	0.621	0.238
10000975	N	<i>Pongo</i>	M	Left	0.335	0.313	0.482	0.418	1.079	0.664	0.263
10000760	N	<i>Pongo</i>	F	Left	0.281	0.326	0.416	0.420	0.979	0.757	0.264
10002622	N	<i>Pongo</i>	F	Right	0.305	0.327	0.452	0.380	1.150	0.637	0.233
10002619	N	<i>Pongo</i>	M	Right	0.350	0.331	0.606	0.869	0.984	0.722	0.294
10000996	N	<i>Pongo</i>	UK	Left	0.308	0.266	0.516	0.884	0.995	0.702	0.303
10002572	N	<i>Pongo</i>	F	Right	0.439	0.299	0.563	0.437	1.173	0.571	0.281

10002628	N	Pongo	M	Left	0.415	0.284	0.538	0.363	1.199	0.575	0.259
10002630	N	Pongo	F	Right	0.366	0.256	0.479	0.367	1.107	0.621	0.282
10000997	Y	Pongo	UK	Right	0.503	0.308	0.644	0.691	0.997	0.600	0.403
10002612	Y	Pongo	F	Right	0.469	0.209	0.602	0.402	1.290	0.491	0.284
X0010287	Y	Pongo	M	Left	0.322	0.281	0.464	0.468	0.934	0.780	0.290

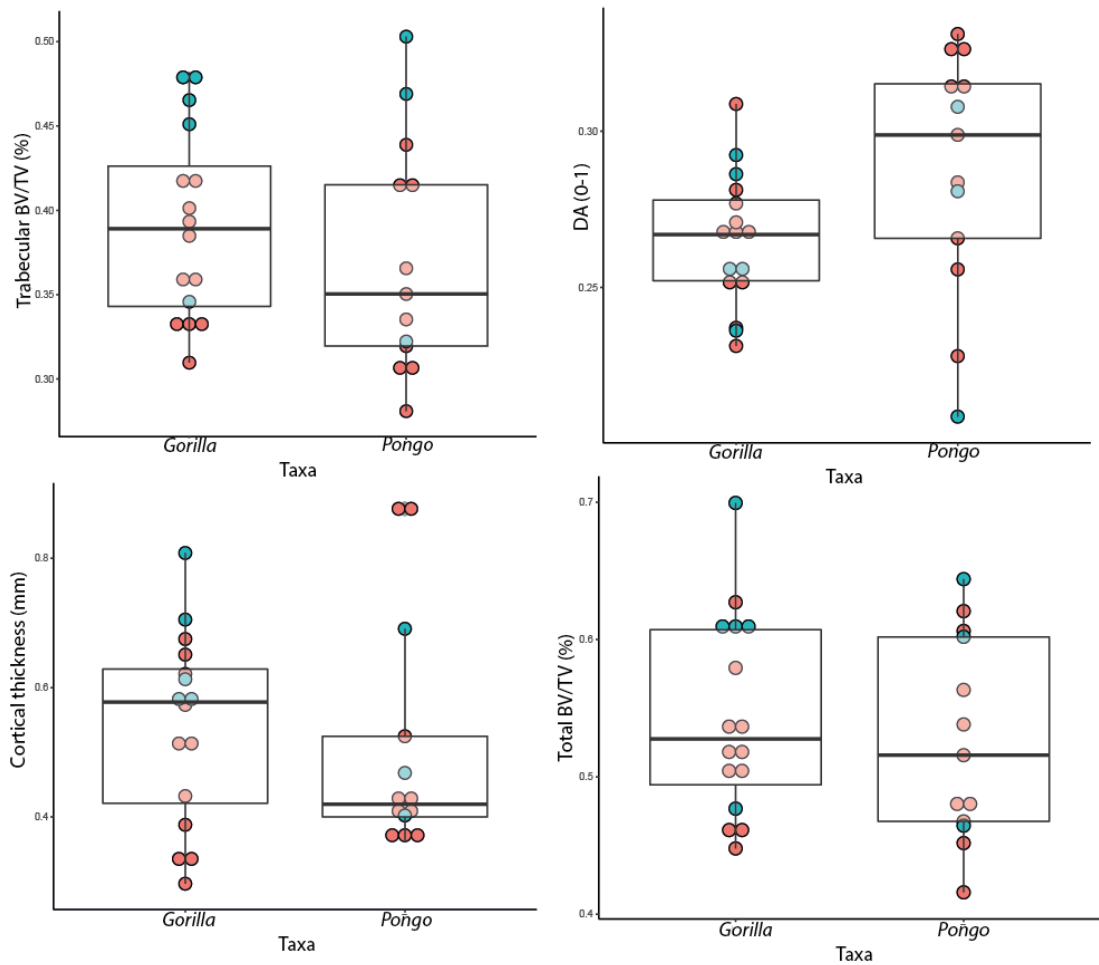


Figure 2.12 Boxplot of trabecular BV/TV, DA, Ct.Th and Total BV/TV results. Red circles = mesh issues present. Blue circles = no mesh issues present.

The parameter results are listed in Table 2.6 and visualised in Figure 2.12. The box-and-whisker plots show the distribution of results between the *Gorilla* and *Pongo* lunates coloured by whether mesh issues were present (blue) or not (red). The results of the Mann-Whitney U tests are listed in Table 2.6. Results indicate that the trabecular BV/TV, Ct.Th and Tb.Th are significantly different between the *Gorilla* groups. No significant differences are identified between the *Pongo* groups. Although there are two outliers in the *Pongo* cortical thickness results, both of these individuals are classified as not having mesh issues. No significant differences are found in Total BV/TV in either *Gorilla* or *Pongo*; however, the *Gorilla* results approach significance at 0.068

Table 2.6 Results of intraspecific Mann-Whitney U tests

Genus	Parameter	<i>p</i> -value
<i>Gorilla</i>	Trabecular BV/TV	0.019

	DA	0.913
	Total BV/TV	0.068
	Ct.Th	0.038
	Tb.N	0.221
	Tb.Sp	0.509
	Tb.Th	0.019
<i>Pongo</i>	Trabecular BV/TV	0.160
	DA	0.286
	Total BV/TV	0.468
	Ct.Th	0.573
	Tb.N	0.811
	Tb.Sp	0.692
	Tb.Th	0.160

Gorilla Total BV/TV results (where measurements are made without tissue segmentation) did not reach significance. This suggests that individuals classified as having mask segmentation issues are not significantly different in overall bone volume; instead, the segmentation process is classifying bone inconsistently due to the porosity, resulting in significantly higher trabecular BV/TV results. It is important to note that the p -value in this test approached significance ($p=0.068$), indicating caution must still be taken when including these specimens in analyses as the small sample sizes may be limiting our capacity to detect a significant result. No significant differences were found in the *Pongo* group, suggesting that including *Pongo* specimens with mask issues may not affect group results. However, the small sample size of *Pongo* with mask issues ($n=3$) may be causing a Type 2 error. In order to minimise errors in interspecific testing, specimens with mask segmentation issues should be excluded from analysis of trabecular BV/TV, Ct.Th and Tb.Th. However, mask segmentation issues do not appear to affect measurements of Total BV/TV, DA, Tb.N and Tb.Sp as strongly as trabecular-only measurements.

2.2.d. Calculating volume

To test for the potential influence of allometry, individual body mass is ideal, but if it is not known, a proxy can be used. Calculating a geometric mean as a proxy for body mass is a common methodology among trabecular functional adaptation studies (Tsegai et al. 2013; Schilling et al. 2014; Tsegai et al. 2017; Kivell et al. 2018b; Komza and Skinner 2019; Ragni 2020) although body mass estimations (Cotter et al. 2009; Barak, Lieberman and Hublin 2013) and linear dimensions (Ryan and Shaw 2013) have also been used.

For this thesis, individual body mass was not available for each specimen, so it was necessary to calculate a proxy. There are currently no protocols to accurately estimate body mass from

linear measurements of hominid carpal bones. Calculating a geometric mean has been applied to the capitate, scaphoid and lunate previously (Schilling et al. 2014; Ragni 2020); however, there are potential limitations as carpal bone morphology is highly variable among primates (Kivell, Barros and Smaers 2013; Kivell 2016a). Therefore, a new method was sought which would quickly and reliably calculate a proxy for body mass with minimal user input. As a solution, each bone's volume (mm³) was calculated using Paraview (4.8.2.). This is a fast, automated process using the inbuilt functionality of the Paraview 4.8.2 software designed to calculate the length, surface area or volume of voxel-based data¹. Firstly, the **OuterMask** is loaded into Paraview. The **OuterMask** contains only a binary representation of bone and background elements. I then applied the “clip by scalar” function to remove the non-bone (background) elements of the scan, leaving only the bone voxels behind. Finally, I applied the Integrate Variables filter to the bone, which calculates and outputs the volume in mm³.

As this is the first study to apply this method, a validity test was run on a phantom to confirm that scan resolution was included in the calculation of volume. A chessboard phantom with known dimensions (created by C. Dunmore) was loaded into Paraview (4.8.2.), and the above methodology was applied. Changing the dimensions of the phantom from one to three tripled the object's volume, verifying that scan resolution was included in the calculation and no adjustments needed to be made.

2.2.e. Statistical analysis

Chapters 3 and 4 contain detailed information on the statistical analyses.

2.2.f. Canonical holistic cone morphometric analysis (cHMA)

As described above, medtool 4.3 creates BV/TV and DA maps that allow visualisation of the distribution of these parameters across the bone of every individual. From these results, we can make assessments as to whether there are inter- or intraspecific patterns present. However, because the size and shape of each bone (and therefore the tetrahedral mesh) of every individual is different (i.e., they are not homologous), we cannot statistically test whether the **distribution** of bone is different between taxa. cHMA provides a solution to this problem by applying statistical deformation modelling (SDM) prior to bone quantification. SDM does not require user-defined landmarks and can be applied to produce 3D shape models from micro-CT or 2D data (Steiner, Synek and Pahr 2021), making it a practical solution to addressing shape issues in multispecies analyses with highly variable morphology (such as carpals).

¹ <https://kitware.github.io/paraview/docs/latest/python/paraview.simple.IntegrateVariables.html>

The full cHMA method, including its testing and validation, has recently been published in Bachmann et al. (2022). The method builds on the theoretical foundations of SDM (Steiner, Synek and Pahr 2021) and applies it to the holistic quantification of bone parameters of medtool (Tsegai et al. 2013; Gross et al. 2014). In short, cHMA addresses the interspecific shape issue by computing a canonical model (or atlas) representing the mean size, position and morphology from a large, multispecies sample of individual bones. Furthermore, by a process described in more detail below, this model allows us to test whether the distribution of bone parameters, such as relative bone volume (RBV), differ statistically between different species.

There are three basic stages of cHMA (1) canonical bone registration, (2) meshing, and (3) morphometry. The first iteration of canonical bone registration registers the mean shape, size and position in space from the **OuterMask** of each individual. This step takes place in a python virtual environment and requires Python 3. A random individual is selected as the reference image. In this study, *H. sapiens* NHMW_J2 right capitata was used. It has been demonstrated that the final canonical shape does not result in a strong bias towards the reference image (Rueckert, Frangi and Schnabel 2003; Bachmann et al. 2022). The cHMA program then runs the SDM, an iterative process of rigid (similarity) and non-rigid (b-spline) registrations (Steiner, Synek and Pahr 2021; Bachmann et al. 2022). Similarity registrations do not change the size or shape of the **OuterMask**, but move it in 3D space. B-spline registrations apply sheer and dilation manipulations to the object and alter its shape and size. On completion, an 'atlas' is produced, representing the sample's mean size, position and morphology. This atlas represents only the mean external morphology and does not contain any internal architectural information. It is important that every bone included in the sample expresses the morphology from the same side of the body. Therefore, prior to undertaking this step, all left capitates were flipped as a mirror image in Avizo (6 or 9) such that they represented the morphology of a right. At the end of the registration process, the surface distances, which measure in milometers (mm) the distance between the original specimen and the canonical bone (i.e., the deformation), can be assessed at the species or individual level. Registration of the capitates used in Chapter 5 had a median surface distance movement of less than .5mm, with a range within that registered during the testing phases as published in Bachmann et al. (2022) (Appendix A Figure 8.2 and Appendix A Figure 8.3). Data on the deformation and transformation of each individual during the SDM process is saved as a .tfm file, which is then used to warp the **InnerMask** data to produce a new canonical atlas of the internal trabecular region of the bone. As the registration of the

InnerMask (the internal trabecular space) does not need to re-run the deformation process individually, it does not need Python 3 and can be run in medtool, which uses Python 2. In time, the intention is to migrate medtool to Python 3 and run the entire process there.

The second step, meshing, is also conducted in medtool using an in-house script. Firstly, medtool fills the canonical mesh with tetrahedral finite elements to build a canonical finite element mesh. Then, the **InnerMask** segmentation of each individual is registered onto the canonical **InnerMask** model, using the same method of rigid and non-rigid transformations. During this process, new .tfm files are saved, and that transformation data is used to warp the tetrahedral canonical mesh onto the individual data. Only the nodes of the mesh are warped so that no holes appear in the mesh. Finally, morphometry can take place on the warped meshes. Firstly, bone parameters such as BV/TV are measured in the same way as outlined for medtool. A 2.5mm grid is placed over the specimen, and a 5mm sampling sphere moves from node to node in the grid, measuring bone parameters iteratively across the entire bone or specified sub-region. The datum from each node is interpolated back onto the canonical finite element mesh and can be visualised in Paraview 4.8.2. Since data were collected from canonical meshes, the datum collected at each node in each individual is homologous and can be analysed statistically. Using a grouping factor, medtool can also produce a model representing the mean RBV of each taxon with three or more representatives. A figure outlining this process is in Chapter 5.

2.2.f.1. Region-specific analysis

As detailed in Chapter 3, the distal capitate of non-human hominids has extremely thick bone at the internal cortical-trabecular boundary and segmenting the two tissues in these instances was methodologically challenging. In some individuals, the internal bone was so thick that it was classified as cortical bone the entire way through the bone, leaving large holes within the **InnerMask**; for an example, see Supplementary Figure 3.1. The cHMA method has not been tested and validated on specimens displaying this methodology, and it is unclear how the registration and mesh morphing would deal with large holes within the **InnerMask** and trabecular structure. Therefore, it was decided that the proximal capitate only would be analysed. cHMA has been validated on metacarpal epiphyses, where the morphology is broadly similar to the proximal capitate, i.e., a roughly spherical shape with a relatively thin cortex surrounding the internal trabecular bone. Further, as demonstrated in Chapter 3, the capitate head is biomechanically distinct from the base.

To analyse the proximal and distal portions of the bone separately, a subset of the canonical mesh was generated using Paraview and R. Firstly, the canonical mesh was loaded into

Paraview. Using the 'select through' tool, the cells of interest were selected (Figure 2.13A). The selection was made at the distal extent of the lunate articulation, as in Bird et al. (2021). This splits the capitate into two sections, the proximal section, which encapsulates the capitate head only, and the distal section, which encapsulates the waist and base of the bone. Paraview lists the mesh numbers of the selected cells, which can be exported and saved as a .txt file (Figure 2.13B). The cells of the distal section, that is, the inverse of the first cell selection can be created by simply taking the full list of mesh cells and removing the cell numbers contained in the proximal cell selection. This resulted in two separate meshes with no overlap (Figure 2.13D). As every specimen in the sample has had its data interpolated onto this canonical mesh, it is not necessary to cut specimens individually. The boundary between the two portions appears slightly jagged because the cell selection will not cut through the tetrahedral elements. Using the list of cells, the two new meshes were generated in R and saved as new canonical meshes. The parameter data were then interpolated onto the new meshes using the cell numbers.

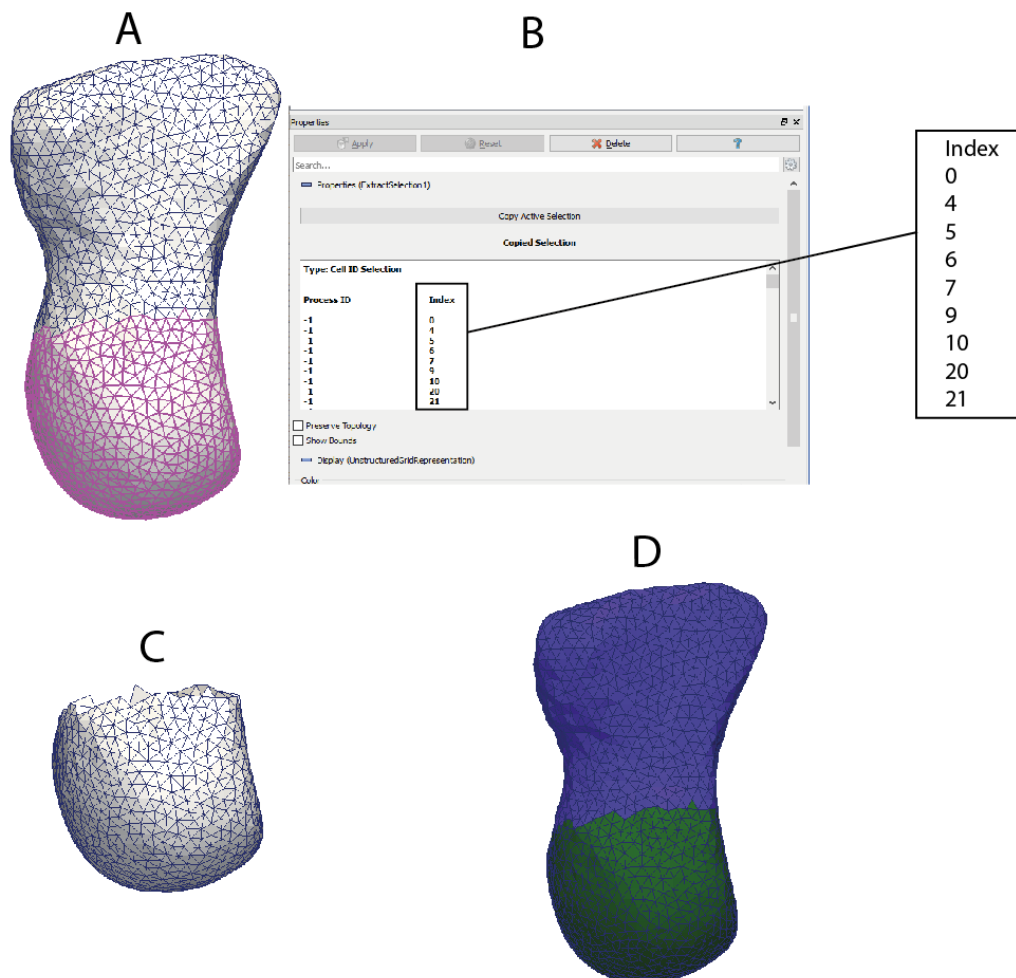


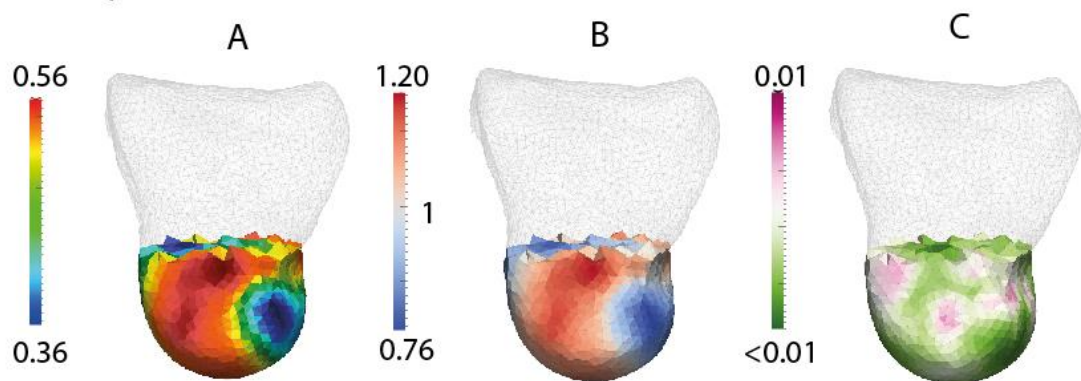
Figure 2.13 Process of cell selection to analyse the proximal and distal capitate separately.

A) Selected cells are in pink; B) Snapshot from the Paraview console. The zoomed box shows the list of cells selected from the mesh; C) Selected cells extracted from the whole mesh; D) The proximal (green) and distal (purple) portions of the two extracted meshes.

2.2.f.2. Data analysis

CHMA has several in-built options for visualising and comparing the collected data; an example is shown in Figure 2.14. Firstly, using a grouping factor, cHMA can build a model of the mean RBV distribution across multiple (3+) individuals. For Chapter 5, taxon-specific mean models were made of each extant taxon and Neanderthals.

Intraspecific visualisations



Interspecific visualisations

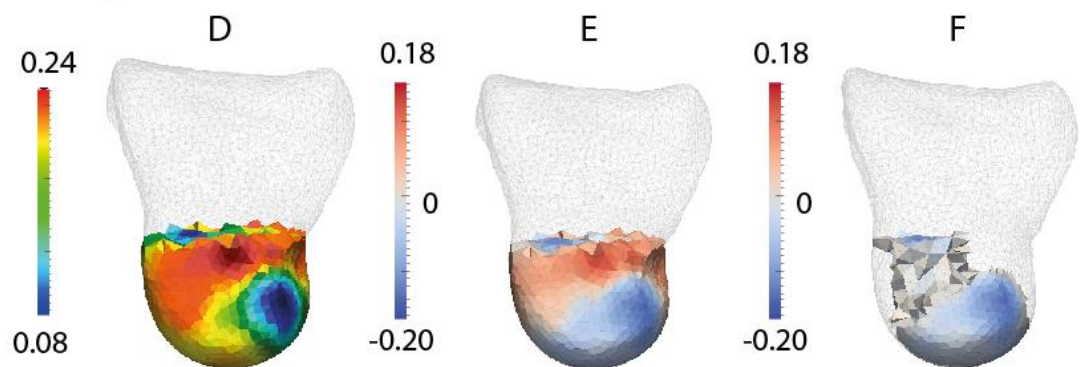


Figure 2.14 cHMA visualisation options.

Top row: Intraspecific visualisations - A) Mean *Gorilla* BV/TV distribution on an absolute scale; B) Mean *Gorilla* RBV distribution; C) BV/TV variance around the mean at each voxel. Bottom row: Interspecific visualisations – D) Difference between *Gorilla* and *Homo* on an absolute BV/TV scale. The scale bar indicates how much *Gorilla* differs relative to *Homo*; E) Difference between *Gorilla* and *Homo* in RBV. The scale bar indicates how much *Gorilla* differs relative to *Homo* - the white region is 0 indicating no relative differences while the positive values indicate higher RBV in *Gorilla*, and the negative values indicate higher RBV in *Homo*; F) This is model E, with a threshold applied in Paraview such that only negative values (where *Homo* have higher RBV) are shown.

Secondly, since the mesh is homologous, a PCA can be run on the datum of every tetrahedron. The PCA is run in R using the 'stats' package (v.4.1.0) and a 2D visualisation produced with the 'factoextra' package (v.1.0.7). Alongside the standard PCA visualisation, it is possible to produce models of the PC loadings, i.e., produce an RBV map representative of any standard deviation along any PC (Figure 2.15). This creates a model illustrating the RBV distributions driving variation along the PCs within the sample.

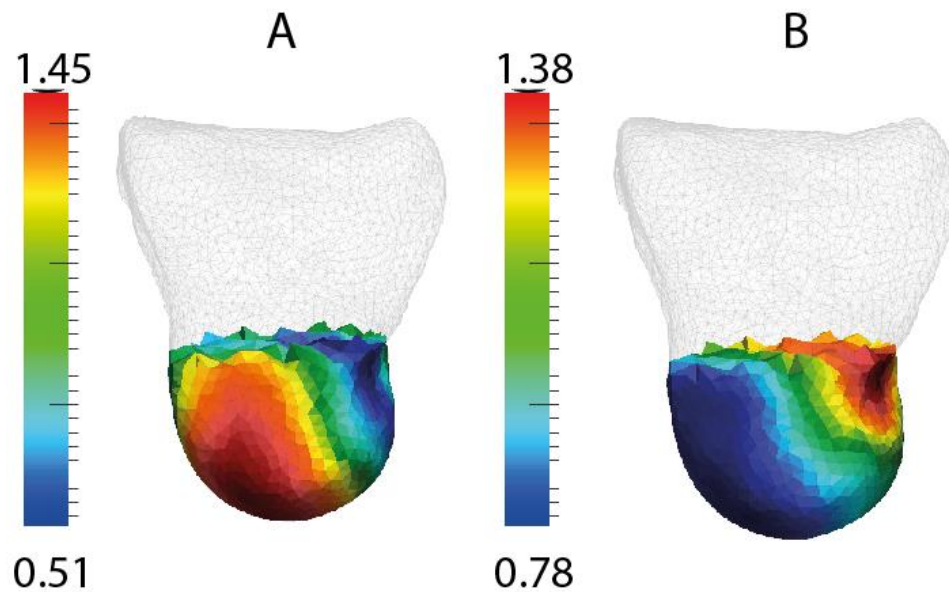


Figure 2.15 Examples of the PC loadings models.
 A) 3 standard deviations along the positive first principle component; B) 3 standard deviations along the negative first principle component.

PCAs were run in R using the 'prcomp' function of the 'stats' package (R core team, v4.1.1). As a dimension reduction method, a PCA has the benefit of reducing the 4,872 data points (tetrahedra in the canonical mesh) to a list of 75 new variables (the PCs). The first three PCs explain >50% of the variance among the sample and can be easily visualised together in two or three-dimensional space. As the remaining PCs explained <5% of the variation, all subsequent statistics were performed only on the first three PCs.

To test for group differences in the distribution of the first three PCs, a permutational omnibus MANOVA test was conducted on the extant taxa, as their sample size was large enough to be included. Omnibus MANOVA tests carry an assumption of normality that the data did not meet, and thus, permutations were run to correct for this violation. The MANOVA was run using the adonis function of the 'vegan' package (M.H.H Stevens, v2.5-7). If the MANOVA tests were significant, permutational pairwise comparisons were run using

the 'pairwise.perm.manova' function of the 'RVAideMemoire' package (M. Hervé, v0.9-80). The pairwise comparisons used the Wilks' Lambda test and applied a Bonferroni correction.

2.2.g. Allometry

The effect of body size, or allometry, is investigated in Chapter 3 and follows the same methodology outlined in Ryan and Shaw (2013). Using the capitate bone volume as a proxy for body mass (as detailed in section 2.2.d), a reduced major axis regression was applied to analyse the relationship between body mass and bone volume. The logged absolute BV/TV (not RBV) from the whole bone (not the values from the proximal and distal segment separately) were used in the regression. As per Ryan and Shaw (2013), shape parameters (BV/TV or RBV, DA and Tb.N) have an isometric slope of zero (or confidence intervals incorporating zero), while size parameters (Ct.Th, Tb.Th and Tb.Sp) have an isometric slope of one, (or confidence intervals incorporating one).

3. Cortical and trabecular bone structure in the hominoid capitate

Published article: Bird, E. E., Kivell, T. L., & Skinner, M. M. (2021). Cortical and trabecular bone structure of the hominoid capitate. *Journal of Anatomy* 239(2), pgs. 351-373. DOI: 10.1111/joa.13437 see 8.3 for copyright information

This manuscript has had minor edits for clarity of understanding and differs from the original publication.

3.1. Abstract

Morphological variation in the hominoid capitate has been linked to differences in habitual locomotor activity due to its importance in movement and load transfer at the midcarpal joint proximally and CMC joints distally. While the shape of bones and their articulations are linked to joint mobility, the internal structure of bones has been shown experimentally to reflect, at least in part, the loading direction and magnitude experienced by the bone. To date, it is uncertain whether locomotor differences among hominoids are reflected in the bone microarchitecture of the capitate. Here, we apply a whole-bone methodology to quantify the cortical and trabecular architecture (separately and combined) of the capitate across bipedal (modern *Homo sapiens*), knuckle-walking (*Pan paniscus*, *Pan troglodytes*, *Gorilla* sp.), and suspensory (*Pongo* sp.) hominoids (n=69). It is hypothesized that variation in bone microarchitecture will differentiate these locomotor groups, reflecting differences in habitual postures and presumed loading force and direction. Additionally, it is hypothesized that trabecular and cortical architecture in the proximal and distal regions, as a result of being part of mechanically divergent joints proximally and distally, will differ across these portions of the capitate. Results indicate that the capitate of knuckle-walking and suspensory hominoids is differentiated from bipedal *Homo* primarily by significantly thicker distal cortical bone. Knuckle-walking taxa are further differentiated from suspensory and bipedal taxa by more isotropic trabeculae in the proximal capitate. In all taxa, bone parameters across the two capitate regions consistently differ, suggesting a variable loading environment between the proximal and distal regions. An allometric analysis indicates that size is not a significant determinant of bone variation across hominoids, although sexual dimorphism may influence some parameters within *Gorilla*. Results suggest that partitioning the capitate (and possibly other short bones) into biomechanically meaningful segments may provide more informative functional analyses for future research. Additionally, while separating

trabecular and cortical bone is normal protocol of current whole-bone methodologies, this study shows that when applied to carpals, removing or studying the cortical bone separately potentially obfuscates functionally relevant signals in bone structure.

3.2. Introduction

Primates use their hands in a diverse set of postures to manipulate and navigate their environment (Fragaszy and Crast 2016). The many articulations within the wrist are central to the capacity of the hand to move through multiple planes of space and, in combination with soft tissue morphology, joint congruence determines the degree of stability, flexibility and dexterity within the wrist and hand (Orr 2010). The capitate articulates proximally with the scaphoid and lunate and distally with the trapezoid, hamate, and metacarpals 2, 3 and, sometimes, 4 (Kivell 2016a). As such, the external morphology of the capitate plays a key role in the range of motion at the wrist as it is a central component of the midcarpal joint proximally and the CMc joints distally (Jenkins and Fleagle 1975; Lewis 1989; Jouffroy and Medina 2002; Crisco et al. 2005; Kijima and Viegas 2009; Orr 2010, 2017).

The external morphology of the hominoid capitate has featured in hypotheses about the locomotor behaviour in the last common ancestor of *Pan* and Hominini (Dainton and Macho 1999; Richmond, Begun and Strait 2001; Begun 2004; Tocheri 2007; Kivell and Schmitt 2009) and the evolution of hominin dexterity and tool-related behaviours (Marzke 1983; Niewoehner, Weaver and Trinkaus 1997; Wolfe et al. 2006; Rein and Harvati 2013). However, drawing locomotor or postural inferences based on external morphology is potentially confounded by the retention of primitive features that are no longer functionally significant (Lieberman 1997; Ward 2002; Pontzer et al. 2006b; Ruff, Holt and Trinkaus 2006; Zeininger, Richmond and Hartman 2011; Kivell 2016b). Furthermore, making biomechanical inferences from external morphology requires in-depth knowledge of the form-function relationship of the bone as well as its surrounding soft tissue and articular environment. This is a particular challenge for carpal research as imaging and analysing the small, closely compacted bones of the wrist is difficult without disrupting the normal kinematic chain (Wolfe, Neu and Crisco 2000; Wolfe et al. 2006; Brainerd et al. 2010; Gatesy et al. 2010; Orr 2016). While advances in 3D imaging and computational techniques have begun to improve our knowledge of wrist biomechanics in *H. sapiens* (see Orr, 2016 for review), our understanding of non-human hominid biomechanics remains more limited (but see Orr, 2017 and 2018). Moreover, the functional relationship between cortical and trabecular tissue within short bones is not well understood, and it is not clear how they may interact to provide whole bone functionality under the high mechanical loads of locomotion and manipulation. To date, it has yet to be

determined whether the internal bone structure of the capitate might reflect differences in hand and wrist use across extant hominoids. Here we apply a whole-bone methodology to investigate how the internal cortical and trabecular bone structure potentially varies within the capitate in a broad sample of *Homo* (recent *H. sapiens*), *Gorilla*, *Pan* (chimpanzees and bonobos) and *Pongo* (orangutans).

3.2.a. Trabecular bone: the relationship between behaviour and structure

In addition to some important clade-specific synapomorphies (Sarmiento 1988; Lewis 1989; Tocheri et al. 2008), the wrists of extant hominoids are adapted to their specialised behaviours and are habitually loaded in different ways. The *Homo* hand is conspicuous among the ape clade as the only species not to habitually utilise the hand for locomotion. Instead, the wrist experiences forces generated predominantly during tool use and other forms of manipulation. High compressive loads are imposed across the wrist by muscle contractions arising from the strong and forceful thumb as well as flexion of the fingers (Napier 1956; Marzke 1997; Tocheri 2007; Marzke 2009; Bardo et al. 2018). Bones must also withstand and transmit sheer and tensional strains as force is transferred radio-ulnarly across the wrist (Tocheri 2007; Marzke 2013). There is clinical evidence to support the hypothesis that the dart-thrower's motion (DTM) is the functional axis of wrist movement in *H. sapiens* (Crisco et al. 2005; Crisco et al. 2011; Schuind et al. 2013; Brigstocke et al. 2014). The DTM runs from radial deviation in extension to ulnar deviation in flexion and is used across numerous activities, from throwing an object to pouring water from a jug (Brigstocke et al. 2014). During this movement, the capitate is very mobile against a stabilized proximal row, with the rotation axis perpendicular to the wrist movement (Crisco et al. 2005).

In contrast, non-human hominids utilise their forelimbs during locomotion. *Pongo* utilises a range of torso orthograde suspensory and climbing postures in an almost exclusively arboreal environment (Thorpe and Crompton 2006; Thorpe, Holder and Crompton 2009; Manduell, Morrogh-Bernard and Thorpe 2011). In these positions, the wrist experiences substantial tensile loading from gravitational forces and stabilising ligaments, as well as compressive stress from muscle contractions (Swartz, Parker and Huo 1998; Isler and Thorpe 2003). *Gorilla* and *Pan* are primarily terrestrial knuckle-walkers but also engage in various types and frequencies of arboreal locomotion depending on the species, population or sex (van Lawick-Goodall 1968; Hunt 1992; Doran 1993a; Remis 1995, 1998; Neufuss et al. 2017; Thompson et al. 2018). During knuckle-walking, the wrist must resist compressive loading from both muscle contractions stabilizing the joints and gravitation forces acting on the body mass (Carlson et al. 2006). However, the knuckle-walking posture differs somewhat between

the two genera. When compared to *Gorilla*, *Pan* typically use more variable hand and forelimb postures, do not bear weight as evenly across the digits and more frequently engages a palm-in forelimb posture (Inouye 1994; Wunderlich and Jungers 2009; Matarazzo 2013; Finestone et al. 2018). *Gorilla* typically knuckle-walk on digits 2-5 and more regularly utilise a palm-backwards forelimb posture (Tuttle 1969; Inouye 1994; Matarazzo 2013), although hand postures in the wild are more variable (Thompson et al. 2018). Although *Gorilla* has been hypothesised to use a more neutral, columnar wrist posture than *Pan* (Kivell and Schmitt 2009), recent kinematic studies of captive African apes found that *Gorilla* and *Pan* were generally similar in their degree of wrist of extension during knuckle-walking (Finestone et al. 2018; Thompson 2020).

Bone functional adaptation (BFA) describes the biological process of bone altering its structure to optimize resistance against peak mechanical loads habitually experienced throughout the lifetime of the individual (Martin, Burr and Sharkey 1998; Ruff, Holt and Trinkaus 2006; Barak, Lieberman and Hublin 2011; Doube et al. 2011). Numerous experimental studies suggest that variation in structure reflects, at least in part, load experienced during life (see Kivell 2016b for review) and thus provides an opportunity to draw behavioural inferences better linked to actual, rather than potential, behaviour (Frost 1987; Ruff and Runestad 1992). BFA research not only facilitates a greater understanding of the joint loading and kinematics of extant species but may also provide an informative avenue for behavioural reconstruction in fossil taxa (Griffin et al. 2010; DeSilva and Devlin 2012; Skinner et al. 2015; Su and Carlson 2017; Kivell et al. 2018b; Dunmore et al. 2020a; Georgiou et al. 2020). Previous studies of primate trabecular bone structure within the capitate have used a volume of interest (VOI) sampling sphere but have found limited functional correlation with locomotor behaviour (Schilling et al. 2014; Ragni 2020). However, using a whole epiphysis/bone methodology has been more functionally informative for hand bone studies (Tsegai et al. 2013; Stephens et al. 2016; Stephens et al. 2018; Dunmore et al. 2019; Dunmore et al. 2020a). Furthermore, a whole-bone approach to carpal functional adaptation is preferable given their irregular shapes and variation across different taxa (Tsegai et al. 2013; Gross et al. 2014; Schilling et al. 2014).

However, inferring a form-function relationship between bone microarchitecture and behaviour is not always straightforward due to several potentially confounding variables (for a comprehensive review and discussion see Kivell 2016b). Firstly, bone modelling (*sensu* Barak 2019) is influenced by the genetic blueprint of the individual, as well as life history factors such as lactation or pregnancy (Kalkwarf and Specker 1995; Lieberman 1996; Parsons

et al. 1997; Lovejoy et al. 2003; Pettersson et al. 2010; Yeni et al. 2011; Paternoster et al. 2013; Tsegai et al. 2017). Systemic features such as these potentially undermine our ability to differentiate between functional and non-functional patterns expressed in bone structure across different individuals or species. Secondly, there is a higher capacity for functional adaptation to occur during the juvenile and young adult periods, and the extent to which bone microarchitectural patterns can be linked to adult behaviour has been debated (Bertram and Swartz 1991; Pearson and Lieberman 2004; Ruff, Holt and Trinkaus 2006). This is particularly salient when analysing African apes because locomotor behaviour is known to differ across age categories (Doran 1992, 1997). Finally, there is also uncertainty regarding the loading frequency and magnitude necessary to induce a BFA response (Frost 1987; Ruff, Holt and Trinkaus 2006; Barak, Lieberman and Hublin 2011; Wallace et al. 2015). Consequently, microarchitecture will never represent the mechanical ideal of the bone as competing demands on bone tissue will result in a compromise morphology (Ruff 2008).

3.2.b. Cortical bone: contribution to bone structure and functional adaptation

Carpal bones function within an intricate biomechanical environment. The bones and ligaments are interdependent and work together, making minor adjustments and movements in concert to create overall hand motion (Lewis 1989; Kijima and Viegas 2009; Orr 2017). Among the carpus, the central role of the capitate within the midcarpal joint and its articulation with the metacarpus makes it an ideal bone to investigate functional differences in wrist loading. The distal capitate is not only compressed via its CMC articulations, but it also receives tensional strain via the attachment of several extrinsic (between carpals and other hand bones) and intrinsic (between carpal bones) ligaments (Schuind et al. 1995; Kijima and Viegas 2009; Regal, Maschke and Li 2020). In contrast, the proximal capitate does not receive any ligaments but forms the 'ball' component of the ball and socket midcarpal joint within the highly mobile proximal row and is thus loaded predominantly in compression (Lewis 1989; Garcia-Elias et al. 1994; Kivell 2016a; Orr 2017).

Unlike long bones, short bones like carpals generally have a thin cortical shell, and the entire internal space is filled with trabeculae (Currey 2002; Schilling et al. 2014). During movement, short bones are likely to bear a significant portion of the load imposed upon the region as they resist compressive forces and transfer load through the bone from one joint articulation to another while also being strained via tensional loads from attached ligaments (Currey 2002; Yao et al. 2020). Cortical and trabecular bone have divergent material properties due to differences in porosity, mineralization and cellular constitution (Currey 2002). Cortical bone is stiffer and stronger than trabecular bone (Martin, Burr and Sharkey 1998; Guo 2001),

but due to its lower porosity, it is slower than trabecular bone to model and is less compliant (Martin, Burr and Sharkey 1998; Hart et al. 2017). While the two tissues work together to create the functionality of the whole bone, their relative contributions to stiffness, strength and homeostasis differs across regions of the same bone (Doubé et al. 2009; Barak, Weiner and Shahar 2010). It is not currently understood how cortical and trabecular bone work together to meet the mechanical demands of the carpus, particularly under the high mechanical demands of locomotion.

By quantifying the internal bone architecture of the hominoid capitate using a whole-bone methodology, this study aims to investigate whether differences in trabecular and cortical architecture among hominoids may relate to the divergent hand use across the clade. We also examine the proximal and distal segments of the capitate separately due to the differences in the soft tissue and articular relationships with the surrounding bones.

3.2.c. Allometry: body size and bone structure

As functional adaptation research aims to identify markers of behaviour rather than body size, analysing bone parameters for allometric effects has been integral to interspecific analyses (Ruff 1984). Decades of research across various species has yet to find consistent patterns; however, some research suggests there may be a general pattern across Mammals and birds whereby bone volume to total volume (BV/TV) and degree of anisotropy (DA) are independent of body mass (Cotter et al. 2009; Barak, Lieberman and Hublin 2011; Doubé et al. 2011; Schilling et al. 2014; Christen, Ito and van Rietbergen 2015; Tsegai et al. 2017; Kivell et al. 2018b; Komza and Skinner 2019) while trabecular thickness (Tb.Th), trabecular number (Tb.N) and trabecular separation (Tb.Sp) scale with negative allometry (Barak et al. 2013; Ryan and Shaw 2013; Kivell et al. 2018b; Ragni 2020). Cortical thickness (Ct.Th) is often reported to be isometric or slightly positively allometric (Runestad 1997; Demes, Jungers and Walker 2000; Fajardo et al. 2013). However, not all studies find BV/TV and DA to be independent of body mass (Fajardo et al. 2013; Ryan and Shaw 2013; Mielke et al. 2018; Ragni 2020) nor the negative relationship with Tb.Th, Tb.N and Tb.Sp (Doubé et al. 2011; Fajardo et al. 2013; Tsegai et al. 2017; Komza and Skinner 2019). Few allometric studies have been undertaken on short bones. Tsegai et al. (2017) found no correlation between trabecular parameters or Ct.Th with size in intraspecific analyses of the *Homo* and *Pan* talus. Similarly, an interspecific analysis in Schilling et al. (2014) of the primate capitate found only Tb.N to scale with negative allometry. Ragni (2020) found a greater number of significant relationships within the capitate of *Pan* and *Gorilla* with Tb.Th, Tb.N and Tb.Sp showing negative allometry and DA and BV/TV expressing isometry. These conflicting results may be

due in part to methodological differences for sampling trabeculae or calculating size. Nevertheless, the effects of allometry on the hominoid capitate remain unclear.

3.2.d. Hominoid capitate morphology

3.2.d.1. Distal capitate

In all hominoids, the distal capitate is bound to the surrounding bones via strong ligaments which are often described as a unit that moves in unison during extension and flexion (Richmond, Begun and Strait 2001; Moojen et al. 2003; Crisco et al. 2005; Richmond 2006; Orr 2010; Tang et al. 2011). The capitate articulates disto-radially with the trapezoid (although this articulation is almost always absent in *Gorilla*), Mc2, and distally with the third and sometimes fourth metacarpals (Lewis 1989; Kivell 2016a). The topology of the Mc joint surfaces in the distal row is more complex and irregular in *Pan* and *Gorilla* compared to the smoother surfaces in *Pongo*; however, the capacity for extension is linked to the range of movement at the midcarpal joint rather than at the CMc junction (Richmond, Begun and Strait 2001; Begun 2004; Orr 2017). The distal capitate in modern *Homo sapiens* is considered to have several derived features linked to committed manipulation and increased efficiency of radio-ulnar force transfer (Tocheri 2007; Tocheri et al. 2008). A distally-oriented capitate-Mc2 articulation allows pronation of the second finger towards the thumb facilitating precision grip, while a palmarly-positioned and expanded capitate-trapezoid articulation is thought to better resist high radio-ulnarly oriented forces incurred by the thumb during tool-related activities (Tocheri et al. 2007; Tocheri et al. 2008). Furthermore, the disto-dorso-radial corner is truncated to accommodate the third Mc3 styloid process, providing a stable joint for transmitting high forces and resisting subluxation of the third ray during tool use (Marzke and Marzke 1987; Riley and Trinkaus 1989; Niewoehner, Weaver and Trinkaus 1997; Tocheri et al. 2008; Ward et al. 2014). In non-human hominids, load transfer also occurs radio-ulnarly as bones of the distal carpal row are compressed against one another. However, in contrast to *H. sapiens*, the orientations of the articular surfaces of the capitate (and distal carpal row more generally) indicate the wrist is better adapted to withstand and transfer proximo-distally oriented forces, which arise during use of the forelimb in locomotion (Tocheri 2007; Tocheri et al. 2008). Only a small proportion of the dorsal surface of the distal capitate is without articular surfaces. In this distal segment, compression is induced at the distal, radial and ulnar articular surfaces, while tension is induced by the supporting intrinsic ligaments surrounding these articulations. Tension further arises from the several intrinsic and extrinsic ligaments attached to the palmar and dorsal surfaces (Kijima and Viegas 2009; Regal, Maschke and Li 2020).

3.2.d.2. Proximal capitate

In hominids, the rounded proximal surface of the capitate articulates with the bones of the proximal row to form the crux of the midcarpal joint (Kivell 2016a). No ligaments attach directly onto the proximal capitate thus compared to the distal row, the bones of the midcarpal joint are able to move more independently of one another (Moojen et al. 2003; Crisco et al. 2005; Kijima and Viegas 2009; Regal, Maschke and Li 2020). In *Pongo*, the proximal capitate is radio-ulnarly narrow in comparison to the other (Figure 3.1) (Richmond, Begun and Strait 2001). Notably, the os centrale is not fused to the scaphoid as it is in the other hominids and thus excludes the scaphoid from articulating with the capitate resulting in relatively greater freedom of movement at the midcarpal joint (Begun 2004; Orr 2018). In *Pan* and *Gorilla*, the proximal capitate is enlarged on the radial aspect, which produces a “waisted” mid-region forming an embrasure with the trapezoid (Richmond, Begun and Strait 2001; Wolfe et al. 2006; Kivell 2016a; Orr 2018). There is also a notable radio-ulnar ridge along the distal extent of the dorsal articular surface that extends onto the hamate (Richmond, Begun and Strait 2001). These features contribute to the so called “screw-clamp mechanism” that describes the functional complex limiting extension at the midcarpal joint. During extension, the scaphoid is wedged in between the capitate and trapezoid, providing stability between the proximal and distal row (Tuttle 1969; Jenkins and Fleagle 1975; Richmond, Begun and Strait 2001; Orr 2005; Richmond 2006; Orr 2017). *Homo* also exhibits the fused scaphoid-os centrale and radially expanded proximal capitate; however, an enlargement of the bone in the radial-palmar region results in a less dramatic “waisting” of the bone, resulting in a range of extension intermediate between the other hominoids (Lewis 1977, 1989; Orr 2017). Notably, the proximal capitate is the crux of the functional axis of the DTM (Crisco et al. 2005). During motion, the rotation axis of the capitate is perpendicular to the movement of the DTM as it moves across a virtually motionless scaphoid and lunate (Crisco et al. 2005). Thus, although a small bone, the proximal and distal portion of the capitate functions within notably different ligamentous and articular environments.

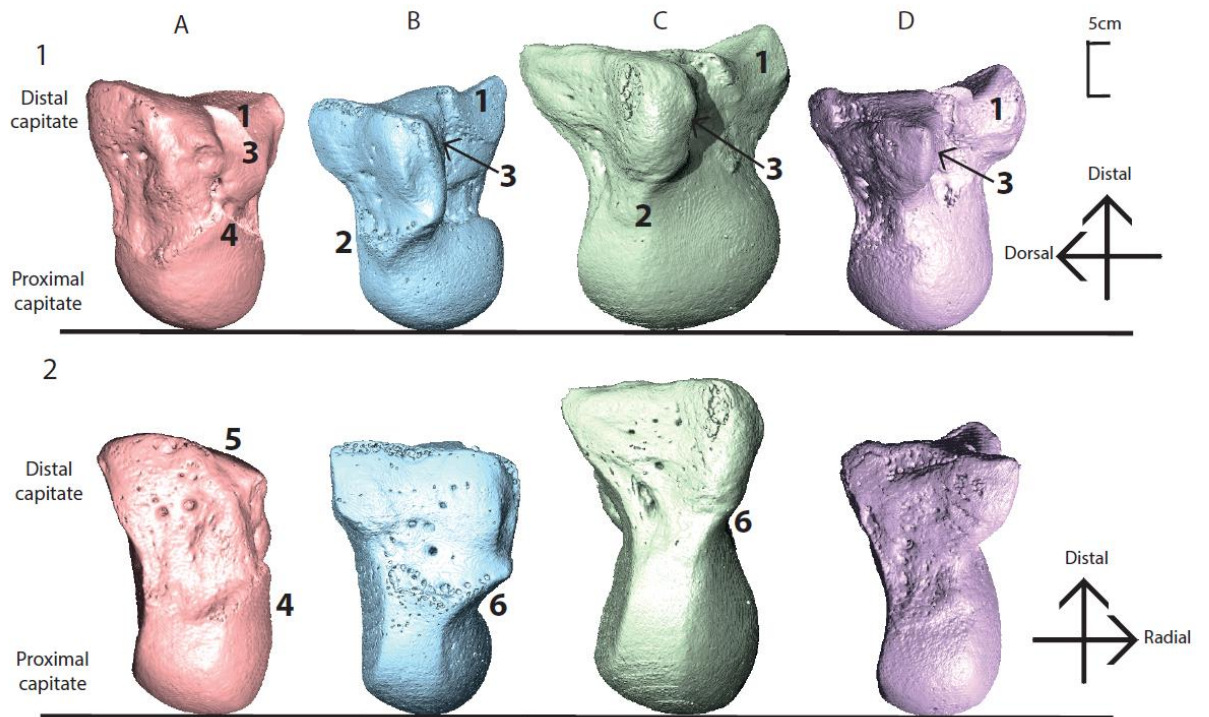


Figure 3.1 CT-derived surface models of a left capitate from each genus showing variation in external morphology.

Capitates have been scaled to relative size. Rows: 1) Capitates are oriented dorso-radially 2) Capitates are oriented dorsally. Columns: A) *Homo sapiens* (DCW_AM_10_0_182), B) *Pan troglodytes* (SMF_4104), C) *Gorilla gorilla* (ZMB_Mam_83587), D) *Pongo pygmaeus* (ZMB_Mam_6948). Numbers representing anatomical features: '1' MC2 articulation, '2' Dorsal ridge, '3' trapezoid articulation, '4' radial-palmar expansion of the proximal capitate, '5' Mc3 styloid process articulation, '6' waisted mid-capitate.

3.3. Hypotheses

This research centres on two interrelated hypotheses for both trabecular and cortical bone that are summarized in Table 3.1 and elaborated below.

Table 3.1 Summary of the hypotheses, predictions and statistical tests used in this study.

Hypothesis	Predictions	Statistical tests
#1	Between species	
Locomotor and behavioural differences among extant hominoids will result in significantly different trabecular and cortical architecture in their capitates	Knuckle-walking taxa will exhibit high BV/TV and DA <i>Pongo</i> will show intermediate BV/TV and low DA <i>Homo</i> will exhibit low BV/TV and intermediate DA Cortical bone will be thickest in <i>Gorilla</i> and <i>Pan</i> , followed by <i>Pongo</i> , then <i>Homo</i> .	Kruskal-Wallis test by ranks and post-hoc Pairwise Wilcoxon rank-sum tests
#2	Between species	
Proximal and distal segments will show significantly differentiated internal bone architecture	Distal to proximal ratios will be statistically undifferentiated among the study taxa	Wilcoxon signed-rank test
	Within Species	
	The distal aspect will have higher BV/TV and DA compared to the proximal aspect across all species The distal cortex will be significantly thicker than the proximal across all species	Kruskal-Wallis test by ranks and post-hoc Pairwise Wilcoxon rank-sum test
#3	Between species	
Allometry	Only Tb.N will show a significant negative relationship to body size, while all other parameters will be uncorrelated	Reduced major axis regression
	Within species	
	No parameters will exhibit significant correlations with body size	Reduced major axis regression

3.3.a. Trabecular bone architecture

We predict that the capitate of knuckle-walking *Gorilla* and *Pan* will have high relative BV/TV and high DA (Table 3.1, hypothesis 1) due to the presumed high compressive forces and reduced mobility from their more extension-limiting midcarpal joint. In contrast, we predict that the *Pongo* capitate will have intermediate BV/TV and low DA due to their predominantly suspensory behaviour, resulting in reduced compression but greater mobility. We expect *Homo* to exhibit low BV/TV and intermediate DA because their capitate is not loaded during

locomotion and presumably has the least compressive loading but more predictable movement along the DTM axis.

Given the differences in mobility and presumed loading between the proximal and distal portions of the capitate, we hypothesize that there will be differences in the trabecular bone structure between these segments (measured as ratios). It is predicted that the distal aspect will have higher BV/TV and DA compared to the proximal aspect across all species (Table 3.1, hypothesis 2). As there are no previous studies that have addressed this question for the capitate, we test the null hypothesis that these ratios will be similar among the study taxa. Although we report Tb.Th, Tb.N and Tb.Sp, we do not make explicit predictions about these parameters because all contribute, potentially in a variety of different combinations, to BV/TV.

3.3.b. Cortical bone thickness

The contribution of cortical bone to the functional adaptation of the capitate in hominoids has never been investigated. Given the assumed loading differences described above, we predict that the cortical bone will be thickest in *Gorilla* and *Pan*, followed by *Pongo*, with *Homo* exhibiting the thinnest cortex (Table 3.1, hypothesis 1). Also following the predictions for trabecular bone, it is predicted that the cortex of the distal capitate should be significantly thicker than the proximal capitate for all genera.

In long bones, the joint surface tends to have a thin layer of cortical bone covering a dense trabecular network that transfers load towards the thicker and stronger diaphyseal cortex (Currey, 2002). In short bones, the cortex is similarly described as thin; however, the relationship between cortical and trabecular bone has never been quantified among hominoids. Additionally, it is unclear whether the behavioural differences among ape genera will result in different ratios of cortical to trabecular bone. Therefore this study will investigate the relative contribution of cortical bone to total bone volume, testing the null hypothesis that these ratios will be similar among the study taxa (Table 3.1, hypothesis 2).

3.3.c. Inter- and intraspecific allometry in internal bone structure

As this study incorporates hominoids of diverse body size, inter- and intraspecific allometry is also investigated. Predictions are outlined in Table 3.1 (hypothesis 3) and follow the results of Schilling et al. (2014) for the interspecific and Tsegai et al. (2017) for the intraspecific predictions.

3.4. Materials and methods

3.4.a. Sample

The study sample includes capitates (n=69) from *Homo sapiens* (n=26), *Pan troglodytes* and *Pan paniscus* (n=14), *Gorilla* sp. (n=16) and *Pongo* sp. (n=13) (Table 3.2; Supp. Table 1). These taxa are categorized into three behavioural groups based on their most frequent locomotor behaviours: bipedal (*Homo*) knuckle-walking (*Gorilla* and *Pan*) and suspensory (*Pongo*). Capitates from non-human hominids were wild-shot adults with no obvious signs of pathology. Consideration was given to ensuring a sex balance for each taxon when possible; however, 16 specimens had unknown sex.

Table 3.2 Summary of the study sample

Taxon	N	Side		Sex			Behavioural Group
		Right	Left	Female	Male	Unknown	
<i>Homo sapiens</i>	26	14	12	5	9	12	Bipedal/Manipulative
<i>Pan paniscus</i>	8	5	3	4	4		Knuckle-Walking
<i>Pan troglodytes</i>	6	3	3	3	3		Knuckle-Walking
<i>Gorilla beringei</i>	1		1			1	Knuckle-Walking
<i>Gorilla gorilla</i>	15	8	7	7	7	1	Knuckle-Walking
<i>Pongo abelii</i>	2	1	1	1	1		Suspensory
<i>Pongo pygmaeus</i>	11	6	5	5	4	2	Suspensory

3.4.b. Computed tomography

Capitate specimens were scanned with either a BIR ACTIS 225/300 high-resolution microCT scanner or a Diondo D3 high-resolution microCT scanner at the Department of Human Evolution, Max Planck Institute for Evolutionary Anthropology, Germany, or a Nikon 225/XTH scanner at the Cambridge Biotomography Centre, University of Cambridge, United Kingdom. Specimens were scanned with an acceleration voltage of 100-160 kV and 100-140 μ A using a 0.2-0.5mm copper or brass filter. Images were reconstructed as 16-bit TIFF stacks. To ensure accurate post-scan segmentation of thin trabeculae, scan resolution was limited to a maximum of 0.048mm (average 0.032mm) for non-human hominids and 0.035mm (average 0.029mm) for the *Homo* sample. This resolution is below the suggested range for minimal error detection (Isaksson et al. 2011; Christen et al. 2016). Post-scanning, each capitate was positioned into approximately the same orientation using Avizo 6.0 (Visualization Sciences

Group, SAS). Segmentation of trabecular bone, including identification and removal of extraneous non-bone material, used the medical image analysis (MIA) clustering method (Dunmore, Wollny and Skinner 2018). The MIA-clustering method increases the reproducibility of results by reducing subjective input parameters required for other segmentation methods (Dunmore, Wollny and Skinner 2018).

3.4.c. Data collection

This study uses the medtool 4.3 software package (<http://www.dr-pahr.at/medtool/>) to quantify bone parameters throughout the entire capitata utilising the method outlined in Gross et al. (2014). In brief, medtool utilises a series of morphological filters to identify the cortical, trabecular, internal (marrow) and background elements of the segmented CT scans. After MIA segmentation, medtool projects a series of rays onto the outside of the bone (Figure 3.2B) that continue to move internally through the bone until a non-bone voxel is reached (Pahr and Zysset 2009b). By using a value of average trabeculae thickness, morphological filters fill and close small holes present in the porous cortex allowing a smooth boundary contour between cortical and trabecular bone to be identified (Pahr and Zysset 2009b, a; Gross et al. 2014). Two *Gorilla*, one *Pan* and two *Pongo* specimens were excluded from the sample as the internal cortical-trabecular boundary could not be confidently defined due to extreme cortical porosity (an example is provided in Supplementary Figure 3.1). Medtool then superimposes the trabecular-cortical boundary to the original image such that the pores within the cortex are maintained for analysis. Porosity is important to maintain within the cortical bone when quantifying microarchitecture as it has been linked to strength and elastic modulus (Cooper et al. 2016). Unique scalars are applied to the background, cortical, trabecular and internal elements of the scan. A series of image stacks are created and include a cortex-only stack (Figure 3.2C), trabecular and internal-only stack (Figure 3.2D) and a trabecular and cortical combined stack (Figure 3.2E). A 3D grid with 2.5mm spaced nodes is then superimposed on an image stack, and a 5mm sampling sphere moves from node to node to measure parameters across the entire bone (Figure 3.2F) (Pahr and Zysset 2009b).

BV/TV is calculated as the ratio of bone to non-bone voxels. DA is calculated via the Mean Intercept Length (MIL) method (Whitehouse 1974) and is calculated as $1 - (\text{min. eigenvalue}/\text{max. eigenvalue})$, which produces a number limited between 1 and 0, with 1 being complete anisotropy and 0 being complete isotropy. Tb.Th, Ct.Th and Tb.Sp are computed in a similar way to the more well-known BoneJ® plugin (Doube et al. 2010) for ImageJ. Spheres are grown within the trabecular or cortical bone, and medtool calculates the

diameter of the largest sphere that fits within the bone (Hildebrand and Rüegsegger 1997). For the calculation of Tb.Sp, medtool inverts the greyscale values of the image stack (Figure 3.2E) such that the 'internal' voxels are now represented by the 'bone' scalar. Similar to Tb.Th and Ct.Th, spheres are then grown within the internal voxels until a trabecular or cortical voxel is reached. The results of Tb.Sp and Tb.Th are used to calculate Tb.N using the formula $1/(Tb.Th+Tb.Sp)$.

Cortical and trabecular parameters were quantified in the whole capitate, as well as proximal and distal VOIs. To produce these VOIs, each capitate was cut just distal to the ulnar-most point of the ridge, delineating the extent of the lunate articulation on the dorsal proximal capitate, as per the measurement made in Richmond (2006) (Figure 3.3D). These VOIs are subjected to the same data collection process as outlined in Figure 3.2, quantifying all of the trabecular or trabecular and cortical bone within the proximal or distal segment. This delineation separates the proximal VOI as the section of the bone that does not contain any ligament attachment sites, from the distal VOI, which does receive ligamentous attachments. To assess and compare the relative contribution of cortical bone to total bone volume, BV/TV was measured twice: firstly, in only the trabecular region of the bone (Figure 3.3D) as determined using medtool (see above) and, secondly, in the original MIA segmented specimen in which there is no partitioning between cortical and trabecular bone (Figure 3.2B). This provides a measure of BV/TV that combines cortical and trabecular bone (referred to as 'total BV/TV' throughout). Relative thickness maps of Ct.Th and Tb.Th are generated by loading the Tb.Th output into ImageJ (1.50b) (<https://imagej.nih.gov/ij/>) and visualized using the 3D Volume Viewer plugin (<http://rsb.info.nih.gov/ij/plugins/volume-viewer.html>)

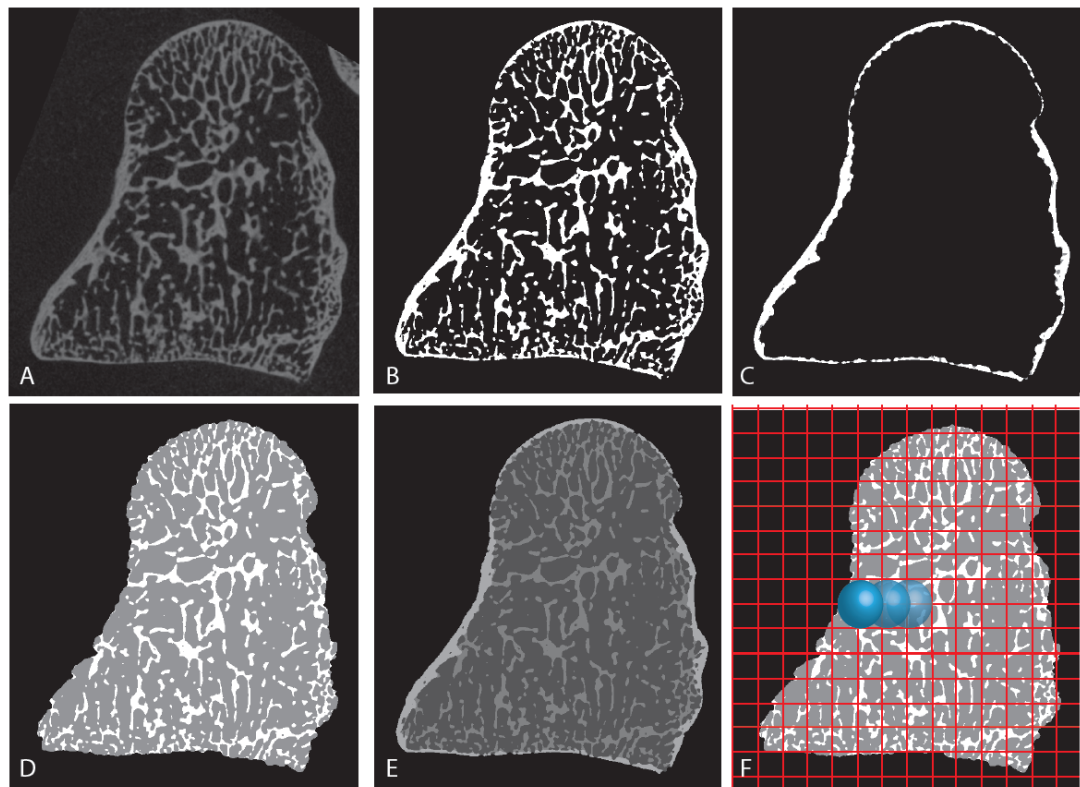


Figure 3.2 Images showing the morphological filters applied in medtool 4.3 for the whole-bone analysis.

A) Original microCT of a *Homo sapiens* capitata, B) MicroCT scan after MIA-clustering segmentation, C) Cortical thickness image stack, allowing analysis of the cortex only, D) Trabecular bone image stack, allowing analysis of the trabeculae (white) only, E) Combined mask overlay, identifying cortical (lightest grey), trabecular (mid-grey) and air (darkest grey internally and black externally) voxels, F) Sampling sphere (blue) moving across each node of the overlaid 3D grid (red) measuring bone parameters in the trabecular bone image stack.

3.4.d. Statistical analysis

3.4.d.1. Trabecular bone hypotheses

The proximal and distal trabecular parameters (trabecular BV/TV, DA, Tb.Th, Tb.N, Tb.Sp) were compared interspecifically using a Kruskal-Wallis one-way ANOVA and post hoc pairwise Wilcoxon rank-sum tests using the Holm p adjust method (*R* Core Team, stats package v3.6.1) (Table 3.1). A Wilcoxon signed-rank test was applied within-genus to test whether the mean values of each trabecular parameter were statistically different between the proximal and distal segment. A distal to proximal ratio was then calculated for each parameter. A Kruskal-Wallis test by ranks and pairwise Wilcoxon rank-sum test examined interspecific differences in the ratios.

3.4.d.2. Cortical bone hypotheses

To test for differences in cortical bone, mean differences in total BV/TV and Ct.Th were compared interspecifically in the proximal and distal segments using a Kruskal-Wallis one-way ANOVA and pairwise Wilcoxon rank-sum tests using the Holm p adjust method (*R* Core Team, stats package v3.6.1).

A Wilcoxon signed-rank test was applied within-genus to test whether the mean values of each parameter were statistically different between the proximal and distal segments. A distal to proximal ratio was then calculated for each parameter. Additionally, we examined taxonomic differences in these ratios using a Kruskal-Wallis one-way ANOVA and pairwise Wilcoxon rank-sum tests.

Two additional ratios were calculated in order to test for taxonomic differences in the relative proportion of cortical and trabecular bone. These ratios were compared between species, using a Kruskal-Wallis one-way ANOVA and pairwise Wilcoxon rank-sum tests using the Holm p adjust method (*R* Core Team, stats package v3.6.1).

3.4.d.3. Inter- and intra-specific allometry

To test for allometric trends in the capitata, each whole-bone cortical and trabecular parameter was inter- and intra-specifically analysed in a reduced major axis regression (RMA). As a proxy for body mass, the volume (mm³) of each capitata was calculated in Paraview (4.8.2) using the Integrate Variables filter. The logged cube root of the volume was regressed against the logged bone parameters using the lmodel2 package in *R* (v1.7-3; Legendre, 2018). Interpretation follows Ryan and Shaw (2013); the shape parameters of BV/TV, DA and Tb.N will have an isometric slope equal to 0; values greater than 0 indicate positive allometry while values less than 0 are indicative of negative allometry. Size parameters, such as Ct.Th, Tb.Th and Tb.Sp will have an isometric slope of 1; positive allometry is indicated by a value greater than one and negative allometry by values of less than 1. All statistical tests conducted for hypotheses 1, 2 and 3 are considered significant if $p \leq 0.05$.

3.5. Results

3.5.a. Trabecular bone

Cross-sections of each genus in Figure 3.3 provide an example of the internal structure of the capitata within three planes of view. The red dotted line in Figure 3.3D indicates where the capitata was partitioned into the proximal and distal segments.

3.5.b. Bone volume to total volume

Proximal and distal trabecular BV/TV differ significantly across the study sample ($p < 0.001$ for both tests, Supplementary Table 3.3). *Gorilla* has the highest proximal and distal BV/TV followed by *Pan*, then *Pongo*, with *Homo* having the lowest BV/TV values (Supplementary Table 3.2). Proximally, pairwise comparisons show that *Pongo* is not differentiated from any other taxa, while other pairwise comparisons are significant. Distally, all pairwise comparisons are significant except between *Pongo* and *Pan* (Figure 3.4A, Supplementary Table 3.3).

Intraspecific comparisons of the BV/TV ratio (distal BV/TV relative to proximal BV/TV) reveal that all genera have greater trabecular BV/TV in the proximal aspect (Figure 3.5A, Supplementary Table 3.4, Supplementary Table 3.5). The differences between the two VOIs reach statistical significance in *Homo*, *Pan* and *Gorilla* ($p < 0.001$ for three tests; Supplementary Table 3.4) but are non-significant in *Pongo*. The Kruskal-Wallis test on the BV/TV ratio reveals that it does not differ significantly among the study sample ($p = 0.429$), indicating that although BV/TV differs between the proximal and distal capitata, the way it differs is similar among the hominoids.

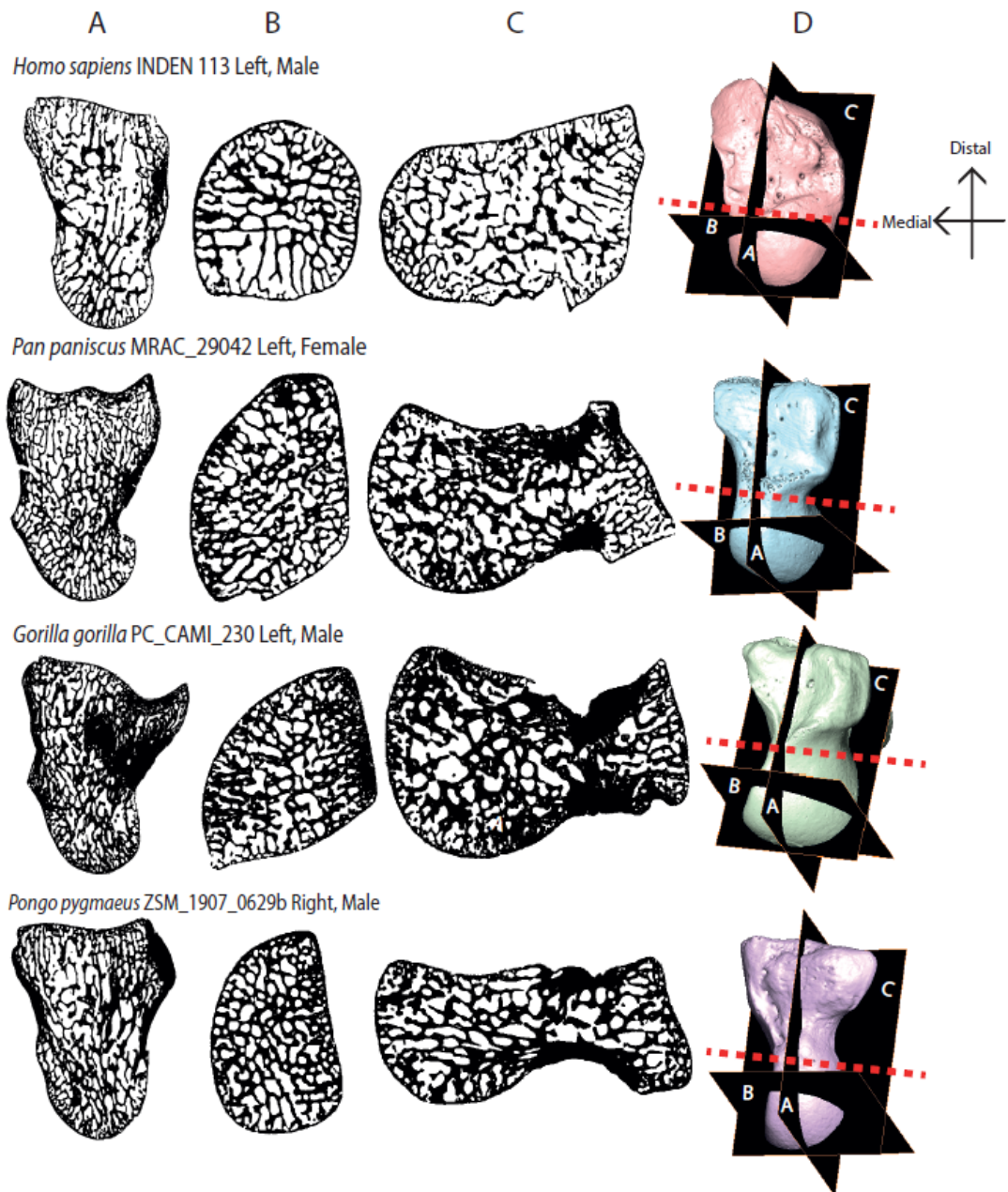


Figure 3.3 Three cross-sections from the four study genera showing internal bone patterning. A) Y-Z dimension, radio-ulnar cross-section, slice taken from mid-section of bone. Distal is up; dorsal is left. B) X-Y dimension, proximal-distal cross-section, slice taken from proximal mid-capitate. Dorsal is up; radial is left. C) X-Z dimension, dorsal-palmar cross-section, slice taken from midsection of bone. Ulnar is up; proximal is left. D) Surface models of each bone showing the location of cross-section A, B and C. The red dotted line indicates where capitates were partitioned into a distal and proximal VOI. Capitates are not to scale. Left capitates have been mirrored.

3.5.c. Degree of anisotropy

Proximal DA differs significantly among the study sample ($p < 0.001$) however distal DA does not ($p = 0.593$, Supplementary Table 3.3). Notably, DA is the only trabecular parameter which has a different significance result for the proximal and distal VOI. *Homo* and *Pongo* have the highest proximal DA with 0.30 followed by *Pan* and *Gorilla*, both with 0.24 (Figure 3.4B, Supplementary Table 3.2). Distal DA differs by only 0.02 between the genera, with the highest value from *Gorilla* at 0.28 and lowest from *Pan* at 0.26 (Supplementary Table 3.2). Pairwise comparisons reveal that proximally, *Homo* and *Pongo* are differentiated from *Pan* and *Gorilla* ($p < 0.001$ for all four significant tests). Distally, there are no significant pairwise results (Figure 3.4B, Supplementary Table 3.3).

Both *Gorilla* and *Pan* have a higher DA in the distal VOI whereas *Homo* and *Pongo* both have higher DA in the proximal and the difference between the proximal and distal VOIs is significant for all genera (Figure 3.5B, Supplementary Table 3.4). The DA ratio differs significantly across the genera ($p < 0.001$) and pairwise comparisons reveal that *Homo* and *Pongo* are differentiated from *Pan* and *Gorilla* ($p < 0.001$ for all four significant tests, Supplementary Table 3.4).

3.5.d. Trabecular thickness

Tb.Th differs significantly across both the proximal and distal capitata of the study sample ($p < 0.001$ for both tests, Supplementary Table 3.3). *Gorilla* has the highest mean thickness followed by *Pongo*, with *Homo* having the thinnest (Supplementary Table 3.2). Distally, all pairwise comparisons are significant except between *Homo* and *Pan*. Proximally, *Gorilla* is differentiated from all other taxa (Figure 3.4C, Supplementary Table 3.3).

Homo, *Pan* and *Gorilla* have thicker trabeculae in the proximal aspect and *Pongo* in the distal aspect (Supplementary Table 3.4 and Supplementary Table 3.5). The difference between the two segments is statistically significant for *Pan*, *Gorilla* and *Pongo* but not for *Homo* (Figure 3.5C, Supplementary Table 3.4). The Tb.Th ratio differs significantly among the study sample ($p < 0.001$) and all pairwise comparisons are significant except between *Homo* and *Gorilla* (Supplementary Table 3.4).

3.5.e. Trabecular number

Proximal and distal Tb.N differs significantly among the study sample ($p < 0.001$ for both tests, Supplementary Table 3.3). *Gorilla* has the lowest trabecular number while *Pan* has the highest number (Supplementary Table 3.2). Distally, all pairwise comparisons are significant

except between *Pongo* and *Homo*, and *Pongo* and *Gorilla*. Proximally, only *Gorilla* is differentiated from all other taxa (Figure 3.4D, Supplementary Table 3.3).

The Tb.N ratio indicates that *Homo*, *Gorilla* and *Pongo* have a higher trabecular number in the proximal aspect, and *Pan* have a higher number in the distal (Figure 3.5D). The differences between the proximal and distal VOI is significant for all taxa. While the Tb.N ratio differs significantly among the study sample ($p < 0.001$) only *Pan* shows significant pairwise results with all other taxa ($p < 0.001$ for all three significant tests, Supplementary Table 3.4 and Supplementary Table 3.5).

3.5.f. Trabecular separation

Tb.Sp differs significantly in the distal ($p < 0.001$) and proximal ($p = 0.038$, Supplementary Table 3.3) capitata of the study sample. *Gorilla* has the most widely spaced trabeculae, while *Pan* has the most tightly packed (Supplementary Table 3.2). Pairwise comparisons indicate that distally, *Pan* is differentiated from all other taxa (Supplementary Table 3.3). Proximally, the only significant pairwise result is between *Pan* and *Gorilla* (Fig. 3.4D).

The Tb.Sp ratio shows that *Homo*, *Gorilla* and *Pongo* have greater trabecular separation in the distal capitata whereas *Pan* has greater separation in the proximal (Figure 3.5D, Supplementary Table 3.5). The difference between the separation in the distal and proximal capitata is significant for all genera (Supplementary Table 3.4). The Tb.Sp ratio differs significantly among the study sample ($p < 0.001$) and the results of the pairwise comparisons mirror those of the distal segment as the only significant tests are between *Pan* and the other taxa ($p < 0.001$ for the three significant tests, Supplementary Table 3.4).

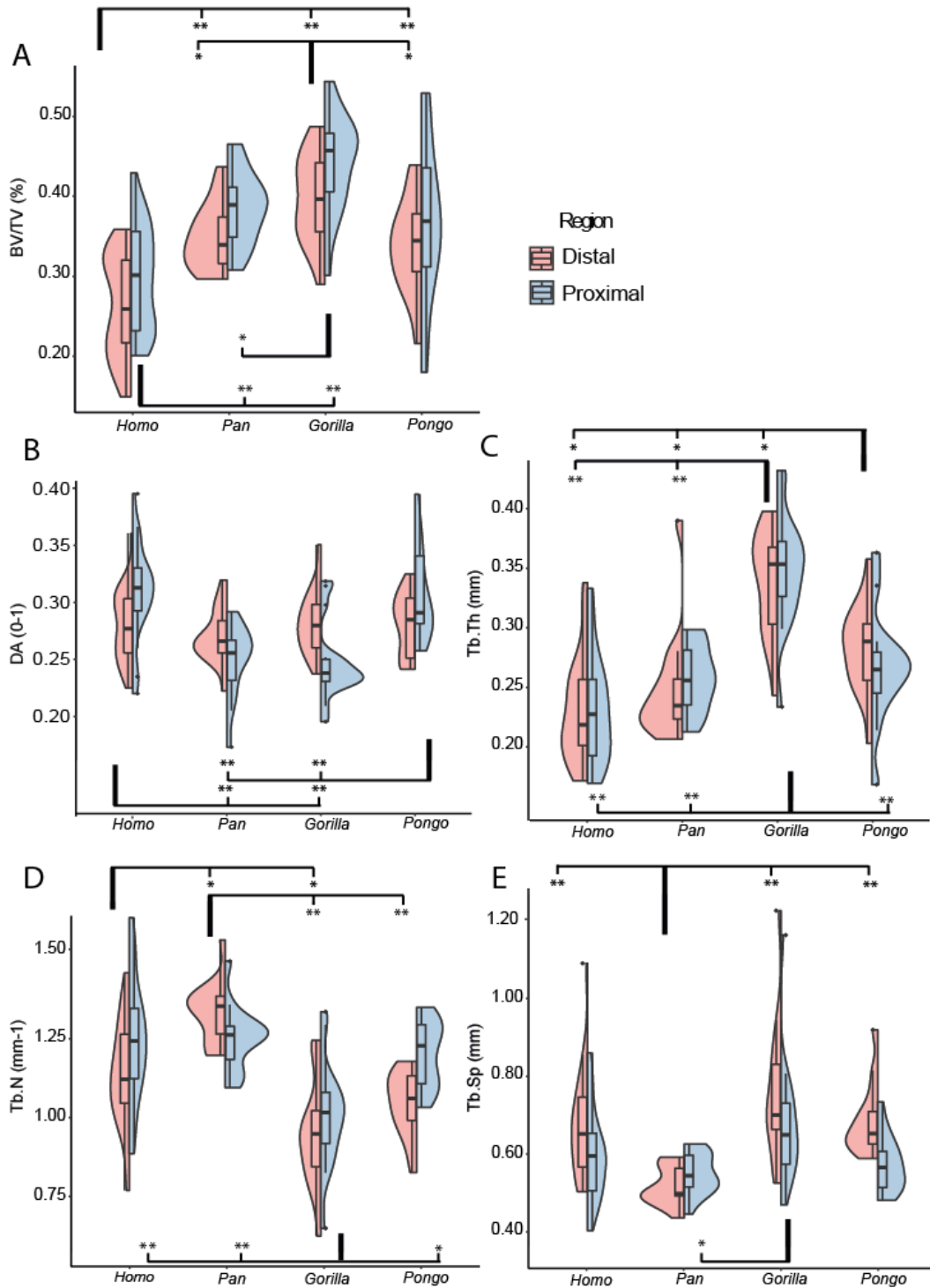


Figure 3.4 Split violin plots showing the distribution of trabecular results in the proximal and distal VOI of each genus.

Images are generated using ggplot2 in R (v. 1.2.1335) and utilise the default (Gaussian) kernel density estimation. Colored contours indicate the density of results across the data range. A) Trabecular bone volume to total volume; B) Degree of anisotropy; C) trabecular thickness; D) trabecular number; E) trabecular separation. Outliers are identified with ● and represent values 1.5 times above the fourth or below the first interquartile range. For all plots: significant pairwise comparisons are indicated by the square brackets for the distal VOI tests (top of graph) and proximal VOI tests (bottom of graph), * = $p \leq 0.05$; ** = $p \leq 0.001$.

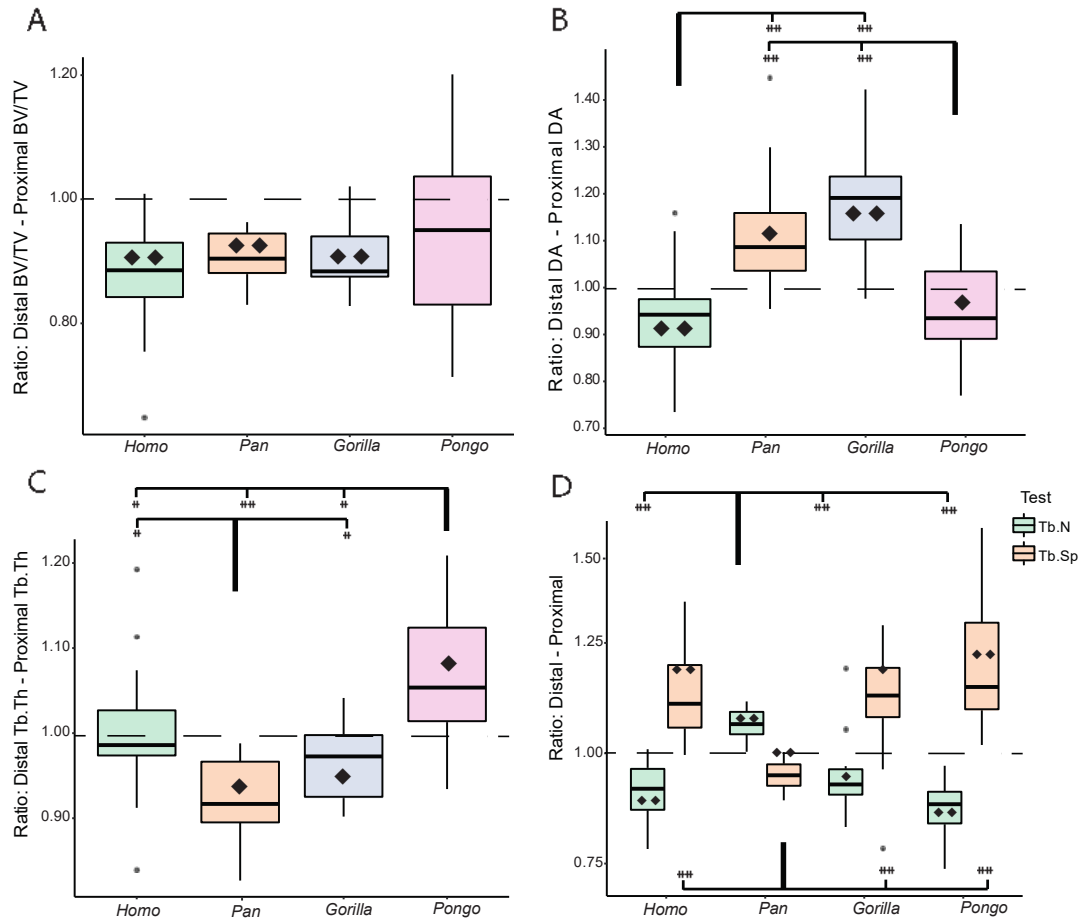


Figure 3.5 Boxplots of the five trabecular ratios for each genus as well as results for the intraspecific Wilcoxon signed-rank test and interspecific pairwise rank-sum tests.

A) Ratio of distal to proximal trabecular BV/TV; B) Ratio of distal to proximal DA; C) Ratio of distal to proximal Tb.Th.; D) Ratio of distal to proximal Tb.N (green) and Tb.Sp (orange). For all figures: Values above the dotted line (ratio = 1) indicate greater trabecular variable in the distal capitata. Significant pairwise comparisons of the ratios are indicated by the square brackets. For D, the top brackets indicate the tests for Tb.N and the bottom brackets indicate those for Tb.Sp. * = $p \leq 0.05$; ** = $p \leq 0.001$. Significant intraspecific Wilcoxon signed-rank tests between the proximal and distal means are represented by the \blacklozenge symbol thus indicates whether the difference between the mean distal and proximal trabecular variable was significantly different. \blacklozenge = $p \leq 0.05$; $\blacklozenge\blacklozenge$ = $p \leq 0.001$.

3.5.g. Total relative bone volume

Total BV/TV, which incorporates both trabecular and cortical bone, differs significantly across the study sample for both the proximal and distal capitata ($p < 0.001$ for both tests, Supplementary Table 3.3). *Gorilla* has the highest total BV/TV in both VOIs, followed by *Pan*, *Pongo* then *Homo* Figure 3.6A, Supplementary Table 3.2). Pairwise comparisons reveal that distally, *Homo* has significantly lower total BV/TV than all other taxa ($p < 0.001$ for all tests, Supplementary Table 3.3). Proximally, the results remain the same between *Homo* and

Gorilla, and *Homo* and *Pan*, although in this region, *Homo* is undifferentiated from *Pongo*. The only significant non-human pairwise comparison among the proximal and distal results is in the distal VOI between *Pongo* and *Gorilla* ($p=0.014$).

The total BV/TV ratio of the proximal and distal capitata differs significantly across the study sample ($p<0.001$). Pairwise comparisons reveal that *Homo* is differentiated from all non-human hominids ($p<0.001$ for all significant tests, Supplementary Table 3.4) while the non-human hominids are not differentiated from one another ($p=0.51$ for all three tests) (Figure 3.6C, Supplementary Table 3.4). The Wilcoxon signed-rank tests indicate that the differences in the total BV/TV between the two segments is statistically significant for all genera. As outlined in the above section, trabecular BV/TV is consistently higher in the proximal segment compared to the distal segment in all genera (Figure 3.4A, Supplementary Table 3.2). However, when total BV/TV is measured, *Pan*, *Gorilla* and *Pongo* show significantly higher values in the distal capitata (Figure 3.6A, Supplementary Table 3.2 and Supplementary Table 3.4). In contrast, *Homo* maintains the trabecular BV/TV pattern, with higher total BV/TV in the proximal segment.

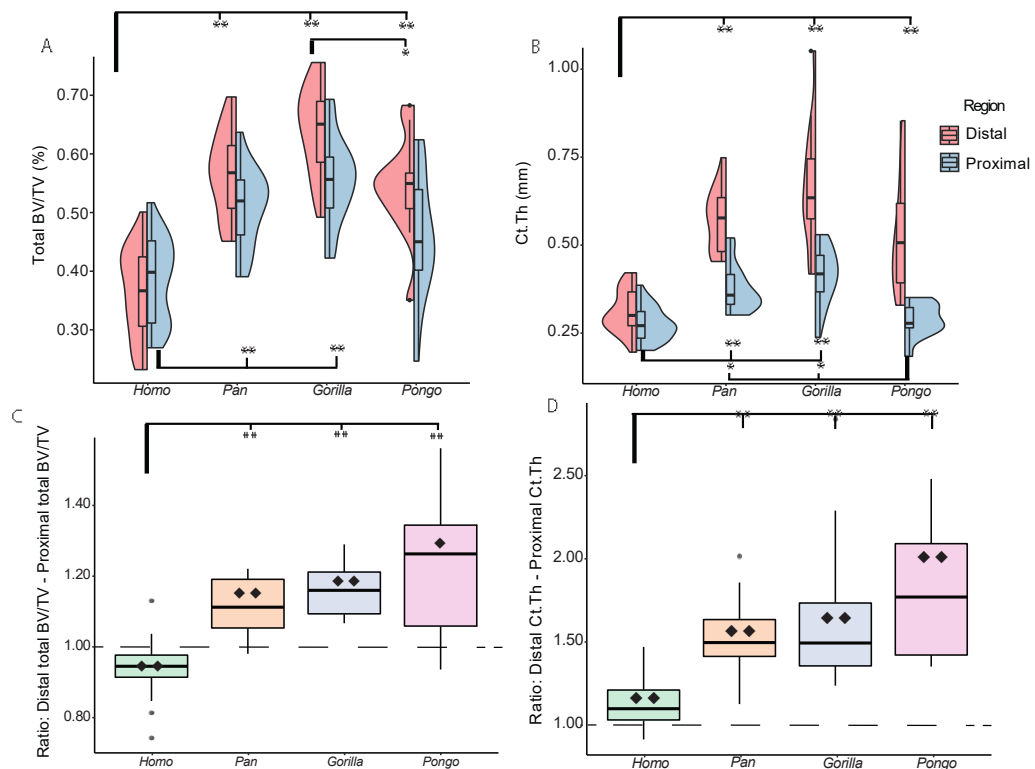


Figure 3.6 Split violin plots showing the distribution of total BV/TV (A) and Ct.Th (B) results in the proximal and distal VOI of each genus.

Images are generated using *ggplot2* in *R* (v. 1.2.1335) and utilise the default (Gaussian) kernel density estimation. Colored contours indicate the density of results across the data range. Outliers are identified with ● and represent values 1.5 times above the fourth or below the

first interquartile range. Significant pairwise comparisons are indicated by the square brackets for the distal tests (top of graph) and proximal tests (bottom of graph), * = $p \leq 0.05$; ** = $p \leq 0.001$. C-D: Boxplots showing the distribution of the distal to proximal ratios of the total BV/TV (C) and Ct.Th (D) of each genus. Boxplots also show the results of the intraspecific Wilcoxon signed-rank test and interspecific pairwise rank-sum tests. Values above the dotted line (ratio = 1) indicate greater cortical variable in the distal capitate. Significant pairwise comparisons of the ratios are indicated by the square brackets, * = $p \leq 0.05$; ** = $p \leq 0.001$. Significant intraspecific Wilcoxon signed-rank tests between the proximal and distal means are represented by the \blacklozenge symbol thus indicate whether the difference between the mean distal and proximal trabecular variable was significantly different. \blacklozenge = $p \leq 0.05$; $\blacklozenge\blacklozenge$ = $p \leq 0.001$.

In the proximal capitate, the ratio of cortical bone to trabecular bone is similar among all genera, and pairwise comparisons reveal no significant results (Supplementary Table 3.4 and Supplementary Table 3.5). In this segment, the inclusion of cortical bone increases BV/TV by 24% in *Gorilla*, 29% in *Pan*, 28% in *Homo* and 24% in *Pongo*. Conversely, in the distal capitate, the ratio of cortical bone to trabecular bone is statistically differentiated among the study sample ($p < 0.001$). Pairwise comparisons indicate this is driven by *Homo*, as the cortical bone represents a significantly lower proportion of total BV/TV compared to all other non-human hominids (Supplementary Table 3.4). The relative portions of distal cortical and trabecular bone are similar among the non-human hominids with cortical bone contributing 59% of total BV/TV in *Pan* and *Pongo* and 58% for *Gorilla*. In *Homo*, cortical bone represents 38% of distal total BV/TV.

3.5.h. Cortical bone thickness

Ct.Th differs significantly among the study genera in both proximal and distal capitate ($p < 0.001$ for both tests, Supplementary Table 3.3). In both segments, *Gorilla* has the thickest mean cortical bone, followed by *Pan*, *Pongo* and finally *Homo* (Figure 3.6B, Supplementary Table 3.2). In the distal capitate, *Homo* has significantly thinner Ct.Th than the non-human hominid ($p < 0.001$ for all tests, Supplementary Table 3.3), while the non-human hominid are not differentiated from one another. In the proximal capitate, *Homo* has significantly thinner cortical bone than *Pan* and *Gorilla* ($p < 0.001$) but is undifferentiated from *Pongo* ($p = 0.386$). Across the non-human hominids, *Pongo* has significantly thinner cortical bone than *Gorilla* and *Pan* ($p = 0.001$ for both)

All genera have thicker cortical bone in the distal VOI and the difference between the proximal and distal segments is statistically significant in all genera ($p < 0.001$ for all tests) (Figure 3.6D, Supplementary Table 3.4 and Supplementary Table 3.5). *Pongo* has the greatest relative cortical thickening in the distal VOI with the distal cortex being 79% thicker than the proximal, followed by *Gorilla* (62% thicker), *Pan* (52% thicker) and finally *Homo* (12% thicker).

Pairwise comparisons of the ratio indicate that *Homo* is differentiated from all non-human hominids ($p < 0.001$ for all tests, Supplementary Table 3.4). There are no significant pairwise comparisons between the non-human hominids. The relative thickness of the cortex and trabeculae is visualized in Figure 3.7. In non-human hominids, the thickest bone is consistently seen within the distal cortex. In *Homo*, the cortex and trabeculae have a similar thickness across the entire bone.

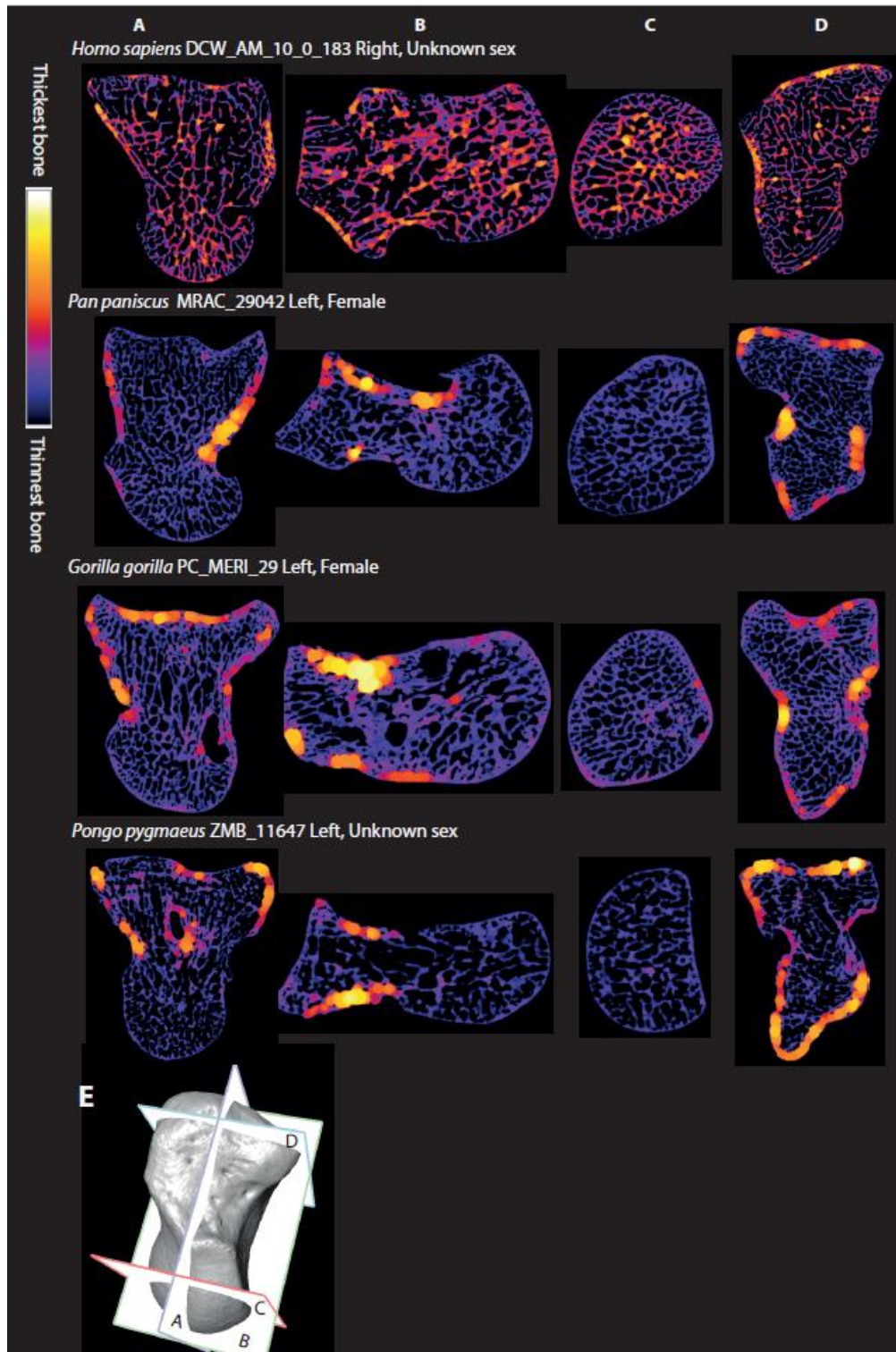


Figure 3.7 Cross-sections from representative individuals of each genus showing relative trabeculae and cortex thickness across the capitate.

A) Y-Z dimension, radio-ulnar cross-section. Distal is up; dorsal is left. B) X-Z dimension, dorsal-palmar cross-section. Ulnar is up; distal is left. C) X-Y dimension, proximal-distal cross-section. Cross-section taken at the proximal mid-capitate. Dorsal is up; radial is left. D) X-Y dimension, proximal-distal cross-section. Cross-section taken at the distal capitate. Dorsal is up; ulnar is left. E) Shows the positions of cross-sections A-D on a *Pan* specimen. Left capitates have been mirrored. Capitates not to scale.

3.5.i. Allometry

The results of the allometry tests are reported in Table 3.3 and a figure plotting the regressions is provided in the supplementary material (Supplementary Figure 3.2). Trabecular and total BV/TV show a significant positive allometric relationship with capitate volume across hominids; however, there are no significant allometric trends intraspecifically. In all inter- and intraspecific tests, DA is independent of capitate volume. Tb.Th shows significant positive allometry across the hominoids as well as in *Homo* and *Pongo*. In *Gorilla*, Tb.Th scales with isometry and in *Pan* it is uncorrelated. Across hominoids, Tb.N scales with negative allometry. Intraspecifically, only *Gorilla* has a significant relationship with Tb.N, scaling with negative allometry. Tb.Sp scales with positive allometry across hominoids. Intraspecifically only *Gorilla* has a significant relationship with Tb.Sp, scaling with positive allometry. Ct.Th scales with positive allometry across the hominoids, as well as in *Homo*, *Gorilla* and *Pongo*.

Table 3.3 RMA regression results of the inter- and interspecific allometry.

CL- and CL+ indicate the 95% lower and upper limits for the confidence interval. Significant test are in bold.

	Variable	Isometric slope	Slope	CL-	CL+	r ²	Intercept	p-value	Allometry
Whole sample	BV/TV	0	1.800	1.440	2.250	0.133	-2.550	0.001	Positive
	DA	0	-0.759	-0.966	-0.596	0.005	0.310	0.559	Uncorrelated
	Tb.Th	1	1.480	1.240	1.770	0.460	-2.280	<0.001	Positive
	Tb.N	0	-1.140	-1.390	-0.940	0.362	1.360	<0.001	Negative
	Tb.Sp	1	1.290	1.040	1.600	0.187	-1.680	<0.001	Positive
	Total BV/TV	0	1.830	1.460	2.280	0.150	-2.420	0.001	Positive
	Ct.Th	1	2.430	1.980	2.980	0.278	-3.160	<0.001	Positive
<i>Homo</i>	BV/TV	0	2.600	1.760	3.840	0.095	-3.510	0.125	Uncorrelated
	DA	0	1.190	0.799	1.760	0.068	-1.880	0.198	Uncorrelated
	Tb.Th	1	1.970	1.370	2.810	0.244	-2.860	0.010	Positive
	Tb.N	0	-1.630	-2.420	-1.100	0.066	1.900	0.205	Uncorrelated
	Tb.Sp	1	1.990	1.320	2.990	0.009	-2.440	0.629	Uncorrelated
	Total BV/TV	0	2.160	1.450	3.210	0.064	-2.880	0.212	Uncorrelated
	Ct.Th	1	1.980	1.370	2.870	0.194	-2.760	0.024	Positive
<i>Pan</i>	BV/TV	0	-1.770	-3.140	-0.998	0.070	1.550	0.341	Uncorrelated
	DA	0	1.390	0.785	2.470	0.070	-2.160	0.344	Uncorrelated
	Tb.Th	1	-1.520	-2.710	-0.850	0.068	1.100	0.384	Uncorrelated
	Tb.N	0	1.140	0.628	2.060	<0.001	-1.170	0.976	Uncorrelated
	Tb.Sp	1	1.480	0.823	2.680	0.011	-1.950	0.071	Uncorrelated
	Total BV/TV	0	-1.850	-3.310	-1.030	0.032	1.800	0.536	Uncorrelated
	Ct.Th	1	-2.230	-4.000	-1.250	0.040	2.230	0.493	Uncorrelated
<i>Gorilla</i>	BV/TV	0	-1.010	-1.720	-0.597	0.064	0.859	0.342	Uncorrelated
	DA	0	0.712	0.418	1.210	0.050	-1.450	0.403	Uncorrelated
	Tb.Th	1	0.959	0.678	1.360	0.618	-1.650	<0.001	Isometry
	Tb.N	0	-1.220	-1.670	-0.895	0.693	1.490	<0.001	Negative
	Tb.Sp	1	1.450	1.020	2.070	0.602	-1.940	<0.001	Positive
	Total BV/TV	0	-0.833	-1.430	-0.484	0.011	0.802	0.698	Uncorrelated
	Ct.Th	1	1.670	1.080	2.560	0.402	-2.280	0.008	Positive

<i>Pongo</i>	BV/TV	0	2.570	1.410	4.690	0.077	-3.320	0.358	Uncorrelated
	DA	0	-1.180	-2.010	-0.690	0.291	0.761	0.057	Uncorrelated
	Tb.Th	1	1.690	1.010	2.850	0.328	-2.440	0.040	Positive
	Tb.N	0	-1.030	-1.880	-0.567	0.079	1.180	0.351	Uncorrelated
	Tb.Sp	1	1.330	0.711	2.470	<0.001	-1.660	0.980	Uncorrelated
	Total BV/TV	0	2.040	1.160	3.580	0.203	-2.560	0.123	Uncorrelated
	Ct.Th	1	3.250	2.000	5.280	0.425	-3.940	0.015	Positive

3.6. Discussion

This study quantified the internal bone structure of the hominoid capitate using a whole-bone methodology to examine 1) whether relative and absolute differences in trabecular and cortical parameters across hominoid taxa could be correlated to inferred habitual behaviour and 2) how the parameters differed inter- and intra-specifically across the proximal and distal portion of the capitate.

3.6.a. Allometry in the capitate

Interspecifically, the predictions for Tb.N and DA were supported while all others were rejected. The two parameters most strongly correlated with size were Tb.Th and Tb.N. This was particularly true for *Gorilla*, which had relatively strong positive scaling for Tb.Th, Tb.N and Tb.Sp, with r-squared values between 0.60-0.69. This suggests these parameters may be linked to sexual dimorphism, which is extreme in *Gorilla* (Smith and Jungers 1997). Indeed, the largest Tb.Th and Tb.Sp, and smallest Tb.N values among the gorillas were from males. *Pan* was the only genus that did not report at least one significant intraspecific allometric test. This indicates that capitate size differences (as a proxy for body mass differences) between *Pan troglodytes* and *Pan paniscus* have not influenced results.

The positive relationship found in BV/TV does not corroborate results of either previous study on allometry in the primate capitate (Schilling et al. 2014; Ragni 2020) or the talus (Tsegai et al. 2017). Differences in results between this study and others may be driven by the variation in the methodologies for calculating size or body mass. While this study used the cube root of the capitate, other studies have used the geometric mean (Schilling et al. 2014; Tsegai et al. 2017), body mass (Cotter et al. 2009; Barak, Lieberman and Hublin 2013), or linear dimensions of the bone (Ryan and Shaw 2013). Furthermore, this study used a whole-bone mean of trabecular parameters whereas other studies have used a VOI sampling sphere (Cotter et al. 2009; Ryan and Shaw 2013; Schilling et al. 2014; Ragni 2020). Results are likely also affected by the species constituting the study sample or the bone used for analysis (Ruff 1987; Doube et al. 2009; Ryan and Shaw 2013; Tsegai et al. 2017). Nevertheless, as BV/TV is widely reported as being independent of body mass/size, results here may indicate carpals are more likely than other skeletal elements to increase BV/TV in response to size, across hominoids. However, given the similarity in capitate size between *Homo*, *Pan* and *Pongo*, the positive relationship found here is likely driven by the larger size of *Gorilla*, rather than reflecting a hominoid trend.

Ct.Th also scaled positively with size across hominoids and within *Homo*, *Gorilla* and *Pongo*. Notably, the r-squared value for *Pongo* and *Gorilla* were high relative to other significant tests with 0.42 and 0.40 reported, respectively. These results may reflect sexually dimorphism in *Gorilla*, as the highest Ct.Th values were all found in males; however, the results were not so clear-cut in *Pongo*, with females represented within some of the highest values. The four highest Ct.Th values in *Homo* were male; however, there was a large number of specimens with unknown sex. These results, particularly the relative strength of the r-squared value, deviate from other Ct.Th studies that, for example, reported isometry in the lumbar vertebrae (Fajardo et al. 2013), positive allometry with confidence intervals incorporating isometry in the femoral neck (Demes, Jungers and Walker 2000) or negative allometry in the radius and humerus (Doubé et al. 2009).

BV/TV and Ct.Th are a primary component of bone strength and are thus critical to inferring function and functional adaptation from form (Maquer et al. 2015). The positive allometric relationship of BV/TV and Ct.Th to size found in this study potentially limits the interpretive value of these measures. However, in both measurements the coefficient of determination was small at 0.13 and 0.27, respectively. Although the average *Gorilla* capitate volume is only 3000 cubic millimeters larger than the pooled average of the other taxa, the significant results may be strongly driven by this size difference. While the significant allometric relationships of Tb.Th, Tb.N and Tb.Sp are notable, these measures are highly correlated with BV/TV and thus each is less important as a single measure than that of BV/TV for understanding bone strength and drawing behavioural inferences. Allometry is undoubtedly complex and not yet fully understood by bone biologists. The generally low r-squared values found here indicate that size did not exert a strong influence on bone parameters in our sample, but these somewhat unexpected results indicate allometry cannot be overlooked in multispecies comparisons.

3.6.b. Can internal bone architecture differentiate locomotor modes of hominoids? Predictions for BV/TV were broadly supported. In trabecular and total BV/TV, knuckle-walking African apes had the highest values, *Homo* had the lowest and *Pongo* generally fell out as intermediate between the two. These intermediate values in *Pongo* were not consistently differentiated from the other taxa. For example, although *Pongo* trabecular and total BV/TV in the distal capitate was significantly greater than that of *Homo*, it was not statistically different in the proximal capitate. This pattern was not predicted given the presumed higher forces acting on the *Pongo* capitate during locomotion compared with that of *Homo* manipulation. However, previous research has found similar results with BV/TV in

Pongo being statistically undifferentiated from *Homo* within the capitate (Schilling et al. 2014) and other skeletal elements, including the talus (DeSilva and Devlin 2012; Tsegai et al. 2013), humerus (Kivell et al. 2018b) and femur (Georgiou et al. 2019).

DA in the capitate was predicted to be highest in *Gorilla* and *Pan*, intermediate in *Homo* and lowest in *Pongo*, and results did not support this prediction. DA in the distal capitate was not significantly different between the genera, suggesting that the numerous, relatively immobile articulations within this region result in a similar DA value, irrespective of hand use. *Homo* and *Pongo* had higher DA in the proximal capitate compared to the distal segment, which statistically separated them from the knuckle-walking taxa. High DA is correlated with strength along predictable loading trajectories within joints (Cotter et al. 2009; Hart et al. 2017; Hammond et al. 2018). In *Homo*, DA in the proximal capitate may be explained by load predictability as the DTM constitutes the path of motion in a large proportion of daily activities (Schuind et al. 1995; Crisco et al. 2005; Brigstocke et al. 2014; Moritomo et al. 2014; Kaufman-Cohen et al. 2019). However, the relatively high DA in the *Pongo* proximal capitate was unexpected as it was assumed that the highly mobile joint and presumed variability in wrist postures adopted during arboreal locomotion would result in diverse loading of the proximal capitate and low DA. High DA is potentially linked to methodological limitations in quantifying directionality due to high Tb.Th or low Tb.N encapsulated by the sampling sphere (Dunmore 2019). However, in this study, *Pongo* Tb.N and Tb.Th were intermediate between *Gorilla* and *Pan*, and thus this result is unlikely a consequence of methodological limitations. Although some trabecular functional adaptation studies have found low DA values for *Pongo* as predicted (Tsegai et al. 2013; Matarazzo 2015; Georgiou et al. 2018; Kivell et al. 2018b) others have also found higher than expected values (Dunmore et al. 2019; Georgiou et al. 2019). Although arboreal locomotion is associated with mobile joints capable of receiving load from multiple directions, our knowledge of *Pongo* hand and wrist kinematics and kinetics is limited (but see Orr et al. 2010; Orr 2017; Orr 2018). The few studies of captive apes have provided invaluable data on the kinematics of vertical climbing (Isler and Thorpe 2003; Isler 2005) and quadrupedal walking (Watson et al. 2011; Finestone et al. 2018), but these behaviours constitute a small proportion of the *Pongo* locomotor repertoire (Cant 1987; Thorpe and Crompton 2006). Additionally, we currently lack manual pressure research on *Pongo* similar to that by Wunderlich and Jungers (2009) or Matarazzo (2013) on African apes. This research landscape may be limiting our ability to predict and interpret functional adaptation in the wrist and hand of wild *Pongo*. Nevertheless, the DA results here indicate

that *Pongo* may have less variation in its wrist or hand postures than predicted with bone aligning to high loads from a low number of habitual postures.

The significantly more isotropic structure in the proximal capitate of knuckle-walkers was also unexpected as the low range of extension during knuckle-walking was assumed to result in high DA. Nevertheless, the DA results are contained within the range of values reported by Ragni (2020) for the *Gorilla* and *Pan* proximal capitate. Dunmore et al. (2019) similarly found the sub-articular trabecular structure of the metacarpophalangeal joint in African apes to be more isotropic than predicted. While African apes are categorized as terrestrial knuckle-walkers, they also utilise arboreal substrates variably across their lifetimes to nest and exploit high quality food resources (Remis 1995; Thorpe and Crompton 2006; Neufuss et al. 2017). The isotropic structure may be a reflection of diverse hand postures and loading patterns from their mixed terrestrial and arboreal locomotor repertoire. It is possible these isotropic results are an artefact of high BV/TV lowering overall DA measurements and indeed in this study the lower proximal BV/TV values of *Homo* and *Pongo* are associated with higher DA. However, the similar DA values in the distal capitate, despite diverse BV/TV values, suggests our method is able to capture variation in DA across a range of BV/TV values.

This study also investigated potential differences in ratios of bone parameters across the proximal and distal capitate, testing the null hypothesis that these ratios would be similar across hominoids. This hypothesis was generally not supported as only two ratios were statistically similar across all genera: distal trabecular BV/TV relative to proximal trabecular BV/TV and proximal total BV/TV relative to proximal trabecular BV/TV. Thus, although proximal Ct.Th in *Homo* and *Pongo* was significantly thinner than that of *Pan* and *Gorilla*, the relative proportion of cortex to trabeculae is similar across all taxa. Similarly, although eight of the 12 pairwise comparisons indicated statistically different trabecular BV/TV across the taxa (Figure 3.4A), the way trabecular volume differs between the two segments is consistent across hominoids. Although it was not predicted that ratio calculations would differentiate locomotor groups, three ratios distinguished *Homo* from the suspensory and knuckle-walking taxa: 1) distal total BV/TV relative to proximal total BV/TV, 2) distal total BV/TV relative to distal trabecular BV/TV, and 3) distal Ct.Th relative to proximal Ct.Th. Together, these ratios indicate that relatively low Ct.Th in the *Homo* distal capitate is distinctive compared with the thicker cortex in non-human hominids. As Ct.Th is correlated to bone strength (Augat and Schorlemmer 2006), the distal capitate in non-human hominids is likely to be better able to resist fracture or failure and withstand high mechanical loads imposed upon the region.

This distinctive cortical morphology in non-human hominids may reflect arboreal behaviours. All non-human hominids engage in suspensory locomotion and climb vertical supports (Remis 1995; Thorpe and Crompton 2006; Neufuss et al. 2017), and in both behaviours the forelimbs are loaded in tension (Swartz, Bertram and Biewener 1989; Hunt et al. 1996; Hanna et al. 2017). The distal capitate has numerous ligament attachments that induce tensional strain onto the capitate (Kijima and Viegas 2009; Regal, Maschke and Li 2020). Bones loaded in tension have a lower failure point than those loaded in compression (Caler and Carter 1989; Pattin, Caler and Carter 1996) and therefore greater BV/TV or Ct.Th would be required to prevent failure at ligament attachment sites (Doube et al. 2009).

When comparing differences in Tb.Th, Tb.N and Tb.Sp across our study sample, results were similar to those of previous studies of different skeletal elements; *Pan* had high Tb.N and low Tb.Th and Tb.Sp, *Gorilla* showed the inverse, while *Homo* and *Pongo* were intermediate for all of these measures (Scherf, Harvati and Hublin 2013; Schilling et al. 2014; Ryan and Shaw 2015; Georgiou et al. 2018; Kivell et al. 2018b; Georgiou et al. 2019; Komza and Skinner 2019; Ragni 2020). The consistent pattern within these parameters may represent systemic, rather than strongly functionally adaptive features of bone. DA and BV/TV have been shown to account for up to 98% of bone's elastic modulus (Maquer et al. 2015) and as Tb.Th, Tb.N and Tb.Sp interact via various combinations to produce BV/TV, individual measures of Tb.Th, Tb.N and Tb.Sp may be less useful for differentiating locomotor or postural modes.

3.6.c. Do the proximal and distal segments reflect divergent strain patterns across the capitate?

Given differences in the articulations and mobility between the proximal and distal capitate, we hypothesized that each portion would show statistically different bone structure. This hypothesis was broadly supported but there was only partial support for the specific predictions. With only two exceptions (*Pongo* distal BV/TV relative to proximal BV/TV, and *Homo* distal Tb.Th relative to proximal Tb.Th), bone parameters differed significantly between the proximal and distal regions. This suggests that the internal bone is subjected to different forces and functional adaptation responses across the capitate. Ct.Th, DA and BV/TV were predicted to be higher in the distal relative to the proximal capitate due to the immobility in the distal carpal row and numerous ligament attachments. Ct.Th results in all genera supported this prediction while the DA prediction was only supported for *Gorilla* and *Pan*. All genera had significantly higher trabecular BV/TV in the proximal capitate; however, due to the great cortical thickening in non-human hominids, total BV/TV was higher in the distal capitate of *Gorilla*, *Pan* and *Pongo*. In contrast, despite a 12% increase in distal Ct.Th,

Homo maintained significantly higher total BV/TV in the proximal capitate. These differences in bone architecture were only revealed by holistically analysing biomechanically meaningful sub-regions of the capitate, while whole-bone measures or the exclusion of cortical bone, likely would have obscured or failed to pick up these trends.

While we argue that the results of this study indicate that force transfer differs across the proximal and distal capitate, additional analyses comparing different portions of the capitate are warranted to further test this conclusion. While this study averaged parameters across entire segments, bone volume distribution methods such as those used in Tsegai et al. (2013) and Tsegai et al. (2017) would allow more nuanced analysis between the regions under compression versus tension. Further, these methods would allow a deeper exploration of the biomechanical consequences of waisted versus non-waisted capitates and whether this aspect of morphology impacts the functional independence of the proximal and distal regions.

3.6.d. The relationship between trabecular and cortical bone in the capitate

This study reveals the importance of considering both cortical and trabecular bone in functional adaptation research, rather than investigating each tissue separately. As exhibited in Figure 3.6 and Figure 3.7, and discussed above, the cortical bone of the non-human hominid capitate varied substantially from that of *H. sapiens*. Thus, the null hypothesis that the ratios of cortical to trabecular bone would be similar across the hominoids was not supported. However, there was one notable exception, namely that all the study taxa had similar cortical to trabeculae ratios in the proximal capitate.

The differences between the proximal and distal Ct.Th across the locomotor groups provide support for the hypothesis that thick distal cortex in the non-human hominids is a result of functional adaptation. However, research indicates modern *Homo sapiens* have systemically low BV/TV and Ct.Th, which has been hypothesized to correlate with increased sedentism after the transition to an agricultural lifestyle (Ruff 2005; Chirchir et al. 2015; Ryan and Shaw 2015; Saers et al. 2016; Tsegai et al. 2018). Thus it would be valuable to assess the distal Ct.Th of pre-Holocene *Homo sapiens* to further interrogate whether thick distal Ct.Th can be correlated simply with higher loading more generally, or, as hypothesized here, is related to forelimb involvement in arboreal behaviour among the non-human hominids. Further, there are important limitations to our interpretation of cortical BFA in short bones. Although cortical bone does model its structure during adulthood in response to load, the genetic blueprint and the process of modelling during ontogeny greatly determines cortical bone

geometry (Martin, Burr and Sharkey 1998; Lovejoy et al. 2003). Investigation on the changes to cortical bone geometry as a result of functional adaptation have predominantly focused on changes at the mid-shaft of long bones (for examples and summary see Ruff et al. (2006) and references therein). In short bones there is unlikely to be the same capacity for the cortical bone to substantially change its geometry with modelling processes because, unlike the diaphysis of a long bone, there is not substantial room to expand (Martin, Burr and Sharkey 1998). During adulthood, cortical bone commonly adapts its mechanical properties via changes to porosity, apparent mineral density or cellular anisotropy (Martin, Burr and Sharkey 1998; Currey 2002), changes that require different methodologies to assess (e.g histology). Finally, when segmenting different bone tissues, it can be challenging to identify the boundary between cortex and trabeculae, particularly when the cortex is porous or trabeculae are especially thick. This was a particular challenge in some of the non-human hominid capitate specimens (see Supplementary Figure 3.1) and will likely be a limitation for many short bones, depending on the question being addressed.

3.7. Conclusion

The capitate of knuckle-walking African apes and suspensory *Pongo* was differentiated from bipedal *Homo*, primarily, by thick distal cortical bone. African apes were further differentiated from *Pongo* and *Homo* by relatively isotropic trabeculae in the proximal capitate, which was not expected given the (presumably) more stereotypical loading of the wrist during knuckle-walking. However this higher than expected DA of the capitate head in *Homo* may indicate preferential alignment of trabeculae along the DTM. Although the wrist is often conceptualized as broadly being under compression or tension, the differentiated bone architecture in the proximal and distal regions of the capitate suggests that the loading environment can differ significantly even within the small bones of the carpus and highly localized functional adaptation responses may be taking place. Further, differences in cortical bone were critical for differentiating *Homo* from non-human hominids. While an unexpected positive relationship was found between bone volume and capitate size, the low coefficient of determination indicated size did not strongly influence group differences in bone microstructure. Given the complex biomechanical environment, and our limited understanding of inter-carpal motion, (particularly in non-human hominids) functional adaptation research of the carpals should take a holistic approach, including incorporated analysis of cortical bone.

3.8. Supplementary Tables

Supplementary Table 3.1 See Appendix A Table 1. Full list of extant and extinct specimens used in this thesis

Supplementary Table 3.2 Descriptive statistics for this study.

Capitate size (mm³) is reported for the whole bone. Trabecular and cortical bone parameters are reported for the proximal, distal and whole bone separately. ± indicates one standard deviation above and below the mean

Capitate size (mm ³)		<i>Homo</i>	<i>Pan</i>	<i>Gorilla</i>	<i>Pongo</i>
Whole bone	Mean	2495 ± 652	2418 ± 505	5376 ± 2,403	2171 ± 568
	Range	1190 – 3606	1670 – 3634	2452 – 10200	1452 – 3182
Trabecular BV/TV (%)		<i>Homo</i>	<i>Pan</i>	<i>Gorilla</i>	<i>Pongo</i>
Proximal	Mean	0.29±0.07	0.38±0.04	0.43±0.06	0.36±0.10
	Range	0.20-0.42	0.30-0.46	0.30-0.54	0.17-0.52
Distal	Mean	0.26±0.06	0.34±0.04	0.39±0.05	0.33±0.06
	Range	0.14-0.35	0.29-0.43	0.28-0.48	0.21-0.43
Whole	Mean	0.27±0.06	0.36±0.04	0.41±0.05	0.34±0.07
	Range	0.16-0.35	0.30-0.44	0.29-0.50	0.20-0.47
DA (0-1)		<i>Homo</i>	<i>Pan</i>	<i>Gorilla</i>	<i>Pongo</i>
Proximal	Mean	0.30±0.04	0.24±0.03	0.24±0.03	0.30±0.04
	Range	0.21-0.39	0.17-0.29	0.19-0.31	0.25-0.39
Distal	Mean	0.27±0.03	0.26±0.02	0.28±0.02	0.27±0.02
	Range	0.22-0.36	0.22-0.31	0.23-0.34	0.24-0.32
Whole	Mean	0.28±0.03	0.25±0.02	0.26±0.02	0.28±0.02
	Range	0.23-0.36	0.20-0.29	0.23-0.33	0.24-0.32
Tb.Th (mm)		<i>Homo</i>	<i>Pan</i>	<i>Gorilla</i>	<i>Pongo</i>
Proximal	Mean	0.23±0.05	0.25±0.02	0.34±0.04	0.26±0.04
	Range	0.16-0.33	0.21-0.29	0.23-0.43	0.16-0.36
Distal	Mean	0.22±0.04	0.24±0.04	0.33±0.04	0.28±0.03
	Range	0.16-0.33	0.20-0.38	0.24-0.39	0.20-0.35
Whole	Mean	0.22±0.04	0.24±0.02	0.34±0.04	0.27±0.03
	Range	0.17-0.32	0.20-0.28	0.23-0.41	0.19-0.35
Tb.N (mm ⁻¹)		<i>Homo</i>	<i>Pan</i>	<i>Gorilla</i>	<i>Pongo</i>
Proximal	Mean	1.23±0.18	1.25±0.10	1.00±0.16	1.19±0.10
	Range	0.88-1.63	1.09-1.49	0.64-1.33	1.03-1.34
Distal	Mean	1.13±0.15	1.33±0.09	0.95±0.17	1.04±0.10
	Range	0.76-1.45	1.19-1.56	0.62-1.24	0.82-1.17
Whole	Mean	1.16±0.16	1.29±0.09	0.97±0.16	1.08±0.09
	Range	0.78-1.47	1.15-1.53	0.63-1.27	0.91-1.20
Tb.Sp (mm)		<i>Homo</i>	<i>Pan</i>	<i>Gorilla</i>	<i>Pongo</i>
Proximal	Mean	0.59±0.12	0.54±0.05	0.67±0.15	0.57±0.07
	Range	0.40-0.85	0.44-0.62	0.46-1.15	0.47-0.73
Distal	Mean	0.66±0.12	0.51±0.04	0.74±0.17	0.68±0.09
	Range	0.50-1.08	0.43-0.58	0.52-1.21	0.58-0.91
Whole	Mean	0.64±0.12	0.53±0.05	0.71±0.16	0.65±0.07
	Range	0.48-1.03	0.43-0.62	0.51-1.19	0.56-0.81
Total BV/TV (%)		<i>Homo</i>	<i>Pan</i>	<i>Gorilla</i>	<i>Pongo</i>
Proximal	Mean	0.37±0.07	0.50±0.06	0.54±0.07	0.45±0.10
	Range	0.26-0.50	0.38-0.62	0.41-0.67	0.24-0.61

Distal	Mean	0.35±0.07	0.55±0.07	0.62±0.07	0.53±0.08
	Range	0.23-0.49	0.44-0.68	0.48-0.74	0.34-0.66
Whole	Mean	0.36±0.06	0.53±0.06	0.60±0.06	0.51±0.08
	Range	0.25-0.46	0.43-0.65	0.47-0.71	0.32-0.66
Ct.Th (mm)		<i>Homo</i>	<i>Pan</i>	<i>Gorilla</i>	<i>Pongo</i>
Proximal	Mean	0.27±0.05	0.37±0.06	0.41±0.08	0.28±0.04
	Range	0.20-0.38	0.30-0.52	0.23-0.52	0.18-0.35
Distal	Mean	0.31±0.07	0.57±0.09	0.65±0.17	0.52±0.16
	Range	0.19-0.42	0.45-0.74	0.41-1.05	0.32-0.61
Whole	Mean	0.30±0.05	0.52±0.07	0.60±0.14	0.47±0.13
	Range	0.19-0.39	0.42-0.67	0.39-0.97	0.31-0.75

Supplementary Table 3.3 Results of the Kruskal-Wallis and post-hoc pairwise comparison tests of the mean parameters in the proximal and distal segments.

In the pairwise comparisons table, values above the diagonal represent the pairwise results for the distal capitata and those below the diagonal represent the results of the proximal. Significant results are in bold.

Kruskal-Wallis		Proximal	Distal			
Trabecular BV/TV		<0.001	<0.001			
DA		<0.001	0.593			
Tb.Th		<0.001	<0.001			
Tb.N		<0.001	<0.001			
Tb.Sp		0.038	<0.001			
Total BV/TV		<0.001	<0.001			
Ct.Th		<0.001	<0.001			
Pairwise Comparisons						
Trabecular BV/TV		<i>Homo</i>	<i>Pan</i>	<i>Gorilla</i>	<i>Pongo</i>	
<i>Homo</i>	Proximal		0.001	<0.001	0.011	Distal
<i>Pan</i>		<0.001		0.044	0.685	
<i>Gorilla</i>		<0.001	0.047		0.040	
<i>Pongo</i>		0.111	0.550	0.111		
DA		<i>Homo</i>	<i>Pan</i>	<i>Gorilla</i>	<i>Pongo</i>	
<i>Homo</i>	Proximal		1	1	1	Distal
<i>Pan</i>		<0.001		1	1	
<i>Gorilla</i>		<0.001	0.846		1	
<i>Pongo</i>		0.846	<0.001	<0.001		
Tb.Th		<i>Homo</i>	<i>Pan</i>	<i>Gorilla</i>	<i>Pongo</i>	
<i>Homo</i>	Proximal		0.278	<0.001	0.004	Distal
<i>Pan</i>		0.072		<0.001	0.004	
<i>Gorilla</i>		<0.001	<0.001		0.007	
<i>Pongo</i>		0.069	0.650	<0.001		
Tb.N		<i>Homo</i>	<i>Pan</i>	<i>Gorilla</i>	<i>Pongo</i>	
<i>Homo</i>	Proximal		0.001	0.004	0.173	Distal
<i>Pan</i>		1		<0.001	<0.001	
<i>Gorilla</i>		0.001	<0.001		0.173	
<i>Pongo</i>		1	1	0.004		
Tb.Sp		<i>Homo</i>	<i>Pan</i>	<i>Gorilla</i>	<i>Pongo</i>	
<i>Homo</i>	Proximal		<0.001	0.290	0.580	Distal
<i>Pan</i>		0.630		<0.001	<0.001	
<i>Gorilla</i>		0.450	0.020		0.580	
<i>Pongo</i>		0.980	0.980	0.180		
Total BV/TV		<i>Homo</i>	<i>Pan</i>	<i>Gorilla</i>	<i>Pongo</i>	
<i>Homo</i>	Proximal		<0.001	<0.001	<0.001	Distal
<i>Pan</i>		<0.001		0.034	0.519	
<i>Gorilla</i>		<0.001	0.202		0.014	
<i>Pongo</i>		0.112	0.220	0.089		
Ct.Th		<i>Homo</i>	<i>Pan</i>	<i>Gorilla</i>	<i>Pongo</i>	
<i>Homo</i>	Proximal		<0.001	<0.001	<0.001	Distal
<i>Pan</i>		<0.001		0.360	0.360	
<i>Gorilla</i>		<0.001	0.386		0.110	
<i>Pongo</i>		0.386	0.001	0.001		

Supplementary Table 3.4 Results of the nine ratios and the associated inter- and intraspecific Wilcoxon tests.

The results of the ratios are shown within the grey shaded cells on the diagonal. Results above 1 indicate the parameter is higher in the distal segment. Asterisks within these cells specify the results of the intraspecific Wilcoxon signed-rank test indicating whether the proximal and distal results are significantly different from one another; * = $p \leq 0.05$; ** = $p \leq 0.001$. Below the diagonal, the ratio values are the results of the interspecific pairwise comparisons of the ratio. Significant results are in bold. Descriptive statistics of the ratios can be found in Supplementary Table 3.5

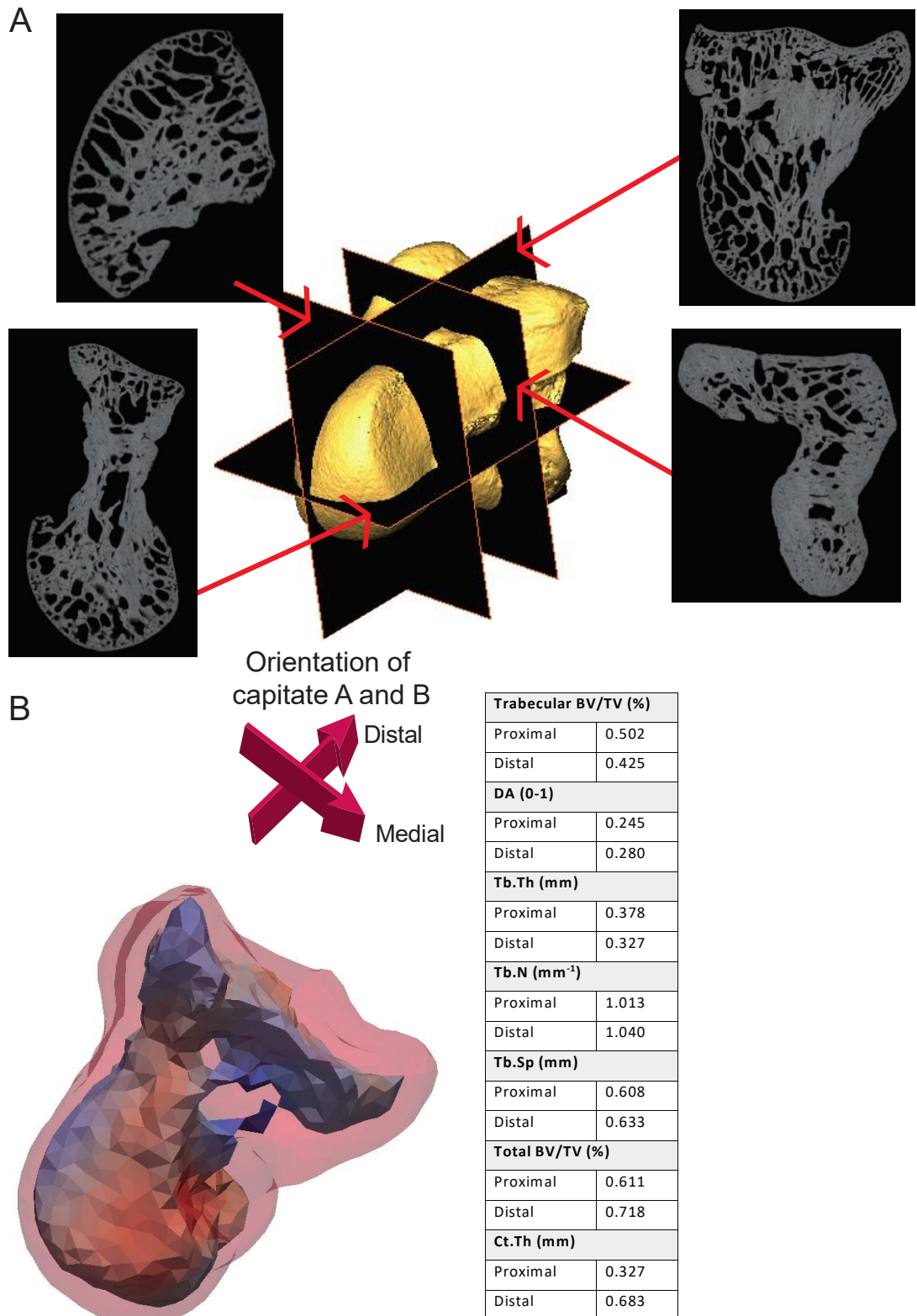
Segment (distal/proximal) differences		<i>Homo</i>	<i>Pan</i>	<i>Gorilla</i>	<i>Pongo</i>
Trabecular BV/TV	<i>Homo</i>	0.87**			
	<i>Pan</i>	1	0.90**		
	<i>Gorilla</i>	1	1	0.91**	
	<i>Pongo</i>	1	1	1	0.95
DA	<i>Homo</i>	0.91**			
	<i>Pan</i>	<0.001	1.09*		
	<i>Gorilla</i>	<0.001	0.283	1.15**	
	<i>Pongo</i>	0.981	0.001	<0.001	0.90*
Tb.Th	<i>Homo</i>	0.99			
	<i>Pan</i>	0.001	0.92*		
	<i>Gorilla</i>	0.184	0.041	0.96*	
	<i>Pongo</i>	0.041	<0.001	0.005	1.07*
Tb.N	<i>Homo</i>	0.92**			
	<i>Pan</i>	<0.001	1.06**		
	<i>Gorilla</i>	0.513	<0.001	0.94*	
	<i>Pongo</i>	0.093	<0.001	0.039	0.87**
Tb.Sp	<i>Homo</i>	1.12**			
	<i>Pan</i>	<0.001	0.94**		
	<i>Gorilla</i>	0.788	<0.001	1.11*	
	<i>Pongo</i>	0.356	<0.001	0.498	1.20**
Total BV/TV	<i>Homo</i>	0.94**			
	<i>Pan</i>	<0.001	1.11**		
	<i>Gorilla</i>	<0.001	0.51	1.15**	
	<i>Pongo</i>	<0.001	0.51	0.51	1.21*
Ct.Th	<i>Homo</i>	1.12**			
	<i>Pan</i>	<0.001	1.52**		
	<i>Gorilla</i>	<0.001	0.810	1.62**	
	<i>Pongo</i>	<0.001	0.380	0.400	1.79**
BV/TV (total/trabecular) differences		<i>Homo</i>	<i>Pan</i>	<i>Gorilla</i>	<i>Pongo</i>
Proximal		<i>Homo</i>	1.28		

	<i>Pan</i>	1	1.29		
	<i>Gorilla</i>	0.22	0.29	1.24	
	<i>Pongo</i>	0.36	0.31	1	1.24
	<i>Homo</i>	<i>Pan</i>	<i>Gorilla</i>	<i>Pongo</i>	
Distal	<i>Homo</i>	1.38			
	<i>Pan</i>	<0.001	1.59		
	<i>Gorilla</i>	<0.001	1	1.58	
	<i>Pongo</i>	<0.001	1	1	1.59

Supplementary Table 3.5 Descriptive statistics for the nine ratios calculated in this study
± indicates one standard deviation above or below the mean.

Regional differences (distal/proximal)		<i>Homo</i>	<i>Pan</i>	<i>Gorilla</i>	<i>Pongo</i>
Trabecular BV/TV	Mean	0.87±0.07	0.90±0.03	0.90±0.04	0.94±0.14
	Range	0.64-1.00	0.82-0.96	0.82-1.20	0.71-1.20
DA	Mean	0.91±0.10	1.09±0.13	1.15±0.12	0.92±0.10
	Range	0.69-1.14	0.92-1.44	0.95-1.41	0.73-1.11
Tb.Th	Mean	0.99±0.06	0.92±0.04	0.96±0.04	1.07±0.06
	Range	0.83-1.19	0.82-0.98	0.90-1.04	0.93-1.20
Tb.N	Mean	0.92±0.05	1.06±0.03	0.94±0.07	0.87±0.06
	Range	0.78-1.00	1.00-1.11	0.83-1.19	0.73-0.97
Tb.Sp	Mean	1.12±0.09	0.94±0.03	1.11±0.11	1.20±0.14
	Range	0.99-1.34	0.89-1.00	0.78-1.29	1.01-1.51
Total BV/TV	Mean	0.94±0.08	1.11±0.07	1.15±0.05	1.21±0.17
	Range	0.75-1.12	0.98-1.21	1.06-1.27	0.93-1.53
Ct.Th	Mean	1.12±0.13	1.52±0.21	1.62±0.40	1.79±0.36
	Range	0.92-1.46	1.13-2.00	1.23-2.80	1.35-2.45
BV/TV (total/trabecular) differences		<i>Homo</i>	<i>Pan</i>	<i>Gorilla</i>	<i>Pongo</i>
Proximal	Mean	1.28±0.06	1.29±0.07	1.24±0.06	1.24±0.06
	Range	1.13-1.40	1.19-1.45	1.15-1.38	1.15-1.42
Distal	Mean	1.38±0.12	1.59±0.16	1.58±0.14	1.59±0.14
	Range	1.25-1.66	1.43-1.73	1.41-1.78	1.42-1.84

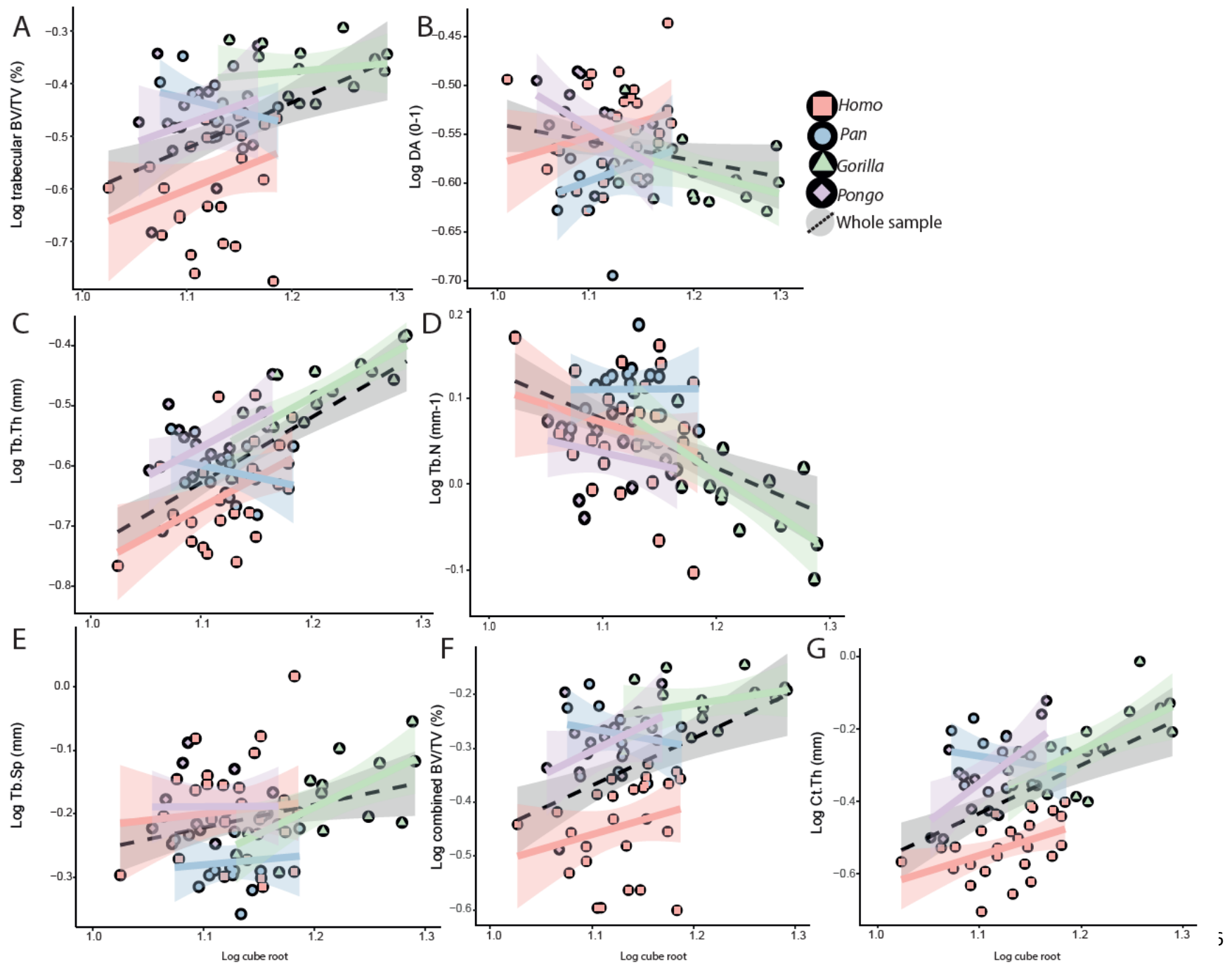
3.9. Supplementary Figures



Supplementary Figure 3.1 Example of excluded *Pan troglodytes* specimen

A) CT-derived surface model of *Pan* capitata showing the location of four cross-sections. Cross-sections show dense and porous bone is continuous throughout the entire capitata.
 B) *Pan* specimen visualized after medtool data collection. The whole bone is shown

transparent in pink, allowing visualization of the constricted and discontinuous trabecular bone region within. Results of the medtool analysis of this specimen are given in the table.



Supplementary Figure 3.2 Plots of the seven RMA regressions testing for allometry.

Individual data points are colored by genus and the hominoid trend is indicated by the dotted black line and grey confidence interval. The log cube root of the volume (mm³) is seen across the x axis. A) Trabecular BV/TV; B) DA; C) Tb.Th.; D) Tb.N.; E) Tb.Sp.; E) Total BV/TV; G) Ct.Th.

4. Patterns of internal bone structure and functional adaptation in the hominoid scaphoid, lunate, and triquetrum

Published article: Bird, E. E., Kivell, T. L., & Skinner, M. M. (2022). Patterns of internal bone structure and functional adaptation in the hominoid scaphoid, lunate, and triquetrum. *American Journal of Biological Anthropology*, 177(2), pgs. 266-285. DOI: 10.1002/ajpa.24449 see 8.3 for copyright information.

This manuscript has had minor edits for clarity of understanding and differs from the original publication.

4.1. Abstract

The morphology of the proximal carpals (scaphoid, lunate, triquetrum) are linked to the range of motion (ROM) at the radiocarpal and midcarpal joints. While the relationship between ROM and habitual locomotor mode is well established, it has yet to be investigated whether relative patterns of internal bone architecture reflect the kinematics and kinetics at the proximal row. As internal bone is known to model its structure to habitually incurred forces, internal architecture has the potential to provide insight into how joints have been loaded during the lifetime of an individual. Using a broad sample of extant hominids (n=177 total bones), this study investigates whether relative differences in the bone volume to total volume (BV/TV) and degree of anisotropy (DA) across the scaphoid, lunate and triquetrum correlate with the presumed force transfer and biomechanics of the hominoid wrist. Results reveal that broad patterns in BV/TV and DA differentiate hominoids by their predominant locomotor mode. The human pattern suggests the lunate may be the most highly strained bone within the proximal row. Both knuckle-walking taxa (*Gorilla*, *Pan*) exhibited similar architectural patterns suggesting they are adapted to resist similar forces in this region of the wrist. The relatively high DA across all *Pongo* carpals suggests it may have more stereotypical wrist loading than commonly assumed. Finally, the distinctly low DA in the triquetrum across all taxa suggests force transfer via the synapomorphic Triangular Fibrocartilage Complex may leave a distinctive signature in the internal bone architecture that requires further investigation.

4.2. Introduction

As a clade, primates exhibit a large range of locomotor strategies, adapted to the diversity of environments they inhabit globally (Schmitt, Zeininger and Granatosky 2016). Morphological variation and concomitant range of motion differences of hand and wrist bones of living primate taxa have been successfully linked to different locomotor strategies and habitual hand postures (Napier 1960; Tuttle 1969; Jenkins and Fleagle 1975; Sarmiento 1988; Lewis 1989; Hamrick 1996; Richmond 2006; Tocheri 2007; Kivell 2016a; Orr 2017), and thus often used as a proxy for inferring the locomotor mode or behaviours of fossil specimens (Marzke 1983; Marzke and Marzke 1987; Lewis 1989; Tocheri et al. 2007; Kivell et al. 2011; Marzke 2013; Kivell et al. 2015; Bardo et al. 2020). Although hominoids are united by a synapomorphic reduction in ulnocarpal articulation (Kivell 2016a), differences in the morphology of the scaphoid, lunate, and triquetrum (the proximal carpal bones) are linked to the diversity of postural modes that characterise the clade (Sarmiento 1988; Orr 2010, 2017, 2018). Among these bones, the scaphoid has received the greatest research attention, due in part to the apomorphic fusion to the os centrale in *Gorilla*, *Pan*, and *Homo*. Although there is limited understanding of the biomechanics of the lunate and triquetrum, the wrist is a series of interdependent joints and thus the morphology of each individual bone affects the movement and functionality of the entire hand.

While the external shape of carpal bones is critical to the functional integrity of the wrist, primates display behavioural and postural flexibility such that external morphology will not accurately reflect all aspects of a species' or individual's behaviour (Nowak and Lee 2013; Kivell 2016b; Schmitt, Zeininger and Granatosky 2016). Furthermore, with fossil specimens it can be challenging to discern functionally significant features from non-functional aspects of morphology representative of phylogenetic lag, particularly as behavioural adaptations precede morphological ones (Lieberman 1997; Ward 2002; Tocheri 2007; Kivell 2016b). Aspects of bone that are responsive to behaviourally induced biomechanical loading have the potential to inform how a bone has been loaded over the lifetime of an individual. For example, cortical cross-sectional area and trabecular architecture have been shown experimentally to adapt in functionally meaningful ways to contrived alterations to normal joint angle or loading (Biewener et al. 1996; Robling et al. 2002; Pontzer et al. 2006a; van der Meulen et al. 2006; Fajardo et al. 2007; Ryan and Walker 2010; Barak, Lieberman and Hublin 2011; Shaw and Ryan 2012; Wallace et al. 2015). Given the link between the morphology of the proximal row carpus to hand posture and habitual locomotor mode (Jenkins and Fleagle 1975; Sarmiento 1988; Hamrick 1996; Tocheri 2007; Orr 2017, 2018), identifying

biomechanically sensitive markers of behaviour among extant taxa would provide a powerful framework from which to reconstruct locomotion from hominoid fossils.

Variation in internal bone architecture is most commonly analysed through the quantification of bone volume to total volume fraction (BV/TV) and degree of anisotropy (DA). BV/TV is the principle component of bone strength while DA indicates the degree to which trabeculae struts are aligned as a proxy for homogenous (anisotropic arrangement) or heterogeneous (isotropic arrangement) direction of loading (Fajardo et al. 2007). In combination, BV/TV and DA have been shown to contribute up to 98% of the Young's Modulus (stiffness) of bone (Cotter et al. 2009; Maquer et al. 2015; Hart et al. 2017). Importantly, BV/TV and DA have been shown to be independent of one another (Tsegai et al. 2013; Georgiou et al. 2018; Kivell et al. 2018b; Komza and Skinner 2019) and not strongly correlated with body mass (Doubé et al. 2011; Barak, Lieberman and Hublin 2013; Ryan and Shaw 2013; Schilling et al. 2014; Saers, Ryan and Stock 2019b; Bird, Kivell and Skinner 2021).

There are distinct challenges to identifying functional adaptation signals in the carpus, particularly since even elements of the skeleton experiencing high, predictable loads, such as the proximal femur, have often failed to conform to predictions (MacLatchy and Müller 2002; Ryan and Ketcham 2002; Carlson et al. 2006; Fajardo et al. 2007; Kivell 2016b; Tsegai et al. 2018). Firstly, all bones are under a multitude of biological demands and genetic influences that can confound functional signals, affecting not only the structure and architecture of bone, but also its capacity to respond to biomechanical signals (Bertram and Swartz 1991; Lieberman 1997; Currey 2003; Lovejoy et al. 2003; Ruff, Holt and Trinkaus 2006). Importantly, interspecific analyses have shown that some structural parameters, such as BV/TV or trabecular thickness, have systemic patterning at the genus level, independent of locomotion and predicted stress magnitude. For example, *Pan* has been shown to have consistently higher BV/TV across multiple skeletal elements, including the humerus, femur, third metacarpal, and vertebra, compared with *Pongo* and modern *Homo sapiens* (Cotter et al. 2009; DeSilva and Devlin 2012; Shaw and Ryan 2012; Scherf, Harvati and Hublin 2013; Tsegai et al. 2013; Su and Carlson 2017; Georgiou et al. 2018; Kivell et al. 2018b; Komza and Skinner 2019; Ragni 2020; Bird, Kivell and Skinner 2021).

Secondly, it is still not well understood how trabecular and cortical bone modelling (sensu Barak 2019) is triggered by variable aspects of biomechanical force such as strain magnitude and loading frequencies (Lieberman 1997; Ruff, Holt and Trinkaus 2006; Doubé et al. 2011). Many hypotheses have focused on the magnitude of strain, suggesting that functional adaptation reflects the peak strain imposed on a joint (Frost 1987; Currey 2002). However,

research by Rubin et al. (2002) suggests that low magnitude but high frequency loads (i.e. habitual postures such as standing) do have the potential to influence trabecular, although not cortical, modelling. Cortical and trabecular bone have divergent material properties and work together to resist fracture and transfer load, however they are unlikely to respond to load in the same way (Martin, Burr and Sharkey 1998; Currey 2002; Rubin et al. 2002; Shaw and Ryan 2012). Furthermore, and critical to this study, it is not clear how the cortex and trabeculae of short bones of the carpus (and tarsus), adapt symbiotically to strain, particularly within a complex articular and ligamentous anatomical region (Martin, Burr and Sharkey 1998; Currey 2002).

Finally, there is a limited amount of detailed kinematic and kinetic research on the wrist, particularly in non-human hominids. Historically, quantifying movement in this complex region has been difficult as x-rays superimpose bones on top of one another and implanted devices disrupt normal kinematics (Rainbow et al. 2016). Defining kinetics at the wrist has also been challenging because, unlike the phalanges or metacarpals that directly contact the substrate, load occurs in the wrist indirectly. Movement and force within the carpus arise from bone-to-bone articulation, the limitations of the articular geometry and joint capsule, as well as the tensional strain imposed by the surrounding ligaments (Garcia-Elias 1997; Wolfe, Neu and Crisco 2000; Jouffroy and Medina 2002; Crisco et al. 2011). In *H. sapiens*, substantial variation has been reported on range of motion (Stirling et al. 2021), carpal shape (Marzke, Wullstein and Viegas 1994; Rainbow et al. 2008; Buijze et al. 2011; Bain et al. 2015), ligament properties (Garcia-Elias et al. 1995; Buijze et al. 2011; Kamal, Starr and Akelman 2016; Garcia-Elias, de la Bellacasa and Schouten 2017), force transfer (Gíslason et al. 2009; Gíslason et al. 2012), and axes of movement (Wolfe, Neu and Crisco 2000; Moojen et al. 2003; Moritomo et al. 2004; Crisco et al. 2005; Kaufman-Cohen et al. 2018; Best et al. 2019). The limited amount of research on non-human hominids indicates that this variability is probably not limited to *H. sapiens* (Carlson et al. 2006; Orr 2018; Casado et al. 2021). For example, although mean intercarpal range of motion differs between *Pan* and *Pongo*, their interspecific ranges overlap (Orr 2017). Thus, while we may be able to describe postural, behavioural, and kinematic trends within species, it is likely that the way in which carpals move in relation to one another to achieve the same behavioural activity has a degree of variability between individuals of the same taxa.

Despite these challenges, BFA research has provided valuable insight into joint loading in extant primates and has yielded meaningful behavioural reconstructions of fossil specimens, including in the proximal femur (Georgiou et al. 2020), proximal humerus (Kivell et al. 2018b),

metacarpals (Skinner et al. 2015; Stephens et al. 2018; Dunmore et al. 2020b), metatarsals (Komza and Skinner 2019), talus (DeSilva and Devlin 2012; Su and Carlson 2017; Tsegai et al. 2017) and tibia (Barak et al. 2013). To date, interspecific functional adaptation research on the carpus has predominantly focused on comparing single elements of the wrist and has reached limited conclusions. Using an extracted volume of interest (VOI), Schilling et al. (2014) analysed the trabecular structure of the capitate, scaphoid and lunate across extant hominoids but failed to find a functionally informative signal. Ragni (2020) extracted a trabecular VOI from the capitate head in *Pan* and *Gorilla* to analyse architecture across different age ranges. While ontogenetic hypotheses were supported, functional interpretations related to interspecific differences remained limited. Bird et al. (2021) used a whole-bone methodology to study the trabecular and cortical architecture of the capitate among hominids. Results indicated that signals of functional adaptation differed across the proximal and distal portion and averaging BV/TV and DA results across an entire bone may obscure functionally discriminating signals (Bird, Kivell and Skinner 2021).

Nevertheless, whole-bone analyses (e.g. the carpal analysis in Stephens et al. 2018) may still be preferable for some research questions particularly given the potential difficulty in identifying homologous regions in carpals across multiple species and the functional interdependence between different regions of the small bones. Given the complexity of kinematics and the known inter- and intraspecific variability, establishing relative patterns of bone architecture across a larger region of the carpus may be a more functionally informative approach to whole-bone carpal analysis. Due to the known systemic control of BV/TV, interspecific differences in this measure, in particular, are unlikely to be strongly correlated to locomotion. Therefore, establishing relative differences across the internal structure of multiple bones may allow us to discern intraspecific patterns while minimising the effects of individual and species-level differences.

4.2.a. Morphology, kinematics, and kinetics of the proximal carpal row.

In all hominoids the articular relationship between the distal radius and ulna and the proximal carpus (the radiocarpal joint) distinguishes them from most other primates (Kivell 2016a). This derived radiocarpal joint configuration features a novel Triangular Fibrocartilage Complex (TFCC) that is linked to distinct kinetics during ulnar deviation and the use of forearm rotation (supination), a defining characteristic of hominoids considered adaptive for suspensory locomotion (Lewis 1972; Sarmiento 1988; Jouffroy and Medina 2002; Kivell 2016a). The ulnar portion of the TFCC (the meniscus homologue) either fully (*Homo*, *Gorilla* and *Pongo*) or partially (*Pan*, *Symphalangus* and *Hylobates*) excludes the ulna from

articulating with the triquetrum (Lewis 1971; Sarmiento 1988; Lewis 1989; Kivell 2016a). However, compared to other groups of primates (e.g. cercopithecoids), hominoid carpals are morphologically variable (Figure 4.1), reflecting the diverse positional and locomotor modes of the clade (Lewis 1971, 1972; Ward 2007; Kivell, Barros and Smaers 2013). Below we describe the morphology and what is currently known about the kinematics (movement) and kinetics (force transfer) of the hominoid proximal carpal row.

4.2.a.1. *Pongo*

Pongo locomotes in a predominantly arboreal environment using torso-orthograde suspensory positions (Hunt 1991b; Isler and Thorpe 2003; Thorpe and Crompton 2006; Manduelli, Morrogh-Bernard and Thorpe 2011). The environmental complexity and range of supportive substrates is thought to require a diversity of hand postures and resistance against multiple origins of force (Sarmiento 1988; Swartz, Bertram and Biewener 1989; Demes et al. 2001; Isler and Thorpe 2003; Carlson 2005; Thorpe and Crompton 2006, 2009). Indeed, anatomical and kinematic analyses show that *Pongo* has a greater range of motion in the midcarpal and radiocarpal joints compared to the other hominids, which may facilitate a greater number of possible hand positions (Tuttle 1969; Orr 2018). In suspension, the wrist is held in a neutral position and force is thought to be predominantly tensile (Sarmiento 1988; Swartz, Bertram and Biewener 1989; Isler and Thorpe 2003; Tocheri 2007). The lunate is relatively large compared to other apes, which suggests the bone is critical to a more central transfer of load through the fingers to the forearm (Sarmiento, 1988). The diminutive, cylindrically shaped triquetrum is distally migrated as a result of the increased lunate size and variably participates in the proximal or distal row throughout different phases of motion (Orr 2010; Orr and Atkinson 2016). Together with the highly convex radiocarpal contour, the morphology and joint configuration of the ulnar-side carpus indicates an increased capacity for pronation-supination, but limited ability for proximo-distal load transfer at the ulnar-side carpus (Sarmiento 1988; Begun 2004). Radially, the independent os centrale allows greater freedom of movement at the midcarpal joint relative to the fused morphology in the non-human hominids (Sarmiento 1988; Richmond, Begun and Strait 2001; Begun 2004; Orr 2018; Püschel et al. 2020).

4.2.a.2. *Gorilla* and *Pan*

Both *Pan* and *Gorilla* are primarily terrestrial knuckle-walkers (Doran 1993a, b, 1997; Thompson et al. 2018). Although non-knuckle-walking hand postures as well as arboreal substrates are utilised in variable proportions dependent on age, sex, sub-species, substrate size and seasonality (Susman, Badrian and Badrian 1980; Doran 1992; Hunt 1992; Doran

1993b; Remis 1995, 1998; Neufuss et al. 2017; Thompson et al. 2018), knuckle-walking is considered to produce greater peak pressures than climbing and suspension (Samuel et al. 2018; although see Synek et al. 2020). Knuckle-walking is thought to induce primarily compressive forces, requiring greater stability at the wrist compared with Asian apes (Sarmiento 1988; Isler and Thorpe 2003; Begun 2004). The compromise between stability and mobility (needed for arboreal locomotor behaviours) in the African ape wrist is achieved via the screw-clamp movement of the scaphoid (with fused os centrale) coming into full congruence with the capitate early on during wrist extension (Lewis 1989; Richmond, Begun and Strait 2001; Begun 2004). During knuckle-walking, the wrist is held in slight extension in both taxa (Finestone et al. 2018; Thompson 2020), although *Pan* shows greater variability utilising a mixture of palm-in and palm-back postures, compared to the consistent adoption of palm-back postures in *Gorilla* (Tuttle 1967, 1969; Inouye 1994; Wunderlich and Jungers 2009; Matarazzo 2013). Substrate reaction force is experienced directly by the intermediate phalanges and load is thought to be transferred proximally through the wrist (Sarmiento 1988; Tocheri 2007). The ulnar phalanges make initial contact with the substrate at touch-down, and weight is transferred onto radial phalanges during the stance phase (Wunderlich and Jungers 2009; Matarazzo 2013; Thompson 2020 [although Samuel et al., 2018 note a slightly different kinematic motion for bonobos]).

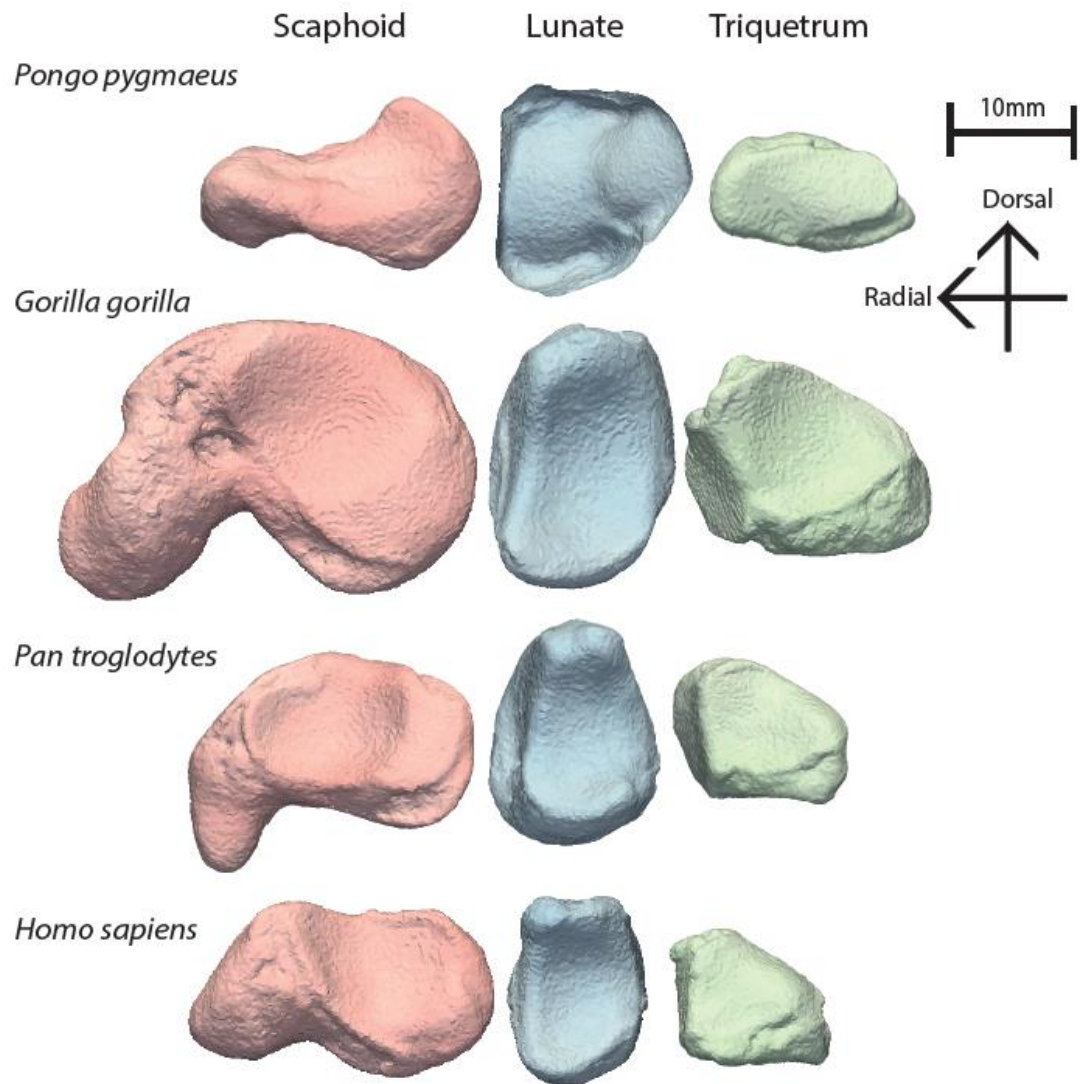


Figure 4.1 External morphology of the scaphoid, lunate and triquetrum of the proximal carpal row from one representative individual of each taxon.

Bones shown in (approximately) distal view, showing the capitate (or os centrale in *Pongo*) and lunate facets of the scaphoid, capitate facet of the lunate, and hamate facet of the triquetrum. All bones show morphology of a left hand (right-sided specimens have been flipped) and are scaled to relative size. *Pongo pygmaeus* ZSM 1907 0633b; *Gorilla gorilla* PC MER 300; *Pan troglodytes* MPITC 11778; *Homo sapiens* NHMW-Nubian K5-2.

4.2.a.3. *Homo*

The human hand is seldom used for locomotion and instead forceful and precise manipulation (Napier 1956; Marzke 1997; Tocheri et al. 2005; Marzke et al. 2010; Marzke 2013; Bardo et al. 2017; Key, Merritt and Kivell 2018). Compressive forces from strong muscle contractions arise predominantly from the robust thumb and second digit and are thought to be directed radio-ulnarly across the hand (Tocheri et al. 2005; Tocheri 2007; Williams, Gordon and Richmond 2012; Marzke 2013; Key and Dunmore 2015; Williams-Hatala et al.

2018; Williams-Hatala et al. 2021). There is a broad consensus amongst clinical researchers that the functional axis of the human wrist is the “Dart-Throwers Motion” (DTM), an arc of motion where the wrist moves from radial deviation in extension to ulnar deviation in flexion (Crisco et al. 2005; Wolfe et al. 2006; Rohde, Crisco and Wolfe 2010; Crisco et al. 2011; Schuind et al. 2013; Brigstocke et al. 2014; Moritomo et al. 2014; Rainbow et al. 2015; Rainbow et al. 2016; Kaufman-Cohen et al. 2018; Kaufman-Cohen et al. 2019). It has yet to be established whether this arc of motion is also utilised by non-human hominids and, if so, therefore represents an exaptation for manipulation in *H. sapiens* (Wolfe et al. 2006). However, during manipulation, *H. sapiens* appear to express little deviation from this path of motion, using it for almost all activities of daily living, from hammering to answering a mobile phone (Rohde, Crisco and Wolfe 2010; Kaufman-Cohen et al. 2018; Kaufman-Cohen et al. 2019). When combined with a power-squeeze grip and/or a power swing, the DTM increases force on impact, providing a mechanical advantage to tool use (Wolfe et al. 2006; Rohde, Crisco and Wolfe 2010). Despite noted ligament laxity between the bones of the proximal row, during the DTM, intercarpal movement at the proximal row is minimised while the capitate head moves against the lunate and scaphoid (Garcia-Elias et al. 1995; Wolfe, Neu and Crisco 2000; Wolfe et al. 2006; Edirisinghe et al. 2014; Garcia-Elias, Alomar Serrallach and Monill Serra 2014).

Using a whole-bone method, we quantify structural parameters of internal bone architecture of the scaphoid, lunate, and triquetrum to determine whether taxa-specific patterns correlate to known or expected differences in radiocarpal and midcarpal kinematics/kinetics. Specifically, we quantify BV/TV (trabecular and cortical bone combined) and DA across these three bones in *Pongo* (Sumatran and Bornean), *Gorilla* (western lowland), *Pan* (bonobos and chimpanzees), and a diverse sample of recent *Homo sapiens*. We predict that African apes would have relatively higher BV/TV and DA in the scaphoid relative to their lunate and triquetrum due to presumed greater, habitual loading of the radial wrist during knuckle-walking (Wunderlich and Jungers 2009; Matarazzo 2013). In *Pongo*, the lunate is notably large and dominates the proximal row, and it is therefore assumed that it will receive and transfer a greater proportion of load relative to the scaphoid and triquetrum and is thus predicted to have the highest relative BV/TV. Low DA is predicted across all carpal bones in *Pongo* because of the variable hand postures required for arboreal locomotion (Sarmiento 1988). Finally, we predict *H. sapiens* will follow the pattern found in Stephens et al. (2018). As the key element to stability during motion (Garcia-Elias and Lluch 2001; Edirisinghe et al. 2014), the lunate is predicted to have the highest BV/TV, followed by the scaphoid and then

the triquetrum. DA is predicted to show the highest values in the scaphoid due to its limited arc of motion (Edirisinghe et al. 2014), and lowest in the triquetrum. For all taxa, we expect the triquetrum to have the relatively lowest BV/TV and DA given its lack of direct articulation with the ulna. As the purpose of this research is to establish whether patterns within species correlate to known or expected kinematics/kinetics we do not specifically test for interspecific differences, particularly as the systemic control over BV/TV reduces its value as a functionally informative parameter. However, the general differences or similarities in patterns across the taxa will be discussed.

4.3. Materials and methods

4.3.a. Sample

This study included associated scaphoids, lunates, and triquetra (n=177) for individuals of *Pongo* sp. (n=14), *Gorilla gorilla* (n=14), *Pan* sp. (*Pan troglodytes* and *Pan paniscus* n=7 each), and *Homo sapiens* (n=17). Taxa were categorised by their major behavioural/locomotor mode; suspensory (*Pongo*), knuckle-walking (*Gorilla* and *Pan*) and bipedal/manipulative (*Homo*) (Table 4.1; Supplementary Table 4.1). Non-human specimens were wild shot except for three *Pongo* individuals (SMF 84218, SMF 74303, and ZSM 1982-0092) who were zoo animals. Across modern *H. sapiens*, there is a relationship between the degree of population mobility and systemic levels of BV/TV (Saers et al. 2016). At one end of the spectrum, hunter-gathering and foraging, which require high levels of population mobility, are correlated to systemically higher levels of BV/TV, while at the other end, population sedentism related to industrialisation is correlated to systemically lower levels of BV/TV; agricultural or mixed agricultural-foraging strategies fall out as intermediate (Nikita et al. 2011; Chirchir et al. 2015; Ryan and Shaw 2015; Saers et al. 2016; Stephens et al. 2018; Saers, Ryan and Stock 2019a). To encapsulate known BV/TV variation among modern *H. sapiens*, the *Homo* sample includes individuals from diverse global populations. This includes five from post-industrialised and 12 from pre-industrialised societies (more information on populations and subsistence strategies, where available, is found in Supplementary Table 4.1).

Each individual in the sample had all the three bones represented from the same side and was free of any signs of pathology. Specimens from left and right hands were included in each taxon. There was a predominance of right hands in the *Homo* sample however research indicates that kinematics of the DTM do not significantly differ bilaterally within individuals (Kaufman-Cohen et al. 2018). Effort was made to balance sex in each taxon, but this was not always possible due to sample constraints and in 7 *Homo*, sex could not be determined.

Table 4.1 Summary of study sample.

Taxon	N	Side		Sex			Major behavioural mode
		Right	Left	Female	Male	Unknown	
<i>Pongo sp.</i>	14	8	6	8	6	0	Suspensory
<i>Gorilla gorilla</i>	14	7	7	6	8	0	Knuckle-Walking
<i>Pan troglodytes</i>	7	3	4	2	5	0	Knuckle-Walking
<i>Pan paniscus</i>	7	4	3	4	3	0	Knuckle-Walking
<i>Homo sapiens</i>	17	11	6	4	6	7	Bipedal/Manipulative

4.3.b. Computed tomography scanning

Specimens were scanned either at the Department of Human Evolution, Max Planck Institute for Evolutionary Anthropology, Germany or at the Cambridge Biotomography Centre, University of Cambridge, United Kingdom. In Germany, specimens were scanned with either the BIR ACTIS 225/300 or the Diondo D3 high-resolution microCT scanner with an acceleration voltage of 100-160 kV and a 0.5mm brass filter. In the UK specimens were scanned with a Nikon 225/XTH scanner with an acceleration voltage of 100-140µA and a 0.2mm copper filter. All scans were reconstructed as 16-bit tiff stacks. Voxel resolution was constrained to ensure accurate segmentation of thin trabeculae (Isaksson et al. 2011; Christen et al. 2016). The maximum resolution was 0.038µ in *Homo* and 0.039µ in non-human hominids (Supplementary Table 4.1). All scans were segmented (thresholded) using the clustering-algorithm based Medical Image Analysis (MIA) protocol, Figure 4.2A-B (Dunmore, Wollny and Skinner 2018).

4.3.c. Data Collection

Data were collected using an in-house script for the medtool 4.3 software (<http://www.dr-pahr.at/medtool/>). The medtool protocol is well-established within the palaeoanthropological literature (Tsegai et al. 2013; Skinner et al. 2015; Stephens et al. 2016; Georgiou et al. 2018; Kivell et al. 2018b; Stephens et al. 2018; Tsegai et al. 2018; Dunmore et al. 2019; Georgiou et al. 2019; Komza and Skinner 2019; Dunmore et al. 2020a; Georgiou et al. 2020) and the methodology has been published in detail (Pahr and Zysset 2009b, a; Gross et al. 2014). Briefly, by running a series of morphological filters, medtool quantifies architectural parameters within an entire bone or epiphysis by identifying and applying unique scalars to the background, cortical, trabecular, and marrow (internal) voxels of the MIA segmented scan (Figure 4.2B). Firstly, a series of mathematical rays are projected across the scan to identify the external contour of the bone. Rays continue to move inwards until a non-bone voxel is identified. This iterative process results in the identification of the internal

cortical and trabecular boundary (Figure 4.2C) (Pahr and Zysset 2009b; Gross et al. 2014). Users can collect data on the whole bone (Figure 4.2B), cortical-only region (white voxels of Figure 4.2C) or the trabeculae-only region (white voxels of Figure 4.2D). A 3D grid with 2.5mm spaced nodes is superimposed on the image stack and a 5mm sphere at each node measures bone parameters in 3D (Figure 4.2E).

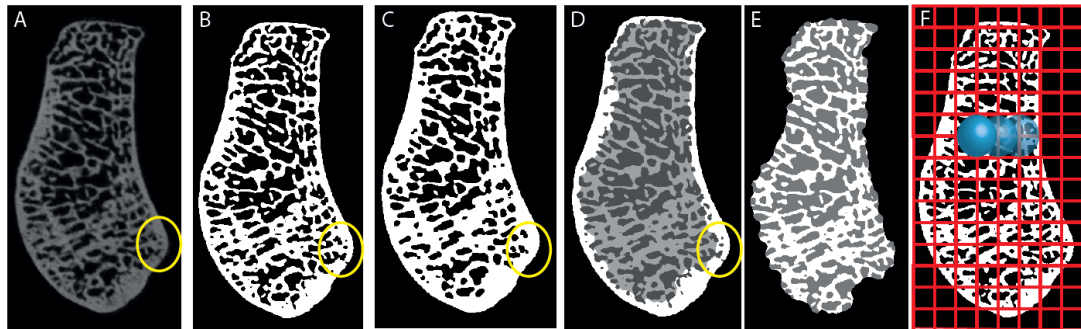


Figure 4.2 Process of μ -CT segmentation and data collection using MIA-clustering and medtool.

A) One cross-sectional slice from the original μ -CT scan from a *Homo sapiens* scaphoid (ID: NHMW-Nubian K5-2). B) Result of MIA-clustering segmentation. C) Filtered image stack showing unique scalar values applied to the cortical (white), trabeculae (light-grey), marrow (dark-grey) and background (black) voxels. D) Image with the cortical bone removed, leaving the trabecular-only region for data analysis. E) Representation of 3D grid imposed over the image stack and a sampling sphere moves between nodes, iteratively collecting data. The yellow circle demonstrates where cortical pores have been maintained for the analytical stack.

BV/TV was calculated on the whole bone, inclusive of the cortex and trabeculae (Figure 4.2B). It is expressed as a ratio of bone voxels to non-bone voxels and reported as a number between 0-1. BV/TV inclusive of trabecular and cortical bone, rather than trabecular-only BV/TV, is measured as it was shown to be more functionally informative in an interspecific analysis of the capitate (Bird, Kivell and Skinner 2021). Further, differentiation of cortical and trabecular tissue is not always straightforward in non-human carpal bones as the internal boundary is characterized by thick but highly porous bone (Bird, Kivell and Skinner 2021). This combined BV/TV value (hereafter referred to as simply BV/TV) therefore provides a holistic measure of whole bone strength. DA was measured on the trabecular only image stack (Figure 4.2D) and calculated using the Mean Intercept Length method (Whitehouse 1974). The calculation $1 - (\text{min. eigenvalue} - \text{max. eigenvalue})$ produces a ratio which expresses the relative strength of the alignment in the trabeculae, in which 0 indicates total isotropy and 1 indicates total anisotropy.

4.3.d. Statistical analysis

A Friedman’s test was used to test for significant differences in BV/TV and DA across the scaphoid, lunate and triquetrum within each taxon (*R* Core Team, stats package v3.6.2). The Friedman’s test is a non-parametric test similar to a one-way analysis of variance by ranks for repeated measures, although the Friedman’s test allows one to consider the bone as a blocking variable prior to ranking. A blocking variable is a factor that potentially affects the dependent variable. Thus, the Friedman’s test indicates whether BV/TV and DA ranks consistently differently across the bones (the blocks) of each individual (Kendall and Smith 1939). Kendall’s *W*, also known as the effect size, was calculated and interpretation followed Cohen’s guidelines (Cohen 2013). Kendall’s *W* normalizes the Friedman’s test result into a number between 0-1 to give an intuitive indication of the importance of the bone to the mean rank. An effect size of 0-0.29 is classified as small, 0.3-0.49 as moderate and ≥ 0.5 as large (Cohen 2013). Finally, three intraspecific post-hoc pairwise comparisons were calculated (all using *R* Core Team, stats package v3.6.2). Firstly, to test for significant differences between the bones, a Kruskal-Wallis signed-rank test with Bonferroni correction was calculated for all genera. Secondly, to test for potential sex differences within genera, a Wilcoxon signed-rank test with Bonferroni correction was calculated for all genera. Finally, to test for potential bilateral asymmetry in modern *H. sapiens*, a Wilcoxon test rank-sum with Bonferroni correction was calculated on the rights and lefts. As the only genera with well-documented and consistent bilateral asymmetry of the limbs, the tests for bilateral asymmetry were only carried out on *Homo*. All reported *p*-values are considered significant if $p \leq 0.05$.

4.4. Results

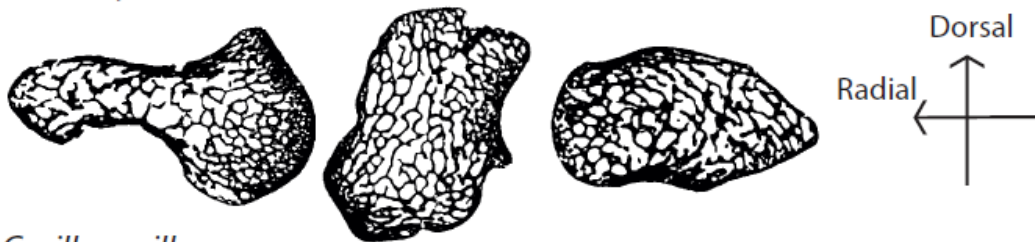
Descriptive statistics for all carpal bones across taxa are reported in Table 4.1. Data by individual specimen including sub-species, sex and side are reported in Supplementary Table 4.1. Figure 4.3 exemplifies the qualitative differences in internal architecture via one cross-section of each bone from a representative individual of each taxon.

Table 4.2 Descriptive statistics for BV/TV and DA across the study taxa. ‘S.D.’ indicates one standard deviation above and below the mean.

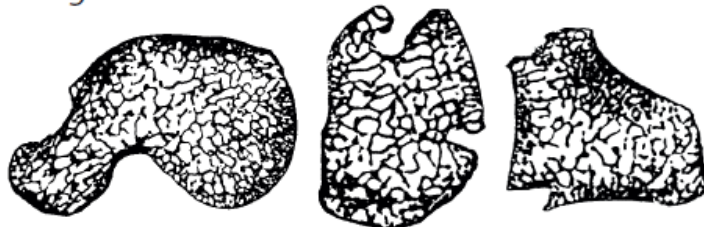
BV/TV		<i>Pongo</i>	<i>Gorilla</i>	<i>Pan</i>	<i>Homo</i>
Scaphoid	Mean and S.D.	0.583 ± 0.089	0.560 ± 0.079	0.564 ± 0.080	0.383 ± 0.081
	Range	0.459 - 0.743	0.438 - 0.716	0.399 - 0.685	0.240 - 0.514
Lunate	Mean and S.D.	0.505 ± 0.066	0.550 ± 0.070	0.567 ± 0.070	0.418 ± 0.075

	Range	0.451 - 0.620	0.447 - 0.699	0.426 - 0.689	0.297 - 0.582
Triquetrum	Mean and S.D.	0.502 ± 0.098	0.612 ± 0.086	0.626 ± 0.101	0.366 ± 0.064
	Range	0.359 - 0.673	0.443 - 0.797	0.425 - 0.786	0.269 - 0.496
DA		<i>Pongo</i>	<i>Gorilla</i>	<i>Pan</i>	<i>Homo</i>
Scaphoid	Mean and S.D.	0.261 ± 0.035	0.261 ± 0.036	0.254 ± 0.036	0.301 ± 0.030
	Range	0.200 - 0.333	0.217 - 0.338	0.199 - 0.348	0.259 - 0.378
Lunate	Mean and S.D.	0.279 ± 0.041	0.262 ± 0.021	0.286 ± 0.037	0.281 ± 0.026
	Range	0.206 - 0.331	0.231 - 0.308	0.228 - 0.346	0.236 - 0.320
Triquetrum	Mean and S.D.	0.241 ± 0.038	0.232 ± 0.029	0.224 ± 0.040	0.255 ± 0.026
	Range	0.172 - 0.293	0.184 - 0.279	0.180 - 0.268	0.206 - 0.326

Pongo pygmaeus



Gorilla gorilla



Pan troglodytes



Homo sapiens



Figure 4.3 Cross-sections of each carpal specimen represented in Figure 4.1 showing differences in the internal architecture.

As in Figure 4.1, bones are shown in (approximate) distal view, showing a coronal slice through the mid-section of the bone. All bones show morphology of a left hand and right specimens have been flipped. Bones are not to scale.

4.4.a. *Pongo*

BV/TV differed significantly across the three bones ($p < 0.001$) with bone type having a large effect on result ($W = 0.770$) (Table 4.3). Box-and-whisker plots in Figure 4.4A show the distribution of BV/TV results and the significant pairwise comparisons, individual results are plotted in Figure 4.5A. The mean rank of the scaphoid was 3.000 indicating that all individuals had highest BV/TV in this bone (Figure 4.5A). BV/TV was more variable between the lunate and triquetrum with the mean rank falling at 1.642 and 1.357, respectively. The scaphoid was significantly differentiated from the lunate and triquetrum in the pairwise comparisons ($p < 0.001$ for both tests) (Table 4.4; Figure 4.4A). DA differed significantly across the three bones ($p < 0.001$) with bone type having a large effect on result ($W = 0.679$). Figure 4.4B illustrates the distribution of DA results and the strength of the pairwise comparisons. The lunate had the highest mean rank (2.785), followed by the scaphoid (2.071) and the triquetrum (1.142) (Figure 4.5B). Pairwise comparisons revealed the triquetrum had significantly lower DA compared with the scaphoid and lunate ($p = 0.050$ and < 0.001 respectively; Figure 4.5B). There were no significant differences between the sexes (Supplementary Table 4.2).

Table 4.3 Mean rank of each bone by taxa with Friedman's test p -value and Kendall's effect size (W).

Significant p -values are in bold.

Taxa		Rank	
<i>Pongo</i>	Element	BV/TV	DA
	Scaphoid	3.000	2.071
	Lunate	1.642	2.785
	Triquetrum	1.357	1.142
	p -value	<0.001	<0.001
	Effect Size	0.770 (Large)	0.679 (Large)
<i>Gorilla</i>	Element	BV/TV	DA
	Scaphoid	1.714	2.214
	Lunate	1.714	2.500
	Triquetrum	2.571	1.285
	p -value	0.032	0.003
	Effect Size	0.245 (Small)	0.403 (Moderate)
<i>Pan</i>	Element	BV/TV	DA
	Scaphoid	1.785	2.071

	Lunate	1.571	2.785
	Triquetrum	2.642	1.142
	<i>p</i> -value	0.011	<0.001
	Effect size	0.321 (Moderate)	0.679 (Large)
<i>Homo</i>	Element	BV/TV	DA
	Scaphoid	1.941	2.764
	Lunate	2.588	1.941
	Triquetrum	1.470	1.294
	<i>p</i> -value	0.004	<0.001
	Effect size	0.315 (Moderate)	0.543 (Large)

Table 4.4 Intraspecific differences between carpal bones using Wilcoxon rank-sum tests with Bonferroni correction for BV/TV (bottom left of table) and DA (top right of table). Significant *p*-values are in bold.

<i>Pongo</i>		Scaphoid	Lunate	Triquetrum	
Scaphoid	BV/TV		0.061	0.050	DA
Lunate		<0.001		<0.001	
Triquetrum		<0.001	1		
<i>Gorilla</i>		Scaphoid	Lunate	Triquetrum	
Scaphoid	BV/TV		1	0.009	DA
Lunate		1		<0.001	
Triquetrum		0.061	0.016		
<i>Pan</i>		Scaphoid	Lunate	Triquetrum	
Scaphoid	BV/TV		0.009	0.012	DA
Lunate		1		<0.001	
Triquetrum		0.074	0.005		
<i>Homo</i>		Scaphoid	Lunate	Triquetrum	
Scaphoid	BV/TV		0.020	<0.001	DA
Lunate		0.134		<0.001	
Triquetrum		0.852	0.020		

4.4.b. *Gorilla*

BV/TV differed significantly across the three bones ($p=0.032$) with bone type having a small effect on the result ($W=0.245$) (Table 4.3). Similar to *Pan* (see below), the triquetrum had the highest mean rank (2.571), while the lunate and scaphoid showed identical mean ranks (1.714) (Figure 4.5A). Pairwise comparisons revealed that triquetrum BV/TV was only significantly higher than the lunate ($p=0.016$) (Table 4.4A). DA differed significantly across the bones ($p=0.003$) with bone type having a moderate effect on results ($W=0.403$). The lunate had the highest mean rank (2.500) followed by the scaphoid (2.214) and triquetrum (1.285) (Figure 4.5B). The triquetrum had significantly lower DA compared with the scaphoid

and lunate ($p=0.009$ and <0.001 , respectively; Figure 4B). There were no significant differences between the sexes (Supplementary Table 4.2).

4.4.c. *Pan*

BV/TV differed significant across the scaphoid, lunate and triquetrum ($p=0.011$) and bone type showed a moderate effect on result ($W = 0.321$) (Table 4.3). The triquetrum had the highest mean rank (2.642), then the scaphoid (1.785), followed closely by the lunate (1.571) (Figure 5A). Only one pairwise comparison was significant, with the triquetrum having higher BV/TV than the lunate ($p=0.005$) (Table 4.4; Figure 4.4A). DA differed significantly across the three bones ($p<0.001$) with bone type having a large effect on parameter result ($W=0.679$). The lunate recorded the highest mean rank (2.785), followed by the scaphoid (2.071), and finally the triquetrum (1.142) (Figure 4.5B). Significant results were recorded for all pairwise comparisons with the following p -values; scaphoid-lunate 0.009, scaphoid-triquetrum 0.012 and lunate-triquetrum <0.001 (Figure 4.4B). There were no significant differences between the sexes (Supplementary Table 4.2).

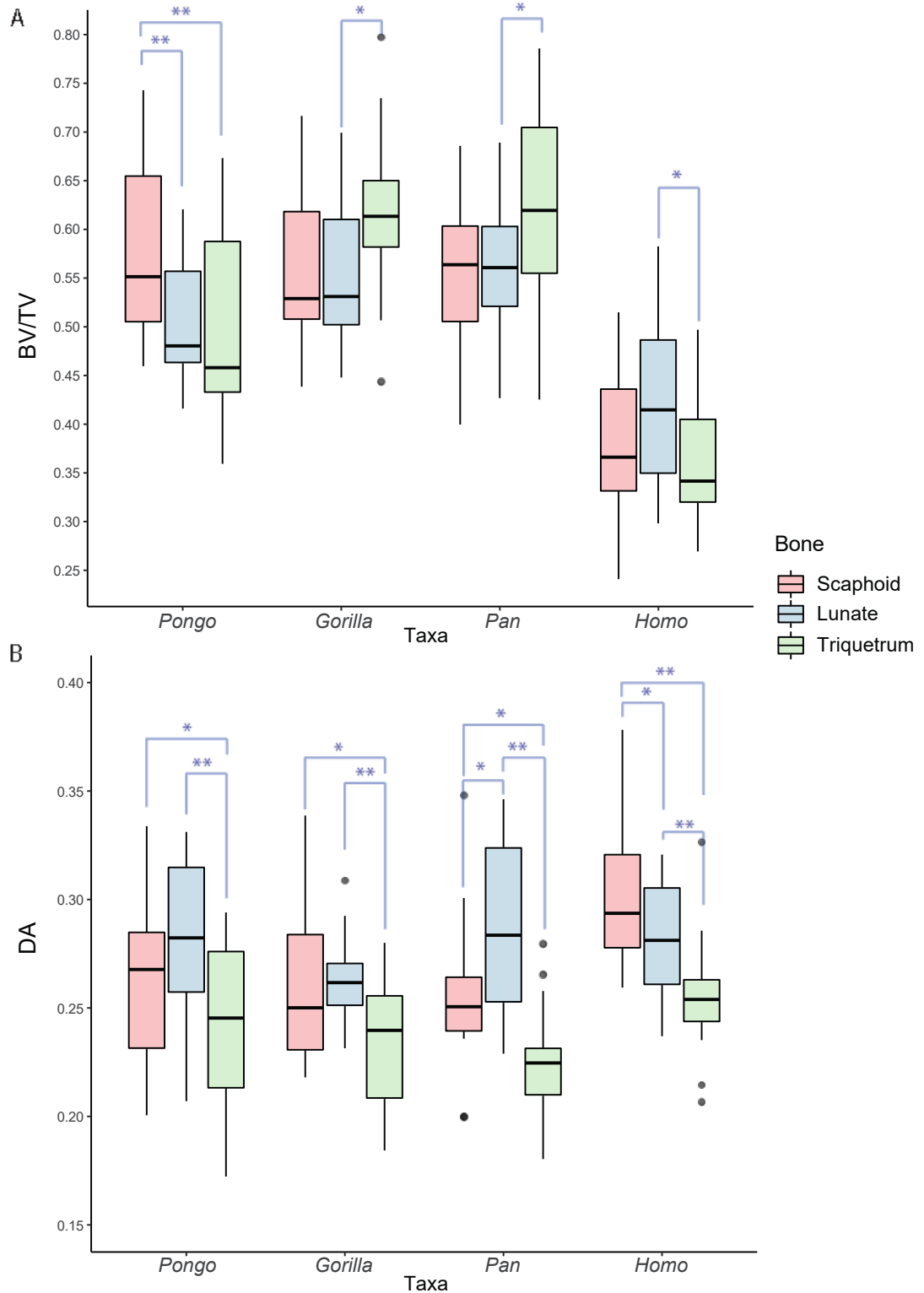


Figure 4.4 Box-and-whisker plots showing the distribution of BV/TV (A) and DA (B) results by bone and taxon.

Significant pairwise comparisons are indicated by the square brackets, with the strength of the p -value indicated by the asterisk; * = a p -value of ≤ 0.05 ; ** = a p -value of ≤ 0.001 . Outliers are identified with \bullet and represent values 1.5 times above the fourth or below the first interquartile range.

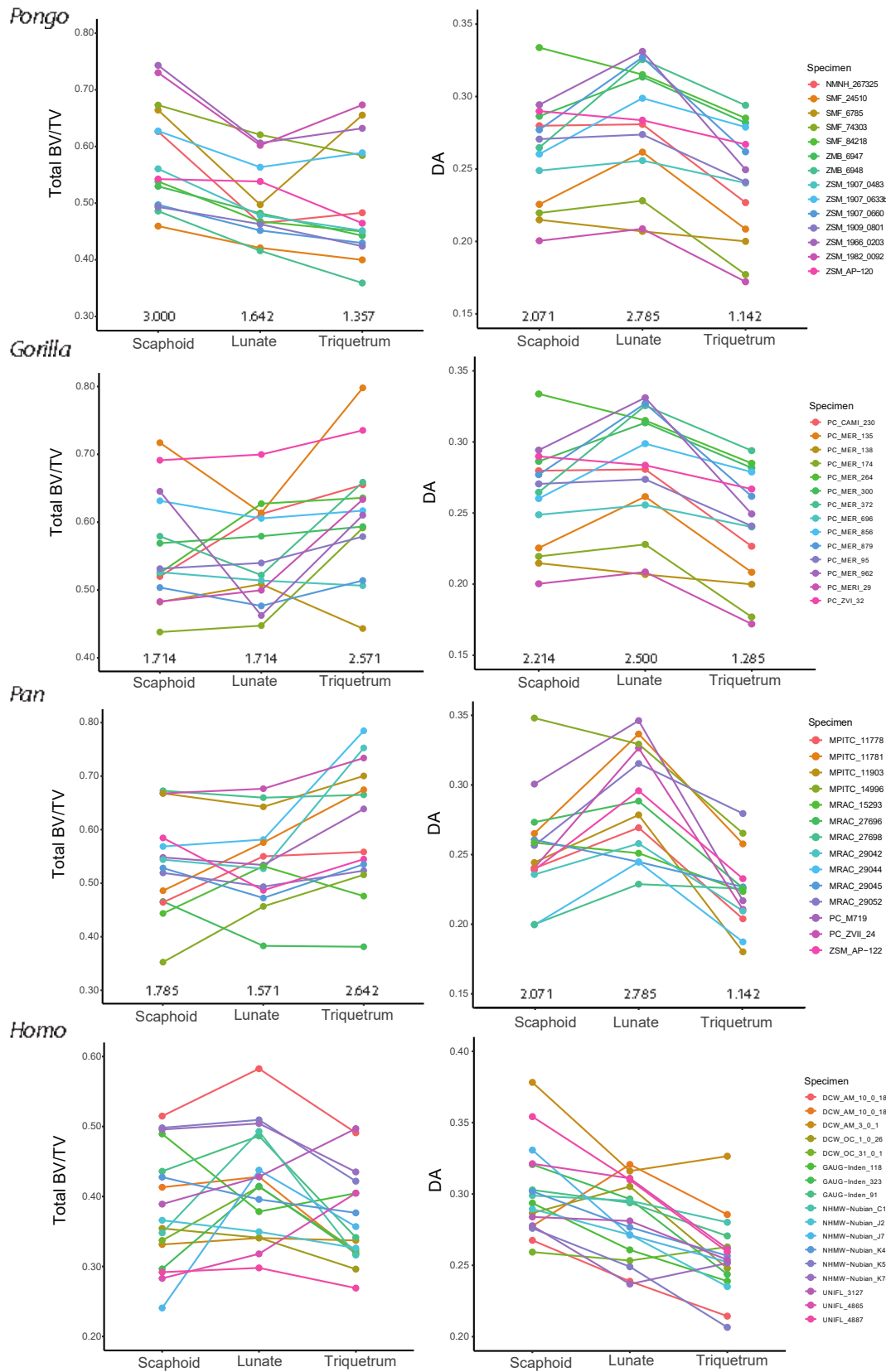


Figure 4.5 Line graphs plotting BV/TV (A) and DA (B) results across each bone by individual and taxon.

Mean rank for each bone (as per Table 4.3) is listed along the x axis. Supplementary table 1 lists the rank of each bone by individual.

4.4.d. *Homo*

BV/TV differed significantly across the three bones ($p=0.004$) with the bone type having a moderate effect on the parameter outcome ($W=0.315$) (Figure 4.4A; Table 4.3). The lunate had the highest mean rank (2.588), then the scaphoid (1.941), with the triquetrum showing the lowest mean rank (1.470) (Figure 4.5A). The only significant pairwise comparisons indicated the lunate had significantly higher BV/TV than the triquetrum ($p=0.020$) (Table 4.4). DA differed significantly across the three bones ($p<0.001$) with the bone type having a large effect on the parameter outcome ($W=0.543$). The scaphoid had the highest mean rank (2.764), followed by the lunate (1.941) then the triquetrum (1.249) (Figure 4.5B). In DA, all three bones were significantly differentiated from one another with the following pairwise comparison p -values; scaphoid-lunate 0.020, scaphoid-triquetrum <0.001 , and lunate-triquetrum <0.001 (Figure 4.5B). There were no significant differences between the sexes (Supplementary table 2). The only statistically significant difference between the left and right bones was in the DA values of the triquetrum ($p=0.003$).

4.5. Discussion

To date, interspecific functional adaptation research of the hominoid carpus has focused on comparing internal bone architecture of single carpal elements across species, but has either failed to find a functional signal or reached limited functional conclusions (Schilling et al. 2014; Ragni 2020; Bird, Kivell and Skinner 2021). This may be due, in part, to the known range of interspecific variation in carpal kinematics in human and non-human hominids (Moritomo et al. 2007; Orr et al. 2010; Chirchir et al. 2017) as well as the systemic differences between genera in BV/TV (Tsegai et al. 2018). The aim of this study was to establish whether relative patterns across a larger region of the carpus, namely the three bones of the proximal row, could be correlated to the known or predicted joint kinematics/kinetics of the radiocarpal and midcarpal joints. BV/TV and DA differed across the three bones of each taxa indicating these bones are subjected to different forces and functional adaptation responses across the proximal row of the carpus. Although interspecific testing was not carried out, distinct patterns in structural architecture differentiating locomotor mode emerged. Below we discuss to what extent the results reflect known or predicted joint kinematics and kinetics across each locomotor group, and then across hominoids as a group.

4.5.a. Suspensory *Pongo*

Pongo is highly arboreal using predominantly suspensory postures for locomotion, with smaller amounts of climbing and arboreal quadrupedalism (Thorpe and Crompton 2006). Hand posture during locomotion has not been studied in as much detail as it has in African apes, however *Pongo* is thought to adopt variable hand postures to navigate the irregular substrates of an arboreal environment (Isler and Thorpe 2003; Carlson 2005). Given its relatively large size, the lunate was predicted to have the highest BV/TV, with low DA across all three bones indicative of diverse loading during arboreal locomotion. In this study, bone type had a large effect on the result of BV/TV and DA, indicating that load magnitude and directionality is not uniformly distributed across the radiocarpal joint. The results did not support the predictions as the structural parameters of the lunate relative to the triquetrum (and scaphoid) did not suggest that the lunate incurs relatively higher load across variable joint positions.

The *Pongo* triquetrum had the lowest mean BV/TV of the three bones. The morphology and joint configuration of the proximal row of *Pongo* has been described as the most derived among the hominids (Sarmiento 1988; Lewis 1989). Due to the enlarged lunate and the more limited development of the TFCC, the triquetrum does not participate in the antebrachial joint via hard or soft tissue mechanisms and must transfer load from the hamate to the lunate rather than to the forearm directly (Sarmiento 1988; Lewis 1989). Functionally, these features have been interpreted as increasing forearm supination and increasing the mechanical advantage of the flexor carpi ulnaris muscle, although the efficiency of ulnar-side load transfer is assumed to be reduced (Sarmiento 1988). This joint configuration may explain why the triquetrum exhibits the lowest mean BV/TV of the three bones. However, it was not significantly lower than the lunate, which was predicted to have the highest BV/TV due to its enlarged size and presumed importance to load transfer to the forearm. Given this, it appears as though the lunate has less BV/TV than expected, rather than the triquetrum having more. Although the lunate had lower than predicted BV/TV, it did have significantly higher anisotropy relative to the triquetrum and, although this may provide strength in lieu of bone volume, higher DA suggests more stereotypical loading than would be predicted for a taxon using diverse hand positions to navigate its arboreal environment.

While these results are somewhat unexpected, higher than predicted DA has been found in other *Pongo* elements such as the proximal capitate (Bird, Kivell and Skinner 2021) and Mc heads (Dunmore et al., 2019, Chirchir et al., 2017b, although see Tsegai et al., 2013). The DA values of *Pongo* fall within the ranges of the other taxa in our study who have lower ranges

of motion and are presumed to use more stereotypical hand postures. These results within the context of previous research, may indicate *Pongo* utilises fewer hand postures during locomotion, or that load is transferred through the hand and wrist in a similar way despite the use of variable hand postures (Synek et al. 2020). The significantly higher BV/TV in the scaphoid relative to the lunate may be related to joint movement and/or force transfer through the unfused os centrale to scaphoid. Although these bones are united by strong ligaments, the os centrale is capable of motion independent of the scaphoid (Lewis 1989; Orr 2018). Bird et al. (2021) found that regions of the capitate that had ligament attachment sites had greater BV/TV than regions without. As bones loaded in tension from ligaments have lower failure points than those loaded in compression (Pattin, Caler and Carter 1996), high BV/TV in the scaphoid may indicate strength to resist strain from the stout and strong scaphocentrale ligaments.

4.5.b. Knuckle-walking in *Gorilla* and *Pan*

In BV/TV, the same pattern and significant differences were seen among the knuckle-walking taxa. The triquetrum had the highest BV/TV, which was significantly higher than the lunate only, while the scaphoid and lunate showed very similar mean values and did not differ significantly. Similar to BV/TV, in DA both taxa expressed the same pattern across the three bones: the lunate showed the highest DA, followed by the scaphoid then the lunate. In *Pan* all three pairwise comparisons were significant however in *Gorilla*, the difference between the scaphoid and lunate was not statistically significant. Although locomotion is reported to differ between the sexes in both African apes (Doran 1993b; Remis 1999), this was not reflected in the results as there were no significant differences detected between males and females across the three bones.

In combination, these results suggest greater loading of the ulnar side of the carpus than predicted. Experimental studies of captive *Pan* and *Gorilla* have reported that, in general, terrestrial knuckle-walking produces the highest peak and mean pressure on digit 2, and decreases ulnarly with the lowest values recorded on digit 5, but with limited statistical differences across the digits (Wunderlich and Jungers 2009; Matarazzo 2013). The similar BV/TV values in the scaphoid and lunate are consistent with this loading pattern. However the higher BV/TV of the lunate does not align with the traditional assumption that the ulnar carpus should incur less load (Tuttle 1969; Sarmiento 1988; Wunderlich and Jungers 2009; Matarazzo 2013). In the only 3D kinematic study of chimpanzee and macaque locomotion, knuckle-walking in the chimpanzee is shown to have a strikingly high degree of ulnar deviation compared to palmigrady or digitigrady postures used by the macaque (Thompson

2020). While 3D knuckle-walking kinematics in *Gorilla* have not yet been studied, they have been shown to exhibit higher degrees of ulnar deviation during climbing than chimpanzees (Sarmiento 1988; Neufuss et al. 2017). Although the kinematics of the triquetrum in African apes is not well understood, in *H. sapiens* the triquetrum is described as a bony stopper to ulnar deviation (Kamal et al. 2012; Edirisinghe et al. 2014) and ligaments attached to the triquetrum are critical to providing carpal stability in axial compression (Garcia-Elias, de la Bellacasa and Schouten 2017). Given the similar morphology and articular relationship of the *Pan* and *Gorilla* triquetrum and hamate to *H. sapiens* (Lewis 1989), the triquetrum in the African apes possibly fulfils a similar role. Stabilizing tensional forces imposed by ligaments during ulnar deviation are not captured by experimental studies of substrate reaction force (e.g. Wunderlich & Jungers, 2009), and thus the high relative BV/TV in the triquetrum may be reflecting stability during ulnar deviation.

Sub-chondral mineralisation research on the distal radius further contextualises the importance of ulnar deviation to functional adaptation in knuckle-walkers and may explain some of the differences observed here between *Pan* and *Gorilla*. Patel and Carlson (2007) found that in the distal radius of *Pan*, the lunate articular surface had higher mineralization and higher strength relative to the scaphoid articular surface. They suggested that the ulnar deviation associated with palm-in postures of knuckle-walking places the lunate in maximum congruence with the distal radius during mid-stance. The lunate is therefore transferring load to and from the ulnar carpus during ulnar deviation in lieu of direct ulnocarpal articulation (Patel and Carlson 2007 and references therein). *Pan* more regularly adopt palm-in postures compared to *Gorilla* (Sarmiento 1988; Matarazzo 2013) thus the greater differentiation between the lunate and scaphoid in *Pan* compared to *Gorilla* may reflect a higher proportion of ulnar deviation during locomotion. A greater use of ulnar deviation provides further support for the BV/TV results discussed above, as the relative difference between the mean BV/TV in the triquetrum and the other bones is greater in *Pan* than in *Gorilla*.

4.5.c. Tool use and manipulation in *Homo*

The pattern in BV/TV across the *Homo* sample supported our predictions. The lunate expressed the highest mean BV/TV which was statistically higher than the triquetrum, although not the scaphoid. While the scaphoid mean value fell between the two other bones, it was not statistically higher than the triquetrum. This pattern suggests there is a relatively similar magnitude of load experienced across the proximal row carpus. Although this pattern was predicted based on previous research (Stephens et al. 2018), it may initially appear counterintuitive. Conventionally, it has been concluded that the scaphoid receives and

transfers a greater magnitude of force than the other proximal row bones given its proximity to the thumb as the primary origin of force, its relatively larger size, and larger articulation with the radius (Viegas et al. 1987; Koebke 1993; Schuind et al. 1995). However, more recent finite element modelling using advanced biological models and realistic loading regimes found that once corrected for contact area, force directed through the radiolunate joint was higher than that of the radioscapoid (Gíslason et al. 2009; Gíslason et al. 2012). Further, in these studies force was higher at the capitulunate and triquetrolunate joint than at any of the intercarpal joints of the scaphoid.

The importance of the lunate, particularly to force transfer during tool use, has been overshadowed by the scaphoid in palaeoanthropological research. Some of the earliest kinematic analyses of the hand identified the capitate and lunate as the most highly stressed bones in the carpus (e.g., Wood Jones 1942) and indeed the most recent kinematic research emphasizes the importance of the lunate to the kinematic chain of the proximal row in *H. sapiens* (Garcia-Elias and Lluch 2001; Edirisinghe et al. 2014). The lunate has been demonstrated to be the key to maintaining stability during the DTM as it resists the flexion moment of the scaphoid and extension moment of the triquetrum, holding the entire row in balance (Garcia-Elias and Lluch 2001; Kamal et al. 2012; Kamal, Starr and Akelman 2016). The lunate also forms the crux of the DTM, as the hinge of the movement is located at the capitulunate joint (Edirisinghe et al. 2014). A phylogenetic analysis of lunate morphology among a broad range of extinct and extant primate taxa suggests the human lunate is primitive, resembling the inferred morphology of the last common ancestor of all hominids (Kivell, Barros and Smaers 2013). Interestingly, the morphology of the Neanderthal lunate appears more derived than the morphology of the modern human (Kivell, Barros and Smaers 2013). Thus, while the lunate is critical to the DTM kinematics, its morphology is plesiomorphic for the hominoid clade. Currently, it is unknown whether the derived proximal row carpus would result in different wrist kinematics in Neanderthals. To begin to resolve these questions, further work is needed to understand whether the lunate in non-human hominids fulfils a similar kinematic role as it does in *H. sapiens* and whether the DTM arc is similarly canalized in other hominoids. The high DA in the *Pan* and *Gorilla* lunate suggests it may fulfil a stabilisation role within the proximal row, however its lower relative BV/TV compared to the human pattern suggest it may not be as heavily loaded.

Given the lack of bony contact and overall low degree of force transferred from the ulna to the carpus, the similar BV/TV values between the scaphoid and triquetrum was an unexpected result, suggesting the triquetrum is probably receiving higher loads from the

hand than is commonly assumed. The morphology facilitating uniquely human manipulative capacities is relatively well studied in the thumb, Mc 2, and Mc3 (Marzke 1983; Marzke and Marzke 1987; Lewis 1989; Marzke 1997), as are the pressures incurred at these digits during tool use and activities of daily living (Rolian, Lieberman and Zermeno 2011; Williams, Gordon and Richmond 2012; Kulothungan, Meyyappan Nachiappan and Rajasekaran 2013; Key and Dunmore 2015; Key et al. 2017; Riddle et al. 2020). Despite the morphology of Mc4 and 5 being critical to human precision and power grips, and in-hand manipulation (Marzke and Shackley 1986; Lewis 1989; Marzke, Wullstein and Viegas 1992; Koebke 1993; Marzke 2013), relatively less research has focused on the pressures experienced by these digits. The robust morphology of the Mc5, in particular, has been argued to provide a critical buttress to stabilise the hand during high impact behaviours such as knapping or swinging a bat (Marzke and Shackley 1986; Marzke, Wullstein and Viegas 1992; Marzke et al. 1998b; Domalain, Bertin and Daver 2017) Indeed, in a recent study Key et al. (2019) found that the pressure experienced by the 5th digit of the non-dominant hand during stone tool production often matched that experienced by the thumb and index finger. Mc4 and 5 have a direct bony contact with the triquetrum via the hamate and high loading would transfer proximally through the ulnar side of the carpus (Sarmiento 1988; Marzke, Wullstein and Viegas 1992).

DA conformed to predictions showing the scaphoid had the highest DA and the triquetrum the lowest. Indeed, the human scaphoid had the highest mean DA of any bone across all taxa, indicating failure from the strong loads arising from the thumb may be mitigated by trabecular anisotropy rather than relatively greater BV/TV. Although movement at the scaphotrapezotrapezoid joint has not been quantified as frequently as the radiocarpal or midcarpal joints, research has emphasized a relatively prescribed arc of motion with a single axis of freedom due to ligamentous constraints and the narrow articular congruence of the distal scaphoid (Moritomo et al. 2000a; Moritomo et al. 2000b; Edirisinghe et al. 2014). Interestingly, the DA in the left triquetra of the human sample were statistically higher than that of the right. As lower DA is correlated to greater diversity in loading, this difference may reflect a greater number of hand postures adopted by the dominant right hand. However, further work is needed; there were only six left triquetra included in our sample and the handedness of the individuals is not known. No differences were detected between the sexes. There are relatively few studies looking specifically at sexual dimorphism in trabecular bone. Saers et al. (2019a) analysed sexual dimorphism in several foot bones (including short bones) of modern *H. sapiens* but reported a general lack of differences between the sexes. Mulder et al. (2020) analysed the trabecular structure in the epiphyses of long bones in

modern *H. sapiens*, and while there were a number of significant differences between the sexes, the patterns of these differences were not consistent across the skeleton. Unlike significant sexual dimorphism frequently reported in long bone diaphyses (Ruff 1987, 2008; Marchi, Sparacello and Shaw 2011; Nikita et al. 2011), the mechanisms underlying sexual dimorphism in trabecular bone may be controlled by more complex mechanisms (Saers, Ryan and Stock 2019a).

To assess whether consistent interspecific patterns of bone parameters were present across the radiocarpal bones, a temporogeographically diverse group of modern *H. sapiens* were included in this study. This includes populations of foragers, agriculturalists and industrialists with diverse daily activities and mobility levels (Supplementary Table 4.1). Differences in trabecular structure correlated to subsistence strategy across the modern human hand has been analysed recently by Stephens et al. (2018) who found correlates of greater strength in foragers relative to industrialists. Our study found a generally consistent relative pattern in BV/TV and DA across the whole *Homo* sample which implies it reflects the innate wrist biomechanics of *Homo sapiens*. This result is consistent with clinical data suggesting that despite diverse hand postures and activities, the *Homo sapiens* wrist moves in a prescribed path across the DTM (Edirisinghe et al. 2014; Kaufman-Cohen et al. 2018; Kaufman-Cohen et al. 2019). The consistent kinematics of the wrist may result in similar force transfer across the carpus, despite differences in behaviours correlated to subsistence strategy. Biomechanically, results suggest the magnitude of load experienced by the scaphoid may not be as different from the lunate and triquetrum as is sometimes assumed and further research on the loading and kinetics (including bilateral asymmetry) of the ulnar side of the hand and wrist is warranted.

4.5.d. Patterns across the hominoids

Research suggests DA is not under strong genetic control (Tsegai et al. 2018) although it has not consistently differentiated locomotor mode in other studies (Cotter et al. 2009; DeSilva and Devlin 2012; Dunmore et al. 2019). In this study, the statistical differences in DA between bones suggests this may be a particularly informative parameter for future interspecific research on the carpus. Among the study taxa two broad patterns are apparent: (1) the *Homo* pattern, which has a continual decrease in DA from the scaphoid to the triquetrum and (2) the non-human hominid pattern, where the lunate has the highest value followed by the scaphoid and finally the triquetrum.

As predicted, the triquetrum consistently shows the lowest DA values in all taxa. The triquetrum is one of the least studied bones across the hominoid carpus and yet its morphology and articular relationships are central to pronation-supination, one of the most important and characteristic movements of the hominoid wrist (Lewis 1989; Jouffroy and Medina 2002). Interestingly, in *H. sapiens* most of the proprioceptive ligaments attach onto the triquetrum indicating that its movement within the wrist is a critical informant to the central nervous system about wrist function (Garcia-Elias, de la Bellacasa and Schouten 2017). As there is little to no bony articulation between the ulna and the proximal carpal row in hominoids, the TFCC (the articular disc, meniscus homologue and associated ligaments) is an important load transfer structure for the ulnar carpus (Sarmiento 1988; Lewis 1989; Burkett and Geissler 2015). Histological analyses in *H. sapiens* indicates the articular disc receives multidirectional loads and excision of the ulnar-most portion leads to greater stress directed to the radius (Burkett and Geissler 2015 and references therein). It has been suggested that load transfer from the articular disc to the lunate in hominoids is diffuse, resulting in distinctly isotropic trabecular structure (Koebke 1993). While the radial portion of the triquetrum articulates with the articular disc, the remaining proximal surface articulates with the meniscus homologue. Unlike the articular disc and ligaments, the meniscus homologue lacks strong collagen fibres and it is unclear whether load transfer with the meniscus results in isotropic trabecular structures (Burkett and Geissler 2015). If load transfer with the TFCC does indeed result in characteristically isotropic trabecular structure, the overall high DA in the lunate suggests it must have localized areas with extremely high DA. Whether the novel TFCC of the hominoid wrist is responsible for the pattern of low DA of the triquetrum is an intriguing hypothesis but it cannot be resolved here. Investigation of this hypothesis is warranted as identification of bony evidence in the triquetrum of the TFCC would provide important insight into the evolution of this hominoid adaptation. Investigation would require the quantification of multiple DA values across the lunate and triquetrum, such as in Dunmore et al. (2019), and ideally inclusions of taxa which do not have the TFCC such as cercopithecoids.

Compared to DA, BV/TV had fewer significant pairwise comparisons and larger standard deviations. Given the known variability in carpal kinematics, a degree of individual variation is to be expected, but these results suggest that the degree of anisotropy, rather than magnitude, varies more substantially across the proximal row carpus (Figure 4.4 and Supplementary Table 4.1). Nevertheless, significant differences between bones within taxa and distinct patterns between the taxa suggest that bone volume is subject to functional

adaptation across the proximal row bones. The lower BV/TV in *H. sapiens* is in line with the systemically low BV/TV across the post-Neolithic human skeleton (Chirchir et al. 2015; Ryan and Shaw 2015; Saers et al. 2016; Chirchir et al. 2017; Stephens et al. 2018; Tsegai et al. 2018) and therefore as a single measure has limited functional value. Given the variation between individuals within taxa, in isolation, relationships between BV/TV in individual fossil specimens may not provide a strong signal of hand use and will likely need to be combined with other measures.

Quantifying BV/TV as trabecular and cortical bone combined rather than the conventional trabecular-measure is a response to a) the lack of clarity around how cortical and trabecular bone interact and disperse load in short bones and b) the difficulty in identifying and segmenting cortical bone from trabecular bone in the carpus of non-human hominids (Bird, Kivell and Skinner 2021). However, there are important considerations to the interpretation of the combined BV/TV measure. Firstly, combined BV/TV is not necessarily directly comparable to studies measuring trabecular-only BV/TV, limiting the ability to compare these results to other studies. Stephens et al. (2018) quantified trabecular bone parameters across the entire hand and carpus in pre- and post-Neolithic modern *H. sapiens*. The pattern between the average trabecular BV/TV results of the two populations in the scaphoid (0.28), lunate (0.30) and triquetrum (0.26) reflect the results of this study suggesting cortical thickness is relatively uniform across the proximal row carpus. However, significant differences were found between trabecular and combined BV/TV in the capitate of non-human hominids (Bird, Kivell and Skinner 2021) thus results in this study may not be comparable to any future trabecular bone results in non-human hominids. Secondly, due to its increased porosity, trabecular bone is considered to have a greater dynamic capacity to model its volume compared to cortical bone (Kivell 2016b and references therein). It is thought that cortical thickness is largely determined during ontogeny with a more limited capacity to model during adulthood, in part due to the geometric confines of short bones (Martin, Burr and Sharkey 1998; Currey 2002; Lovejoy et al. 2003). Therefore, BV/TV in this study provides a holistic measure of overall bone strength and probably reflects forces experienced during both ontogeny and adulthood.

Many of the interpretations offered here rely on assumptions or predictions of force transfer and magnitude. In particular, the kinetics of ligaments and soft tissue structures are central to functional interpretations in this study and also on the capitate (Bird, Kivell and Skinner 2021); however, our knowledge of ligament function is drawn predominantly from human research. While muscles in non-human hominids are relatively well studied (Lemelin and

Diogo 2016 for a review) the ligaments are less so (although see Sarmiento 1988; Lewis 1989; Orr 2018). Recent kinematic research has increased the nuance of our knowledge on non-human hominid locomotion (Neufuss et al. 2017; Thompson et al. 2018) and sometimes challenged conventional theories (Finestone et al. 2018; Synek et al. 2020) but in many cases detailed kinematic studies are lacking, particularly on wild animals.

4.6. Conclusion

Distinct patterns differentiating locomotor modes were evident among the study genera. In *Homo*, the scaphoid appears to resist failure from the high loads arising from the thumb during tool use by a combination of moderate BV/TV and high DA. The high BV/TV and moderate DA of the lunate is indicative of its central role to the DTM and as the stabilising block of the proximal row kinematic chain. *Pan* and *Gorilla* showed similar patterns in BV/TV and DA suggesting a comparable functional adaptation response in the proximal row carpus of both knuckle-walking taxa. The higher DA in the *Pan* lunate may be due to greater proportions of ulnar deviation and radiolunate force transfer during palm-in knuckle-walking posture. The patterns in *Pongo* indicate that the magnitude and directionality of load is not uniformly distributed across the wrist, but that *Pongo* may adopt fewer hand postures than is commonly assumed. The triquetrum had the lowest mean DA of the three bones within all taxa which may be indicative of load transfer with the Triangular Fibrocartilage Complex, unique to hominoids. This conclusion warrants further investigation within a larger comparative context including non-hominid species. The functional morphology of the lunate and triquetrum is understudied in palaeoanthropology and further research is warranted in regards to their role in knuckle-walking and tool use, particularly given the distinctly different morphology across all three proximal row carpals in Neanderthals relative to *Homo sapiens*.

4.7. Supplementary Tables

Supplementary Table 4.1 Specimen information and individual parameter results. DA and BV/TV rank is given by individual; a rank of 1 indicates lowest rank of the three bones and 3 indicates highest. The specimen column records the curatorial institutions as abbreviations; DCW = The Duckworth Collection, University of Cambridge; INDEN = Georg-August-University Goettingen, Anthropology Collection; MPI_TC = Max Planck Institute for Evolutionary Anthropology Primatology, Tai Collection; MRAC = Royal Museum for Central Africa Tervuren; NHMW = Natural History Museum Vienna; NMNH = National Museum Natural History Smithsonian; PC = Powell-Cotton Museum; SMF = Senckenberg Natural History Museum, Frankfurt; UNI_FL = University of Florence; ZMB_Mam = the Natural History Museum, Berlin; ZSM = Bavarian State Collection Zoology. Abbreviations: Taxon - Ggor = *Gorilla gorilla*; Hsap = *Homo sapiens*; Pabe = *Pongo abelii*; Ppan = *Pan paniscus*; Ppyg = *Pongo pygmaeus*; Ptro = *Pan troglodytes*. Sex - M = male; F = female; UK = unknown. Side - L = left; R = right. Element - Ln = lunate; Sc = scaphoid; Tq = triquetrum.

Specimen	Taxon	Sex	Provenance	Resolution (mm)	Side	Element	DA (0-1)	DA rank	BV/TV (%)	BV/TV rank
PC_CAMI_230	Ggor	M	Wild	0.031	L	Ln	0.257	3	0.612	2
PC_CAMI_230	Ggor	M	Wild	0.018	L	Sc	0.243	2	0.520	1
PC_CAMI_230	Ggor	M	Wild	0.031	L	Tq	0.239	1	0.655	3
PC_MER_135	Ggor	M	Wild	0.036	L	Ln	0.255	2	0.614	1
PC_MER_135	Ggor	M	Wild	0.036	L	Sc	0.339	3	0.717	2
PC_MER_135	Ggor	M	Wild	0.036	L	Tq	0.240	1	0.797	3
PC_MER_138	Ggor	F	Wild	0.034	L	Ln	0.253	1	0.509	3
PC_MER_138	Ggor	F	Wild	0.034	L	Sc	0.253	2	0.483	2
PC_MER_138	Ggor	F	Wild	0.034	L	Tq	0.258	3	0.444	1
PC_MER_174	Ggor	M	Wild	0.032	R	Ln	0.271	3	0.448	2
PC_MER_174	Ggor	M	Wild	0.032	R	Sc	0.226	1	0.438	1
PC_MER_174	Ggor	M	Wild	0.032	R	Tq	0.228	2	0.592	3
PC_MER_264	Ggor	M	Wild	0.036	R	Ln	0.267	3	0.627	2
PC_MER_264	Ggor	M	Wild	0.036	R	Sc	0.244	2	0.525	1
PC_MER_264	Ggor	M	Wild	0.036	R	Tq	0.241	1	0.636	3
PC_MER_300	Ggor	F	Wild	0.034	R	Ln	0.237	3	0.579	2
PC_MER_300	Ggor	F	Wild	0.034	R	Sc	0.218	2	0.569	1
PC_MER_300	Ggor	F	Wild	0.034	R	Tq	0.191	1	0.594	3
PC_MER_372	Ggor	M	Wild	0.035	R	Ln	0.266	3	0.522	1
PC_MER_372	Ggor	M	Wild	0.035	R	Sc	0.259	2	0.579	2
PC_MER_372	Ggor	M	Wild	0.035	R	Tq	0.207	1	0.659	3
PC_MER_696	Ggor	F	Wild	0.028	R	Ln	0.251	3	0.514	2
PC_MER_696	Ggor	F	Wild	0.028	R	Sc	0.225	2	0.526	3
PC_MER_696	Ggor	F	Wild	0.028	R	Tq	0.184	1	0.507	1
PC_MER_856	Ggor	F	Wild	0.037	L	Ln	0.286	3	0.605	1
PC_MER_856	Ggor	F	Wild	0.037	L	Sc	0.279	1	0.631	3
PC_MER_856	Ggor	F	Wild	0.037	L	Tq	0.280	2	0.617	2
PC_MER_879	Ggor	M	Wild	0.036	L	Ln	0.292	2	0.477	1
PC_MER_879	Ggor	M	Wild	0.036	L	Sc	0.303	3	0.504	2

PC_MER_879	Ggor	M	Wild	0.036	L	Tq	0.273	1	0.514	3
PC_MER_95	Ggor	F	Wild	0.035	L	Ln	0.231	3	0.540	2
PC_MER_95	Ggor	F	Wild	0.035	L	Sc	0.224	2	0.532	1
PC_MER_95	Ggor	F	Wild	0.035	L	Tq	0.198	1	0.579	3
PC_MER_962	Ggor	M	Wild	0.034	R	Ln	0.269	2	0.463	1
PC_MER_962	Ggor	M	Wild	0.034	R	Sc	0.285	3	0.645	3
PC_MER_962	Ggor	M	Wild	0.034	R	Tq	0.260	1	0.610	2
PC_MERI_29	Ggor	F	Wild	0.031	L	Ln	0.309	2	0.500	2
PC_MERI_29	Ggor	F	Wild	0.031	L	Sc	0.321	3	0.483	1
PC_MERI_29	Ggor	F	Wild	0.031	L	Tq	0.249	1	0.633	3
PC_ZVI_32	Ggor	M	Wild	0.034	R	Ln	0.236	2	0.699	2
PC_ZVI_32	Ggor	M	Wild	0.034	R	Sc	0.247	3	0.691	1
PC_ZVI_32	Ggor	M	Wild	0.034	R	Tq	0.212	1	0.735	3
DCW_AM_10_0_182	Hsap	UK	Pre-industrial: Americas	0.031	R	Ln	0.239	2	0.583	3
DCW_AM_10_0_182	Hsap	UK	Pre-industrial: Americas	0.031	R	Sc	0.268	3	0.515	2
DCW_AM_10_0_182	Hsap	UK	Pre-industrial: Americas	0.031	R	Tq	0.214	1	0.491	1
DCW_AM_10_0_183	Hsap	UK	Pre-industrial: Americas	0.029	L	Ln	0.321	3	0.428	3
DCW_AM_10_0_183	Hsap	UK	Pre-industrial: Americas	0.029	L	Sc	0.278	1	0.413	2
DCW_AM_10_0_183	Hsap	UK	Pre-industrial: Americas	0.029	L	Tq	0.286	2	0.318	1
DCW_AM_3_0_1	Hsap	UK	Pre-industrial: Americas	0.035	L	Ln	0.316	1	0.341	3
DCW_AM_3_0_1	Hsap	UK	Pre-industrial: Americas	0.035	L	Sc	0.378	3	0.331	1
DCW_AM_3_0_1	Hsap	UK	Pre-industrial: Americas	0.035	L	Tq	0.326	2	0.337	2
DCW_OC_1_0_26	Hsap	UK	Pre-industrial: Oceania	0.029	R	Ln	0.305	3	0.341	2
DCW_OC_1_0_26	Hsap	UK	Pre-industrial: Oceania	0.026	R	Sc	0.287	2	0.354	3
DCW_OC_1_0_26	Hsap	UK	Pre-industrial: Oceania	0.026	R	Tq	0.248	1	0.296	1
DCW_OC_31_0_1	Hsap	UK	Pre-industrial: Oceania	0.030	L	Ln	0.253	1	0.414	3
DCW_OC_31_0_1	Hsap	UK	Pre-industrial: Oceania	0.030	L	Sc	0.259	2	0.337	2
DCW_OC_31_0_1	Hsap	UK	Pre-industrial: Oceania	0.030	L	Tq	0.263	3	0.323	1
GAUG-Inden_118	Hsap	F	Post-industrial: Inden, Germany	0.025	R	Ln	0.261	2	0.378	1
GAUG-Inden_118	Hsap	F	Post-industrial: Inden, Germany	0.025	R	Sc	0.294	3	0.489	3

GAUG-Inden_118	Hsap	F	Post-industrial: Inden, Germany	0.025	R	Tq	0.239	1	0.405	2
GAUG-Inden_323	Hsap	UK	Post-industrial: Inden, Germany	0.025	R	Ln	0.296	2	0.415	3
GAUG-Inden_323	Hsap	UK	Post-industrial: Inden, Germany	0.025	R	Sc	0.321	3	0.296	1
GAUG-Inden_323	Hsap	UK	Post-industrial: Inden, Germany	0.025	R	Tq	0.244	1	0.320	2
GAUG-Inden_91	Hsap	M	Post-industrial: Inden, Germany	0.030	R	Ln	0.294	2	0.486	3
GAUG-Inden_91	Hsap	M	Post-industrial: Inden, Germany	0.025	R	Sc	0.303	3	0.436	2
GAUG-Inden_91	Hsap	M	Post-industrial: Inden, Germany	0.025	R	Tq	0.271	1	0.341	1
NHMW-Nubian_C1-31	Hsap	M	Pre-industrial: Nubian Egypt	0.030	L	Ln	0.295	2	0.493	3
NHMW-Nubian_C1-31	Hsap	M	Pre-industrial: Nubian Egypt	0.030	L	Sc	0.299	3	0.348	2
NHMW-Nubian_C1-31	Hsap	M	Pre-industrial: Nubian Egypt	0.003	L	Tq	0.280	1	0.316	1
NHMW-Nubian_J2	Hsap	M	Pre-industrial: Nubian Egypt	0.030	R	Ln	0.271	2	0.350	2
NHMW-Nubian_J2	Hsap	M	Pre-industrial: Nubian Egypt	0.030	R	Sc	0.289	3	0.366	3
NHMW-Nubian_J2	Hsap	M	Pre-industrial: Nubian Egypt	0.030	R	Tq	0.235	1	0.326	1
NHMW-Nubian_J7	Hsap	F	Pre-industrial: Nubian Egypt	0.030	R	Ln	0.271	2	0.438	3
NHMW-Nubian_J7	Hsap	F	Pre-industrial: Nubian Egypt	0.030	R	Sc	0.331	3	0.241	1
NHMW-Nubian_J7	Hsap	F	Pre-industrial: Nubian Egypt	0.030	R	Tq	0.252	1	0.357	2
NHMW-Nubian_K41-2	Hsap	UK	Pre-industrial: Nubian Egypt	0.030	R	Ln	0.277	2	0.396	2
NHMW-Nubian_K41-2	Hsap	UK	Pre-industrial: Nubian Egypt	0.030	R	Sc	0.302	3	0.428	3
NHMW-Nubian_K41-2	Hsap	UK	Pre-industrial: Nubian Egypt	0.030	R	Tq	0.257	1	0.377	1
NHMW-Nubian_K5-2	Hsap	M	Pre-industrial: Nubian Egypt	0.030	R	Ln	0.249	2	0.509	3
NHMW-Nubian_K5-2	Hsap	M	Pre-industrial: Nubian Egypt	0.030	R	Sc	0.276	3	0.498	2
NHMW-Nubian_K5-2	Hsap	M	Pre-industrial: Nubian Egypt	0.030	R	Tq	0.207	1	0.422	1
NHMW-Nubian_K78-2	Hsap	F	Pre-industrial: Nubian Egypt	0.030	R	Ln	0.237	1	0.504	3
NHMW-Nubian_K78-2	Hsap	F	Pre-industrial: Nubian Egypt	0.030	R	Sc	0.278	3	0.496	2
NHMW-Nubian_K78-2	Hsap	F	Pre-industrial: Nubian Egypt	0.030	R	Tq	0.252	2	0.435	1
UNIFL_3127	Hsap	M	Pre-industrial: Tierra Del Fuego	0.038	L	Ln	0.281	2	0.428	2
UNIFL_3127	Hsap	M	Pre-industrial: Tierra Del Fuego	0.038	L	Sc	0.284	3	0.389	1
UNIFL_3127	Hsap	M	Pre-industrial: Tierra Del Fuego	0.038	L	Tq	0.254	1	0.497	3
UNIFL_4865	Hsap	M	Post-industrial: Syracuse, Italy	0.030	L	Ln	0.311	2	0.318	2
UNIFL_4865	Hsap	M	Post-industrial: Syracuse, Italy	0.030	L	Sc	0.321	3	0.283	1

UNIFL_4865	Hsap	M	Post-industrial: Syracuse, Italy	0.030	L	Tq	0.262	1	0.405	3
UNIFL_4887	Hsap	F	Post-industrial: Syracuse, Italy	0.030	R	Ln	0.310	2	0.298	3
UNIFL_4887	Hsap	F	Post-industrial: Syracuse, Italy	0.030	R	Sc	0.354	3	0.292	2
UNIFL_4887	Hsap	F	Post-industrial: Syracuse, Italy	0.030	R	Tq	0.259	1	0.269	1
NMNH_267325	Pabe	M	Wild	0.040	L	Ln	0.281	3	0.464	1
NMNH_267325	Pabe	M	Wild	0.040	L	Sc	0.280	2	0.626	3
NMNH_267325	Pabe	M	Wild	0.040	L	Tq	0.227	1	0.483	2
SMF_6785	Pabe	M	Wild	0.030	R	Ln	0.207	2	0.497	1
SMF_6785	Pabe	M	Wild	0.030	R	Sc	0.215	3	0.664	3
SMF_6785	Pabe	M	Wild	0.030	R	Tq	0.200	1	0.655	2
MRAC_15293	Ppan	F	Wild	0.030	L	Ln	0.251	2	0.560	3
MRAC_15293	Ppan	F	Wild	0.030	L	Sc	0.259	3	0.481	1
MRAC_15293	Ppan	F	Wild	0.030	L	Tq	0.224	1	0.510	2
MRAC_27696	Ppan	M	Wild	0.030	L	Ln	0.288	3	0.427	2
MRAC_27696	Ppan	M	Wild	0.030	L	Sc	0.273	2	0.501	3
MRAC_27696	Ppan	M	Wild	0.030	L	Tq	0.226	1	0.425	1
MRAC_27698	Ppan	F	Wild	0.030	L	Ln	0.229	3	0.674	1
MRAC_27698	Ppan	F	Wild	0.030	L	Sc	0.200	1	0.686	3
MRAC_27698	Ppan	F	Wild	0.030	L	Tq	0.226	2	0.679	2
MRAC_29042	Ppan	F	Wild	0.030	R	Ln	0.258	3	0.556	1
MRAC_29042	Ppan	F	Wild	0.030	R	Sc	0.236	2	0.571	2
MRAC_29042	Ppan	F	Wild	0.030	R	Tq	0.210	1	0.757	3
MRAC_29044	Ppan	M	Wild	0.030	R	Ln	0.245	3	0.604	2
MRAC_29044	Ppan	M	Wild	0.030	R	Sc	0.200	2	0.593	1
MRAC_29044	Ppan	M	Wild	0.030	R	Tq	0.187	1	0.786	3
MRAC_29045	Ppan	F	Wild	0.030	L	Ln	0.245	2	0.507	1
MRAC_29045	Ppan	F	Wild	0.030	L	Sc	0.261	3	0.557	2
MRAC_29045	Ppan	F	Wild	0.030	L	Tq	0.227	1	0.563	3
MRAC_29052	Ppan	M	Wild	0.030	R	Ln	0.315	3	0.526	1
MRAC_29052	Ppan	M	Wild	0.030	R	Sc	0.257	1	0.549	3

MRAC_29052	Ppan	M	Wild	0.030	R	Tq	0.280	2	0.552	2
SMF_24510	Ppyg	F	Wild	0.034	R	Ln	0.262	3	0.421	2
SMF_24510	Ppyg	F	Wild	0.034	R	Sc	0.226	2	0.460	3
SMF_24510	Ppyg	F	Wild	0.034	R	Tq	0.209	1	0.400	1
SMF_74303	Ppyg	F	Wild	0.030	L	Ln	0.228	3	0.621	2
SMF_74303	Ppyg	F	Wild	0.030	L	Sc	0.220	2	0.673	3
SMF_74303	Ppyg	F	Wild	0.030	L	Tq	0.177	1	0.584	1
SMF_84218	Ppyg	F	Captive	0.030	L	Ln	0.315	2	0.468	2
SMF_84218	Ppyg	F	Captive	0.030	L	Sc	0.334	3	0.538	3
SMF_84218	Ppyg	F	Captive	0.030	L	Tq	0.285	1	0.450	1
ZMB_Mam_6947	Ppyg	M	Wild	0.032	L	Ln	0.313	3	0.482	2
ZMB_Mam_6947	Ppyg	M	Wild	0.032	L	Sc	0.286	2	0.530	3
ZMB_Mam_6947	Ppyg	M	Wild	0.032	L	Tq	0.282	1	0.443	1
ZMB_Mam_6948	Ppyg	F	Wild	0.029	L	Ln	0.326	3	0.416	2
ZMB_Mam_6948	Ppyg	F	Wild	0.029	L	Sc	0.265	2	0.486	3
ZMB_Mam_6948	Ppyg	F	Wild	0.029	L	Tq	0.294	1	0.359	1
ZSM_1907_0483	Ppyg	F	Wild	0.028	R	Ln	0.256	3	0.479	2
ZSM_1907_0483	Ppyg	F	Wild	0.028	R	Sc	0.249	2	0.561	3
ZSM_1907_0483	Ppyg	F	Wild	0.028	R	Tq	0.240	1	0.451	1
ZSM_1907_0633b	Ppyg	F	Wild	0.028	R	Ln	0.299	3	0.563	1
ZSM_1907_0633b	Ppyg	F	Wild	0.028	R	Sc	0.260	1	0.627	3
ZSM_1907_0633b	Ppyg	F	Wild	0.028	R	Tq	0.279	2	0.589	2
ZSM_1907_0660	Ppyg	F	Wild	0.029	R	Ln	0.327	3	0.452	2
ZSM_1907_0660	Ppyg	F	Wild	0.029	R	Sc	0.277	2	0.497	3
ZSM_1907_0660	Ppyg	F	Wild	0.029	R	Tq	0.262	1	0.430	1
ZSM_1909_0801	Ppyg	M	Wild	0.028	R	Ln	0.274	3	0.463	2
ZSM_1909_0801	Ppyg	M	Wild	0.028	R	Sc	0.271	2	0.493	3
ZSM_1909_0801	Ppyg	M	Wild	0.028	R	Tq	0.241	1	0.424	1
ZSM_1966_0203	Ppyg	M	Captive	0.029	R	Ln	0.331	3	0.606	1
ZSM_1966_0203	Ppyg	M	Captive	0.029	R	Sc	0.294	2	0.743	3

ZSM_1966_0203	Ppyg	M	Captive	0.029	R	Tq	0.249	1	0.632	2
ZSM_1982_0092	Ppyg	F	Captive	0.029	R	Ln	0.209	3	0.602	1
ZSM_1982_0092	Ppyg	F	Captive	0.029	R	Sc	0.200	2	0.730	3
ZSM_1982_0092	Ppyg	F	Captive	0.029	R	Tq	0.172	1	0.673	2
ZSM_AP-120	Ppyg	M	Wild	0.028	L	Ln	0.284	2	0.538	2
ZSM_AP-120	Ppyg	M	Wild	0.028	L	Sc	0.290	3	0.542	3
ZSM_AP-120	Ppyg	M	Wild	0.034	L	Tq	0.267	1	0.465	1
MPITC_11778	Ptro	F	Wild	0.030	L	Ln	0.269	3	0.576	2
MPITC_11778	Ptro	F	Wild	0.030	L	Sc	0.240	2	0.499	1
MPITC_11778	Ptro	F	Wild	0.030	L	Tq	0.204	1	0.584	3
MPITC_11781	Ptro	M	Wild	0.030	L	Ln	0.337	3	0.599	2
MPITC_11781	Ptro	M	Wild	0.030	L	Sc	0.265	2	0.519	1
MPITC_11781	Ptro	M	Wild	0.030	L	Tq	0.258	1	0.688	3
MPITC_11903	Ptro	M	Wild	0.030	L	Ln	0.279	3	0.659	1
MPITC_11903	Ptro	M	Wild	0.030	L	Sc	0.244	2	0.682	2
MPITC_11903	Ptro	M	Wild	0.030	L	Tq	0.180	1	0.711	3
MPITC_14996	Ptro	F	Wild	0.030	L	Ln	0.329	2	0.493	2
MPITC_14996	Ptro	F	Wild	0.030	L	Sc	0.348	3	0.400	1
MPITC_14996	Ptro	F	Wild	0.030	L	Tq	0.265	1	0.545	3
PC_M719	Ptro	M	Wild	0.031	R	Ln	0.346	3	0.562	1
PC_M719	Ptro	M	Wild	0.031	R	Sc	0.301	2	0.575	2
PC_M719	Ptro	M	Wild	0.031	R	Tq	0.217	1	0.656	3
PC_ZVII_24	Ptro	M	Wild	0.032	R	Ln	0.326	3	0.689	2
PC_ZVII_24	Ptro	M	Wild	0.032	R	Sc	0.241	2	0.681	1
PC_ZVII_24	Ptro	M	Wild	0.032	R	Tq	0.211	1	0.741	3
ZSM_AP-122	Ptro	M	Wild	0.034	R	Ln	0.296	3	0.519	1
ZSM_AP-122	Ptro	M	Wild	0.034	R	Sc	0.239	2	0.607	3
ZSM_AP-122	Ptro	M	Wild	0.034	R	Tq	0.233	1	0.572	2

Supplementary Table 4.2 Results of the Wilcoxon intraspecific pairwise comparisons. The first four sets of results show whether there are sex differences in BV/TV and DA for *Pongo*, *Gorilla*, *Pan* and *Homo*. The final set of results shows whether there are differences in BV/TV and DA between the right and left bones of *Homo*. Significant results are in bold.

Taxon	Test	Bone	BV/TV <i>p</i> -value	DA <i>p</i> -value
<i>Pongo</i>	Sex Male = 6 Female = 8	Scaphoid	0.662	0.181
		Lunate	0.662	0.949
		Triquetrum	0.572	1
<i>Gorilla</i>	Sex Male = 8 Female = 6	Bone	BV/TV <i>p</i> -value	DA <i>p</i> -value
		Scaphoid	0.572	0.345
		Lunate	0.754	0.490
<i>Pan</i>	Sex Male = 8 Female = 6	Bone	BV/TV <i>p</i> -value	DA <i>p</i> -value
		Scaphoid	0.228	0.851
		Lunate	0.572	0.081
<i>Homo</i>	Sex Male = 6 Female = 4	Bone	BV/TV <i>p</i> -value	DA <i>p</i> -value
		Scaphoid	0.914	0.476
		Lunate	0.761	0.352
	Side Left = 6 Right = 11	Triquetrum	0.914	0.609
		Scaphoid	0.216	0.883
		Lunate	0.383	0.078
	Triquetrum	0.807	0.003	

5. Internal structure of the capitate and its implications for hand use in fossil hominins

5.1. Abstract

The capitate sits within the centre of the wrist and is a critical functional link between the fingers and forearm. Variable hominid capitate morphology is hypothesised to reflect the divergent force vectors experienced by a hand used primarily for manipulation (as in *Homo sapiens*) versus locomotion (as in *Pongo*, *Gorilla* and *Pan*). While the external morphology of bones reflects evolutionary adaptation, the microarchitecture of trabecular bone is known to alter its microstructure to the strain experienced by the bone over a lifetime. Differences in trabecular microarchitecture therefore may be an additional avenue to identify habitual behaviour among fossils where the degree of arboreality or tool behaviour is uncertain. It has already been established that *H. sapiens* express a distinctive microstructure in the proximal capitate hypothesised to reflect the 'dart-thrower's motion' (DTM) axis of the wrist (Stephens et al. 2018). Using micro-computed tomographic scans of extant and extinct (*Australopithecus sediba*, *Homo naledi*, *Homo floresiensis*, Neanderthals) hominid taxa, this study investigates differences in the distribution of trabecular bone volume in the proximal capitate. We determine 1) whether the distribution in *H. sapiens* is different to the other extant hominids and 2) what can be inferred about hand loading history in fossil hominins. Results indicated that modern and fossil *H. sapiens*, and Neanderthal expressed a unique pattern of bone distribution, differentiating them from the other extant hominids, suggesting this pattern may be a strong indicator of a functional commitment to tool behaviour. All hominids exhibited high bone volume at the capitulunate joint suggesting high strain at this joint may be a shared feature of hominid wrist kinetics. Despite being the geologically oldest fossil, *A. sediba* was the only other taxa to have bone volume distribution resembling modern *H. sapiens*. *Homo floresiensis* and *H. naledi* had a similar distribution of bone, indicative of high ulnar side loading of the hand. This suggests they likely used different hand postures and gripping strategies to late *Homo*. Results support hypotheses of hand use diversity across the hominin fossil record, but more work is needed to understand whether the *H. sapiens* pattern reflects the kinematics of the DTM, or the kinetics of forceful precision gripping.

5.2. Introduction

The external shape of carpal bones facilitates mobility or stability at the numerous interdependent joints of the wrist (Hamrick 1996). Among primates, shape and range of

motion variation in these joints are correlated to differences in the primary function of the hand (Richmond 2006; Orr 2017; Preuschoft 2019). Carpal morphology and concomitant range of motion are more variable among the hominids than in other groups of primates due to the diverse locomotor strategies within the clade (Kivell, Barros and Smaers 2013). As such, there is a long history of using carpal morphology to infer the arboreality and capacity for tool behaviour among fossil hominins (Napier 1962b; Lewis 1972; Orr et al. 2013). Sitting within the centre of the wrist (Figure 5.1A), morphological differences in the hominid capitate reflect variable adaptations to the biomechanically distinct force vectors imposed upon the midcarpal joint during manipulation and forelimb locomotion (Sarmiento 1988; Lewis 1989; Richmond 2006; Tocheri 2007). The capitate has therefore been the focus of several studies inferring hand use in fossil hominins (Marzke 1983; McHenry 1983; Orr et al. 2013); however, there are limitations to drawing behavioural inferences from the external morphology of fossil material. The external shape of bones provides evidence of potential joint movement; however, as numerous genetic and non-genetic factors determine shape, skeletal morphology has the potential to reflect features that are no longer functionally significant (Lieberman 1997; Ward 2002; Tocheri 2007). In order to investigate questions about behaviour in fossils, palaeoanthropologists need to investigate phenotypically plastic aspects of bone (Lieberman 1997). Beneath the external cortical bone, the internal, porous trabecular bone is known to model aspects of its architectural properties to loading experienced during life (Pontzer et al. 2006a; Barak, Lieberman and Hublin 2011). Therefore, quantifying trabecular architecture within a comparative context provides an avenue to explore the actual, rather than the potential, behaviour of an individual or species. As a key component of midcarpal kinematics, trabecular architecture within the proximal capitate may hold insights into how Plio-Pleistocene hominins, who often combine aspects of ape-like and human-like hand morphology, interacted with their environment.

The highly compacted and complex wrist region makes understanding the form-function of wrist morphology challenging (Orr 2016). Some studies have used live animal motion capture to report how the wrist moves during locomotion (Tuttle 1967; Jenkins and Fleagle 1975; Sarmiento 1988; Doran 1997; Pontzer, Raichlen and Rodman 2014; Finestone et al. 2018), while 2D cineradiographs have been used to quantify the movement of individual carpal bones between static postures (Jenkins and Fleagle 1975; Ruby et al. 1988; Moritomo et al. 2000b; Jouffroy and Medina 2002). Both types of studies traditionally report movement with respect to the traditional anatomical planes (e.g., radial-ulnar deviation, flexion-extension, pronation-supination). From these studies, it has been well-demonstrated that the range of

motion in extension at the midcarpal joint varies with habitual locomotor mode, with hominids being characterised by high degrees of ulnar deviation relative to cercopithecoids (Sarmiento 1988; Jouffroy and Medina 2002). Functional movement, however, combines variable degrees of flexion-extension, radial-ulnar deviation and pronation-supination (Tuttle 1967; Wunderlich and Jungers 2009; Matarazzo 2013; Thompson 2020), and there is currently less quantitative data on these concomitant out-of-plane movements that accompany motion along the anatomical axes.

The development of computational techniques for reconstructing and quantifying intercarpal motion in 3D (Crisco et al. 2005; Crisco et al. 2011) led to the hypothesis that the “dart-thrower’s motion” characterises the functional axis of *H. sapiens* wrist movement. The DTM was first named by Fisk (1981) to describe the distinctive out-of-plane movement of the human wrist when, for example, casting a fishing line or throwing a dart (Figure 5.1B). It describes movement of the hand from extension with radial deviation to flexion with ulnar deviation (Crisco et al. 2005) (Figure 5.1b). Many studies using 3D techniques for quantifying intercarpal movement have demonstrated that the proximal capitate (also known as the capitate head) is the central component of this motion as its rotation axis is always perpendicular to hand movement, essentially tracking the path of the DTM (Crisco et al. 2005; Crisco et al. 2011; Rainbow et al. 2013; Brigstocke et al. 2014; Edirisinghe et al. 2014; Garcia-Elias, Alomar Serrallach and Monill Serra 2014). Throughout this oblique (i.e., out-of-plane) motion, the loosely tethered lunate and scaphoid are continuously tightly compacted against one another, resulting in a stable articular surface for the capitate at a joint which is usually highly unstable (Crisco et al. 2005; Edirisinghe et al. 2014; Garcia-Elias, Alomar Serrallach and Monill Serra 2014). The DTM is used for almost all activities of daily living, from manoeuvring a screwdriver, and pouring water from a jug, to turning a door handle (Brigstocke et al. 2014; Edirisinghe et al. 2014; Kaufman-Cohen et al. 2018; Stirling et al. 2021; Williams-Hatala et al. 2021).

In living *H. sapiens*, the DTM is used for normal day-to-day behaviours; however, it has been demonstrated to increase the accuracy and velocity of strikes during high-impact vocational behaviours such as hammering, clubbing, and throwing, while also decreasing the risk of injury from the resultant reaction forces (Wolfe et al. 2006; Williams, Gordon and Richmond 2010, 2014). Furthermore, despite the power generated by the DTM, forearm muscles are only minimally activated, and when the wrist is allowed to fall passively against gravity, extension or flexion is always accompanied by degrees of radial or ulnar deviation, suggesting the intrinsic structures of the human wrist are highly adapted to the motion (Moritomo et

al. 2007). While such high-impact activities may not be routinely performed by the majority of living *H. sapiens* today, the functional consequences of the DTM have been used to support hypotheses that it may have evolved in adaptation to knapping activities (Wolfe et al. 2006; Williams, Gordon and Richmond 2010, 2014). Furthermore, when analysing the distribution of trabecular bone volume in the proximal capitate of modern *H. sapiens*, Stephens et al. (2018) found that high bone volume coincided with the axis of the DTM axis.

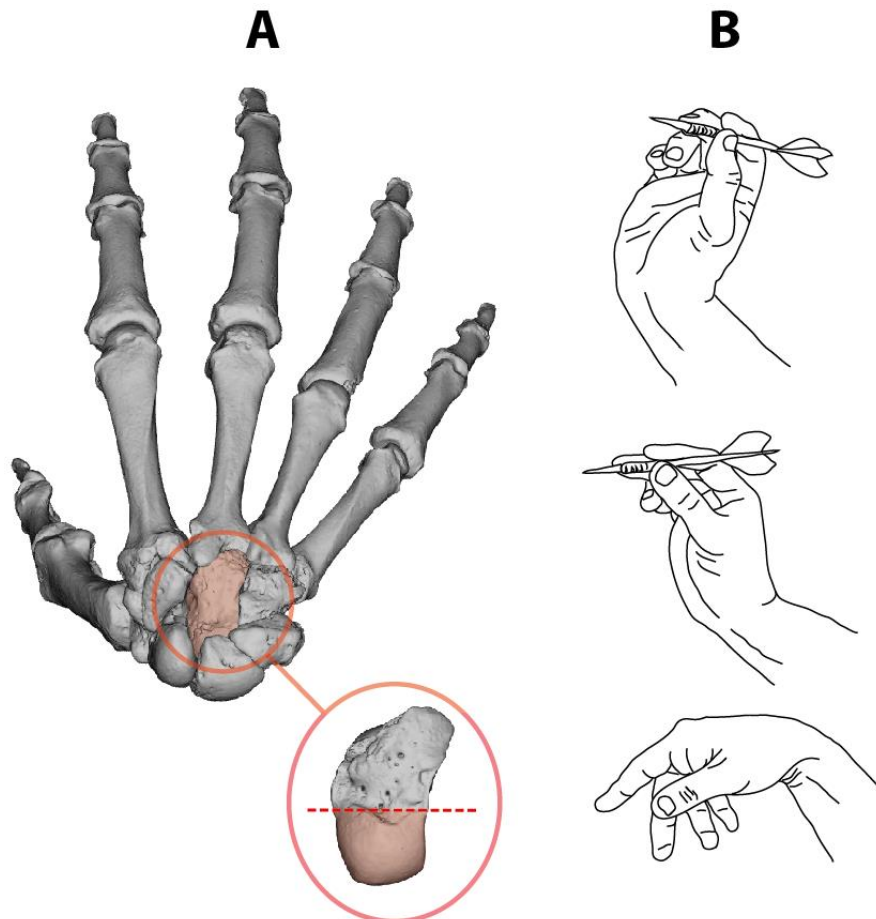


Figure 5.1 Anatomy of the capitate and function in the wrist.

A) A modern *H. sapiens* right hand shows the position of the capitate (in red) in the centre of the wrist. The capitate is also shown in isolation; the dotted line illustrates where the proximal capitate (in red) was separated from the distal capitate (in grey). B) A hand moving through the dart-thrower's motion

Like *H. sapiens*, the scaphoid and lunate form an unstable joint in non-human hominids (Lewis 1989; Orr 2017). Thus, a similar biomechanical solution may be needed to stabilise the proximal midcarpal joint surface (i.e., the scapholunate joint), as the DTM does for *H. sapiens*. Using the method published originally by Crisco et al. (2005) to study the DTM, Orr (2010) quantified intercarpal motion in 3D to investigate how the so-called “screw-clamp” mechanism of the midcarpal joint may provide stability to the midcarpal joint of African apes

(*Pan* sp and *Gorilla* sp). The screw-clamp mechanism was first described by MacConnaill (1941) in relation to *H. sapiens* as a two-phase motion: 1) the scaphoid “twists” around the proximal capitate bringing the two bones into full congruence, linking the scaphoid to the motion of the capitate, and 2) the twisting motion of the triquetrohamate joint pins the lunate between the triquetrum and the scaphoid. Orr (2010) found that the scaphoid and triquetrum helical axis of rotation in *Pan troglodytes* has a higher degree of obliquity than in *Pongo*, which resulted in a lower range of motion in midcarpal extension and a more inherently stable radial-side wrist.

Both the DTM and the screw-clamp mechanism provide hypotheses for how an inherently unstable midcarpal joint uses out-of-plane movements to achieve stability. Some of the morphological features underlying these hypotheses are shared, i.e., the lunate is the central component holding the proximal row in balance; the usually unstable scapholunate joint is kept in close congruence (Garcia-Elias 1997; Orr 2010; Edirisinghe et al. 2014). However, it has yet to be formally tested whether the oblique wrist axis used by non-human hominids is functionally or mechanically similar to the DTM. As such, it is unclear whether 1) the underlying biomechanical structures of the wrist that facilitate the DTM were inherited from a hominid common ancestor, or 2) the DTM evolved in response to intensified tool behaviours among hominins (Wolfe et al. 2006).

It has been demonstrated *in vivo* that architectural aspects of trabecular bone are sensitive to behaviourally induced force and capable of adapting its structure (at least to some degree) to improve resistance to strain and deformation from habitual loading regimes (Pontzer et al. 2006a; Ruff, Holt and Trinkaus 2006; Barak, Lieberman and Hublin 2011). While there are challenges to detecting functional signals in bone structure, particularly given genetic influences and the physiological role bone plays within the body (for comprehensive reviews see, Ruff, Holt and Trinkaus 2006; Kivell 2016b), studies have found functionally meaningful differences in the structure and pattern of trabecular bone across numerous skeletal elements among primates (e.g., Ryan and Shaw 2012; Barak et al. 2013; Tsegai et al. 2013; Skinner et al. 2015; Su and Carlson 2017; Georgiou et al. 2019; Dunmore et al. 2020a). It has already been established that the proximal capitate in modern *H. sapiens* shows a pattern of trabecular bone distribution consistent with the DTM axis (Stephens et al. 2018). Thus, extending this analysis to non-human hominids will provide insight into whether aspects of the DTM loading kinetics are unique (or not) to *H. sapiens* and help better understand the adaptive significance of the DTM.

Currently, there is a 3 million year gap between the first evidence for stone tool technology (Harmand et al. 2015) and use (McPherron et al. 2010) and the full-suite of morphological adaptations to that technology in the carpus (Tocheri et al. 2008). Like *H. sapiens*, Neanderthals are obligate tool users, and share the full suite of wrist features indicative of a functional commitment to precise and forceful gripping (Tocheri et al. 2008). While these morphological features are thought to have been inherited from a common ancestor, the current paucity of hominin carpals, particularly those of *Homo erectus*, means it is not possible to precisely identify when each of these features arose during hominin evolution (Tocheri et al. 2008; Lorenzo et al. 2015). Outside the Neanderthals, all other fossil hominins show variable combinations of human-like and ape-like morphology in their wrist bones (Tocheri et al. 2008; Kivell 2015). These combinations are not reflected in any living taxa, making it challenging to draw functional conclusions as to their capacity for tool behaviour (Tocheri et al. 2008; Orr et al. 2013). Three Plio-Pleistocene hominins, *Australopithecus sediba*, *Homo naledi*, and *Homo floresiensis*, have well-preserved capitate bones providing an opportunity to compare their trabecular architecture to habitually arboreal (*Pongo*, *Gorilla*, *Pan*) and obligate tool-using (fossil and modern *H. sapiens*, and Neanderthals) hominids.

In South Africa, *A. sediba* (1.977ma, Pickering et al., 2011) and *H. naledi* (235-335ka, Dirks et al., 2017) both exhibit adaptations for climbing and arboreality in the upper limb such as long, ape-like forelimbs for overhead reaching and curved phalanges for powerful flexion and grasping (Kivell et al. 2011; Churchill et al. 2013; Feuerriegel et al. 2017; Kivell et al. 2018a). However, they also both exhibit a long thumb capable of opposing the non-pollical digits and some carpal joint adaptations indicative of human-like tool behaviour, including aspects of a human-like capitate (see Kivell 2015 for a comprehensive review). Unfortunately, no stone tools are associated with either species and thus there is no direct evidence of their tool behaviour. In contrast to the South African hominins, the late surviving *H. floresiensis* from Indonesia (100-60ka, Sutikna et al., 2016) is associated with Oldowan-like tools recovered from the Liang Bua Cave (Moore & Brumm, 2009). However, the *H. floresiensis* carpals are ape-like and do not possess any derived, human-like features (Marzke 1997; Tocheri et al. 2008; Orr et al. 2013). The *H. floresiensis* phalanges are curved, similar to the degree found in australopiths, but the remaining hand bones are fragmentary, and its thumb-to-finger length ratio is currently unclear (Tocheri et al. 2007; Larson et al. 2009; Orr et al. 2013).

The distribution of trabecular bone in the proximal capitate of *H. sapiens* has yet to be compared to other taxa; thus, it is unclear whether the pattern identified by Stephens et al.

(2018) is unique to *H. sapiens* and could be considered a signal of habitual, human-like tool behaviour. In order to quantify bone volume and investigate signals of functional adaptation, we use microtomography to test whether patterns of relative bone volume (RBV) distribution are different across the proximal capitate in extant and extinct hominids. We predict the results of *H. sapiens* will reflect those of Stephens (2018); *H. sapiens* will have high RBV at the capitulum and capitolunate joint. We also predict that the non-human hominids will express high RBV at the capitulum joint, reflecting the biomechanics of the screw-clamp mechanism, but will not have high RBV at the capitolunate joint, reflecting lower loading of the radial-side hand compared to *H. sapiens*. We make no specific predictions for the fossil hominids. To quantify and statistically compare the distribution of RBV within the proximal capitate, this study uses canonical holistic morphometric analysis (cHMA), which combines statistical deformation modelling and holistic morphometric analysis (Steiner, Synek and Pahr 2021; Bachmann et al. 2022). This novel method is applied to a diverse sample of extant hominids (*Pongo*, *Gorilla*, *Pan*, modern *H. sapiens*) and fossil hominins (*A. sediba*, *H. naledi* and *H. floresiensis*, Neanderthals, and fossil *H. sapiens*) with the aim to provide insights into the loading history of the midcarpal joints of these fossil hominins.

5.3. Materials

This study used micro-CT scans of left and right capitates from five extant genera (*Pongo* sp. n=12, *Gorilla* sp. n=11, *Pan* sp. n=10, and *H. sapiens* n=29). The human sample derives from spatio-temporally diverse populations to capture behavioural and bone volume variation (Chirchir et al. 2015; Ryan and Shaw 2015; Stephens et al. 2018). From earliest to latest dates, this includes individuals from early 20th century Italy; 18th-19th century Germany; crewmen from the Mary Rose Tudor warship (Stirland 2005); late 19th century Duckworth North American and Oceania collection; late 19th Century Tierra Del Fuego, (Marangoni et al. 2011), Medieval England (Hicks and Hicks 2001); and 6th and 11th century Egyptian Nubia (Paoli et al. 1993) (for more detailed information see Appendix A Table 8.1). We also included three *H. sapiens* from Late Pleistocene populations: Arene Candide 2 from Western Liguria, Italy, dated at 12-11ka (Sparacello et al. 2018); from the same region, Barma Grande 2, dated at 15-17ka (Formicola, Pettitt and Dellucchese 2004); and Ohalo 2, dated to 19ka from Israel (Hershkovitz et al. 1995). Seven fossil hominins from four extinct genera were analysed. All three Neanderthals are from Israel: Tabun C1, dated at 143 ± 37 ka (Coppa et al. 2005); Amud 1, dated at 50-70ka (Valladas et al. 1999), and Kebara 2, dated to 50-60ka (Schwarcz et al. 1989). *Homo floresiensis* is represented by two individuals, the left capitate of Liang Bua 1

(ID: LB1) and the right capitate probably belonging to Liang Bua 6 (ID: LB6). *H. naledi* is represented by one right capitate (ID: UW101_1730) from the Hand 1 skeleton. *Australopithecus sediba* is represented by one individual, Malapa Hominin 2 (MH2), with both the right (ID: UW88_156) and left (ID: UW88_105) capitate included. All specimens were adults with no signs of pathology. Non-human hominids were wild-shot except for one *P. pygmaeus* individual (SMF_84218), who was a captive zoo animal.

5.4. Methods

5.4.a. Data collection

Specimens were scanned either at the Max Planck Institute for Evolutionary Anthropology, Germany, using a BIR ACTIS 225/300 or Diondo D3 microCT scanner or at the University of Cambridge Biotomography Centre with a Nikon 225/XTH scanner. Scans used a 0.2-0.5mm copper or brass filter at an acceleration voltage of 100-160 kV and 100-140 μ A. To ensure that thin trabecular struts were accurately measured, scan resolution was between 0.02 and 0.03 μ . Images were reconstructed as 16-bit volumetric tiff stacks. Using Avizo 6.3 or 9 (Visualization Sciences Group, SAS), these tiff stacks were then oriented into a similar anatomical position, and all left specimens were flipped along the sagittal plane so that they looked like right capitates. The medical imaging analysis (MIA) clustering method was used to remove non-bone material from the scans and produce a binary segmentation (Figure 5.2B) (Dunmore, Wollny and Skinner 2018). MIA uses a semi-automated clustering algorithm, which reduces the subjective decision-making of the cleaning and segmentation process, increasing the reproducibility of results compared to other segmentation protocols (Dunmore, Wollny and Skinner 2018). I performed all fossil segmentations, which were then approved by C. Dunmore, T. Kivell and M. Skinner (Appendix A Figure 8.1). Image segmentations were then tissue segmented using medtool 4.3 (<http://www.dr-pahr.at/medtool/>). Medtool is a medical image analysis software capable of identifying and quantifying structural parameters across the entire 3D bone or a user-defined region (Gross et al. 2014). By projecting a series of arbitrary mathematical rays across the scan, medtool identifies the bone and non-bone voxels in a scan and builds a series of image stacks, assigning unique scalars to the trabecular, cortical, internal and background voxels (Tsegai et al. 2013; Gross et al. 2014). Medtool is able to identify cortical bone from trabecular bone by using a local measurement of average trabecular thickness to determine pores in the cortical bone (defined as less than the thickness of average trabeculae) from inter-trabecular space (equal to or greater than the average thickness of one trabecular strut). By assigning a unique greyscale value to the two tissues, they can be separated and analysed separately. The

'InnerMask' image stack has had the cortical bone voxels removed and defines the shape of the internal trabecular space but contains no architectural information (Figure 5.2C). The InnerMask segmentation (Figure 5.2D) is the InnerMask with the trabecular bone and internal space defined by separate scalars (white and light grey, respectively).

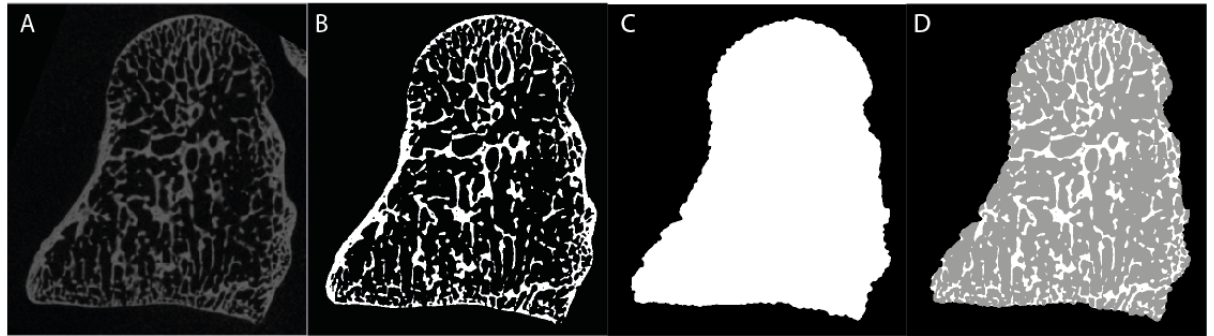


Figure 5.2 MIA segmentation and medtool analysis used in this study.

A) the original micro-CT scan of a human capitulum. B) The result of MIA segmentation. C) The InnerMask has had the cortical bone removed, leaving only the internal trabecular space (white). D) the InnerMask segmentation. The cortical bone has been removed, leaving only the trabecular bone (white) and internal space (light grey).

The cHMA protocol builds on previous work on whole-bone internal analysis (Tsegai et al. 2013; Gross et al. 2014; Steiner, Synek and Pahr 2021) and uses statistical deformation modelling to register the mean shape, position and size of all capitulates in the sample in 3D space (Steiner, Synek and Pahr 2021; Bachmann et al. 2022). The full methodology, including testing and validation, is described in Bachmann et al. (2022); here, we will briefly describe the process undertaken to register the trabecular bone for analysis. Using an in-house script for medtool, two iterations of a similarity and b-spline registration were run on the 'InnerMask' image stack of each capitulum (Figure 5.3A), using individual NHMW J2 (*H. sapiens*) as the initial fixed image (Steiner, Synek and Pahr 2021). It has been demonstrated that this process produces a model with minimal bias toward the reference individual (Bachmann et al. 2022). The registration process results in a canonical capitulum model representing the mean size, shape and position of the internal trabecular bone space of the entire sample (Figure 5.3B). This model contains no inherent architectural information (i.e., trabecular thickness or number) beyond the mean shape and size. All specimens were included in the shape registration except *H. naledi* due to preservation issues. The canonical model was then filled with finite elements (tetrahedral) to produce a canonical mesh (Figure 5.3C). The individual InnerMask segmentations (Figure 2.1D) were then backtransformed onto the canonical InnerMask (Figure 5.3D). Then, using the transformation data from this step, the individual canonical InnerMasks are morphed onto the canonical mesh (Figure

5.3E). This results in the entire sample interpolated onto identical finite element meshes. Finally, using Paraview (3.98.0), the canonical mesh was split into a proximal and distal part, so that the capitate head could be analysed separately (Figure 5.3F, in pink). The separation was made at the distal extent of the lunate articular surface on the capitate head, as per Bird et al. (2021). Each tetrahedron in the mesh is represented by a number and as every individual is represented by the same mesh, only one separation needed to be defined for the whole sample.

Standard medtool protocols (as per Tsegai et al. 2013; Gross et al. 2014) were used to quantify bone volume across the sample of canonical meshes. In short, a 3D grid with nodes spaced 2.5mm apart (Figure 5.3G, red box) was placed over each canonical mesh. Next, a 5mm sampling sphere moved from node to node, iteratively measuring trabecular bone volume to total volume (Figure 5.3G, blue sphere). Once the data are collected, they are interpolated back onto the canonical mesh, and colour maps representing bone volume distribution are available to be viewed in Paraview (Figure 5.3H). Since data were collected from the canonical mesh, the datum collected at each node in the 3D grid is homologous between individuals. Next, the bone volume of each tetrahedron was divided by the overall average to give a measure of relative bone volume (RBV). As baseline bone volume is correlated to systemic, taxon-specific patterns (Chirchir et al. 2015; Tsegai et al. 2018), RBV demonstrates where bone volume has increased or decreased relative to the mean, allowing meaningful comparisons between individuals and genera (Dunmore et al. 2020a).

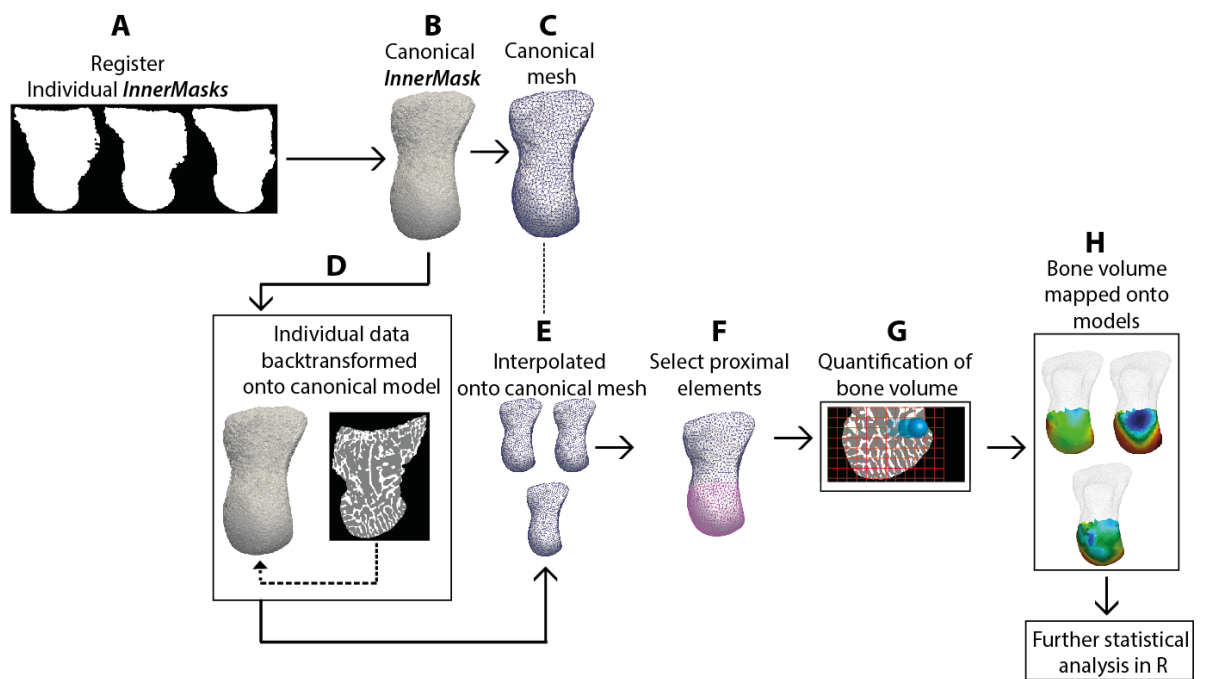


Figure 5.3 Overview of the canonical holistic morphometric analysis (cHMA) workflow.

5.4.b. Statistics

Using the in-house script for medtool, the mean RBV distribution of each extant taxon and the fossil *H. sapiens* and Neanderthals was calculated by aggregating the data of each tetrahedron of each individual and dividing by the group mean. As part of this process, medtool produces the RBV standard deviation for each tetrahedron. This taxon-specific distribution was mapped to the canonical mesh and visualised in Paraview (v.3.98.0). The remainder of the statistical processes were conducted in R (v4.1.1). Firstly, as the dataset contained 4,872 data points per individual (i.e., tetrahedra in each canonical mesh), a Principle Component Analysis (PCA) was run (R, 'stats' package v4.1.0) in order to reduce the dimensionality while maintaining the majority of the variance. Principle Components (PCs) 1 to 3 were visualised in 2D (R, 'factoextra' package v1.0.7) and 3D (R, 'plot3d' package v1.4). All subsequent statistical tests were run on the first three PCs as they explain $\sim >50\%$ of the variance while the remainders explain $\leq 5\%$ each. To test for group differences among the extant taxa (*Pongo*, *Gorilla*, *Pan*, modern *H. sapiens*), a one-way permutational MANOVA was run (R, *vegan* v2.5-7). Following a significant MANOVA test, permutational multivariate pairwise comparisons with a Bonferroni correction were run (R, 'RVAideMemoire' package v0.9-80). Using the PCA standard deviations, a capitate model representing extreme RBV variation along the PCs was built (R, *base*, v4.2.0). To build this model, the standard deviation of PC1 was multiplied by three. This new dataset represents values at each tetrahedron three standard deviations above the mean along the positive PC1 axis. This process was repeated

using a multiplication of negative three, which produced a dataset representing the distribution three standard deviations away from the mean of negative PC1. These calculations were made for each positive and negative axis of PC1-3. These new datasets were interpolated onto the canonical mesh and visualised in Paraview. In Paraview, the threshold function was used to identify the tetrahedra at the 40th percentile, allowing visualisation of the capitate regions most strongly driving variation along the PC axes.

5.5. Results

5.5.a. Extant

Figure 5.4 illustrates the mean RBV distribution of each extant taxon; the standard deviations around this mean are found in Supplementary Figure 5.1. Individual RBV maps and two cross sections of the original trabecular structure are in Supplementary Figure 5.2. A summary of the qualitative descriptions of the taxon-specific mean RBV distribution is given in Supplementary Table 5.2. *Pongo* is characterised by moderate RBV at the lunate articular surface. This increase moves distally through the capitate, with the highest RBV seen in the central and distal components of the capitate head. *Gorilla* is characterised by high RBV at the ulnar and radial sides of the head. Increased RBV is seen at the proximal-most portion of the head, with higher values at the lunate-side compared to the scaphoid-side. High RBV does not extend distally, as the high values appear at the subchondral trabeculae only. *Pan* exhibits increased RBV at the proximal lunate articular surface, which extends ulnarly onto the hamate surface but not onto the radial articular surface of the scaphoid. *Pan* is the only extant species to typically show high RBV on the palmar surface, which is confluent with the ulnar side band of high RBV. The sagittal cross section shows high RBV on the palmar, and the ulnar side extends disto-palmarly through the centre of the capitate. The modern *H. sapiens* pattern is characterised by a subchondral band of high RBV across the proximal-most portion of the capitate. This band runs from the hamate articulation on the ulnar side to the radial scaphoid articulation. In contrast to the non-human hominids, both the scaphoid and lunate proximal articular surface express high RBV, although the highest values are typically on the lunate side. This high RBV extends from the subchondral trabeculae through the capitate distally.

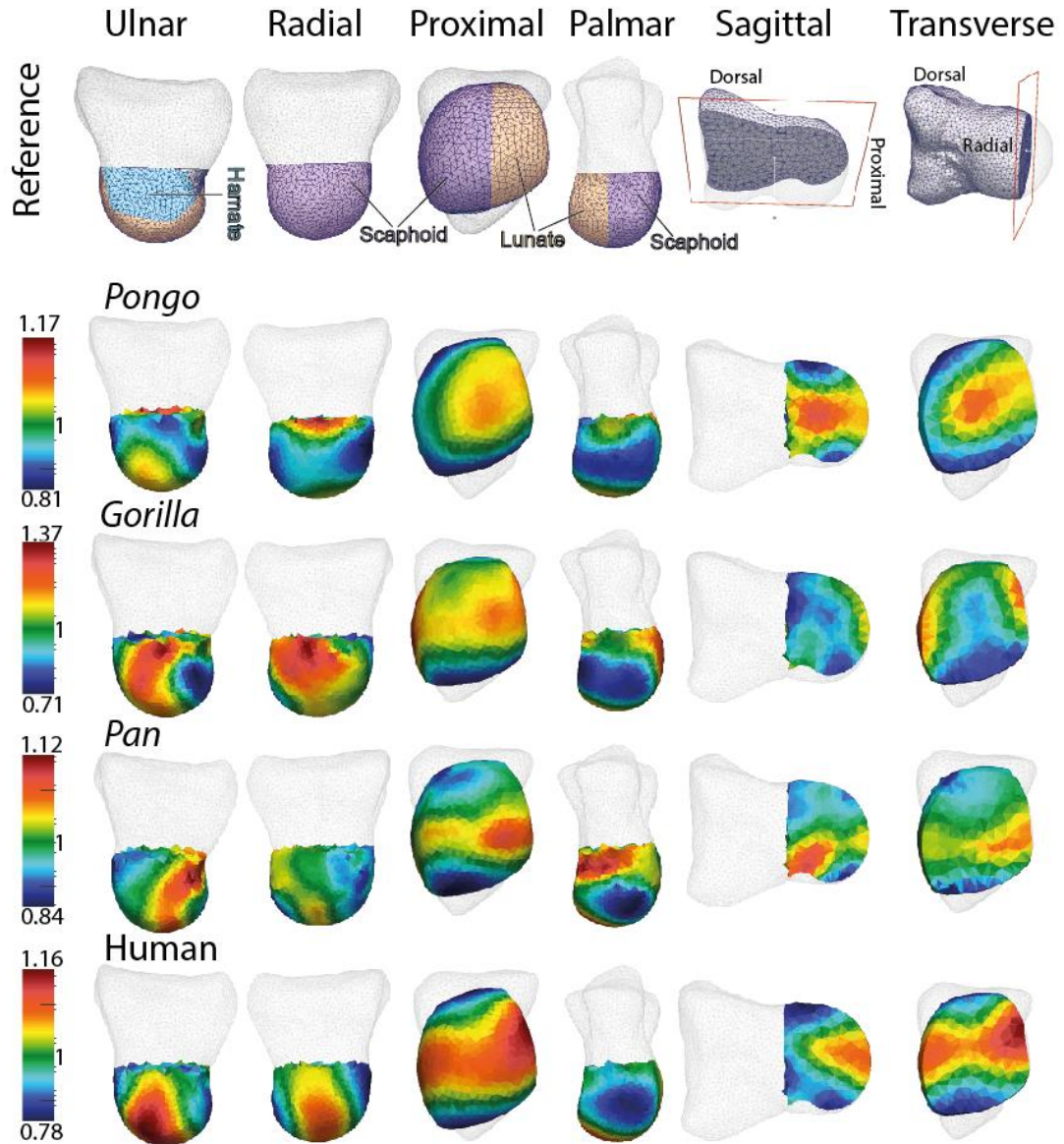
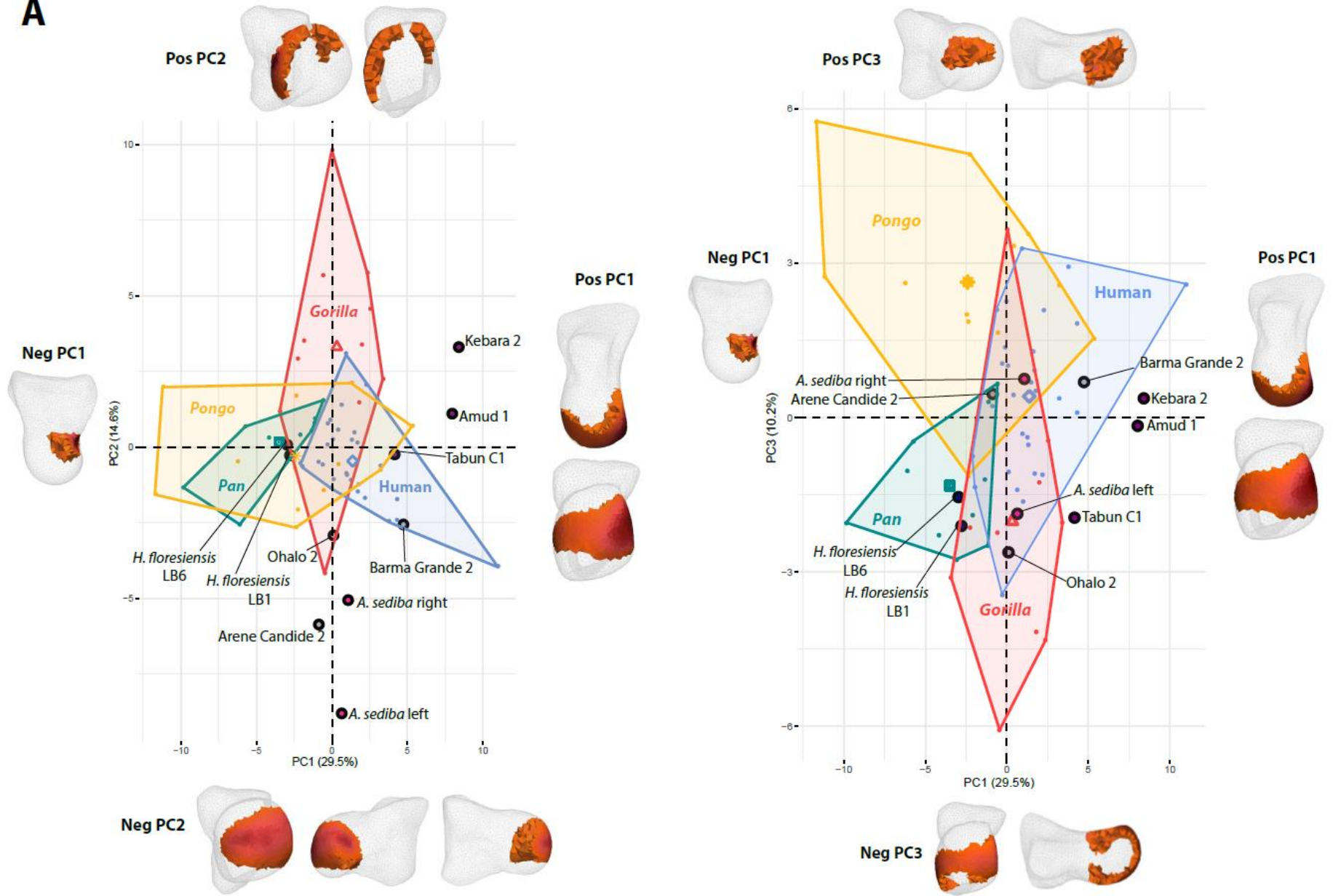


Figure 5.4 The average relative bone distribution in the capitate head of each extant taxon. The first four columns of the reference images illustrate the articular surfaces of the proximal capitate. The last two columns of the reference images illustrate where a slice has been placed in the canonical model to show the internal structure. The average RBV value for each taxon is represented by green (1). Warmer colours represent higher than average bone volume, and cooler colours represent lower than average.

A one-way permutational MANOVA indicates that the distribution of RBV statistically differs extant hominids ($p < 0.001$). All permutational multivariate pairwise comparisons are significant ($p < 0.001$ for all tests, Supplementary Table 5.3). The PCA illustrates the variance in RBV distribution (Figure 5.5). Principle component (PC) 1 explains 29.5% of the variance and generally separates *H. sapiens* (high PC1 scores) from *Pongo* and *Pan*, with *Gorilla* falling almost exactly at the intersection of the PC1 and 2. Positive PC1 scores correlate to high RBV

across the proximal-most capitate, extending radially, ulnarly, and distally (Figure 5.5A). This pattern closely resembles the typical modern *H. sapiens* pattern (Figure 5.4), explaining why they generally fall along positive PC1. Negative PC1 scores correlate to high RBV in the palmar portion of the distal-most aspect of the capitate head, as typically seen in *Pan* (Figure 5.4). PC2 explains 14.6% of the variance, where only *Gorilla* has a mean PC2 score substantially above 0. Positive PC2 scores correlate to high RBV at the subchondral distodorsal and radial surfaces. Negative PC2 scores correlate to high RBV at the subchondral lunate and proximal hamate and scaphoid articular surfaces, which extend distally through the capitate head. PC3 explains 10.2% of the variance and generally separates *Pongo* and *H. sapiens* (high PC3 scores) from *Gorilla* and *Pan*. Positive values correlate with high RBV in the centre of the distal-most portion of the head, as typical in *Pongo* (Figure 5.4). Negative PC3 values correlate with high RBV at the subchondral trabeculae at the scaphoid, lunate and hamate surfaces, extending onto the palmar surface, as typically seen in *Gorilla*.

A

B

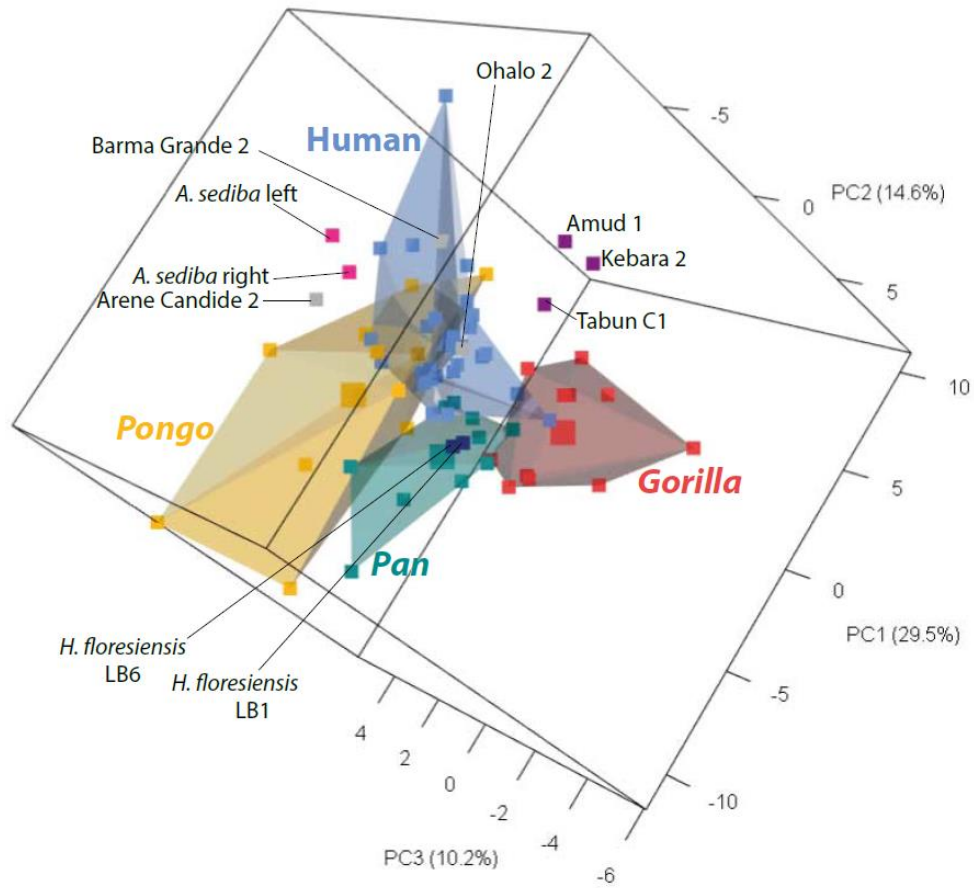


Figure 5.5 Results of the PCA analysis.

A) PC1 and 2 (left), and PC2 and 3 (right). Models at the end of each axis represent the regions of high RBV (in red) driving variance along those PCs. B) PCA showing the separation in 3D space. Fossils are labelled individually in both figures.

5.5.b. Fossil hominins

Figure 5.6 illustrates the mean fossil *H. sapiens* pattern; individual maps of Ohalo 2, Barma Grande 2 and Arene Candide 2 are in Supplementary Figure 5.2. The RBV distribution in Ohalo 2 and Barma Grande 2 resembles the typical modern *H. sapiens* pattern, although Arene Candide 2 has lower RBV at the scaphoid articular surface and higher RBV at the proximo-palmar lunate surface than is typical for modern *H. sapiens*. In the PCA, Barma Grande 2 falls within the range of modern *H. sapiens* variation. Ohalo 2 and Arene Candide 2 fall close to, but outside, the modern *H. sapiens* variation due to extremely low values on negative PC2, which is driven by the dorsopalmar expansion of the high subchondral RBV on the proximal-most portion of the head. The average Neanderthal pattern is illustrated in Figure 5.6; the individual maps of Amud 1, Kebara 2, and Tabun C1 are in Supplementary Figure 5.2. The typical Neanderthal resembles the typical modern *H. sapiens* pattern, exhibiting a subchondral radio-ulnar band of high RBV at the proximal-most aspect of the capitate, which extends radially, ulnarly, and distally. Individually, Kebara 2 and Tabun C1 exemplify the typical human pattern, while Amud 1 exhibits slightly lower RBV on the scaphoid than is typical for modern *H. sapiens*. All three Neanderthal individuals fall close to one another outside modern *H. sapiens* variation, primarily due to higher scores along positive PC1.

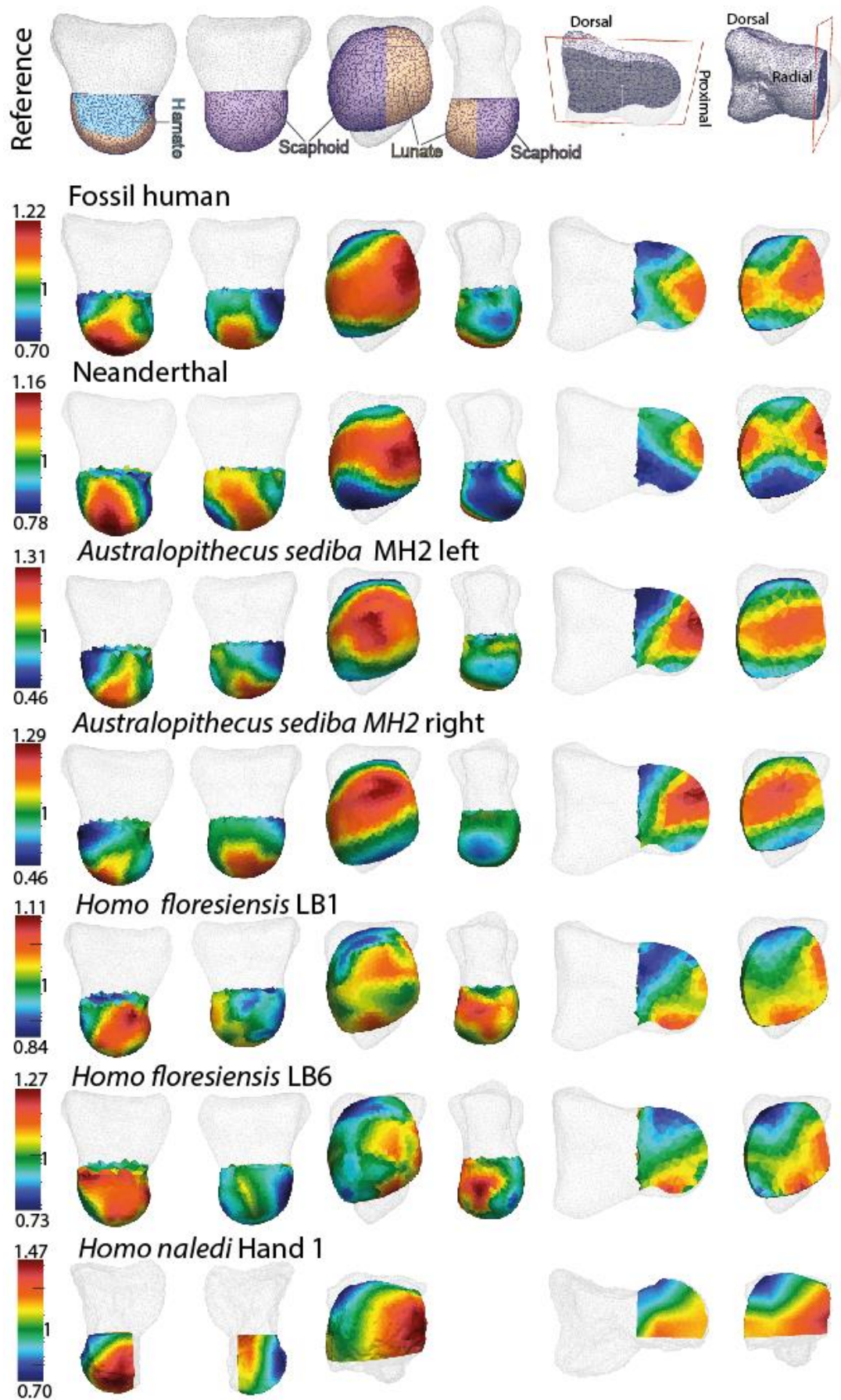


Figure 5.6 Relative bone volume (RBV) distribution maps of the fossil specimens. Neanderthals and fossil *H. sapiens* are represented by a mean map, *A. sediba*, *H. naledi* and *H. floresiensis* are represented individually. In the reference image, the first four images illustrate the articular surfaces of the proximal capitate, and the last two illustrate where a slice has been placed in the canonical model to show the internal RBV. The average RBV value for each taxon is represented by green (1). Warmer colours represent higher than average bone volume, and cooler colours represent lower than average. *Homo naledi* Hand 1 is represented on its actual shape as the broken palmar portion excluded it from statistical analysis. The broken element has been removed from the visualisation. High resolution images of the bone, including the extent of the damage, can be seen in Kivell et al. (2015).

The RBV distribution of the right and left *A. sediba* capitates are illustrated in Figure 5.6. In the PCA, both capitates fall on positive PC1 and negative PC2, outside the range of variation of any extant hominid, although the right capitate falls very close to fossil human Arene Candide 2. The RBV on the subchondral bone reflects the typical modern *H. sapiens* pattern, as both the left and right bones show a distinct radio-ulnar band of high RBV distribution. Although this band is dorsopalmarly taller than is typically seen in *H. sapiens* and Neanderthals, it includes the hamate, scaphoid and lunate subchondral surfaces. The band extends disto-palmarly through the trabeculae, distinguishing it from the predominantly distal orientation in *H. sapiens* and Neanderthals. While *Pan* also shows a disto-palmar orientation of high RBV, it only originates from the lunate, while in *A. sediba* it originates at both the scaphoid and lunate. With this combination, *A. sediba* expresses a unique pattern of RBV among the extant hominids.

The *H. floresiensis* capitates from LB1 and LB6 fall close to one another on the PCA, very near to the *Pan* centroid (Figure 5.5). Both capitates have high RBV on the lunate and hamate articular surfaces (Figure 5.6), as well as widely distributed across the palmar surface. Both individuals are clearly distinguished from the typical modern *H. sapiens* and Neanderthal pattern as neither express high RBV at the scaphoid articular surface nor a band of distally oriented high RBV within the central component of the head. The palmo-ulnar concentration of high RBV aligns the *H. floresiensis* RBV pattern with *Pan*, as *Pan* is the only extant taxon to typically have high RBV at the palmar region (Figure 5.3) and higher RBV at the ulnar relative to the radial side of the capitate.

Due to the broken element on the palmar surface, the *H. naledi* capitate is not included in the PCA, and the distribution of RBV is analysed on its actual shape (Figure 5.6). Hand 1 showed several similarities with the typical *Pan* pattern, including high RBV at the capitoulunate and capitohamate joint, although the distribution is dorsopalmarly taller in *H.*

naledi than is typical of *Pan*. The high RBV at the lunate surface does not extend radially onto the scaphoid articular surface, clearly differentiating *H. naledi* from the typical late *Homo* pattern. The disto-radial portion of the scaphoid expresses higher RBV values, somewhat resembling the typical *Gorilla* pattern (Figure 5.4). Again similar to *Pan*, high RBV is concentrated on the ulnar side of the bone and appears to extend towards the palmar aspect. However, as this component is broken in *H. naledi*, this must be interpreted with caution.

5.6. Discussion

5.6.a. Is the distribution of trabecular bone in *Homo sapiens* unique among extant hominids?

Stephens et al. (2018) identified that the modern *H. sapiens* proximal capitate expresses a distinctive pattern of high RBV from the proximal scaphoid to the lunate articular surface on the capitate. It was hypothesised that this pattern reflected habitual use of the DTM, where the capitate takes an oblique axis of motion across the confluent scaphoid and lunate joints. In line with our prediction, our study replicated that result on a larger, more diverse modern *H. sapiens* sample and demonstrated for the first time that this pattern differentiates *H. sapiens* from non-human hominids. Two features appeared consistently among *H. sapiens*: firstly, no other species consistently expressed high RBV at both the proximal scaphoid and lunate joints; secondly, the distal extension of high RBV into the body of the capitate was distinctive from *Gorilla* (where there was typically no distal extension), *Pan* and *Pongo*, as only *H. sapiens* had this band originate from both the proximal scaphoid and the lunate articular surfaces. This suggests that in the proximal capitate, peak loading is experienced by both the capitulunate and capitoscapoid joints, although RBV tended to be higher on the capitulunate.

The low degree of variability within the expression of this pattern is particularly notable as *H. sapiens* are known to show high degrees of morphological variability in the carpals, which has been demonstrated in the ligaments (Buijze et al. 2011; Casado et al. 2021), geometry (Lewis 1989; Marzke, Wullstein and Viegas 1994; Bain et al. 2015) and kinematics (Garcia-Elias et al. 1994; Crisco et al. 2005; Orr 2017). Further, it is reasonable to assume that there was behavioural variation among the modern *H. sapiens* sample, as it derives from spatio-temporally diverse populations. Despite this, only two individuals did not exhibit the typical radio-ulnar band of high RBV at the subchondral bone. Individual DCW_AM_10_0_183, an indigenous person from 19th Century Greenland (unknown sex), had low RBV at the

capitoscaphoid joint; and individual NHMW_J3, a Nubian Egyptian (unknown sex) from a population dated between the 6th and 11th century (Paoli et al. 1993), showed low RBV at the capitolunate joint. Although variation in RBV may be noted in the other *H. sapiens* (e.g., some have high RBV on the palmar capitolunate joint; there is disto-palmar height variation in high RBV on the capitolunate joint, see Supplementary Figure 5.2), all other individuals express these two features which distinguish *H. sapiens* from non-human hominids. The consistency of these results accords with the conclusions of clinical research, which has underscored the consistent use of the DTM, despite variability in wrist morphology or hand use (Kaufmann et al. 2005; Brigstocke et al. 2014; Rainbow et al. 2015; Kamal, Starr and Akelman 2016; Kaufman-Cohen et al. 2019).

The presence of high RBV suggests which joints are highly strained, as increased bone volume is correlated to strength and habitual strain (Pontzer et al. 2006a; Barak, Lieberman and Hublin 2011; Maquer et al. 2015; Hart et al. 2017); however, high RBV is not *ipso facto* evidence of bone kinematics (i.e., intercarpal motion). Although the RBV distribution in the *H. sapiens* sample reflects what one may expect to see given what is known about the DTM (e.g., Crisco et al. 2005; Edirisinghe et al. 2014; Garcia-Elias, Alomar Serrallach and Monill Serra 2014), it can not be considered direct evidence of the DTM kinematics. The human scaphocapitate joint is larger than non-human hominids, which is considered an adaptation to the high forces arising from the thumb during tool behaviour (Tocheri 2007). Thus, high RBV at this joint on the capitate may also be reasonably linked to the forces incurred via high-impact manipulative behaviours, i.e., the kinetics of forceful precision gripping, rather than midcarpal movement.

There is a relative paucity of studies looking at manual posture and kinematics in behaviours associated with Holocene *H. sapiens*, which would include a diverse range of activities from agriculture to hand-writing and typing on a computer (but see Li 2002; Riddle et al. 2020). Functional adaptation is likely to occur in response to habitual behaviours that induce the highest loading on the joints (Huiskes et al. 2000; Currey 2002). As such, it is currently unclear what functional adaptation might look like among living *H. sapiens* who do not regularly load their hands heavily for vocational work. It is important to note that loading magnitude increases proximally through the hand such that forces experienced at the intercarpal joints will be higher than what is experienced at the fingers (Currey 2002; Gíslason et al. 2009; Gíslason et al. 2012). Nevertheless, it remains to be confirmed that activities of living *H. sapiens*, such as opening a jar or pouring a glass of water, result in a functional adaptation at the midcarpal joint, similar to the historic sample of modern *H. sapiens* in this study.

5.6.b. What does the relative bone volume distribution in non-human hominids suggest about load transfer in the midcarpal joint?

The RBV distribution was statistically distinct in all extant hominids, suggesting distinctive loading is associated with hand use. Supporting the prediction, all non-human hominids had higher RBV at the capitulate compared to the capitoscapoid joint. There was some overlap in the PCA between *H. sapiens* and *Pongo* due to this capitulate feature (positive PC1) in combination with a band of high RBV moving distally into the capitate body (positive PC3). However, the pattern in *Pongo* is clearly differentiated from *H. sapiens* as *Pongo* exhibited relatively greater ulnar side loading. The *Pongo* pattern is consistent with the assumption that the hypertrophied lunate incurs higher loading relative to the other proximal carpal bones (scaphoid, triquetrum) (Sarmiento 1988). In addition, the predominantly distally-oriented high RBV suggests the highest forces directed through the *Pongo* capitate are in a neutral midcarpal position, which may reflect the frequent use of suspensory postures (Thorpe and Crompton 2006).

The pattern of RBV in *Gorilla* suggested high load was experienced relatively evenly across the subchondral surface, which may reflect resistance to the high biomechanical loading associated with habitual knuckle-walking. During knuckle-walking, the midcarpal joint must resist load from all articulations as it is highly compressed by the forces of gravity and the body mass held above the wrist (Carlson and Patel 2006). Despite also using high proportions of knuckle-walking (Doran and Hunt 1994; Doran 1996), the RBV patterns in *Pan* were clearly distinguished from *Gorilla*. Higher degrees of midcarpal extension in *Pan* might explain the distinctive disto-palmarly oriented band of high RBV through the central body of the capitate. A higher proportion of arboreal locomotion has been hypothesised to result in greater use of extended wrist postures in *Pan* (Kivell and Schmitt 2009). However, very few studies have quantified wrist posture during arboreality in wild animals. Palmigrady, which uses high degrees of wrist extension, has been observed in wild unhabituated *P. paniscus*; although studies of habituated *P. paniscus* suggests it has similarly low levels of long distance arboreal locomotion as *P. troglodytes* (Doran 1993a; Doran and Hunt 1994; Ramos III 2014). The higher RBV at the ulnar-side of the capitate in *Pan* compared to *Gorilla* may be more reasonably linked to greater use of ulnar deviation, which is thought to be high during the palm-in postures frequently adopted by *Pan* during knuckle-walking (Tuttle 1967; Inouye 1992; Wunderlich and Jungers 2009; Matarazzo 2013; Thompson 2020) (but see Samuel et al. 2018). Although *Gorilla* is demonstrated to use higher degrees of ulnar deviation during vertical climbing (Neufuss et al. 2017), this behaviour is performed at lower frequencies than

knuckle-walking is in both taxa (Doran 1996). Locomotor mode among African apes is variable and correlated with several ecological (Doran and Hunt 1994; Remis 1998, 1999; Neufuss et al. 2017) and life history factors (Doran, 1992, 1993b, 1997; Remis 1995, 1998, 1999), the differences in our results suggest the nuanced locomotor differences between the two African apes is reflected in their underlying midcarpal joint RBV distribution.

Although the RBV patterns in non-human hominids are differentiated from *H. sapiens*, it is not to imply that non-human hominids do not use an oblique path of motion at the midcarpal joint. Further kinematic analysis is needed to confirm whether the functional axis of the midcarpal joint in non-human hominids is oblique, as it is in *H. sapiens*. A shared feature between the extant hominids was higher RBV at the capitulate joint compared to the capitolunate, supporting our prediction for the non-human hominids. In *H. sapiens*, the capitulate joint has been demonstrated via 4D CT to be the hinge of the DTM as movement between the proximal and distal rows pivot on this joint (Edirisinghe et al. 2014; Garcia-Elias, Alomar Serrallach and Monill Serra 2014). Although it was not predicted, if this joint is acting as a hinge between the proximal and distal carpal row in *H. sapiens*, one may expect the highest RBV to appear here. While both joints in *H. sapiens* had high RBV, the capitulate did typically have the highest values, supporting that assumption. While descriptions of the screw-clamp mechanism have not emphasised the role of the lunate, it is similarly held securely in place by the oblique movement of the triquetrum and scaphoid (MacConaill 1941; Orr 2010). Given the similar pattern of RBV distribution, the capitulate joint in non-human hominids may also play an important hinge role between the proximal and distal carpal rows. Recently, Bird et al. (2022) found higher than expected RBV in the lunate compared to the scaphoid and triquetrum in *Gorilla*, *Pan*, and *H. sapiens*, further supporting the hypothesis that it plays an important role in force transfer between the forearm and distal carpus. In light of this, it remains unclear whether the *H. sapiens* pattern identified in our research is 1) a function of high capitolunate strain from a primarily manipulative thumb in combination with high capitulate strain as a shared feature of hominid wrist kinetics or 2) a direct result of habitual movement across the DTM axis at the midcarpal joint. In either scenario, the results of our research suggest that the strain induced at the proximal capitate in the primarily manipulative hand of *H. sapiens* is distinct from that in non-human hominids using their hands primarily for locomotion.

5.6.c. What can be inferred about hand use among fossil hominins?

Fossil *H. sapiens* broadly expressed the same RBV distribution as the typical modern *H. sapiens*, suggesting that high strain at the capitulate and capitolunate joints are a

common biomechanical feature of all *H. sapiens*. Arene Candide 2 had higher RBV in the palmar aspect of the proximal capitate than is typical for modern *H. sapiens*, which may indicate frequent use of wrist flexion, as the lunate and palmar capitate head have congruence in this posture (Edirisinghe et al. 2014). Hammering and knapping do not induce highly flexed wrist postures (Williams, Gordon and Richmond 2014; Williams-Hatala et al. 2021); thus, this distribution suggests Arene Candide 2 may have habitually engaged in different high-impact behaviour. Less kinematic research has been conducted on wrist posture during stone tool use compared to manufacture (e.g., Williams, Gordon and Richmond 2010; Williams-Hatala et al. 2021). Although one such analysis that quantified muscle recruitment during a cutting task with Palaeolithic tools reported that while flexed wrist postures were rare, they were used when smaller flakes were scraped across materials (Key et al. 2020). Scraping tasks, such as hide preparation, are a potential behaviour which may leave this distinctive signature, although greater understanding of hand posture during Plio-Pleistocene tool use is needed to understand the full range of correlated behaviours.

In this study, the RBV distribution in the three Neanderthals (Amud 1, Kebara 2 and Tabun C1) resembled the typical modern *H sapiens* pattern. The Neanderthals clustered together on the PCA, outside the range of modern *H. sapiens* variation, primarily because they exhibited a more “extreme” version of the typical *H. sapiens* pattern (high PC1 scores). This result emphasises the similarity between the proximal capitate loading in *H. sapiens* and Neanderthals, which is somewhat in contrast to other functional adaptation analyses that have found differences in the microarchitecture of *H. sapiens* and Neanderthal hands. Dunmore et al. (2020a) analysed the subchondral RBV distribution of the hominid first metacarpal. The pattern in Neanderthal Feldhofer 1 was similar to *H. sapiens*, reflecting habitual use of abducted thumb postures correlated with pad-to-pad precision gripping, while Kebara 2 and El Sidrón were distinct from the typical *H. sapiens* pattern, instead reflecting the RBV distribution of habitual adducted thumb postures correlated with transverse power grips. Other studies, such as Bardo et al. (2020) and Karakostis et al. (2018), have also emphasised inter- and intraspecific variation in functional adaptation signals in late *Homo* hands. In combination, these results suggest that behavioural variation among Middle to Late Pleistocene *Homo* results in detectable differences in the microarchitecture of the hand. However, the similarity of the proximal capitate trabecular architecture across Neanderthals, fossil and modern *H. sapiens* in our study suggest that behavioural variation among hominins whose hand is used primarily for manipulation is not detectable in the RBV distribution of the proximal capitate. This low variation indicates that the *H. sapiens* pattern

is potentially a very insightful marker of functional commitment to tool use among hominins. Variation in grip preferences between *H. sapiens* and Neanderthals might be detected via functional adaptation analyses within different functional units of the hand and wrist. As transverse power grips are likely to induce greater ulnar-side loading than oblique grips (Marzke, Wullstein and Viegas 1992), comparing RBV between the proximal metacarpal epiphyses or distal row carpus may be an insightful avenue to explore this question.

The distribution of RBV in the *A. sediba* right and left capitate were similar to one another, expressing a unique combination of features seen in *Pan* and *H. sapiens*. The subchondral bone resembled the typical late *Homo* pattern, suggesting MH2 was heavily and consistently loading the capitulunate and capitoscapoid joints and, therefore, potentially using the DTM axis. Dunmore et al. (2020b) compared the subchondral trabecular RBV distribution in *A. sediba* to a sample of extant hominids and found the pattern in the thumb metacarpal resembled the typical pattern of *H. sapiens*, while the pattern in the non-pollical metacarpals resembled *Pongo*. They concluded that these patterns of functional adaptation were consistent with a behavioural repertoire including significant proportions of both flexed power grasping for arboreality and human-like manipulation with the thumb (Dunmore et al. 2020b). The results of our study fit well with these conclusions as the subchondral patterning in the *A. sediba* proximal capitate suggests consistent and high loading at the capitoscapoid joint, which is correlated with habitual loading of the thumb during manipulation (Williams, Gordon and Richmond 2012; Key et al. 2017; Key, Dunmore and Marzke 2019; Williams-Hatala et al. 2021). The trabeculae within the centre of the capitate head suggest wrist posture during peak loading was distinctive from modern *H. sapiens*, and thus the kinetics and kinematics of the midcarpal joint in *A. sediba* remain distinctive from typical *H. sapiens*.

The similarity in the RBV distribution of the right and left *A. sediba* capitates suggests the midcarpal joints are loaded similarly between the hands. Although *H. sapiens* overwhelmingly exhibit a right-handedness bias, clinical literature indicates that the midcarpal joint uses similar axes of motion in both hands (Kaufman-Cohen et al. 2018). Thus even though the role of the hands is often differentiated, it is reasonable to assume RBV distribution would be similar in the midcarpal joint of the dominant and non-dominant hands. Investigating lateralisation was outside the scope of this research, although this assumption of bilateral similarity in the midcarpal RBV distribution does require further investigation. Indeed, the presence of the right and left hand bones from one individual provides a rare opportunity to study lateralisation in fossil hominins. Nevertheless, the

similarity in the distribution in the right and left MH2 capitate in this research cannot yet be considered evidence for lack of manual lateralisation.

Although they are geologically younger than *A. sediba*, neither *H. naledi* nor *H. floresiensis* exhibited a human-like pattern of subchondral bone. Both *H. floresiensis* specimens (LB1 and LB6) clustered closely to the *Pan* centroid in 3D morphospace, primarily due to the relatively higher ulnar and palmar loading of the capitate. This pattern suggests *H. floresiensis* made Oldowan-style tools without using typical human-like loading of the midcarpal joint. The inherent flexibility of the hominid hand means it is challenging to precisely infer the grips used by fossil hominins based on their external wrist morphology; however, the abundance of stone tools, in combination with the well-developed soft tissue attachments on the thumb (Larson et al. 2009), suggests *H. floresiensis* was using forceful, precision gripping (Orr et al. 2013). Some aspects of the ulnar-side wrist morphology suggest *H. floresiensis* may have had a mechanical advantage for loading this aspect of the hand (Orr et al. 2013). The robust hamulus potentially indicates hypertrophied hypothenar musculature and more powerful flexion and ulnar deviation at the wrist (Orr et al. 2013). Emphasis on high loading of the ulnar-side digits has been correlated to transverse grips, for example, the cradle grip (Niewoehner, Weaver and Trinkaus 1997; Marzke et al. 1998a; Niewoehner 2006; Key, Dunmore and Marzke 2019; Williams-Hatala et al. 2021). The cradle grip is one of the main postures used by modern *H. sapiens* when reproducing Oldowan tools, and they are used in particularly high proportions by non-expert/unexperienced stone knappers (Marzke 1997; Key, Merritt and Kivell 2018; Williams-Hatala et al. 2021). The higher RBV on the ulnar-side of the *H. floresiensis* capitate head supports a hypothesis for the use of transverse-type grips as relatively high loading from the fourth and fifth digits would be transferred to the proximal capitate via the hamate. Further, the ape-like carpal joint configurations would have been well-adapted to resist proximo-distally oriented force vectors from the ulnar-side digits during these grips (Marzke 1997; Niewoehner, Weaver and Trinkaus 1997; Orr et al. 2013).

Locomotion that uses the forelimb, such as climbing, has demonstrated a similar kinetic pattern at the fingers as transverse tool gripping. Although kinetic research of climbing has not been quantified extensively in hominids (but see Fuss & Niegl, (2012) and Quaine (2003) for human research, and Samuel et al. (2018) for bonobos), research indicates that the force exerted on the third and fourth digits can be equal to or greater than the second (Quaine, Vigouroux and Martin 2003; Amca et al. 2012; Fuss and Niegl 2012; Samuel et al. 2018). Like non-human hominids, when modern *H. sapiens* climb, the thumb is rarely recruited or heavily loaded (Sarmiento 1988; Amca et al. 2012; Samuel et al. 2018), which is in stark

contrast to manipulative tasks, where it is usually the highest or among the highest loaded digit (Williams, Gordon and Richmond 2012; Key and Dunmore 2015; Key et al. 2017; Williams-Hatala et al. 2018; Williams-Hatala et al. 2021). Climbing and transverse-type grips such as the cradle grip may be highly compatible from a kinetic point of view as they both emphasise ulnar-side loading of the hand. A reliance on transverse-type grips may allow a species to improve the functional efficiency of stone tool behaviour without highly compromising climbing ability. The degree to which *H. floresiensis* relied on arboreal substrates is still largely unknown, although it has been hypothesised that they were more capable climbers than *H. sapiens* due to possessing a relatively long foot with moderately curved pedal (and manual) phalanges and generally australopith-like body proportions (Brown et al. 2004; Jungers et al. 2009a). The trade-off, however, is that the predominant use of transverse-type grips to produce Plio-Pleistocene tools limits the sophistication and mechanical efficiency of these behaviours (Marzke 1997; Williams-Hatala et al. 2021).

Climbing has also been a key discussion point in relation to *H. naledi* as because, despite the carpus being highly derived toward the human condition, its curved fingers and the ape-like upper limb suggest climbing and arboreality continued to be an important component of its behavioural repertoire (Kivell 2015; Feuerriegel et al. 2017). Indeed, it has been hypothesised that habitual climbing differentiated the niche of *H. naledi* from contemporaneous *H. sapiens* such that they could coexist within the same south African grassland habitat (Dusseldorp and Lombard 2021). The broken component in *H. naledi* means we cannot confidently infer the loading of the proximo-palmar joints of the capitate; however, there are notable similarities in the RBV distribution between *H. naledi* and the two *H. floresiensis* capitates. From what is preserved, *H. naledi* seemed to have higher ulnar-side loading of the midcarpal joint. Therefore, despite having a more human-like capitate based on external morphology and being geologically younger than *A. sediba*, *H. naledi* does not appear to resist habitual and high loading from the capitoscapoid joint. If *H. naledi* was regularly performing tool behaviours, as parsimony would suggest, the forces arising from the radial-side of the hand, and being transferred at the capitoscapoid joint, were relatively much lower than what is observed in the patterns among late *Homo* and *A. sediba*.

Although statistical differences have been identified in the RBV of the extant apes, detecting signals of arboreal and manipulative behaviour from the proximal capitate of fossils in isolation has limitations, particularly as different behaviours use similar hand postures and loading patterns at the midcarpal joint. For example, the relatively higher ulnar-side loading in both *H. naledi* and *H. floresiensis* may indicate climbing, the use of a cradle grip for tool

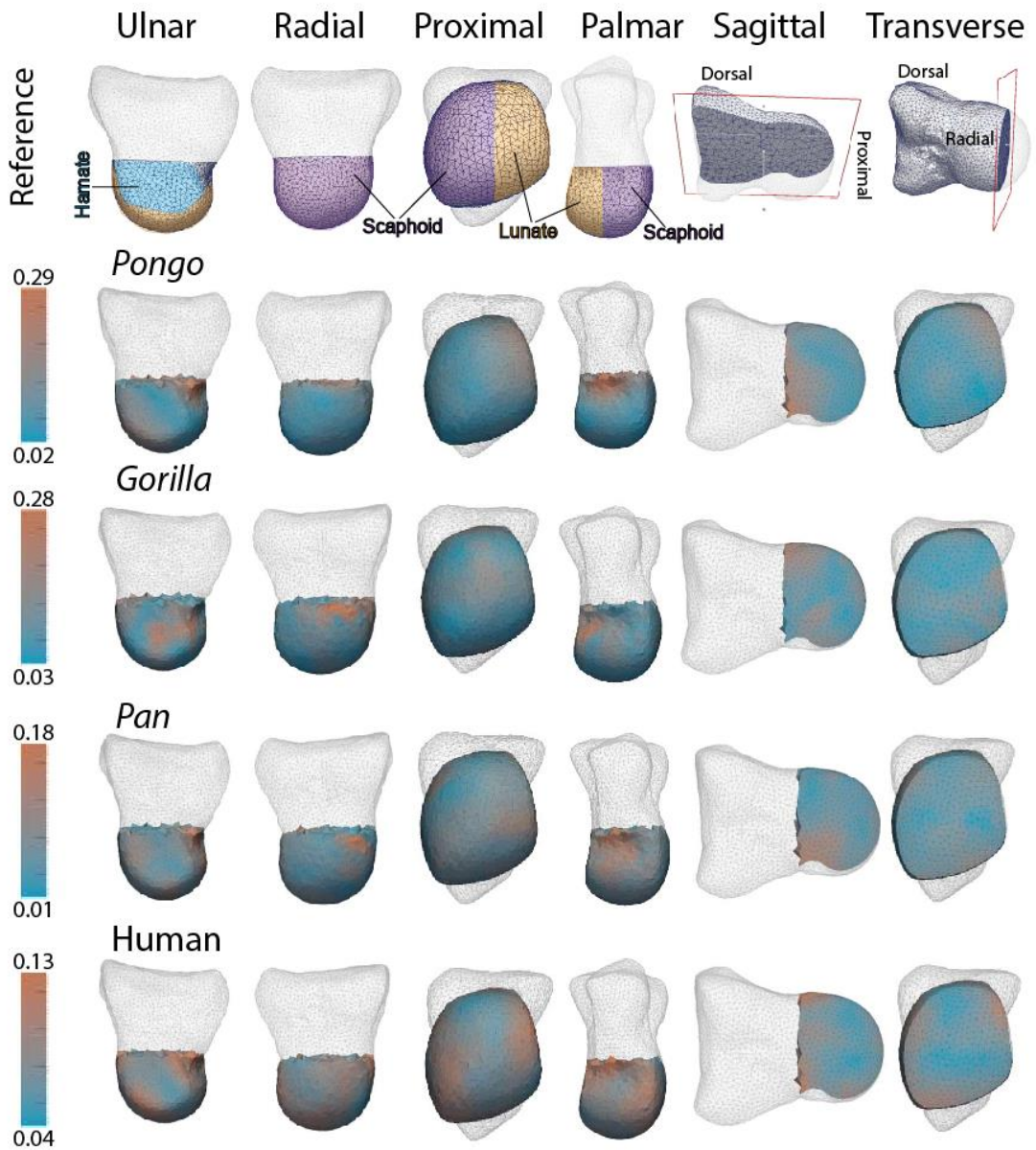
behaviour, or another as yet unidentified behaviour. *Australopithecus sediba*, *H. naledi* and *H. floresiensis* all had opportunities to climb within the forests, caves and rocky outcrops present in their environments (Holt et al. 2016; Sutikna et al. 2016; Dusseldorp and Lombard 2021), and although the clinical literature on climbing in *H. sapiens* provides invaluable kinematic and kinetic data for the interpretation of our results, data are often collected from experiments using artificial climbing walls (e.g., Amca et al. 2012), which may not necessarily replicate the substrate of a fossil hominin. Hand posture and the concomitant force induced at each digit differ depending on the size and shape of the surface or diameter of support (Sarmiento 1988; Amca et al. 2012; Fuss and Niegl 2012). Furthermore, the curved phalanges in these fossil species suggest that the strain induced by climbing may be modulated differently through the hand and wrist compared to modern *H. sapiens* (e.g., Richmond 2007). Analysing the distribution of RBV across a greater number of carpal elements may be particularly beneficial in alleviating some of these limitations. This approach has shown to be functionally informative in previous research (Stephens et al. 2018; Bird, Kivell and Skinner 2022) and may help to contextualise and differentiate similar RBV patterns within single joints. This may be particularly insightful for detecting signals of climbing, as the high degrees of ulnar deviation used by non-human hominids (Sarmiento 1988; Neufuss et al. 2017) has been hypothesised to result in high bone volume of the triquetrum (as per Bird, Kivell and Skinner 2022).

5.7. Conclusion

Our study replicated the results of Stephens et al. (2018), which found that the proximal capitate of *H. sapiens* had a distinctive radio-ulnar band of high trabecular bone volume across the scaphoid and lunate joints, coincident with the well-known functional axis of the midcarpal joint, known as the dart-thrower's motion (DTM). We demonstrated for the first time that this pattern differentiates *H. sapiens* from non-human hominids (*Pongo*, *Gorilla* and *Pan*). All extant hominids exhibited high bone volume at the capitulunate joint suggesting its importance to force transfer within the wrist may be a shared biomechanic of the hominids. It therefore still remains unclear whether this pattern identified in modern *H. sapiens* is a unique adaptation to the DTM axis. The analysis of fossil hominins within this comparative context revealed insights into the loading history of their midcarpal joints. Neanderthals and fossil *H. sapiens* exhibited the same pattern as modern *H. sapiens* suggesting high loading of the capitulunate and capitoscapoid joints is a shared feature of a hand used primarily for manipulation. Despite being the oldest fossil in this study, *A. sediba* exhibited high loading of the capitoscapoid and capitulunate joints, making it the only other

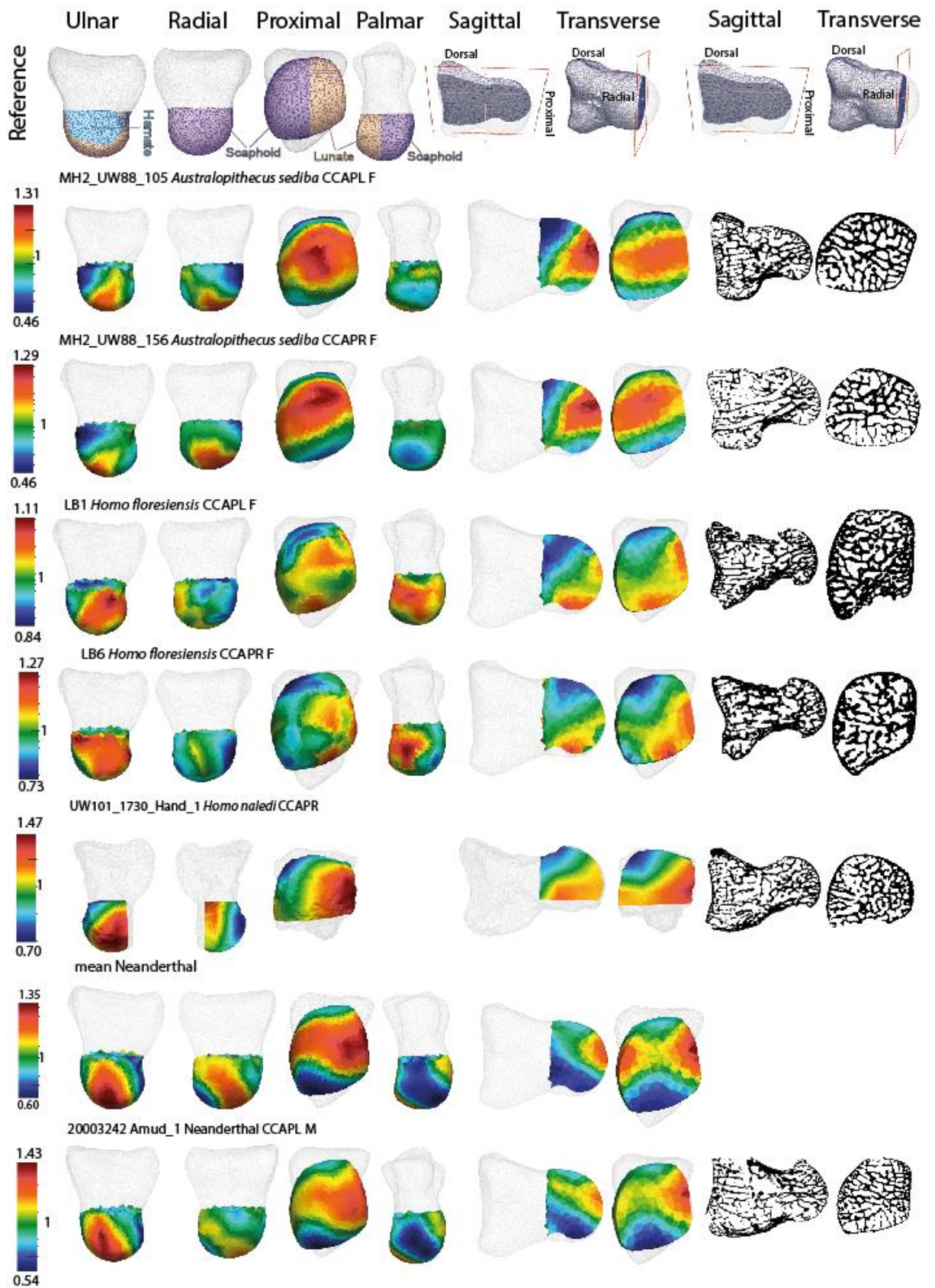
fossil species to exhibit aspects of the human-like pattern. The high ulnar-side loading of the *H. floresiensis* capitate suggests they made Oldowan-style tools without using human-like loading of the midcarpal joint. The loading pattern detected is consistent with the presumed loading of transverse-type grips, which emphasise ulnar-side loading of the hand. High ulnar-side loading of the midcarpal joint is also correlated with climbing, and thus, the use of transverse-type grips may present a potential kinetic solution for combining tool behaviour with arboreality in hominins. The palmar aspect of the *H. naledi* capitate was broken, limiting the functional inferences we could draw. However, like *H. floresiensis*, *H. naledi* appears to have high ulnar-side loading and lower loading of the capitoscapoid joint. Therefore, despite having a human-like scaphoid and capitate, there is no evidence in the Hand 1 capitate that *H. naledi* was resisting relatively high radially-derived loads correlated with human-like tool behaviour.

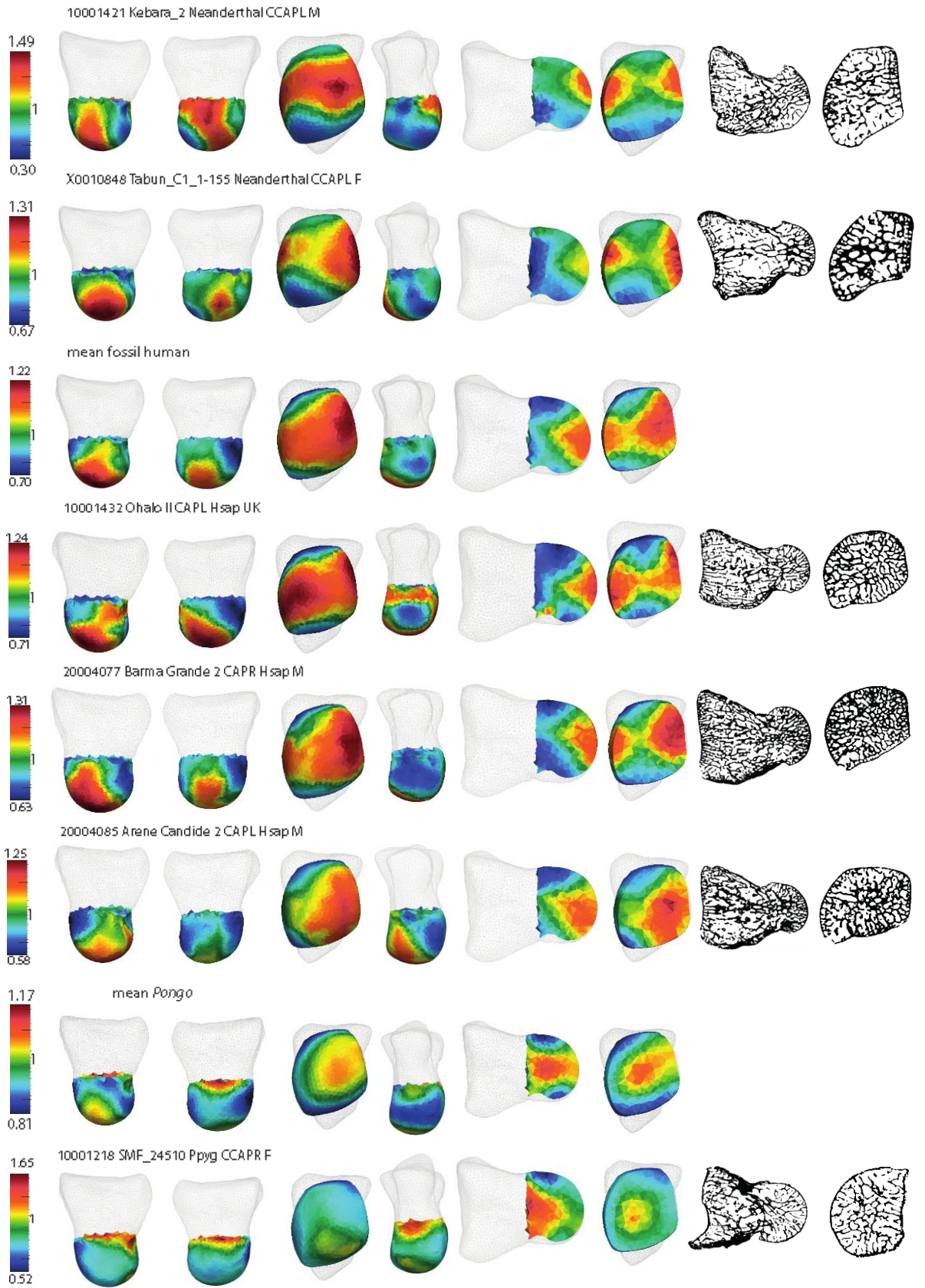
5.8. Supplementary Figures

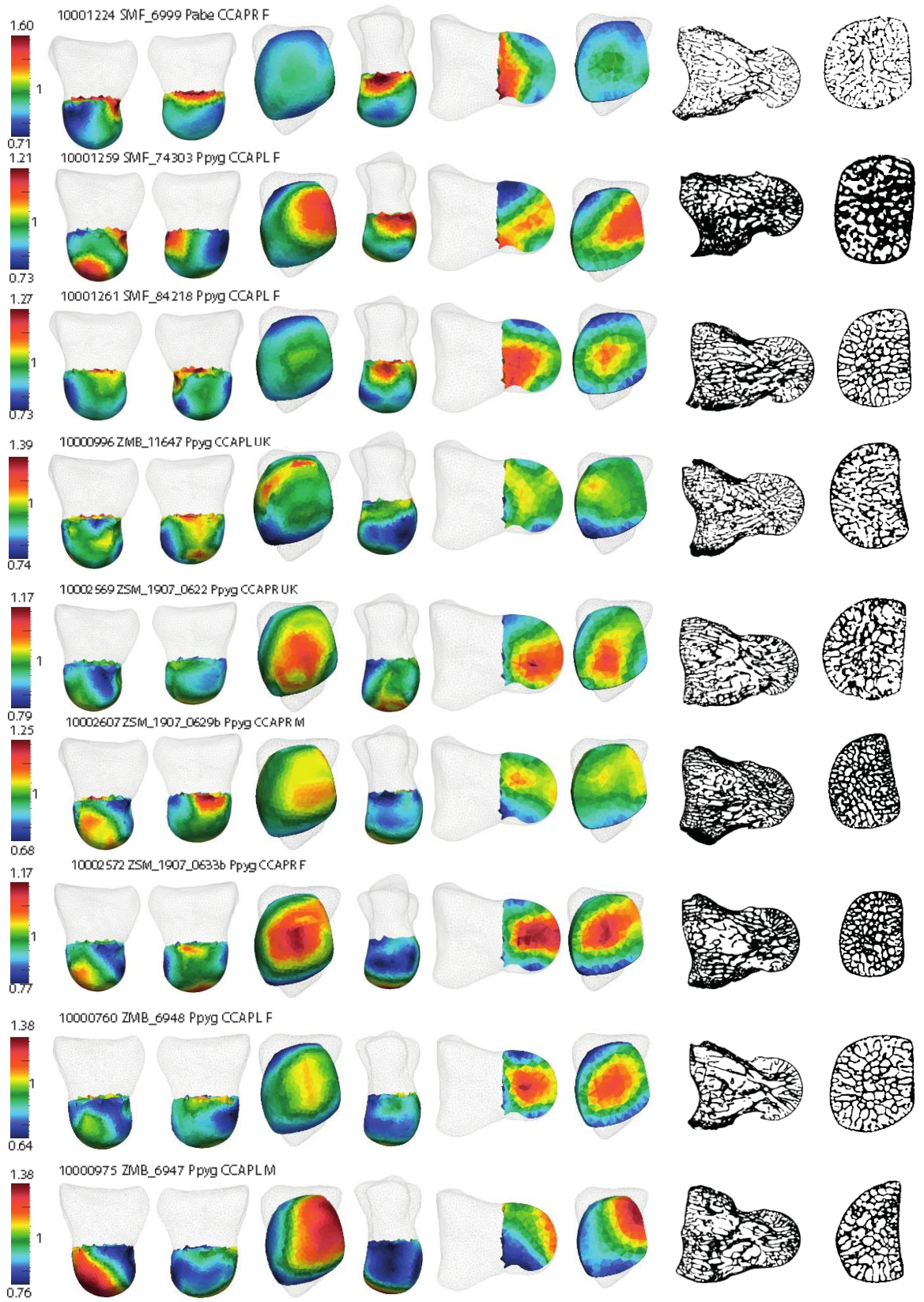


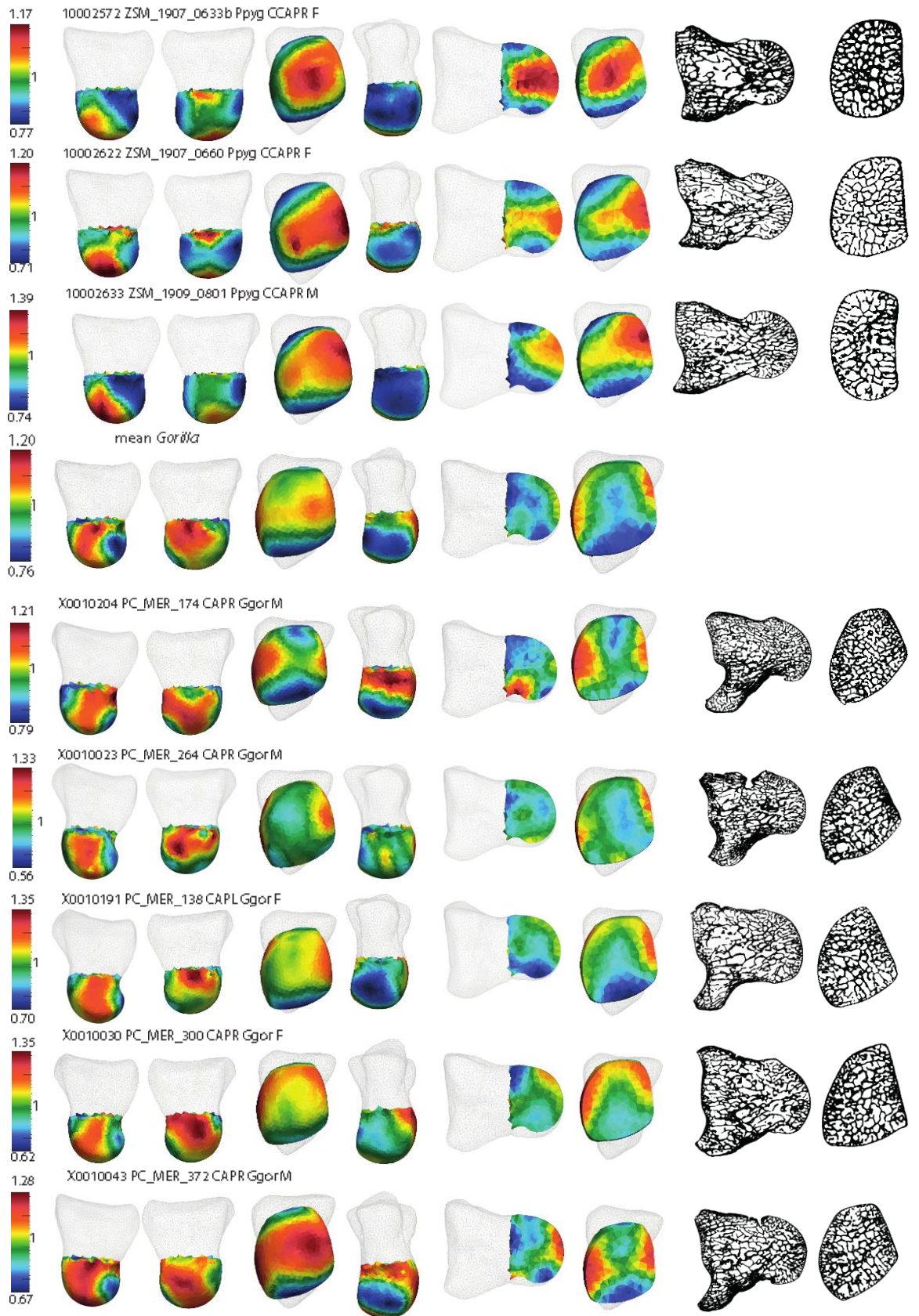
Supplementary Figure 5.1 Maps illustrating the standard deviations in the taxon-specific distribution of relative bone volume.

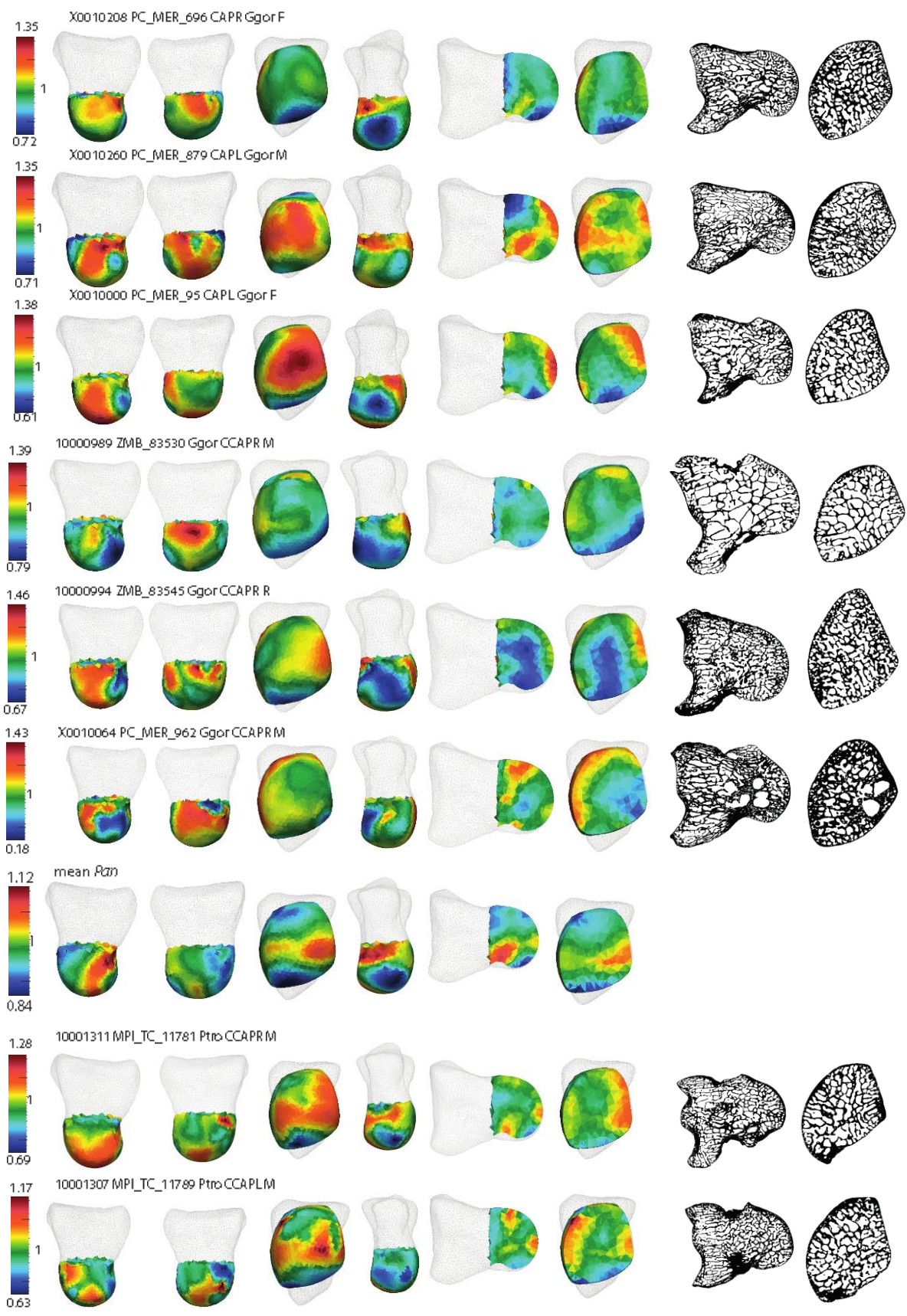
In the reference image, the first four images illustrate the articular surfaces of the proximal capitate, the last two illustrate where a slice has been placed in the canonical model to show the internal RBV. Pink values represent higher standard deviations within that region of the bone, and teal values represent the lowest standard deviations.

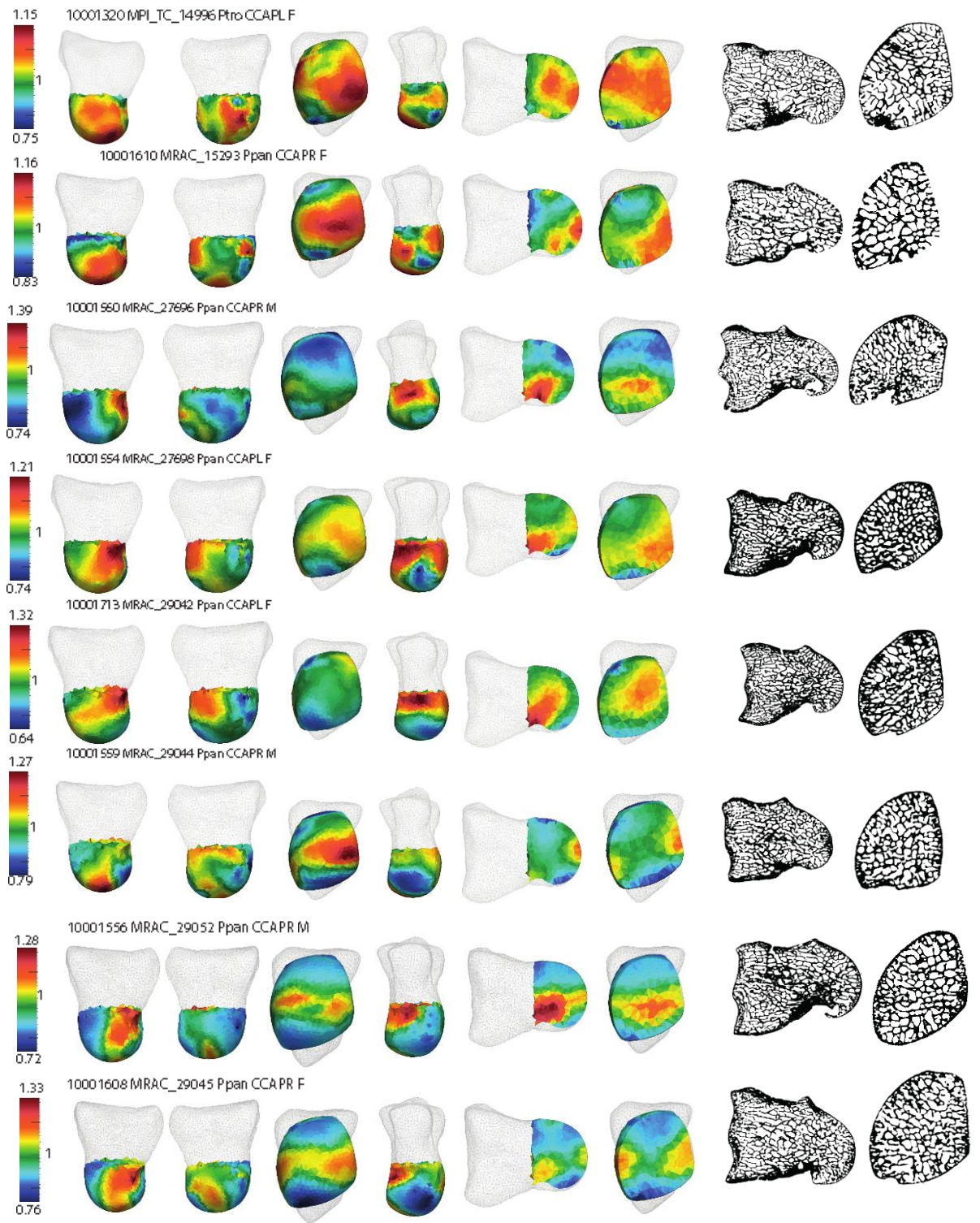


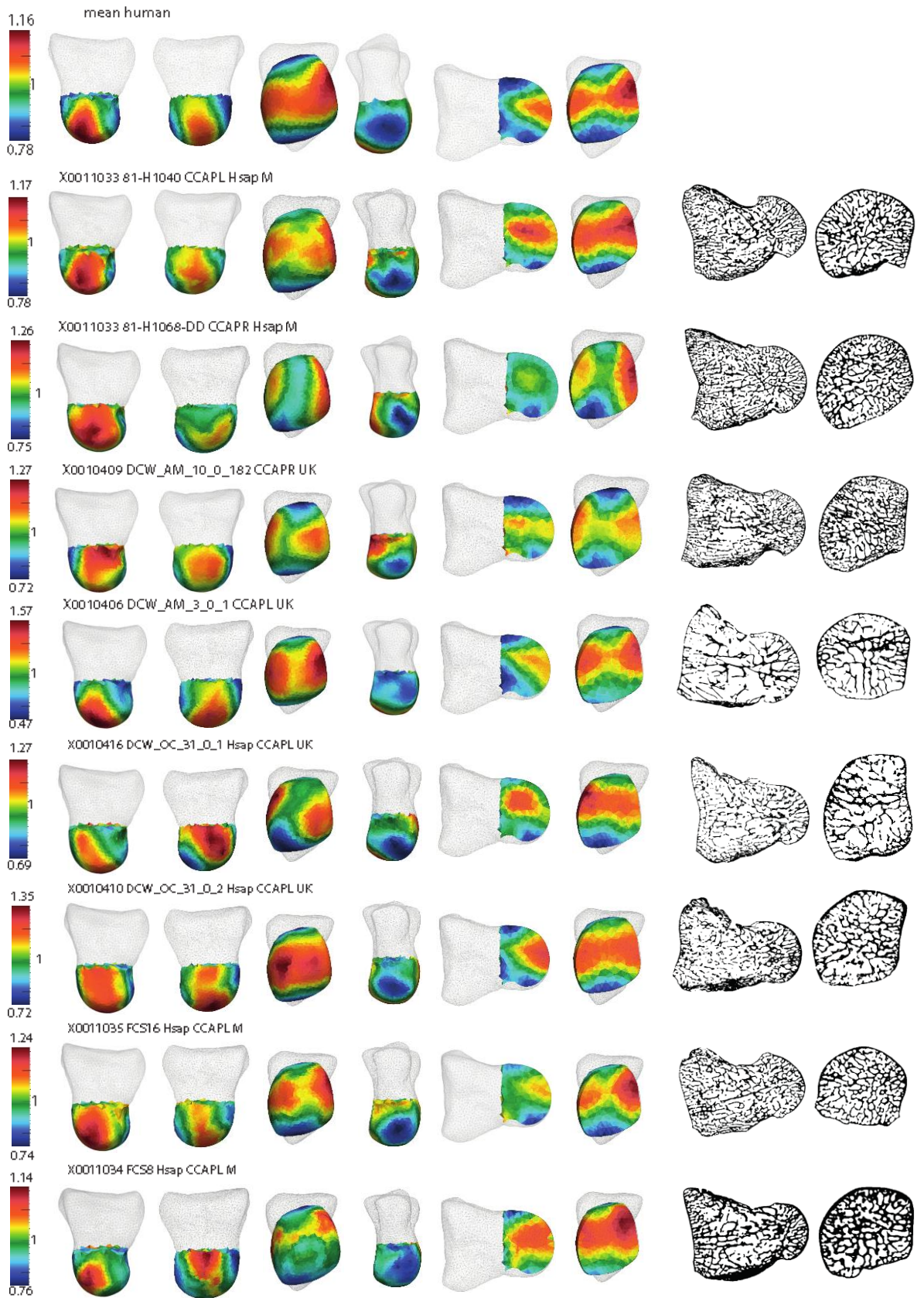


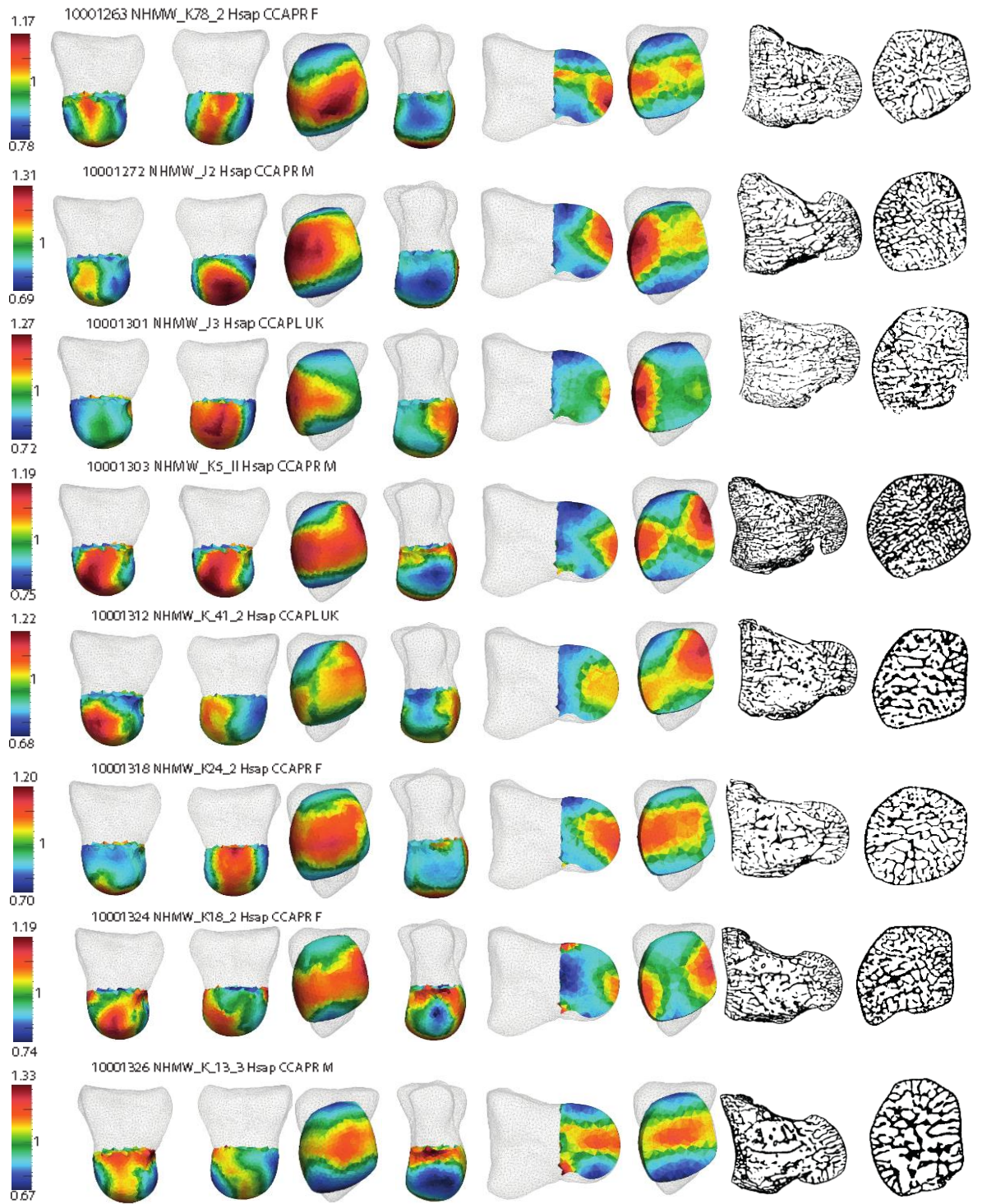


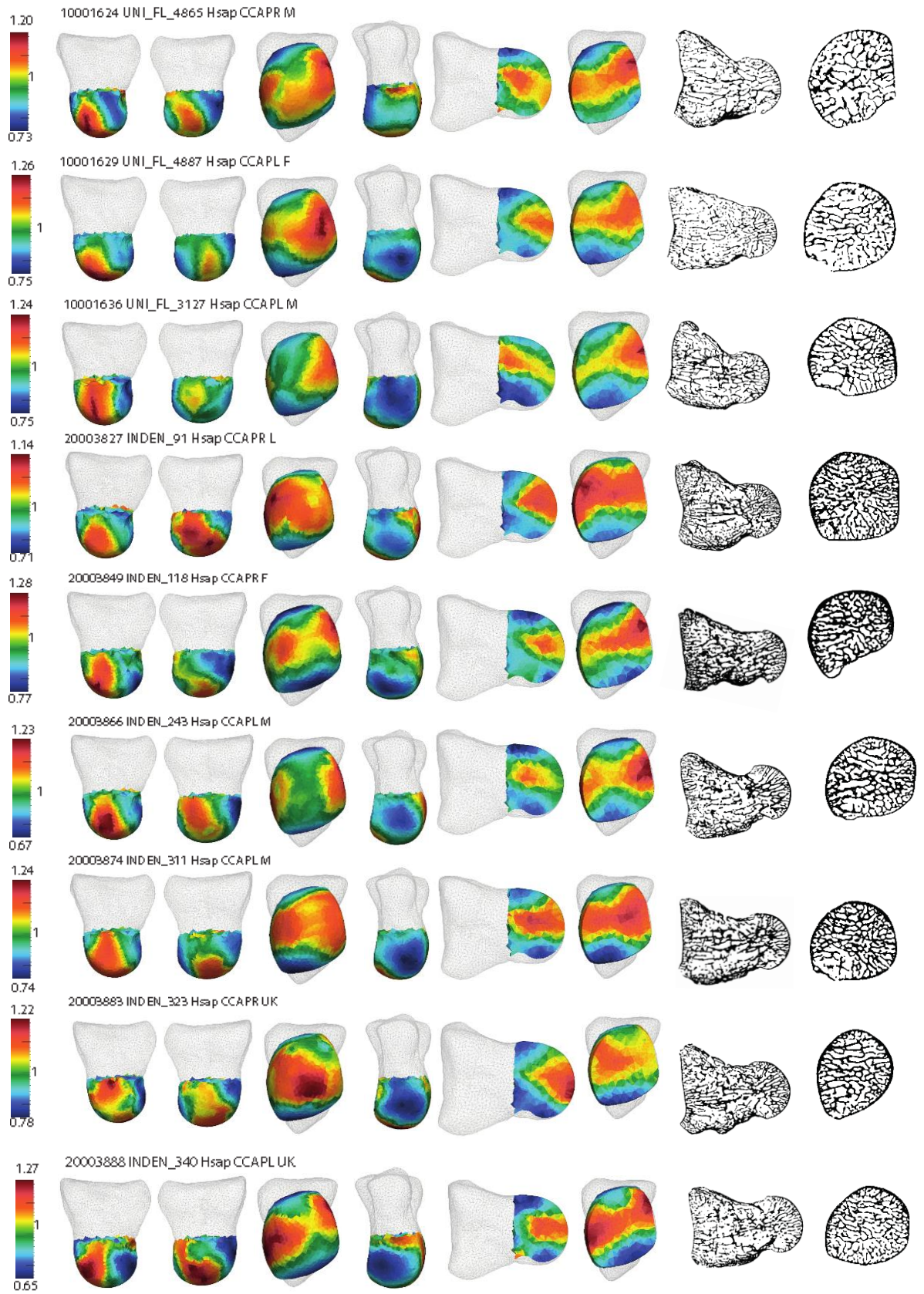


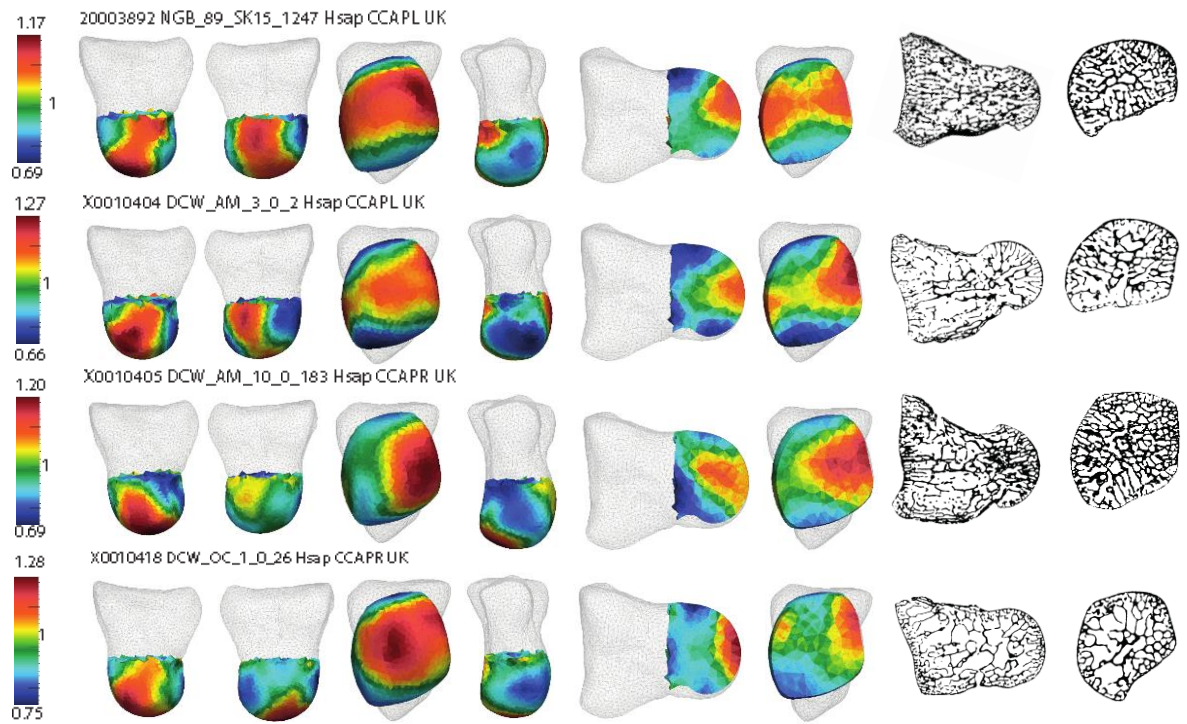












Supplementary Figure 5.2 Maps illustrating the relative bone volume distribution of every individual in the sample.

Fossils are presented first, then Pongo, Gorilla, Pan and *H. sapiens*. The mean distribution of each taxon group is present first, and each individual within that group follows. In the reference image, the first four images illustrate the articular surfaces of the proximal capitate, the last four illustrate where a slice has been placed in the canonical model (first two) or original micro-CT scan (last two) to show the internal structure of the bone

5.9. Supplementary Tables

Supplementary Table 5.1 Specimen information and individual parameter values.

The specimen column records the curatorial institutions as abbreviations; DCW = The Duckworth Collection, University of Cambridge; INDEN = Georg-August-University Goettingen, Anthropology Collection; MPI_TC = Max Planck Institute for Evolutionary Anthropology Primatology, Tai Collection; MRAC = Royal Museum for Central Africa Tervuren; NGB = University of Kent; NHMW = Natural History Museum Vienna; NMNH = National Museum Natural History Smithsonian; PC = Powell-Cotton Museum; SMF = Senckenberg Natural History Museum, Frankfurt; UNI_FL = University of Florence; ZMB_Mam = the Natural History Museum, Berlin; ZSM = Bavarian State Collection Zoology.

* The right and left *A. sediba* specimens are antonyms of each other from specimen MH2. ** the BV/TV measurement on *H. naledi* is made on the entire proximal capitata including the broken palmar component.

Specimen	Taxon	Sex	Side	Resolution (mm)	BV/TV (%)
MH2_UW88_156	<i>A. sediba</i>	Female	Right*	0.0217	0.3219
MH2_UW88_105	<i>A. sediba</i>	Female	Left*	0.0234	0.3324
ZMB_Mam_83530	<i>G. gorilla</i>	Male	Right	0.0302	0.3108
ZMB_Mam_83545	<i>G. gorilla</i>	Male	Right	0.0301	0.4798
PC_MER_95	<i>G. gorilla</i>	Female	Left	0.0318	0.3983
PC_MER_264	<i>G. gorilla</i>	Male	Right	0.0369	0.5383
PC_MER_300	<i>G. gorilla</i>	Female	Right	0.0363	0.5059
PC_MER_372	<i>G. gorilla</i>	Male	Right	0.0352	0.5150
PC_MER_962	<i>G. gorilla</i>	Male	Right	0.0344	0.5518
PC_MER_138	<i>G. gorilla</i>	Female	Left	0.0353	0.4352
PC_MER_174	<i>G. gorilla</i>	Male	Right	0.0282	0.5104
PC_MER_696	<i>G. gorilla</i>	Female	Right	0.0308	0.4910
PC_MER_879	<i>G. gorilla</i>	Male	Left	0.0319	0.4426
LB1	<i>H. floresiensis</i>	Female	Left	0.0281	0.5289
LB6	<i>H. floresiensis</i>	Female	Right	0.0281	0.4527
UW101_1730_Hand_1	<i>H. naledi</i>	Unknown	Right	0.0330	0.4193**
NHMW_K78_2	<i>H. sapiens</i>	Female	Right	0.0319	0.2239
NHMW_J2	<i>H. sapiens</i>	Male	Right	0.0300	0.2628
NHMW_J3	<i>H. sapiens</i>	Unknown	Left	0.0301	0.2404
NHMW_K5_II	<i>H. sapiens</i>	Male	Right	0.0301	0.4408
NHMW_K_41_2	<i>H. sapiens</i>	Unknown	Left	0.0302	0.3088
NHMW_K24_2	<i>H. sapiens</i>	Female	Right	0.0202	0.2142
NHMW_K18_2	<i>H. sapiens</i>	Female	Right	0.0301	0.3292
NHMW_K_13_3	<i>H. sapiens</i>	Male	Right	0.0300	0.3266
UNI_FL_4865	<i>H. sapiens</i>	Male	Right	0.0302	0.2260
UNI_FL_4887	<i>H. sapiens</i>	Female	Left	0.0301	0.1977
UNI_FL_3127	<i>H. sapiens</i>	Male	Left	0.0302	0.2789
INDEN_91	<i>H. sapiens</i>	Male	Right	0.0301	0.3734
INDEN_118	<i>H. sapiens</i>	Female	Right	0.0251	0.3505
INDEN_243	<i>H. sapiens</i>	Male	Left	0.0301	0.3672
INDEN_311	<i>H. sapiens</i>	Male	Left	0.0301	0.3636

INDEN_323	<i>H. sapiens</i>	Unknown	Right	0.0301	0.3577
INDEN_340	<i>H. sapiens</i>	Unknown	Left	0.0301	0.2861
NGB_89_SK15_1247	<i>H. sapiens</i>	Unknown	Left	0.0300	0.3163
DCW_AM_3_0_2	<i>H. sapiens</i>	Unknown	Left	0.0294	0.2151
DCW_AM_10_0_183	<i>H. sapiens</i>	Unknown	Right	0.0315	0.3960
DCW_AM_3_0_1	<i>H. sapiens</i>	Unknown	Left	0.0345	0.2227
DCW_AM_10_0_182	<i>H. sapiens</i>	Unknown	Right	0.0314	0.3245
DCW_OC_31_0_2	<i>H. sapiens</i>	Unknown	Left	0.0306	0.2793
DCW_OC_31_0_1	<i>H. sapiens</i>	Unknown	Left	0.0302	0.2222
DCW_OC_1_0_26	<i>H. sapiens</i>	Unknown	Right	0.0264	0.1910
81-H1068-DD	<i>H. sapiens</i>	Male	Right	0.0445	0.3261
81-H1040	<i>H. sapiens</i>	Male	Left	0.0445	0.3234
FCS8	<i>H. sapiens</i>	Male	Left	0.0433	0.4303
FCS16	<i>H. sapiens</i>	Male	Left	0.0433	0.2858
Ohalo_II_H2	<i>H. sapiens</i>	Male	Left	0.0301	0.3214
Barma_Grande_2	<i>H. sapiens</i>	Male	Right	0.0350	0.3912
Arene_Candide_2	<i>H. sapiens</i>	Male	Left	0.0350	0.3601
Kebara_2	Neanderthal	Male	Left	0.0301	0.3148
Amud_1	Neanderthal	Male	Left	0.0300	0.3548
Tabun_C1_1-155	Neanderthal	Female	Left	0.0281	0.3753
MRAC_27698	<i>P. paniscus</i>	Female	Left	0.0302	0.4939
MRAC_29052	<i>P. paniscus</i>	Male	Right	0.0340	0.3914
MRAC_29044	<i>P. paniscus</i>	Male	Right	0.0400	0.3911
MRAC_27696	<i>P. paniscus</i>	Male	Right	0.0302	0.3233
MRAC_29045	<i>P. paniscus</i>	Female	Right	0.0309	0.3500
MRAC_15293	<i>P. paniscus</i>	Female	Right	0.0302	0.3629
MRAC_29042	<i>P. paniscus</i>	Female	Left	0.0302	0.4474
MPI_TC_11789	<i>P. troglodytes</i>	Male	Left	0.0302	0.3802
MPI_TC_11781	<i>P. troglodytes</i>	Male	Right	0.0302	0.4256
MPI_TC_14996	<i>P. troglodytes</i>	Female	Left	0.0302	0.3016
SMF_6999	<i>P. abelii</i>	Female	Right	0.0294	0.2044
ZMB_Mam_6948	<i>P. pygmaeus</i>	Female	Left	0.0321	0.3084
ZMB_Mam_6947	<i>P. pygmaeus</i>	Male	Left	0.0318	0.4464
ZMB_Mam_11647	<i>P. pygmaeus</i>	Unknown	Left	0.0481	0.3084
SMF_24510	<i>P. pygmaeus</i>	Female	Right	0.0318	0.2305
SMF_74303	<i>P. pygmaeus</i>	Female	Left	0.0301	0.5871
SMF_84218	<i>P. pygmaeus</i>	Female	Left	0.0302	0.3636
ZSM_1907_0622	<i>P. pygmaeus</i>	Unknown	Right	0.0293	0.3644
ZSM_1907_0633b	<i>P. pygmaeus</i>	Female	Right	0.0293	0.5270
ZSM_1907_0629b	<i>P. pygmaeus</i>	Male	Right	0.0284	0.5352
ZSM_1907_0660	<i>P. pygmaeus</i>	Female	Right	0.0284	0.3199
ZSM_1909_0801	<i>P. pygmaeus</i>	Male	Right	0.0343	0.4090

Supplementary Table 5.2 Summary of the qualitative descriptions of the typical RBV for key regions in the proximal capitate. For the trabeculae within the centre of the bone, the description includes the direction or extent of high RBV if present.

	Central trabeculae	Lunate	Proximal scaphoid	Radial scaphoid	Distal scaphoid	Hamate	Palmar
<i>Pongo</i>	High, distally oriented, restricted to ulnar-side	Moderate-high	Low	Low	Low	Moderate	Low
<i>Pan</i>	High, disto-palmarly oriented, restricted to ulnar-side	High	Low-Moderate	Low-Moderate	Low-Moderate	High	High
<i>Gorilla</i>	Low	Moderate-High	Low-Moderate	Moderate-High	High	High	Low
<i>H. sapiens</i>	High, distally oriented, originates from proximal scaphoid and lunate	High	High	High	Low	High	Low
Fossil <i>H. sapiens</i>	High, distally oriented, originates from proximal scaphoid and lunate	High	High	High	Low	High	Low
Neanderthals	High, distally oriented, originates from proximal scaphoid and lunate	High	High	High	Low	High	Low
<i>Australopithecus sediba</i>	High, distally oriented, originates from proximal scaphoid and lunate	High	High	High	Low	Moderate-High	Low
<i>Homo floresiensis</i>	High, disto-palmarly oriented, restricted to ulnar-side	High	Low	Low	Low	High	High
<i>Homo naledi</i>	High, disto-palmarly oriented, restricted to ulnar-side	High	Low	Low	High	High	n/a

Supplementary Table 5.3 Permutational multivariate pairwise comparisons of extant hominoids.

	<i>Gorilla</i>	<i>H. sapiens</i>	<i>Pan</i>
<i>H. sapiens</i>	<0.001	/	/
<i>Pan</i>	0.001	0.001	/
<i>Pongo</i>	<0.001	<0.001	<0.001

6. Discussion and Conclusions

The primate hand is highly dexterous, and all extant hominids are capable of tool behaviours under varying conditions and degrees (Lewis 1989; Marzke 2013; Fragaszy and Crast 2016). But what sets human manipulation apart is the degree of precision, control and force that can be applied by the hand (Marzke 1997). A central theme in palaeoanthropology is when, why and how tool use moved from facultative, as it is in non-human hominids, to obligate, as it is in modern *H. sapiens*.

Hominids are a behaviourally diverse group of primates (Hunt 1991b), and their carpals' morphological variation reflects adaptations to the primary function of their hands, and the divergent loading these behaviours induce (Tocheri 2007; Preuschoft 2019). Therefore, biomechanically sensitive aspects of bone tissue, such as bone volume to total volume (BV/TV) and the degree of anisotropy (DA) among the trabeculae, provide an avenue for researchers to explore questions of load transmission and hand use among fossil hominins. While the trabecular architecture in human carpals has been shown to be congruent with the force vectors associated with manipulation (Stephens et al. 2018), prior to this thesis, whole-bone analytical techniques had yet to be applied to the non-human hominid carpus. **The central aim of this thesis was to explore how and why wrist bone structure differs among extant and extinct hominids.** The first question investigated by this thesis, which was explored throughout all three projects, was: **Do differences exist between extant hominids, and how do we best detect these differences within the distinct biomechanical environment of the wrist?**

6.1. Do differences exist between extant species?

All three research projects indicated that statistically significant differences exist in the carpal microarchitecture of extant hominids. Furthermore, the intraspecific statistical differences in DA and relative BV/TV (RBV) across the scaphoid, lunate, triquetrum, and proximal and distal capitate indicated load magnitude and directionality are not evenly distributed across the wrist. Thus while we often conceptualise the hominid wrist as being broadly under compression or tension, there are highly localised responses to strain.

Although differences between the extant apes were detected, predictions were not always supported. The hominids are behaviourally versatile, and quantifying hand use *in vivo* is complicated by the difficulty in observing behaviours (particularly among wild animals) who may be high up in trees, obscured by foliage, or unhabituated to observers. Studies on captive animals provide invaluable data on behaviour (e.g., Bardo et al. 2017; Finestone et

al. 2018; Samuel et al. 2018; Thompson 2020) but will not necessarily reflect the full diversity of behaviours expressed by wild animals (Birkett and Newton-Fisher 2011; Ross and Shender 2016). Predicting and interpreting functional adaptation is further complicated by the challenge of drawing kinetic (force and loading induced by movement) inferences from kinematic (movement alone) observations. Two pertinent examples are drawn in Samuel et al. (2018) and Synek et al. (2020). Samuel et al. (2018) quantified hand posture and pressure experienced by the palm, fingers and thumb by bonobos during arboreal locomotion. They found that although the thumb routinely contacted the substrate, it exerted low or no pressure onto that surface. Synek et al. (2020) found that forces induced by the muscles significantly influence the force vectors experienced by a skeletal element such that estimations made from joint position alone may not necessarily accurately reflect the actual force vectors experienced by the bone. Quantifying human muscle activity during manual activity has been relatively well studied (e.g., Hamrick et al. 1998; Marzke et al. 1998b; Key et al. 2020; Key et al. 2021) compared to other hominids, where such studies are constrained ethically and practically (Marzke 2013). Thus while the differences observed in my results can be correlated to what we know or presume about locomotor differences in the extant apes, interpretations of fossil material will be improved by more *in vivo* research on hand use and manual pressure, particularly in *Pongo* for which no pressure studies currently exist.

6.1.a. Summary of bone microstructure in *Pongo*

Pongo is a highly arboreal ape and has been assumed to utilise numerous hand postures to navigate its complex 3D environment (Isler and Thorpe 2003; Thorpe and Crompton 2006). Although the *Pongo* midcarpal joint has a high capacity for movement (Orr 2017), my results suggested the capitulate joint, as part of the midcarpal joint, may be more stable during hand use than has been commonly assumed. The higher than expected DA in the lunate and the distribution of RBV in the proximal capitate suggested these two bones are relatively stable and highly stressed in a predominantly neutral posture. The high RBV at the capitolunate joint supported the prediction that load would be preferentially directed towards the large lunate by the ulnar carpals. Higher than expected DA has also been found in other *Pongo* skeletal elements, such as the metacarpus (Dunmore 2019) and proximal femur (Georgiou et al. 2019). *Pongo* kinetics and kinematics are particularly understudied, which may be why functional adaptation predictions often do not align with results. **In totality, the patterns across the *Pongo* carpus suggested that a relatively stable midcarpal joint receives its peak loading in a neutral posture, with relatively greater strain in the large lunate and a reduced capacity for force transfer at the ulnocarpal joint.**

6.1.b. Summary of bone microstructure in *Gorilla*

The patterns across the *Gorilla* wrist differentiated it from all other extant taxa, although it did share some patterns with *Pan*. *Gorilla* is the most terrestrial non-human extant ape, typically adopting palm-backwards knuckle-walking, with slight extension at the wrist (Doran 1997; Remis 1998; Matarazzo 2013; Finestone et al. 2018; Thompson et al. 2018). As such, forces transferred through the wrist are assumed to be high as all intercarpal joints must resist compression from gravity alongside its large body mass held above the wrist (Carlson and Patel 2006). In the carpals of the proximal row, *Gorilla* showed a lower magnitude of difference in RBV and DA across the three bones compared to the other taxa, suggesting the three bones experience more similar degrees of loading. This conclusion is consistent with the study by Matarazzo (2013), which found that *Gorilla* phalanges experienced more similar vertical pressure during knuckle-walking compared to *Pan*. The high RBV in the triquetrum was an unexpected result. Due to the complete lack of ulnocarpal contact, it has been assumed that the ulnar side of the *Gorilla* hand has a reduced capacity for force transfer and resistance to strain (Sarmiento 1988; Lewis 1989; Matarazzo 2013). The high RBV in the triquetrum suggests it may be providing important stability to the wrist during ulnar deviation. *Gorilla* uses varying degrees of ulnar deviation during climbing and knuckle-walking (Sarmiento 1988; Neufuss et al. 2017, 2018; Thompson et al. 2018), and in lieu of direct ulnocarpal contact, ligaments likely play an important part of the stabilising mechanisms at the wrist (Garcia-Elias, de la Bellacasa and Schouten 2017).

Gorilla displayed greater isotropy in the proximal capitate compared to *H. sapiens* or *Pongo*. This pattern (also present in *Pan*) was unexpected as it was assumed the predominance of knuckle-walking and low range of midcarpal extension in African apes (Orr 2017) would result in a low variability of joint postures and force vectors. While these results may reflect the use of a greater number of hand postures than usually assumed in *Gorilla* (see also Thompson et al., 2018), the cHMA results provide an alternative explanation. The RBV maps showed a wide distribution of moderate-to-high trabecular bone across the proximal capitate, creating a band of thick trabeculae across the radial, proximal and ulnar capitate. These trabeculae may be isotopically distributed across this region in a 'fan-like' structure, providing support across all joints. A future analysis of the distribution of DA using the cHMA method could investigate this hypothesis. **In totality, the carpal bones examined in this thesis suggested that the *Gorilla* wrist is loaded relatively evenly across the intercarpal joints, with peak forces likely incurred in a roughly neutral posture.** The role of ligaments are likely to be providing extremely important stabilisation, particularly at the ulnar side of

the wrist; however, a more nuanced understanding of wrist ligaments in non-human hominids is needed to support this hypothesis.

6.1.c. Summary of bone microstructure in *Pan*

Pan was differentiated from the other taxa in all three chapters, although it shared some similarities with *Gorilla*. In Chapter 3, *Pan* generally expressed the same relative patterns across the proximal and distal subregion of the capitate as *Gorilla*. However, when the distribution of RBV in the proximal capitate was quantified in Chapter 5, the distribution of this bone was statistically different. Similarly, in Chapter 4, *Pan* expressed the same relative patterns across the scaphoid, lunate and triquetrum as *Gorilla*; however, the statistical relationships between the bones were different, with *Pan* exhibiting a greater magnitude of difference between the bones. These results suggest that while the broad kinetic forces across the knuckle-walking wrist are similar, the nuanced differences in their locomotion result in detectable differences in bone functional adaptation. As in *Gorilla*, the unexpectedly high RBV in the triquetrum is potentially a result of ligamentous stabilisation during ulnar deviation, which is thought to be adopted by *Pan* due to the use of palm-in knuckle-walking postures (Tuttle 1969; Wunderlich and Jungers 2009; Matarazzo 2013), and may further explain the greater magnitude of difference in the DA between the lunate and triquetrum. During palm-in knuckle-walking, the lunate is stabilised in maximum congruence with the radius, while simultaneously, the ulnar-most side of the proximal row would need to provide stability to resist axial compression (Patel and Carlson 2007; Garcia-Elias, de la Bellacasa and Schouten 2017). **In totality, the results suggested that force is variable across the *Pan* wrist, perhaps with more frequent loading of the joints at the ROM extremes compared to *Gorilla*.**

6.1.d. Summary of bone microstructure *H. sapiens*

This thesis demonstrated that the primarily manipulative hand of *H. sapiens* has statistically distinct bone architecture within the carpus relative to non-human hominids that use the hand primarily for locomotion. Stephens et al. (2018) first used whole-bone methods to map bone architecture across *H. sapiens* and found a distinctive distribution of bone across the proximal capitate, hypothesised to reflect habitual use of the dart-thrower's motion (DTM). Using a larger and more diverse sample of *H. sapiens*, I replicated these results in Chapter 5, but showed for the first time that the characteristic *H. sapiens* pattern in the proximal capitate statistically differentiates them from non-human hominids. As predicted, high trabecular bone volume was found in the capitoscaphoid and capitolunate joints, which is coincident with the axis of the DTM (Crisco et al. 2005; Crisco et al. 2011; Brigstocke et al.

2014; Edirisinghe et al. 2014; Garcia-Elias, Alomar Serrallach and Monill Serra 2014). This distribution was ubiquitous across the sample, including in the Pleistocene *H. sapiens*, suggesting that this kinetic pattern is a shared feature of all *H. sapiens* across spatio-temporally and behaviourally diverse populations. The results from Chapters 4 and 5, which emphasise the relative importance of the lunate and capitulate joint in force transfer, align with analyses showing the capitulate joint to be the hinge of the DTM (Edirisinghe et al. 2014; Garcia-Elias, Alomar Serrallach and Monill Serra 2014), transferring a greater amount of force relative to the capitolunate joint (Gíslason et al. 2009; Gíslason et al. 2012). However, the trend for higher bone volume at the capitulate joint relative to the capitolunate joint was a general trend across all hominids, including in the extinct taxa. Despite being the functional crux of the DTM, a phylogenetic analysis of lunate morphology found it resembled the hypothesised lunate morphology of the hominoid last common ancestor (Kivell, Barros and Smaers 2013). This suggests that non-human hominids share (at least) two fundamental components of the DTM (lunate shape, high capitulate force transfer), and thus some of the underlying morphological features of this axis may have been inherited from a common ancestor. It thus remains unclear whether the pattern found in modern and fossil *H. sapiens* represents: 1) high capitolunate joint loading as a result of compressive forces from the thumb, in combination with high capitulate joint loading as a shared feature of hominid wrist biomechanics; or 2) a reflection of habitual movement and loading across the DTM axis. While more kinetic research is needed to investigate this open question, **the distinctive pattern across the human carpals suggests habitual patterns of loading associated with a primarily manipulative hand are distinctive relative to non-human hominids.**

6.2. Limitations and implications for future functional adaptation analyses of short bones

The bone functional adaptation methodologies used in this thesis have been developed on long bones (e.g., Gross et al. 2014; Bachmann et al. 2022), and the application of these methodologies rests on a simple assumption that differences in the biomechanics and cellular organisation of trabecular and cortical bone result in distinct morphological and architectural differences. The method has been demonstrated to reliably and efficiently differentiate cortical and trabecular bone in the epiphyses of many long bones, including the metacarpals (Tsegai et al. 2013; Skinner et al. 2015; Dunmore et al. 2019), metatarsals (Komza and Skinner 2019), femur (Georgiou et al. 2018; Georgiou et al. 2019) and humerus (Kivell et al. 2018b). This thesis found that trabecular and cortical bone can be difficult to differentiate in short bones, such as carpals. Notably, every species had roughly the same

ratio of cortical bone to trabecular bone in the proximal capitate; however, in the distal capitate, non-human hominids had a far greater proportion of cortical bone than *H. sapiens*. This indicated that relatively thick cortical bone is not simply an underlying, systemic feature of non-human hominid carpals but is likely to be a functional adaptation to strain. It was concluded that this might be a signal of arboreality due to tensional strain induced by ligaments, as tensional strain has a lower failure point relative to compressive strain (Caler and Carter 1989; Patten, Caler and Carter 1996). Further investigation of this hypothesis is warranted as if it can be validated, it may be a meaningful functional adaptation signal of habitual arboreality in fossil species.

The capitate has two regions with biomechanically distinct joint complexes. This made it an ideal bone to separate and test whether the two subregions had statistically differentiated microarchitecture. Although not all the specific predictions were supported, the six measured parameters (trabecular BV/TV, Total BV/TV, cortical thickness, trabecular thickness, trabecular number, and trabecular separation) were significantly different in 26 of the 28 tests conducted across the four taxa. This provided strong support for the hypothesis that carpal bones experience highly localised functional adaptation responses. It was argued that analysing the carpals within functional subregions may provide more meaningful results than looking at whole-bone averages in isolation. Based on these conclusions, Chapter 5 applied cHMA to the proximal capitate only. The cHMA method addressed some limitations and critiques of the functional adaptation methods used to date, in particular, that it has not been possible to apply statistical tests to compare the interspecific differences in bone distribution. cHMA is a significant step forward in BFA studies and was thus an important contribution to the first aim of this thesis.

By using the cHMA method, it was possible to produce a PCA with high statistical power as the RBV at each of the 4,872 homologous finite elements could be compared across every individual in the sample. The ability to build taxon-specific mean models (with standard deviations) saved time and reduced the subjective nature of identifying taxon-specific patterns across numerous individuals. However, there were still some notable limitations. For example, t-tests (and their non-parametric counterparts) can be conducted on each finite element within the canonical mesh; however, results are still limited by the original small sample sizes. Further testing is also needed to validate the methodology on irregular shapes. I analysed only the proximal capitate, which is similar in shape to the epiphysis of a long bone, on which this methodology was tested and validated (Bachmann et al. 2022). It is not clear how the shape registration protocol will deal with more irregular shapes or the very

restricted internal space of the distal capitate in non-human hominids. A final limitation, which arose during the interpretation of the cHMA results, is that different behaviours use similar joint postures, and so when only a single bone, or subregion of that bone, is analysed, it can be impossible to differentiate between two or more possible interpretations. For example, midcarpal extension is used by numerous behaviours from terrestrial or arboreal palmigrady to vertical rock climbing. Looking at RBV distribution patterns across a greater number of bones is likely to ameliorate this limitation.

This thesis benefited from several recent papers identifying that species tend to exhibit a genetically determined baseline bone volume value (e.g., Chirchir et al. 2015; Ryan and Shaw 2015; Chirchir et al. 2017; Tsegai et al. 2018). Systemic differences in bone volume were addressed by analysing and visualising relative bone volume (RBV). This approach will continue to be important, particularly when studying fossil species, as modern *H. sapiens* have systemically low bone volume (Chirchir et al. 2015) and thus, absolutely higher mean bone volumes among other hominins have limited functional meaning.

One of the most pervasive limitations, common to almost all palaeoanthropological research, is the sample size. Although the sample sizes used in this thesis are the largest known to me for internal carpal analyses, the highly nuanced locomotor repertoires of non-human hominids are still likely underrepresented. This is particularly true for *G. beringei*, for which we only have one capitate. Although a very simple analysis found higher DA in the left compared to the right triquetra in *H. sapiens*, the sample sizes limit our ability to analyse potentially significant intraspecific factors, such as sex, handedness, age, etc. Chapter 5 had fewer *Pan troglodytes* than *Pan paniscus*; however, *Pan troglodytes* is thought to use less arboreal quadrupedalism and palmigrady than *Pan paniscus* (Doran 1993a); separating these for analyses may enhance our understanding of arboreality on the midcarpal trabecular microarchitecture. Although bootstrapping and non-parametric statistical tests help us address some issues of small sample sizes, the statistical power remains low such that small but potentially significant differences may be missed.

An additional limitation that arose as a discussion point during the *viva voce* of this thesis was the prediction of “no difference”, i.e., a prediction of the null hypothesis. A prediction of the null hypothesis is not standard statistical methodology as statistical tests are designed to test the likelihood of an alternative hypothesis being true. For example, in Chapter 3, hypothesis 2 stated, “Proximal and distal segments will show significantly differentiated internal bone architecture”. The following prediction should have outlined an alternative hypothesis to explain significant differences if found; however, the prediction stated the null

hypothesis: “Distal to proximal ratios will be statistically undifferentiated among the study taxa”. If predictions are hard to formulate due to a lack of pre-existing literature, it would be more appropriate to discuss the research as exploratory rather than to predict the null hypothesis and potentially invalidate the statistical methodology.

In light of these results, **do differences exist between extant species, and how do we best detect these differences within the distinct biomechanical environment of the wrist?** The statistical differences found in the microarchitecture of the carpus suggest functionally meaningful differences exist. Because of the complex biomechanical environment of the wrist, careful consideration is needed during research design to ensure the right data are captured to answer the research question. Analysing larger subregions of the wrist will likely be more informative than analyses of single joints, even with the statistical advances of the CHMA method.

6.3. What does the internal structure of the capitate suggest about hand use among extinct Plio-Pleistocene hominins?

6.3.a. Neanderthals load their proximal capitate in the same way as modern *H. sapiens*

Based on the archaeological record, Shea (2017) proposed a model to identify shifts from facultative (tools are used in optional tasks with small fitness benefits) to habitual (stereotypical tools, engaged periodically with fitness benefits for users) to obligate (cannot survive within their ecological niche without the application of tools) tool use within the archaeological record. Neanderthals were the only extinct species included in this thesis who are known, obligate tool users. While *H. floresiensis* has been found in association with Oldowan-type tools (Moore and Brumm 2009; Brumm et al. 2010; Brumm et al. 2016; Van den Bergh et al. 2016), their hand morphology is primitive, and thus it is unclear where they fall on Shea's (2017) scale. All three Neanderthals included in this thesis (Amud 1, Kebara 2, Tabun C1) expressed a human-like pattern of trabecular architecture in the proximal capitate, suggesting that, like *H. sapiens*, they were consistently and heavily loading the capitulum and capitolunate and capitolunate joints, and potentially using the DTM. If this pattern does indeed reflect the use of the DTM, the results suggest this axis of motion was inherited from a common ancestor.

The similar results in *H. sapiens* and Neanderthals is somewhat in contrast to other functional adaptation studies. My thesis used a similar sample of fossil and modern *H. sapiens*, and Neanderthals as the PhD thesis of N. Stephens (2018), which compared the distribution of

trabecular bone volume across the entire hand. It was concluded that the higher BV/TV and lower DA across the palm and fingers of Neanderthals reflected a greater diversity of grip postures than *H. sapiens*, with greater force applied and a preference for transverse power grips. Bardo et al. (2020) analysed the covariation of shape in the trapezium-Mc1 across *H. sapiens* and Neanderthals. While *H. sapiens* tended towards a joint shape advantageous for precision grips and Neanderthals for transverse power grips, there was a high degree of interspecific variation within both groups. Karakostis et al. (2018) analysed the manual enthesal patterns from a sample of fossil *H. sapiens* and Neanderthals (including Kebara 2) to a population of modern *H. sapiens* who routinely used either precision grips or power grips vocationally. Unlike the other two above papers that emphasised interspecific variation, the patterns of manual entheses were relatively consistent. Neanderthals clustered with *H. sapiens* who routinely performed precision tasks, and never with *H. sapiens* who routinely performed heavy manual work. While discrepancies in results between all these studies are potentially due to variations in sample and methodology, in combination, they suggest that behavioural variation among late *Homo* results in detectable differences in the microarchitecture of hand bones.

High RBV at the capitulum and capitolunate joint that moved distally through the capitate was a shared pattern of RBV distribution across my diverse late *Homo* sample. While this suggests that this pattern may be a useful signal of a primarily manipulative hand, more work is needed to evaluate whether behavioural variation can be detected in the proximal capitate, or elsewhere in the carpals. Arene Candide 2 has high RBV on the palmar capitolunate joint, which was not typically expressed by *H. sapiens*, although a small number of individuals had high RBV at the distal-most aspect of the capitolunate joint, including Ohalo 2, and one male and one female from the Egyptian Nubian population. It is unclear what sort of behaviour this feature may be correlated to as kinematic studies of Plio-Pleistocene tool use are rare (but see Key et al. 2020). Further research on *in vivo* tool use or large skeletal assemblages with correlated vocational information is needed to address this question. Analysing broader functional units across the wrist may also provide avenues to investigate the inferences drawn here, as well as new questions. For example, it is notable that in the results from Karakostis et al. (2018), Neanderthals never show entheses patterns indicative of tools held obliquely across the palm. Grips hypothesised to be associated with the Neanderthal entheses pattern are either cradle grips, where the object is held with the pads of all five digits, with or without the palm, or pinch grips, where the tool is held between the Mc1 and Mc2/3 (see Karakostis et al. 2018 for illustrations). Analyses of the distal row

carpus or metacarpal proximal epiphyses may be insightful for investigating evidence of variation in grip preferences between the two late *Homo* groups. If Neanderthals adopted transverse grips at a greater frequency than *H. sapiens*, the ulnar carpus and metacarpus may show higher RBV compared to the radial carpus and metacarpus.

Australopithecus sediba, *Homo naledi* and *Homo floresiensis* all have relatively well-preserved capitate bones and thus provided a unique opportunity to investigate functional adaptation in fossil hominins whose commitment to arboreality and tool use is uncertain. *Australopithecus sediba* was the geologically oldest fossil included in this thesis; however, it was the only fossil taxa alongside the Neanderthals that had similarities to the human RBV distribution. Specifically, the distribution of subchondral bone reflected the typical human pattern, suggesting *A. sediba* loaded the capitulum and capitolunate and capitolunate joints similarly to *H. sapiens* and potentially used the DTM axis. However, the disto-palmarly oriented high RBV within the body of the proximal capitate was similar to the pattern seen in *Pan* and suggests that peak loading of the midcarpal joint in *A. sediba* was in a different posture than is typical for late *Homo*. With this unique combination, loading and force transfer of the *A. sediba* midcarpal joint was distinctive from all extant taxa.

6.3.b. Evidence supports the use of transverse-type grips for tool behaviour in *Homo floresiensis*

Based on its overall primitive carpal morphology, in combination with a rugous attachment for the *flexor pollicis longus* (Tocheri et al. 2007; Larson et al. 2009; Orr et al. 2013), it has been hypothesised that precision gripping in *H. floresiensis* was likely to have different biomechanical consequences than in *H. sapiens* (Tocheri et al. 2007; Orr et al. 2013). *H. floresiensis* exhibited high RBV at the ulnar capitate, without evidence for high capitolunate loading, as seen in late *Homo*. Relatively high ulnar side loading of the hand is commensurate with the presumed loading regime of transverse grips, such as cradle grips (Marzke, Wullstein and Viegas 1992; Niewoehner 2001; Stephens et al. 2018; Williams-Hatala et al. 2021). Cradle grips are one of the main postures used by *H. sapiens* when making and using Plio-Pleistocene tools (Marzke 1997; Key, Merritt and Kivell 2018; Williams-Hatala et al. 2021). Although, in a recent study comparing the kinetics of Plio-Pleistocene tool manufacture between experts and novices, Williams-Hatala et al. (2021) demonstrated that cradle grips are used predominantly by inexperienced stone knappers. Furthermore, this study found that when using cradle grips, modern *H. sapiens* tended to load their third, fourth, and fifth digits higher than experienced stone knappers, who typically used 2-jaw precision grips (Williams-Hatala et al. 2021). This RBV distribution provides support for the

hypotheses that *H. floresiensis* used transverse grips, potentially cradle grips, to produce tools. The ape-like carpal morphology of *H. floresiensis* exhibits radially oriented intercarpal joint surfaces, which are well-suited to resist sheer and compression from proximally oriented force vectors via heavily loaded ulnar side digits (Niewoehner, Weaver and Trinkaus 1997; Tocheri 2007). In sum, the results from my research suggest that Oldowan-type tools were made and used by *H. floresiensis* without typical human-like midcarpal load transfer.

Similar to *Pan* and some *Australopithecus* species, *H. floresiensis* exhibits a J-hook morphology at the proximo-radial capitate (Larson et al. 2009; Orr et al. 2013). Although this morphology has yet to receive formal biomechanical analysis, during extension, the scaphoid would engage with this portion of the capitate, and it has been hypothesized to improve midcarpal load transfer at the capitoscapoid joint (Larson et al. 2009; Orr et al. 2013). It is unclear whether the J-hook would reduce the range of motion at the midcarpal joint, although the engagement of the scaphoid into the curved facet may reduce movement in extension. The distribution of RBV at this joint was low and therefore does not suggest a high magnitude of stress and force transfer at the capitoscapoid joint.

The broken component in the *H. naledi* capitate meant that it could not be included in the cHMA modelling or the PCA, and the RBV distribution was analysed on its actual shape. From what was preserved, the RBV distribution in the *H. naledi* capitate had several similarities with both *H. floresiensis* capitates. Specifically, *H. naledi* also appeared to have high ulnar-side loading of the capitate. Although the extent that high RBV moved into the palmar component of the capitate cannot be confidently inferred, the lower RBV at the capitoscapoid joint suggested that this joint was not heavily or consistently loaded by the radial side of the hand. Thus, despite *H. naledi* having a morphologically human-like capitate and scaphoid, a large scaphocapitate joint and being geologically younger than *A. sediba*, the capitate does not have a human-like RBV distribution.

6.3.c. The kinetics and kinematics of climbing

While we only have direct evidence for tool behaviour in *H. floresiensis*, parsimony would suggest that *A. sediba* and *H. naledi* were also capable of tool manipulation and use. Based on morphological evidence, all three fossils have also been hypothesised to maintain a degree of arboreality (Larson et al. 2007; Churchill et al. 2013; DeSilva et al. 2013; Kivell et al. 2015; Rein et al. 2017; Kivell et al. 2018a; Feuerriegel et al. 2019; Dunmore et al. 2020b; Dusseldorp and Lombard 2021). In *A. sediba*, functional adaptation analyses support the morphological ones and suggest use of arboreal substrates. For example, a recent analysis

of the RBV and DA in the metacarpal heads of MH2 indicated orangutan-like, flexed-finger power grasping in Mc2-5, while the architecture in the thumb suggested human-like manipulation (Dunmore et al., 2020b). Further, analysis of calculus and microwear on the teeth indicates MH2 favoured arboreal food sources such as fruit, tree leaves and bark, more closely resembling a chimpanzee's diet than other australopiths who consume predominantly terrestrial savannah plant foods (Henry et al., 2012). Similar functional adaptation analyses have yet to be applied to *H. naledi* or *H. floresiensis*. However, dental analyses of *H. naledi* do not indicate a predominance of arboreal food sources like *A. sediba*, instead, they suggest *H. naledi* consumed hard and gritty foods such as nuts or underground tubers (Towle, Irish and De Groote 2017; Berthaume, Delezene and Kupczik 2018; Ungar and Berger 2018).

The biomechanical requirements of manipulation versus locomotion are frequently in opposition to one another (Alba, Moyà-Solà and Köhler 2003; Preuschoft 2019), and it is uncertain how a hand required to perform both behaviours may look. Recently, Neufuss et al. (2019) proposed that the functional morphology of the African ape hand that facilitates climbing also facilitates their capacity for complex manipulation. This is because non-human hominids often use the same power and hook grips for suspension and climbing as they do for manipulative tasks, such as termite fishing or processing tough plant foods prior to consumption (Marzke et al. 2015; Bardo et al. 2016; Bardo et al. 2017; Neufuss et al. 2019). While they cannot exert the same degree of force as *H. sapiens*, the longer *Gorilla* thumb also appears to provide a degree of stability and enhanced control during manipulation (Neufuss et al. 2019), and they have also been observed to perform a 2-jaw chuck grip (Bardo et al. 2017; Neufuss et al. 2019). In light of this, it is notable that when living *H. sapiens* climb, they tend to use similar transverse power and hook grips as the African apes (Sarmiento 1988; Sims 2022).

Climbing (in *H. sapiens* and non-human hominids) is correlated with high loading on the ulnar side of the hand and relatively low loading of the thumb (Quaine, Vigouroux and Martin 2003; Amca et al. 2012; Fuss and Niegl 2012; Samuel et al. 2018). Although climbing is likely to induce a higher magnitude of strain on the fingers, it may be highly biomechanically compatible with transverse-type grips, as the force directionality and relative loading across the hand are similar between the two behaviours. As such, the use of transverse-type grips may have provided a biomechanical solution to increasing tool behaviour efficiency without the need to reconfigure hand morphology and subsequently reduce arboreal competency. The downside to this solution is that cradle grips cannot produce or manoeuvre tools as

effectively or efficiently compared to oblique or precision grips (Marzke 1997; Williams-Hatala et al. 2021). If tool use among hominins began with transverse grips, natural selection might have favoured individuals who were able to exert higher pressures on the thumb and second metacarpal, increasing their control of the object and exertion of force, all increasing the mechanical efficiency to the use of the tool.

Analyses of broader regions of the wrist are necessary to further investigate signals of climbing or manipulation in these hominins. This is primarily because similar midcarpal joint postures are correlated with divergent behaviours. For example, high degrees of wrist extension is correlated with terrestrial palmigrady for locomotion as well the DTM (Sarmiento 1988; Williams, Gordon and Richmond 2014; Orr 2017). The fossil hominin results of this thesis may indicate high ulnar-side loading from tool behaviours, climbing, or another not yet identified behaviour. Future analyses of the triquetrum may be particularly insightful as the high RBV in *Pan* and *Gorilla* found in Chapter 4 was hypothesised to be a signal of climbing.

In summary, my results suggested that using the hand as a primarily manipulative organ leaves detectable and statistically distinct signatures in the underlying microarchitecture of carpal bones. The consistent expression of high capitulate and capitolunate bone volume on the proximal capitate among late *Homo* makes it a strong indicator of human-like tool manufacture and use. However, it is not useful as a single measure to detect a diversity of tool behaviours across the fossil record. For example, *H. floresiensis* is a known tool maker; however, it did not display this characteristic bone volume distribution in the proximal capitate. Recent evidence has suggested that there were potentially many adaptive radiations for hand use among hominins, some that appear to have combined tool behaviours with arboreal locomotion, including *A. sediba* and *H. naledi* (Kivell et al. 2011; Kivell et al. 2015; Skinner et al. 2015; Dunmore et al. 2020a; Dusseldorp and Lombard 2021). The unique trabecular architecture across late *Homo* (*H. sapiens*, Neanderthals), *A. sediba*, *H. naledi*, and *H. floresiensis* provides support for a model of hominin hand use diversity.

6.4. Conclusion

To date, it has been unclear whether signals of functional adaptation to locomotion and manipulation are detectable in the microarchitecture of hominid carpal bones, as multispecies analyses had reached limited interspecific functional conclusions (Schilling et al. 2014; Ragni 2020). This thesis addressed this gap by applying whole-bone techniques (e.g., Gross et al. 2014; Bachmann et al. 2022) to quantify and analyse the internal structure of

wrist bones within a broad sample of extant and extinct hominids. The central aim was to assess how and why the internal structure of wrist bones differs among extant and extinct hominids. I undertook three research projects to achieve this aim that applied different approaches to ‘whole-bone’ analyses. The results showed that the microarchitecture of the capitate, scaphoid, lunate and triquetrum differentiates *H. sapiens* from non-human hominids suggesting that using the hand as a primarily manipulative organ leaves detectable and statistically distinct signatures in the underlying microarchitecture of wrist bones. The wrist, however, is biomechanically complex, and when applying bone functional adaptation research to the carpus, research design needs to carefully consider which functional subregions should be quantified in order to meaningfully answer the research question.

Within this comparative context, I inferred the loading and hand use from the capitate midcarpal joint of extinct hominin species. Fossil and modern *H. sapiens* and Neanderthals exhibited the same pattern of relative bone volume (RBV) distribution, which has previously been correlated to the axis of the dart-thrower’s motion of the wrist (Stephens et al. 2018). This suggested that this pattern may be an adaptive signal of a primarily manipulative hand and potentially an identifying feature of a functional commitment to tool behaviour within fossil species. However, the low variability in the expression of this feature among the late *Homo* sample suggests that as a single measure, it may not be able to detect tool behaviours that are not human-like. The distribution of RBV in *A. sediba* placed it in a unique part of the morphospace among the extant hominids, suggesting it was loading its wrist with a unique combination of force vectors relative to the extant sample. Notably, it was the only fossil species aside from Neanderthals to exhibit the distinctive RBV distribution at the proximal capitate, suggesting that it loaded its capitulunate and capitoscapoid joint in a manner similar to *H. sapiens*. Despite having an anatomically modern capitate and being geologically younger than *A. sediba*, the RBV in *H. naledi* did not reflect *H. sapiens*. This suggests that if it did make and use tools, it did so without inducing high, habitual loading from the radial side of the hand. The RBV distribution in *H. floresiensis* closely resembled that of *Pan*, suggesting that it made and used Oldowan-style tools without the use of human-like hand and wrist postures. The relatively higher ulnar-side loading of the capitate in both *H. floresiensis* individuals is consistent with the presumed force vectors induced by transverse-type grips, such as cradle grips. Notably, the loading patterns associated with cradle grips are similar to those induced by climbing (Quaine, Vigouroux and Martin 2003; Fuss and Niegler 2012; Williams-Hatala et al. 2021). This inference suggests a scenario where a hominin may use cradle grips to improve the functional efficiency of tool behaviours without compromising

climbing ability. Further research comparing the signals found in the proximal capitate to a broader anatomical region of the hand and wrist is needed to support and provide further nuance to these hypotheses.

6.5. Future directions

There continues to be a significant opportunity to investigate the functional morphology of the ulnar wrist and hand. If differences exist in hand grip preferences between *H. sapiens* and Neanderthals, it may be found with an analysis of the Mc5 and ulnar-side carpus as transverse power grips are likely to induce greater load on the ulnar-side hand compared to oblique grips. The inclusion of cercopithecoids into the comparative sample is another future research opportunity, as it would allow the exploration of broader questions of primate wrist evolution. For example, a functional adaptation study of the triquetrum across a broad sample of hominoid and non-hominoid primates may illustrate the consequences of ulnocarpal reduction on the RBV and DA in the hominoid triquetrum. However, this would introduce further potential limitations. Firstly, there are currently fewer μ CT scans of cercopithecoid carpus than there are hominoids. Secondly, the body mass of the chosen species would need to be quite large to ensure there are a sufficient number of trabeculae to quantify within the internal space. Small carpal bones from primates with low body mass have absolutely fewer trabeculae (Barak, Lieberman and Hublin 2013; Ryan and Shaw 2013). Because we measure DA with numerous small sampling spheres, a low trabecular number is potentially correlated to obtaining results of high DA that may not accurately reflect the actual alignment of trabeculae across the whole subregion of interest. More research is needed here as this correlation has not yet been formally analysed; however, using samples of similar-sized primates removes this potential methodological limitation.

Applying cHMA to the DA across the carpus would be particularly valuable for further investigating some of the inferences drawn from my results. The whole-bone measures of DA limit our ability to understand the highly localised functional adaptation responses across these complex multi-jointed bones. Three hypotheses were drawn from the results, which would benefit in particular from such an analysis. Firstly, the high DA in the proximal capitate may result from aligned trabeculae across the DTM axis. If this is so, it will strengthen the conclusion that this axis represents the consistent use of the DTM among *H. sapiens*. Secondly, the high DA of the scaphoid was not predicted as it was assumed that the wide range of thumb postures used during manipulation would load the scaphoid heterogeneously. In combination with the low RBV, these results suggested that either the scaphoid joints are not as highly strained as assumed or that highly stable joints and fewer

joint positions allow for trabecular alignment, rather than volume, to resist high degrees of strain. Finally, the low DA across the triquetrum of all taxa suggests that force transfer with the TFCC soft tissue structures may result in isotropic trabeculae. A confirmation of this would provide an informative avenue to investigate the evolution of these soft tissue structures. Developing techniques to study DA presents a significant future research opportunity more generally. Although medtool does allow us to visualise the primary eigenvector with the eigenvalue as a scalar, we currently have no statistical method for analysing DA in 3D.

The wrist is biomechanically complex, and the integration of newer modelling techniques may provide new opportunities to advance our understanding of how force is transferred through the carpus (and, ultimately, how to infer these signals in fossil hominins). Finite element modelling approximates stress and strain experienced by a structure under different loading conditions (Orr 2016). To date, these models have only been applied to *H. sapiens*. The finite models constructed by Gíslason et al. (2009; 2012) provided a critical context for interpreting the results I found in the human midcarpal joint. Finite element modelling requires input on numerous aspects of loading conditions, which in the carpus would include the geometry and Young's modulus of hard and soft tissue, ligament attachment sites, and substrate reaction forces (Gíslason et al. 2009; Gíslason et al. 2012). It would be particularly informative to better understand how articular cartilage affects load dissipation and force transfer through the carpals. Articular cartilage is a viscoelastic soft tissue that sits between the intercarpal joints, facilitating force transmission between the joint surfaces (Fox, Bedi and Rodeo 2009). How articular cartilage potentially affects trabecular adaptation is unclear and may be particularly important for understanding why surfaces with ligamentous attachments have notably thick cortices (i.e., the proximal versus the distal capitate).

Before finite element modelling method can be applied to non-human hominid carpus, basic biomechanical data needs to be collected, which will require further *in vivo* research. For example, the vertical substrate reaction forces acting upon the phalanges during knuckle-walking in African apes have been quantified previously (Matarazzo 2013); however, no analogous studies currently exist for *Pongo*. Human research could be extended by altering the loading conditions to reflect what is known about the force experienced by the fingers during stone tool production (e.g., Williams, Gordon and Richmond 2012; Key et al. 2017). Another advanced modelling technique with potential for future palaeoanthropological research is 4D CT (also called X-Ray Reconstruction of Moving Morphology). 4D CT takes and reconstructs in 3D numerous high-resolution x-rays during movement, providing a gold

standard for quantifying joint position *in vivo*. To date, the human wrist has only been quantified with 4D CT while performing the DTM, without holding an object or performing a specific task (Edirisinghe et al. 2014; Garcia-Elias, Alomar Serrallach and Monill Serra 2014). Although the application of 4D CT to non-human hominids may be limited for practical and ethical reasons, more research could be conducted on the human hand performing a range of behaviours, such as those of interest to palaeoanthropologists like stone tool manufacture and use. Finally, it remains to be confirmed that the use of the DTM for activities of living *H. sapiens*, such as opening a jar or pouring a glass of water, results in diagnostic, functional adaptation at the midcarpal joint. Loading of the human skeleton has decreased over time (Ryan and Shaw 2015; Saers et al. 2016; Chirchir et al. 2017), and it is unclear how hand loading in living *H. sapiens*, which is likely to be much lower than during Plio-Pleistocene tool behaviour, would impact functional adaptation.

7. References

- Aiello, L. C. (2010). Five years of *Homo floresiensis*. *American Journal of Physical Anthropology*, 142(2), 167-179.
- Aiello, L. C. and Dean, C. (1990). *An introduction to human evolutionary anatomy*, UK, Academic Press.
- Alba, D. M., Moyà-Solà, S. and Köhler, M. (2003). Morphological affinities of the *Australopithecus afarensis* hand on the basis of manual proportions and relative thumb length. *Journal of Human Evolution*, 44(2), 225-254.
- Alberich-Bayarri, Á., Moratal, D., Martí-Bonmatí, L., Salmerón-Sánchez, M., Vallés-Lluch, A., Nieto-Charques, L. and Rieta, J. J. (2007). Volume mesh generation and finite element analysis of trabecular bone magnetic resonance images. *29th Annual International Conference of the IEEE Engineering in Medicine and Biology Society*. IEEE.
- Amca, A. M., Vigouroux, L., Aritan, S. and Berton, E. (2012). Effect of hold depth and grip technique on maximal finger forces in rock climbing. *Journal of sports sciences*, 30(7), 669-677.
- Ancrenaz, M., Sollmann, R., Meijaard, E., Hearn, A. J., Ross, J., Samejima, H., Loken, B., Cheyne, S. M., Stark, D. J. and Gardner, P. C. (2014). Coming down from the trees: Is terrestrial activity in Bornean orangutans natural or disturbance driven? *Scientific Reports*, 4(1), 1-5.
- Argue, D., Donlon, D., Groves, C. and Wright, R. (2006). *Homo floresiensis*: microcephalic, pygmoid, *Australopithecus*, or *Homo*? *Journal of Human Evolution*, 51(4), 360-374.
- Augat, P. and Schorlemmer, S. (2006). The role of cortical bone and its microstructure in bone strength. *Age and Ageing*, 35(suppl_2), ii27-ii31.
- Ayhan, Ç. and Ayhan, E. 2020. Kinesiology of the Wrist and the Hand. In: ANGIN, S. & ŞİMŞEK, I. E. (eds.) *Comparative Kinesiology of the Human Body: Normal and Pathological Conditions*. London: Elsevier. pp. 211-282.
- Bachmann, S., Dunmore, C. J., Skinner, M. M., Pahr, D. H. and Synek, A. (2022). A computational framework for canonical holistic morphometric analysis of trabecular bone. *Scientific Reports*, 12(1), 1-13.
- Bain, G. I., Clitherow, H. D., Millar, S., Fraysse, F., Costi, J. J., Eng, K., McGuire, D. T. and Thewlis, D. (2015). The effect of lunate morphology on the 3-dimensional kinematics of the carpus. *The Journal of hand surgery*, 40(1), 81-89.
- Barak, M. M. (2019). Bone modeling or bone remodeling: That is the question. *American journal of physical anthropology*, 172(2), 153-155.
- Barak, M. M., Lieberman, D. E. and Hublin, J.-J. (2011). A Wolff in sheep's clothing: trabecular bone adaptation in response to changes in joint loading orientation. *Bone*, 49(6), 1141-1151.
- Barak, M. M., Lieberman, D. E. and Hublin, J.-J. (2013). Of mice, rats and men: trabecular bone architecture in mammals scales to body mass with negative allometry. *Journal of structural biology*, 183(2), 123-131.
- Barak, M. M., Lieberman, D. E., Raichlen, D., Pontzer, H., Warrener, A. G. and Hublin, J.-J. (2013). Trabecular evidence for a human-like gait in *Australopithecus africanus*. *PLoS One*, 8(11), e77687.
- Barak, M. M., Weiner, S. and Shahar, R. (2008). Importance of the integrity of trabecular bone to the relationship between load and deformation of rat femora: an optical metrology study. *Journal of Materials Chemistry*, 18(32), 3855-3864.
- Barak, M. M., Weiner, S. and Shahar, R. (2010). The contribution of trabecular bone to the stiffness and strength of rat lumbar vertebrae. *Spine*, 35(22), E1153-9.

- Bardo, A., Borel, A., Meunier, H., Guéry, J. P. and Pouydebat, E. (2016). Behavioral and functional strategies during tool use tasks in bonobos. *American Journal of Physical Anthropology*, 161(1), 125-140.
- Bardo, A., Cornette, R., Borel, A. and Pouydebat, E. (2017). Manual function and performance in humans, gorillas, and orangutans during the same tool use task. *American Journal of Physical Anthropology*, 164(4), 821-836.
- Bardo, A., Moncel, M.-H., Dunmore, C. J., Kivell, T. L., Pouydebat, E. and Cornette, R. (2020). The implications of thumb movements for Neanderthal and modern human manipulation. *Scientific Reports*, 10(1), 1-12.
- Bardo, A., Vigouroux, L., Kivell, T. L. and Pouydebat, E. (2018). The impact of hand proportions on tool grip abilities in humans, great apes and fossil hominins: A biomechanical analysis using musculoskeletal simulation. *Journal of Human Evolution*, 125106-121.
- Baum, D. A. and Larson, A. (1991). Adaptation reviewed: a phylogenetic methodology for studying character macroevolution. *Systematic Biology*, 40(1), 1-18.
- Begun, D. R. 2004. Knuckle-walking and the origin of human bipedalism. In: HILTON, C. E. & MELDRUM, D. J. (eds.) *From Biped to Strider*. New York: Springer. pp. 9-33.
- Berger, L. (2012). *Australopithecus sediba* and the earliest origins of the genus *Homo*. *Journal of Anthropological Sciences*, 90117-131.
- Berger, L. R., De Ruiter, D. J., Churchill, S. E., Schmid, P., Carlson, K. J., Dirks, P. H. and Kibii, J. M. (2010). *Australopithecus sediba*: a new species of *Homo*-like australopith from South Africa. *Science*, 328(5975), 195-204.
- Berger, L. R., Hawks, J., de Ruiter, D. J., Churchill, S. E., Schmid, P., Deleuzene, L. K., Kivell, T. L., Garvin, H. M., Williams, S. A. and DeSilva, J. M. (2015). *Homo naledi*, a new species of the genus *Homo* from the Dinaledi Chamber, South Africa. *elife*, 4e09560.
- Berger, L. R., Hawks, J., Dirks, P. H., Elliott, M. and Roberts, E. M. (2017). *Homo naledi* and Pleistocene hominin evolution in subequatorial Africa. *elife*, 6e24234.
- Berthaume, M. A., Deleuzene, L. K. and Kupczik, K. (2018). Dental topography and the diet of *Homo naledi*. *Journal of Human Evolution*, 11814-26.
- Bertram, J. E. A. and Swartz, S. M. (1991). The 'law of bone transformation': a case of crying Wolff? *Biological Reviews*, 66(3), 245-273.
- Best, A., Holt, B., Troy, K. and Hamill, J. (2017). Trabecular bone in the calcaneus of runners. *PLoS One*, 12(11), e0188200.
- Best, G. M., Mack, Z. E., Pichora, D. R., Crisco, J. J., Kamal, R. N. and Rainbow, M. J. (2019). Differences in the rotation axes of the scapholunate joint during flexion-extension and radial-ulnar deviation motions. *The Journal of hand surgery*, 44(9), 772-778.
- Biewener, A. A., Fazzalari, N. L., Konieczynski, D. and Baudinette, R. V. (1996). Adaptive changes in trabecular architecture in relation to functional strain patterns and disuse. *Bone*, 19(1), 1-8.
- Bird, E. E., Kivell, T. L. and Skinner, M. M. (2021). Cortical and trabecular bone structure of the hominoid capitate. *Journal of anatomy* 239(2), 351-373.
- Bird, E. E., Kivell, T. L. and Skinner, M. M. (2022). Patterns of internal bone structure and functional adaptation in the hominoid scaphoid, lunate, and triquetrum. *American Journal of Biological Anthropology*, 177(2), 266-285.
- Birkett, L. P. and Newton-Fisher, N. E. (2011). How abnormal is the behaviour of captive, zoo-living chimpanzees? *PloS One*, 6(6), e20101.
- Birkhold, A. I., Razi, H., Duda, G. N., Weinkamer, R., Checa, S. and Willie, B. M. (2014). The influence of age on adaptive bone formation and bone resorption. *Biomaterials*, 35(34), 9290-9301.
- Blinkhorn, J., Zanolli, C., Compton, T., Groucutt, H. S., Scerri, E. M., Crété, L., Stringer, C., Petraglia, M. D. and Blockley, S. (2021). Nubian Levallois technology associated with southernmost Neanderthals. *Scientific Reports*, 11(1), 1-13.

- Bloch, J. I. and Boyer, D. M. (2002). Grasping primate origins. *Science*, 298(5598), 1606-1610.
- Boesch, C. and Boesch, H. 1993. Different hand postures for pounding nuts with natural hammers by wild chimpanzees. In: PREUSCHOFT, H. & CHIVERS, D. J. (eds.) *Hands of primates*. Vienna: Springer-Verlag. pp. 31-43.
- Borel, A., Dobosi, V. and Moncel, M.-H. (2017). Neanderthal's microlithic tool production and use, the case of Tata (Hungary). *Quaternary International*, 4355-20.
- Brainerd, E. L., Baier, D. B., Gatesy, S. M., Hedrick, T. L., Metzger, K. A., Gilbert, S. L. and Crisco, J. J. (2010). X-ray reconstruction of moving morphology (XROMM): precision, accuracy and applications in comparative biomechanics research. *Journal of Experimental Zoology Part A: Ecological Genetics and Physiology*, 313(5), 262-279.
- Bramble, D. M. and Lieberman, D. E. (2004). Endurance running and the evolution of *Homo*. *Nature*, 432(7015), 345-352.
- Breuer, T., Ndoundou-Hockemba, M. and Fishlock, V. (2005). First observation of tool use in wild gorillas. *PLoS biology*, 3(11), e380.
- Bright, C. M. (2014). *A History of Rock Climbing Gear Technology and Standards*. BSc, University of Arkansas
- Brigstocke, G. H. O., Hearnden, A., Holt, C. and Whatling, G. (2014). In-vivo confirmation of the use of the dart thrower's motion during activities of daily living. *The Journal of hand surgery*, 39(4), 373-378.
- Brown, P., Sutikna, T., Morwood, M. J., Soejono, R. P., Saptomo, E. W. and Due, R. A. (2004). A new small-bodied hominin from the Late Pleistocene of Flores, Indonesia. *Nature*, 431(7012), 1055-1061.
- Brumm, A., Aziz, F., Van Den Bergh, G. D., Morwood, M. J., Moore, M. W., Kurniawan, I., Hobbs, D. R. and Fullagar, R. (2006). Early stone technology on Flores and its implications for *Homo floresiensis*. *Nature*, 441(7093), 624-628.
- Brumm, A., Jensen, G. M., van den Bergh, G. D., Morwood, M. J., Kurniawan, I., Aziz, F. and Storey, M. (2010). Hominins on Flores, Indonesia, by one million years ago. *Nature*, 464(7289), 748-752.
- Brumm, A., van Den Bergh, G. D., Storey, M., Kurniawan, I., Alloway, B. V., Setiawan, R., Setiyabudi, E., Grün, R., Moore, M. W. and Yurnaldi, D. (2016). Age and context of the oldest known hominin fossils from Flores. *Nature*, 534(7606), 249-253.
- Buijze, G. A., Lozano-Calderon, S. A., Strackee, S. D., Blankevoort, L. and Jupiter, J. B. (2011). Osseous and ligamentous scaphoid anatomy: Part I. A systematic literature review highlighting controversies. *The Journal of hand surgery*, 36(12), 1926-1935.
- Burkett, J. L. and Geissler, W. B. 2015. Anatomy of the Triangular Fibrocartilage Complex. In: GEISSLER, W. B. (ed.) *Wrist and Elbow Arthroscopy*. New York: Springer. pp. 47-58.
- Buzug, T. M. 2011. Computed tomography. In: KRAMME, R., HOFFMANN, K.-P. & POZOS, R. S. (eds.) *Springer Handbook of Medical Technology*. Germany: Springer. pp. 311-342.
- Caler, W. E. and Carter, D. R. (1989). Bone creep-fatigue damage accumulation. *Journal of Biomechanics*, 22(6-7), 625-635.
- Cant, J. G. (1987). Positional behavior of female Bornean orangutans (*Pongo pygmaeus*). *American Journal of Primatology*, 12(1), 71-90.
- Carlson, K. J. (2005). Investigating the form-function interface in African apes: Relationships between principal moments of area and positional behaviors in femoral and humeral diaphyses. *American Journal of Physical Anthropology*, 127(3), 312-334.
- Carlson, K. J., Doran-Sheehy, D. M., Hunt, K. D., Nishida, T., Yamanaka, A. and Boesch, C. (2006). Locomotor behavior and long bone morphology in individual free-ranging chimpanzees. *Journal of Human Evolution*, 50(4), 394-404.
- Carlson, K. J. and Patel, B. A. (2006). Habitual use of the primate forelimb is reflected in the material properties of subchondral bone in the distal radius. *Journal of anatomy*, 208(6), 659-670.

- Carlson, K. J., Stout, D., Jashashvili, T., De Ruiter, D. J., Tafforeau, P., Carlson, K. and Berger, L. R. (2011). The endocast of MH1, *Australopithecus sediba*. *Science*, 333(6048), 1402-1407.
- Cartmill, M. (1992). New views on primate origins. *Evolutionary Anthropology: Issues, News, and Reviews*, 1(3), 105-111.
- Cartmill, M. and Milton, K. (1977). The lorisiform wrist joint and the evolution of "brachiating" adaptations in the Hominoidea. *American Journal of Physical Anthropology*, 47(2), 249-272.
- Casado, A., Avià, Y., Llorente, M., Riba, D., Pastor, J. F. and Potau, J. M. (2021). Effects of Captivity on the Morphology of the Insertion Sites of the Palmar Radiocarpal Ligaments in Hominoid Primates. *Animals*, 11(7), 1856.
- Chappell, J., Phillips, A. C., van Noordwijk, M. A., Setia, T. M. and Thorpe, S. K. S. (2015). The Ontogeny of gap crossing behaviour in Bornean orangutans (*Pongo pygmaeus wurmbii*). *PLoS One*, 10(7), e0130291.
- Chazan, M., Ron, H., Matmon, A., Porat, N., Goldberg, P., Yates, R., Avery, M., Sumner, A. and Horwitz, L. K. (2008). Radiometric dating of the Earlier Stone Age sequence in excavation I at Wonderwerk Cave, South Africa: preliminary results. *Journal of Human Evolution*, 55(1), 1-11.
- Chirchir, H., Kivell, T. L., Ruff, C. B., Hublin, J. J., Carlson, K. J., Zipfel, B. and Richmond, B. G. (2015). Recent origin of low trabecular bone density in modern humans. *Proceedings of the National Academy of Sciences*, 112(2), 366-371.
- Chirchir, H., Ruff, C. B., Junno, J. A. and Potts, R. (2017). Low trabecular bone density in recent sedentary modern humans. *American Journal of Physical Anthropology*, 162(3), 550-560.
- Christen, P., Ito, K. and van Rietbergen, B. (2015). A potential mechanism for allometric trabecular bone scaling in terrestrial mammals. *Journal of anatomy*, 226(3), 236-243.
- Christen, P., Schulte, F. A., Zwahlen, A., Van Rietbergen, B., Boutroy, S., Melton III, L. J., Amin, S., Khosla, S., Goldhahn, J. and Müller, R. (2016). Voxel size dependency, reproducibility and sensitivity of an in vivo bone loading estimation algorithm. *Journal of The Royal Society Interface*, 13(114), 20150991.
- Churchill, S. E. (2001). Hand morphology, manipulation, and tool use in Neandertals and early modern humans of the Near East. *Proceedings of the National Academy of Sciences*, 98(6), 2953-2955.
- Churchill, S. E., Holliday, T. W., Carlson, K. J., Jashashvili, T., Macias, M. E., Mathews, S., Sparling, T. L., Schmid, P., de Ruiter, D. J. and Berger, L. R. (2013). The upper limb of *Australopithecus sediba*. *Science*, 340(6129), 1233-1237.
- Coddington, J. A. (1988). Cladistic tests of adaptational hypotheses. *Cladistics*, 4(1), 3-22.
- Cohen, J. (2013). *Statistical power analysis for the behavioral sciences*, New York, Academic press.
- Cooney, W. P. and Chao, E. Y. (1977). Biomechanical analysis of static forces in the thumb during hand function. *The Journal of bone and joint surgery*, 59(1), 27-36.
- Cooper, D., Kawalilak, C., Harrison, K., Johnston, B. and Johnston, J. (2016). Cortical bone porosity: what is it, why is it important, and how can we detect it? *Current osteoporosis reports*, 14(5), 187-198.
- Coppa, A., Grün, R., Stringer, C., Eggins, S. and Vargiu, R. (2005). Newly recognized Pleistocene human teeth from Tabun cave, Israel. *Journal of Human Evolution*, 49(3), 301-315.
- Corruccini, R. S. (1978). Comparative osteometrics of the hominoid wrist joint, with special reference to knuckle-walking. *Journal of Human Evolution*, 7(4), 307-321.

- Cotter, M. M., Simpson, S. W., Latimer, B. M. and Hernandez, C. J. (2009). Trabecular microarchitecture of hominoid thoracic vertebrae. *The Anatomical Record*, 292(8), 1098-1106.
- Cowin, S. C. (2001). *Bone mechanics handbook*, New York, CRC press.
- Crast, J., Fragaszy, D., Hayashi, M. and Matsuzawa, T. (2009). Dynamic in-hand movements in adult and young juvenile chimpanzees (*Pan troglodytes*). *American Journal of Physical Anthropology*, 138(3), 274-285.
- Crisco, J. J., Coburn, J. C., Moore, D. C., Akelman, E., Weiss, A.-P. C. and Wolfe, S. W. (2005). In vivo radiocarpal kinematics and the dart thrower's motion. *The Journal of bone and joint surgery*, 87(12), 2729-2740.
- Crisco, J. J., Heard, W. M., Rich, R. R., Paller, D. J. and Wolfe, S. W. (2011). The mechanical axes of the wrist are oriented obliquely to the anatomical axes. *The Journal of bone and joint surgery*, 93(2), 169-177.
- Currey, J. D. (2002). *Bones; Structure and Mechanics*, Oxford, Princeton University Press.
- Currey, J. D. (2003). The many adaptations of bone. *Journal of Biomechanics*, 36(10), 1487-1495.
- Dainton, M. and Macho, G. A. (1999). Did knuckle walking evolve twice? *Journal of Human Evolution*, 36(2), 171-194.
- Davies, A. B., Ancrenaz, M., Oram, F. and Asner, G. P. (2017). Canopy structure drives orangutan habitat selection in disturbed Bornean forests. *Proceedings of the National Academy of Sciences*, 114(31), 8307-8312.
- Demes, B., Jungers, W. L. and Walker, C. (2000). Cortical bone distribution in the femoral neck of strepsirrhine primates. *Journal of Human Evolution*, 39(4), 367-379.
- Demes, B., Qin, Y. X., Stern, J. T., Larson, S. G. and Rubin, C. T. (2001). Patterns of strain in the macaque tibia during functional activity. *American Journal of Physical Anthropology*, 116(4), 257-265.
- DeSilva, J. M. (2010). Revisiting the "midtarsal break". *American Journal of Physical Anthropology*, 141(2), 245-258.
- DeSilva, J. M., Carlson, K. J., Claxton, A. G., Harcourt-Smith, W. E., McNutt, E. J., Sylvester, A. D., Walker, C. S., Zipfel, B., Churchill, S. E. and Berger, L. R. (2018). *Australopithecus sediba*---The Anatomy of the Lower Limb Skeleton of *Australopithecus sediba*. *PaleoAnthropology*, 2018357-405.
- DeSilva, J. M. and Devlin, M. J. (2012). A comparative study of the trabecular bony architecture of the talus in humans, non-human primates, and *Australopithecus*. *Journal of Human Evolution*, 63(3), 536-551.
- DeSilva, J. M., Holt, K. G., Churchill, S. E., Carlson, K. J., Walker, C. S., Zipfel, B. and Berger, L. R. (2013). The lower limb and mechanics of walking in *Australopithecus sediba*. *Science*, 340(6129), 1232999.
- Dirks, P. H., Kibii, J. M., Kuhn, B. F., Steininger, C., Churchill, S. E., Kramers, J. D., Pickering, R., Farber, D. L., Mériaux, A.-S. and Herries, A. I. (2010). Geological setting and age of *Australopithecus sediba* from southern Africa. *Science*, 328(5975), 205-208.
- Dirks, P. H., Roberts, E. M., Hilbert-Wolf, H., Kramers, J. D., Hawks, J., Dosseto, A., Duval, M., Elliott, M., Evans, M. and Grün, R. (2017). The age of *Homo naledi* and associated sediments in the Rising Star Cave, South Africa. *elife*, 6e24231.
- Doblaré, M., Garcia, J. M. and Gómez, M. J. (2004). Modelling bone tissue fracture and healing: a review. *Engineering Fracture Mechanics*, 71(13-14), 1809-1840.
- Domalain, M., Bertin, A. and Daver, G. (2017). Was *Australopithecus afarensis* able to make the Lomekwian stone tools? Towards a realistic biomechanical simulation of hand force capability in fossil hominins and new insights on the role of the fifth digit. *Comptes Rendus Palevol*, 16(5-6), 572-584.

- Doran, D. M. (1992). The ontogeny of chimpanzee and pygmy chimpanzee locomotor behavior: a case study of paedomorphism and its behavioral correlates. *Journal of Human Evolution*, 23(2), 139-157.
- Doran, D. M. (1993a). Comparative locomotor behavior of chimpanzees and bonobos: the influence of morphology on locomotion. *American Journal of Physical Anthropology*, 91(1), 83-98.
- Doran, D. M. (1993b). Sex differences in adult chimpanzee positional behavior: the influence of body size on locomotion and posture. *American Journal of Physical Anthropology*, 91(1), 99-115.
- Doran, D. M. 1996. Comparative positional behavior of the African apes. In: MCGREW, W. C., MARCHANT, L. F. & NISHIDA, T. (eds.) *Great ape societies*. Cambridge: Cambridge University Press. pp. 213-224.
- Doran, D. M. (1997). Ontogeny of locomotion in mountain gorillas and chimpanzees. *Journal of Human Evolution*, 32(4), 323-344.
- Doran, D. M. and Hunt, K. D. 1994. Comparative Locomotor Behavior of Chimpanzees and Bonobos: Species and Habitat Differences. In: WRANGHAM, R. W. M., W. C & DE WAAL, F. (eds.) *Chimpanzee Cultures*. USA: Harvard University Press. pp. 93.
- Doube, M., Conroy, A. W., Christiansen, P., Hutchinson, J. R. and Shefelbine, S. (2009). Three-dimensional geometric analysis of felid limb bone allometry. *PLoS One*, 4(3), e4742.
- Doube, M., Kłosowski, M. M., Arganda-Carreras, I., Cordelières, F. P., Dougherty, R. P., Jackson, J. S., Schmid, B., Hutchinson, J. R. and Shefelbine, S. J. (2010). BoneJ: free and extensible bone image analysis in ImageJ. *Bone*, 47(6), 1076-1079.
- Doube, M., Kłosowski, M. M., Wiktorowicz-Conroy, A. M., Hutchinson, J. R. and Shefelbine, S. J. (2011). Trabecular bone scales allometrically in mammals and birds. *Proceedings of the Royal Society B: Biological Sciences*, 278(1721), 3067-3073.
- Du, A. and Alemseged, Z. (2019). Temporal evidence shows *Australopithecus sediba* is unlikely to be the ancestor of *Homo*. *Science advances*, 5(5), eaav9038.
- Duckworth, W. (1900). On a collection of crania, with two skeletons, of the Mori-ori, or aborigines of the Chatham Islands. With a note on some crania from the same islands now in the Museum of the Royal College of Surgeons. *Journal of the Anthropological Institute of Great Britain and Ireland*, 141-152.
- Dunmore, C. J. (2019). *Evolution in the palm of the human hand: Functional inferences from internal bone architecture in great apes and fossil hominins*. PhD, University of Kent.
- Dunmore, C. J., Bardo, A., Skinner, M. M. and Kivell, T. L. (2020a). Trabecular variation in the first metacarpal and manipulation in hominids. *American Journal of Physical Anthropology*, 171(2), 219-241.
- Dunmore, C. J., Kivell, T. L., Bardo, A. and Skinner, M. M. (2019). Metacarpal trabecular bone varies with distinct hand-positions used in hominid locomotion. *Journal of anatomy*, 235(1), 45-66.
- Dunmore, C. J., Skinner, M. M., Bardo, A., Berger, L. R., Hublin, J.-J., Pahr, D. H., Rosas, A., Stephens, N. B. and Kivell, T. L. (2020b). The position of *Australopithecus sediba* within fossil hominin hand use diversity. *Nature Ecology & Evolution*, 4(7), 911-918.
- Dunmore, C. J., Wollny, G. and Skinner, M. M. (2018). MIA-Clustering: a novel method for segmentation of paleontological material. *PeerJ*, 6e4374.
- Dusseldorp, G. L. and Lombard, M. (2021). Constraining the likely technological niches of late Middle Pleistocene hominins with *Homo naledi* as case study. *Journal of Archaeological Method and Theory*, 28(1), 11-52.
- Dusseldorp, G. L., Lombard, M. and Wurz, S. (2013). Pleistocene *Homo* and the updated stone age sequence of South Africa. *South African Journal of Science*, 109(5), 1-7.
- Edirisinghe, Y., Troupis, J., Patel, M., Smith, J. and Crossett, M. (2014). Dynamic motion analysis of dart throwers motion visualized through computerized tomography and

- calculation of the axis of rotation. *The Journal of hand surgery (European Volume)*, 39(4), 364-372.
- Eriksen, E. F. (2010). Cellular mechanisms of bone remodeling. *Reviews in Endocrine and Metabolic Disorders*, 11(4), 219-227.
- Eriksen, E. F., Melsen, F., Sod, E., Barton, I. and Chines, A. (2002). Effects of long-term risedronate on bone quality and bone turnover in women with postmenopausal osteoporosis. *Bone*, 31(5), 620-625.
- Fajardo, R. J., Desilva, J. M., Manoharan, R. K., Schmitz, J. E., Maclatchy, L. M. and Bouxsein, M. L. (2013). Lumbar vertebral body bone microstructural scaling in small to medium-sized strepsirhines. *The Anatomical Record*, 296(2), 210-226.
- Fajardo, R. J. and Müller, R. (2001). Three-dimensional analysis of nonhuman primate trabecular architecture using micro-computed tomography. *American Journal of Physical Anthropology*, 115(4), 327-336.
- Fajardo, R. J., Müller, R., Ketcham, R. A. and Colbert, M. (2007). Nonhuman anthropoid primate femoral neck trabecular architecture and its relationship to locomotor mode. *The Anatomical Record*, 290(4), 422-436.
- Falk, D., Hildebolt, C., Smith, K., Morwood, M. J., Sutikna, T., Brown, P., Jatmiko, Saptomo, E. W., Brunnsden, B. and Prior, F. (2005). The brain of LB1, *Homo floresiensis*. *Science*, 308(5719), 242-245.
- Falótico, T., Proffitt, T., Ottoni, E. B., Staff, R. A. and Haslam, M. (2019). Three thousand years of wild capuchin stone tool use. *Nature Ecology & Evolution*, 3(7), 1034-1038.
- Feuerriegel, E. M., Green, D. J., Walker, C. S., Schmid, P., Hawks, J., Berger, L. R. and Churchill, S. E. (2017). The upper limb of *Homo naledi*. *Journal of Human Evolution*, 104, 155-173.
- Feuerriegel, E. M., Voisin, J.-L., Churchill, S., Haeusler, M., Mathews, S., Schmid, P., Hawks, J. and Berger, L. R. (2019). Upper limb fossils of *Homo naledi* from the lesedi chamber, rising Star System, South Africa. *PaleoAnthropology*, 2019, 311-349.
- Finestone, E. M., Brown, M. H., Ross, S. R. and Pontzer, H. (2018). Great ape walking kinematics: Implications for hominoid evolution. *American Journal of Physical Anthropology*, 166(1), 43-55.
- Fisk, G. 1981. Biomechanics of the wrist joint. In: TUBIANA, R. (ed.) *The Hand*. Philadelphia: WB Saunders. pp. 136-141.
- Formicola, V., Pettitt, P. and DelLucchese, A. (2004). A direct AMS radiocarbon date on the Barma Grande 6 Upper Paleolithic skeleton. *Current Anthropology*, 45(1), 114-118.
- Fox, A. J. S., Bedi, A. and Rodeo, S. A. (2009). The basic science of articular cartilage: structure, composition, and function. *Sports health*, 1(6), 461-468.
- Fragaszy, D. M. and Crast, J. 2016. Functions of the hand in primates. In: KIVELL, T. L., LEMELIN, P., RICHMOND, B. G. & SCHMITT, D. (eds.) *The evolution of the primate hand*. New York: Springer. pp. 313-344.
- Frost, H. M. (1987). Bone "mass" and the "mechanostat": a proposal. *The Anatomical Record*, 219(1), 1-9.
- Fuss, F. K. and Niegl, G. (2012). Finger load distribution in different types of climbing grips. *Sports Technology*, 5(3-4), 151-155.
- Galletta, L., Stephens, N. B., Bardo, A., Kivell, T. L. and Marchi, D. (2019). Three-dimensional geometric morphometric analysis of the first metacarpal distal articular surface in humans, great apes and fossil hominins. *Journal of Human Evolution*, 132, 119-136.
- Garcia-Elias, M. (1997). Kinetic analysis of carpal stability during grip. *Hand clinics*, 13(1), 151-158.
- Garcia-Elias, M., Alomar Serrallach, X. and Monill Serra, J. (2014). Dart-throwing motion in patients with scapholunate instability: a dynamic four-dimensional computed tomography study. *The Journal of hand surgery (European Volume)*, 39(4), 346-352.

- Garcia-Elias, M., de la Bellacasa, I. P. and Schouten, C. (2017). Carpal ligaments: a functional classification. *Hand clinics*, 33(3), 511-520.
- Garcia-Elias, M. and Lluch, A. (2001). Partial excision of scaphoid: is it ever indicated? *Hand clinics*, 17(4), 687-95.
- Garcia-Elias, M., Ribe, M., Rodriguez, J., Cots, M. and Casas, J. (1995). Influence of joint laxity on scaphoid kinematics. *The Journal of hand surgery*, 20(3), 379-382.
- Garcia-Elias, M., Smith, D. K., Ruby, L. K., Horii, E., An, K.-N., Linscheid, R. L., Chao, E. Y. S. and Cooney, W. P. 1994. Normal and abnormal carpal kinematics. In: SCHUIND, F., AN, K. N., COONEY III, W. P. & GARCIA-ELIAS, M. (eds.) *Advances in the biomechanics of the hand and wrist*. New York: Springer. pp. 247-253.
- Gatesy, S. M., Baier, D. B., Jenkins, F. A. and Dial, K. P. (2010). Scientific rotoscoping: a morphology-based method of 3-D motion analysis and visualization. *Journal of Experimental Zoology Part A: Ecological Genetics and Physiology*, 313(5), 244-261.
- Georgiou, L., Dunmore, C. J., Bardo, A., Buck, L. T., Hublin, J. J., Pahr, D. H., Stratford, D., Synek, A., Kivell, T. L. and Skinner, M. M. (2020). Evidence for habitual climbing in a Pleistocene hominin in South Africa. *Proceedings of the National Academy of Sciences*, 117(15), 8416-8423.
- Georgiou, L., Kivell, T. L., Pahr, D. H., Buck, L. T. and Skinner, M. M. (2019). Trabecular architecture of the great ape and human femoral head. *Journal of anatomy*, 234(5), 679-693.
- Georgiou, L., Kivell, T. L., Pahr, D. H. and Skinner, M. M. (2018). Trabecular bone patterning in the hominoid distal femur. *PeerJ*, 6e5156.
- Gíslason, M. K., Nash, D. H., Nicol, A., Kanellopoulos, A., Bransby-Zachary, M., Hems, T., Condon, B. and Stansfield, B. (2009). A three-dimensional finite element model of maximal grip loading in the human wrist. *Proceedings of the Institution of Mechanical Engineers, Part H: Journal of Engineering in Medicine*, 223(7), 849-861.
- Gíslason, M. K., Stansfield, B., Bransby-Zachary, M., Hems, T. and Nash, D. (2012). Load transfer through the radiocarpal joint and the effects of partial wrist arthrodesis on carpal bone behaviour: a finite element study. *The Journal of hand surgery (European Volume)*, 37(9), 871-878.
- Gordon, A. D., Nevell, L. and Wood, B. (2008). The *Homo floresiensis* cranium (LB1): Size, scaling, and early *Homo* affinities. *Proceedings of the National Academy of Sciences*, 105(12), 4650-4655.
- Granger, D. E., Gibbon, R. J., Kuman, K., Clarke, R. J., Bruxelles, L. and Caffee, M. W. (2015). New cosmogenic burial ages for Sterkfontein member 2 *Australopithecus* and member 5 Oldowan. *Nature*, 522(7554), 85-88.
- Green, D. J. and Gordon, A. D. (2008). Metacarpal proportions in *Australopithecus africanus*. *Journal of Human Evolution*, 54(5), 705-719.
- Griffin, N. L., D'Août, K., Ryan, T. M., Richmond, B. G., Ketcham, R. A. and Postnov, A. (2010). Comparative forefoot trabecular bone architecture in extant hominids. *Journal of Human Evolution*, 59(2), 202-213.
- Gross, T., Kivell, T. L., Skinner, M. M., Nguyen, H. and Pahr, D. H. (2014). Holistic analysis of bone. *Palaeontologia Electronica*, 17(3), 1.
- Grün, R. and Stringer, C. B. (1991). Electron spin resonance dating and the evolution of modern humans. *Archaeometry*, 33(2), 153-199.
- Gruss, L. T. and Schmitt, D. (2015). The evolution of the human pelvis: changing adaptations to bipedalism, obstetrics and thermoregulation. *Philosophical Transactions of the Royal Society B: Biological Sciences*, 370(1663), 20140063.
- Guo, X. E. (2001). Mechanical properties of cortical bone and cancellous bone tissue. *Bone mechanics handbook*, 101-23.

- Hadjidakis, D. J. and Androulakis, I. I. (2006). Bone remodeling. *Annals of the New York Academy of Sciences*, 1092(1), 385-396.
- Hagert, E., Forsgren, S. and Ljung, B. O. (2005). Differences in the presence of mechanoreceptors and nerve structures between wrist ligaments may imply differential roles in wrist stabilization. *Journal of Orthopaedic Research*, 23(4), 757-763.
- Hammond, M. A., Wallace, J. M., Allen, M. R. and Siegmund, T. (2018). Incorporating tissue anisotropy and heterogeneity in finite element models of trabecular bone altered predicted local stress distributions. *Biomechanics and modeling in mechanobiology*, 17(2), 605-614.
- Hamrick, M. W. (1996). Functional morphology of the lemuriform wrist joints and the relationship between wrist morphology and positional behavior in arboreal primates. *American Journal of Physical Anthropology*, 99(2), 319-344.
- Hamrick, M. W., Churchill, S. E., Schmitt, D. and Hylander, W. L. (1998). EMG of the human flexor pollicis longus muscle: implications for the evolution of hominid tool use. *Journal of Human Evolution*, 34(2), 123-136.
- Hanna, J. B., Granatosky, M. C., Rana, P. and Schmitt, D. (2017). The evolution of vertical climbing in primates: evidence from reaction forces. *Journal of Experimental Biology*, 220(17), 3039-3052.
- Hara, T., Horii, E., An, K.-N., Cooney, W. P., Linscheid, R. L. and Chao, E. Y. S. (1992). Force distribution across wrist joint: application of pressure-sensitive conductive rubber. *The Journal of hand surgery*, 17(2), 339-347.
- Harcourt-Smith, W. E., Throckmorton, Z., Congdon, K. A., Zipfel, B., Deane, A. S., Drapeau, M. S., Churchill, S. E., Berger, L. R. and DeSilva, J. M. (2015). The foot of *Homo naledi*. *Nature Communications*, 6(1), 1-8.
- Hardy, B. L., Moncel, M.-H., Daujeard, C., Fernandes, P., Béarez, P., Desclaux, E., Navarro, M. G. C., Puaud, S. and Gallotti, R. (2013). Impossible Neanderthals? Making string, throwing projectiles and catching small game during Marine Isotope Stage 4 (Abri du Maras, France). *Quaternary Science Reviews*, 8223-40.
- Hardy, B. L., Moncel, M.-H., Kerfant, C., Lebon, M., Bellot-Gurlet, L. and Mélard, N. (2020). Direct evidence of Neanderthal fibre technology and its cognitive and behavioral implications. *Scientific Reports*, 10(1), 1-9.
- Harmand, S., Lewis, J. E., Feibel, C. S., Lepre, C. J., Prat, S., Lenoble, A., Boës, X., Quinn, R. L., Brenet, M. and Arroyo, A. (2015). 3.3-million-year-old stone tools from Lomekwi 3, West Turkana, Kenya. *Nature*, 521(7552), 310-315.
- Hart, N. H., Nimphius, S., Rantalainen, T., Ireland, A., Sifarakas, A. and Newton, R. (2017). Mechanical basis of bone strength: influence of bone material, bone structure and muscle action. *Journal of Musculoskeletal and Neuronal Interactions*, 17(3), 114.
- Havill, L. M., Allen, M. R., Bredbenner, T. L., Burr, D. B., Nicoletta, D. P., Turner, C. H., Warren, D. M. and Mahaney, M. C. (2010). Heritability of lumbar trabecular bone mechanical properties in baboons. *Bone*, 46(3), 835-840.
- Hawks, J., Elliott, M., Schmid, P., Churchill, S. E., de Ruiter, D. J., Roberts, E. M., Hilbert-Wolf, H., Garvin, H. M., Williams, S. A. and Delezene, L. K. (2017). New fossil remains of *Homo naledi* from the Lesedi Chamber, South Africa. *elife*, 6e24232.
- Heinonen, A., Oja, P., Kannus, P., Sievänen, H., Mänttari, A. and Vuori, I. (1993). Bone mineral density of female athletes in different sports. *Bone and mineral*, 23(1), 1-14.
- Hershkovitz, I., Speirs, M. S., Frayer, D., Nadel, D., Wish-Baratz, S. and Arensburg, B. (1995). Ohalo II H2: A 19,000-year-old skeleton from a water-logged site at the Sea of Galilee, Israel. *American Journal of Physical Anthropology*, 96(3), 215-234.
- Hicks, M. and Hicks, A. (2001). *St Gregory's Priory, Northgate, Canterbury: Excavations 1988-1991*, Canterbury, UK, Canterbury Archaeological Trust Limited.

- Hildebrand, T. and Rügsegger, P. (1997). A new method for the model-independent assessment of thickness in three-dimensional images. *Journal of microscopy*, 185(1), 67-75.
- Holloway, R. L., Hurst, S. D., Garvin, H. M., Schoenemann, P. T., Vanti, W. B., Berger, L. R. and Hawks, J. (2018). Endocast morphology of *Homo naledi* from the Dinaledi Chamber, South Africa. *Proceedings of the National Academy of Sciences*, 115(22), 5738-5743.
- Holt, E., Dirks, P., Placzek, C. and Berger, L. (2016). The stable isotope setting of *Australopithecus sediba* at Malapa, South Africa. *South African Journal of Science*, 112(7-8), 1-9.
- Huiskes, R., Ruimerman, R., Van Lenthe, G. H. and Janssen, J. D. (2000). Effects of mechanical forces on maintenance and adaptation of form in trabecular bone. *Nature*, 405(6787), 704.
- Hunt, K. D. (1991a). Mechanical implications of chimpanzee positional behavior. *American Journal of Physical Anthropology*, 86(4), 521-536.
- Hunt, K. D. (1991b). Positional behavior in the Hominoidea. *International Journal of Primatology*, 12(2), 95-118.
- Hunt, K. D. (1992). Positional behavior of *Pan troglodytes* in the Mahale mountains and Gombe stream national parks, Tanzania. *American Journal of Physical Anthropology*, 87(1), 83-105.
- Hunt, K. D., Cant, J. G., Gebo, D. L., Rose, M. D., Walker, S. E. and Youlatos, D. (1996). Standardized descriptions of primate locomotor and postural modes. *Primates*, 37(4), 363-387.
- Inouye, S. E. (1992). Ontogeny and allometry of African ape manual rays. *Journal of Human Evolution*, 23(2), 107-138.
- Inouye, S. E. (1994). Ontogeny of knuckle-walking hand postures in African apes. *Journal of Human Evolution*, 26(5-6), 459-485.
- Isaksson, H., Töyräs, J., Hakulinen, M., Aula, A., Tamminen, I., Julkunen, P., Kröger, H. and Jurvelin, J. (2011). Structural parameters of normal and osteoporotic human trabecular bone are affected differently by microCT image resolution. *Osteoporosis International*, 22(1), 167-177.
- Isler, K. (2005). 3D-kinematics of vertical climbing in hominoids. *American Journal of Physical Anthropology*, 126(1), 66-81.
- Isler, K. and Thorpe, S. K. (2003). Gait parameters in vertical climbing of captive, rehabilitant and wild Sumatran orang-utans (*Pongo pygmaeus abelii*). *Journal of Experimental Biology*, 206(22), 4081-4096.
- Izard, R. M., Fraser, W. D., Negus, C., Sale, C. and Greeves, J. P. (2016). Increased density and periosteal expansion of the tibia in young adult men following short-term arduous training. *Bone*, 8813-19.
- Jenkins, F. A. and Fleagle, J. G. 1975. Knuckle-walking and the functional anatomy of the wrists in living apes. In: TUTTLE, R. (ed.) *Primate functional morphology and evolution*. The Hague: Mouton. pp. 213-227.
- Jouffroy, F. K. and Medina, M. F. (2002). Radio-ulnar deviation of the primate carpus: an X-ray study. *Zeitschrift für Morphologie und Anthropologie*, 275-289.
- Jungers, W. L. (1982). Lucy's limbs: skeletal allometry and locomotion in *Australopithecus afarensis*. *Nature*, 297(5868), 676-678.
- Jungers, W. L. (1984). Aspects of size and scaling in primate biology with special reference to the locomotor skeleton. *American Journal of Physical Anthropology*, 27(S5), 73-97.
- Jungers, W. L., Harcourt-Smith, W. E., Wunderlich, R., Tocheri, M. W., Larson, S. G., Sutikna, T., Due, R. A. and Morwood, M. J. (2009a). The foot of *Homo floresiensis*. *Nature*, 459(7243), 81-84.

- Jungers, W. L., Larson, S. G., Harcourt-Smith, W., Morwood, M. J., Sutikna, T., Awe, R. D. and Djubiantono, T. (2009b). Descriptions of the lower limb skeleton of *Homo floresiensis*. *Journal of Human Evolution*, 57(5), 538-554.
- Kalkwarf, H. J. and Specker, B. L. (1995). Bone mineral loss during lactation and recovery after weaning. *Obstetrics & Gynecology*, 86(1), 26-32.
- Kamal, R. N., Rainbow, M. J., Akelman, E. and Crisco, J. J. (2012). In vivo triquetrum-hamate kinematics through a simulated hammering task wrist motion. *The Journal of bone and joint surgery*, 94(12), e85.
- Kamal, R. N., Starr, A. and Akelman, E. (2016). Carpal kinematics and kinetics. *The Journal of hand surgery*, 41(10), 1011-1018.
- Karakostis, F. A., Hotz, G., Tournloukis, V. and Harvati, K. (2018). Evidence for precision grasping in Neandertal daily activities. *Science advances*, 4(9), eaat2369.
- Kaufman-Cohen, Y., Friedman, J., Levanon, Y., Jacobi, G., Doron, N. and Portnoy, S. (2018). Wrist plane of motion and range during daily activities. *American Journal of Occupational Therapy*, 72(6), 7206205080p1-7206205080p10.
- Kaufman-Cohen, Y., Portnoy, S., Levanon, Y. and Friedman, J. (2019). Does Object Height Affect the Dart Throwing Motion Angle during Seated Activities of Daily Living? *Journal of motor behavior*, 52(4), 456-465.
- Kaufmann, R., Pfaeffle, J., Blankenhorn, B., Stabile, K., Robertson, D. and Goitz, R. (2005). Kinematics of the midcarpal and radiocarpal joints in radioulnar deviation: an in vitro study. *The Journal of hand surgery*, 30(5), 937-942.
- Kendall, M. G. and Smith, B. B. (1939). The problem of m rankings. *The annals of mathematical statistics*, 10(3), 275-287.
- Kent, G. N., Price, R. I., Gutteridge, D. H., Allen, J. R., Rosman, K. J., Smith, M., Bhagat, C. I., Wilson, S. G. and Retallack, R. W. (1993). Effect of pregnancy and lactation on maternal bone mass and calcium metabolism. *Osteoporosis International*, 344-47.
- Kerr, D., Morton, A., Dick, I. and Prince, R. (1996). Exercise effects on bone mass in postmenopausal women are site-specific and load-dependent. *Journal of Bone and Mineral Research*, 11(2), 218-225.
- Key, A. and Dunmore, C. J. (2015). The evolution of the hominin thumb and the influence exerted by the non-dominant hand during stone tool production. *Journal of Human Evolution*, 7860-69.
- Key, A., Dunmore, C. J., Hatala, K. G. and Williams-Hatala, E. M. (2017). Flake morphology as a record of manual pressure during stone tool production. *Journal of Archaeological Science*, 1243-53.
- Key, A., Dunmore, C. J. and Marzke, M. W. (2019). The unexpected importance of the fifth digit during stone tool production. *Scientific Reports*, 9(1), 1-8.
- Key, A., Farr, I., Hunter, R., Mika, A., Eren, M. I. and Winter, S. L. (2021). Why invent the handle? Electromyography (EMG) and efficiency of use data investigating the prehistoric origin and selection of hafted stone knives. *Archaeological and Anthropological Sciences*, 13(10), 1-16.
- Key, A., Farr, I., Hunter, R. and Winter, S. L. (2020). Muscle recruitment and stone tool use ergonomics across three million years of Palaeolithic technological transitions. *Journal of Human Evolution*, 144102796.
- Key, A., Merritt, S. R. and Kivell, T. L. (2018). Hand grip diversity and frequency during the use of Lower Palaeolithic stone cutting-tools. *Journal of Human Evolution*, 125137-158.
- Kibij, J. M., Churchill, S. E., Schmid, P., Carlson, K. J., Reed, N. D., De Ruiter, D. J. and Berger, L. R. (2011). A partial pelvis of *Australopithecus sediba*. *Science*, 333(6048), 1407-1411.
- Kijima, Y. and Viegas, S. F. (2009). Wrist anatomy and biomechanics. *The Journal of hand surgery*, 34(8), 1555-1563.

- Kivell, T. L. (2011). A comparative analysis of the hominin triquetrum (SKX 3498) from Swartkrans, South Africa. *South African Journal of Science*, 107(5-6), 60-69.
- Kivell, T. L. (2015). Evidence in hand: recent discoveries and the early evolution of human manual manipulation. *Philosophical Transactions of the Royal Society B: Biological Sciences*, 370(1682), 20150105.
- Kivell, T. L. 2016a. The primate wrist. In: KIVELL, T. L., LEMELIN, P., RICHMOND, B. G. & SCHMITT, D. (eds.) *The evolution of the primate hand*. New York: Springer. pp. 17-54.
- Kivell, T. L. (2016b). A review of trabecular bone functional adaptation: what have we learned from trabecular analyses in extant hominoids and what can we apply to fossils? *Journal of anatomy*, 228(4), 569-594.
- Kivell, T. L., Barros, A. P. and Smaers, J. B. (2013). Different evolutionary pathways underlie the morphology of wrist bones in hominoids. *BMC evolutionary biology*, 13(1), 229.
- Kivell, T. L. and Begun, D. R. (2007). Frequency and timing of scaphoid-centrale fusion in hominoids. *Journal of Human Evolution*, 52(3), 321-340.
- Kivell, T. L., Churchill, S. E., Kibii, J. M., Schmid, P. and Berger, L. R. (2018a). The hand of *Australopithecus sediba*. *PaleoAnthropology*, 282-333.
- Kivell, T. L., Davenport, R., Hublin, J. J., Thackeray, J. F. and Skinner, M. M. (2018b). Trabecular architecture and joint loading of the proximal humerus in extant hominoids, *Ateles*, and *Australopithecus africanus*. *American Journal of Physical Anthropology*, 167(2), 348-365.
- Kivell, T. L., Deane, A. S., Tocheri, M. W., Orr, C. M., Schmid, P., Hawks, J., Berger, L. R. and Churchill, S. E. (2015). The hand of *Homo naledi*. *Nature Communications*, 68431.
- Kivell, T. L., Kibii, J. M., Churchill, S. E., Schmid, P. and Berger, L. R. (2011). *Australopithecus sediba* hand demonstrates mosaic evolution of locomotor and manipulative abilities. *Science*, 333(6048), 1411-1417.
- Kivell, T. L., Lemelin, P., Richmond, B. G. and Schmitt, D. (2016). *The evolution of the primate hand*, New York, Springer.
- Kivell, T. L., Rosas, A., Estalrich, A., Huguet, R., García-Taberner, A., Ríos, L. and de la Rasilla, M. (2018c). New Neandertal wrist bones from El Sidron, Spain (1994–2009). *Journal of Human Evolution*, 11445-75.
- Kivell, T. L. and Schmitt, D. (2009). Independent evolution of knuckle-walking in African apes shows that humans did not evolve from a knuckle-walking ancestor. *Proceedings of the National Academy of Sciences*, 106(34), 14241-14246.
- Koebke, J. 1993. Functional morphology of the human carpus. In: PREUSCHOFT, H. & CHIVERS, D. J. (eds.) *Hands of primates*. Vienna: Springer. pp. 235-244.
- Komza, K. and Skinner, M. M. (2019). First metatarsal trabecular bone structure in extant hominoids and Swartkrans hominins. *Journal of Human Evolution*, 1311-21.
- Kraft, T. S., Venkataraman, V. V. and Dominy, N. J. (2014). A natural history of human tree climbing. *Journal of Human Evolution*, 71105-118.
- Kubo, D., Kono, R. T. and Kaifu, Y. (2013). Brain size of *Homo floresiensis* and its evolutionary implications. *Proceedings of the Royal Society B: Biological Sciences*, 280(1760), 20130338.
- Kulothungan, G., Meyyappan Nachiappan, M. S. K. and Rajasekaran, S. (2013). Comparative study of forces involved in different styles of handwriting. *Journal of Automation and Control Engineering*, 1(3), 260-264.
- Kuman, K. and Clarke, R. J. (2000). Stratigraphy, artefact industries and hominid associations for Sterkfontein, Member 5. *Journal of Human Evolution*, 38(6), 827-847.
- Kuman, K., Granger, D. E., Gibbon, R. J., Pickering, T. R., Caruana, M. V., Bruxelles, L., Clarke, R. J., Heaton, J. L., Stratford, D. and Brain, C. (2021). A new absolute date from

- Swartkrans Cave for the oldest occurrences of *Paranthropus robustus* and Oldowan stone tools in South Africa. *Journal of Human Evolution*, 156103000.
- Laird, M. F., Schroeder, L., Garvin, H. M., Scott, J. E., Dembo, M., Radovčić, D., Musiba, C. M., Ackermann, R. R., Schmid, P. and Hawks, J. (2017). The skull of *Homo naledi*. *Journal of Human Evolution*, 104100-123.
- Larson, S. G., Jungers, W. L., Morwood, M. J., Sutikna, T., Saptomo, E. W., Due, R. A. and Djubiantono, T. (2007). *Homo floresiensis* and the evolution of the hominin shoulder. *Journal of Human Evolution*, 53(6), 718-731.
- Larson, S. G., Jungers, W. L., Tocheri, M. W., Orr, C. M., Morwood, M. J., Sutikna, T., Awe, R. D. and Djubiantono, T. (2009). Descriptions of the upper limb skeleton of *Homo floresiensis*. *Journal of Human Evolution*, 57(5), 555-570.
- Latimer, B. 1991. Locomotor adaptations in *Australopithecus afarensis*: the issue of arboreality. In: COPPENS, Y. S., B. (ed.) *Origine(s) de la Bipédie chez les Hominidés*. Paris: CNRS. pp. 169-176.
- Leakey, L. S., Tobias, P. V. and Napier, J. R. (1964). A new species of the genus *Homo* from Olduvai Gorge. *Nature*, 202(4927), 7-9.
- Leakey, L. S., Tobias, P. V. and Napier, J. R. (1965). A new species of genus *Homo* from Olduvai Gorge. *Current Anthropology*, 6(4), 424-427.
- Leder, D., Hermann, R., Hüls, M., Russo, G., Hoelzmann, P., Nielbock, R., Böhner, U., Lehmann, J., Meier, M. and Schwalb, A. (2021). A 51,000-year-old engraved bone reveals Neanderthals' capacity for symbolic behaviour. *Nature Ecology & Evolution*, 5(9), 1273-1282.
- Lemelin, P. and Diogo, R. 2016. Anatomy, Function, and Evolution of the Primate Hand Musculature. In: KIVELL, T. L., LEMELIN, P., RICHMOND, B. G. & SCHMITT, D. (eds.) *The evolution of the primate hand*. New York: Springer. pp. 155-193.
- Lemelin, P. and Schmitt, D. 2016. On primitiveness, prehensility, and opposability of the primate hand: the contributions of Frederic Wood Jones and John Russell Napier. In: KIVELL, T. L., LEMELIN, P., RICHMOND, B. G. & SCHMITT, D. (eds.) *The evolution of the primate hand*. New York: Springer. pp. 5-13.
- Lewis, O. J. (1971). Biological Sciences: Brachiation and the Early Evolution of the Hominoidea. *Nature*, 230(5296), 577-579.
- Lewis, O. J. (1972). Osteological features characterizing the wrists of monkeys and apes, with a reconsideration of this region in *Dryopithecus (Proconsul) africanus*. *American Journal of Physical Anthropology*, 36(1), 45-58.
- Lewis, O. J. (1977). Joint remodelling and the evolution of the human hand. *Journal of anatomy*, 123(Pt 1), 157-201.
- Lewis, O. J. (1989). *Functional morphology of the evolving hand and foot*, New York, Oxford University Press, USA.
- Li, J., Bao, Q., Chen, S., Liu, H., Feng, J., Qin, H., Li, A., Liu, D., Shen, Y. and Zhao, Y. (2017). Different bone remodeling levels of trabecular and cortical bone in response to changes in Wnt/ β -catenin signaling in mice. *Journal of Orthopaedic Research*, 35(4), 812-819.
- Li, Z.-M. (2002). The influence of wrist position on individual finger forces during forceful grip. *The Journal of hand surgery*, 27(5), 886-896.
- Lieberman, D. E. (1996). How and why humans grow thin skulls: experimental evidence for systemic cortical robusticity. *American Journal of Physical Anthropology*, 101(2), 217-236.
- Lieberman, D. E. (1997). Making behavioral and phylogenetic inferences from hominid fossils: considering the developmental influence of mechanical forces. *Annual Review of Anthropology*, 26(1), 185-210.

- Lindsay, R., Nieves, J., Formica, C., Henneman, E., Woelfert, L., Shen, V., Dempster, D. and Cosman, F. (1997). Randomised controlled study of effect of parathyroid hormone on vertebral-bone mass and fracture incidence among postmenopausal women on oestrogen with osteoporosis. *The Lancet*, 350(9077), 550-555.
- Lorenzo, C., Arsuaga, J. L. and Carretero, J. M. (1999). Hand and foot remains from the Gran Dolina early Pleistocene site (Sierra de Atapuerca, Spain). *Journal of Human Evolution*, 37(3-4), 501-522.
- Lorenzo, C., Pablos, A., Carretero, J. M., Huguet, R., Valverdú, J., Martín-Torres, M., Arsuaga, J. L., Carbonell, E. and de Castro, J. M. B. (2015). Early Pleistocene human hand phalanx from the Sima del Elefante (TE) cave site in Sierra de Atapuerca (Spain). *Journal of Human Evolution*, 78114-121.
- Lovejoy, C. O., McCollum, M. A., Reno, P. L. and Rosenman, B. A. (2003). Developmental biology and human evolution. *Annual Review of Anthropology*, 32(1), 85-109.
- MacConaill, M. (1941). The mechanical anatomy of the carpus and its bearings on some surgical problems. *Journal of anatomy*, 75(Pt 2), 166.
- MacLatchy, L. and Müller, R. (2002). A comparison of the femoral head and neck trabecular architecture of Galago and Perodicticus using micro-computed tomography (μ CT). *Journal of Human Evolution*, 43(1), 89-105.
- Malaivijitnond, S., Lekprayoon, C., Tandavanittj, N., Panha, S., Cheewatham, C. and Hamada, Y. (2007). Stone-tool usage by Thai long-tailed macaques (*Macaca fascicularis*). *American Journal of Primatology*, 69(2), 227-233.
- Manduell, K. L., Morrogh-Bernard, H. C. and Thorpe, S. K. S. (2011). Locomotor behavior of wild orangutans (*Pongo pygmaeus wurmbii*) in disturbed peat swamp forest, Sabangau, Central Kalimantan, Indonesia. *American Journal of Physical Anthropology*, 145(3), 348-359.
- Maquer, G., Musy, S. N., Wandel, J., Gross, T. and Zysset, P. K. (2015). Bone volume fraction and fabric anisotropy are better determinants of trabecular bone stiffness than other morphological variables. *Journal of bone and mineral research*, 30(6), 1000-1008.
- Marangoni, A., Belli, M. L., Caramelli, D., Moggi Cecchi, J., Zavattaro, M. and Manzi, G. (2011). Tierra del Fuego, its ancient inhabitants, and the collections of skeletal remains in the Museum of Anthropology of Florence and Rome. *Museologia Scientifica*, 5(1-2), 88-96.
- Marchi, D., Sparacello, V. and Shaw, C. 2011. Mobility and lower limb robusticity of a pastoralist Neolithic population from North-Western Italy. In: PINHASI, R. & STOCK, J. (eds.) *Human bioarchaeology of the transition to agriculture*. Chichester: John Wiley & Sons. pp. 317-346.
- Marchi, D., Walker, C. S., Wei, P., Holliday, T. W., Churchill, S. E., Berger, L. R. and DeSilva, J. M. (2017). The thigh and leg of *Homo naledi*. *Journal of Human Evolution*, 104174-204.
- Martin, R. B., Burr, D. B. and Sharkey, N. A. (1998). *Skeletal tissue mechanics*, New York, Springer.
- Marzke, M. W. (1983). Joint functions and grips of the *Australopithecus afarensis* hand, with special reference to the region of the capitate. *Journal of Human Evolution*, 12(2), 197-211.
- Marzke, M. W. (1997). Precision grips, hand morphology, and tools. *American Journal of Physical Anthropology*, 102(1), 91-110.
- Marzke, M. W. (2009). Upper-limb evolution and development. *JBSJ*, 91(Supplement_4), 26-30.
- Marzke, M. W. (2013). Tool making, hand morphology and fossil hominins. *Philosophical Transactions of the Royal Society B: Biological Sciences*, 368(1630), 1-8.

- Marzke, M. W., Marchant, L. F., McGrew, W. C. and Reece, S. P. (2015). Grips and hand movements of chimpanzees during feeding in Mahale Mountains National Park, Tanzania. *American Journal of Physical Anthropology*, 156(3), 317-326.
- Marzke, M. W. and Marzke, R. F. (1987). The third metacarpal styloid process in humans: origin and functions. *American Journal of Physical Anthropology*, 73(4), 415-431.
- Marzke, M. W. and Shackley, M. S. (1986). Hominid hand use in the Pliocene and Pleistocene: evidence from experimental archaeology and comparative morphology. *Journal of Human Evolution*, 15(6), 439-460.
- Marzke, M. W., Tocheri, M. W., Steinberg, B., Femiani, J. D., Reece, S. P., Linscheid, R. L., Orr, C. M. and Marzke, R. F. (2010). Comparative 3D quantitative analyses of trapeziometacarpal joint surface curvatures among living catarrhines and fossil hominins. *American Journal of Physical Anthropology*, 141(1), 38-51.
- Marzke, M. W., Toth, N., Schick, K., Reece, S., Steinberg, B., Hunt, K., Linscheid, R. and An, K. N. (1998a). EMG study of hand muscle recruitment during hard hammer percussion manufacture of Oldowan tools. *American Journal of Physical Anthropology: The Official Publication of the American Association of Physical Anthropologists*, 105(3), 315-332.
- Marzke, M. W., Toth, N., Schick, K., Reece, S., Steinberg, B., Hunt, K., Linscheid, R. and An, K. N. (1998b). EMG study of hand muscle recruitment during hard hammer percussion manufacture of Oldowan tools. *American Journal of Physical Anthropology*, 105(3), 315-332.
- Marzke, M. W., Wullstein, K. and Viegas, S. F. (1992). Evolution of the power ("squeeze") grip and its morphological correlates in hominids. *American Journal of Physical Anthropology*, 89(3), 283-298.
- Marzke, M. W., Wullstein, K. L. and Viegas, S. F. (1994). Variability at the carpometacarpal and midcarpal joints involving the fourth metacarpal, hamate, and lunate in catarrhini. *American Journal of Physical Anthropology*, 93(2), 229-240.
- Matarazzo, S. (2013). Manual pressure distribution patterns of knuckle-walking apes. *American Journal of Physical Anthropology*, 152(1), 44-50.
- Matarazzo, S. (2015). Trabecular architecture of the manual elements reflects locomotor patterns in primates. *PLoS One*, 10(3), e0120436.
- Maxwell, J. J. (2015). *The Moriori. The integration of Arboriculture and Agroforestry in an East Polynesian Society*. PhD, University of Otago.
- McGuigan, F. E. A., Murray, L., Gallagher, A., Davey-Smith, G., Neville, C. E., Van't Hof, R., Boreham, C. and Ralston, S. H. (2002). Genetic and environmental determinants of peak bone mass in young men and women. *Journal of bone and mineral research*, 17(7), 1273-1279.
- McHenry, H. M. (1983). The capitate of *Australopithecus afarensis* and *A. africanus*. *American Journal of Physical Anthropology*, 62(2), 187-198.
- McHenry, H. M. and Coffing, K. (2000). *Australopithecus* to *Homo*: transformations in body and mind. *Annual Review of Anthropology*, 29(1), 125-146.
- McPherron, S. P., Alemseged, Z., Marean, C. W., Wynn, J. G., Reed, D., Geraads, D., Bobe, R. and Béarat, H. A. (2010). Evidence for stone-tool-assisted consumption of animal tissues before 3.39 million years ago at Dikika, Ethiopia. *Nature*, 466(7308), 857-860.
- Meulman, E. J. and van Schaik, C. P. 2013. Orangutan tool use and the evolution of technology. In: SANZ, C. M., CALL, J. & BOESCH, C. (eds.) *Tool use in animals: Cognition and ecology*. USA: Cambridge University Press. pp. 176-202.
- Micklesfield, L. K., Norris, S. A. and Pettifor, J. M. (2011). Ethnicity and bone: a South African perspective. *Journal of bone and mineral metabolism*, 29(3), 257.

- Mielke, M., Wölfer, J., Arnold, P., van Heteren, A. H., Amson, E. and Nyakatura, J. A. (2018). Trabecular architecture in the sciuriform femoral head: allometry and functional adaptation. *Zoological letters*, 4(1), 10.
- Mittra, E. S., Smith, H. F., Lemelin, P. and Jungers, W. L. (2007). Comparative morphometrics of the primate apical tuft. *American Journal of Physical Anthropology*, 134(4), 449-459.
- Moojen, T. M., Snel, J. G., Ritt, M. J., Venema, H. W., Kauer, J. M. and Bos, K. E. (2003). In vivo analysis of carpal kinematics and comparative review of the literature. *The Journal of hand surgery*, 28(1), 81-87.
- Moore, M. W. and Brumm, A. 2009. *Homo floresiensis* and the African Oldowan. In: HOVERS, E. & BRAUN, D. R. (eds.) *Interdisciplinary approaches to the Oldowan*. The Netherlands: Springer. pp. 61-69.
- Morel, J., Combe, B., Francisco, J. and Bernard, J. (2001). Bone mineral density of 704 amateur sportsmen involved in different physical activities. *Osteoporosis International*, 12(2), 152-157.
- Moritomo, H., Apergis, E. P., Herzberg, G., Werner, F. W., Wolfe, S. W. and Garcia-Elias, M. (2007). 2007 IFSSH committee report of wrist biomechanics committee: biomechanics of the so-called dart-throwing motion of the wrist. *The Journal of hand surgery*, 32(9), 1447-1453.
- Moritomo, H., Apergis, E. P., Herzberg, G., Werner, F. W., Wolfe, S. W. and Garcia-Elias, M. (Year) Published. IFSSH scientific committee on anatomy and biomechanics wrist biomechanics and instability: Wrist dart-throwing motion updated. International Federation of Societies for Surgery of the Hand, 2014. pp. 23-28.
- Moritomo, H., Murase, T., Goto, A., Oka, K., Sugamoto, K. and Yoshikawa, H. (2004). Capitate-based kinematics of the midcarpal joint during wrist radioulnar deviation: an in vivo three-dimensional motion analysis¹. *The Journal of hand surgery*, 29(4), 668-675.
- Moritomo, H., Viegas, S. F., Elder, K., Nakamura, K., DaSilva, M. F. and Patterson, R. M. (2000a). The scaphotrapezio-trapezoidal joint. Part 2: a kinematic study. *The Journal of hand surgery*, 25(5), 911-920.
- Moritomo, H., Viegas, S. F., Nakamura, K., DaSilva, M. F. and Patterson, R. M. (2000b). The scaphotrapezio-trapezoidal joint. Part 1: An anatomic and radiographic study. *The Journal of hand surgery*, 25(5), 899-910.
- Morwood, M. J., Brown, P., Sutikna, T., Saptomo, E. W., Westaway, K. E., Due, R. A., Roberts, R. G., Maeda, T., Wasisto, S. and Djubiantono, T. (2005). Further evidence for small-bodied hominins from the Late Pleistocene of Flores, Indonesia. *Nature*, 437(7061), 1012-1017.
- Morwood, M. J., Soejono, R. P., Roberts, R. G., Sutikna, T., Turney, C. S., Westaway, K. E., Rink, W. J., Zhao, J.-X., Van Den Bergh, G. D. and Due, R. A. (2004). Archaeology and age of a new hominin from Flores in eastern Indonesia. *Nature*, 431(7012), 1087-1091.
- Mulder, B., Stock, J. T., Saers, J. P., Inskip, S. A., Cessford, C. and Robb, J. E. (2020). Intrapopulation variation in lower limb trabecular architecture. *American Journal of Physical Anthropology*, 173(1), 112-129.
- Müller, R., Koller, B., Hildebrand, T., Laib, A., Gianolini, S. and Rügsegger, P. (1996). Resolution dependency of microstructural properties of cancellous bone based on three-dimensional μ -tomography. *Technology and Health Care*, 4(1), 113-119.
- Müller, R. and Rügsegger, P. (1995). Three-dimensional finite element modelling of non-invasively assessed trabecular bone structures. *Medical Engineering & Physics*, 17(2), 126-133.
- Müller, R., Van Campenhout, H., Van Damme, B., Van der Perre, G., Dequeker, J., Hildebrand, T. and Rügsegger, P. (1998). Morphometric analysis of human bone biopsies: a

- quantitative structural comparison of histological sections and micro-computed tomography. *Bone*, 23(1), 59-66.
- Musgrave, J. H. (1973). The phalanges of Neanderthal and Upper Palaeolithic hands. *Human evolution*, 1159-85.
- Napier, J. (1956). The prehensile movements of the human hand. *The Journal of bone and joint surgery*, 38(4), 902-913.
- Napier, J. 1960. Studies of the hands of living primates. *Proceedings of the Zoological Society of London*. Oxford: Blackwell Publishing. pp. 647-657.
- Napier, J. (1962a). The evolution of the hand. *Scientific American*, 207(6), 56-65.
- Napier, J. (1962b). Fossil hand bones from Olduvai Gorge. *Nature*, 196(4853), 409-411.
- Napier, J. and Tuttle, R. H. (1993). *Hands*, New Jersey, Princeton University Press.
- Naylor, K. E., Iqbal, P., Fledelius, C., Fraser, R. B. and Eastell, R. (2000). The effect of pregnancy on bone density and bone turnover. *Journal of Bone and Mineral Research*, 15(1), 129-137.
- Neufuss, J., Robbins, M. M., Baeumer, J., Humle, T. and Kivell, T. L. (2017). Comparison of hand use and forelimb posture during vertical climbing in mountain gorillas (*Gorilla beringei beringei*) and chimpanzees (*Pan troglodytes*). *American Journal of Physical Anthropology*, 164(4), 651-664.
- Neufuss, J., Robbins, M. M., Baeumer, J., Humle, T. and Kivell, T. L. (2018). Gait characteristics of vertical climbing in mountain gorillas and chimpanzees. *Journal of Zoology*, 306(2), 129-138.
- Neufuss, J., Robbins, M. M., Baeumer, J., Humle, T. and Kivell, T. L. (2019). Manual skills for food processing by mountain gorillas (*Gorilla beringei beringei*) in Bwindi Impenetrable National Park, Uganda. *Biological Journal of the Linnean Society*, 127(3), 543-562.
- Nguyen, N. H., Pahr, D. H., Gross, T., Skinner, M. M. and Kivell, T. L. (2014). Micro-finite element (μ FE) modeling of the siamang (*Symphalangus syndactylus*) third proximal phalanx: The functional role of curvature and the flexor sheath ridge. *Journal of Human Evolution*, 6760-75.
- Niewoehner, W. A. (2001). Behavioral inferences from the Skhul/Qafzeh early modern human hand remains. *Proceedings of the National Academy of Sciences*, 98(6), 2979-2984.
- Niewoehner, W. A. 2006. Neanderthal hands in their proper perspective. In: HARVATI, K. & HARRISON, T. (eds.) *Neanderthals revisited: New approaches and perspectives*. The Netherlands: Springer. pp. 157-190.
- Niewoehner, W. A., Weaver, A. H. and Trinkaus, E. (1997). Neandertal capitate-metacarpal articular morphology. *American Journal of Physical Anthropology*, 103(2), 219-233.
- Nikita, E., Ysi Siew, Y., Stock, J., Mattingly, D. and Mirazón Lahr, M. (2011). Activity patterns in the Sahara Desert: An interpretation based on cross-sectional geometric properties. *American Journal of Physical Anthropology*, 146(3), 423-434.
- Nowak, K. and Lee, P. C. 2013. "Specialist" primates can be flexible in response to habitat alteration. In: MARSH, L. K. (ed.) *Primates in fragments*. New York: Springer. pp. 199-211.
- Orr, C. M. (2005). Knuckle-walking anteater: A convergence test of adaptation for purported knuckle-walking features of african Hominidae. *American Journal of Physical Anthropology*, 128(3), 639-658.
- Orr, C. M. (2010). *Adaptations to knuckle-walking and digitigrady: a three-dimensional kinematic and morphometric analysis of the anthropoid wrist*. PhD Thesis, Arizona State University.
- Orr, C. M. 2016. Functional morphology of the primate hand: Recent approaches using biomedical imaging, computer modeling, and engineering methods. In: KIVELL, T. L.,

- LEMELIN, P., RICHMOND, B. G. & SCHMITT, D. (eds.) *The evolution of the primate hand*. New York: Springer. pp. 227-257.
- Orr, C. M. (2017). Locomotor hand postures, carpal kinematics during wrist extension, and associated morphology in anthropoid primates. *The Anatomical Record*, 300(2), 382-401.
- Orr, C. M. (2018). Kinematics of the anthropoid os centrale and the functional consequences of scaphoid-centrale fusion in African apes and hominins. *Journal of Human Evolution*, 114102-117.
- Orr, C. M. and Atkinson, R. (2016). Carpal kinematics and morphological correlates of ulnar deviation mobility in anthropoids. In: COMMITTEE, A. S. P. (ed.) *85th Annual Meeting of the American Association of Physical Anthropologists*. Atlanta, Georgia: American Journal of Physical Anthropology.
- Orr, C. M., Leventhal, E. L., Chivers, S. F., Marzke, M. W., Wolfe, S. W. and Crisco, J. J. (2010). Studying Primate Carpal Kinematics in Three Dimensions Using a Computed-Tomography-Based Markerless Registration Method. *The Anatomical Record*, 293(4), 692-709.
- Orr, C. M., Tocheri, M. W., Burnett, S. E., Awe, R. D., Saptomo, E. W., Sutikna, T., Wasisto, S., Morwood, M. J. and Jungers, W. L. (2013). New wrist bones of *Homo floresiensis* from Liang Bua (Flores, Indonesia). *Journal of Human Evolution*, 64(2), 109-129.
- Otoni, E. B. and Izar, P. (2008). Capuchin monkey tool use: overview and implications. *Evolutionary Anthropology: Issues, News, and Reviews: Issues, News, and Reviews*, 17(4), 171-178.
- Paciulli, L. (1995). Ontogeny of phalangeal curvature and positional behavior in chimpanzees. *American Journal of Physical Anthropology*, 20(Suppl), 165.
- Pahr, D. H. and Zysset, P. K. (2009a). A comparison of enhanced continuum FE with micro FE models of human vertebral bodies. *Journal of Biomechanics*, 42(4), 455-462.
- Pahr, D. H. and Zysset, P. K. (2009b). From high-resolution CT data to finite element models: development of an integrated modular framework. *Computer methods in biomechanics and biomedical engineering*, 12(1), 45-57.
- Paoli, G., Tarli, S. M. B., Klír, P., Strouhal, E., Tofanelli, S., Del Santo Valli, M. T. and Pavelcová, B. (1993). Paleoserology of the Christian population at Sayala (Lower Nubia): an evaluation of the reliability of the results. *American Journal of Physical Anthropology*, 92(3), 263-272.
- Parsons, T. J., Van Dusseldorp, M., van Der Vliet, M., Van De Werken, K., Schaafsma, G. and Van Staveren, W. A. (1997). Reduced bone mass in Dutch adolescents fed a macrobiotic diet in early life. *Journal of Bone and Mineral Research*, 12(9), 1486-1494.
- Patel, B. A. and Carlson, K. J. (2007). Bone density spatial patterns in the distal radius reflect habitual hand postures adopted by quadrupedal primates. *Journal of Human Evolution*, 52(2), 130-141.
- Paternoster, L., Lorentzon, M., Lehtimäki, T., Eriksson, J., Kähönen, M., Raitakari, O., Laaksonen, M., Sievänen, H., Viikari, J. and Lyytikäinen, L.-P. (2013). Genetic determinants of trabecular and cortical volumetric bone mineral densities and bone microstructure. *PLoS genetics*, 9(2), e1003247.
- Pattin, C. A., Caler, W. E. and Carter, D. R. (1996). Cyclic mechanical property degradation during fatigue loading of cortical bone. *Journal of Biomechanics*, 29(1), 69-79.
- Pearson, O. M. and Lieberman, D. E. (2004). The aging of Wolff's "law": ontogeny and responses to mechanical loading in cortical bone. *American Journal of Physical Anthropology*, 125(S39), 63-99.

- Pettersson, U., Nilsson, M., Sundh, V., Mellström, D. and Lorentzon, M. (2010). Physical activity is the strongest predictor of calcaneal peak bone mass in young Swedish men. *Osteoporosis International*, 21(3), 447-455.
- Pham, D. L. and Prince, J. L. (1999). An adaptive fuzzy C-means algorithm for image segmentation in the presence of intensity inhomogeneities. *Pattern recognition letters*, 20(1), 57-68.
- Pickering, R., Dirks, P. H., Jinnah, Z., De Ruiter, D. J., Churchill, S. E., Herries, A. I., Woodhead, J. D., Hellstrom, J. C. and Berger, L. R. (2011). *Australopithecus sediba* at 1.977 Ma and implications for the origins of the genus *Homo*. *Science*, 333(6048), 1421-1423.
- Pollitzer, W. S. and Anderson, J. J. (1989). Ethnic and genetic differences in bone mass: a review with a hereditary vs environmental perspective. *The American Journal of Clinical Nutrition*, 50(6), 1244-1259.
- Pontzer, H., Lieberman, D. E., Momin, E., Devlin, M. J., Polk, J., Hallgrímsson, B. and Cooper, D. (2006a). Trabecular bone in the bird knee responds with high sensitivity to changes in load orientation. *Journal of Experimental Biology*, 209(1), 57-65.
- Pontzer, H., Lieberman, D. E., Momin, E., Devlin, M. J., Polk, J. D., Hallgrímsson, B. and Cooper, D. M. (2006b). Trabecular bone in the bird knee responds with high sensitivity to changes in load orientation. *Journal of Experimental Biology*, 209(Pt 1), 57-65.
- Pontzer, H., Raichlen, D. A. and Rodman, P. S. (2014). Bipedal and quadrupedal locomotion in chimpanzees. *Journal of Human Evolution*, 6664-82.
- Pontzer, H., Raichlen, D. A. and Sockol, M. D. (2009). The metabolic cost of walking in humans, chimpanzees, and early hominins. *Journal of Human Evolution*, 56(1), 43-54.
- Popp, K. L., Hughes, J. M., Martinez-Betancourt, A., Scott, M., Turkington, V., Caksa, S., Guerriere, K. I., Ackerman, K. E., Xu, C. and Unnikrishnan, G. (2017). Bone mass, microarchitecture and strength are influenced by race/ethnicity in young adult men and women. *Bone*, 103200-208.
- Preuschoft, H. (2019). Power grip or precision handling? What determines hand morphology in primates, including Hominidae? *Biological Journal of the Linnean Society*, 127(3), 694-706.
- Püschel, T. A., Marcé-Nogué, J., Chamberlain, A. T., Yoxall, A. and Sellers, W. I. (2020). The biomechanical importance of the scaphoid-centrale fusion during simulated knuckle-walking and its implications for human locomotor evolution. *Scientific Reports*, 10(1), 1-7.
- Quaine, F., Vigouroux, L. and Martin, L. (2003). Effect of simulated rock climbing finger postures on force sharing among the fingers. *Clinical Biomechanics*, 18(5), 385-388.
- Raggatt, L. J. and Partridge, N. C. (2010). Cellular and molecular mechanisms of bone remodeling. *The Journal of biological chemistry*, 285(33), 25103-25108.
- Ragni, A. J. (2020). Trabecular architecture of the capitate and third metacarpal through ontogeny in chimpanzees (*Pan troglodytes*) and gorillas (*Gorilla gorilla*). *Journal of Human Evolution*, 138102702.
- Raichlen, D. A., Gordon, A. D., Harcourt-Smith, W. E., Foster, A. D. and Haas Jr, W. R. (2010). Laetoli footprints preserve earliest direct evidence of human-like bipedal biomechanics. *PLoS One*, 5(3), e9769.
- Rainbow, M. J., Crisco, J. J., Moore, D. C. and Wolfe, S. W. (2008). Gender differences in capitate kinematics are eliminated after accounting for variation in carpal size. *Journal of biomechanical engineering*, 130(4), 041003:1-041003:5.
- Rainbow, M. J., Kamal, R. N., Leventhal, E., Akelman, E., Moore, D. C., Wolfe, S. W. and Crisco, J. J. (2013). In vivo kinematics of the scaphoid, lunate, capitate, and third metacarpal in extreme wrist flexion and extension. *The Journal of hand surgery*, 38(2), 278-288.

- Rainbow, M. J., Kamal, R. N., Moore, D. C., Akelman, E., Wolfe, S. W. and Crisco, J. J. (2015). Subject-specific carpal ligament elongation in extreme positions, grip, and the dart thrower's motion. *Journal of biomechanical engineering*, 137(11), 111006:1-111006:10.
- Rainbow, M. J., Wolff, A. L., Crisco, J. J. and Wolfe, S. W. (2016). Functional kinematics of the wrist. *The Journal of hand surgery*, 41(1), 7-21.
- Ramos III, G. L. (2014). *Positional behavior of Pan paniscus at Lui Kotale, Democratic Republic of Congo*. PhD, Indiana University.
- Regal, S., Maschke, S. and Li, Z.-M. 2020. Hand and Wrist Biomechanics. In: CHENG, C.-K. & WOO, S. L.-Y. (eds.) *Frontiers in Orthopaedic Biomechanics*. Singapore: Springer. pp. 89-104.
- Rein, T. R., Harrison, T., Carlson, K. J. and Harvati, K. (2017). Adaptation to suspensory locomotion in *Australopithecus sediba*. *Journal of Human Evolution*, 104:1-12.
- Rein, T. R. and Harvati, K. (2013). Exploring third metacarpal capitate facet shape in early hominins. *The Anatomical Record*, 296(2), 240-249.
- Rein, T. R., Harvati, K. and Harrison, T. (2015). Inferring the use of forelimb suspensory locomotion by extinct primate species via shape exploration of the ulna. *Journal of Human Evolution*, 78:70-79.
- Remis, M. J. (1995). Effects of body size and social context on the arboreal activities of lowland gorillas in the Central African Republic. *American Journal of Physical Anthropology*, 97(4), 413-433.
- Remis, M. J. 1998. The gorilla paradox. In: STRASSER, E., FLEAGLE, J., ROSENBERGER, A. L. & MCHENRY, H. (eds.) *Primate locomotion*. Boston: Springer. pp. 95-106.
- Remis, M. J. (1999). Tree structure and sex differences in arboreality among western lowland gorillas (*Gorilla gorilla gorilla*) at Bai Hokou, Central African Republic. *Primates*, 40(2), 383.
- Rho, J. Y., Ashman, R. B. and Turner, C. H. (1993). Young's modulus of trabecular and cortical bone material: ultrasonic and microtensile measurements. *Journal of Biomechanics*, 26(2), 111-119.
- Richmond, B. G. 2006. Functional morphology of the midcarpal joint in knuckle-walkers and terrestrial quadrupeds. In: ISHIDA, H., TUTTLE, R., PICKFORD, M., OGIHARA, N. & NAKATSUKASA, M. (eds.) *Human origins and environmental backgrounds*. USA: Springer. pp. 105-122.
- Richmond, B. G. (2007). Biomechanics of phalangeal curvature. *Journal of Human Evolution*, 53(6), 678-690.
- Richmond, B. G., Begun, D. R. and Strait, D. S. (2001). Origin of human bipedalism: the knuckle-walking hypothesis revisited. *American Journal of Physical Anthropology*, 116(S33), 70-105.
- Richmond, B. G. and Jungers, W. L. (2008). *Orrorin tugenensis* femoral morphology and the evolution of hominin bipedalism. *Science*, 319(5870), 1662-1665.
- Riddle, M., MacDermid, J., Robinson, S., Szekeres, M., Ferreira, L. and Lalone, E. (2020). Evaluation of individual finger forces during activities of daily living in healthy individuals and those with hand arthritis. *Journal of Hand Therapy*, 33(2), 188-197.
- Riley, G. and Trinkaus, E. (Year) Published. Neandertal capitate-metacarpal 2 articular morphology and Neandertal manipulative behavior. *American Journal of Physical Anthropology*, 1989. *American Journal of Physical Anthropology*, pp. 290.
- Robling, A. G., Hinant, F. M., Burr, D. B. and Turner, C. H. (2002). Improved bone structure and strength after long-term mechanical loading is greatest if loading is separated into short bouts. *Journal of Bone and Mineral Research*, 17(8), 1545-1554.
- Rodríguez-Vidal, J., d'Errico, F., Pacheco, F. G., Blasco, R., Rosell, J., Jennings, R. P., Queffelec, A., Finlayson, G., Fa, D. A. and López, J. M. G. (2014). A rock engraving made by

- Neanderthals in Gibraltar. *Proceedings of the National Academy of Sciences*, 111(37), 13301-13306.
- Rohde, R. S., Crisco, J. J. and Wolfe, S. W. (2010). The advantage of throwing the first stone: how understanding the evolutionary demands of *Homo sapiens* is helping us understand carpal motion. *The Journal of the American Academy of Orthopaedic Surgeons*, 18(1), 51-58.
- Rolian, C., Lieberman, D. E. and Zermeno, J. P. (2011). Hand biomechanics during simulated stone tool use. *Journal of Human Evolution*, 61(1), 26-41.
- Rose, M. D. (1984). A hominine hip bone, KNM-ER 3228, from East Lake Turkana, Kenya. *American Journal of Physical Anthropology*, 63(4), 371-378.
- Rose, M. D. (1992). Kinematics of the trapezium-1st metacarpal joint in extant anthropoids and Miocene hominoids. *Journal of Human Evolution*, 22(4-5), 255-266.
- Ross, C. F., Lockwood, C. A., Fleagle, J. G. and Jungers, W. L. 2002. Adaptation and behavior in the primate fossil record. In: PLAVCAN, J. M., KAY, R. F., JUNGERS, W. L. & SCHAIK, C. P. V. (eds.) *Reconstructing behavior in the primate fossil record*. Boston: Springer. pp. 1-41.
- Ross, S. R. and Shender, M. A. (2016). Daily travel distances of zoo-housed chimpanzees and gorillas: implications for welfare assessments and space requirements. *Primates*, 57(3), 395-401.
- Rubin, C., Turner, A., Mallinckrodt, C., Jerome, C., McLeod, K. and Bain, S. (2002). Mechanical strain, induced noninvasively in the high-frequency domain, is anabolic to cancellous bone, but not cortical bone. *Bone*, 30(3), 445-452.
- Ruby, L., Conney III, W., An, K., Linscheid, R. and Chao, E. (1988). Relative motion of selected carpal bones: a kinematic analysis of the normal wrist. *The Journal of hand surgery*, 13(1), 1-10.
- Rueckert, D., Frangi, A. F. and Schnabel, J. A. (2003). Automatic construction of 3-D statistical deformation models of the brain using nonrigid registration. *IEEE transactions on medical imaging*, 22(8), 1014-1025.
- Ruff, C. B. (1984). Allometry between length and cross-sectional dimensions of the femur and tibia in *Homo sapiens sapiens*. *American Journal of Physical Anthropology*, 65(4), 347-358.
- Ruff, C. B. (1987). Structural allometry of the femur and tibia in Hominoidea and *Macaca*. *Folia primatologica*, 48(1-2), 9-49.
- Ruff, C. B. (2005). Mechanical determinants of bone form: insights from skeletal remains. *Journal of Musculoskeletal and Neuronal Interactions*, 5(3), 202.
- Ruff, C. B. 2008. Biomechanical analyses of archaeological human skeletons. In: KATZENBERG, M. A. & GRAUER, A. L. (eds.) *Biological anthropology of the human skeleton*. Hoboken, NJ: Wiley Online Library. pp. 183-206.
- Ruff, C. B., Burgess, M. L., Bromage, T. G., Mudakikwa, A. and McFarlin, S. C. (2013). Ontogenetic changes in limb bone structural proportions in mountain gorillas (*Gorilla beringei beringei*). *Journal of Human Evolution*, 65(6), 693-703.
- Ruff, C. B., Holt, B. and Trinkaus, E. (2006). Who's afraid of the big bad Wolff?: "Wolff's law" and bone functional adaptation. *American Journal of Physical Anthropology*, 129(4), 484-498.
- Ruff, C. B. and Runestad, J. A. (1992). Primate limb bone structural adaptations. *Annual Review of Anthropology*, 21(1), 407-433.
- Runestad, J. A. (1997). Postcranial adaptations for climbing in Loridae (Primates). *Journal of Zoology*, 242(2), 261-290.
- Ryan, T. M. and Ketcham, R. A. (2002). The three-dimensional structure of trabecular bone in the femoral head of strepsirrhine primates. *Journal of Human Evolution*, 43(1), 1-26.

- Ryan, T. M. and Shaw, C. N. (2012). Unique suites of trabecular bone features characterize locomotor behavior in human and non-human anthropoid primates. *PLoS One*, 7(7), e41037.
- Ryan, T. M. and Shaw, C. N. (2013). Trabecular bone microstructure scales allometrically in the primate humerus and femur. *Proceedings of the Royal Society B: Biological Sciences*, 280(1758), 20130172.
- Ryan, T. M. and Shaw, C. N. (2015). Gracility of the modern *Homo sapiens* skeleton is the result of decreased biomechanical loading. *Proceedings of the National Academy of Sciences*, 112(2), 372-377.
- Ryan, T. M. and Walker, A. (2010). Trabecular bone structure in the humeral and femoral heads of anthropoid primates. *The Anatomical Record*, 293(4), 719-729.
- Saers, J. P., Ryan, T. M. and Stock, J. T. (2019a). Trabecular bone functional adaptation and sexual dimorphism in the human foot. *American Journal of Physical Anthropology*, 168(1), 154-169.
- Saers, J. P., Ryan, T. M. and Stock, J. T. (2019b). Trabecular bone structure scales allometrically in the foot of four human groups. *Journal of Human Evolution*, 135102654.
- Saers, J. P. P., Cazorla-Bak, Y., Shaw, C. N., Stock, J. T. and Ryan, T. M. (2016). Trabecular bone structural variation throughout the human lower limb. *Journal of Human Evolution*, 9797-108.
- Samuel, D. S., Nauwelaerts, S., Stevens, J. M. and Kivell, T. L. (2018). Hand pressures during arboreal locomotion in captive bonobos (*Pan paniscus*). *Journal of Experimental Biology*, 221(8), e170910.
- Sanz, C. M., Call, J. and Boesch, C. (2013). *Tool use in animals: cognition and ecology*, Cambridge, Cambridge University Press.
- Sarmiento, E. E. (1988). Anatomy of the hominoid wrist joint: its evolutionary and functional implications. *International Journal of Primatology*, 9(4), 281-345.
- Scherf, H., Harvati, K. and Hublin, J. J. (2013). A comparison of proximal humeral cancellous bone of great apes and humans. *Journal of Human Evolution*, 65(1), 29-38.
- Schilling, A. M., Tofanelli, S., Hublin, J. J. and Kivell, T. L. (2014). Trabecular bone structure in the primate wrist. *Journal of Morphology*, 275(5), 572-585.
- Schmitt, D., Zeininger, A. and Granatosky, M. C. 2016. Patterns, variability, and flexibility of hand posture during locomotion in primates. In: KIVELL, T. L., LEMELIN, P., RICHMOND, B. G. & SCHMITT, D. (eds.) *The evolution of the primate hand*. New York: Springer. pp. 345-369.
- Schmitz, R. W., Serre, D., Bonani, G., Feine, S., Hillgruber, F., Krainitzki, H., Pääbo, S. and Smith, F. H. (2002). The Neandertal type site revisited: interdisciplinary investigations of skeletal remains from the Neander Valley, Germany. *Proceedings of the National Academy of Sciences*, 99(20), 13342-13347.
- Schuind, F., An, K. N., Cooney lii, W. P. and Garcia-Elias, M. (2013). *Advances in the Biomechanics of the Hand and Wrist*, New York, Springer Science & Business Media.
- Schuind, F., Cooney, W. P., Linscheid, R. L., An, K. N. and Chao, E. Y. S. (1995). Force and pressure transmission through the normal wrist. A theoretical two-dimensional study in the posteroanterior plane. *Journal of Biomechanics*, 28(5), 587-601.
- Schwarcz, H., Buhay, W., Grün, R., Valladas, H., Tchernov, E., Bar-Yosef, O. and Vandermeersch, B. (1989). ESR dating of the Neanderthal site, Kebara Cave, Israel. *Journal of Archaeological Science*, 16(6), 653-659.
- Shaar, R., Matmon, A., Horwitz, L. K., Ebert, Y., Chazan, M., Arnold, M., Aumaître, G., Boursès, D. and Keddadouche, K. (2021). Magnetostratigraphy and cosmogenic dating of Wonderwerk Cave: New constraints for the chronology of the South African Earlier Stone Age. *Quaternary Science Reviews*, 259106907.

- Shaw, C. N. and Ryan, T. M. (2012). Does skeletal anatomy reflect adaptation to locomotor patterns? Cortical and trabecular architecture in human and nonhuman anthropoids. *American Journal of Physical Anthropology*, 147(2), 187-200.
- Shea, J. J. (2017). Occasional, obligatory, and habitual stone tool use in hominin evolution. *Evolutionary Anthropology: Issues, News, and Reviews*, 26(5), 200-217.
- Short, W. H., Werner, F. W., Green, J. K. and Masaoka, S. (2002). Biomechanical evaluation of ligamentous stabilizers of the scaphoid and lunate. *The Journal of hand surgery*, 27(6), 991-1002.
- Sims, L. A. (2022). Upper Extremity Injuries in Rock Climbers: Diagnosis and Management. *The Journal of hand surgery*, online early access.
- Skinner, M. M., Stephens, N. B., Tsegai, Z. J., Foote, A. C., Nguyen, N. H., Gross, T., Pahr, D. H., Hublin, J. J. and Kivell, T. L. (2015). Human-like hand use in *Australopithecus africanus*. *Science*, 347(6220), 395-399.
- Smith, D. M., Nance, W. E., Kang, K. W., Christian, J. C. and Johnston, C. C., Jr. (1973). Genetic factors in determining bone mass. *The Journal of clinical investigation*, 52(11), 2800-2808.
- Smith, R. J. and Jungers, W. L. (1997). Body mass in comparative primatology. *Journal of Human Evolution*, 32(6), 523-559.
- Sparacello, V. S., Rossi, S., Pettitt, P., Roberts, C., Salvatore, J. and Formicola, V. (2018). New insights on Final Epigravettian funerary behaviour at Arene Candide Cave (Western Liguria, Italy) from osteological and spatial analysis of secondary bone deposits. *Journal of Anthropological Sciences*, 961-24.
- Steiner, L., Synek, A. and Pahr, D. H. (2021). Femoral strength can be predicted from 2D projections using a 3D statistical deformation and texture model with finite element analysis. *Medical Engineering & Physics*, 9372-82.
- Stengel, S. V., Kemmler, W., Pintag, R., Beeskow, C., Weineck, J., Lauber, D., Kalender, W. A. and Engelke, K. (2005). Power training is more effective than strength training for maintaining bone mineral density in postmenopausal women. *Journal of applied physiology*, 99(1), 181-188.
- Stephens, N. B. (2018). *Functional morphology of the hand: Detecting behaviour during life through variation in internal trabecular architecture*. Ph.D, University of Leipzig.
- Stephens, N. B., Kivell, T. L., Gross, T., Pahr, D. H., Lazenby, R. A., Hublin, J. J., Hershkovitz, I. and Skinner, M. M. (2016). Trabecular architecture in the thumb of *Pan* and *Homo*: implications for investigating hand use, loading, and hand preference in the fossil record. *American Journal of Physical Anthropology*, 161(4), 603-619.
- Stephens, N. B., Kivell, T. L., Pahr, D. H., Hublin, J.-J. and Skinner, M. M. (2018). Trabecular bone patterning across the human hand. *Journal of Human Evolution*, 1231-23.
- Stern, J. T., Jungers, W. L. and Susman, R. L. (1995). Quantifying phalangeal curvature: an empirical comparison of alternative methods. *American Journal of Physical Anthropology*, 97(1), 1-10.
- Stern, J. T. and Susman, R. L. (1983). The locomotor anatomy of *Australopithecus afarensis*. *American Journal of Physical Anthropology*, 60(3), 279-317.
- Stirland, A. J. (2005). *The men of the Mary Rose: Raising the dead*, UK, The History Press.
- Stirling, P. H., Chan, C. C., Cliff, N. J. and Rust, P. A. (2021). A Reference Range of Dart-Thrower's Motion at the Wrist in a Healthy Adult Population. *The Journal of hand surgery*, 46(6), 519.e1-519.e6.
- Stout, D., Toth, N., Schick, K. and Chaminade, T. (2008). Neural correlates of Early Stone Age toolmaking: technology, language and cognition in human evolution. *Philosophical Transactions of the Royal Society B: Biological Sciences*, 363(1499), 1939-1949.
- Su, A. and Carlson, K. J. (2017). Comparative analysis of trabecular bone structure and orientation in South African hominin tali. *Journal of Human Evolution*, 1061-18.

- Sundaramurthy, A., Xu, C., Hughes, J. M., Gaffney-Stomberg, E., Guerriere, K. I., Popp, K. L., Bouxsein, M. L., Reifman, J. and Unnikrishnan, G. (2019). Regional Changes in Density and Microarchitecture in the Ultradistal Tibia of Female Recruits After US Army Basic Combat Training. *Calcified tissue international*, 105(1), 1-9.
- Susman, R. L. (1974). Facultative terrestrial hand postures in an orangutan (*Pongo pygmaeus*) and pongid evolution. *American Journal of Physical Anthropology*, 40(1), 27-37.
- Susman, R. L., Badrian, N. L. and Badrian, A. J. (1980). Locomotor behavior of *Pan paniscus* in Zaire. *American Journal of Physical Anthropology*, 53(1), 69-80.
- Sutikna, T., Tocheri, M. W., Faith, J. T., Awe, R. D., Meijer, H. J., Saptomo, E. W. and Roberts, R. G. (2018). The spatio-temporal distribution of archaeological and faunal finds at Liang Bua (Flores, Indonesia) in light of the revised chronology for *Homo floresiensis*. *Journal of Human Evolution*, 12452-74.
- Sutikna, T., Tocheri, M. W., Morwood, M. J., Saptomo, E. W., Awe, R. D., Wasisto, S., Westaway, K. E., Aubert, M., Li, B. and Zhao, J.-x. (2016). Revised stratigraphy and chronology for *Homo floresiensis* at Liang Bua in Indonesia. *Nature*, 532(7599), 366-369.
- Swartz, S. M., Bertram, J. E. A. and Biewener, A. A. (1989). Telemetered in vivo strain analysis of locomotor mechanics of brachiating gibbons. *Nature*, 342(6247), 270.
- Swartz, S. M., Parker, A. and Huo, C. (1998). Theoretical and empirical scaling patterns and topological homology in bone trabeculae. *Journal of Experimental Biology*, 201(Pt 4), 573-590.
- Sykes, R. W. 2015. To see a world in a hafted tool: birch pitch composite technology, cognition and memory in Neanderthals. In: COWARD, F., HOSFIELD, R., POPE, M. & WENBAN-SMITH, F. (eds.) *Settlement, Society and Cognition in Human Evolution: Landscapes in the Mind*. Cambridge: Cambridge University Press. pp. 117-137.
- Sylvester, A. D. (2006). Locomotor decoupling and the origin of hominin bipedalism. *Journal of theoretical biology*, 242(3), 581-590.
- Synek, A., Lu, S.-C., Nauwelaerts, S., Pahr, D. H. and Kivell, T. L. (2020). Metacarpophalangeal joint loads during bonobo locomotion: model predictions versus proxies. *Journal of The Royal Society Interface*, 17(164), 20200032.
- Taaffe, D. R., Snow-Harter, C., Connolly, D. A., Robinson, T. L., Brown, M. D. and Marcus, R. (1995). Differential effects of swimming versus weight-bearing activity on bone mineral status of eumenorrhic athletes. *Journal of Bone and Mineral Research*, 10(4), 586-593.
- Taleisnik, J. (1976). The ligaments of the wrist. *The Journal of hand surgery*, 1(2), 110-118.
- Tanck, E., Bakker, A. D., Kregting, S., Cornelissen, B., Klein-Nulend, J. and Van Rietbergen, B. (2009). Predictive value of femoral head heterogeneity for fracture risk. *Bone*, 44(4), 590-595.
- Tang, J. B., Gu, X. K., Xu, J. and Gu, J. H. (2011). In vivo length changes of carpal ligaments of the wrist during dart-throwing motion. *The Journal of hand surgery*, 36(2), 284-290.
- Thackeray, J. F. (2015). Estimating the age and affinities of *Homo naledi*. *South African Journal of Science*, 111(11-12), 1-2.
- Thompson, N. E. (2020). The biomechanics of knuckle-walking: 3-D kinematics of the chimpanzee and macaque wrist, hand and fingers. *Journal of Experimental Biology*, 223(14), jeb224360.
- Thompson, N. E., Ostrofsky, K. R., McFarlin, S. C., Robbins, M. M., Stoinski, T. S. and Almécija, S. (2018). Unexpected terrestrial hand posture diversity in wild mountain gorillas. *American Journal of Physical Anthropology*, 166(1), 84-94.
- Thorpe, S. K. S. and Crompton, R. H. (2005). Locomotor ecology of wild orangutans (*Pongo pygmaeus abelii*) in the Gunung Leuser Ecosystem, Sumatra, Indonesia: A

- multivariate analysis using log-linear modelling. *American Journal of Physical Anthropology*, 127(1), 58-78.
- Thorpe, S. K. S. and Crompton, R. H. (2006). Orangutan positional behavior and the nature of arboreal locomotion in Hominoidea. *American Journal of Physical Anthropology*, 131(3), 384-401.
- Thorpe, S. K. S. and Crompton, R. H. 2009. Orangutan positional behavior: interspecific variation and ecological correlates. In: WICH, S. A., ATMOKO, U. S. U., SETIA, T. M. & VAN SCHAİK, C. P. (eds.) *Orangutans: Geographic variation in behavioral ecology and conservation*. New York: Oxford University Press pp. 33-47.
- Thorpe, S. K. S., Holder, R. and Crompton, R. H. (2009). Orangutans employ unique strategies to control branch flexibility. *Proceedings of the National Academy of Sciences*, 106(31), 12646-12651.
- Thorpe, S. K. S., McClymont, J. M. and Crompton, R. H. (2014). The arboreal origins of human bipedalism. *Antiquity*, 88(341), 906-914.
- Tocheri, M. W. (2007). *Three-dimensional riddles of the radial wrist: derived carpal and carpometacarpal joint morphology in the genus Homo and the implications for understanding the evolution of stone tool-related behaviors in Hominins*. PhD Thesis, Arizona State University.
- Tocheri, M. W., Marzke, M. W., Liu, D., Bae, M., Jones, G. P., Williams, R. C. and Razdan, A. (2003). Functional capabilities of modern and fossil hominid hands: Three-dimensional analysis of trapezia. *American Journal of Physical Anthropology*, 122(2), 101-112.
- Tocheri, M. W., Orr, C. M., Jacofsky, M. C. and Marzke, M. W. (2008). The evolutionary history of the hominin hand since the last common ancestor of *Pan* and *Homo*. *Journal of anatomy*, 212(4), 544-562.
- Tocheri, M. W., Orr, C. M., Larson, S. G., Sutikna, T., Jatmiko, Saptomo, E. W., Due, R. A., Djubiantono, T., Morwood, M. J. and Jungers, W. L. (2007). The primitive wrist of *Homo floresiensis* and its implications for hominin evolution. *Science*, 317(5845), 1743-1745.
- Tocheri, M. W., Razdan, A., Williams, R. C. and Marzke, M. W. (2005). A 3D quantitative comparison of trapezium and trapezoid relative articular and nonarticular surface areas in modern humans and great apes. *Journal of Human Evolution*, 49(5), 570-586.
- Toth, N., Schick, K. D., Savage-Rumbaugh, E. S., Sevcik, R. A. and Rumbaugh, D. M. (1993). *Pan* the tool-maker: investigations into the stone tool-making and tool-using capabilities of a bonobo (*Pan paniscus*). *Journal of Archaeological Science*, 20(1), 81-91.
- Towle, I., Irish, J. D. and De Groote, I. (2017). Behavioral inferences from the high levels of dental chipping in *Homo naledi*. *American Journal of Physical Anthropology*, 164(1), 184-192.
- Trinkaus, E. (1983). *The Shanidar Neandertals*, London, Academic Press.
- Trinkaus, E. 2016. The evolution of the hand in Pleistocene *Homo*. In: KIVELL, T. L., LEMELIN, P., RICHMOND, B. G. & SCHMITT, D. (eds.) *The evolution of the primate hand*. New York: Springer. pp. 545-571.
- Trinkaus, E., Churchill, S. E., Villedure, I., Riley, K. G., Heller, J. A. and Ruff, C. B. (1991). Robusticity versus shape: the functional interpretation of Neandertal appendicular morphology. *Journal of the Anthropological Society of Nippon*, 99(3), 257-278.
- Trinkaus, E. and Villedure, I. (1991). Mechanical advantages of the Neandertal thumb in flexion: a test of an hypothesis. *American Journal of Physical Anthropology*, 84(3), 249-260.

- Tsegai, Z. J., Kivell, T. L., Gross, T., Nguyen, N. H., Pahr, D. H., Smaers, J. B. and Skinner, M. M. (2013). Trabecular bone structure correlates with hand posture and use in hominoids. *PLoS One*, 8(11), e78781.
- Tsegai, Z. J., Skinner, M. M., Gee, A. H., Pahr, D. H., Treece, G. M., Hublin, J. J. and Kivell, T. L. (2017). Trabecular and cortical bone structure of the talus and distal tibia in *Pan* and *Homo*. *American Journal of Physical Anthropology*, 163(4), 784-805.
- Tsegai, Z. J., Skinner, M. M., Pahr, D. H., Hublin, J. J. and Kivell, T. L. (2018). Systemic patterns of trabecular bone across the human and chimpanzee skeleton. *Journal of anatomy*, 232(4), 641-656.
- Tsuzuku, S., Shimokata, H., Ikegami, Y., Yabe, K. and Wasnich, R. D. (2001). Effects of high versus low-intensity resistance training on bone mineral density in young males. *Calcified tissue international*, 68(6), 342-347.
- Turner, A., Chen, T. C., Barber, T. W., Malabanan, A. O., Holick, M. F. and Tangpricha, V. (2004). Testosterone increases bone mineral density in female-to-male transsexuals: A case series of 15 subjects. *Clinical endocrinology*, 61(5), 560-566.
- Turner, C. H., Rho, J., Takano, Y., Tsui, T. Y. and Pharr, G. M. (1999). The elastic properties of trabecular and cortical bone tissues are similar: results from two microscopic measurement techniques. *Journal of Biomechanics*, 32(4), 437-441.
- Turner, R. T. (2001). Skeletal adaptation to external loads optimizes mechanical properties: fact or fiction. *Current opinion in orthopaedics*, 12(5), 384-388.
- Tuttle, R. H. (1967). Knuckle-walking and the evolution of hominoid hands. *American Journal of Physical Anthropology*, 26(2), 171-206.
- Tuttle, R. H. (1969). Quantitative and functional studies on the hands of the Anthroidea. I. The Hominoidea. *Journal of Morphology*, 128(3), 309-363.
- Tuttle, R. H. and Watts, D. P. 1985. The positional behavior and adaptive complexes of *Pan gorilla*. In: KONDO, S. (ed.) *Primate morphophysiology, locomotor analysis and human bipedalism*. Tokyo: Tokyo University Press. pp. 261-288.
- Ulrich, D., van Rietbergen, B., Weinans, H. and R egsegger, P. (1998). Finite element analysis of trabecular bone structure: a comparison of image-based meshing techniques. *Journal of Biomechanics*, 31(12), 1187-1192.
- Ungar, P. S. and Berger, L. R. (2018). Brief communication: Dental microwear and diet of *Homo naledi*. *American Journal of Physical Anthropology*, 166(1), 228-235.
- Valladas, H., Mercier, N., Froget, L., Hovers, E., Joron, J.-L., Kimbel, W. H. and Rak, Y. (1999). TL dates for the Neanderthal site of the Amud Cave, Israel. *Journal of Archaeological Science*, 26(3), 259-268.
- Van den Bergh, G. D., Kaifu, Y., Kurniawan, I., Kono, R. T., Brumm, A., Setiyabudi, E., Aziz, F. and Morwood, M. J. (2016). *Homo floresiensis*-like fossils from the early Middle Pleistocene of Flores. *Nature*, 534(7606), 245-248.
- van der Meulen, M. C., Morgan, T. G., Yang, X., Baldini, T. H., Myers, E. R., Wright, T. M. and Bostrom, M. P. (2006). Cancellous bone adaptation to in vivo loading in a rabbit model. *Bone*, 38(6), 871-877.
- van Lawick-Goodall, J. (1968). The behaviour of free-living chimpanzees in the Gombe Stream Reserve. *Animal behaviour monographs*, 1161-IN12.
- Vanhoof, M. J., Galletta, L., De Groote, I. and Vereecke, E. E. (2021). Functional signals and covariation in triquetrum and hamate shape of extant primates using 3D Geometric Morphometrics. *Journal of Morphology*, 282(9), 1382-1401.
- Viegas, S. F., Patterson, R. M., Todd, P. D. and McCarty, P. (1993). Load mechanics of the midcarpal joint. *The Journal of hand surgery*, 18(1), 14-18.
- Viegas, S. F., Tencer, A. F., Cantrell, J., Chang, M., Clegg, P., Hicks, C., O'Meara, C. and Williamson, J. B. (1987). Load transfer characteristics of the wrist. Part I. The normal joint. *The Journal of hand surgery*, 12(6), 971-978.

- Villa, P. and Roebroeks, W. (2014). Neandertal demise: an archaeological analysis of the modern human superiority complex. *PLoS One*, 9(4), e96424.
- Volkman, S. K., Galecki, A. T., Burke, D. T., Paczas, M. R., Moalli, M. R., Miller, R. A. and Goldstein, S. A. (2003). Quantitative trait loci for femoral size and shape in a genetically heterogeneous mouse population. *Journal of Bone and Mineral Research*, 18(8), 1497-1505.
- Wallace, I. J., Burgess, M. L. and Patel, B. A. (2020). Phalangeal curvature in a chimpanzee raised like a human: Implications for inferring arboreality in fossil hominins. *Proceedings of the National Academy of Sciences*, 117(21), 11223-11225.
- Wallace, I. J., Pagnotti, G. M., Rubin-Sigler, J., Naeher, M., Copes, L. E., Judex, S., Rubin, C. T. and Demes, B. (2015). Focal enhancement of the skeleton to exercise correlates with responsiveness of bone marrow mesenchymal stem cells rather than peak external forces. *Journal of Experimental Biology*, 218(19), 3002-3009.
- Ward, C. V. (2002). Interpreting the posture and locomotion of *Australopithecus afarensis*: where do we stand? *American Journal of Physical Anthropology*, 119(S35), 185-215.
- Ward, C. V. 2007. Postcranial and locomotor adaptations of hominoids. In: HENKE, W. & TATTERSALL, I. (eds.) *Handbook of paleoanthropology*. Berlin: Springer. pp. 1011-1030.
- Ward, C. V. 2013a. Postcranial and locomotor adaptations of hominoids. In: HENKE, W. & TATTERSALL, I. (eds.) *Handbook of Paleoanthropology: Vol I: Principles, Methods and Approaches Vol II: Primate Evolution and Human Origins Vol III: Phylogeny of Hominids*. USA: Springer. pp. 1-22.
- Ward, C. V. 2013b. Postural and locomotor adaptations of *Australopithecus* species. In: REED, K. E., FLEAGLE, J. G. & LEAKEY, R. E. (eds.) *The paleobiology of Australopithecus*. New York: Springer. pp. 235-245.
- Ward, C. V., Tocheri, M. W., Plavcan, J. M., Brown, F. H. and Manthi, F. K. (2014). Early Pleistocene third metacarpal from Kenya and the evolution of modern human-like hand morphology. *Proceedings of the National Academy of Sciences*, 111(1), 121-124.
- Washburn, S. L. (1960). Tools and human evolution. *Scientific American*, 203(3), 62-75.
- Watson, J., Payne, R., Chamberlain, A., Jones, R. and Sellers, W. 2011. The influence of load carrying on gait parameters in humans and apes: implications for the evolution of human bipedalism. In: STRASSER, E., FLEAGLE, J., ROSENBERGER, A. L. & MCHENRY, H. (eds.) *Primate Locomotion*. Boston: Springer. pp. 109-134.
- Whitehouse, W. J. (1974). The quantitative morphology of anisotropic trabecular bone. *Journal of microscopy*, 101(2), 153-168.
- Williams-Hatala, E. M., Hatala, K. G., Gordon, M., Key, A., Kasper, M. and Kivell, T. L. (2018). The manual pressures of stone tool behaviors and their implications for the evolution of the human hand. *Journal of Human Evolution*, 119, 14-26.
- Williams-Hatala, E. M., Hatala, K. G., Key, A., Dunmore, C. J., Kasper, M., Gordon, M. and Kivell, T. L. (2021). Kinetics of stone tool production among novice and expert tool makers. *American Journal of Physical Anthropology*, 174(4), 714-727.
- Williams, E. M., Gordon, A. D. and Richmond, B. G. (2010). Upper limb kinematics and the role of the wrist during stone tool production. *American Journal of Physical Anthropology*, 143(1), 134-145.
- Williams, E. M., Gordon, A. D. and Richmond, B. G. (2012). Hand pressure distribution during Oldowan stone tool production. *Journal of Human Evolution*, 62(4), 520-532.
- Williams, E. M., Gordon, A. D. and Richmond, B. G. (2014). Biomechanical strategies for accuracy and force generation during stone tool production. *Journal of Human Evolution*, 72, 52-63.

- Williams, S. A., Prang, T. C., Meyer, M. R., Nalley, T. K., Van Der Merwe, R., Yelverton, C., García-Martínez, D., Russo, G. A., Ostrofsky, K. R. and Eyre, J. (2021). New fossils of *Australopithecus sediba* reveal a nearly complete lower back. *bioRxiv*, 10e70447.
- Wilson, D. E. and Reeder, D. M. (2005). *Mammal species of the world: a taxonomic and geographic reference*, JHU Press.
- Wolfe, S. W., Crisco, J. J., Orr, C. M. and Marzke, M. W. (2006). The dart-throwing motion of the wrist: is it unique to humans? *The Journal of hand surgery*, 31(9), 1429-1437.
- Wolfe, S. W., Neu, C. and Crisco, J. J. (2000). In vivo scaphoid, lunate, and capitate kinematics in flexion and in extension. *The Journal of hand surgery*, 25(5), 860-869.
- Wolff, J. (1892). *der Knochen, Das Gesetz der Transformation*; Verlag von August Hirschwald.
- Wood, B. and Collard, M. (1999). The human genus. *Science*, 284(5411), 65-71.
- Wood Jones, F. (1942). *The principles of anatomy as seen in the hand*, London, J. & A. Churchill.
- Wu, J. Z., Sinsel, E. W., Shroyer, J. F., Warren, C. M., Welcome, D. E., Zhao, K. D., An, K.-N. and Buczek, F. L. (2014). Analysis of the musculoskeletal loading of the thumb during pipetting—A pilot study. *Journal of Biomechanics*, 47(2), 392-399.
- Wunderlich, R. E. and Jungers, W. L. (2009). Manual digital pressures during knuckle-walking in chimpanzees (*Pan troglodytes*). *American Journal of Physical Anthropology*, 139(3), 394-403.
- Yao, J., Lian, Z., Yang, B. and Fan, Y. 2020. Biomechanics of Ligaments. In: CHENG, C.-K. & WOO, S. L.-Y. (eds.) *Frontiers in Orthopaedic Biomechanics*. Singapore: Springer. pp. 75-87.
- Yeni, Y. N., Zinno, M. J., Yerramshetty, J. S., Zuel, R. and Fyhrie, D. P. (2011). Variability of trabecular microstructure is age-, gender-, race-and anatomic site-dependent and affects stiffness and stress distribution properties of human vertebral cancellous bone. *Bone*, 49(4), 886-894.
- Young, R. W. (2003). Evolution of the human hand: the role of throwing and clubbing. *Journal of anatomy*, 202(1), 165-174.
- Zeininger, A., Richmond, B. G. and Hartman, G. (2011). Metacarpal head biomechanics: A comparative backscattered electron image analysis of trabecular bone mineral density in *Pan troglodytes*, *Pongo pygmaeus*, and *Homo sapiens*. *Journal of Human Evolution*, 60(6), 703-710.
- Zipfel, B., DeSilva, J. M., Kidd, R. S., Carlson, K. J., Churchill, S. E. and Berger, L. R. (2011). The foot and ankle of *Australopithecus sediba*. *Science*, 333(6048), 1417-1420.

8. Appendices

8.1. Appendix A Sample preparation

Appendix A Table 8.1 Full list of extinct and extant specimens used in this thesis.

The extinct taxa are listed first, followed by the extant taxa. In the capitata column the side used for analysis is reported and the superscript indicates which chapters it was included in: 1 = Chapter 3; 2 = Chapter 5; 3 = it was prepared but dropped from analysis. The proximal row column refers to the use of the scaphoid, lunate and triquetrum in Chapter 4, all bones derive from the same side, which is noted in this column. In the sex column, UK indicates unknown sex, F = female and M = male. In the subsistence column PRE indicates the individual derives from a pre-industrialised population and POST indicates a post-industrialised population.

Specimen	Taxon	Sex	Subsistence	Curatorial Institution	Capitata	Date	Reference
UW88_156	<i>A. sediba</i>	F	PRE	University of the Witwatersrand	Right ²	1.98ma	Dirks et al. (2010)
UW88_105	<i>A. sediba</i>	F	PRE	University of the Witwatersrand	Left ²	As above	As above
LB1	<i>H. floresiensis</i>	F	PRE	National Archaeology Institute, Jakarta, Indonesia	Left ²	100-60ka	Sutikna et al. (2016)
LB6	<i>H. floresiensis</i>	F	PRE	National Archaeology Institute, Jakarta, Indonesia	Right ²	As above	As above
UW101_1730_Hand_1	<i>H. naledi</i>	UK	PRE	University of the Witwatersrand, Johannesburg, South Africa	Right ²	235-335ka	Dirks et al. (2017)
Kebara_2	Neanderthal	M	PRE	the Sackler School of Medicine at Tel Aviv University	Left ²	50-60ka	Schwarcz et al. (1989)
Amud_1	Neanderthal	M	PRE	the Sackler School of Medicine at Tel Aviv University	Left ²	50-70ka	Valladas et al. (1999)

LVRB_NN21	Neanderthal	M	PRE	State Museum, Bonn	Left ³	40ka	Schmitz et al. (2002)	
SD-1034	Neanderthal	UK	PRE	Museo Nacional de Ciencias Naturales, Madrid Spain	Left ³	49ka	Kivell et al. (2018c)	
Tabun_C1_1-155	Neanderthal	F	PRE	the Sackler School of Medicine at Tel Aviv University	Left ²	143ka ± 37ka	Coppa et al. (2005)	
Arene_Candide_2	<i>H. sapiens</i>	M	PRE	the Museo Archeologico del Finale	Left ²	12-11ka	Sparacello et al. (2018)	
Barma_Grande_2	<i>H. sapiens</i>	M	PRE	Museo Nazionale Preistorico dei Balzi Rossi	Right ²	15-17ka	Formicola et al. (2004)	
Ohalo_II_H2	<i>H. sapiens</i>	M	PRE	the Sackler School of Medicine at Tel Aviv University	Left ²	19ka	Hershkovitz et al. (1995)	
Qafzeh_9	<i>H. sapiens</i>	M	PRE	the Sackler School of Medicine at Tel Aviv University	Right ³	90-120ka	Grün and Stringer (1991)	
Specimen	Taxon	Sex	Subsistence	Collection	Capitate	Proximal Row	Date	Reference (if available)
81-H1040	<i>H. sapiens</i>	M	POST	Mary Rose Trust	Left ²	/	16 th Century England	Stirland (2005)
81-H1068-DD	<i>H. sapiens</i>	M	POST	Mary Rose Trust	Right ²	/	As above	As above
DCW_AM_10_0_182	<i>H. sapiens</i>	UK	PRE	The Duckworth Collection, University of Cambridge, North American Collection	Right ^{1,2}	Right	late 19th century, Greenland	NA
DCW_AM_10_0_183	<i>H. sapiens</i>	UK	PRE	The Duckworth Collection, University of Cambridge, North American Collection	Right ^{1,2}	Left	late 19th century, Greenland	NA

DCW_AM_3_0_1	<i>H. sapiens</i>	UK	PRE	The Duckworth Collection, University of Cambridge, North American Collection	Left ^{1,2}	Left	late 19th century, Greenland	NA
DCW_AM_3_0_2	<i>H. sapiens</i>	UK	PRE	The Duckworth Collection, University of Cambridge, North American Collection	Left ^{1,2}	/	late 19th century, Greenland	NA
DCW_OC_1_0_26	<i>H. sapiens</i>	UK	PRE	The Duckworth Collection, University of Cambridge, Oceania Collection	Right ^{1,2}	Right	late 19th century, Australia	NA
DCW_OC_31_0_1	<i>H. sapiens</i>	UK	PRE	The Duckworth Collection, University of Cambridge, Oceania Collection	Left ^{1,2}	Left	late 19th century, Chatham Islands	Maxwell (2015)
DCW_OC_31_0_2	<i>H. sapiens</i>	UK	PRE	The Duckworth Collection, University of Cambridge, Oceania Collection	Left ^{1,2}	/	As above	As above
FCS16	<i>H. sapiens</i>	M	POST	Mary Rose Trust	Left ²	/	16 th Century England	(2005)
FCS8	<i>H. sapiens</i>	M	POST	Mary Rose Trust	Left ²	/	As above	As above
INDEN_113	<i>H. sapiens</i>	M	POST	Georg-August-University Goettingen, Anthropology Collection	Right ¹	/	18th-19th century, Inden, Germany	Stephens et al. (2018)
INDEN_118	<i>H. sapiens</i>	F	POST	Georg-August-University Goettingen, Anthropology Collection	Right ^{1,2}	Right	As above	As above
INDEN_243	<i>H. sapiens</i>	M	POST	Georg-August-University Goettingen,	Left ^{1,2}	/	As above	As above

				Anthropology Collection				
INDEN_311	<i>H. sapiens</i>	M	POST	Georg-August-University Goettingen, Anthropology Collection	Left ^{1,2}	/	As above	As above
INDEN_323	<i>H. sapiens</i>	UK	POST	Georg-August-University Goettingen, Anthropology Collection	Right ^{1,2}	Right	As above	As above
INDEN_340	<i>H. sapiens</i>	UK	POST	Georg-August-University Goettingen, Anthropology Collection	Left ^{1,2}	/	As above	As above
INDEN_91	<i>H. sapiens</i>	M	POST	Georg-August-University Goettingen, Anthropology Collection	Right ^{1,2}	Right	As above	As above
NGB_89_SK15_1247	<i>H. sapiens</i>	UK	POST	University of Kent	Left ^{1,2}	/	Medieval Canterbury, UK	Hicks and Hicks (2001)
NHMW_C1-31	<i>H. sapiens</i>	M	PRE	Natural History Museum Vienna	/	Left	Egyptian Nubian dated between the 6th and 11th century	Paoli et al. (1993)
NHMW_J2	<i>H. sapiens</i>	M	PRE	Natural History Museum Vienna	Right ^{1,2}	Right	As above	As above
NHMW_J3	<i>H. sapiens</i>	UK	PRE	Natural History Museum Vienna	Left ^{1,2}	/	As above	As above
NHMW_J7	<i>H. sapiens</i>	F	PRE	Natural History Museum Vienna	/	Right	As above	As above

NHMW_K_13_3	<i>H. sapiens</i>	M	PRE	Natural History Museum Vienna	Right ^{1,2}	/	As above	As above
NHMW_K_41_2	<i>H. sapiens</i>	UK	PRE	Natural History Museum Vienna	Left ^{1,2}	Right	As above	As above
NHMW_K18_2	<i>H. sapiens</i>	F	PRE	Natural History Museum Vienna	Right ^{1,2}	/	As above	As above
NHMW_K24_2	<i>H. sapiens</i>	F	PRE	Natural History Museum Vienna	Right ^{1,2}	/	As above	As above
NHMW_K5_2	<i>H. sapiens</i>	M	PRE	Natural History Museum Vienna	Right ^{1,2}	Right	As above	As above
NHMW_K78_2	<i>H. sapiens</i>	F	PRE	Natural History Museum Vienna	Right ^{1,2}	Right	As above	As above
UNI_FL_3127	<i>H. sapiens</i>	M	PRE	University of Florence	Left ^{1,2}	Left	late 19th Century, Tierra del Fuego	Marangoni et al. (2011)
UNI_FL_4865	<i>H. sapiens</i>	M	POST	University of Florence	Right ^{1,2}	Left	early 20th century, Syracuse, Italy	NA
UNI_FL_4887	<i>H. sapiens</i>	F	POST	University of Florence	Left ^{1,2}	Right	As above	NA
Specimen	Taxon	Sex	Subsistence	Collection	Capitate	Proximal Row		
MRAC_27698	<i>P. paniscus</i>	F	Wild	Royal Museum for Central Africa, Tervuren	Left ^{1,2}	Left		
MRAC_29052	<i>P. paniscus</i>	M	Wild	Royal Museum for Central Africa, Tervuren	Right ^{1,2}	Right		
MRAC_29044	<i>P. paniscus</i>	M	Wild	Royal Museum for Central Africa, Tervuren	Right ^{1,2}	Right		

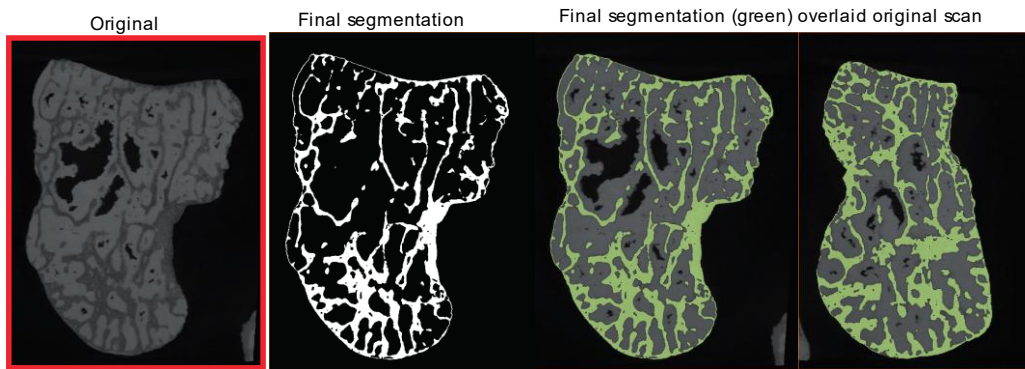
MRAC_27696	<i>P. paniscus</i>	M	Wild	Royal Museum for Central Africa, Tervuren	Right ^{1,2}	Left
MRAC_15294	<i>P. paniscus</i>	M	Wild	Royal Museum for Central Africa, Tervuren	Left ¹	/
MRAC_29045	<i>P. paniscus</i>	F	Wild	Royal Museum for Central Africa, Tervuren	Right ^{1,2}	Left
MRAC_15293	<i>P. paniscus</i>	F	Wild	Royal Museum for Central Africa, Tervuren	Right ^{1,2}	Left
MRAC_29042	<i>P. paniscus</i>	F	Wild	Royal Museum for Central Africa, Tervuren	Left ^{1,2}	Right
SMF_4104	<i>P. troglodytes</i>	UK	Wild	Senckenberg Natural History Museum, Frankfurt	Left ¹	/
MPI_TC_11903	<i>P. troglodytes</i>	M	Wild	Max Planck Institute for Evolutionary Anthropology, Tai Chimpanzee Collection	/	Left
MPI_TC_11789	<i>P. troglodytes</i>	M	Wild	Max Planck Institute for Evolutionary Anthropology, Tai Chimpanzee Collection	Left ^{1,2}	/
MPI_TC_11781	<i>P. troglodytes</i>	M	Wild	Max Planck Institute for Evolutionary Anthropology, Tai Chimpanzee Collection	Right ^{1,2}	Left
MPI_TC_11778	<i>P. troglodytes</i>	F	Wild	Max Planck Institute for Evolutionary	Right ¹	Left

				Anthropology, Tai Chimp Collection		
MPI_TC_14996	<i>P. troglodytes</i>	F	Wild	Max Planck Institute for Evolutionary Anthropology, Tai Chimp Collection	Left ^{1,2}	Left
ZSM_AP_122	<i>P. troglodytes</i>	M	Wild	Bavarian State Collection of Zoology	Right ¹	Right
PC_ZVII_24	<i>P. troglodytes</i>	M	Wild	Powell-Cotton Museum	/	Right
PC_M719	<i>P. troglodytes</i>	M	Wild	Powell-Cotton Museum	/	Right
SMF_63976	<i>G. beringei</i>	UK	Wild	Senckenberg Natural History Museum, Frankfurt	Left ¹	/
ZMB_Mam_83587	<i>G. gorilla</i>	F	Wild	Natural History Museum, Berlin	Left ¹	/
ZMB_Mam_18516	<i>G. gorilla</i>	UK	Wild	Natural History Museum, Berlin	Right ¹	/
ZMB_Mam_83530	<i>G. gorilla</i>	M	Wild	Natural History Museum, Berlin	Right ^{1,2}	/
ZMB_Mam_83545	<i>G. gorilla</i>	M	Wild	Natural History Museum, Berlin	Right ^{1,2}	/
PC_MER_95	<i>G. gorilla</i>	F	Wild	Powell-Cotton Museum	Left ^{1,2}	Left
PC_MER_135	<i>G. gorilla</i>	M	Wild	Powell-Cotton Museum	/	Left
PC_MER_264	<i>G. gorilla</i>	M	Wild	Powell-Cotton Museum	Right ^{1,2}	Right
PC_MER_300	<i>G. gorilla</i>	F	Wild	Powell-Cotton Museum	Right ^{1,2}	Right
PC_MER_372	<i>G. gorilla</i>	M	Wild	Powell-Cotton Museum	Right ^{1,2}	Right

PC_MER_962	<i>G. gorilla</i>	M	Wild	Powell-Cotton Museum	/	Right
PC_MERI_29	<i>G. gorilla</i>	F	Wild	Powell-Cotton Museum	Left ¹	Left
PC_CAMI_230	<i>G. gorilla</i>	M	Wild	Powell-Cotton Museum	Left ¹	Left
PC_MER_138	<i>G. gorilla</i>	F	Wild	Powell-Cotton Museum	Left ^{1,2}	Left
PC_MER_174	<i>G. gorilla</i>	M	Wild	Powell-Cotton Museum	Right ^{1,2}	Right
PC_MER_696	<i>G. gorilla</i>	F	Wild	Powell-Cotton Museum	Right ^{1,2}	Right
PC_MER_856	<i>G. gorilla</i>	F	Wild	Powell-Cotton Museum	Left ¹	Left
PC_MER_879	<i>G. gorilla</i>	M	Wild	Powell-Cotton Museum	Left ^{1,2}	Left
PC_ZVI_32	<i>G. gorilla</i>	M	Wild	Powell-Cotton Museum	/	Right
SMF_6999	<i>P. abelii</i>	F	Wild	Senckenberg Natural History Museum, Frankfurt	Right ^{1,2}	/
SMF_6785	<i>P. abelii</i>	M	Wild	Senckenberg Natural History Museum, Frankfurt	/	Right
NMNH_267325	<i>P. abelii</i>	M	Wild	Smithsonian Institution National Museum of Natural History	Left ¹	Left
ZMB_Mam_6948	<i>P. pygmaeus</i>	F	Wild	Natural History Museum, Berlin	Left ^{1,2}	Left
ZMB_Mam_6947	<i>P. pygmaeus</i>	M	Wild	Natural History Museum, Berlin	Left ^{1,2}	Left

ZMB_Mam_11647	<i>P. pygmaeus</i>	UK	Wild	Natural History Museum, Berlin	Left ^{1,2}	/
SMF_24510	<i>P. pygmaeus</i>	F	Wild	Senckenberg Natural History Museum, Frankfurt	Right ^{1,2}	Right
SMF_74303	<i>P. pygmaeus</i>	F	Wild	Senckenberg Natural History Museum, Frankfurt	/	Left
SMF_84218	<i>P. pygmaeus</i>	F	Captive	Senckenberg Natural History Museum, Frankfurt	Left ^{1,2}	Left
ZSM_1907_0622	<i>P. pygmaeus</i>	UK	Wild	Bavarian State Collection of Zoology	Right ^{1,2}	/
ZSM_1907_0633b	<i>P. pygmaeus</i>	F	Wild	Bavarian State Collection of Zoology	Right ^{1,2}	Right
ZSM_1907_0629b	<i>P. pygmaeus</i>	M	Wild	Bavarian State Collection of Zoology	Right ^{1,2}	/
ZSM_1982_0092	<i>P. pygmaeus</i>	F	Captive	Bavarian State Collection of Zoology	/	Right
ZSM_1966_0203	<i>P. pygmaeus</i>	M	Captive	Bavarian State Collection of Zoology	/	Right
ZSM_1907_0660	<i>P. pygmaeus</i>	F	Wild	Bavarian State Collection of Zoology	Right ^{1,2}	Right
ZSM_AP_120	<i>P. pygmaeus</i>	M	Wild	Bavarian State Collection of Zoology	Left ¹	Left
ZSM_1907_0483	<i>P. pygmaeus</i>	F	Wild	Bavarian State Collection of Zoology	/	Right
ZSM_1909_0801	<i>P. pygmaeus</i>	M	Wild	Bavarian State Collection of Zoology	Right ^{1,2}	Right

Australopithecus sediba, MH2 Left

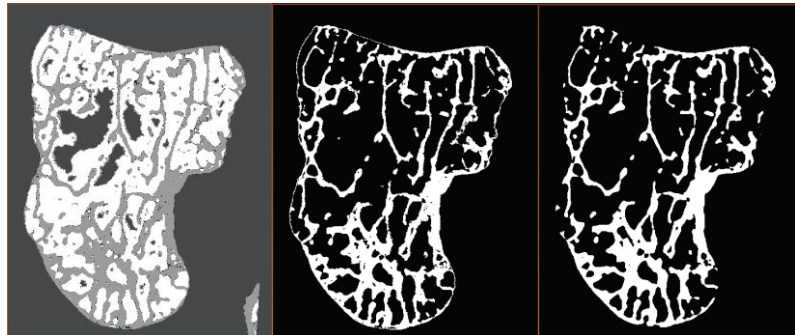


Steps

MIA segment m3-g100-060

Bone material only

Median filter applied

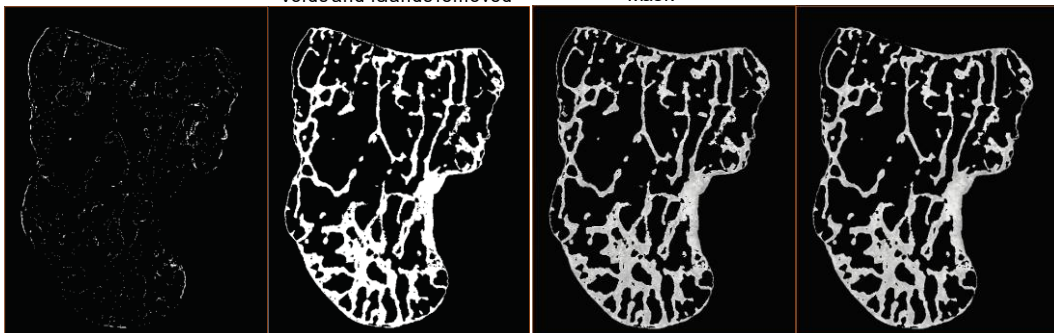


Voids and islands

Voids and islands removed

Mask

Median filter

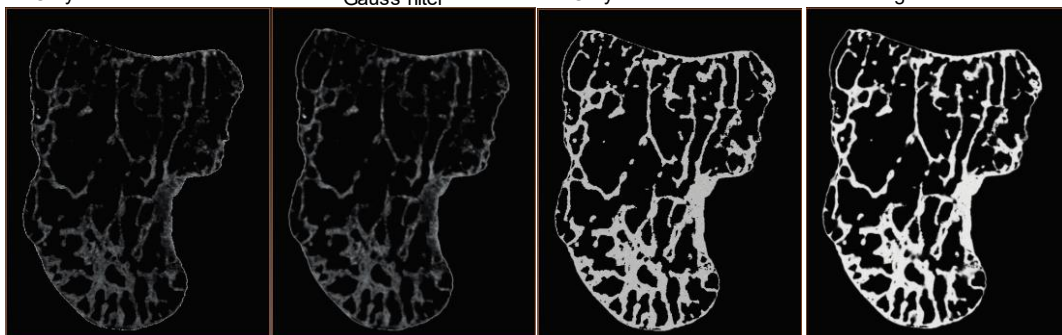


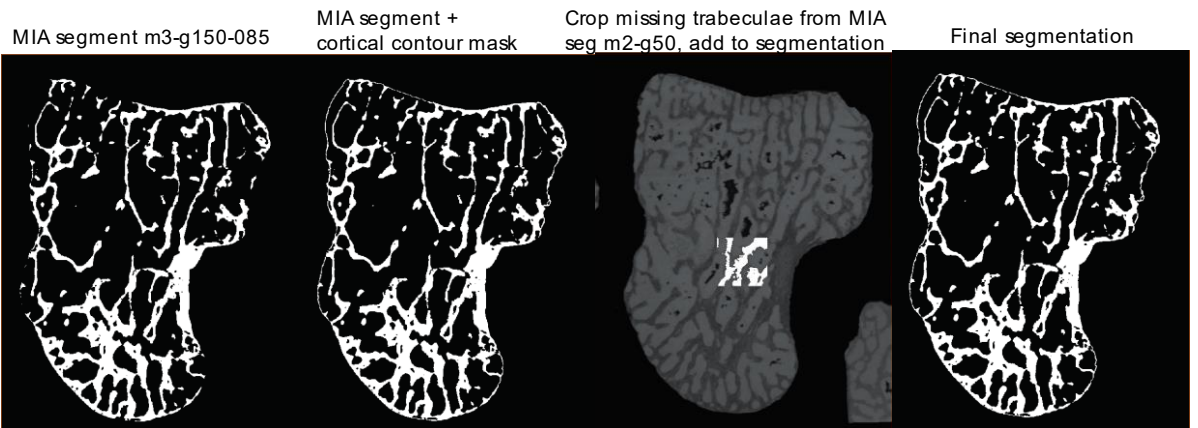
Greyscale inversion

Gauss filter

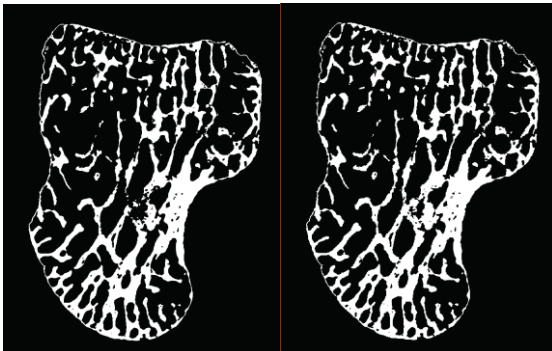
Greyscale smoothed

Final gauss filter

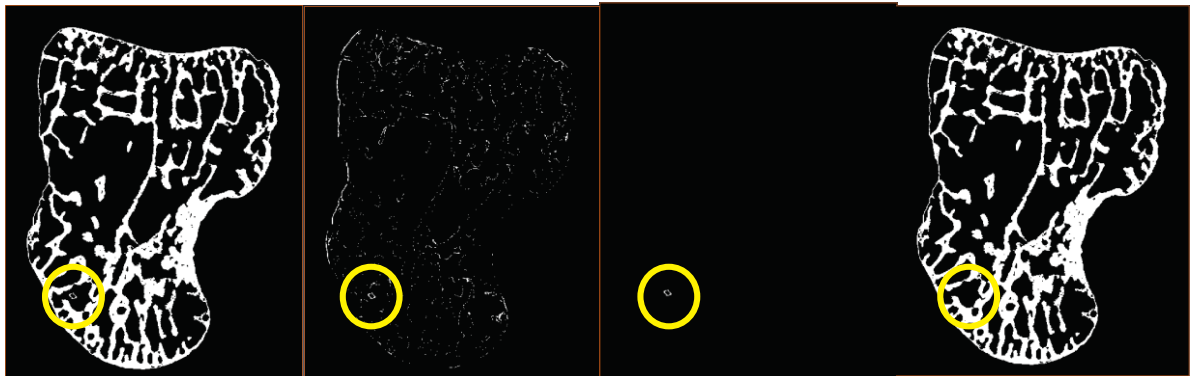




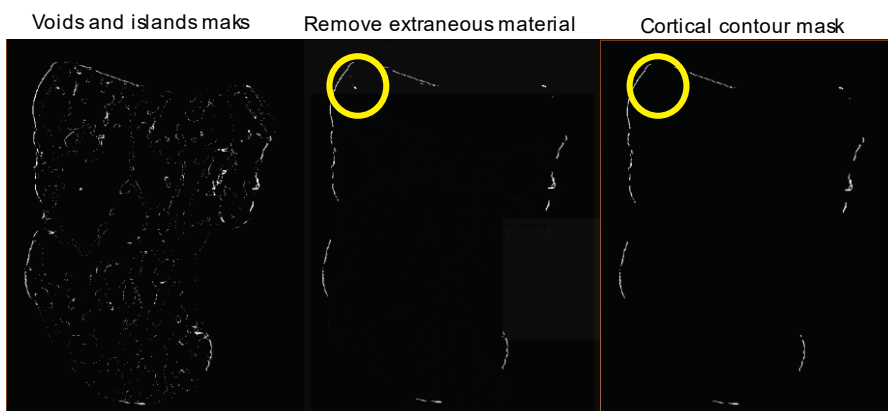
Example: Slice 228 without trabecular plates re-added Slice 228, with trabecular plates added



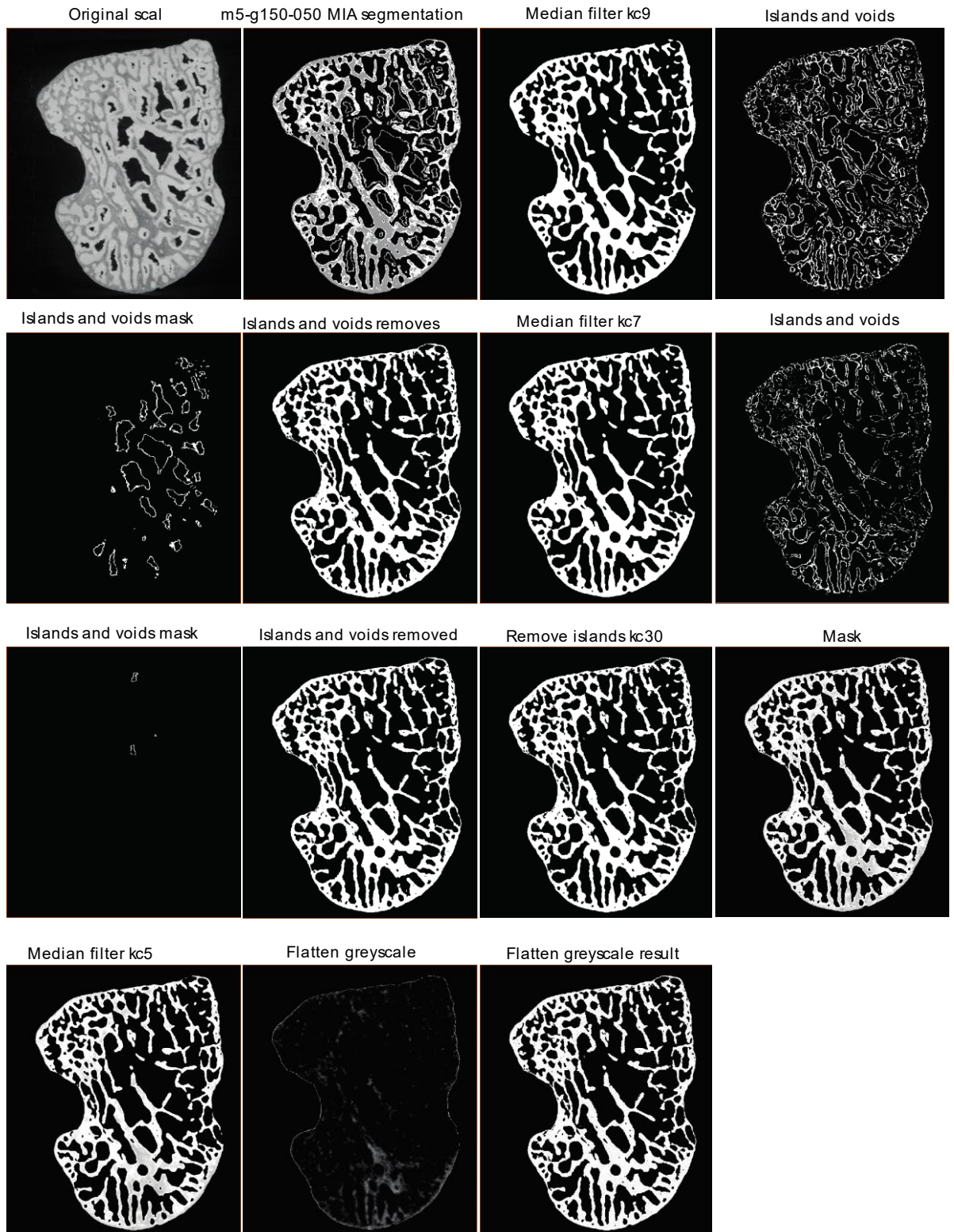
Example: creating voids and islands masks on slice yz 266

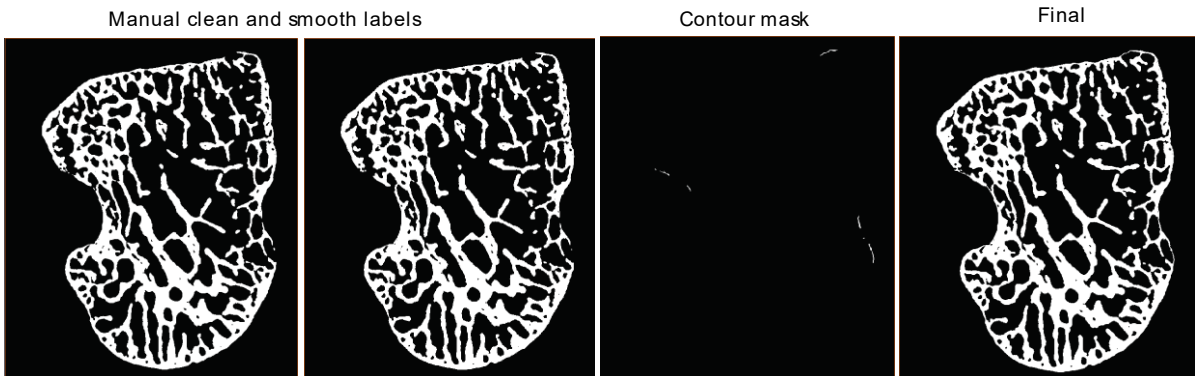
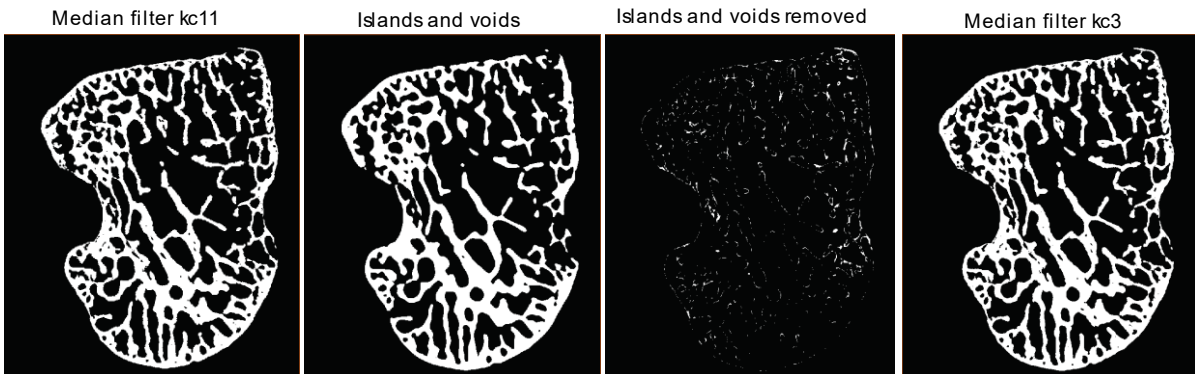
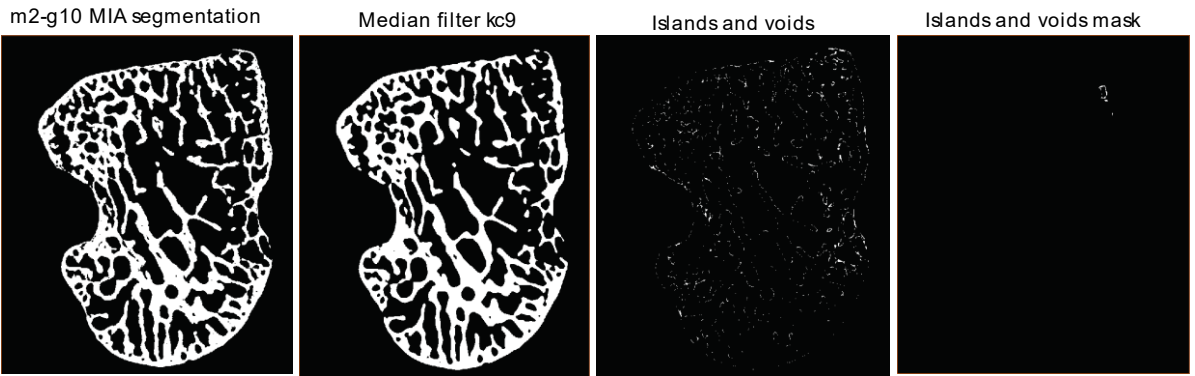


Example: creating cortical contour mask from voids and islands masks

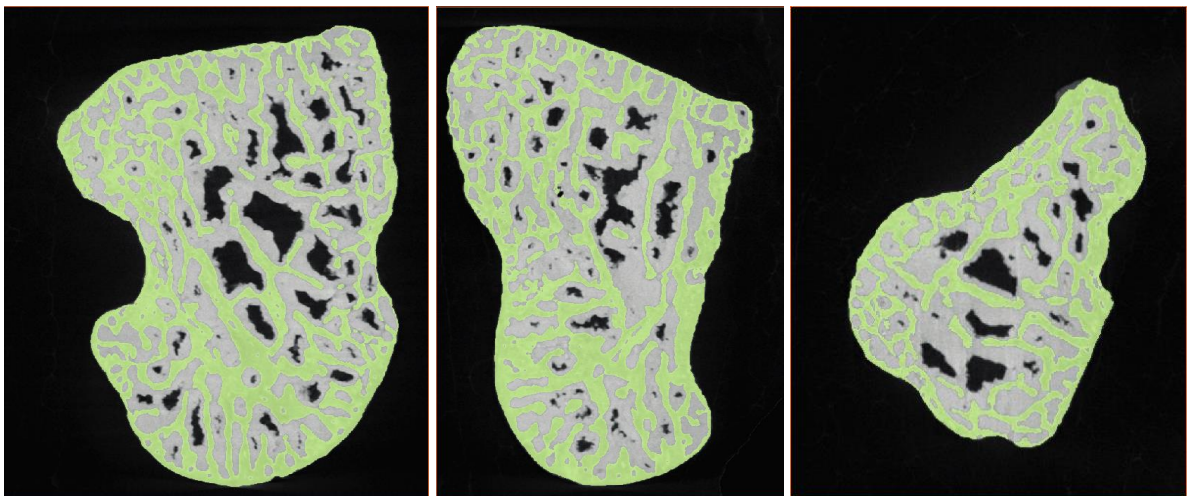


Australopithecus sediba, MH2 right



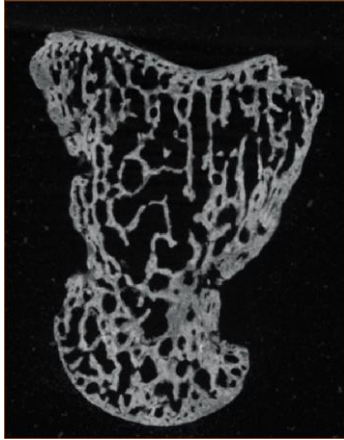


Final segmentation (green) overlaid original scal

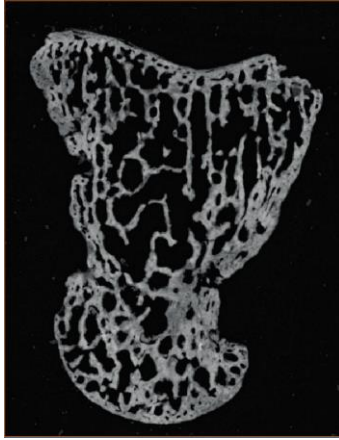


Homo floresiensis LB1, left

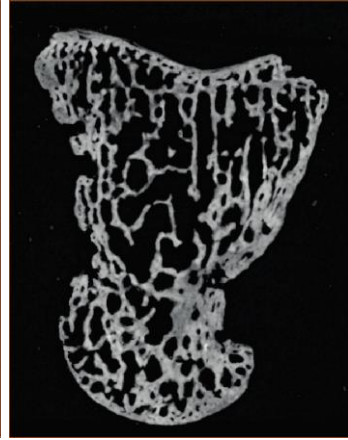
Original scal



Background noise removed,
enhanced boundaries



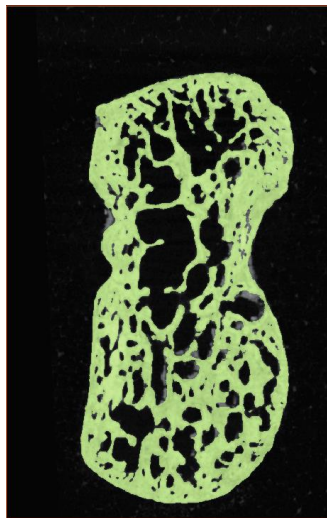
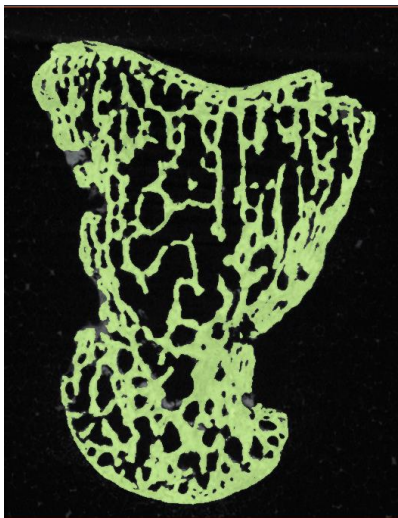
Manual clean, median filter kc3



MIA segment m2-g10

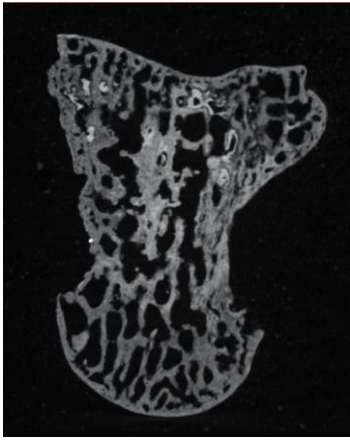


Final segmentation (green) overlaid original scal

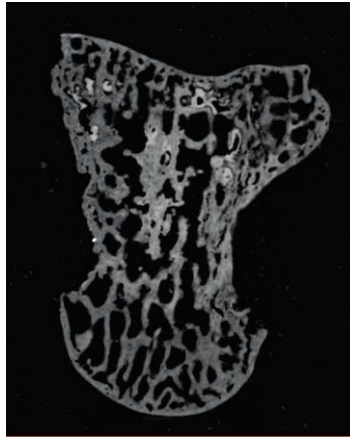


Homo floresiensis LB6, right

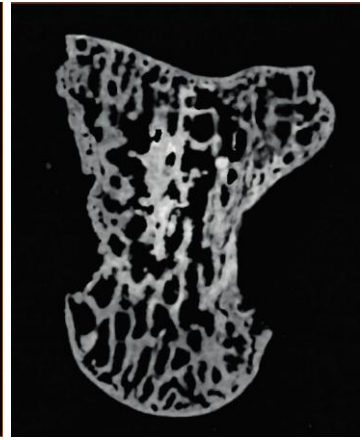
Original scal



Background noise removed,
enhanced boundaries



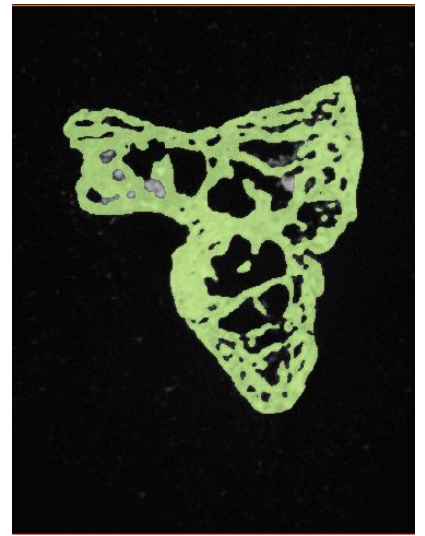
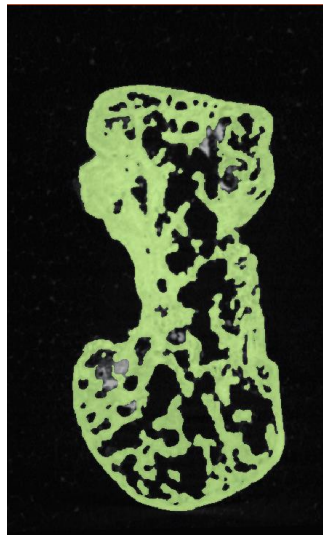
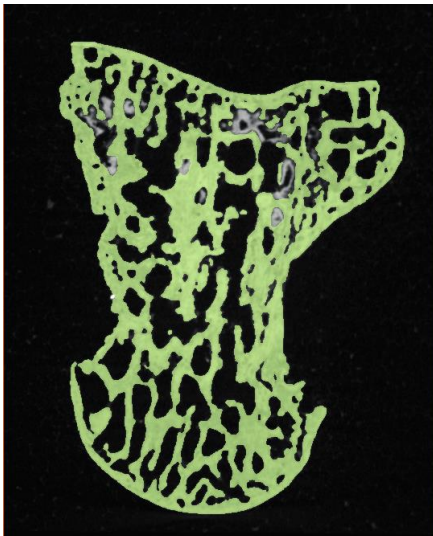
Manual clean, median filter kc3



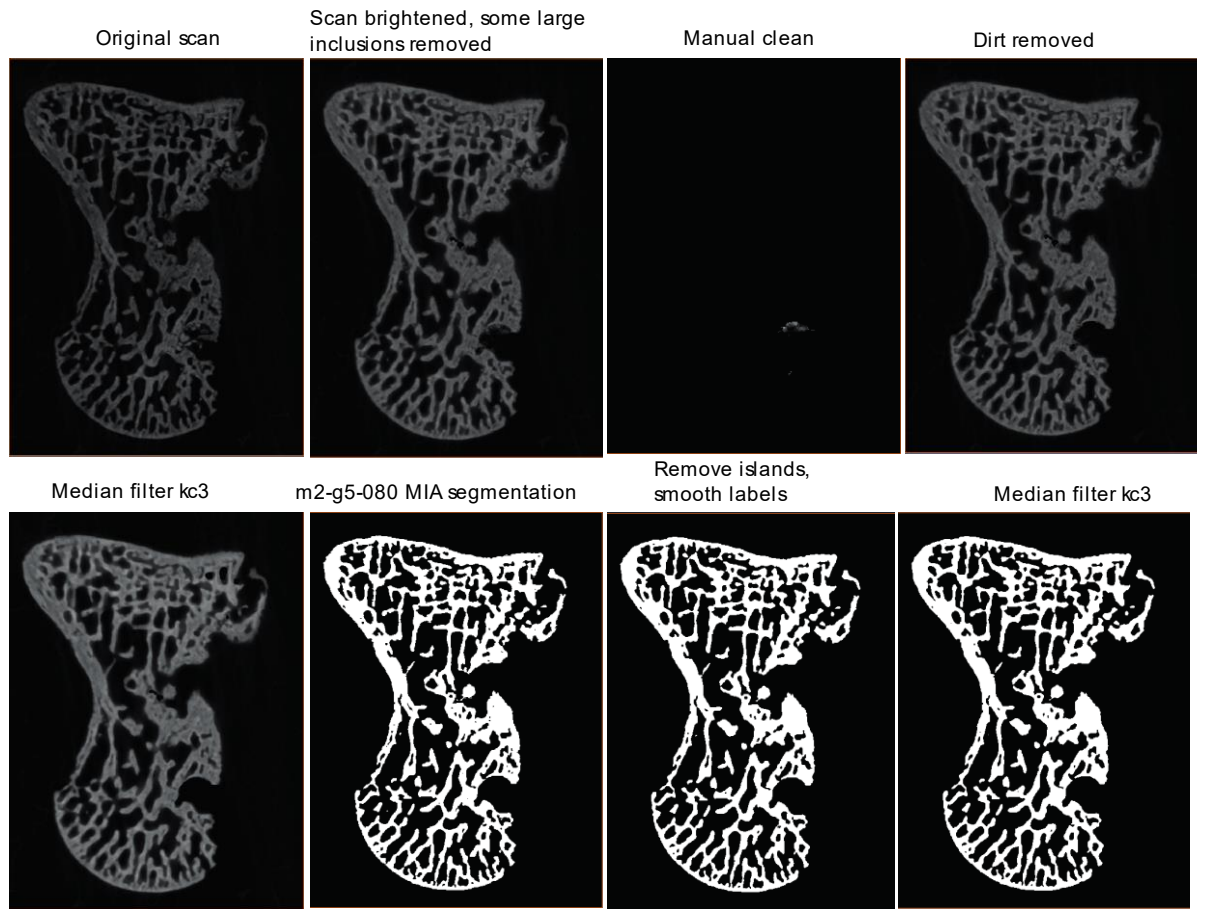
MIA segment m2-g8



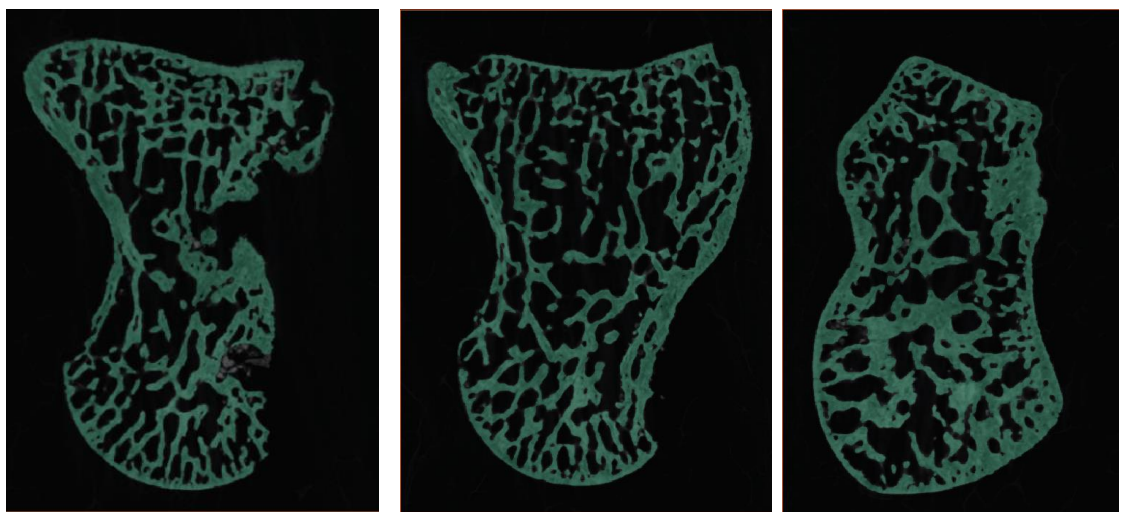
Final segmentation (green) overlaid original scal



Homo naledi, Hand 1, right



Final segmentation (green) overlaid original scan

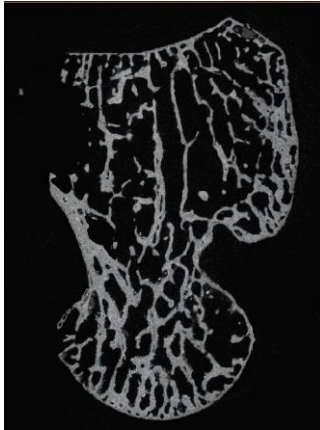


Neanderthal, Amud 1 left

Original



Bright inclusions removed



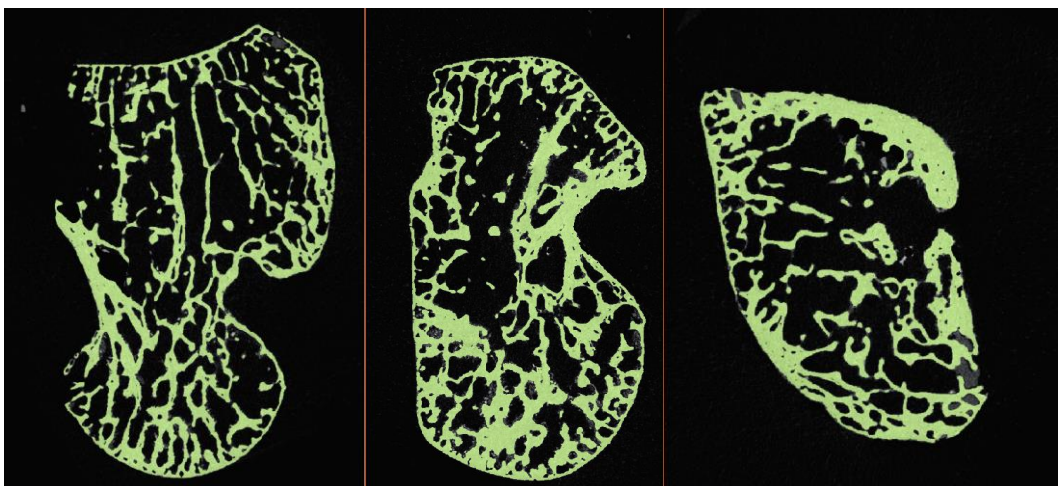
m2-g20-085
with smooth labels



Median filter kc3



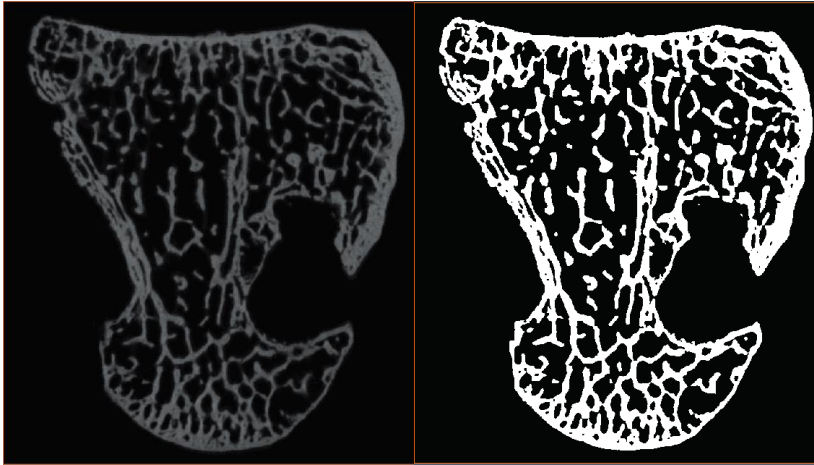
Final segmentation (green) overlaid original scan



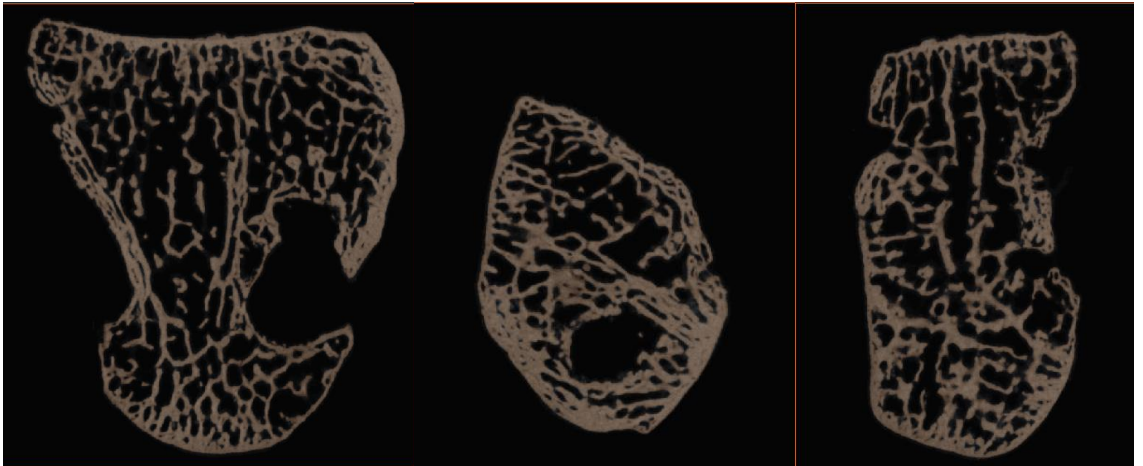
Neanderthal, Kebara 2 left

Original

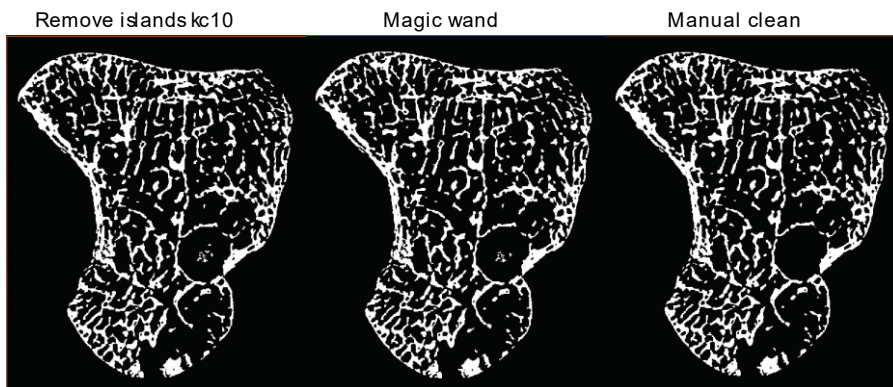
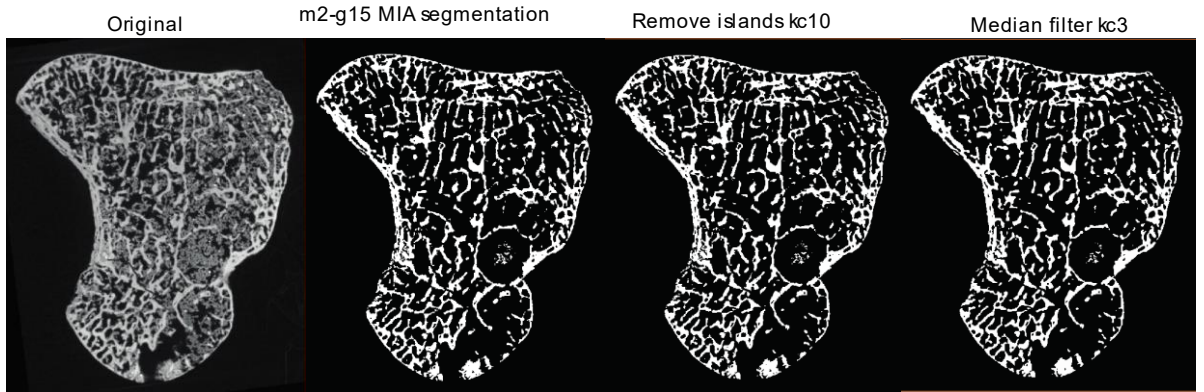
m2-g15 MIA segmentation



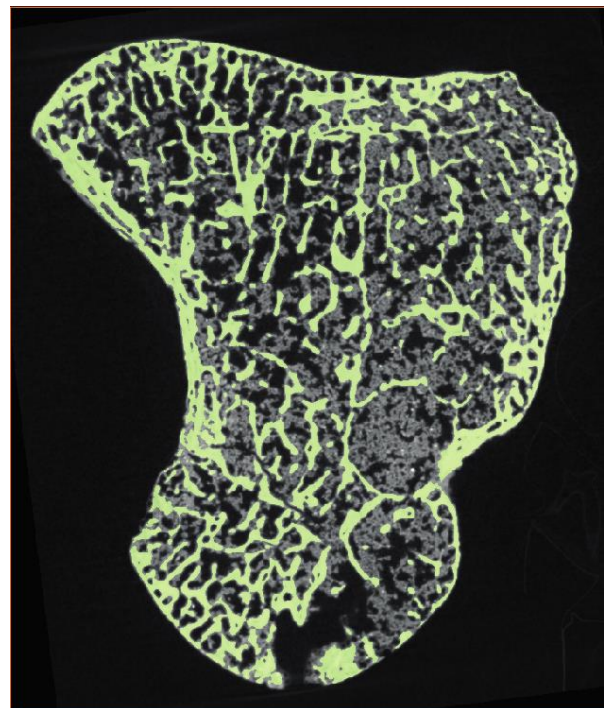
Final segmentation (orange) overlaid original scan



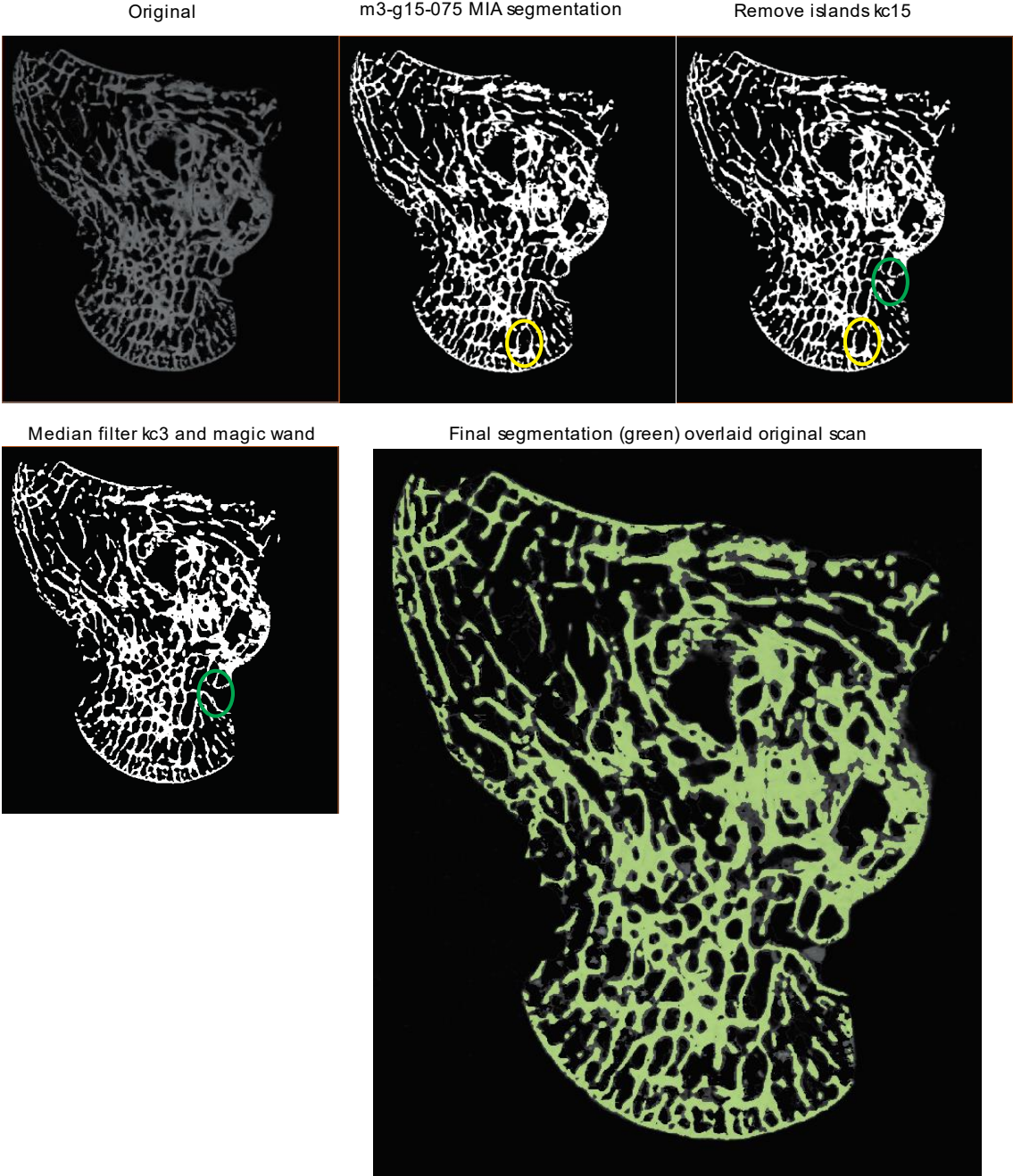
Neanderthal, SD-1034 left



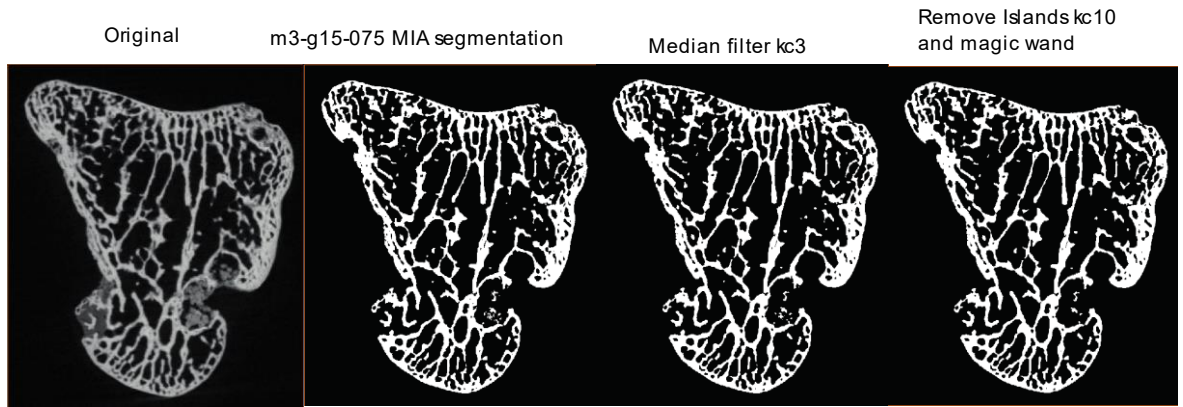
Final segmentation (green) overlaid original scan



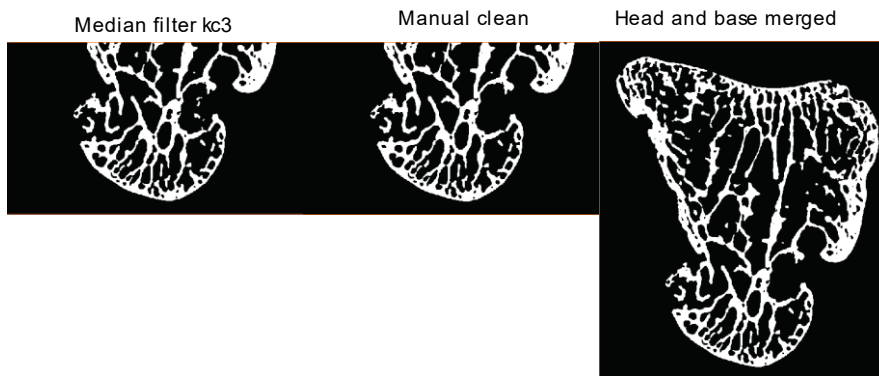
Neanderthal, LVRB-NN21 left



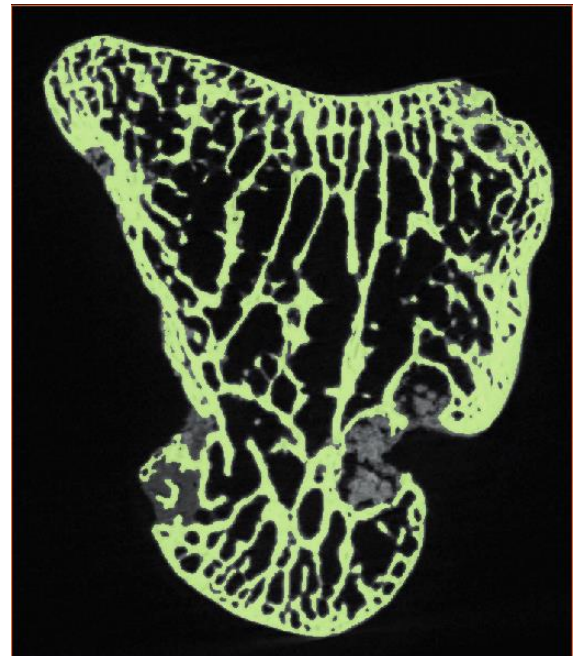
Neanderthal, Tabun C1 left



Head only

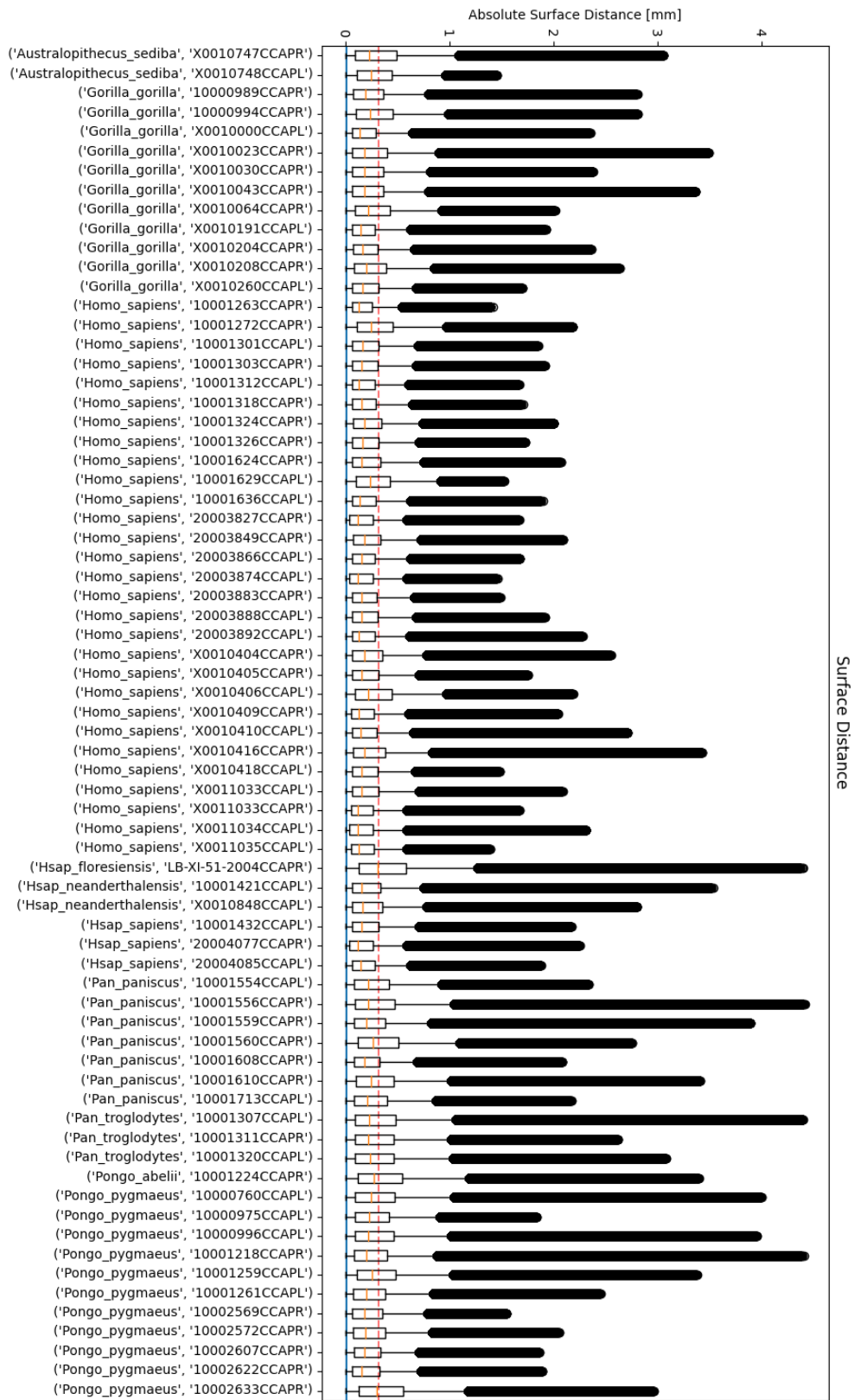


Final segmentation (green) overlaid original scan



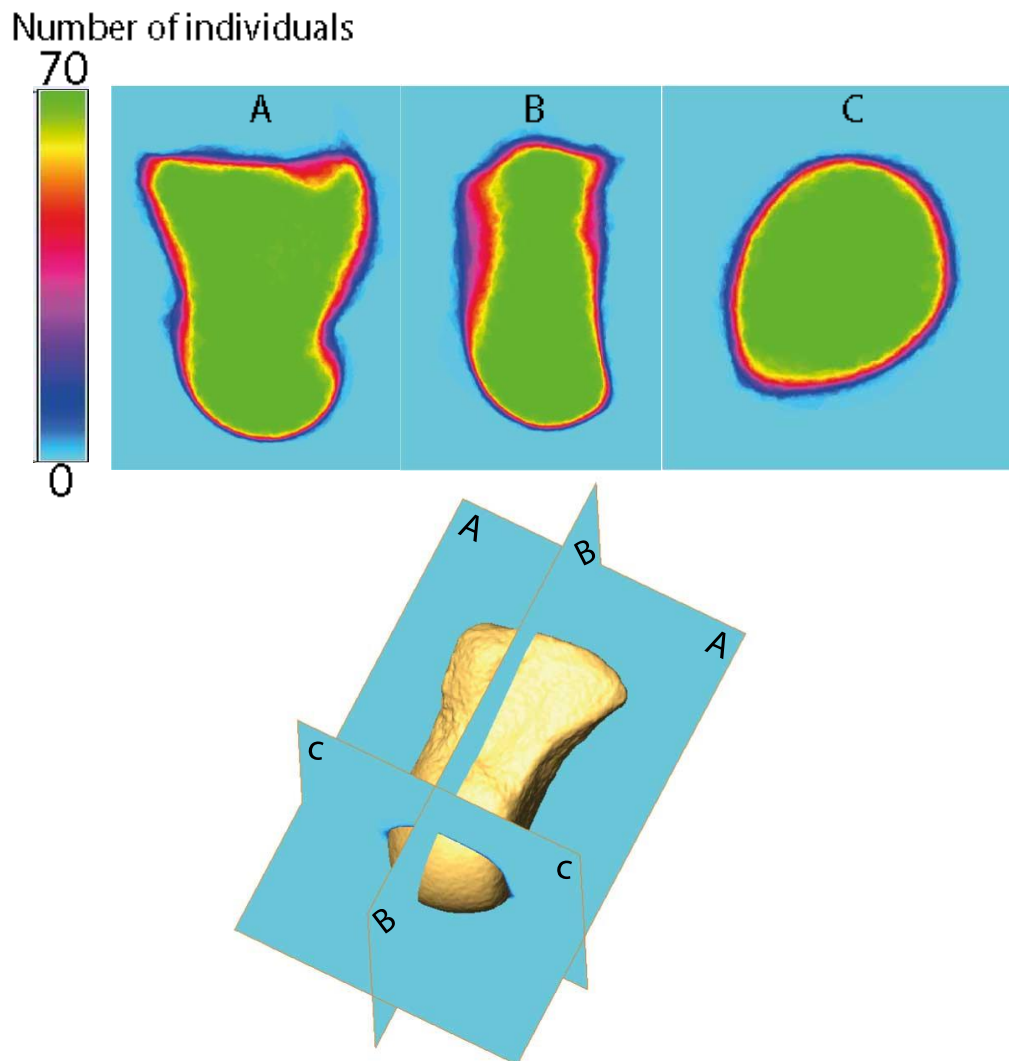
Appendix A Figure 8.1 Illustrations of the step by step process of tissue segmenting the fossil specimens.

Each step is labelled with the step undertaken. Kc = kernel size; m = number of materials specified to MIA; g = grid size used in MIA.



Appendix A Figure 8.2 Box and whisker plots of absolute surface distance movements during the registration of mean capitae shape for cHMA analysis.

The absolute surface distance reflects the amount of deformation (movement) the surface of the capitates underwent after both iterations of the similarity and b-spline protocols. These graph the mean movement for the registration of the whole capitate, including the distal component that was not included in analysis, as the proximal capitate was partitioned for analysis after the initial shape registration. LB1, Amud 1 and *Homo naledi* are not included in this figure as they were not included in the shape registration due to broken components. Each of those fossils was registered separately onto the mean capitate model.



Appendix A Figure 8.3 Visual representation of individuals registered in the mean capitate shape.

The original shape of the 70 capitate bones used to register the mean capitate shape are superimposed onto the inner mean mesh (yellow model in the bottom figure). The scale bar indicates how many capitates overlap in that space based on their original geometry, i.e., the green space indicates that the original shape of all 70 capitates overlap in that space. The bright blue indicates zero individuals were in that space. Only the proximal capitate was included in the final analysis, although the original registration was undertaken on the whole bone.

8.2. Appendix B: Published Work

Cortical and trabecular bone structure of the hominoid capitate

Emma E. Bird¹  | Tracy L. Kivell^{1,2} | Matthew M. Skinner^{1,2}

¹Skeletal Biology Research Centre, School of Anthropology and Conservation, University of Kent, Canterbury, UK

²Department of Human Evolution, Max Planck Institute for Evolutionary Anthropology, Leipzig, Germany

Correspondence

Emma E. Bird, School of Anthropology and Conservation, University of Kent, Marlowe Building, Canterbury, CT2 7NR, UK.

Email: eeb8@kent.ac.uk

Funding information

University of Kent, Grant/Award Number: 50th Anniversary Research Scholarship; Horizon 2020 Framework Programme, Grant/Award Number: 819960; Max Planck Society; FP7 Ideas: European Research Council, Grant/Award Number: 336301

Abstract

Morphological variation in the hominoid capitate has been linked to differences in habitual locomotor activity due to its importance in movement and load transfer at the midcarpal joint proximally and carpometacarpal joints distally. Although the shape of bones and their articulations are linked to joint mobility, the internal structure of bones has been shown experimentally to reflect, at least in part, the loading direction and magnitude experienced by the bone. To date, it is uncertain whether locomotor differences among hominoids are reflected in the bone microarchitecture of the capitate. Here, we apply a whole-bone methodology to quantify the cortical and trabecular architecture (separately and combined) of the capitate across bipedal (modern *Homo sapiens*), knuckle-walking (*Pan paniscus*, *Pan troglodytes*, *Gorilla* sp.), and suspensory (*Pongo* sp.) hominoids ($n = 69$). It is hypothesized that variation in bone microarchitecture will differentiate these locomotor groups, reflecting differences in habitual postures and presumed loading force and direction. Additionally, it is hypothesized that trabecular and cortical architecture in the proximal and distal regions, as a result of being part of mechanically divergent joints proximally and distally, will differ across these portions of the capitate. Results indicate that the capitate of knuckle-walking and suspensory hominoids is differentiated from bipedal *Homo* primarily by significantly thicker distal cortical bone. Knuckle-walking taxa are further differentiated from suspensory and bipedal taxa by more isotropic trabeculae in the proximal capitate. An allometric analysis indicates that size is not a significant determinate of bone variation across hominoids, although sexual dimorphism may influence some parameters within *Gorilla*. Results suggest that internal trabecular and cortical bone is subjected to different forces and functional adaptation responses across the capitate (and possibly other short bones). Additionally, while separating trabecular and cortical bone is normal protocol of current whole-bone methodologies, this study shows that when applied to carpals, removing or studying the cortical bone separately potentially obfuscates functionally relevant signals in bone structure.

KEYWORDS

cancellous bone, functional morphology, locomotion, primates, wrist

This is an open access article under the terms of the Creative Commons Attribution License, which permits use, distribution and reproduction in any medium, provided the original work is properly cited.

© 2021 The Authors. *Journal of Anatomy* published by John Wiley & Sons Ltd on behalf of Anatomical Society

1 | INTRODUCTION

Primates use their hands in a diverse set of postures to manipulate and navigate their environment (Fragaszy & Crast, 2016). The many articulations within the wrist are central to the capacity of the hand to move through multiple planes of space and, in combination with soft tissue morphology, joint congruence determines the degree of stability, flexibility and dexterity within the wrist and hand (Orr, 2010). The capitate articulates proximally with the scaphoid and lunate and distally with the trapezoid, hamate, and metacarpals 2, 3, and, sometimes, 4 (Kivell, 2016a). As such, the external morphology of the capitate plays a key role in the range of motion at the wrist as it is a central component of the midcarpal joint proximally and the carpometacarpal joints distally (Crisco et al., 2005; Jenkins & Fleagle, 1975; Jouffroy & Medina, 2002; Kijima & Viegas, 2009; Lewis, 1989; Orr, 2017; Orr et al., 2010).

The external morphology of the hominoid capitate has featured in hypotheses about the locomotor behavior in the last common ancestor of *Pan* and Hominini (Begun, 2004; Dainton & Macho, 1999; Kivell & Schmitt, 2009; Richmond et al., 2001; Tocheri et al., 2007) and the evolution of hominin dexterity and tool-related behaviors (Marzke, 1983; Niewoehner et al., 1997; Rein & Harvati, 2013; Wolfe et al., 2006). However, drawing locomotor or postural inferences based on external morphology is potentially confounded by the retention of primitive features that are no longer functionally significant (Kivell, 2016b; Lieberman, 1997; Pontzer et al., 2006; Ruff et al., 2006; Ward, 2002; Zeininger et al., 2011). Furthermore, making biomechanical inferences from external morphology requires in-depth knowledge of the form-function relationship of the bone as well as its surrounding soft tissue and articular environment. This is a particular challenge for carpal research as understanding the kinematics and kinetics of the wrist is inherently difficult due to complications in imaging and analyzing the small, closely compacted bones without disrupting the normal kinematic chain (Brainerd et al., 2010; Gatesy et al., 2010; Orr, 2016; Wolfe et al., 2000, 2006). Although advances in 3D imaging and computational techniques have begun to improve our knowledge of human wrist biomechanics (see Orr, 2016 for review), our understanding of nonhuman ape biomechanics remains more limited (but see Orr, 2017, 2018). Moreover, the functional relationship between cortical and trabecular tissue within short bones is not well understood, and it is not clear how they may interact to provide whole bone functionality under the high mechanical loads of locomotion and manipulation. To date, it has yet to be determined whether the internal bone structure of the capitate might reflect differences in hand and wrist use across extant hominoids. Here we apply a whole-bone methodology to investigate how the internal cortical and trabecular bone structure potentially varies within the capitate in a broad sample of *Homo* (recent humans), *Pan* (chimpanzees and bonobos), *Gorilla*, and *Pongo* (orangutans).

1.1 | Trabecular bone: The relationship between behavior and structure

In addition to some important clade specific synapomorphies (Lewis, 1989; Sarmiento, 1988; Tocheri et al., 2008), the wrists of extant hominoids are adapted to their specialized behaviors and are habitually loaded in different ways. The *Homo* hand is conspicuous among the ape clade as the only species not to habitually utilize the hand for locomotion. Instead, the wrist experiences forces generated predominantly during tool use and other forms of manipulation. High compressive loads are imposed across the wrist by muscle contractions arising from the strong and forceful human thumb as well as flexion of the fingers (Bardo et al., 2018; Marzke, 1997; Napier, 1956; Tocheri, 2007). Bones must also withstand and transmit shear and tensional strains as force is transferred radio-ulnarly across the wrist (Marzke, 2013; Tocheri, 2007). There is an abundance of clinical evidence to support the hypothesis that the Dart Throwers Motion (DTM) is the functional axis of human wrist movement (Brigstocke et al., 2014; Crisco et al., 2005, 2011; Schuind et al., 1994). The DTM runs from radial deviation in extension to ulnar deviation in flexion and is used across numerous activities from throwing an object to pouring water from a jug (Brigstocke et al., 2014). During this movement, the capitate is very mobile against a stabilized proximal row, with the rotation axis perpendicular to the wrist movement (Crisco et al., 2005).

In contrast, nonhuman apes utilize their forelimbs during locomotion. *Pongo* utilize a range of torso orthograde suspensory and climbing postures in an almost exclusively arboreal environment (Manduell et al., 2011; Thorpe & Crompton, 2006, 2009). In these positions, the wrist experiences substantial tensile loading from gravitational forces and stabilising ligaments, as well as compressive stress from muscle contractions (Isler & Thorpe, 2004; Swartz et al., 1989). *Gorilla* and *Pan* are primarily terrestrial knuckle-walkers but also engage in various types and frequencies of arboreal locomotion depending on the species, population or sex (Doran, 1993; Hunt, 1992; van Lawick-Goodall, 1968; Neufuss et al., 2017; Remis, 1995, 1998; Thompson et al., 2018). During knuckle-walking, the wrist must resist compressive loading from both muscle contractions stabilizing the joints and gravitation forces acting on the body mass (Carlson & Patel, 2006). However, the knuckle-walking posture differs somewhat between the two genera. When compared to *Gorilla*, *Pan* typically use more variable hand and forelimb postures, do not bear weight as evenly across the digits, and more frequently engage a palm-in forelimb posture (Finestone et al., 2018; Inouye, 1994; Matarazzo, 2013; Wunderlich & Jungers, 2009). *Gorilla* typically knuckle-walk on digits 2–5 and more regularly utilize a palm-backwards forelimb posture (Inouye, 1994; Matarazzo, 2013; Tuttle, 1969), although hand postures in the wild are more variable (Thompson et al., 2018). Although *Gorilla* are hypothesised to use a more neutral, columnar wrist posture than *Pan* (Kivell & Schmitt, 2009), recent kinematic studies of captive African apes found that *Gorilla* and *Pan* were generally similar in their degree of wrist of extension during knuckle-walking (Finestone et al., 2018; Thompson, 2020).

Bone functional adaptation describes the biological process of bone altering its structure to optimize resistance against peak mechanical loads habitually experienced throughout the lifetime of the individual (Barak et al., 2011; Doube et al., 2011; Martin et al., 1998; Ruff et al., 2006). Numerous experimental studies suggest that variation in structure reflects, at least in part, load experienced during life (see Kivell, 2016b for review) and thus provides an opportunity to draw behavioral inferences better linked to actual, rather than potential, behavior (Frost, 1987; Ruff & Runestad, 1992). Bone functional adaptation research cannot only facilitate a greater understanding of the joint loading and kinematics of extant species but may also provide an informative avenue for behavioral reconstruction in fossil taxa (DeSilva & Devlin, 2012; Dunmore et al., 2020; Georgiou et al., 2020; Griffin et al., 2010; Kivell et al., 2018; Skinner et al., 2015; Su & Carlson, 2017). Previous studies of primate trabecular bone structure within the capitate have used a volume of interest (VOI) sampling sphere but have found limited functional correlation with locomotor behavior (Ragni, 2020; Schilling et al., 2014). However, using a whole epiphysis/bone methodology has been more functionally informative for hand bone studies (Dunmore et al., 2019; Stephens et al., 2016, 2018; Tsegai et al., 2013, 2017). Furthermore, a whole-bone approach to carpal functional adaptation is preferable given their irregular shapes and variation across different taxa (Gross et al., 2014; Schilling et al., 2014; Tsegai et al., 2013).

However, inferring a form-function relationship between bone microarchitecture and behavior is not always straightforward due to several potentially confounding variables (for a comprehensive review and discussion see Kivell, 2016b). Firstly, bone modelling (*sensu* Barak, 2019) is influenced by the genetic blueprint of the individual, as well as life history factors such as lactation or pregnancy (Kalkwarf & Specker, 1995; Lieberman, 1996; Lovejoy et al., 2003; Parsons et al., 1997; Paternoster et al., 2013; Pettersson et al., 2010; Tsegai et al., 2017; Yeni et al., 2011). Systemic features such as these potentially undermine our ability to differentiate between functional and nonfunctional patterns expressed in bone structure across different individuals or species. Secondly, there is a higher capacity for functional adaptation to occur during the juvenile and young adult periods and the extent to which bone microarchitectural patterns can be linked to adult behavior has been debated (Bertram & Schwartz, 1991; Pearson & Lieberman, 2004; Ruff et al., 2006). This is particularly salient when analyzing African apes because locomotor behavior is known to differ across age categories (Doran, 1992, 1997). Finally, there is also uncertainty regarding the loading frequency and magnitude necessary to induce a functional adaptation response (Barak et al., 2011; Frost, 1987; Ruff et al., 2006; Wallace et al., 2015). Consequently, microarchitecture will never represent the mechanical ideal of the bone as competing demands on bone tissue will result in a compromise morphology (Ruff et al., 2006).

1.2 | Cortical bone: Contribution to bone structure and functional adaptation

Carpal bones function within an intricate biomechanical environment. The bones and ligaments are interdependent and work together making minor adjustments and movements in concert to create overall hand motion (Kijima & Viegas, 2009; Lewis, 1989; Orr, 2017). Among the carpus, the central role of the capitate within the midcarpal joint and its articulation with the metacarpus makes it an ideal bone to investigate functional differences in wrist loading. The distal capitate is not only compressed via its carpometacarpal articulations but it also receives tensional strain via the attachment of several extrinsic (between carpals and other hand bones) and intrinsic (between carpal bones) ligaments (Kijima & Viegas, 2009; Regal et al., 2020; Schuind et al., 1995). In contrast, the proximal capitate does not receive any ligaments but forms the “ball” component of the ball and socket midcarpal joint within the highly mobile proximal row and is thus loaded predominantly in compression (Garcia-Elias et al., 1994; Kivell, 2016a; Lewis, 1989; Orr, 2017).

Unlike long bones, short bones like carpals generally have a thin cortical shell and the entire internal space is filled with trabeculae (Currey, 2002; Schilling et al., 2014). During movement, short bones are likely to bear a significant portion of the load imposed upon the region as they resist against compressive forces and transfer load through the bone from one joint articulation to another, while also being strained via tensional loads from attached ligaments (Currey, 2002; Yao et al., 2020). Cortical and trabecular bone have divergent material properties due to differences in porosity, mineralization and cellular constitution (Currey, 2002). Cortical bone is stiffer and stronger than trabecular bone (Guo, 2001; Martin et al., 1998), but due to its lower porosity, it is slower than trabecular bone to model and is less compliant (Hart et al., 2017; Martin et al., 1998). While the two tissues work together to create the functionality of the whole bone, their relative contributions to stiffness, strength and homeostasis differs across regions of the same bone (Barak et al., 2010; Doube et al., 2009). It is not currently understood how cortical and trabecular bone work together to meet the mechanical demands of the carpus, particularly under the high mechanical demands of locomotion.

By quantifying the internal bone architecture of the hominoid capitate using a whole-bone methodology, this study aims to investigate whether differences in trabecular and cortical architecture among hominoids may relate to the divergent hand use across the clade. We also examine the proximal and distal segments of the capitate separately, due to the differences in the soft tissue and articular relationships with the surrounding bones.

1.3 | Allometry: Body size and bone structure

As functional adaptation research aims to identify markers of behavior rather than body size, analyzing bone parameters for allometric effects has been integral to interspecific analyses (Ruff, 1984). Decades of research across various species has yet to find consistent patterns;

however, some research suggests there may be a general pattern across mammals and birds whereby bone volume to total volume (BV/TV) and degree of anisotropy (DA) are independent of body mass (Barak et al., 2013; Christen et al., 2015; Cotter et al., 2009; Doube et al., 2011; Kivell et al., 2018; Komza & Skinner, 2019; Schilling et al., 2014; Tsegai et al., 2017) while trabecular thickness (Tb.Th), trabecular number (Tb.N) and trabecular separation (Tb.Sp) scale with negative allometry (Barak et al., 2013; Kivell et al., 2018; Ragni, 2020; Ryan & Shaw, 2013). Cortical thickness (Ct.Th) is often reported to be isometric or slightly positively allometric (Demes et al., 2000; Fajardo et al., 2013; Runestad, 1997). However, not all studies find BV/TV and DA to be independent of body mass (for example Fajardo et al., 2013; Mielke et al., 2018; Ragni, 2020; Ryan & Shaw, 2013) nor the negative relationship with Tb.Th, Tb.N and Tb.Sp (for example Doube et al., 2011; Fajardo et al., 2013; Komza & Skinner, 2019; Tsegai et al., 2017). Few allometric studies have been undertaken on short bones. Tsegai et al. (2017) found no correlation between trabecular parameters or Ct.Th with size in intraspecific analyses of the *Homo* and *Pan* talus. Similarly, an interspecific analysis in Schilling et al. (2014) of the primate capitate found only Tb.N to scale with negative allometry. Ragni (2020) found a greater number of significant relationships within the capitate of *Pan* and *Gorilla* with Tb.Th, Tb.N, and Tb.Sp showing negative allometry and DA and BV/TV expressing isometry. These conflicting results may be due in part to methodological differences for sampling trabeculae or calculating size. Nevertheless, the effects of allometry on the hominoid capitate remain unclear.

1.4 | Hominoid capitate morphology

1.4.1 | Distal capitate

In all hominoids, the distal capitate is bound to the surrounding bones via strong ligaments which are often described as a unit that moves in unison during extension and flexion (Crisco et al., 2005; Moojen et al., 2003; Orr, 2010; Richmond, 2006; Richmond et al., 2001; Tang et al., 2011). The capitate articulates distoradially with the trapezoid (although this articulation can be absent in *Gorilla*) and second metacarpal (Mc2), and distally with the third and sometimes fourth metacarpals (Kivell, 2016a; Lewis, 1989). The topology of the metacarpal joint surfaces in the distal row is more complex and irregular in *Pan* and *Gorilla* compared to the smoother surfaces in *Pongo*; however, the capacity for extension is linked to the range of movement at the midcarpal joint rather than at the carpometacarpal junction (Begun, 2004; Orr, 2017; Richmond et al., 2001). The distal capitate in modern *Homo sapiens* is considered to have several derived features linked to committed manipulation and increased efficiency of radio-ulnar force transfer (Tocheri, 2007; Tocheri et al., 2008). A distally oriented capitate-Mc2 articulation allows pronation of the second finger towards the thumb facilitating precision grip, while a palmarly positioned and expanded capitate-trapezoid articulation is thought to better resist high radio-ulnarly oriented forces incurred by the thumb during tool-related activities (Marzke, 1997; Tocheri, 2007; Tocheri et al., 2008).

Furthermore, the disto-dorso-radial corner is truncated to accommodate the third metacarpal (Mc3) styloid process, providing a stable joint for transmitting high forces and resisting subluxation of the third ray during tool use (Marzke & Marzke, 1987; Niewoehner et al., 1997; Riley & Trinkaus, 1989; Tocheri et al., 2008; Ward et al., 2014). In nonhuman apes, load transfer also occurs radio-ulnarly as bones of the distal carpal row are compressed against one another. However, in contrast to humans, the orientations of the articular surfaces of the capitate (and distal carpal row more generally) indicate the wrist is better adapted to withstand and transfer proximo-distally oriented forces, which arise during use of the forelimb in locomotion (Tocheri, 2007; Tocheri et al., 2008). Only a small proportion of the dorsal surface of the distal capitate is without articular surfaces. In this distal segment, compression is induced at the distal, radial and ulna articular surfaces, while tension is induced by the supporting intrinsic ligaments surrounding these articulations. Tension further arises from the several intrinsic and extrinsic ligaments attached to the palmar and dorsal surfaces (Kijima & Viegas, 2009; Regal et al., 2020).

1.4.2 | Proximal capitate

In great apes, the rounded proximal surface of the capitate articulates with the bones of the proximal row to form the crux of the midcarpal joint (Kivell, 2016b). No ligaments attach directly onto the proximal capitate thus compared to the distal row, the bones of the midcarpal joint are able to move more independently of one another (Crisco et al., 2005; Kijima & Viegas, 2009; Moojen et al., 2003; Regal et al., 2020). In *Pongo*, the proximal capitate is radio-ulnarly narrow in comparison to the other great apes (Figure 1; Richmond et al., 2001). Notably, the os centrale is not fused to the scaphoid as it is in the other hominids and thus excludes the scaphoid from articulating with the capitate resulting in relatively greater freedom of movement at the midcarpal joint (Begun, 2004; Orr, 2018). In *Pan* and *Gorilla*, the proximal capitate is enlarged on the radial aspect, which produces a "waisted" mid-region forming an embrasure with the trapezoid (Kivell, 2016a; Orr, 2018; Richmond et al., 2001; Wolfe et al., 2006). There is also a notable radio-ulnar ridge along the distal extent of the dorsal articular surface that extends onto the hamate (Richmond et al., 2001). These features contribute to the so called "screw-clamp mechanism" that describes the functional complex limiting extension at the midcarpal joint. During extension, the scaphoid is wedged in between the capitate and trapezoid, providing stability between the proximal and distal row (Jenkins & Fleagle, 1975; Orr, 2005, 2017; Richmond, 2006; Richmond et al., 2001; Tuttle, 1969). *Homo* also exhibits the fused scaphoid-os centrale and radially expanded proximal capitate; however, an enlargement of the bone in the radial-palmar region results in a less dramatic "waisting" of the bone, resulting in a range of extension intermediate between the other hominoids (Lewis, 1977; Lewis, 1989; Orr, 2017). Notably, the proximal capitate is the crux of the functional axis of the DTM (Crisco et al., 2005). During motion, the rotation axis of the capitate is perpendicular to the movement of the DTM as it moves across a virtually

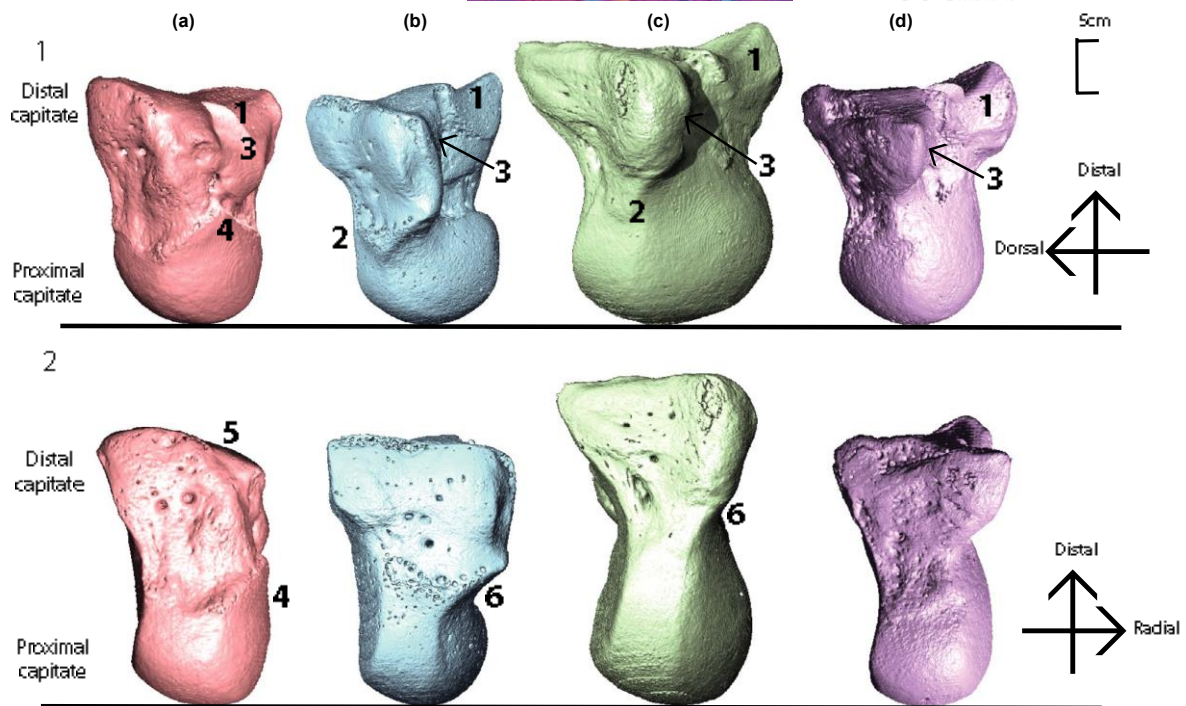


FIGURE 1 CT-derived surface models of a left capitate from each genus showing variation in external morphology. Capitates have been scaled to relative size. Rows: (1) Capitates are oriented dorso-radially and (2) capitates are oriented dorsally. Columns: (a) *Homo sapiens* (DCW_AM_10_0_182), (b) *Pan troglodytes* (SMF_4104), (c) *Gorilla gorilla* (ZMB_83587), (d) *Pongo pygmaeus* (ZMB_6948). Numbers representing anatomical features: “1” Mc2 articulation, “2” Dorsal ridge, “3” trapezoid articulation, “4” radial-palmar expansion of the proximal capitate, “5” Mc3 styloid process articulation, “6” waisted mid-capitate

motionless scaphoid and lunate (Crisco et al., 2005). Thus, although a small bone, the proximal and distal portion of the capitate functions within notably different ligamentous and articular environments.

1.5 | Hypotheses

This research centers on three interrelated hypotheses for both trabecular and cortical bone that are summarized in Table 1 and elaborated below.

1.6 | Trabecular bone architecture

We predict that the capitate of knuckle-walking *Gorilla* and *Pan* will have high relative BV/TV and high DA (Table 1, Hypothesis 1) due to the presumed high compressive forces and reduced mobility from their more extension-limiting midcarpal joint. In contrast, we predict that the *Pongo* capitate will have intermediate BV/TV and low DA due to their predominantly suspensory behavior, resulting in reduced compression but greater mobility. We expect *Homo* to exhibit low BV/TV and intermediate DA because their capitate is not loaded during locomotion and presumably has the least compressive loading but more predictable movement along the DTM axis.

Given the differences in mobility and presumed loading between the proximal and distal portions of the capitate, we hypothesize that there will be differences in the trabecular bone structure between these segments (measured as ratios). It is predicted that the distal aspect will have higher BV/TV and DA compared to the proximal aspect across all species (Table 1, Hypothesis 2). As there are no previous studies that have addressed this question for the capitate, we test the null hypothesis that these ratios will be similar among the study taxa. Although we report Tb.Th, Tb.N and Tb.Sp, we do not make explicit predictions about these parameters because all contribute, potentially in a variety of different combinations, to BV/TV.

1.7 | Cortical bone thickness

The contribution of cortical bone to the functional adaptation of the capitate in hominoids has never been investigated. Given the assumed loading differences described above, we predict that the cortical bone will be thickest in *Gorilla* and *Pan*, followed by *Pongo*, with *Homo* exhibiting the thinnest cortex (Table 1, Hypothesis 1). Also following the predictions for trabecular bone, it is predicted that the cortex of the distal capitate should be significantly thicker than the proximal capitate for all genera.

In long bones, the joint surface tends to have a thin layer of cortical bone covering a dense trabecular network that transfers load towards

TABLE 1 Summary of the hypotheses, predictions, and statistical tests used in this study

Hypothesis	Predictions	Statistical tests
#1		
Locomotor and behavioral differences among extant hominoids will result in significantly different trabecular and cortical architecture in their capitates	<p>Between species</p> <ul style="list-style-type: none"> • Knuckle-walking taxa will exhibit high BV/TV and DA • <i>Pongo</i> will show intermediate BV/TV and low DA • <i>Homo</i> will exhibit low BV/TV and intermediate DA • Cortical bone will be thickest in <i>Gorilla</i> and <i>Pan</i>, followed by <i>Pongo</i>, then <i>Homo</i>. 	<ul style="list-style-type: none"> • Kruskal-Wallis one-way ANOVA • Pairwise Wilcoxon rank-sum tests
#2		
Proximal and distal segments will show significantly differentiated internal bone architecture	<p>Between Species</p> <ul style="list-style-type: none"> • Distal to proximal ratios will be statistically undifferentiated among the study taxa <p>Within Species</p> <ul style="list-style-type: none"> • The distal aspect will have higher BV/TV and DA compared to the proximal aspect across all species • The distal cortex will be significantly thicker than the proximal across all species 	<ul style="list-style-type: none"> • Wilcoxon signed-rank test • Kruskal-Wallis one-way ANOVA • Pairwise Wilcoxon rank-sum test
#3		
Allometry	<p>Between species</p> <ul style="list-style-type: none"> • Only Tb.N will show a significant negative relationship to body size, while all other parameters will be uncorrelated <p>Within species</p> <ul style="list-style-type: none"> • No parameters will exhibit significant correlations with body size 	<ul style="list-style-type: none"> • Reduced major axis regression • Reduced major axis regression

TABLE 2 Summary of study sample

Taxon	N	Side		Sex			Behavioral group
		Right	Left	Female	Male	Unknown	
<i>Homo sapiens</i>	26	14	12	5	9	12	Bipedal/manipulative
<i>Pan paniscus</i>	8	5	3	4	4		Knuckle-walking
<i>Pan troglodytes</i>	6	3	3	3	3		Knuckle-walking
<i>Gorilla beringei</i>	1		1			1	Knuckle-walking
<i>Gorilla gorilla</i>	15	8	7	7	7	1	Knuckle-walking
<i>Pongo abelii</i>	2	1	1	1	1		Suspensory
<i>Pongo pygmaeus</i>	11	6	5	5	4	2	Suspensory

the thicker and stronger diaphyseal cortex (Currey, 2002). In short bones, the cortex is similarly described as thin; however, the relationship between cortical and trabecular bone has never been quantified among hominoids. Additionally, it is unclear whether the behavioral differences among ape genera will result in different ratios of cortical to trabecular bone. Therefore, this study will investigate the relative contribution of cortical bone to total bone volume, testing the null hypothesis that these ratios will be similar among the study taxa (Table 1, Hypothesis 2).

1.8 | Interspecific and intraspecific allometry in internal bone structure

As this study incorporates hominoids of diverse body size, interspecific and intraspecific allometry is also investigated. Predictions are

outlined in Table 1 (Hypothesis 3) and follow the results of Schilling et al. (2014) for the interspecific and Tsegai et al. (2017) for the intraspecific predictions.

2 | MATERIALS AND METHODS

2.1 | Sample

The study sample includes capitates ($n = 69$) from *Homo sapiens* ($n = 26$), *Pan troglodytes* and *Pan paniscus* ($n = 14$), *Gorilla* sp. ($n = 16$) and *Pongo* sp. ($n = 13$) (Table 2 and Table S1). These taxa are categorized into three behavioral groups based on their most frequent locomotor behaviors: bipedal (*Homo*) knuckle-walking (*Gorilla* and *Pan*) and suspensory (*Pongo*). Capitates from nonhuman apes were wild-shot adults with no obvious

signs of pathology. Consideration was given to ensuring a sex balance for each taxon when possible; however, 16 specimens had unknown sex.

2.2 | Computed tomography

Capitate specimens were scanned with either a BIRACTIS 225/300 high-resolution microCT scanner or a Diondo D3 high-resolution microCT scanner at the Department of Human Evolution, Max Planck Institute for Evolutionary Anthropology, Germany, or a Nikon 225/XTH scanner at the Cambridge Biotomography Centre, University of Cambridge, United Kingdom. Specimens were scanned with an acceleration voltage of 100–160 kV and 100–140 μ A using a 0.2- to 0.5-mm copper or brass filter. Images were reconstructed as 16-bit TIFF stacks. To ensure accurate post-scan segmentation of thin trabeculae, scan resolution was limited to a maximum of 0.048 mm (average 0.032 mm) for nonhuman apes, and 0.035 mm (average 0.029 mm) for the *Homo* sample (Table S1). This resolution is below the suggested range for minimal error detection (Christen et al., 2016; Isaksson et al., 2011). Post-scanning, each capitate was positioned into approximately the same orientation using Avizo 6.0 (Visualization Sciences Group, SAS). Segmentation of trabecular bone, including identification and removal of extraneous nonbone material, used the medical image analysis (MIA) clustering method (Dunmore et al., 2018). The MIA-clustering method increases the reproducibility of results by reducing subjective input parameters required for other segmentation methods (Dunmore et al., 2018).

2.3 | Data collection

This study uses the medtool 4.3 software package (<http://www.dr-pahr.at/medtool/>) to quantify bone parameters throughout the entire capitate utilizing the method outlined in Gross et al. (2014). In brief, medtool utilizes a series of morphological filters to identify the cortical, trabecular, internal (marrow), and background elements of the segmented CT scans. After MIA segmentation, medtool projects a series of rays onto outside of the bone (Figure 2b) that continue to move internally through the bone until a nonbone voxel is reached (Pahr & Zysset, 2009a). By using a value of average trabeculae thickness, morphological filters fill and close small holes present in the porous cortex allowing a smooth boundary contour between cortical and trabecular bone to be identified (Gross et al., 2014; Pahr & Zysset, 2009a, 2009b). Two *Gorilla*, one *Pan* and two *Pongo* specimens were excluded from the sample as the internal cortical-trabecular boundary could not be confidently defined due to extreme cortical porosity (an example is provided in Figure S1). Medtool then superimposes the trabecular-cortical boundary to the original image such that the pores within the cortex are maintained for analysis. Porosity is important to maintain within the cortical bone when quantifying microarchitecture as it has been linked to strength and elastic modulus (see Cooper et al., 2016 for review). Unique scalars are applied to the background, cortical, trabecular, and internal elements of the scan. A series of image stacks are created and include a cortex only

stack (Figure 2c), trabecular and internal only stack (Figure 2d) and a trabecular and cortical combined stack (Figure 2e). A 3D grid with 2.5-mm spaced nodes is then superimposed on an image stack and a 5-mm sampling sphere moves from node to node to measure parameters across the entire bone (Figure 2f) (Pahr & Zysset, 2009a).

BV/TV is calculated as the ratio of bone to non-bone voxels. DA is calculated via the mean intercept length (MIL) method (Whitehouse, 1974) and is calculated as $1 - (\text{min. eigenvalue} / \text{max. eigenvalue})$ which produces a number limited between 1 and 0, with 1 being complete anisotropy and 0 being complete isotropy. Tb.Th, Ct.Th, and Tb.Sp are computed in a similar way to the more well-known BoneJ[®] plugin (Doube et al., 2010) for ImageJ. Spheres are grown within the trabecular or cortical bone and medtool calculates the diameter of the largest sphere that fits within the bone (Hildebrand & Rüeggsegger, 1997). For the calculation of Tb.Sp, medtool inverts the greyscale values of the image stack (Figure 2E) such that the “internal” voxels are now represented by the “bone” scalar. Similar to Tb.Th and Ct.Th, spheres are then grown within the internal voxels until a trabecular or cortical voxel is reached. The results of Tb.Sp and Tb.Th are used to calculate Tb.N using the formula $1 / (\text{Tb.Th} + \text{Tb.Sp})$.

Cortical and trabecular parameters were quantified in the whole capitate, as well as proximal and distal VOIs. To produce these VOIs, each capitate was cut just distal to the ulnar-most point of the ridge delineating the extent of the lunate articulation on the dorsal proximal capitate, as per the measurement made in Richmond (2006) (Figure 3d). These VOIs are subjected to the same data collection process as outlined in Figure 2, quantifying all of the trabecular or trabecular and cortical bone within the proximal or distal segment. This delineation separates the proximal VOI as the section of the bone that does not contain any ligament attachment sites, from the distal VOI which does receive ligamentous attachments. To assess and compare the relative contribution of cortical bone to total bone volume, BV/TV was measured twice: firstly, in only the trabecular region of the bone (Figure 3d) as determined using medtool (see above) and, secondly, in the original MIA segmented specimen in which there is no partitioning between cortical and trabecular bone (Figure 2b). This provides a measure of BV/TV that combines cortical and trabecular bone (referred to as “total BV/TV” throughout). Relative thickness maps of Ct.Th and Tb.Th are generated by loading the Tb.Th output into ImageJ (1.50b) (<https://imagej.nih.gov/ij/>) and visualized using the 3D Volume Viewer plugin (<http://rsb.info.nih.gov/ij/plugins/volume-viewer.html>).

2.4 | Statistical analysis

2.4.1 | Trabecular bone hypotheses

Mean differences in the proximal and distal trabecular parameters (trabecular BV/TV, DA, Tb.Th, Tb.N, Tb.Sp) were compared interspecifically using a Kruskal–Wallis one-way ANOVA and pairwise Wilcoxon rank-sum tests using the Holm *p* adjust method (R Core Team, stats package v3.6.1) (Table 1). A distal to proximal ratio was calculated for each parameter and a Wilcoxon signed-rank test was applied within-genus to

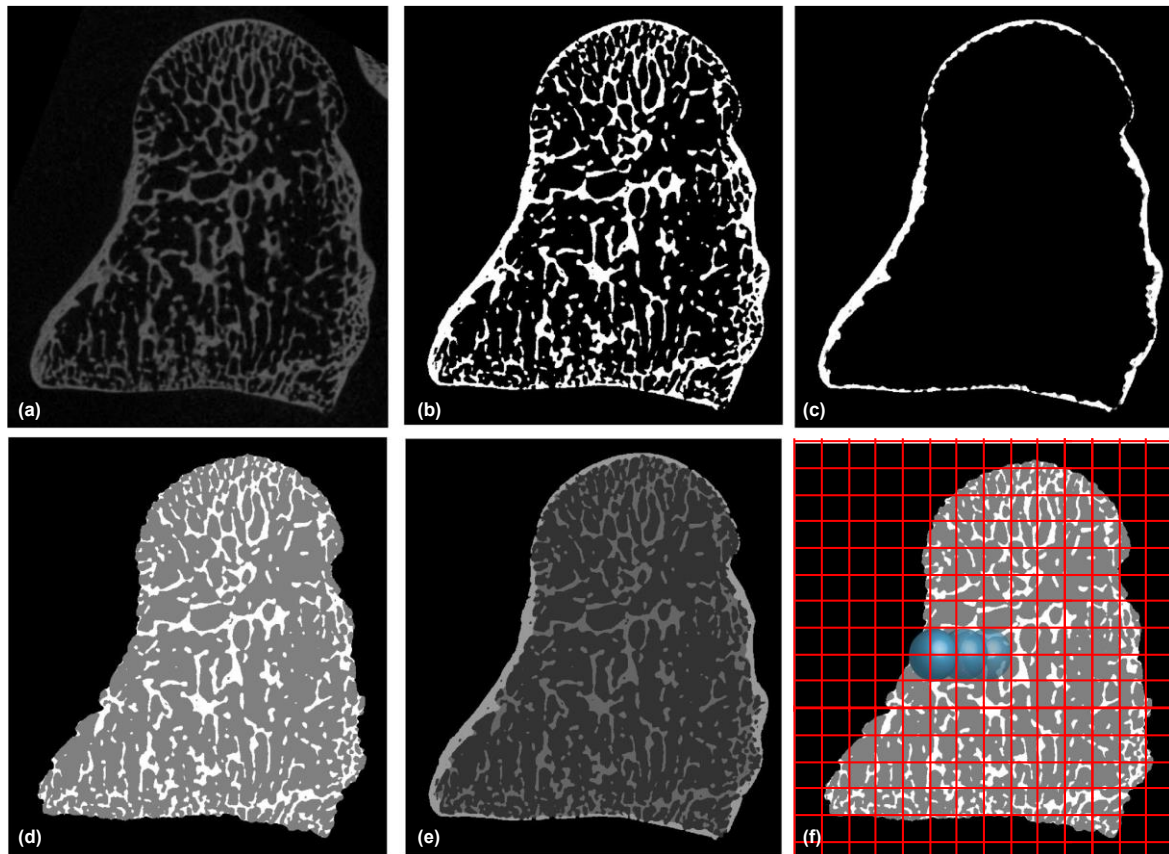


FIGURE 2 Images showing the morphological filters applied in medtool 4.3 for the whole-bone analysis. (a) Original microCT of a *Homo sapiens* capitate, (b) microCT scan after MIA-clustering segmentation, (c) cortical thickness image stack, allowing analysis of the cortex only, (d) trabecular bone image stack, allowing analysis of the trabeculae (white) only, (e) combined mask overlay, identifying cortical (lightest grey), trabecular (mid-grey) and air (darkest grey internally and black externally) voxels, (f) sampling sphere (blue) moving across each node of the overlaid 3D grid (red) measuring bone parameters in the trabecular bone image stack

test whether the mean values of the ratio were statistically significant. A Kruskal-Wallis one-way ANOVA and pairwise Wilcoxon rank-sum test examined interspecific differences in the ratios.

2.4.2 | Cortical bone hypotheses

To test for differences in cortical bone, mean differences in total BV/TV and Ct.Th were compared interspecifically in the proximal and distal segments using a Kruskal-Wallis one-way ANOVA and pairwise Wilcoxon rank-sum tests using the Holm *p* adjust method (R Core Team, stats package v3.6.1).

Within each genus, a distal to proximal ratio was calculated for each parameter and a Wilcoxon signed-rank test was applied to test whether mean values of the ratio were statistically significant. Additionally, we examined taxonomic differences in these ratios using a Kruskal-Wallis one-way ANOVA and pairwise Wilcoxon rank-sum tests.

Two additional ratios were calculated in order to test for taxonomic differences in the relative proportion of cortical and trabecular

bone. These ratios were compared between species, using a Kruskal-Wallis one-way ANOVA and pairwise Wilcoxon rank-sum tests using the Holm *p* adjust method (R Core Team, stats package v3.6.1).

2.4.3 | Interspecific and intraspecific allometry

To test for allometric trends in the capitate, each whole-bone cortical and trabecular parameter was interspecifically and intraspecifically analyzed in a reduced major axis regression (RMA). As a proxy for body mass, the volume (mm^3) of each capitate was calculated in Paraview (4.8.2) using the Integrate Variables filter. The logged cube root of the volume was regressed against the logged bone parameters using the lmodel2 package in R (v1.7-3). Interpretation follows Ryan and Shaw (2013); the shape parameters of BV/TV, DA and Tb.N will have an isometric slope equal to 0; values greater than 0 indicate positive allometry while values less than 0 are indicative of negative allometry. Size parameters, such as Ct.Th, Tb.Th and Tb.Sp will have an isometric slope of 1; positive allometry is indicated by

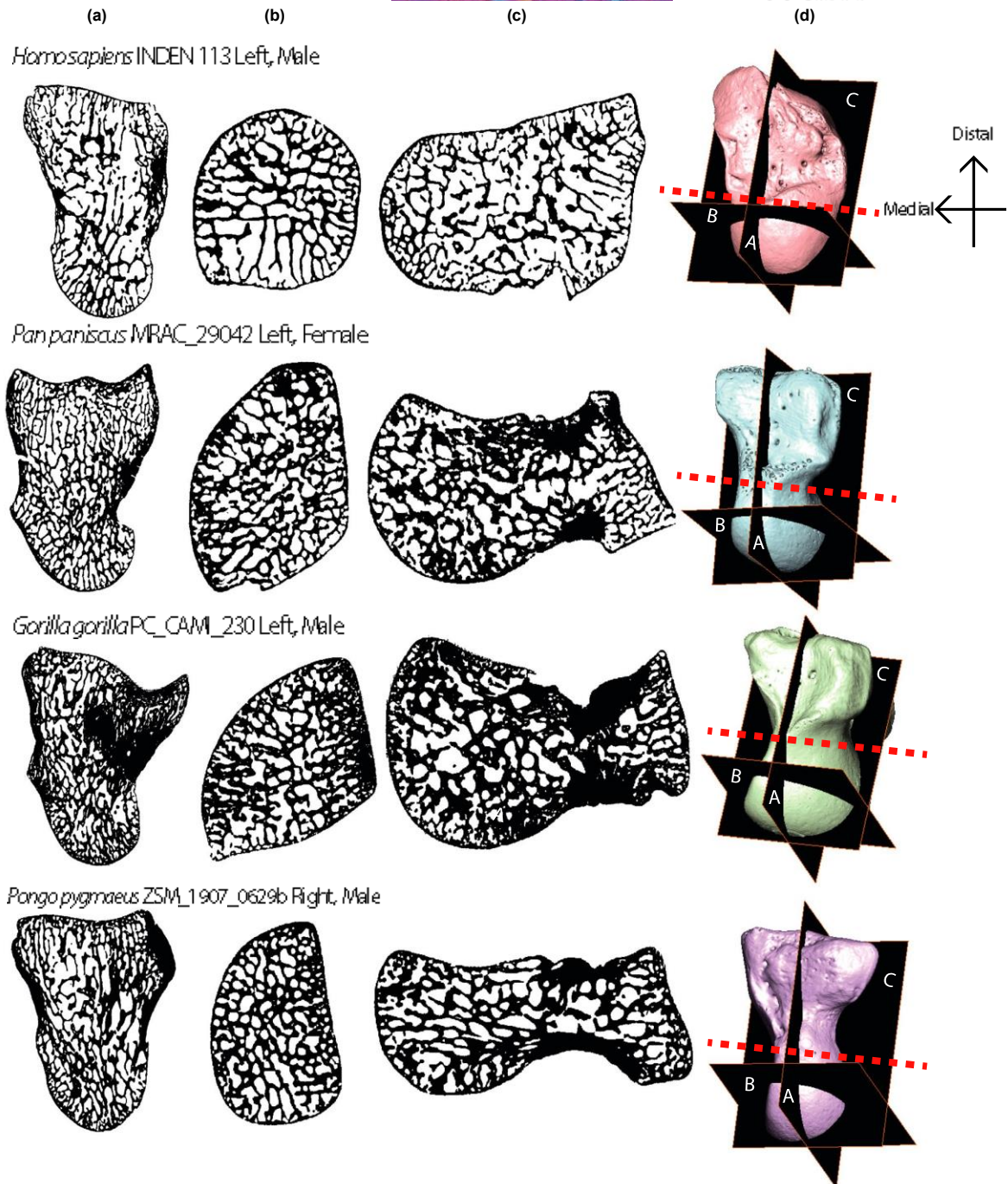


FIGURE 3 Three cross-sections from the four study genera showing internal bone patterning. (a) Y-Z dimension, radial-ulnar cross-section, slice taken from mid-section of bone. Distal is up; dorsal is left. (b) X-Y dimension, proximal-distal cross-section, slice taken from proximal mid-capitate. Dorsal is up; radial is left. (c) X-Z dimension, dorsal-palmar cross-section, slice taken from midsection of bone. Ulnar is up; proximal is left. (d) Surface models of each bone showing the location of cross-section (a, b, and c). The red dotted line indicates where capitates were partitioned into a distal and proximal VOI. Capitates are not to scale. Left capitates have been mirrored

a value greater than one and negative allometry by values of less than 1. All statistical tests conducted for hypotheses 1, 2 and 3 are considered significant if $p \leq 0.05$.

3 | RESULTS

3.1 | Trabecular bone

Cross-sections of each genera in Figure 3 provide an example of the internal structure of the capitate within three planes of view. The red dotted line in Figure 3d indicates where the capitate was partitioned into the proximal and distal VOIs.

3.2 | Bone volume to total volume

Proximal and distal trabecular BV/TV differ significantly across the study sample ($p \leq 0.001$ for both tests, Table S3). *Gorilla* has the highest proximal and distal BV/TV followed by *Pan*, then *Pongo*, with *Homo* having the lowest BV/TV values (Table S2). Proximally, pairwise comparisons show that *Pongo* is not differentiated from any other taxa, while other pairwise comparisons are significant. Distally, all pairwise comparisons are significant except between *Pongo* and *Pan* (Figure 4a, Table S3).

Intraspecific comparisons of the BV/TV ratio (distal BV/TV relative to proximal BV/TV) reveal that all genera have greater trabecular BV/TV in the proximal aspect (Figure 5a; Tables S4 and S5). The differences between the two VOIs reach statistical significance in *Homo*, *Pan*, and *Gorilla* ($p \leq 0.001$ for three tests; Table S4) but are nonsignificant in *Pongo*. The Kruskal-Wallis test on the BV/TV ratio reveal that it does not differ significantly among the study sample ($p = 0.429$) indicating that although BV/TV differs between the proximal and distal capitate, the way it differs is similar among the hominoids.

3.3 | Degree of anisotropy

Proximal DA differs significantly among the study sample ($p \leq 0.001$); however, distal DA does not ($p = 0.593$, Table S3). Notably, DA is the only trabecular parameter which has a different significance result for the proximal and distal VOI. *Homo* and *Pongo* have the highest proximal DA with 0.30 followed by *Pan* and *Gorilla*, both with 0.24 (Figure 4b, Table S2). Distal DA differs by only 0.02 between the genera, with the highest value from

Gorilla at 0.28 and lowest from *Pan* at 0.26 (Table S2). Pairwise comparisons reveal that proximally, *Homo* and *Pongo* are differentiated from *Pan* and *Gorilla* ($p \leq 0.001$ for all four significant tests). Distally, there are no significant pairwise results (Figure 4b, Table S3).

Both *Gorilla* and *Pan* have a higher DA in the distal VOI whereas *Homo* and *Pongo* both have higher DA in the proximal and the difference between the proximal and distal VOIs is significant for all genera (Figure 5b, Table S4). The DA ratio differs significantly across the genera ($p \leq 0.001$) and pairwise comparisons reveal that *Homo* and *Pongo* are differentiated from *Pan* and *Gorilla* ($p \leq 0.001$ for all four significant tests, Table S4).

3.4 | Trabecular thickness

Tb.Th differs significantly across both the proximal and distal capitate of the study sample ($p < 0.001$ for both tests, Table S3). *Gorilla* has the highest mean thickness followed by *Pongo*, with *Homo* having the thinnest (Table S2). Distally, all pairwise comparisons are significant except between *Homo* and *Pan*. Proximally, *Gorilla* is differentiated from all other taxa (Figure 4c, Table S3).

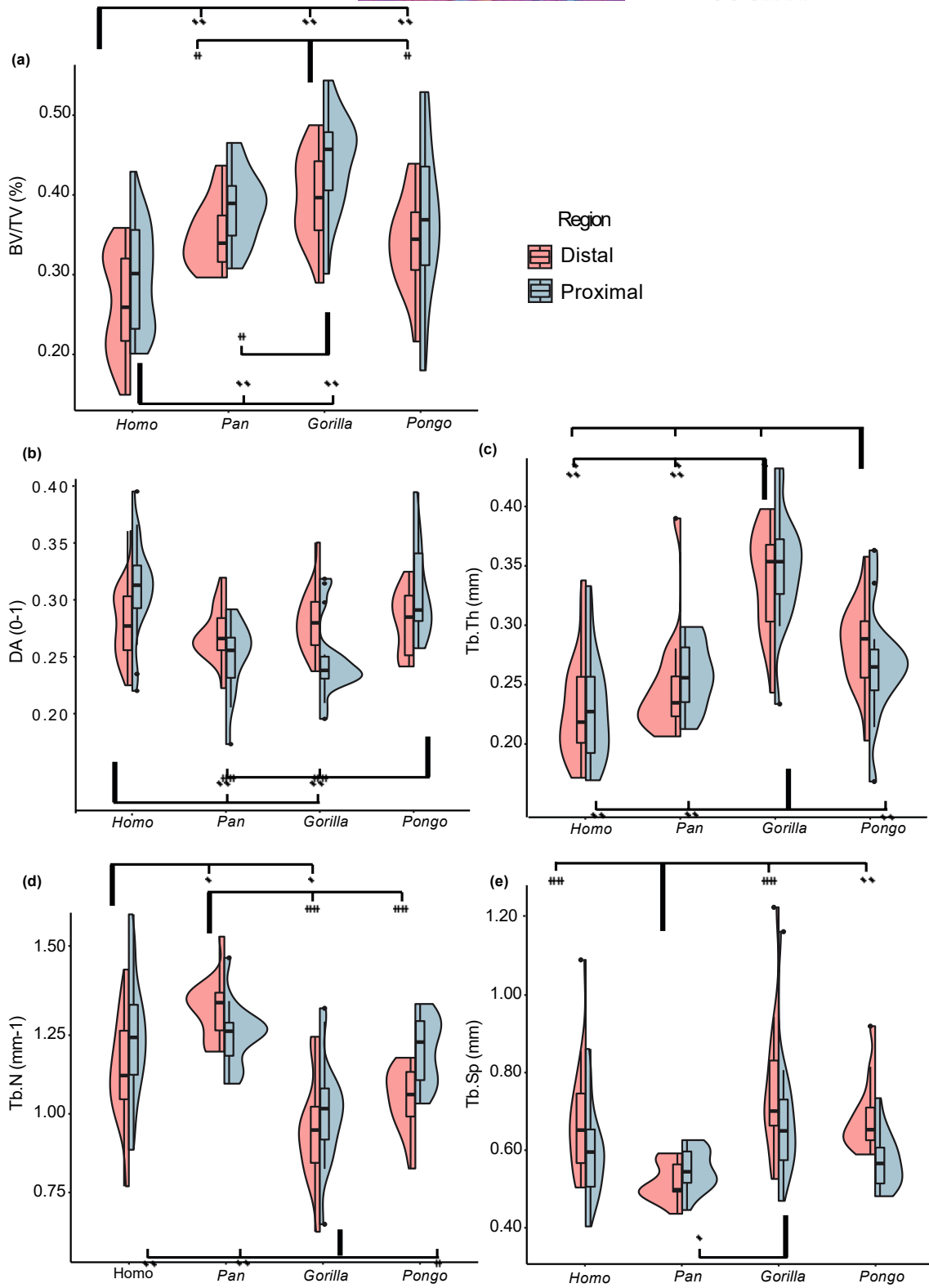
Homo, *Pan*, and *Gorilla* have thicker trabeculae in the proximal aspect and *Pongo* in the distal aspect (Tables S4 and S5). The difference between the two segments is statistically significant for *Pan*, *Gorilla*, and *Pongo* but not for *Homo* (Figure 5c, Table S4). The Tb.Th ratio differs significantly among the study sample ($p \leq 0.001$) and all pairwise comparisons are significant except between *Homo* and *Gorilla* (Table S4).

3.5 | Trabecular number

Proximal and distal Tb.N differs significantly among the study sample ($p \leq 0.001$ for both tests, Table S3). *Gorilla* has the lowest trabecular number while *Pan* has the highest number (Table S2). Distally, all pairwise comparisons are significant except between *Pongo* and *Homo*, and *Pongo* and *Gorilla*. Proximally, only *Gorilla* is differentiated from all other taxa (Figure 4d, Table S3).

The Tb.N ratio indicates that *Homo*, *Gorilla*, and *Pongo* have a higher trabecular number in the proximal aspect, and *Pan* have a higher number in the distal (Figure 5d). The differences between the proximal and distal VOI is significant for all taxa. While the Tb.N ratio differs significantly among the study sample ($p \leq 0.001$) only *Pan* shows significant pairwise results with all other taxa ($p \leq 0.001$ for all three significant tests, Tables S4 and S5).

FIGURE 4 Split violin plots showing the distribution of trabecular results in the proximal and distal VOI of each genus. Images are generated using *ggplot2* in R (v. 1.2.1335) and utilize the default (Gaussian) kernel density estimation. Colored contours indicate the density of results across the data range. (a) Trabecular bone volume to total volume; (b) degree of anisotropy; (c) trabecular thickness; (d) trabecular number; (e) trabecular separation. Outliers are identified with ● and represent values 1.5 times above the fourth or below the first interquartile range. For all plots: significant pairwise comparisons are indicated by the square brackets for the distal VOI tests (top of graph) and proximal VOI tests (bottom of graph), * $p \leq 0.05$; ** $p \leq 0.001$



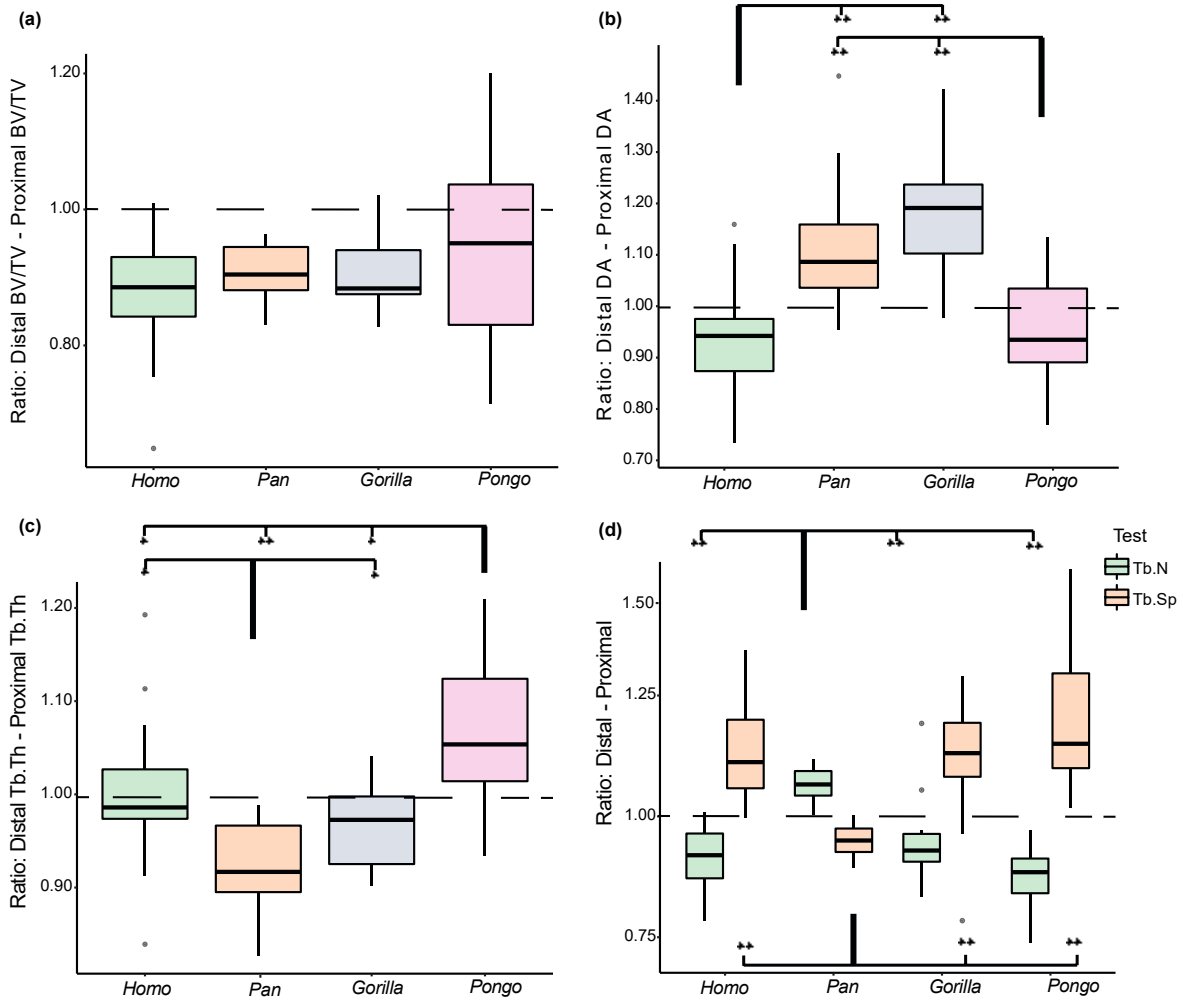


FIGURE 5 Boxplots of the five trabecular ratios for each genus as well as results for the intraspecific Wilcoxon signed-rank test and interspecific pairwise rank-sum tests. (a) Ratio of distal to proximal trabecular BV/TV; (b) ratio of distal to proximal DA; (c) ratio of distal to proximal Tb.Th; (d) ratio of distal to proximal Tb.N (green) and Tb.Sp (orange). For all figures: Values above the dotted line (ratio =1) indicate greater trabecular variable in the distal capitale. Significant pairwise comparisons of the ratios are indicated by the square brackets. For (d), the top brackets indicate the tests for Tb.N and the bottom brackets indicate those for Tb.Sp. * $p \leq 0.05$; ** $p \leq 0.001$. Significant intraspecific Wilcoxon signed-rank tests between the proximal and distal means are represented by the \blacklozenge symbol thus indicate whether the difference between the mean distal and proximal trabecular variable was significantly different. $\blacklozenge p \leq 0.05$; $\blacklozenge\blacklozenge p \leq 0.001$

3.6 | Trabecular separation

Tb.Sp differs significantly in the distal ($p \leq 0.001$) and proximal ($p = 0.038$, Table S3) capitale of the study sample. *Gorilla* has the most widely spaced trabeculae, while *Pan* has the most tightly packed (Table S2). Pairwise comparisons indicate that distally, *Pan* is differentiated from all other taxa (Table S3). Proximally, the only significant pairwise result is between *Pan* and *Gorilla* (Figure 4d).

The Tb.Sp ratio shows that *Homo*, *Gorilla*, and *Pongo* have greater trabecular separation in the distal capitale whereas *Pan* has greater separation in the proximal (Figure 5d, Table S5). The difference between the separation in the distal and proximal capitale is significant for all

genera (Table S4). The Tb.Sp ratio differs significantly among the study sample ($p \leq 0.001$) and the results of the pairwise comparisons mirror those of the distal segment as the only significant tests are between *Pan* and the other taxa ($p \leq 0.001$ for the three significant tests, Table S4).

3.7 | Total relative bone volume

Total BV/TV, which incorporates both trabecular and cortical bone, differs significantly across the study sample for both the proximal and distal capitale ($p \leq 0.001$ for both tests, Table S3). *Gorilla* has the highest total BV/TV in both VOIs, followed by *Pan*, *Pongo*, then *Homo*

(Figure 6a, Table S2). Pairwise comparisons reveal that distally, *Homo* has significantly lower total BV/TV than all other taxa ($p \leq 0.001$ for all tests, Table S3). Proximally, the results remain the same between *Homo* and *Gorilla*, and *Homo* and *Pan*, although in this region *Homo* is undifferentiated from *Pongo*. The only significant nonhuman pairwise comparison among the proximal and distal results is in the distal VOI between *Pongo* and *Gorilla* ($p = 0.014$).

The total BV/TV ratio of the proximal and distal capitae differs significantly across the study sample ($p \leq 0.001$). Pairwise comparisons reveal that *Homo* is differentiated from all nonhuman apes ($p \leq 0.001$ for all significant tests, Table S4) while the nonhuman apes are not differentiated from one another ($p = 0.51$ for all three

tests) (Figure 6c, Table S4). The Wilcoxon signed-rank tests indicate that the differences in the total BV/TV between the two segments is statistically significant for all genera. As outlined in the above section, trabecular BV/TV is consistently higher in the proximal segment compared to the distal segment in all genera (Figure 4a, Table S2). However, when total BV/TV is measured, *Pan*, *Gorilla*, and *Pongo* show significantly higher values in the distal capitae (Figure 6a, Tables S2 and S4). In contrast, *Homo* maintains the trabecular BV/TV pattern, with higher total BV/TV in the proximal segment.

In the proximal capitae, the ratio of cortical bone to trabecular bone is similar among all genera, and pairwise comparisons reveal no significant results (Tables S4 and S5). In this segment, the inclusion

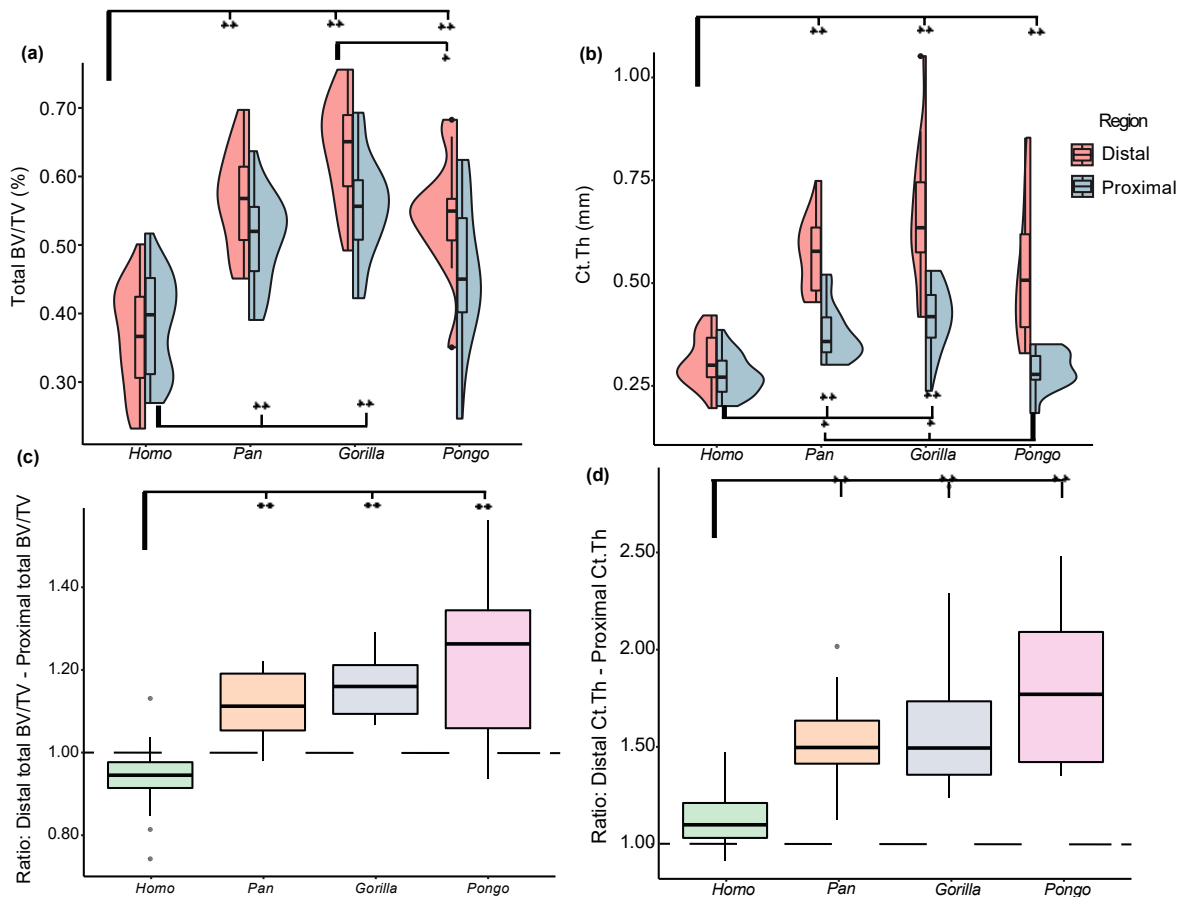


FIGURE 6 (a, b) Split violin plots showing the distribution of total BV/TV (a) and Ct.Th (b) results in the proximal and distal VOI of each genus. Images are generated using *ggplot2* in *R* (v. 1.2.1335) and utilize the default (Gaussian) kernel density estimation. Colored contours indicate the density of results across the data range. Outliers are identified with • and represent values 1.5 times above the fourth or below the first interquartile range. Significant pairwise comparisons are indicated by the square brackets for the distal tests (top of graph) and proximal tests (bottom of graph), * $p \leq 0.05$; ** $p \leq 0.001$. (c, d) Boxplots showing the distribution of the distal to proximal ratios of the total BV/TV (C) and Ct.Th (D) of each genus. Boxplots also show the results of the intraspecific Wilcoxon signed-rank test and interspecific pairwise rank-sum tests. Values above the dotted line (ratio = 1) indicate greater cortical variable in the distal capitae. Significant pairwise comparisons of the ratios are indicated by the square brackets, * $p \leq 0.05$; ** $p \leq 0.001$. Significant intraspecific Wilcoxon signed-rank tests between the proximal and distal means are represented by the ♦ symbol thus indicate whether the difference between the mean distal and proximal trabecular variable was significantly different. ♦ $p \leq 0.05$; ♦♦ $p \leq 0.001$

of cortical bone increases BV/TV by 24% in *Gorilla*, 29% in *Pan*, 28% in *Homo*, and 24% in *Pongo*. Conversely, in the distal capitate the ratio of cortical bone to trabecular bone is statistically differentiated among the study sample ($p \leq 0.001$). Pairwise comparisons indicate this is driven by *Homo*, as the cortical bone represents a significantly lower proportion of total BV/TV compared to all other nonhuman apes (Table S4). The relative portions of distal cortical and trabecular bone are similar among the nonhuman apes with cortical bone contributing 59% of total BV/TV in *Pan* and *Pongo* and 58% for *Gorilla*. In *Homo*, cortical bone represents 38% of distal total BV/TV.

3.8 | Cortical bone thickness

Ct.Th differs significantly among the study genera in both proximal and distal capitate ($p \leq 0.001$ for both tests, Table S3). In both segments *Gorilla* has the thickest mean cortical bone, followed by *Pan*, *Pongo*, and finally *Homo* (Figure 6b, Table S2). In the distal capitate, *Homo* has significantly thinner Ct.Th than the nonhuman apes ($p \leq 0.001$ for all tests, Table S3), while the nonhuman apes are not differentiated from one another. In the proximal capitate, *Homo* has significantly thinner cortical bone than *Pan* and *Gorilla* ($p \leq 0.001$) but is undifferentiated from *Pongo* ($p = 0.386$). Across the nonhuman apes, *Pongo* has significantly thinner cortical bone than *Gorilla* and *Pan* ($p = 0.001$ for both).

All genera have thicker cortical bone in the distal VOI and the difference between the proximal and distal segments is statistically significant in all genera ($p \leq 0.001$ for all tests) (Figure 6d, Tables S4 and S5). *Pongo* has the greatest relative cortical thickening in the distal VOI with the distal cortex being 79% thicker than the proximal, followed by *Gorilla* (62% thicker), *Pan* (52% thicker) and finally *Homo* (12% thicker). Pairwise comparisons of the ratio indicate that *Homo* is differentiated from all nonhuman apes ($p \leq 0.001$ for all tests, Table S4). There are no significant pairwise comparisons between the nonhuman apes. The relative thickness of the cortex and trabeculae is visualized in Figure 7. In nonhuman apes, the thickest bone is consistently seen within the distal cortex. In *Homo*, the cortex and trabeculae have a similar thickness across the entire bone.

3.9 | Allometry

The results of the allometry tests are reported in Table 3 and a figure plotting the regressions is provided in Figure S2. Trabecular and total BV/TV show a significant positive allometric relationship with capitate volume across hominoids; however, there are no significant allometric trends intraspecifically. In all interspecific and intraspecific

tests, DA is independent of capitate volume. Tb.Th shows significant positive allometry across the hominoids as well as in *Homo* and *Pongo*. In *Gorilla*, Tb.Th scales with isometry and in *Pan* it is uncorrelated. Across hominoids, Tb.N scales with negative allometry. Intraspecifically, only *Gorilla* has a significant relationship with Tb.N, scaling with negative allometry. Tb.Sp scales with positive allometry across hominoids. Intraspecifically only *Gorilla* has a significant relationship with Tb.Sp, scaling with positive allometry. Ct.Th scales with positive allometry across the hominoids, as well as in *Homo*, *Gorilla*, and *Pongo*.

4 | DISCUSSION

This study quantified the internal bone structure of the hominoid capitate using a whole-bone methodology to examine (1) whether relative and absolute differences in trabecular and cortical parameters across hominoid taxa could be correlated to inferred habitual behavior and (2) how the parameters differed interspecifically and intraspecifically across the proximal and distal portion of the capitate.

4.1 | Allometry in the capitate

Interspecifically, the predictions for Tb.N and DA were supported while all others were rejected. The two parameters most strongly correlated with size were Tb.Th and Tb.N. This was particularly true for *Gorilla*, which had relatively strong positive scaling for Tb.Th, Tb.N and Tb.Sp, with r-squared values between 0.60 and 0.69. This suggests these parameters may be linked to sexual dimorphism, which is extreme in *Gorilla* (Smith & Jungers, 1997). Indeed, the largest Tb.Th and Tb.Sp, and smallest Tb.N values among the Gorillas were from males. *Pan* was the only genus that did not report at least one significant intraspecific allometric test. This indicates that capitate size differences (as a proxy for body mass differences) between *Pan troglodytes* and *Pan paniscus* have not influenced results.

The positive relationship found in BV/TV does not corroborate results of either previous study on allometry in the primate capitate (Ragni, 2020; Schilling et al., 2014) or the talus (Tsegai et al., 2017). Differences in results between this study and others may be driven by the variation in the methodologies for calculating size or body mass. While this study used the cube root of the capitate, other studies have used the geometric mean (Schilling et al., 2014; Tsegai et al., 2017), body mass (Barak et al., 2013; Cotter et al., 2009), or linear dimensions of the bone (Ryan & Shaw, 2013). Furthermore, this study used a whole-bone mean of trabecular parameters whereas

FIGURE 7 Cross-sections from representative individuals of each genus showing relative trabeculae and cortex thickness across the capitate. (a) Y-Z dimension, radio-ulnar cross-section. Distal is up; dorsal is left. (b) X-Z dimension, dorsal-palmar cross-section. Ulnar is up; distal is left. (c) X-Y dimension, proximal-distal cross-section. Cross-section taken at the proximal mid-capitate. Dorsal is up; radial is left. (d) X-Y dimension, proximal-distal cross-section. Cross-section taken at the distal capitate. Dorsal is up; ulnar is left. (e) Shows the positions of cross-sections (a-d) on a *Pan* specimen. Left capitates have been mirrored. Capitates not to scale

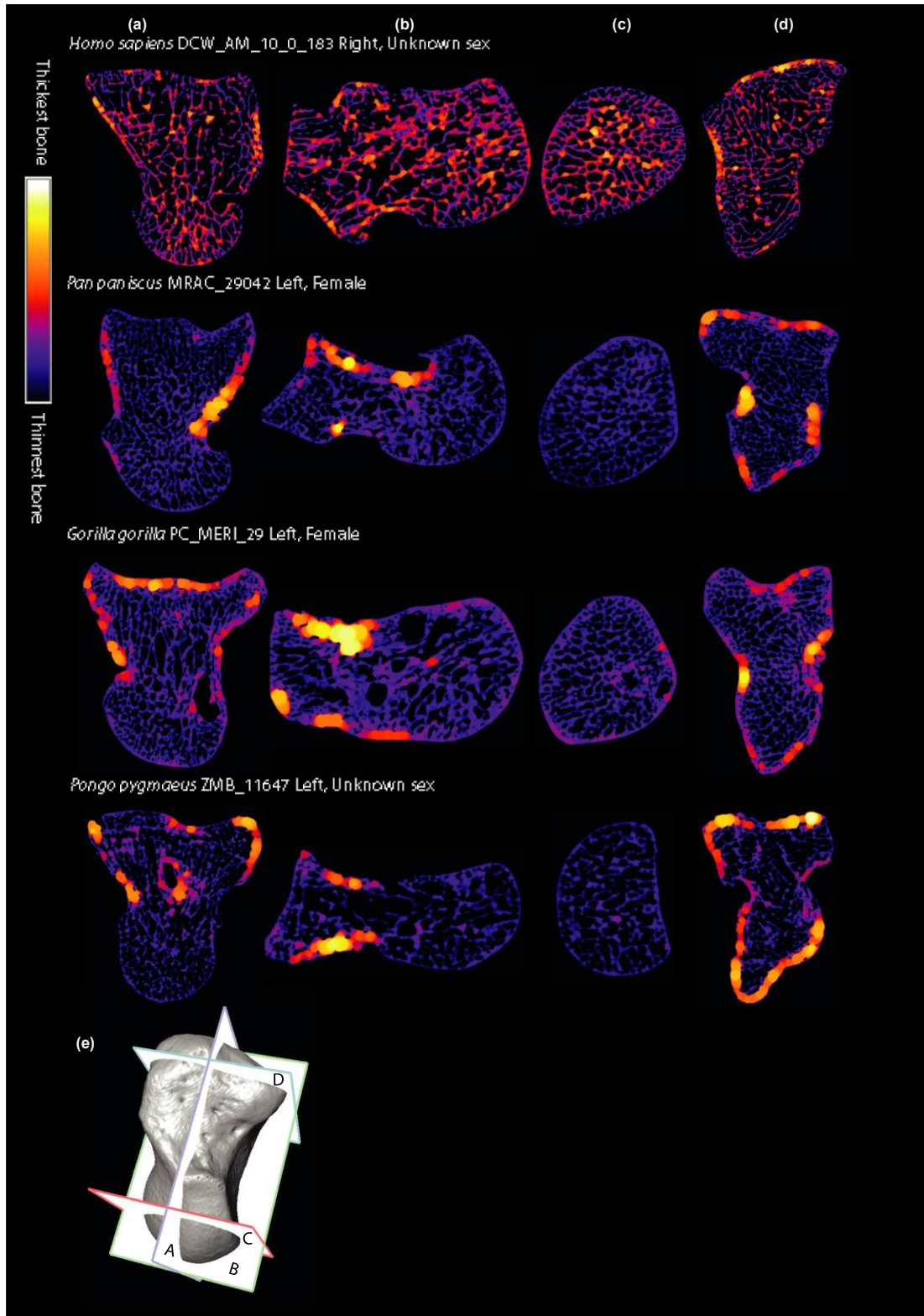


TABLE 3 RMA regression results of the interspecific and interspecific allometry

	Variable	Isometric slope	Slope	CL-	CL+	r ²	Intercept	p value	Allometry
Whole sample	BV/TV	0	1.800	1.440	2.250	0.133	-2.550	0.001	Positive
	DA	0	-0.759	-0.966	-0.596	0.005	0.310	0.559	Uncorrelated
	Tb.Th	1	1.480	1.240	1.770	0.460	-2.280	<0.001	Positive
	Tb.N	0	-1.140	-1.390	-0.940	0.362	1.360	<0.001	Negative
	Tb.Sp	1	1.290	1.040	1.600	0.187	-1.680	<0.001	Positive
	Total BV/TV	0	1.830	1.460	2.280	0.150	-2.420	0.001	Positive
	Ct.Th	1	2.430	1.980	2.980	0.278	-3.160	<0.001	Positive
<i>Homo</i>	BV/TV	0	2.600	1.760	3.840	0.095	-3.510	0.125	Uncorrelated
	DA	0	1.190	0.799	1.760	0.068	-1.880	0.198	Uncorrelated
	Tb.Th	1	1.970	1.370	2.810	0.244	-2.860	0.010	Positive
	Tb.N	0	-1.630	-2.420	-1.100	0.066	1.900	0.205	Uncorrelated
	Tb.Sp	1	1.990	1.320	2.990	0.009	-2.440	0.629	Uncorrelated
	Total BV/TV	0	2.160	1.450	3.210	0.064	-2.880	0.212	Uncorrelated
	Ct.Th	1	1.980	1.370	2.870	0.194	-2.760	0.024	Positive
<i>Pan</i>	BV/TV	0	-1.770	-3.140	-0.998	0.070	1.550	0.341	Uncorrelated
	DA	0	1.390	0.785	2.470	0.070	-2.160	0.344	Uncorrelated
	Tb.Th	1	-1.520	-2.710	-0.850	0.068	1.100	0.384	Uncorrelated
	Tb.N	0	1.140	0.628	2.060	<0.001	-1.170	0.976	Uncorrelated
	Tb.Sp	1	1.480	0.823	2.680	0.011	-1.950	0.071	Uncorrelated
	Total BV/TV	0	-1.850	-3.310	-1.030	0.032	1.800	0.536	Uncorrelated
	Ct.Th	1	-2.230	-4.000	-1.250	0.040	2.230	0.493	Uncorrelated
<i>Gorilla</i>	BV/TV	0	-1.010	-1.720	-0.597	0.064	0.859	0.342	Uncorrelated
	DA	0	0.712	0.418	1.210	0.050	-1.450	0.403	Uncorrelated
	Tb.Th	1	0.959	0.678	1.360	0.618	-1.650	<0.001	Isometry
	Tb.N	0	-1.220	-1.670	-0.895	0.693	1.490	<0.001	Negative
	Tb.Sp	1	1.450	1.020	2.070	0.602	-1.940	<0.001	Positive
	Total BV/TV	0	-0.833	-1.430	-0.484	0.011	0.802	0.698	Uncorrelated
	Ct.Th	1	1.670	1.080	2.560	0.402	-2.280	0.008	Positive
<i>Pongo</i>	BV/TV	0	2.570	1.410	4.690	0.077	-3.320	0.358	Uncorrelated
	DA	0	-1.180	-2.010	-0.690	0.291	0.761	0.057	Uncorrelated
	Tb.Th	1	1.690	1.010	2.850	0.328	-2.440	0.040	Positive
	Tb.N	0	-1.030	-1.880	-0.567	0.079	1.180	0.351	Uncorrelated
	Tb.Sp	1	1.330	0.711	2.470	<0.001	-1.660	0.980	Uncorrelated
	Total BV/TV	0	2.040	1.160	3.580	0.203	-2.560	0.123	Uncorrelated
	Ct.Th	1	3.250	2.000	5.280	0.425	-3.940	0.015	Positive

Note: CL- and CL+ indicate the 95% lower and upper limits for the confidence interval. Significant test are in bold.

other studies have used a VOI sampling sphere (Cotter et al., 2009; Ragni, 2020; Ryan & Shaw, 2013; Schilling et al., 2014). Results are likely also affected by the species constituting the study sample or the bone used for analysis (Doube et al., 2009; Ruff, 1987; Ryan & Shaw, 2013; Tsegai et al., 2017). Nevertheless, as BV/TV is widely reported as being independent of body mass/size, results here may indicate carpals are more likely than other skeletal elements to increase BV/TV in response to size, across hominoids. However, given the similarity in capitate size between *Homo*, *Pan* and *Pongo*, the

positive relationship found here is likely driven by the larger size of *Gorilla*, rather than reflecting a hominoid trend.

Ct.Th also scaled positively with size across hominoids and within *Homo*, *Gorilla*, and *Pongo*. Notably, the r^2 value for *Pongo* and *Gorilla* was high relative to other significant tests with 0.42 and 0.40 reported, respectively. These results may reflect sexually dimorphism in *Gorilla*, as the highest Ct.Th values were all found in males; however, the results were not so clear-cut in *Pongo*, with females represented within some of the highest values. The four

highest Ct.Th values in *Homo* were male; however, there was a large number of specimens with unknown sex. These results, particularly the relative strength of the r -squared value, deviate from other Ct.Th studies that, for example, reported isometry in the lumbar vertebrae (Fajardo et al., 2013), positive allometry with confidence intervals incorporating isometry in the femoral neck (Demes et al., 2000) or negative allometry in the radius and humerus (Doube et al., 2009).

BV/TV and Ct.Th are a primary component of bone strength and are thus critical to inferring function and functional adaptation from form (Maquer et al., 2015). The positive allometric relationship of BV/TV and Ct.Th to size found in this study potentially limits the interpretive value of these measures. However, in both measurements the coefficient of determination was small at 0.13 and 0.27, respectively. Although the average *Gorilla* capitate volume is only 3000 cubic millimeters larger than the pooled average of the other taxa, the significant results may be strongly driven by this size difference. While the significant allometric relationships of Tb.Th, Tb.N and Tb.Sp are notable, these measures are highly correlated with BV/TV and thus each is less important as a single measure than that of BV/TV for understanding bone strength and drawing behavioral inferences. Allometry is undoubtedly complex and not yet fully understood by bone biologists. The generally low r^2 values found here indicate that size did not exert a strong influence on bone parameters in our sample, but these somewhat unexpected results indicate allometry cannot be overlooked in multispecies comparisons.

4.2 | Can internal bone architecture differentiate locomotor modes of hominoids?

Predictions for BV/TV were broadly supported. In trabecular and total BV/TV, knuckle-walking African apes had the highest values, *Homo* had the lowest and *Pongo* generally fell out as intermediate between the two. These intermediate values in *Pongo* were not consistently differentiated from the other taxa. For example, although *Pongo* trabecular and total BV/TV in the distal capitate was significantly greater than that of *Homo*, it was not statistically different in the proximal capitate. This pattern was not predicted given the presumed higher forces acting on the *Pongo* capitate during locomotion compared with that of *Homo* manipulation. However, previous research has found similar results with BV/TV in *Pongo* being statistically undifferentiated from *Homo* within the capitate (Schilling et al., 2014) and other skeletal elements, including the talus (Desilva & Devlin, 2012; Tsegai et al., 2013), humerus (Kivell et al., 2018) and femur (Georgiou et al., 2019).

DA in the capitate was predicted to be highest in *Gorilla* and *Pan*, intermediate in *Homo* and lowest in *Pongo*, and results did not support this prediction. DA in the distal capitate was not significantly different between the genera, suggesting that the numerous, relatively immobile articulations within this region result in a similar DA value, irrespective of hand use. *Homo* and *Pongo* had higher DA in

the proximal capitate compared to the distal segment, which statistically separated them from the knuckle-walking taxa. High DA is correlated with strength along predictable loading trajectories within joints (Cotter et al., 2009; Hammond et al., 2018; Hart et al., 2017). In *Homo*, DA in the proximal capitate may be explained by load predictability as the DTM constitutes the path of motion in a large proportion of daily activities (Brigstocke et al., 2014; Crisco et al., 2005; Kaufman-Cohen et al., 2019; Moritomo et al., 2014; Schuidman et al., 1994). However, the relatively high DA in the *Pongo* proximal capitate was unexpected as it was assumed that the highly mobile joint and presumed variability in wrist postures adopted during arboreal locomotion would result in diverse loading of the proximal capitate and low DA. High DA is potentially linked to methodological limitations in quantifying directionality due to high Tb.Th or low Tb.N encapsulated by the sampling sphere (Dunmore et al., 2019). However, in this study, *Pongo* Tb.N and Tb.Th were intermediate between *Gorilla* and *Pan*, and thus, this result is unlikely a consequence of methodological limitations. Although some trabecular functional adaptation studies have found low DA values for *Pongo* as predicted (Georgiou et al., 2018; Kivell et al., 2018; Matarazzo, 2015; Tsegai et al., 2013) others have also found higher than expected values (Dunmore et al., 2019; Georgiou et al., 2019). Although arboreal locomotion is associated with mobile joints capable of receiving load from multiple directions, our knowledge of *Pongo* hand and wrist kinematics and kinetics is limited (but see Orr, 2010, 2017, 2018). The few studies of captive apes have provided invaluable data on the kinematics of vertical climbing (Isler, 2005; Isler & Thorpe, 2004) and quadrupedal walking (Finestone et al., 2018; Watson et al., 2011), but these behaviors constitute a small proportion of the *Pongo* locomotor repertoire (Cant, 1987; Thorpe & Crompton, 2006). Additionally, we currently lack manual pressure research on *Pongo* similar to that by Wunderlich and Jungers (2009) or Matarazzo (2013) on African apes. This research landscape may be limiting our ability to predict and interpret functional adaptation in the wrist and hand of wild *Pongo*. Nevertheless, the DA results here indicate that *Pongo* may have less variation in its wrist or hand postures than predicted with bone aligning to high loads from a low number of habitual postures.

The significantly more isotropic structure in the proximal capitate of knuckle-walkers was also unexpected as the low range of extension during knuckle-walking was assumed to result in high DA. Nevertheless, the DA results are contained within the range of values reported by Ragni (2020) for the *Gorilla* and *Pan* proximal capitate. Dunmore et al. (2019) similarly found the subarticular trabecular structure of the metacarpophalangeal joint in African apes to be more isotropic than predicted. While African apes are categorized as terrestrial knuckle-walkers, they also utilize arboreal substrates variably across their lifetimes to nest and exploit high quality food resources (Neufuss et al., 2017; Remis, 1995; Thorpe & Crompton, 2006). The isotropic structure may be a reflection of diverse hand postures and loading patterns from their mixed terrestrial and arboreal locomotor repertoire. It is possible these isotropic results are an artefact of high BV/TV lowering overall DA measurements and indeed in this study the lower proximal BV/TV values of

Homo and *Pongo* are associated with higher DA. However, the similar DA values in the distal capitate, despite diverse BV/TV values, suggests our method is able to capture variation in DA across a range of BV/TV values.

This study also investigated potential differences in ratios of bone parameters across the proximal and distal capitate, testing the null hypothesis that these ratios would be similar across hominoids. This hypothesis was generally not supported as only two ratios were statistically similar across all genera: distal trabecular BV/TV relative to proximal trabecular BV/TV and proximal total BV/TV relative to proximal trabecular BV/TV. Thus, although proximal Ct.Th in *Homo* and *Pongo* was significantly thinner than that of *Pan* and *Gorilla*, the relative proportion of cortex to trabeculae is similar across all taxa. Similarly, although eight of the 12 pairwise comparisons indicated statistically different trabecular BV/TV across the taxa (Figure 4a), the way trabecular volume differs between the two segments is consistent across hominoids. Although it was not predicted that ratio calculations would differentiate locomotor groups, three ratios distinguished *Homo* from the suspensory and knuckle-walking taxa: (1) distal total BV/TV relative to proximal total BV/TV, (2) distal total BV/TV relative to distal trabecular BV/TV, and (3) distal Ct.Th relative to proximal Ct.Th. Together, these ratios indicate that relatively low Ct.Th in the *Homo* distal capitate is distinctive compared with the thicker cortex in nonhuman apes. As Ct.Th is correlated to bone strength (Augat & Schorlemmer, 2006), the distal capitate in nonhuman apes is likely to be better able to resist fracture or failure and withstand high mechanical loads imposed upon the region.

This distinctive cortical morphology in nonhuman apes may reflect arboreal behaviors. All nonhuman apes engage in suspensory locomotion and climb vertical supports (Neufuss et al., 2017; Remis, 1995; Thorpe & Crompton, 2006), and in both behaviors the forelimbs are loaded in tension (Hanna et al., 2017; Hunt et al. 1996; Swartz et al., 1989). The distal capitate has numerous ligament attachments that induce tensional strain onto the capitate (Kijima & Viegas, 2009; Regal et al., 2020). Bones loaded in tension have a lower failure point than those loaded in compression (Caler & Carter, 1989; Pattin et al., 1996) and therefore greater BV/TV or Ct.Th would be required to prevent failure at ligament attachment sites (Doube et al., 2009).

When comparing differences in Tb.Th, Tb.N, and Tb.Sp across our study sample, results were similar to those of previous studies of different skeletal elements; *Pan* had high Tb.N and low Tb.Th and Tb.Sp, *Gorilla* showed the inverse, while *Homo* and *Pongo* were intermediate for all of these measures (Georgiou et al., 2019; Georgiou et al., 2018; Kivell et al., 2018; Komza & Skinner, 2019; Ragni, 2020; Ryan & Shaw, 2015; Scherf et al., 2013; Schilling et al., 2014). The consistent pattern within these parameters may represent systemic, rather than strongly functionally adaptive features of bone. DA and BV/TV have been shown to account for up to 98% of bone's elastic modulus (Maquer et al., 2015) and as Tb.Th, Tb.N and Tb.Sp interact via various combinations to produce BV/TV, individual measures of Tb.Th, Tb.N and Tb.Sp may be less useful for differentiating locomotor or postural modes.

4.3 | Do the proximal and distal segments reflect divergent strain patterns across the capitate?

Given differences in the articulations and mobility between the proximal and distal capitate, we hypothesized that these regions would show statistically different bone structure. This hypothesis was broadly supported but there was only partial support for the specific predictions. With only two exceptions (*Pongo* distal BV/TV relative to proximal BV/TV, and *Homo* distal Tb.Th relative to proximal Tb.Th), bone parameters differed significantly between the proximal and distal regions. This suggests that the internal bone is subjected to different forces and functional adaptation responses across the capitate. Ct.Th, DA and BV/TV were predicted to be higher in the distal relative to the proximal capitate due to the immobility in the distal carpal row and numerous ligament attachments. Ct.Th results in all genera supported this prediction while the DA prediction was only supported for *Gorilla* and *Pan*. All genera had significantly higher trabecular BV/TV in the proximal capitate; however, due to the great cortical thickening in nonhuman apes, total BV/TV was higher in the distal capitate of *Gorilla*, *Pan* and *Pongo*. In contrast, despite a 12% increase in distal Ct.Th, *Homo* maintained significantly higher total BV/TV in the proximal capitate. These differences in bone architecture were only revealed by holistically analyzing subregions of the capitate, while whole-bone measures or the exclusion of cortical bone, likely would have obscured or failed to pick up these trends.

While we argue that the results of this study indicate that force transfer differs across the proximal and distal capitate, additional analyses comparing different portions of the capitate are warranted to further test this conclusion. While this study averaged parameters across entire segments, bone volume distribution methods such as those used in Tsegai et al. (2013) and Tsegai et al. (2017) would allow more nuanced analysis between the regions under compression versus tension. Further, these methods would allow a deeper exploration of the biomechanical consequences of waisted versus non-waisted capitates and whether this aspect of morphology impacts the functional independence of the proximal and distal regions.

4.4 | The relationship between trabecular and cortical bone in the capitate

This study reveals the importance of considering both cortical and trabecular bone in functional adaptation research, rather than investigating each tissue separately. As exhibited in Figures 6 and 7, and discussed above, the cortical bone of the nonhuman ape capitate varied substantially from that of humans. Thus, the null hypothesis that the ratios of cortical to trabecular bone would be similar across the hominoids was not supported. However, there was one notable exception, namely, that all the study taxa had similar cortical to trabeculae ratios in the proximal capitate.

The differences between the proximal and distal Ct.Th across the locomotor groups provide support for the hypothesis that thick distal

cortex in the nonhuman apes is a result of functional adaptation. However, research indicates modern *Homo sapiens* have systemically low BV/TV and Ct.Th, which has been hypothesized to correlate with increased sedentism after the transition to an agricultural lifestyle (Chirchir et al., 2015; Ruff et al., 2006; Ryan & Shaw, 2015; Saers et al., 2016; Tsegai et al., 2018). Thus, it would be valuable to assess the distal Ct.Th of pre-Holocene *Homo sapiens* to further interrogate whether thick distal Ct.Th can be correlated simply with higher loading more generally, or, as hypothesized here, is related to forelimb involvement in arboreal behavior among the nonhuman apes. Further, there are important limitations to our interpretation of cortical bone functional adaptation in short bones. Although cortical bone does model its structure during adulthood in response to load, the genetic blueprint and the process of modelling during ontogeny greatly determines cortical bone geometry (Lovejoy et al., 2003; Martin et al., 1998). Investigation on the changes to cortical bone geometry as a result of functional adaptation have predominantly focused on changes at the mid-shaft of long bones (for examples and summary see Ruff et al., 2006 and references therein). In short bones there is unlikely to be the same capacity for the cortical bone to substantially change its geometry with modelling processes because, unlike the diaphysis of a long bone, there is not substantial room to expand (Martin et al., 1998). During adulthood, cortical bone commonly adapts its mechanical properties via changes to porosity, apparent mineral density or cellular anisotropy (Currey, 2002; Martin et al., 1998), changes that require different methodologies to assess (e.g., histology). Finally, when segmenting different bone tissues, it can be challenging to identify the boundary between cortex and trabeculae, particularly when the cortex is porous or trabeculae are especially thick. This was a particular challenge in some of the nonhuman ape capitate specimens (see Figure S1) and will likely be a limitation for many short bones, depending on the question being addressed.

5 | CONCLUSION

The capitate of knuckle-walking African apes and suspensory *Pongo* was differentiated from bipedal *Homo*, primarily, by thick distal cortical bone. African apes were further differentiated from *Pongo* and *Homo* by relatively isotropic trabeculae in the proximal capitate, which was not expected given the (presumably) more stereotypical loading of the wrist during knuckle-walking. However this higher than expected DA of the capitate head in *Homo* may indicate preferential alignment of trabeculae along the DTM. Although the wrist is often conceptualized as broadly being under compression or tension, the differentiated bone architecture in the proximal and distal regions of the capitate suggests that the loading environment can differ significantly even within the small bones of the carpus and highly localized functional adaptation responses may be taking place. Further, differences in cortical bone were critical for differentiating *Homo* from nonhuman apes. While an unexpected positive relationship was found between bone volume and capitate size, the

low coefficient of determination indicated size did not strongly influence group differences in bone microstructure. Given the complex biomechanical environment, and our limited understanding of intercarpal motion, (particularly in nonhuman apes) functional adaptation research of the carpals should take a holistic approach, including incorporated analysis of cortical bone.

ACKNOWLEDGEMENTS

This research was supported by a 50th Anniversary Research Scholarship, University of Kent (EEB), FP7 European Research Council Starting Grant #336301, European Union's Horizon 2020 research and innovation programme Grant #819960, and the Max Planck Society (MMS, TLK). For providing access to the specimens, we would like to acknowledge: G. Haszprunar, Bavarian State Collection of Zoology; Frieder Mayer and Christiane Funk, Berlin Museum für Naturkunde; T. Biers and M. Mirazon Lahr, the Duckworth Collection, University of Cambridge; V. Volpato and K. Krohmann, Frankfurt Senckenberg Museum; B. Großkopf, Georg-August-University Göttingen, Anthropology Collection; C. Boesch, Max Planck Institute for Evolutionary Anthropology; I. Livne, Powell-Cotton Museum; E. Gilissen and W. Wendelen, Royal Museum for Central Africa; J. Moggi-Cecchi and S. Bortoluzzi, University of Florence; M. Teschler-Nicola and R. Muehl, Vienna Natural History Museum. For microCT scanning, we thank R. Freeney, P. Schoenfeld, A. Silvester, K. Smithson, N. Stephens, H. Temming, Z. Tsegai, and A. Winzer. The authors declare no conflicts of interest. We also thank the two anonymous reviewers for their thoughtful commentary on early versions of this manuscript. The authors declare no conflicts of interest.

AUTHOR CONTRIBUTIONS

EEB conceived and designed the experiments, acquired data, performed the experiments, analyzed the data, prepared figures and tables, authored first draft and reviewed drafts of the paper, approved the final draft. TLK and MMS conceived and designed the experiments, contributed data, provided analysis tools, authored and provided critical review of manuscript drafts, approved the final manuscript.

DATA AVAILABILITY STATEMENT

The authors confirm that the data supporting the findings of this study are available within the article and its supplementary materials.

ORCID

Emma E. Bird  <https://orcid.org/0000-0001-8232-7485>

REFERENCES

- Augat, P. & Schorlemmer, S. (2006) The role of cortical bone and its microstructure in bone strength. *Age and Ageing*, 35, ii27–ii31.
- Barak, M.M. (2019) Bone modeling or bone remodeling: That is the question. *American Journal of Physical Anthropology*, 172(2), 153–155.
- Barak, M.M., Lieberman, D.E. & Hublin, J.-J. (2011) A Wolff in sheep's clothing: Trabecular bone adaptation in response to changes in joint loading orientation. *Bone*, 49, 1141–1151.

- Barak, M.M., Lieberman, D.E. & Hublin, J.-J. (2013) Of mice, rats and men: Trabecular bone architecture in mammals scales to body mass with negative allometry. *Journal of structural biology*, 183, 123–131.
- Barak, M.M., Weiner, S. & Shahar, R. (2010) The contribution of trabecular bone to the stiffness and strength of rat lumbar vertebrae. *Spine*, 35, E1153–E1159.
- Bardo, A., Vigouroux, L., Kivell, T.L. & Pouydebat, E. (2018) The impact of hand proportions on tool grip abilities in humans, great apes and fossil hominins: A biomechanical analysis using musculoskeletal simulation. *Journal of human evolution*, 125, 106–121.
- Begun, D.R. (2004) Knuckle-walking and the origin of human bipedalism. In: Meldrum, J. & Hilton, C.E. (Eds.) *From biped to strider: The emergence of modern human walking, running, and resource transport* (pp. 9–33). Springer Science & Business Media.
- Bertram, J.E. & Swartz, S.M. (1991) The 'law of bone transformation': A case of crying Wolff? *Biological Reviews*, 66(3), 245–273.
- Brainerd, E.L., Baier, D.B., Gatesy, S.M. et al. (2010) X-ray reconstruction of moving morphology (XROMM): precision, accuracy and applications in comparative biomechanics research. *Journal of Experimental Zoology Part A: Ecological Genetics and Physiology*, 313, 262–279.
- Brigstocke, G.H.O., Hearnden, A., Holt, C. & Whatling, G. (2014) In-vivo confirmation of the use of the dart thrower's motion during activities of daily living. *Journal of Hand Surgery (European Volume)*, 39, 373–378.
- Caler, W.E. & Carter, D.R. (1989) Bone creep-fatigue damage accumulation. *Journal of Biomechanics*, 22, 625–635.
- Cant, J.G. (1987) Positional behavior of female Bornean orangutans (*Pongo pygmaeus*). *American Journal of Primatology*, 12, 71–90.
- Carlson, K.J. & Patel, B.A. (2006) Habitual use of the primate forelimb is reflected in the material properties of subchondral bone in the distal radius. *Journal of anatomy*, 208, 659–670.
- Chirchir, H., Kivell, T.L., Ruff, C.B., Hublin, J.-J., Carlson, K.J., Zipfel, B. & et al. (2015) Recent origin of low trabecular bone density in modern humans. *Proceedings of the National Academy of Sciences of the United States of America*, 112, 366–371.
- Christen, P., Ito, K. & van Rietbergen, B. (2015) A potential mechanism for allometric trabecular bone scaling in terrestrial mammals. *Journal of anatomy*, 226, 236–243.
- Christen, P., Schulte, F.A., Zwahlen, A. et al. (2016) Voxel size dependency, reproducibility and sensitivity of an in vivo bone loading estimation algorithm. *Journal of the Royal Society Interface*, 13, 20150991.
- Cooper, D., Kawalilak, C., Harrison, K., Johnston, B. & Johnston, J. (2016) Cortical bone porosity: What is it, why is it important, and how can we detect it? *Current Osteoporosis Reports*, 14, 187–198.
- Cotter, M.M., Simpson, S.W., Latimer, B.M. & Hernandez, C.J. (2009) Trabecular microarchitecture of hominoid thoracic vertebrae. *The Anatomical Record: Advances in Integrative Anatomy and Evolutionary Biology: Advances in Integrative Anatomy and Evolutionary Biology*, 292, 1098–1106.
- Crisco, J.J., Coburn, J.C., Moore, D.C., Akelman, E., Weiss, A.-P.-C. & Wolfe, S.W. (2005) In vivo radiocarpal kinematics and the dart thrower's motion. *JBJS*, 87, 2729–2740.
- Crisco, J.J., Heard, W.M., Rich, R.R., Paller, D.J. & Wolfe, S.W. (2011) The mechanical axes of the wrist are oriented obliquely to the anatomical axes. *The Journal of Bone and Joint Surgery. American*, 93, 169–177.
- Currey, J.D. (2002) *Bones: Structure and mechanics*. Princeton University Press.
- Dainton, M. & Macho, G.A. (1999) Did knuckle-walking evolve twice? *Journal of Human Evolution*, 36, 171–194.
- Demes, B., Jungers, W.L. & Walker, C. (2000) Cortical bone distribution in the femoral neck of strepsirhine primates. *Journal of Human Evolution*, 39, 367–379.
- DeSilva, J.M. & Devlin, M.J. (2012) A comparative study of the trabecular bony architecture of the talus in humans, non-human primates, and Australopithecus. *Journal of Human Evolution*, 63, 536–551.
- Doran, D.M. (1992) The ontogeny of chimpanzee and pygmy chimpanzee locomotor behavior: a case study of paedomorphism and its behavioral correlates. *Journal of Human Evolution*, 23(2), 139–157.
- Doran, D.M. (1993) Sex differences in adult chimpanzee positional behavior: The influence of body size on locomotion and posture. *American Journal of Physical Anthropology*, 91, 99–115.
- Doran, D.M. (1997) Ontogeny of locomotion in mountain gorillas and chimpanzees. *Journal of Human Evolution*, 32(4), 323–344.
- Doube, M., Conroy, A.W., Christiansen, P., Hutchinson, J.R. & Shefelbine, S. (2009) Three-dimensional geometric analysis of felid limb bone allometry. *PLoS ONE*, 4, e4742.
- Doube, M., Klosowski, M.M., Arganda-Carreras, I., Cordelières, F.P., Dougherty, R.P., Jackson, J.S. et al. (2010) BoneJ: Free and extensible bone image analysis in ImageJ. *Bone*, 47, 1076–1079.
- Doube, M., Klosowski, M.M., Wiktorowicz-Conroy, A.M., Hutchinson, J.R. & Shefelbine, S.J. (2011) Trabecular bone scales allometrically in mammals and birds. *Proceedings of the Royal Society B: Biological Sciences*, 278, 3067–3073.
- Dunmore, C.J., Bardo, A., Skinner, M.M. & Kivell, T.L. (2020) Trabecular variation in the first metacarpal and manipulation in hominids. *American Journal of Physical Anthropology*, 171, 219–241.
- Dunmore, C.J., Kivell, T.L., Bardo, A. & Skinner, M.M. (2019) Metacarpal trabecular bone varies with distinct hand-positions used in hominid locomotion. *Journal of Anatomy*, 235(1), 45–66.
- Dunmore, C.J., Wollny, G. & Skinner, M.M. (2018) MIA-Clustering: A novel method for segmentation of paleontological material. *PeerJ*, 6, e4374.
- Fajardo, R.J., Desilva, J.M., Manoharan, R.K., Schmitz, J.E., Maclatchy, L.M. & Bouxsein, M.L. (2013) Lumbar vertebral body bone microstructural scaling in small to medium-sized strepsirhines. *The Anatomical Record*, 296, 210–226.
- Finestone, E.M., Brown, M.H., Ross, S.R. & Pontzer, H. (2018) Great ape walking kinematics: Implications for hominoid evolution. *American Journal of Physical Anthropology*, 166, 43–55.
- Fragaszy, D.M. & Crast, J. (2016) Functions of the hand in primates. In: Kivell, T.L., Lemelin, P., Richmond, B.G. & Schmitt, D. (Eds.) *The evolution of the primate hand*. Springer, pp. 313–344.
- Frost, H.M. (1987) Bone "mass" and the "mechanostat": A proposal. *The Anatomical Record*, 219, 1–9.
- García-Elias, M., Smith, D.K., Ruby, L.K., Horii, E., An, K.-N., Linscheid, R.L. & et al. (1994) Normal and abnormal carpal kinematics. In: Schuind, F., An, K.N., Cooney III, W.P. & García-Elias, M. (Eds.) *Advances in the biomechanics of the hand and wrist*, Vol. 256. Springer, pp. 247–253.
- Gatesy, S.M., Baier, D.B., Jenkins, F.A. & Dial, K.P. (2010) Scientific roscoping: A morphology-based method of 3-D motion analysis and visualization. *Journal of Experimental Zoology Part A: Ecological Genetics and Physiology*, 313, 244–261.
- Georgiou, L., Dunmore, C.J., Bardo, A., Buck, L.T., Hublin, J.-J., Pahr, D.H. et al. (2020) Evidence for habitual climbing in a Pleistocene hominin in South Africa. *Proceedings of the National Academy of Sciences of the United States of America*, 117, 8416–8423.
- Georgiou, L., Kivell, T.L., Pahr, D.H., Buck, L.T. & Skinner, M.M. (2019) Trabecular architecture of the great ape and human femoral head. *Journal of Anatomy*, 234, 679–693.
- Georgiou, L., Kivell, T.L., Pahr, D.H. & Skinner, M.M. (2018) Trabecular bone patterning in the hominoid distal femur. *PeerJ*, 6, e5156.
- Griffin, N.L., D'Août, K., Ryan, T.M., Richmond, B.G., Ketcham, R.A. & Postnov, A. (2010) Comparative forefoot trabecular bone architecture in extant hominids. *Journal of Human Evolution*, 59, 202–213.
- Gross, T., Kivell, T.L., Skinner, M.M., Nguyen, H. & Pahr, D.H. (2014) Holistic analysis of bone. *Palaeontologia Electronica*, 17, 1.

- Guo, X.E. (2001) Mechanical properties of cortical bone and cancellous bone tissue. *Bone Mechanics Handbook*, 10, 1–23.
- Hammond, M.A., Wallace, J.M., Allen, M.R. & Siegmund, T. (2018) Incorporating tissue anisotropy and heterogeneity in finite element models of trabecular bone altered predicted local stress distributions. *Biomechanics and Modeling in Mechanobiology*, 17, 605–614.
- Hanna, J.B., Granatosky, M.C., Rana, P. & Schmitt, D. (2017) The evolution of vertical climbing in primates: Evidence from reaction forces. *Journal of Experimental Biology*, 220, 3039–3052.
- Hart, N.H., Nimphius, S., Rantalainen, T., Ireland, A., Siafarikas, A. & Newton, R. (2017) Mechanical basis of bone strength: influence of bone material, bone structure and muscle action. *Journal of Musculoskeletal & Neuronal Interactions*, 17, 114.
- Hildebrand, T. & Rügsegger, P. (1997) A new method for the model-independent assessment of thickness in three-dimensional images. *Journal of Microscopy*, 185, 67–75.
- Hunt, K.D. (1992) Positional behavior of *Pan troglodytes* in the Mahale mountains and Gombe stream national parks, Tanzania. *American Journal of Physical Anthropology*, 87, 83–105.
- Inouye, S.E. (1994) Ontogeny of knuckle-walking hand postures in African apes. *Journal of human evolution*, 26, 459–485.
- Isaksson, H., Töyräs, J., Hakulinen, M., Aula, A.S., Tamminen, I., Julkunen, P. et al. (2011) Structural parameters of normal and osteoporotic human trabecular bone are affected differently by microCT image resolution. *Osteoporosis International*, 22, 167–177.
- Isler, K. (2005) 3D-kinematics of vertical climbing in hominoids. *American Journal of Physical Anthropology: The Official Publication of the American Association of Physical Anthropologists*, 126, 66–81.
- Isler, K. & Thorpe, S.K. (2004) Gait parameters in vertical climbing of captive, rehabilitant and wild Sumatran orang-utans (*Pongo pygmaeus abelii*). *Journal of Experimental Biology*, 206(22), 4081–4096.
- Jenkins, F.A. & Fleagle, J.G. (1975) Knuckle-walking and the functional anatomy of the wrists in living apes. In: Holloway, R.L. & Tuttle, R.H. (Eds.) *Primate functional morphology and evolution*. Mouton Press, pp. 213–227.
- Jouffroy, F.K. & Medina, M.F. (2002) Radio-ulnar deviation of the primate carpus: An X-ray study. *Zeitschrift für Morphologie und Anthropologie*, 83, 275–289.
- Kalkwarf, H.J. & Specker, B.L. (1995) Bone mineral loss during lactation and recovery after weaning. *Obstetrics & Gynecology*, 86, 26–32.
- Kaufman-Cohen, Y., Portnoy, S., Levanon, Y. & Friedman, J. (2019) Does object height affect the dart throwing motion angle during seated activities of daily living? *Journal of Motor Behavior*, 52(4), 456–465.
- Kijima, Y. & Viegas, S.F. (2009) Wrist anatomy and biomechanics. *The Journal of Hand Surgery*, 34, 1555–1563.
- Kivell, T.L. (2016a) The primate wrist. In: Kivell, T.L., Lemelin, P., Richmond, B.G. & Schmitt, D. (Eds.) *The evolution of the primate hand*. Springer, pp. 17–54.
- Kivell, T.L. (2016b) A review of trabecular bone functional adaptation: what have we learned from trabecular analyses in extant hominoids and what can we apply to fossils? *Journal of Anatomy*, 228, 569–594.
- Kivell, T.L., Davenport, R., Hublin, J.J., Thackeray, J.F. & Skinner, M.M. (2018) Trabecular architecture and joint loading of the proximal humerus in extant hominoids, Ateles, and *Australopithecus africanus*. *American Journal of Physical Anthropology*, 167, 348–365.
- Kivell, T.L. & Schmitt, D. (2009) Independent evolution of knuckle-walking in African apes shows that humans did not evolve from a knuckle-walking ancestor. *Proceedings of the National Academy of Sciences of the United States of America*, 106, 14241–14246.
- Komza, K. & Skinner, M.M. (2019) First metatarsal trabecular bone structure in extant hominoids and Swartkrans hominins. *Journal of Human Evolution*, 131, 1–21.
- Lewis, O.J. (1977) Joint remodelling and the evolution of the human hand. *Journal of Anatomy*, 123, 157–201.
- Lewis, O.J. (1989) *Functional morphology of the evolving hand and foot*. Oxford University Press.
- Lieberman, D.E. (1996) How and why humans grow thin skulls: Experimental evidence for systemic cortical robusticity. *American Journal of Physical Anthropology: The Official Publication of the American Association of Physical Anthropologists*, 101, 217–236.
- Lieberman, D.E. (1997) Making behavioral and phylogenetic inferences from hominid fossils: considering the developmental influence of mechanical forces. *Annual Review of Anthropology*, 26, 185–210.
- Lovejoy, C.O., McCollum, M.A., Reno, P.L. & Rosenman, B.A. (2003) Developmental biology and human evolution. *Annual Review of Anthropology*, 32, 85–109.
- Manduell, K.L., Morrogh-Bernard, H.C. & Thorpe, S.K.S. (2011) Locomotor behavior of wild orangutans (*Pongo pygmaeus wurmbii*) in disturbed peat swamp forest, Sabangau, Central Kalimantan, Indonesia. *American Journal of Physical Anthropology*, 145, 348–359.
- Maquer, G., Musy, S.N., Wandel, J., Gross, T. & Zysset, P.K. (2015) Bone volume fraction and fabric anisotropy are better determinants of trabecular bone stiffness than other morphological variables. *Journal of Bone and Mineral Research*, 30, 1000–1008.
- Martin, R.B., Burr, D.B. & Sharkey, N.A. (1998) *Skeletal tissue mechanics*. Springer.
- Marzke, M.W. (1983) Joint functions and grips of the *Australopithecus afarensis* hand, with special reference to the region of the capitate. *Journal of Human Evolution*, 12, 197–211.
- Marzke, M.W. (1997) Precision grips, hand morphology, and tools. *American Journal of Physical Anthropology*, 102, 91–110.
- Marzke, M.W. (2013) Tool making, hand morphology and fossil hominins. *Philosophical Transactions of the Royal Society B: Biological Sciences*, 368(1630), 20120414.
- Marzke, M.W. & Marzke, R.F. (1987) The third metacarpal styloid process in humans: Origin and functions. *American Journal of Physical Anthropology*, 73, 415–431.
- Matarazzo, S. (2013) Manual pressure distribution patterns of knuckle-walking apes. *American Journal of Physical Anthropology*, 152, 44–50.
- Matarazzo, S.A. (2015) Trabecular architecture of the manual elements reflects locomotor patterns in primates. *PLoS ONE*, 10, e0120436.
- Mielke, M., Wölfer, J., Arnold, P., van Heteren, A.H., Amson, E. & Nyakatura, J.A. (2018) Trabecular architecture in the sciuriform femoral head: Allometry and functional adaptation. *Zoological letters*, 4, 10.
- Moojen, T.M., Snel, J.G., Ritt, M.J., Venema, H.W., Kauer, J.M. & Bos, K.E. (2003) In vivo analysis of carpal kinematics and comparative review of the literature. *The Journal of Hand Surgery*, 28, 81–87.
- Moritomo, H., Apergis, E.P., Herzberg, G., Werner, F.W., Wolfe, S.W. & Garcia-Elias, M. (2014) IFSSH scientific committee on anatomy and biomechanics wrist biomechanics and instability: Wrist dart-throwing motion updated. *International Federation of Societies for Surgery of the Hand*, 23–28.
- Napier, J.R. (1956) The prehensile movements of the human hand. *The Journal of Bone and Joint Surgery. British*, 38, 902–913.
- Neufuss, J., Robbins, M.M., Baeumer, J., Humle, T. & Kivell, T.L. (2017) Comparison of hand use and forelimb posture during vertical climbing in mountain gorillas (*Gorilla beringei beringei*) and chimpanzees (*Pan troglodytes*). *American Journal of Physical Anthropology*, 164, 651–664.
- Niewoehner, W.A., Weaver, A.H. & Trinkaus, E. (1997) Neandertal capitate-metacarpal articular morphology. *American Journal of Physical Anthropology: The Official Publication of the American Association of Physical Anthropologists*, 103, 219–233.
- Orr, C.M. (2005) Knuckle-walking anteaater: A convergence test of adaptation for purported knuckle-walking features of african Hominidae. *American Journal of Physical Anthropology: The Official Publication of the American Association of Physical Anthropologists*, 128, 639–658.
- Orr, C.M. (2010) *Adaptations to knuckle-walking and digitigrady: A three-dimensional kinematic and morphometric analysis of the anthropoid wrist*. Arizona State University.

- Orr, C.M. (2016) Functional morphology of the primate hand: Recent approaches using biomedical imaging, computer modeling, and engineering methods. In: Kivell, T.L., Lemelin, P., Richmond, B.G. & Schmitt, D. (Eds.) *The evolution of the primate hand*. Springer, pp. 227–257.
- Orr, C.M. (2017) Locomotor hand postures, carpal kinematics during wrist extension, and associated morphology in anthropoid primates. *The Anatomical Record*, 300, 382–401.
- Orr, C.M. (2018) Kinematics of the anthropoid os centrale and the functional consequences of scaphoid-centrale fusion in African apes and hominins. *Journal of Human Evolution*, 114, 102–117.
- Orr, C.M., Leventhal, E.L., Chivers, S.F., Marzke, M.W., Wolfe, S.W. & Crisco, J.J. (2010) Studying primate carpal kinematics in three dimensions using a computed-tomography-based markerless registration method. *The Anatomical Record: Advances in Integrative Anatomy and Evolutionary Biology*, 293, 692–709.
- Pahr, D.H. & Zysset, P.K. (2009) From high-resolution CT data to finite element models: Development of an integrated modular framework. *Computer Methods in Biomechanics and Biomedical Engineering*, 12, 45–57.
- Pahr, D.H. & Zysset, P.K. (2009) A comparison of enhanced continuum FE with micro FE models of human vertebral bodies. *Journal of Biomechanics*, 42, 455–462.
- Parsons, T.J., Van Dusseldorp, M., van Der Vliet, M., Van De Werken, K., Schaafsma, G. & Van Staveren, W.A. (1997) Reduced bone mass in Dutch adolescents fed a macrobiotic diet in early life. *Journal of Bone and Mineral Research*, 12, 1486–1494.
- Paternoster, L., Lorentzon, M., Lehtimäki, T., Eriksson, J., Kähönen, M., Raitakari, O. et al. (2013) Genetic determinants of trabecular and cortical volumetric bone mineral densities and bone microstructure. *PLoS Genetics*, 9, e1003247.
- Pattin, C.A., Caler, W.E. & Carter, D.R. (1996) Cyclic mechanical property degradation during fatigue loading of cortical bone. *Journal of Biomechanics*, 29, 69–79.
- Pearson, O.M. & Lieberman, D.E. (2004) The aging of Wolff's "law": ontogeny and responses to mechanical loading in cortical bone. *American Journal of Physical Anthropology*, 125(S39), 63–99.
- Pettersson, U., Nilsson, M., Sundh, V., Mellström, D. & Lorentzon, M. (2010) Physical activity is the strongest predictor of calcaneal peak bone mass in young Swedish men. *Osteoporosis International*, 21, 447–455.
- Pontzer, H., Lieberman, D.E., Momin, E., Devlin, M.J., Polk, J.D., Hallgrímsson, B. & et al. (2006) Trabecular bone in the bird knee responds with high sensitivity to changes in load orientation. *The Journal of Experimental Biology*, 209, 57–65.
- Ragni, A.J. (2020) Trabecular architecture of the capitate and third metacarpal through ontogeny in chimpanzees (*Pan troglodytes*) and gorillas (*Gorilla gorilla*). *Journal of Human Evolution*, 138, 102702.
- Regal, S., Maschke, S. & Li, Z.-M. (2020) Hand and wrist biomechanics. In: Cheng, C.K. & Woo, S.L. (Eds.) *Frontiers in orthopaedic biomechanics*. Springer, pp. 89–104.
- Rein, T.R. & Harvati, K. (2013) Exploring third metacarpal capitate facet shape in early hominins. *The Anatomical Record*, 296, 240–249.
- Remis, M. (1995) Effects of body size and social context on the arboreal activities of lowland gorillas in the Central African Republic. *American Journal of Physical Anthropology*, 97, 413–433.
- Remis, M.J. (1998) The gorilla paradox. In: Strasser, E., Fleagle, J., Rosenberger, A.L. & McHenry, H. (Eds.) *Primate locomotion: Recent advances*. Springer, pp. 95–106.
- Richmond, B.G. (2006) Functional morphology of the midcarpal joint in knuckle-walkers and terrestrial quadrupeds. In: Ishida, H., Tuttle, R., Pickford, M., Oghihara, N. & Nakatsukasa, M. (Eds.) *Human origins and environmental backgrounds*. Springer Science & Business Media, pp. 105–122.
- Richmond, B.G., Begun, D.R. & Strait, D.S. (2001) Origin of human bipedalism: The knuckle-walking hypothesis revisited. *American Journal of Physical Anthropology: The Official Publication of the American Association of Physical Anthropologists*, 116, 70–105.
- Riley, G. & Trinkaus, E. (1989) Neandertal capitate-metacarpal 2 articular morphology and Neandertal manipulative behavior. *American Journal of Physical Anthropology*, 78, 290.
- Ruff, C.B. (1984) Allometry between length and cross-sectional dimensions of the femur and tibia in *Homo sapiens sapiens*. *American Journal of Physical Anthropology*, 65, 347–358.
- Ruff, C. (1987) Sexual dimorphism in human lower limb bone structure: relationship to subsistence strategy and sexual division of labor. *Journal of Human Evolution*, 16(5), 391–416.
- Ruff, C., Holt, B. & Trinkaus, E. (2006) Who's afraid of the big bad Wolff?: "Wolff's law" and bone functional adaptation. *American Journal of Physical Anthropology: The Official Publication of the American Association of Physical Anthropologists*, 129, 484–498.
- Ruff, C.B. & Runestad, J.A. (1992) Primate limb bone structural adaptations. *Annual Review of Anthropology*, 21, 407–433.
- Runestad, J.A. (1997) Postcranial adaptations for climbing in Loridae (Primates). *Journal of Zoology*, 242, 261–290.
- Ryan, T.M. & Shaw, C.N. (2013) Trabecular bone microstructure scales allometrically in the primate humerus and femur. *Proceedings of the Royal Society B: Biological Sciences*, 280, 20130172.
- Ryan, T.M. & Shaw, C.N. (2015) Gracility of the modern *Homo sapiens* skeleton is the result of decreased biomechanical loading. *Proceedings of the National Academy of Sciences of the United States of America*, 112, 372–377.
- Saers, J.P.P., Cazorla-Bak, Y., Shaw, C.N., Stock, J.T. & Ryan, T.M. (2016) Trabecular bone structural variation throughout the human lower limb. *Journal of Human Evolution*, 97, 97–108.
- Sarmiento, E.E. (1988) Anatomy of the hominoid wrist joint: its evolutionary and functional implications. *International Journal of Primatology*, 9, 281–345.
- Scherf, H., Harvati, K. & Hublin, J.J. (2013) A comparison of proximal humeral cancellous bone of great apes and humans. *Journal of Human Evolution*, 65, 29–38.
- Schilling, A.M., Tofanelli, S., Hublin, J.J. & Kivell, T.L. (2014) Trabecular bone structure in the primate wrist. *Journal of Morphology*, 275, 572–585.
- Schuidt, F., An, K.N., Cooney III, W.P. & Garcia-Elias, M. (1994) *Advances in the Biomechanics of the Hand and Wrist*. 256, Springer Science & Business Media.
- Schuidt, F., Cooney, W.P., Linscheid, R.L., An, K.N. & Chao, E.Y.S. (1995) Force and pressure transmission through the normal wrist. A theoretical two-dimensional study in the posteroanterior plane. *Journal of Biomechanics*, 28, 587–601.
- Skinner, M.M., Stephens, N.B., Tsegai, Z.J., Foote, A.C., Huynh Nguyen, N., Gross, T. et al. (2015) Human evolution. Human-like hand use in *Australopithecus africanus*. *Science*, 347, 395–399.
- Smith, R.J. & Jungers, W.L. (1997) Body mass in comparative primatology. *Journal of Human evolution*, 32, 523–559.
- Stephens, N.B., Kivell, T.L., Gross, T., Pahr, D.H., Lazenby, R.A., Hublin, J.-J. et al. (2016) Trabecular architecture in the thumb of *Pan* and *Homo*: implications for investigating hand use, loading, and hand preference in the fossil record. *American Journal of Physical Anthropology*, 161, 603–619.
- Stephens, N.B., Kivell, T.L., Pahr, D.H., Hublin, J.-J. & Skinner, M.M. (2018) Trabecular bone patterning across the human hand. *Journal of Human Evolution*, 123, 1–23.
- Su, A. & Carlson, K.J. (2017) Comparative analysis of trabecular bone structure and orientation in South African hominin *tali*. *Journal of Human Evolution*, 106, 1–18.
- Swartz, S.M., Bertram, J.E.A. & Biewener, A.A. (1989) Telemetered in vivo strain analysis of locomotor mechanics of brachiating gibbons. *Nature*, 342, 270.
- Tang, J.B., Gu, X.K., Xu, J. & Gu, J.H. (2011) In vivo length changes of carpal ligaments of the wrist during dart-throwing motion. *The Journal of Hand Surgery*, 36(2), 284–290.

- Thompson, N.E. (2020) The biomechanics of knuckle-walking: 3-D kinematics of the chimpanzee and macaque wrist, hand and fingers. *Journal of Experimental Biology*, 223, jeb235226.
- Thompson, N.E., Ostrofsky, K.R., McFarlin, S.C., Robbins, M.M., Stoinski, T.S. & Alméjida, S. (2018) Unexpected terrestrial hand posture diversity in wild mountain gorillas. *American Journal of Physical Anthropology*, 166, 84–94.
- Thorpe, S.K.S. & Crompton, R.H. (2006) Orangutan positional behavior and the nature of arboreal locomotion in Hominoidea. *American Journal of Physical Anthropology: The Official Publication of the American Association of Physical Anthropologists*, 131, 384–401.
- Thorpe, S.K.S. & Crompton, R.H. (2009) Orangutan positional behavior: Interspecific variation and ecological correlates. In: Wich, S.A., Setia, T.M. & van Schaik, P. (Eds.) *Orangutans: Geographic variation in behavioral ecology and conservation*, OUP Oxford, pp. 33–47.
- Tocheri, M.W. (2007) Three-dimensional riddles of the radial wrist: derived carpal and carpometacarpal joint morphology in the genus *Homo* and the implications for understanding the evolution of stone tool-related behaviors in hominins. Doctoral dissertation, Arizona State University.
- Tocheri, M.W., Orr, C.M., Jacofsky, M.C. & Marzke, M.W. (2008) The evolutionary history of the hominin hand since the last common ancestor of *Pan* and *Homo*. *Journal of Anatomy*, 212, 544–562.
- Tocheri, M.W., Orr, C.M., Larson, S.G., Sutikna, T., Jatmiko, W., Wahyu Saptomo, E. et al. (2007) The primitive wrist of *Homo floresiensis* and its implications for hominin evolution. *Science*, 317, 1743–1745.
- Tsegai, Z.J., Kivell, T.L., Gross, T., Nguyen, N.H., Pahr, D.H., Smaers, J.B. & et al. (2013) Trabecular bone structure correlates with hand posture and use in hominoids. *PLoS ONE*, 8, e78781.
- Tsegai, Z.J., Skinner, M.M., Gee, A.H., Pahr, D.H., Treece, G.M., Hublin, J.J. & et al. (2017) Trabecular and cortical bone structure of the talus and distal tibia in *Pan* and *Homo*. *American Journal of Physical Anthropology*, 163, 784–805.
- Tsegai, Z.J., Skinner, M.M., Pahr, D.H., Hublin, J.J. & Kivell, T.L. (2018) Systemic patterns of trabecular bone across the human and chimpanzee skeleton. *Journal of anatomy*, 232, 641–656.
- Tuttle, R.H. (1969) Quantitative and functional studies on the hands of the Anthropoidea. I. The Hominoidea. *Journal of Morphology*, 128, 309–363.
- van Lawick-Goodall, J. (1968) The behaviour of free-living chimpanzees in the Gombe Stream Reserve. *Animal Behaviour Monographs*, 1, 161–IN12.
- Wallace, I.J., Pagnotti, G.M., Rubin-Sigler, J., Naeher, M., Copes, L.E., Judex, S. et al. (2015) Focal enhancement of the skeleton to exercise correlates to mesenchymal stem cell responsiveness rather than peak external forces. *Journal of Experimental Biology*, 218(19), 3002–3009.
- Ward, C.V. (2002) Interpreting the posture and locomotion of *Australopithecus afarensis*: Where do we stand? *American Journal of Physical Anthropology*, 119, 185–215.
- Ward, C.V., Tocheri, M.W., Plavcan, J.M., Brown, F.H. & Manthi, F.K. (2014) Early Pleistocene third metacarpal from Kenya and the evolution of modern human-like hand morphology. *Proceedings of the National Academy of Sciences of the United States of America*, 111, 121–124.
- Watson, J., Payne, R., Chamberlain, A., Jones, R. & Sellers, W. (2011) The influence of load carrying on gait parameters in humans and apes: Implications for the evolution of human bipedalism. In: D'Août, K. & Vereecke, E.E. (Eds.) *Primate locomotion: Linking field and laboratory research*. Springer Science & Business Media, pp. 109–134.
- Whitehouse, W.J. (1974) The quantitative morphology of anisotropic trabecular bone. *Journal of Microscopy*, 101, 153–168.
- Wolfe, S.W., Crisco, J.J., Orr, C.M. & Marzke, M.W. (2006) The dart-throwing motion of the wrist: is it unique to humans? *The Journal of Hand Surgery*, 31, 1429–1437.
- Wunderlich, R.E. & Jungers, W.L. (2009) Manual digital pressures during knuckle-walking in chimpanzees (*Pan troglodytes*). *American Journal of Physical Anthropology: The Official Publication of the American Association of Physical Anthropologists*, 139, 394–403.
- Yao, J., Lian, Z., Yang, B. & Fan, Y. (2020) Biomechanics of ligaments. In: Cheng, C.K. & Woo, S.L. (Eds.) *Frontiers in orthopaedic biomechanics*. Springer, pp. 75–87.
- Yeni, Y.N., Zinno, M.J., Yerramshetty, J.S., Zael, R. & Fyhrie, D.P. (2011) Variability of trabecular microstructure is age-, gender-, race- and anatomic site-dependent and affects stiffness and stress distribution properties of human vertebral cancellous bone. *Bone*, 49, 886–894.
- Zeininger, A., Richmond, B.G. & Hartman, G. (2011) Metacarpal head biomechanics: A comparative backscattered electron image analysis of trabecular bone mineral density in *Pan troglodytes*, *Pongo pygmaeus*, and *Homo sapiens*. *Journal of Human Evolution*, 60, 703–710.

SUPPORTING INFORMATION

Additional supporting information may be found online in the Supporting Information section.

How to cite this article: Bird EE, Kivell TL, Skinner MM. Cortical and trabecular bone structure of the hominoid capitate. *J Anat.* 2021;00:1–23. <https://doi.org/10.1111/joa.13437>

8.3. Further acknowledgements

This research was supported by a 50th Anniversary Research Scholarship, University of Kent (EEB), FP7 European Research Council Starting Grant #336301, European Union's Horizon 2020 research and innovation programme Grant #819960 and the Max Planck Society (MMS, TLK). For providing access to the specimens, we would like to acknowledge: G. Haszprunar, Bavarian State Collection of Zoology; F. Mayer and C. Funk, Berlin Museum für Naturkunde; T. Biers and M. Mirazon Lahr, the Duckworth Collection, University of Cambridge; V. Volpato and K. Krohmann, Frankfurt Senckenberg Museum; B. Großkopf, Georg-August-University Goettingen, Anthropology Collection; C. Boesch, A. Hildred, the Mary Rose Trust; Max Planck Institute for Evolutionary Anthropology; A. Rosas, Paleoanthropology Group, Museo Nacional de Ciencias Naturales -Consejo Superior de Investigaciones Científicas (CSIC), Madrid, Spain; I. Livne, Powell-Cotton Museum; E. Gilissen and W. Wendelen, Royal Museum for Central Africa; State Museum, Bonn; I. Herskovitz, Tel Aviv University; J. Moggi-Cecchi and S. Bortoluzzi, University of Florence; B. Zipfel, University of the Witwatersrand, Johannesburg; M. Teschler-Nicola and R. Muehl, Vienna Natural History Museum. For microCT scanning, we thank R. Freeney, P. Schoenfeld, A. Silvester, K. Smithson, N. Stephens, H. Temming, Z. Tsegai, and A. Winzer.

Chapter 3 is the peer reviewed version of the following article: Bird, E. E., Kivell, T. L., & Skinner, M. M. (2021). Cortical and trabecular bone structure of the hominoid capitate. *Journal of anatomy*, 239(2), 351-373, which has been published in final form at <https://doi.org/10.1111/joa.13437>. This article may be used for non-commercial purposes in accordance with Wiley Terms and Conditions for Use of Self-Archived Versions. This article may not be enhanced, enriched or otherwise transformed into a derivative work, without express permission from Wiley or by statutory rights under applicable legislation. Copyright notices must not be removed, obscured or modified. The article must be linked to Wiley's version of record on Wiley Online Library and any embedding, framing or otherwise making available the article or pages thereof by third parties from platforms, services and websites other than Wiley Online Library must be prohibited.

Chapter 4 is the peer reviewed version of the following article: Bird, E. E., Kivell, T. L., & Skinner, M. M. (2022). Patterns of internal bone structure and functional adaptation in the hominoid scaphoid, lunate, and triquetrum. *American Journal of Biological Anthropology*, 177(2), 266-285, which has been published in final form at <https://doi.org/10.1002/ajpa.24449>. This article may be used for non-commercial purposes in accordance with Wiley Terms and Conditions for Use of Self-Archived Versions. This article

may not be enhanced, enriched or otherwise transformed into a derivative work, without express permission from Wiley or by statutory rights under applicable legislation. Copyright notices must not be removed, obscured or modified. The article must be linked to Wiley's version of record on Wiley Online Library and any embedding, framing or otherwise making available the article or pages thereof by third parties from platforms, services and websites other than Wiley Online Library must be prohibited.